MICROBIAL CONNECTIONS BETWEEN THE SUBSURFACE SULFUR CYCLE AND OTHER ELEMENTAL CYCLES

EDITED BY: Alexandra V. Turchyn, Orit Sivan, Shuhei Ono and Tanja Bosak
PUBLISHED IN: Frontiers in Microbiology and Frontiers in Earth Science

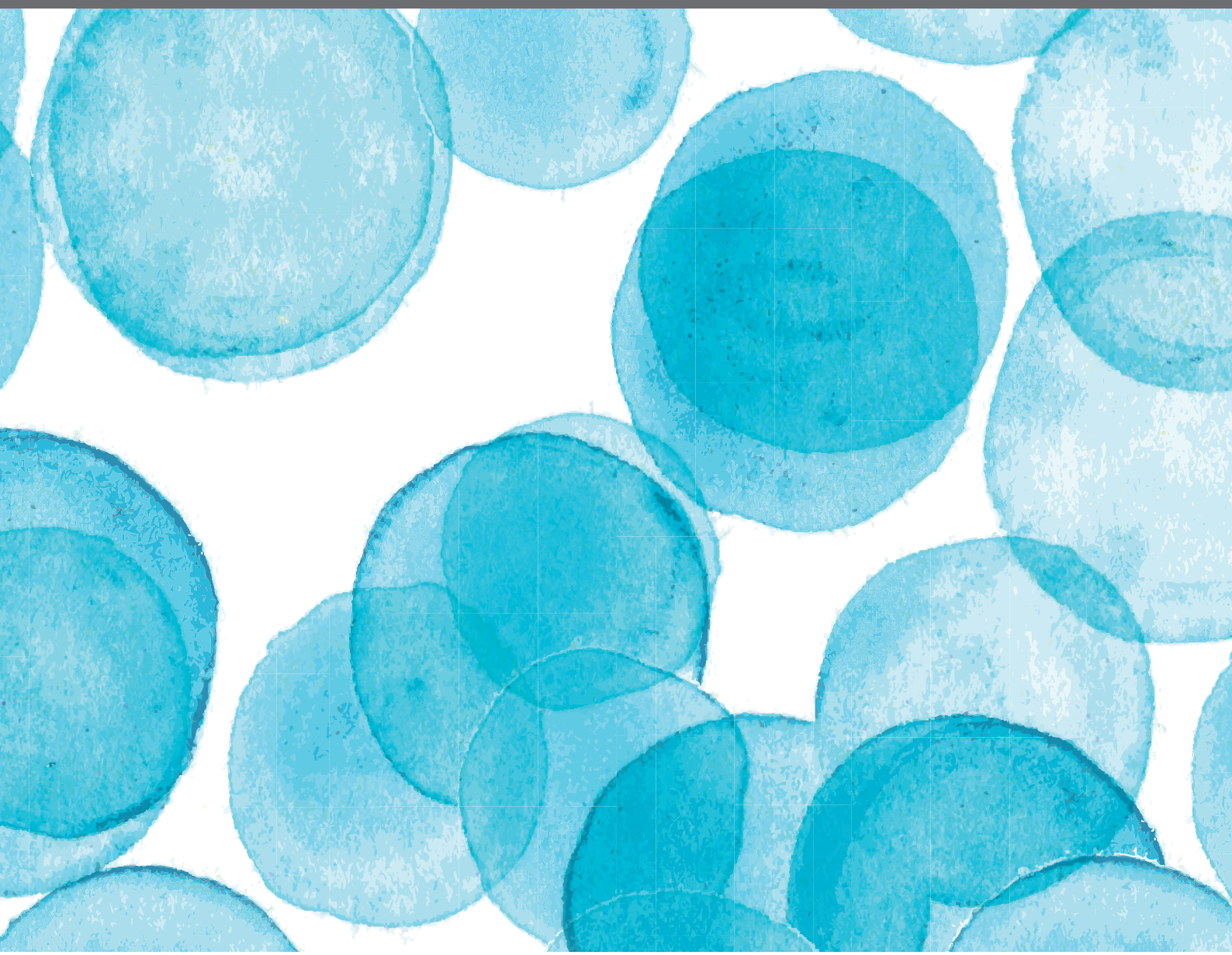

frontiers Research Topics

frontiers

ISSN 1664-8714
ISBN 978-2-88945-652-9
DOI 10.3389/978-2-88945-652-9

About Frontiers

Frontiers is more than just an open-access publisher of scholarly articles: it is a pioneering approach to the world of academia, radically improving the way scholarly research is managed. The grand vision of Frontiers is a world where all people have an equal opportunity to seek, share and generate knowledge. Frontiers provides immediate and permanent online open access to all its publications, but this alone is not enough to realize our grand goals.

Frontiers Journal Series

The Frontiers Journal Series is a multi-tier and interdisciplinary set of open-access, online journals, promising a paradigm shift from the current review, selection and dissemination processes in academic publishing. All Frontiers journals are driven by researchers for researchers; therefore, they constitute a service to the scholarly community. At the same time, the Frontiers Journal Series operates on a revolutionary invention, the tiered publishing system, initially addressing specific communities of scholars, and gradually climbing up to broader public understanding, thus serving the interests of the lay society, too.

Dedication to Quality

Each Frontiers article is a landmark of the highest quality, thanks to genuinely collaborative interactions between authors and review editors, who include some of the world's best academicians. Research must be certified by peers before entering a stream of knowledge that may eventually reach the public - and shape society; therefore, Frontiers only applies the most rigorous and unbiased reviews.
Frontiers revolutionizes research publishing by freely delivering the most outstanding research, evaluated with no bias from both the academic and social point of view. By applying the most advanced information technologies, Frontiers is catapulting scholarly publishing into a new generation.

What are Frontiers Research Topics?

Frontiers Research Topics are very popular trademarks of the Frontiers Journals Series: they are collections of at least ten articles, all centered on a particular subject. With their unique mix of varied contributions from Original Research to Review Articles, Frontiers Research Topics unify the most influential researchers, the latest key findings and historical advances in a hot research area! Find out more on how to host your own Frontiers Research Topic or contribute to one as an author by contacting the Frontiers Editorial Office: researchtopics@frontiersin.org

MICROBIAL CONNECTIONS BETWEEN THE SUBSURFACE SULFUR CYCLE AND OTHER ELEMENTAL CYCLES

Topic Editors:
Alexandra V. Turchyn, University of Cambridge, United Kingdom
Orit Sivan, Ben-Gurion University of the Negev, Israel
Shuhei Ono, Massachusetts Institute of Technology, United States
Tanja Bosak, Massachusetts Institute of Technology, United States

Citation: Turchyn, A. V., Sivan, O., Ono, S., Bosak T., eds (2018). Microbial Connections Between the Subsurface Sulfur Cycle and Other Elemental Cycles. Lausanne: Frontiers Media. doi: 10.3389/978-2-88945-652-9

Table of Contents

frontiers in Microbiology

PERSPECTIVE
published: 06 April 2018
doi: 10.3389/fmicb.2018.00519

A Critical Look at the Combined Use of Sulfur and Oxygen Isotopes to Study Microbial Metabolisms in Methane-Rich Environments

Gilad Antler[1,2,3] and André Pellerin[4]*

[1] Department of Earth Sciences, University of Cambridge, Cambridge, United Kingdom, [2] Department of Geological and Environmental Sciences, Ben-Gurion University of the Negev, Beersheba, Israel, [3] The Interuniversity Institute for Marine Sciences, Eilat, Israel, [4] Center for Geomicrobiology, Department of Bioscience, Aarhus University, Aarhus, Denmark

Separating the contributions of anaerobic oxidation of methane and organoclastic sulfate reduction in the overall sedimentary sulfur cycle of marine sediments has benefited from advances in isotope biogeochemistry. Particularly, the coupling of sulfur and oxygen isotopes measured in the residual sulfate pool ($\delta^{18}O_{SO4}$ vs. $\delta^{34}S_{SO4}$). Yet, some important questions remain. Recent works have observed patterns that are inconsistent with previous interpretations. We differentiate the contributions of oxygen and sulfur isotopes to separating the anaerobic oxidation of methane and organoclastic sulfate reduction into three phases; first evidence from conventional high methane vs. low methane sites suggests a clear relationship between oxygen and sulfur isotopes in porewater and the metabolic process taking place. Second, evidence from pure cultures and organic matter rich sites with low levels of methane suggest the signatures of both processes overlap and cannot be differentiated. Third, we take a critical look at the use of oxygen and sulfur isotopes to differentiate metabolic processes (anaerobic oxidation of methane vs. organoclastic sulfate reduction). We identify that it is essential to develop a better understanding of the oxygen kinetic isotope effect, the degree of isotope exchange with sulfur intermediates as well as establishing their relationships with the cell-specific metabolic rates if we are to develop this proxy into a reliable tool to study the sulfur cycle in marine sediments and the geological record.

Keywords: sulfur isotopes, oxygen isotopes, anaerobic oxidation of methane (AOM), sulfate reduction rates, marine sediments

OPEN ACCESS

Edited by:
Gordon T. Taylor,
Stony Brook University, United States

Reviewed by:
Mustafa Yucel,
Middle East Technical University, Turkey
William D. Leavitt,
Dartmouth College, United States

****Correspondence:***
Gilad Antler
giladantler@gmail.com

Specialty section:
This article was submitted to Microbiological Chemistry and Geomicrobiology, a section of the journal Frontiers in Microbiology

Received: *23 May 2017*
Accepted: *08 March 2018*
Published: *06 April 2018*

Citation:
Antler G and Pellerin A (2018) A Critical Look at the Combined Use of Sulfur and Oxygen Isotopes to Study Microbial Metabolisms in Methane-Rich Environments. Front. Microbiol. 9:519. doi: 10.3389/fmicb.2018.00519

INTRODUCTION

Methane is an important greenhouse gas which moderates the climate of the planet and marine sediments are Earth's largest methane reservoir and production site (Whiticar et al., 1986; Kvenvolden, 1988). In the distant past, fluxes of methane from marine pelagic environments may have triggered abrupt warming periods (Dickens et al., 1995) and understanding the controls on its production and release is of interest for predictions of climate change and reconstruction of Earth's past. A continuous flux of methane from biotic and thermogenic origins diffuses or escapes from production zones toward the surface. The distinct zone where upward diffusion of methane meets with the downward diffusion of sulfate from seawater is called the sulfate methane transition zone. This zone is where the anaerobic oxidation of methane by sulfate (hereafter 'AOM-SR') is

catalyzed by consortia of bacteria and archaea who derive energy for growth by reacting the two together (Boetius et al., 2000). This leads to the quasi-quantitative consumption of both substrates, the establishment of steady state concentration profiles and the oxidation of a large fraction of the flux of methane, which would otherwise diffuses upward into the ocean (Wuebbles and Hayhoe, 2002). Sulfate is also consumed by sulfate reducing microorganisms which couple the oxidation of organic matter deposited on the seafloor with the reduction of sulfate (hereafter organoclastic sulfate reduction – OSR).

Separating the contributions of OSR and AOM-SR to the overall sedimentary sulfur cycle has been challenging but has benefited from recent advances in isotope biogeochemistry. Stable carbon isotopes have been vastly used to address these processes. Recently, the coupling of sulfur and oxygen isotopes measured in the residual sulfate pool ($\delta^{18}O_{SO4}$ vs. $\delta^{34}S_{SO4}$) has also been demonstrated to be instrumental in our understanding of the interactions between the carbon and sulfur cycles. Metabolic processes discriminate between light and heavy isotopologues and the progressive enrichments in heavy isotoplogues observed in the residual sulfate pool can trace this activity. Oxygen and sulfur isotopes are sensitive to the reductive pathway and geochemical conditions under which multiple biological and abiotic reactions occur (Brunner et al., 2005; Turchyn et al., 2006; Wortmann et al., 2007). Yet, similar to other proxies, the combined S-O isotopes in porewater sulfate is propagating on Elderfield's proxy confidence curve [from the 'Optimism phase,' through the 'Pessimism phase,' to the 'Realism phase'–(Elderfield, 2002)]. With recent works observing $\delta^{18}O_{SO4}$ vs. $\delta^{34}S_{SO4}$ patterns that are inconsistent with previously held interpretations, we ask: what are the limits of application of the combined sulfur–oxygen isotope tool to distinguish between AOM-SR and OSR?

THE OPTIMISM PHASE

In a given pore water profile, the slope of the tangent on the $\delta^{18}O_{SO4}$ vs. $\delta^{34}S_{SO4}$ (slope of the apparent linear phase—SALP) is related to the overall sulfate reduction rate (SRR) where lower rates lead to steeper SALP (see **Figure 1**) (Böttcher et al., 1998, 1999; Aharon and Fu, 2000; Brunner et al., 2005; Antler et al., 2013). The negative relationship between SALP and SRR is understood as increased reversibility of the sulfate reducing enzymatic pathway (Fritz et al., 1989; Brunner and Bernasconi, 2005). The SALP is also affected by sulfur cycling extracellularly where waste products of sulfate reduction can be reoxidized. For example, disproportionation will lead to higher SALP values (Böttcher and Thamdrup, 2001; Böttcher et al., 2001, 2005; Blonder et al., 2017). These relationships are utilized to study the sulfur cycle in marine sediments.

In pelagic regions of the oceans, where the sedimentation rate and supply of organic carbon is relatively low, most of the organic matter remineralization occurs through OSR and only a small fraction of mineralization is via methanogenesis. Under these conditions, sulfate reduction proceeds under organic matter limitation (Glombitza et al., 2015). This results in pore

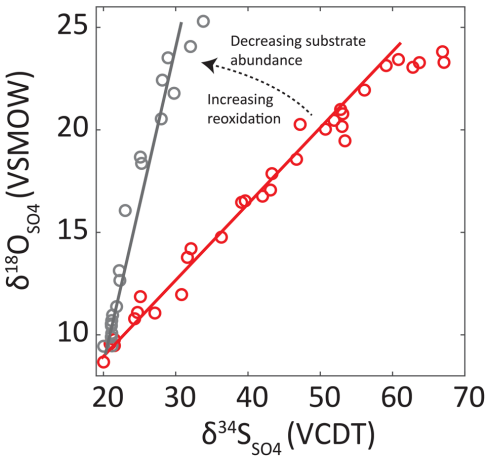

FIGURE 1 | Graphical demonstration of the slope of the apparent linear phase (SALP) and its interpretation. Red line is SALP associated with seep environments while black line is associated with OSR-dominated deep sea sediments. Red circles are data from seeps, black circles from deep sea sediments (Antler et al., 2015). The decreasing substrate refers to the decrease in electron donor supply and 'Increasing reoxidation' refers to the increase in reduced sulfur which is oxidized to sulfate.

water profiles characterized by high SALP numbers (**Figure 2**, gray bars). On the other hand, sites with a high organic carbon flux to the seafloor results in excess methane diffusing upward and leads to low SALP numbers. In fact, methane-rich environments interestingly fall in a very narrow range of SALPs (see highlighted 'seeps' range, **Figure 2**). AOM-SR-dominated sites record maximum SALP values of ∼0.4 (**Figure 2**) and reflect the fact that these environments are not electron donor (methane) limited and thus have low reversibility (Antler et al., 2015). Indeed, low SALP appears to be universal for methane rich environments, regardless of the ambient temperature, water depth (or pressure), salinity and sedimentation rate (Antler et al., 2015; Feng et al., 2016). Therefore, it appears SALP may distinguish between OSR and AOM-SR, even when sulfate concentration profiles are similar in their sulfate penetration depth (Antler et al., 2014). Overall, this tool seems to be robust under different environmental conditions and a great potential for both modern and geological applications.

THE PESSIMISM PHASE

However, observations of low SALP in organic-rich, OSR-dominated sediments of marine mangroves (slope of 0.36 ±0.06; Crémière et al., 2017) questions the robustness of SALP to identify AOM-SR dominated environments. This suggests that low SALPs are not unique to AOM-SR in the environment. (**Figure 2**; green bars). To address this issue, we compiled SALP data from sites that are likely to be AOM-SR dominated as well as sites that are OSR dominated (**Figure 2**, red bars and green bars, respectively). It appears there is no significant difference in SALP between AOM-SR and some OSR dominated environments. This

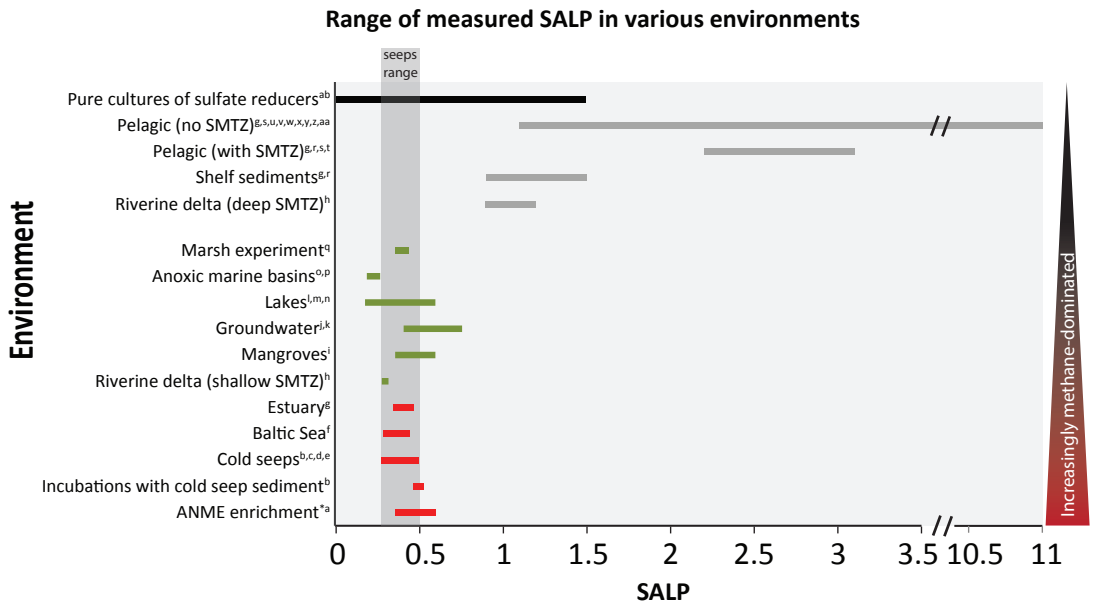

FIGURE 2 | Slope of the apparent linear phase (SALP) measured in various environments. Note the broken axis between 3.5 and 10.5. Black bar indicates pure cultures of dissimilatory sulfate reducers, gray bars specify environments where methane is thought to play a minor role according to the reference. Green bars indicate environments where the presence and contribution of methane to the overall removal of sulfate is questionable. Red bars indicate environments that are thought to be methane dominated. Gray dashed line indicates the SALP measured in methane seeps. Triangle grading from black to red is meant to demonstrate the overall increase in methane in that specific environment. Data (Deusner et al., 2014)[a], (Sivan et al., 2014)[b], (Aharon and Fu, 2000)[c], (Aharon and Fu, 2003)[d], (Rubin-Blum et al., 2014)[e], (Strauss et al., 2012)[f], (Antler et al., 2013)[g], (Aller et al., 2010)[h], (Crémière et al., 2017)[i], (Avrahamov et al., 2014)[j], (Einsiedl et al., 2015)[k], (Knossow et al., 2015)[l], (Gilhooly et al., 2016)[m], (Antler, 2012)[n], (Gomes and Johnston, 2017)[o], (Mandernack and Skei, 2003)[p], (Mills et al., 2016)[q], (Turchyn et al., 2006)[r], (Turchyn et al., 2016)[s], (Riedinger et al., 2010)[t], (Böttcher et al., 1998)[u], (Böttcher et al., 1999)[v], (Böttcher et al., 2006)[w], (Blake et al., 2006)[x], (Turchyn et al., 2006)[y], (Turchyn et al., 2016)[z], (Wortmann et al., 2007)[aa], (Antler et al., 2017)[ab]. *Indicates SALP values are calculated.

means that the SALP does not provide sufficient information to distinguish between these two processes.

Pure cultures of sulfate reducing microorganisms (**Figure 2**, black bar) are analogous in metabolic pathway to OSR in marine sediments and are useful to discuss the limits of SALP associated with this metabolism. They have been demonstrated to produce the entire range of SALPs observed in nature with the exception of pelagic sites (**Figure 2**; gray bars). In pure culture, a near zero SALP indicates the sulfur isotope discrimination of sulfate reduction is being expressed but not the oxygen isotope effect. An absence of oxygen isotope enrichment but presence of sulfur isotope enrichment can be explained if there is no kinetic isotope effect for oxygen, no back reaction of sulfur intermediates (only the entry of sulfate into the cell is reversible) or if the turnover times of the intracellular intermediate pools where oxygen equilibration can happen are so short that it simply is not expressed. Sulfite is the main sulfur intermediate which enables oxygen isotope exchange and does so in a matter of minutes (Betts and Voss, 1970; Horner and Connick, 2003; Müller et al., 2013; Wankel et al., 2014). Recent theoretical work on intracellular APS and sulfite concentrations has predicted sub-micromolar and millimolar levels respectively (Wing and Halevy, 2014) while measurements in pure cultures grown in batch suggest concentrations of around a hundred micromolar and ten micromolar respectively (Sim et al., 2017). In the first instance, (Wing and Halevy, 2014) assumed the reduction of APS and sulfite is coupled to the oxidation of menaquinone (a mildly reducing electron donor), forcing a high ratio of reduced to oxidized menaquinone to generate a favorable redox potential. This produces a low APS to sulfite ratio of 1:1000 and relatively high sulfite concentrations. Ultimately this results in the intracellular sulfite pool having a large turnover time and enable high oxygen isotope exchange. Contrarily, the measurements of (Sim et al., 2017) in (fast growing) batch cultures suggest the ratio of APS to sulfite is ∼10:1 with both having relatively low concentrations resulting in a fast turnover time and therefore, less oxygen isotope exchange. A calculation of the turnover times of sulfur within a cell under conditions which produce SALP close to 0 [cell-specific sulfate reduction rate ≈50 fmol/cell/day and assumptions on cellular and intracellular parameters; cell size = 1.5×10^{-18} m^3, internal adenosine 5′ phosphosulfate concentration = 0.1–0.001 mM, internal sulfite concentration = 10 μM–10 mM (Wing and Halevy, 2014; Sim et al., 2017)] suggests the APS pool is turned over within a fraction of a second (<<1 s) and the sulfite pool in 0.03–30 s. In these conditions only partial oxygen isotope exchange can occur between sulfite and water. Naturally, as the cell specific sulfate reduction rates in the environment are 2–6 orders of magnitude lower than this calculation, e.g., (Holmkvist et al., 2011), turnover of intracellular metabolites increases from seconds to minutes or hours and the oxygen isotope effect becomes significant. These findings are also in

agreement with the finding that low csSRR which produce large sulfur isotope fractionations (such as the ones observed in the environment) can only be driven by modestly negative electron carriers (i.e., menaquinone) whereas very negative electron carriers (i.e., ferredoxins) restrict the net fractionation to around < 22‰ (Wenk et al., 2017). In most cases, SALP is a direct consequence of these intracellular states. In addition, it is possible that the abundance of different sulfoxy isomers might have an effect on the rate of the isotopic exchange with water as well as on the magnitude of isotope fractionation (Müller et al., 2013; Wankel et al., 2014). These should be incorporated into a kinetic-thermodynamic model as it would enable oxygen isotope exchange to be quantified at the cellular level and be an important tool to predict metabolite cycling within sulfate reducing organisms. For environmental studies, it would allow testing whether cellular-level processes associated with OSR are a fair approximation of environmental observations. This should be a priority of future work.

THE REALISM PHASE

Empirical studies on AOM-SR have shown a high dependence of sulfur and oxygen isotope fractionation on methane concentrations (Deusner et al., 2014). Unlike pure cultures of sulfate reducing microorganism, AOM-SR is fundamentally incapable of having a zero contribution from $\delta^{18}O$ in water. In AOM-SR, consortia of archaea and proteobacteria reduce sulfate to sulfide but they do so by disproportionating intermediate sulfur species (Milucka et al., 2012). This leads to the regeneration of $1/8^{th}$ of the reduced sulfate, and an 'inescapable' generation of sulfate with a partial contribution from the isotopic signature of water. However, the oxygen isotope enrichment gained by disproportionation only account partially for the inability of AOM-SR to produce SALP below 0.25. This shunt in the sulfur cycle in AOM-SR accounts for only about 12% of the total sulfur and is not enough to produce the characteristic range of SALP seen methane-dominated environments (Antler et al., 2015). Contrarily to OSR, AOM-SR requires a degree of reversibility which allows the oxygen isotope exchange of intermediates to be expressed in the sulfate pool even at the highest possible metabolic rates (no methane or sulfate limitation). The fact that the range of SALPs observed in AOM-SR is so narrow is something which remains thus far a perplexing issue that will require further empirical work.

The linear progression of $\delta^{18}O_{SO4}$ vs. $\delta^{34}S_{SO4}$ in nature (slope of about 0.25) is mostly interpreted as an indicator for the ratio between the kinetic isotope effects of $\delta^{34}S_{SO4}$ and $\delta^{18}O_{SO4}$, where the oxygen fractionation factor is roughly ¼ of that of sulfur (Mizutani and Rafter, 1969). However, there is no solid evidence for an oxygen kinetic isotope effect in pure cultures of sulfate reducing microorganisms. In fact, pure culture experiments with low SALPs similar to some natural environments and smaller (SALP = 0.25) already show dependence on the oxygen isotope composition of water (Antler et al., 2017), suggesting that the kinetic isotope effect for oxygen isotopes is small or even negligible. Porewater SALPs are evidently more complex than simple kinetic isotope fractionation or equilibrium isotope exchange. An alternative way to reconcile the linear sulfur vs. oxygen isotopes profiles in nature with a small kinetic isotope effect for oxygen may be that SALP is generated by diffusion between two end members, such as seawater sulfate and the enriched ($\delta^{34}S_{SO4}$) and fully equilibrated ($\delta^{18}O_{SO4}$) pool of sulfate near the sulfate methane transition zone.

In environmental samples, determining if a given SALP is produced by AOM-SR or OSR is challenging for multiple reasons. First, the majority of published work on $\delta^{18}O_{SO4}$ and $\delta^{34}S_{SO4}$ does not provide independent, robust evidence of the metabolic processes (AOM-SR or OSR) controlling the pore water profiles. Second, a spatial separation of OSR and AOM-SR at different depths can effectively hide the AOM-SR signature. For example, an abundance of pelagic sites such as from IODP expeditions clearly have a sulfate methane transition zone where sulfate and methane are both consumed. However, OSR in the surface sediment drives $\delta^{18}O_{SO4}$ to equilibrium before AOM-SR has a chance to imprint its signature on the oxygen isotopes. Third, the level of reoxidation occurring in sediments plays an important role in SALP as it increases recycling of the $\delta^{18}O_{H2O}$ signature to $\delta^{18}O_{SO4}$, resulting in a steepening of SALP. Estimating the contribution of reoxidation to the overall sulfur cycle is a large uncertainty in the marine sedimentary sulfur cycle (Jørgensen and Nelson, 2004) and an important aspect of the sulfur cycle where SALP can be a critically important tool, e.g., Brunner et al. (2016).

There is a potential to preserve the SALP signature in sulfate containing minerals, such as barite and celestine and in carbonates (as carbonate associated sulfate) and that it may be a useful indicator of past methane seeps (Feng et al., 2016). Among the three, carbonates are by far more spatially and temporally abundant in the geological record. Authigenic carbonates are more likely to form during AOM-SR due to the reaction stoichiometry, which results in sharp increases in pH (Soetaert et al., 2007). Therefore, although the SALP cannot distinguish between AOM-SR and high activity OSR, high activity OSR is not associated with extensive carbonate precipitation like AOM-SR.

High carbon isotope fractionation during methanogenesis results in the $\delta^{13}C$ of the methane being as low as -100‰ (Whiticar, 1999). Since AOM-SR consumes this isotopically light carbon while OSR does not, AOM-SR results in the production of $\delta^{13}C$ -depleted dissolved inorganic carbon, a marker which can be utilized in a quantitative way to estimate the contributions of AOM-SR and OSR to the DIC pool in marine sediments (Martens et al., 1999; Sivan et al., 2007; Malinverno and Pohlman, 2011; Komada et al., 2016). For example, $\delta^{13}C$ and $\Delta^{14}C$ of the major carbon pools in the Santa Barbara Basin were used to study the discrepancy of methane and sulfate fluxes to the SMT. Based on the carbon isotope signatures in the resulting DIC pools, OSR could account for 35–45% of the sulfate consumption in the sulfate methane transition zone (Komada et al., 2016). Such quantitative work, while tedious, is an effective way to differentiate AOM and OSR, which could be utilized in conjunction with S–O isotopes to further constrain the nature of carbon mineralization in sediments. Since C–S–O

isotopes are preserved over geological timescales (as carbonates and carbonate-associated suflates), they should also be useful when applied to the geological record. Isotopically light carbon isotope in lipids have long been known to be a reliable tracer of methanotrophy because of the distinctly light isotope signature of methane (Hinrichs et al., 1999) and carbon isotopes of carbonates associated with AOM-SR are usually light, a tell tale marker of the methanotrophy associated with AOM-SR (Drake et al., 2015). From a quantitative perspective, these markers have limitations because unknown contributions of carbon from non-methane sources can be incorporated. Non-isotopic quantitative approaches to estimating contributions from AOM-SR and OSR also hold significant promise. For instance, careful comparisons of the fluxes of methane and sulfate into the SMT, combined with in-situ AOM-SR radiotracer incubation experiments e.g., (Beulig et al., 2017) may be able to estimate the relative importance of AOM-SR and OSR in the SMT. A tool which previously held high hopes was molecular approaches to identify microbial community abundances and relate them to process rates, e.g., (Carolan et al., 2015). However, these have thus far been unsuccessful at quantitatively differentiating AOM-SR and OSR. This is in large part because there exists phylogenetic and functional overlap between oxidizing and reducing reactions; for instance ANME and methanogens, e.g., (McGlynn, 2017) or sulfide oxidizers and sulfate reducers, e.g., (Thorup et al., 2017) which makes it impossible to ascertain which organism is doing what in the subsurface. Molecular approaches are unlikely to yield quantitatively useful information by themselves until significant progress is made in connecting genotypes to metabolic functions.

SALP provides a powerful tool to study the sulfur cycle, by sensitively responding to changes in the reduction of sulfate vs. the oxidation of reduce sulfur compounds. In this contribution, we explored the limitation of this tool as a way to distinguish between AOM-SR and OSR. Because of the multiple parameters which control the extent of SALP, the information provided and what it tells of the microbial sulfur transformations are not generally applicable to all circumstances. However, with a careful site-specific approach and in combination with other proxies, SALP can contribute vital information on the microbial and chemical reactions taking place in marine sediments. Further refining (1) our understanding on the magnitude of the oxygen isotope kinetic fractionation during the APS reduction to sulfite, (2) the degree of oxygen isotope exchange between sulfur intermediates and water and (3) its relationship to the cell specific sulfate reduction rate, would greatly improve our ability to interpret the SALP as an indicator of the microbial transformations taking place. Doing so will transform this analytical tool into a reliable proxy of sulfur cycling.

AUTHOR CONTRIBUTIONS

Both authors contributed to the redaction of the manuscript and figures.

ACKNOWLEDGMENTS

We would like to thank Harold J. Bradbury, Sambuddha Misra, Jacquelynn Ward, Felix Beulig, and Alexander Michaud for their comments. AP acknowledges the Danish National Research Foundation [DNRF104] and the European Research Council [294200].

REFERENCES

Aharon, P., and Fu, B. (2000). Microbial sulfate reduction rates and sulfur and oxygen isotope fractionations at oil and gas seeps in deepwater Gulf of Mexico. *Geochim. Cosmochim. Acta* 64, 233–246. doi: 10.1016/S0016-7037(99)00292-6

Aharon, P., and Fu, B. (2003). Sulfur and oxygen isotopes of coeval sulfate–sulfide in pore fluids of cold seep sediments with sharp redox gradients. *Chem. Geol.* 195, 201–218. doi: 10.1016/S0009-2541(02)00395-9

Aller, R. C., Madrid, V., Chistoserdov, A., Aller, J. Y., and Heilbrun, C. (2010). Unsteady diagenetic processes and sulfur biogeochemistry in tropical deltaic muds: implications for oceanic isotope cycles and the sedimentary record. *Geochim. Cosmochim. Acta* 74, 4671–4692. doi: 10.1016/j.gca.2010.05.008

Antler, G. (2012). *Multiple Stable Isotopes a Tool for Studying the Mechanism of Bacterial Sulfate Reduction, Geological Sciences*. Beersheba: Ben-Gurion University of the Negev.

Antler, G., Turchyn, A. V., Herut, B., Davies, A., Rennie, V. C. F., and Sivan, O. (2014). Sulfur and oxygen isotope tracing of sulfate driven anaerobic methane oxidation in estuarine sediments. *Estuar. Coast. Shelf Sci.* 142, 4–11. doi: 10.1016/j.ecss.2014.03.001

Antler, G., Turchyn, A. V., Herut, B., and Sivan, O. (2015). A unique isotopic fingerprint of sulfate-driven anaerobic oxidation of methane. *Geology* 43, 619–622. doi: 10.1130/G36688.1

Antler, G., Turchyn, A. V., Ono, S., Sivan, O., and Bosak, T. (2017). Combined 34S, 33S and 18O isotope fractionations record different intracellular steps of microbial sulfate reduction. *Geochim. Cosmochim. Acta* 203, 364–380. doi: 10.1016/j.gca.2017.01.015

Antler, G., Turchyn, A. V., Rennie, V., Herut, B., and Sivan, O. (2013). Coupled sulfur and oxygen isotope insight into bacterial sulfate reduction in the natural environment. *Geochim. Cosmochim. Acta* 118, 98–117. doi: 10.1016/j.gca.2013.05.005

Avrahamov, N., Antler, G., Yechieli, Y., Gavrieli, I., Joye, S., Saxton, M., et al. (2014). Anaerobic oxidation of methane by sulfate in hypersaline groundwater of the Dead Sea aquifer. *Geobiology* 12, 511–528. doi: 10.1111/gbi.12095

Betts, R. H., and Voss, R. H. (1970). The kinetics of oxygen exchange between the sulfite ion and water. *Can. J. Chem.* 48, 2035–2041. doi: 10.1139/v70-339

Beulig, F., Røy, H., Glombitza, C., and Jørgensen, B. B. (2017). Control on rate and pathway of anaerobic organic carbon degradation in the seabed. *Proc. Natl. Acad. Sci. U.S.A.* 115:201715789. doi: 10.1073/pnas.1715789115

Blake, R. E., Surkov, A. V., Böttcher, M. E., Ferdelman, T. G., and Jørgensen, B. B. (2006). "Oxygen isotope composition of dissolved sulfate in deep-sea sediments: eastern equatorial Pacific Ocean," in *Proceedings of the Ocean Drilling Program, Scientific Results*, eds B. B. Jørgensen, S. L. D'Hondt and D. J. Miller (College Station, TX: Ocean Drilling Program), 1–24. doi: 10.2973/odp.proc.sr.201.116.2006

Blonder, B., Boyko, V., Turchyn, A. V., Antler, G., Sinichkin, U., Knossow, N., et al. (2017). Impact of Aeolian dry deposition of reactive iron minerals on sulfur cycling in sediments of the Gulf of Aqaba. *Front. Microbiol.* 8:1131. doi: 10.3389/fmicb.2017.01131

Boetius, A., Ravenschlag, K., Schubert, C. J., Rickert, D., Widdel, F., Gieseke, A., et al. (2000). A marine microbial consortium apparently mediating anaerobic oxidation of methane. *Nature* 407, 623–626. doi: 10.1038/35036572

Böttcher, M. E., Bernasconi, S. M., and Brumsack, H. J. (1999). Carbon, sulfur, and oxygen isotope geochemistry of interstitial waters from the Western

Mediterranean. *Proc. Ocean Drill. Prog.* 161, 413–421. doi: 10.2973/odp.proc.sr.161.229.1999

Böttcher, M. E., Brumsack, H. J., and de Lange, G. J. (1998). "Sulfate reduction and related stable isotope (34S, 18O) variations in interstitial waters from the eastern Mediterranean," in *Proceedings of the Ocean Drilling Program, Scientific Results* (College Station, TX: Ocean Drilling Program), 365–373. doi: 10.2973/odp.proc.sr.160.002.1998

Böttcher, M. E., Ferdelman, T. G., Jørgensen, B. B., Blake, R. E., Surkov, A. V., and Claypool, G. E. (2006). "Sulfur isotope fractionation by the deep biosphere within sediments of the eastern equatorial Pacific and Peru margin," in *Proceedings of the Ocean Drilling Program, Scientific Results*, eds B. B. Jørgensen, S. L. D'Hondt and D. J. Miller (College Station, TX: Ocean Drilling Program), 1–21. doi: 10.2973/odp.proc.sr.201.109.2006

Böttcher, M. E., and Thamdrup, B. (2001). Anaerobic sulfide oxidation and stable isotope fractionation associated with bacterial sulfur disproportionation in the presence of MnO2. *Geochim. Cosmochim. Acta* 65, 1573–1581. doi: 10.1016/S0016-7037(00)00622-0

Böttcher, M. E., Thamdrup, B., Gehre, M., and Theune, A. (2005). 34S/32S and 18O/16O fractionation during sulfur disproportionation by *Desulfobulbus propionicus*. *Geomicrobiol. J.* 22, 219–226. doi: 10.1080/01490450590947751

Böttcher, M. E., Thamdrup, B., and Vennemann, T. W. (2001). Oxygen and sulfur isotope fractionation during anaerobic bacterial disproportionation of elemental sulfur. *Geochim. Cosmochim. Acta* 65, 1601–1609. doi: 10.1016/S0016-7037(00)00628-1

Brunner, B., Arnold, G. L., Røy, H., Müller, I. A., and Jørgensen, B. B. (2016). Off limits: sulfate below the sulfate-methane transition. *Front. Earth Sci.* 4:75. doi: 10.3389/feart.2016.00075

Brunner, B., and Bernasconi, S. M. (2005). A revised isotope fractionation model for dissimilatory sulfate reduction in sulfate reducing bacteria. *Geochim. Cosmochim. Acta* 69, 4759–4771. doi: 10.1016/j.gca.2005.04.015

Brunner, B., Bernasconi, S. M., Kleikemper, J., and Schroth, M. H. (2005). A model for oxygen and sulfur isotope fractionation in sulfate during bacterial sulfate reduction processes. *Geochim. Cosmochim. Acta* 69, 4773–4785. doi: 10.1016/j.gca.2005.04.017

Carolan, M. T., Smith, J. M., and Beman, J. M. (2015). Transcriptomic evidence for microbial sulfur cycling in the eastern tropical North Pacific oxygen minimum zone. *Front. Microbiol.* 6:334. doi: 10.3389/fmicb.2015.00334

Crémière, A., Strauss, H., Sebilo, M., Hong, W.-L., Gros, O., Schmidt, S., et al. (2017). Sulfur diagenesis under rapid accumulation of organic-rich sediments in a marine mangrove from Guadeloupe (French West Indies). *Chem. Geol.* 454, 67–79. doi: 10.1016/j.chemgeo.2017.02.017

Deusner, C., Holler, T., Arnold, G. L., Bernasconi, S. M., Formolo, M. J., and Brunner, B. (2014). Sulfur and oxygen isotope fractionation during sulfate reduction coupled to anaerobic oxidation of methane is dependent on methane concentration. *Earth Planet. Sci. Lett.* 399, 61–73. doi: 10.1016/j.epsl.2014.04.047

Dickens, G. R., O'Neil, J. R., Rea, D. K., and Owen, R. M. (1995). Dissociation of oceanic methane hydrate as a cause of the carbon isotope excursion at the end of the Paleocene. *Paleoceanography* 10, 965–971. doi: 10.1029/95PA02087

Drake, H., Åström, M. E., Heim, C., Broman, C., Åström, J., Whitehouse, M., et al. (2015). Extreme 13C depletion of carbonates formed during oxidation of biogenic methane in fractured granite. *Nat. Commun.* 6:7020. doi: 10.1038/ncomms8020

Einsiedl, F., Pilloni, G., Ruth-Anneser, B., Lueders, T., and Griebler, C. (2015). Spatial distributions of sulphur species and sulphate-reducing bacteria provide insights into sulphur redox cycling and biodegradation hot-spots in a hydrocarbon-contaminated aquifer. *Geochim. Cosmochim. Acta* 156, 207–221. doi: 10.1016/j.gca.2015.01.014

Elderfield, H. (2002). *Foraminiferal Mg/Ca Paleothermometry: Expected Advances and Unexpected Consequences Goldschmidt Conference*. Davos: Cambridge Publications.

Feng, D., Peng, Y., Bao, H., Peckmann, J., Roberts, H. H., and Chen, D. (2016). A carbonate-based proxy for sulfate-driven anaerobic oxidation of methane. *Geology* 44, 999–1002. doi: 10.1130/G38233.1

Fritz, P., Basharmal, G., Drimmie, R., Ibsen, J., and Qureshi, R. (1989). Oxygen isotope exchange between sulphate and water during bacterial reduction of sulphate. *Chem. Geol. Isot. Geosci. Sect.* 79, 99–105. doi: 10.1016/0168-9622(89)90012-2

Gilhooly, W. P. III, Reinhard, C. T., and Lyons, T. W. (2016). A comprehensive sulfur and oxygen isotope study of sulfur cycling in a shallow, hyper-euxinic meromictic lake. *Geochim. Cosmochim. Acta* 189, 1–23. doi: 10.1016/j.gca.2016.05.044

Glombitza, C., Jaussi, M., Røy, H., Seidenkrantz, M.-S., Lomstein, B. A., and Jørgensen, B. B. (2015). Formate, acetate, and propionate as substrates for sulfate reduction in sub-arctic sediments of Southwest Greenland. *Front. Microbiol.* 6:846. doi: 10.3389/fmicb.2015.00846

Gomes, M. L., and Johnston, D. T. (2017). Oxygen and sulfur isotopes in sulfate in modern euxinic systems with implications for evaluating the extent of euxinia in ancient oceans. *Geochim. Cosmochim. Acta* 205, 331–359. doi: 10.1016/j.gca.2017.02.020

Hinrichs, K.-U., Hayes, J. M., Sylva, S. P., Brewer, P. G., and DeLong, E. F. (1999). Methane-consuming archaebacteria in marine sediments. *Nature* 398, 802–805. doi: 10.1038/19751

Holmkvist, L., Ferdelman, T. G., and Jørgensen, B. B. (2011). A cryptic sulfur cycle driven by iron in the methane zone of marine sediment (Aarhus Bay, Denmark. *Geochim. Cosmochim. Acta* 75, 3581–3599. doi: 10.1016/j.gca.2011.03.033

Horner, D. A., and Connick, R. E. (2003). Kinetics of oxygen exchange between the two isomers of bisulfite ion, disulfite ion (S2O52-), and water as studied by oxygen-17 nuclear magnetic resonance spectroscopy. *Inorg. Chem.* 42, 1884–1894. doi: 10.1021/ic020692n

Jørgensen, B. B., and Nelson, D. C. (2004). Sulfide oxidation in marine sediments: geochemistry meets microbiology. *Geol. Soc. Am. Spec. Pap.* 379, 63–81. doi: 10.1130/0-8137-2379-5.63

Knossow, N., Blonder, B., Eckert, W., Turchyn, A. V., Antler, G., and Kamyshny, A. (2015). Annual sulfur cycle in a warm monomictic lake with sub-millimolar sulfate concentrations. *Geochem. Trans.* 16:7. doi: 10.1186/s12932-015-0021-5

Komada, T., Burdige, D. J., Li, H.-L., Magen, C., Chanton, J. P., and Cada, A. K. (2016). Organic matter cycling across the sulfate-methane transition zone of the Santa Barbara Basin. California Borderland. *Geochim. Cosmochim. Acta* 176, 259–278. doi: 10.1016/j.gca.2015.12.022

Kvenvolden, K. A. (1988). Methane hydrate — a major reservoir of carbon in the shallow geosphere? *Chem. Geol.* 71, 41–51. doi: 10.1016/0009-2541(88)90104-0

Malinverno, A., and Pohlman, J. W. (2011). Modeling sulfate reduction in methane hydrate-bearing continental margin sediments: does a sulfate-methane transition require anaerobic oxidation of methane. *Geochem. Geophys. Geosyst.* 12:Q07006. doi: 10.1029/2011GC003501

Mandernack, K. W., and Skei, J. M. (2003). A stable sulfur and oxygen isotopic investigation of sulfur cycling in an anoxic marine basin, Framvaren Fjord, Norway. *Chem. Geol.* 195, 181–200. doi: 10.1016/S0009-2541(02)00394-7

Martens, C. S., Albert, D., and Alperin, M. J. (1999). Stable isotope tracing of anaerobic methane oxidation in the gassy sediments of Eckernförde Bay, German Baltic Sea. *Am. J. Sci.* 299, 589–610. doi: 10.2475/ajs.299.7-9.589

McGlynn, S. E. (2017). Energy metabolism during anaerobic methane oxidation in ANME archaea. *Microbes Environ.* 32, 5–13. doi: 10.1264/jsme2.ME16166

Mills, J. V., Antler, G., and Turchyn, A. V. (2016). Geochemical evidence for cryptic sulfur cycling in salt marsh sediments. *Earth Planet. Sci. Lett.* 453, 23–32. doi: 10.1016/j.epsl.2016.08.001

Milucka, J., Ferdelman, T. G., Polerecky, L., Franzke, D., Wegener, G., Schmid, M., et al. (2012). Zero-valent sulphur is a key intermediate in marine methane oxidation. *Nature* 491, 541–546. doi: 10.1038/nature11656

Mizutani, Y., and Rafter, T. A. (1969). Oxygen isotopic composition of sulphate. Part 4. Bacterial fractionation of oxygen isotopes in the reduction of sulphate and in the oxidation of sulphur. *N. Z. J. Sci.* 12, 60–68.

Müller, I. A., Brunner, B., and Coleman, M. (2013). Isotopic evidence of the pivotal role of sulfite oxidation in shaping the oxygen isotope signature of sulfate. *Chem. Geol.* 354, 186–202. doi: 10.1016/j.chemgeo.2013.05.009

Riedinger, N., Brunner, B., Formolo, M. J., Solomon, E., Kasten, S., Strasser, M., et al. (2010). Oxidative sulfur cycling in the deep biosphere of the Nankai Trough, Japan. *Geology* 38, 851–854. doi: 10.1130/G31085.1

Rubin-Blum, M., Antler, G., Turchyn, A. V., Tsadok, R., Goodman-Tchernov, B. N., Shemesh, E., et al. (2014). Hydrocarbon-related microbial processes in the deep sediments of the Eastern Mediterranean Levantine Basin. *FEMS Microbiol. Ecol.* 87, 780–796. doi: 10.1111/1574-6941.12264

Sim, M. S., Paris, G., Adkins, J. F., Orphan, V. J., and Sessions, A. L. (2017). Quantification and isotopic analysis of intracellular sulfur metabolites in the dissimilatory sulfate reduction pathway. *Geochim. Cosmochim. Acta* 206, 57–72. doi: 10.1016/j.gca.2017.02.024

Sivan, O., Antler, G., Turchyn, A. V., Marlow, J. J., and Orphan, V. J. (2014). Iron oxides stimulate sulfate-driven anaerobic methane oxidation in seeps. *Proc. Natl. Acad. Sci. U.S.A.* 111, 4139–4147. doi: 10.1073/pnas.1412269111

Sivan, O., Schrag, D. P., and Murray, R. W. (2007). Rates of methanogenesis and methanotrophy in deep-sea sediments. *Geobiology* 5, 141–151. doi: 10.1111/j.1472-4669.2007.00098.x

Soetaert, K., Hofmann, A. F., Middelburg, J. J., Meysman, F. J. R., and Greenwood, J. (2007). The effect of biogeochemical processes on pH. *Mar. Chem.* 105, 30–51. doi: 10.1016/j.marchem.2006.12.012

Strauss, H., Bast, R., Cording, A., Diekrup, D., Fugmann, A., Garbe-Schonberg, D., et al. (2012). Sulphur diagenesis in the sediments of the Kiel Bight, SW Baltic Sea, as reflected by multiple stable sulphur isotopes. *Isotopes Environ. Health Stud.* 48, 166–179. doi: 10.1080/10256016.2012.648930

Thorup, C., Schramm, A., Findlay, A. J., Finster, K. W., and Schreiber, L. (2017). Disguised as a Sulfate Reducer: growth of the Deltaproteobacterium *Desulfurivibrio alkaliphilus* by sulfide oxidation with Nitrate. *mBio* 8:e00671-17. doi: 10.1128/mBio.00671-17

Turchyn, A., Sivan, O., and Schrag, D. (2006). Oxygen isotopic composition of sulfate in deep sea pore fluid: evidence for rapid sulfur cycling. *Geobiology* 4, 191–201. doi: 10.1111/j.1472-4669.2006.00079.x

Turchyn, A. V., Antler, G., Byrne, D., Miller, M., and Hodell, D. A. (2016). Microbial sulfur metabolism evidenced from pore fluid isotope geochemistry at Site U1385. *Glob. Planet. Change* 141, 82–90. doi: 10.1016/j.gloplacha.2016.03.004

Wankel, S. D., Bradley, A. S., Eldridge, D. L., and Johnston, D. T. (2014). Determination and application of the equilibrium oxygen isotope effect between water and sulfite. *Geochim. Cosmochim. Acta* 125, 694–711. doi: 10.1016/j.gca.2013.08.039

Wenk, C. B., Wing, B. A., and Halevy, I. (2017). Electron carriers in microbial sulfate reduction inferred from experimental and environmental sulfur isotope fractionation. *ISME J.* doi: 10.1038/ismej.2017.185 [Epub ahead of print].

Whiticar, M. J. (1999). Carbon and hydrogen isotope systematics of bacterial formation and oxidation of methane. *Chem. Geol.* 161, 291–314. doi: 10.1016/S0009-2541(99)00092-3

Whiticar, M. J., Faber, E., and Schoell, M. (1986). Biogenic methane formation in marine and freshwater environments: CO2 reduction vs. acetate fermentation—Isotope evidence. *Geochim. Cosmochim. Acta* 50, 693–709. doi: 10.1016/0016-7037(86)90346-7

Wing, B. A., and Halevy, I. (2014). Intracellular metabolite levels shape sulfur isotope fractionation during microbial sulfate respiration. *Proc. Natl. Acad. Sci. U.S.A.* 111, 18116–18125. doi: 10.1073/pnas.1407502111

Wortmann, U. G., Chernyavsky, B., Bernasconi, S. M., Brunner, B., Böttcher, M. E., and Swart, P. K. (2007). Oxygen isotope biogeochemistry of pore water sulfate in the deep biosphere: dominance of isotope exchange reactions with ambient water during microbial sulfate reduction (ODP Site 1130). *Geochim. Cosmochim. Acta* 71, 4221–4232. doi: 10.1016/j.gca.2007.06.033

Wuebbles, D. J., and Hayhoe, K. (2002). Atmospheric methane and global change. *Earth Sci. Rev.* 57, 177–210. doi: 10.1016/S0012-8252(01)00062-9

Conflict of Interest Statement: The authors declare that the research was conducted in the absence of any commercial or financial relationships that could be construed as a potential conflict of interest.

frontiers in Microbiology

ORIGINAL RESEARCH
published: 29 August 2017
doi: 10.3389/fmicb.2017.01573

Effect of Thermophilic Nitrate Reduction on Sulfide Production in High Temperature Oil Reservoir Samples

*Gloria N. Okpala[1], Chuan Chen[2], Tekle Fida[1] and Gerrit Voordouw[1]**

[1] *Petroleum Microbiology Research Group, Department of Biological Sciences, University of Calgary, Calgary, AB, Canada,*
[2] *State Key Laboratory of Urban Water Resource and Environment, Harbin Institute of Technology, Harbin, China*

Oil fields can experience souring, the reduction of sulfate to sulfide by sulfate-reducing microorganisms. At the Terra Nova oil field near Canada's east coast, with a reservoir temperature of 95°C, souring was indicated by increased hydrogen sulfide in produced waters (PW). Microbial community analysis by 16S rRNA gene sequencing showed the hyperthermophilic sulfate-reducing archaeon *Archaeoglobus* in Terra Nova PWs. Growth enrichments in sulfate-containing media at 55–70°C with lactate or volatile fatty acids yielded the thermophilic sulfate-reducing bacterium (SRB) *Desulfotomaculum*. Enrichments at 30–45°C in nitrate-containing media indicated the presence of mesophilic nitrate-reducing bacteria (NRB), which reduce nitrate without accumulation of nitrite, likely to N_2. Thermophilic NRB (tNRB) of the genera *Marinobacter* and *Geobacillus* were detected and isolated at 30–50°C and 40–65°C, respectively, and only reduced nitrate to nitrite. Added nitrite strongly inhibited the isolated thermophilic SRB (tSRB) and tNRB and SRB could not be maintained in co-culture. Inhibition of tSRB by nitrate in batch and continuous cultures required inoculation with tNRB. The results suggest that nitrate injected into Terra Nova is reduced to N_2 at temperatures up to 45°C but to nitrite only in zones from 45 to 65°C. Since the hotter zones of the reservoir (65–80°C) are inhabited by thermophilic and hyperthermophilic sulfate reducers, souring at these temperatures might be prevented by nitrite production if nitrate-reducing zones of the system could be maintained at 45–65°C.

Keywords: oil field, seawater, sulfate reduction, nitrate reduction, microbial community

OPEN ACCESS

Edited by:
Tanja Bosak,
Massachusetts Institute of Technology, United States

Reviewed by:
James F. Holden,
University of Massachusetts Amherst, United States
Alexis Templeton,
University of Colorado Boulder, United States

****Correspondence:***
Gerrit Voordouw
voordouw@ucalgary.ca

Specialty section:
This article was submitted to Microbiological Chemistry and Geomicrobiology, a section of the journal Frontiers in Microbiology

Received: *30 March 2017*
Accepted: *03 August 2017*
Published: *29 August 2017*

Citation:
Okpala GN, Chen C, Fida T and Voordouw G (2017) Effect of Thermophilic Nitrate Reduction on Sulfide Production in High Temperature Oil Reservoir Samples. Front. Microbiol. 8:1573. doi: 10.3389/fmicb.2017.01573

INTRODUCTION

Oil reservoir souring, the reduction of sulfate to sulfide by sulfate-reducing microorganisms (SRM), and its control with nitrate has been studied extensively in shallow, low temperature reservoirs, which support the growth of mesophilic microbes throughout. Injection of water with 1 mM sulfate, amended with 2 mM nitrate, caused the emergence of sequential zones of nitrate-reduction, sulfate-reduction and methanogenesis along the water flow path. Although microbial communities in produced waters (PW) were dominated by methanogens, SRB and NRB were present and were readily activated when samples were grown under nitrate- or sulfate-reducing conditions. All three of these activities were, therefore, easily established in bioreactors or microcosms containing

nitrate, sulfate and excess volatile fatty acids irrespective whether the inoculum was a field sample or a derived enrichment (Lambo et al., 2008; Voordouw et al., 2009; Callbeck et al., 2011; Chen et al., 2017). In contrast studying microbial communities derived from deep, high temperature reservoirs is much more complex. Because the zones of microbial activities are superimposed on a steep gradient of increasing temperature in the near injection wellbore region (NIWR).

For instance, in the Terra Nova field, located 350 km from the east coast of Newfoundland, oil is produced from a depth of 3200–3700 m below the sea floor, where the reservoir temperature is 95°C (Haugen et al., 2007). Due to the harsh operating conditions existing in this region, the oilfield is operated through a Floating Production Storage and Offloading (FPSO) vessel from where flexible manifold pipes are connected to the subsea system (Howell et al., 2001). Following its intake, cold seawater is warmed during its downward travel, reaching 30°C upon injection in the reservoir (**Figure 1**). This temperature further increases in the NIWR, in which the temperature changes from that of the injected water to that of the bulk of the reservoir (Eden et al., 1993). The NIWR thus consists of a succession of mesophilic (30–45°C), thermophilic (45–80°C) and abiotic (80–95°C) zones, assuming that microbial life in the reservoir does not extend beyond 80°C (Magot, 2005; Liebensteiner et al., 2014; Fida et al., 2016). Following travel through the abiotic bulk of the reservoir (95°C), the temperature of the PW and oil mixture will cool to 70°C, when it travels upward to the FSPO, allowing renewed growth of thermophilic but not of mesophilic microorganisms. Produced oil and water are then separated in the FPSO with cleaned but still hot PW being discharged into the ocean (**Figure 1**).

A variety of mesophilic and thermophilic NRB (tNRB), SRM, and fermentative bacteria, as well as methanogenic *Archaea* have been obtained from or detected in injected seawater and PW from high temperature reservoirs (Beeder et al., 1995; Nilsen et al., 1996a,b; Slobodkin et al., 1999; Orphan et al., 2003; Nazina et al., 2006; Gittel et al., 2009, 2012; Zhang F. et al., 2012; Aüllo et al., 2013; Lenchi et al., 2013; Agrawal et al., 2014). Their positioning in the NIWR depends on the temperature dependence of their activity. However, data on this for multiple isolates from the same field are lacking. Study of the physiology of pure cultures or enrichments has indicated that tNRB reduce nitrate to nitrite, but do not reduce nitrite, e.g., to di-nitrogen (N_2) (Fida et al., 2016). Hence, addition of nitrate to a culture of thermophilic SRB (tSRB) in which tNRB are present would strongly inhibit tSRB activity, because nitrite is such a strong and specific SRB inhibitor (Greene et al., 2003; Haveman et al., 2004). At low temperature mesophilic NRB can persist in cultures of mesophilic SRB in the absence of nitrate by switching to fermentative metabolism. However, coculturing of tNRB and SRB is more difficult. For example sulfide production by two tSRM enrichments from North Sea fields at 60°C, harboring *Thermodesulforabdus* or *Archaeoglobus*, was not inhibited by 10 mM nitrate, indicating absence of tNRB (Kaster et al., 2007). Both of these enrichments were strongly inhibited by only 0.25 mM nitrite. Likewise, Reinsel et al. (1996), demonstrated that injecting as little as 0.71 mM nitrate inhibited sulfate reduction in souring bioreactors at 60°C due to its reduction to nitrite. However, this inhibition could be lost in bioreactors, which had been injected with sulfate only for a prolonged period of time, requiring re-inoculation with tNRB.

Our objectives in researching the Terra Nova system were to determine the community composition, as well as the temperature dependence of reduction of nitrate to nitrite, of nitrite to nitrogen and of sulfate to sulfide for samples of injection and PWs, of derived enrichments and of pure cultures. This may allow mapping of the location of taxa and their activities in the temperature versus distance profile of the NIWR. Further study of cocultures of tSRB and NRB was also pursued to improve understanding of souring control in systems with a temperature gradient as in the NIWR.

MATERIALS AND METHODS

Sample Collection and Physicochemical Analysis

Samples were collected on-board the FPSO and were sent in sealed containers. Three sets of injection water (IW) and PW samples were received from Terra Nova oil fields in January 2014, January 2015 and May 2015. The samples were either shipped in 3 L airtight metal canisters or in 1 L Nalgene bottles, with 2 or 3 L of each sample provided (**Table 1**). The sample bottles or canisters were filled to the brim and sealed tightly to exclude air. Upon arrival, the samples were stored at room temperature in an anoxic chamber with an atmosphere of 10% CO_2 and 90% N_2 (N_2-CO_2; Praxair, Calgary, AB, Canada). An aliquot of 200 ml of each sample was centrifuged for 15 min at 11,200 × *g* to pellet biomass, the pellets were frozen at −20°C for use in DNA extraction. The salinity as molar equivalent (Meq) of NaCl was determined from the conductivity measured with an Orion conductivity cell (model 013005MD). Sulfide and ammonium concentrations in the water samples were determined spectrophotometrically using the methylene blue method (Cline, 1969) and the indophenol method (Cornish Shartau et al., 2010), respectively.

Nitrate and nitrite concentrations were measured by high performance liquid chromatography (HPLC), using a Waters 600E HPLC (Waters Corp, Milford, MA, United States) which was fitted with a Waters 2489 UV/Visible detector, set at 200 nm and an IC-PAK^{TM} anion column HC (150 × 4.6 mm, waters), and eluted with a sodium borate-gluconate (2%) buffer containing 12% acetonitrile and 2% butanol. Sulfate, was measured with the same column using a Waters 432 conductivity detector at a flowrate of 2 ml/min. Samples for anion assay were prepared by centrifugation at 14,000 rpm for 5 min, after which 100 µl of supernatant was added to 400 µl of the prepared buffer solution in a vial. Volatile fatty acid (VFA) concentrations of field samples were analyzed with a Waters 2487 UV detector at 210 nm, with a Prevail organic acid (OA) 5u column (250 × 4.6 mm, Alltech, Guelph, ON, Canada) at a flow rate of 1.0 ml/min. Field samples (1 ml) were centrifuged and 300 µl of the supernatant was acidified in a vial with 20 µl of 1M H_3PO_4 before elution with 25 mM KH_2PO_4 (pH 2.5).

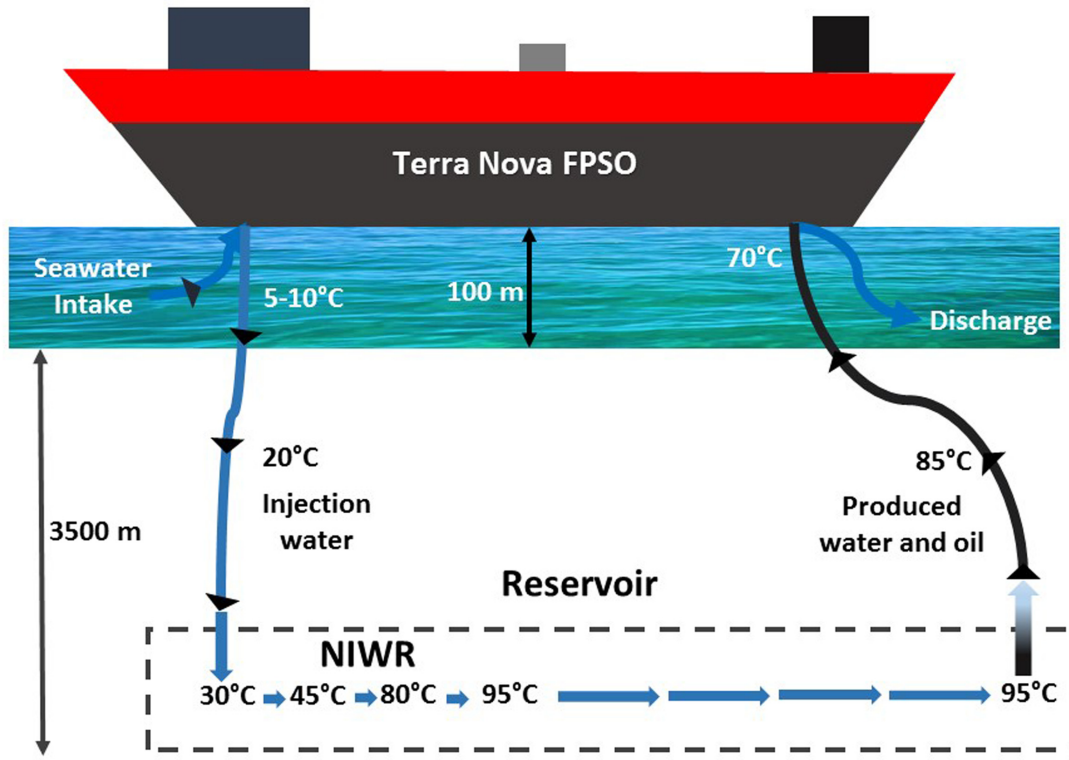

FIGURE 1 | Schematic of seawater injection from the Terra Nova Floating Production Storage and Offloading (FPSO) vessel, as explained in the text. The near injection wellbore region (NIWR) has mesophilic (30–45°C), thermophilic (45–80°C) and abiotic (80–95°C) zones.

TABLE 1 | Physicochemical analyses of injection water (IW) and produced water (PW) samples.

Water chemistry	pH	NaCl (Meq)	Sulfate (mM)	Acetate (mM)	Propionate (mM)	NH_4^+ (mM)
Injection water (IW) 2014-2015						
IW1_14	6.74	0.48	28	0.11	0	0.11
IW1_15	6.51	0.55	27.6	0.02	0	0.34
IW5_15	6.42	0.53	19.8	0	0	0.32
Average ± SD	6.56 ± 0.17	0.52 ± 0.04	25.1 ± 4.6	0.04 ± 0.06	0	0.26 ± 0.13
Produced Water (PW) 2014-2015						
PW1_14	6.75	0.4	16.8	2.26	0.24	1.24
PW1_15	6.97	0.69	22.14	1.85	0.08	1.4
PWC2_5_15	6.7	0.55	13.8	0.28	0.02	0.46
PWF2_5_15	6.7	0.64	8.9	1.76	0.17	1.06
Average ± SD	6.78 ± 0.13	0.57 ± 0.13	15.4 ± 5.5	1.54 ± 0.87	0.13 ± 0.10	1.04 ± 0.41

Microbial Enumeration of SRB and Acid-Producing Bacteria (APB)

Most probable number (MPN) determinations were done using 48-well cell culture plates (Shen and Voordouw, 2015) for enumerating SRB and acid-producing bacteria (APB) using media containing lactate and sulfate or glucose and phenol red, respectively. Plates were incubated at 30°C or 60°C inside an anaerobic jar for 1 month. MPNs were calculated by comparing the pattern of positive wells to a probability table for MPN tests done using triplicate series of dilutions.

Activity of SRB and NRB

Microbial activity tests were done by inoculating 10% (v/v) of sample in modified Coleville synthetic brine (CSB) medium A with 0.5 M NaCl. CSBA medium had the following composition (g/L): NaCl, 29.3; $CaCl_2.2H_2O$, 0.15; $MgCl_2.5H_2O$, 0.4; NH_4Cl, 0.25; KCl, 0.5; KH_2PO_4, 0.2; resazurin (1%), 2–3 drops. After autoclaving, trace elements, 1 ml; selenate-tungstate, 1 ml; 1 M $NaHCO_3$, 30 ml were added and the pH was adjusted to 7.4–7.6 using 1 M HCl (Hubert et al., 2003). Fifty ml of the CSBA medium was added to 122 ml serum bottles, which were sealed with a

butyl rubber stopper, crimped with an aluminum cap and flushed with N_2-CO_2 gas (90–10%) for 5 min to exclude oxygen. Sulfate, nitrate, VFA, lactate and sulfide were added to these media in final concentrations as indicated. The media in the serum bottles were inoculated with 10% (v/v) of IW or PW samples. Following inoculation, the serum bottles were incubated at 30 or 60°C. Aliquots of 0.5 ml were taken at different time intervals to determine the concentrations of sulfide, sulfate, nitrite and nitrate. Sulfide concentrations were determined immediately after each sampling, and the remainders of the samples were frozen (−20°C) for further analysis of sulfate, nitrate and nitrite by HPLC.

Enrichment of Thermophilic SRB and NRB Consortia from Field Samples

To increase the probability of cultivating tSRB and NRB from the water samples, the biomass in the water samples was concentrated by either filtration or centrifugation. For filtration, 250 mL of sample were filtered through a 0.2 μm filter, after which the biomass concentrated on the surface of the filter, was inoculated into 30 mL of the filtrate or of CSBA. For centrifugation, 250 ml of PW or IW were centrifuged at 11,200 × *g* for 15 min. After centrifugation, the supernatant was poured off, and the pellets formed were re-suspended with 5 ml of the supernatant.

Aliquots (20 ml) of CSBA medium were dispensed into 50 ml serum bottles, and sealed with rubber stoppers and aluminum crimps. The medium was flushed with N_2-CO_2. To the SRB media, 20 mM lactate and 10 mM sulfate or 6 mM VFA and 10 mM sulfate were added, while to the NRB media, 20 mM lactate and 10 mM nitrate were added. The inoculated media were incubated at 60°C. Samples were taken periodically with an N_2-CO_2 flushed syringe. The nitrate, sulfate and nitrite concentrations were determined using HPLC, while sulfide was measured colorimetrically.

Temperature Dependence of Sulfate and Nitrate Reduction

IW and PW samples collected in 2015 were inoculated into CSBA medium containing 3 mM VFA (3 mM each of acetate, propionate and butyrate) and 10 mM nitrate or 20 mM lactate and 10 mM sulfate. Following inoculation, the incubations were done at 30, 40, 45, 50, 55, 60, 65, and 70°C. Aliquots of 0.5 ml were withdrawn periodically from the incubations to monitor sulfide, sulfate, nitrate and nitrite concentrations.

Isolation and Identification of tNRB Strains

Thermophilic NRB enrichments derived from IW1_14 grown at 60°C or derived from IW5_15 grown at 50°C were 10-fold serially diluted in CSBA medium and 100 μl of the dilutions was plated on a 2% CSBA-agar medium containing 3 mM VFA and 10 mM nitrate. The plates were incubated at 50°C or 60°C in anaerobic jars flushed with N_2-CO_2. Individual colonies were picked and grown in CSBA medium with 3 mM VFA and 10 mM nitrate. To identify the isolates, DNA was extracted and 16S rRNA gene amplicons were obtained using primers 27F and 1525R. Sanger sequencing of the amplicons was done at the Core DNA Services Laboratory of the University of Calgary.

Effect of Nitrate and Nitrite on Sulfate Reduction by tSRB

To assess the inhibition of sulfide production in tSRB consortia using nitrate or nitrite, 10% (v/v) of tSRB enrichment was grown in CSBA medium containing 20 mM lactate and 10 mM sulfate. Also, a tNRB mixed culture of *Geobacillus* sp. strain TK004 and TK005 was prepared by inoculating glycerol stocks of each strain into CSBA medium with 0.25 M NaCl, containing 20 mM lactate and 10 mM nitrate. The effectiveness of tNRB activity in inhibiting sulfate reduction was monitored by adding tNRB and nitrate at the start (0 h) or in mid-log phase of a tSRB culture.

The effect of nitrate and nitrite on sulfate reduction by tSRB growing in continuous culture was also assessed. A continuous culture of tSRB was started by inoculating 10% of a 48-h tSRB culture into 90 mL CSBA containing 10 mM lactate and 5 mM sulfate. Once all sulfate was reduced, a multichannel peristaltic pump was used to pump the same medium at a flow rate of 33 ml/d (dilution rate 0.33 d^{-1}). To test the effect of nitrate addition on sulfate reduction, CSBA medium containing both 5 mM nitrate and 5 mM sulfate was injected into the tSRB culture in medium with sulfate only. To evaluate the effect of tNRB addition on sulfate reduction, tNRB were grown in CSBA medium containing 5 mM nitrate and 10 mM lactate. The cells were harvested at mid-log phase and washed with CSBA to remove any residual nitrate or nitrite. The cell pellets were re-suspended in CSBA medium and then inoculated into the tSRB culture. The effect of nitrite on sulfate reduction by tSRB was monitored by adding 0.125, 0.25, or 1 mM nitrite to the injection medium.

Microbial Community Analysis

DNA was isolated from 200 ml of PW and IW samples using the Fast DNA Spin Kit for Soil and the FastPrep Instrument (MP Biomedicals, Santa Ana, CA, United States) as per the manufacturer's instructions. The extracted DNA was quantified using a Qubit fluorimeter (Invitrogen). Pyrosequencing of 16S amplicons was done for 2014 samples, whereas Illumina Miseq sequencing was done for 2015 samples.

For pyrosequencing PCR amplification was for 25 cycles with 16S primers 926Fw and 1392R, followed by 10 cycles with FLX titanium primers 454T_RA_X and 454T_FwB, as described in An et al. (2013). Purified 16S amplicons (20 ng each) were sequenced at the Genome Quebec and McGill University Innovation Centre, Montreal, Quebec with a Genome Sequencer FLX Instrument, using a GS FLX Titanium Series Kit XLR70 (Roche Diagnostics Corporation).

For Illumina Miseq sequencing 16S rRNA genes of the extracted DNA were amplified using a two-step PCR procedure with each reaction of 50 μl volume containing premade reagents mixed in proportion as per manufacturer's instructions (Thermo-Scientific). The first PCR used 16S primers 926Fi5 and 1392Ri7, as indicated elsewhere (Menon and Voordouw, 2016). The PCR

product obtained was purified and quantified and was then used for the second PCR reaction, which used primer P5-S50X-OHAF and P7-N7XX-OHAR for 10 cycles, as described elsewhere (Menon and Voordouw, 2016). The resulting purified PCR product was sequenced using the 300PE (paired-end) MiSeq protocol on an Illumina Miseq system at the Department of Geosciences, University of Calgary. The 300PE reads were merged using PEAR 0.9.6 with a 50 bp overlap and were further processed with a 420 bp cutoff of amplicon size using MetaAmp, a 16S rRNA data analysis pipeline, developed by the Energy Bioengineering Group, Department of Geosciences, University of Calgary. MetaAmp was also used for bioinformatic analysis[1].

All sequences have been submitted to NCBI Sequence Read Archive (SRA) under Bioproject accession number PRJNA181037, with biosample number SAMN06645415 and SAMN06645441.

RESULTS

Physicochemical Analyses and Most Probable Numbers

The average salinity of Terra Nova IWs was 0.52 ± 0.04 Meq of NaCl, which was similar to that of produced waters (**Table 1**: 0.57 ± 0.13 Meq of NaCl). The concentrations of sulfate in IW samples (25.1 ± 4.6 mM) were higher than those of produced waters, (15.4 ± 5.5 mM). PW samples had higher concentrations of acetate, propionate and ammonium than IW samples (**Table 1**). All samples had a near neutral pH. Concentrations of nitrate, nitrite and sulfide were zero for all the samples.

The MPNs for SRB, determined by incubation at 30 or 60°C, were below the detection limit in both the IW and PW samples. IW samples had some mesophilic APB (3.6/ml; 30°C), but no thermophilic APB (60°C). No mesophilic or thermophilic APB were detected in the PW samples. Overall these results indicate that only small numbers of bacteria, culturable on the media used, were present in the samples.

Microbial Community Analysis of IW1_14 and PW1_14

Results derived from pyrosequencing of 16S rRNA amplicons for the 2014 samples and from Illumina sequencing of 16S rRNA amplicons for the 2015 samples are presented in Supplementary Tables S1, S2, respectively. The microbial community in PW1_14 had significant fractions of potentially thermophilic *Euryarchaeota* (Supplementary Table S1), including *Methanothermococcus* (7.1%), *Methermicoccus* (2.2%) *Thermococcus* (2.2%) and *Archaeoglobus* (1.7%). The majority of *Bacteria* in the PW1_14 community were thermophiles belonging to the genera *Thermoanaerobacter* (78.2%) and *Thermosipho* (0.7%). Members of the *Deltaproteobacteria* included the tSRB *Desulfonauticus* (0.3%; Piceno et al., 2014). The microbial community in injection water IW1_14 consisted mainly of aerobic mesophilic marine bacteria. About 33.2% of the total reads were affiliated with the genus *Neptuniibacter,* which reduces nitrate to nitrite at temperatures between 4 and 33°C (Arahal et al., 2007; Gutierrez et al., 2013). Other potential hydrocarbon degraders were *Thalassospira* (5.7%), *Alcanivorax* (4.5%) and *Cycloclasticus* (3.0%) (Gutierrez et al., 2013). *Alcanivorax* spp. are moderately halophilic alkane degraders which reduce nitrate to nitrite and N_2 (Nakano et al., 2009; Mayumi et al., 2011; McGenity et al., 2012; Singh et al., 2014). The nitrate-reducing *Marinobacter* was present at 0.5% (Supplementary Table S2) (Li et al., 2013; Stepanov et al., 2016). Contrary to the community in PW1_14, that of IW1_14, harbored no thermophiles (Supplementary Table S1: entries #12, 26-31).

Few potentially thermophilic taxa were found in samples collected in 2015. These were dominated by *Alpha-* and *Gammaproteobacteria*, but lacked *Euryarchaeo*ta. IW5_15 had a high fraction of the sulfur-oxidizing *Thiomicrospira* (Table S2, entry #21, 42%), which was not found in the other samples. Most of the dominating taxa are considered mesophilic. The community in PW1_15 had small fractions of *Methanothermococcus* and *Thermococcus* (Supplementary Table S2: entries #30 and 31).

Thermophilic Enrichments of Field Samples

Because Terra Nova samples had few culturable bacteria, as judged by MPN assays, enrichment of tSRB and tNRB consortia was done with concentrated inocula. Injecting concentrated PW1_14 and IW1_14 in media gave the results indicated in **Figure 2**. Activity of tSRB was detected in lactate-sulfate medium after 3–6 days of incubation at 60°C (**Figure 2A**), whereas tSRB activity was detected in VFA-sulfate medium after 4 to 8 days of incubation (**Figure 2B**). No tSRB activity was detected in medium inoculated with concentrated IW1_14 (results not shown). tNRB activity was observed in medium with 20 mM lactate and 10 mM nitrate inoculated with concentrated IW1_14 (**Figure 2D**). Nitrate was reduced to nitrite, which was not reduced further. No tNRB activity was observed with concentrated PW1_14 (**Figure 2C**).

Nitrate-reducing enrichments using 50-fold concentrated inocula of samples PW1_15 and IW1_15 were done at different temperatures (Supplementary Figure S1). Nitrate was completely reduced within 24 h at 30 and 40°C (Supplementary Figures S1A–D). Nitrite appeared transiently up to 4.8 mM in the incubation with IW1_15 at 40°C (Supplementary Figure S1B), whereas 1.0 mM nitrite persisted in the incubation with PW1_15 at 40°C (Supplementary Figure S1E). At 45°C nitrate was slowly reduced to nitrite in the medium inoculated with concentrated IW1_15 PW (Supplementary Figure S1C). Reduction of 3 mM nitrate was observed with PW1_15 without production of nitrite (Supplementary Figure S1F). Incubations at 50 to 70°C showed no tNRB activity (results not shown). SRB activity was observed for concentrated PW1_15 in medium with VFA and sulfate at 60°C (results not shown).

[1]http://ebg.ucalgary.ca/metaamp

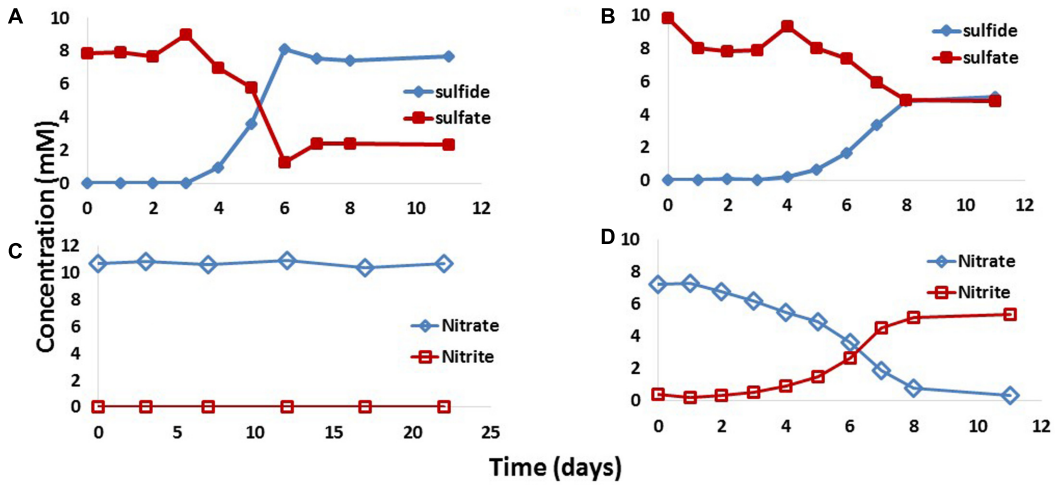

FIGURE 2 | Activity of tSRB and tNRB observed with 50-fold concentrated inocula of Terra Nova produced water PW1_14 and injection water IW1_14. Incubations were with PW1_14 with 10 mM sulfate and 20 mM lactate **(A)**, PW1_14 with 10 mM sulfate and 3 mM VFA **(B)**, PW1_14 with 10 mM nitrate and 20 mM lactate **(C)** and IW1_14 with 10 mM nitrate and 20 mM lactate **(D)**. Data are averages of duplicate incubations.

Use of 50-fold concentrated inocula of IW5_15 indicated rapid reduction of nitrate at 40, 45, and 50°C (**Figures 3A–C**). Nitrite was not detected at 40 and 45°C, but persisted in the 50°C incubation (**Figure 3C**). No NRB activity was found at 55, 60, and 65°C (**Figures 3D–F**). No SRB activity was found at any of these temperatures. No NRB or SRB activity was found with concentrated inocula of PW5_15 at 40–65°C.

Thus, significant tSRB and tNRB activity at 60°C were observed in the produced water and IW samples collected in January of 2014, respectively. Samples collected in January and May 2015 gave tNRB activity at lower temperature (50°C). These results are in agreement with the increased presence of thermophiles in the 2014 samples, as compared to the 2015 samples, indicated by microbial community analyses (Supplementary Tables S1, S2).

NRB Enrichment at 50°C and 60°C and Isolation of tNRB

The tNRB enrichment obtained at 50°C (**Figure 3C**) was further evaluated for effect of temperature on nitrate reduction, growth and community composition. The results in **Figures 3G–I** showed that in incubations at 30, 40, and 50°C, nitrate was reduced to nitrite and no further. Nitrate was completely reduced at 30°C within 72 h (**Figure 3G**), at 40°C within 48 h (**Figure 3H**) and at 50°C within 24 h (**Figure 3I**). Nitrite accumulated at all three temperatures. No nitrate reduction was observed above 50°C. High cell density of these cultures was observed at 30, 40, and 50°C, but not at higher temperatures (Supplementary Figure S2A), indicating the nitrate reducers to be facultative tNRB. Mesophilic NRB, which reduced nitrite (**Figures 3A,B**) were no longer present in this enrichment. Microbial community data for the incubations in **Figures 3G–I** indicated *Marinobacter* spp. as the dominant NRB present at 99.6%, 68 and 99.7% respectively (Supplementary Figure S2B). A pure culture isolate, obtained from the enrichment in **Figure 3I** and grown at 50°C, was identified as *Marinobacter* sp. GN001 (KY818661). Growth of this isolate at temperatures ranging from 30 to 60°C, indicated that it reduced nitrate, but not nitrite, at 30, 40, and 50°C (**Figures 3J–L**). Nitrate was not reduced at 60°C (results not shown). Nitrate reduction proceeded most rapidly at 40 and 50°C and more slowly at 30°C, like the enrichment in **Figures 3G–I**.

Pure culture tNRB isolates TK004 and TK005 were obtained from IW1_14 at 60°C. Both were identified as *Geobacillus* spp. by 16S rRNA sequencing. Nitrate reduction by TK004 as a function of temperature indicated maximal activity at 60°C, lower activity at 50 and 40°C and no activity at 30 and 70°C. Nitrate was reduced to nitrite only (**Figure 4**).

Enrichment of tSRB

The temperature dependence of the rate of sulfate reduction to sulfide was determined for a tSRB consortium previously enriched from PW1_14 at 60°C (**Figure 2A**). Reduction of sulfate to sulfide was observed at 55, 60, and 65°C (**Figures 5A,B**), but not at lower temperatures. Significant increases in biomass were also only observed at 55, 60, and 65°C (**Figure 5C**). Reduction of sulfate to sulfide was observed at 70°C after 300 h at a very slow rate (Supplementary Figure S3). This finding was further supported by the community data from 55 to 65°C incubations, when compared to the inocula used for the experiment (Supplementary Table S3). Bioinformatic analysis of quality controlled Illumina reads indicated that the tSRB consortium was more diverse than the 55, 60, and 65°C incubations (Supplementary Table S3). The tSRB consortium had high fractions of the thermophiles *Thermus* (25%), *Anoxybacillus* (8.8%) and *Desulfotomaculum* (7.6%). However, the 55, 60, and 65°C incubations were dominated by the genus *Desulfotomaculum*, which was present at 98.8, 97.2, and 95.5% respectively (Supplementary Table S4).

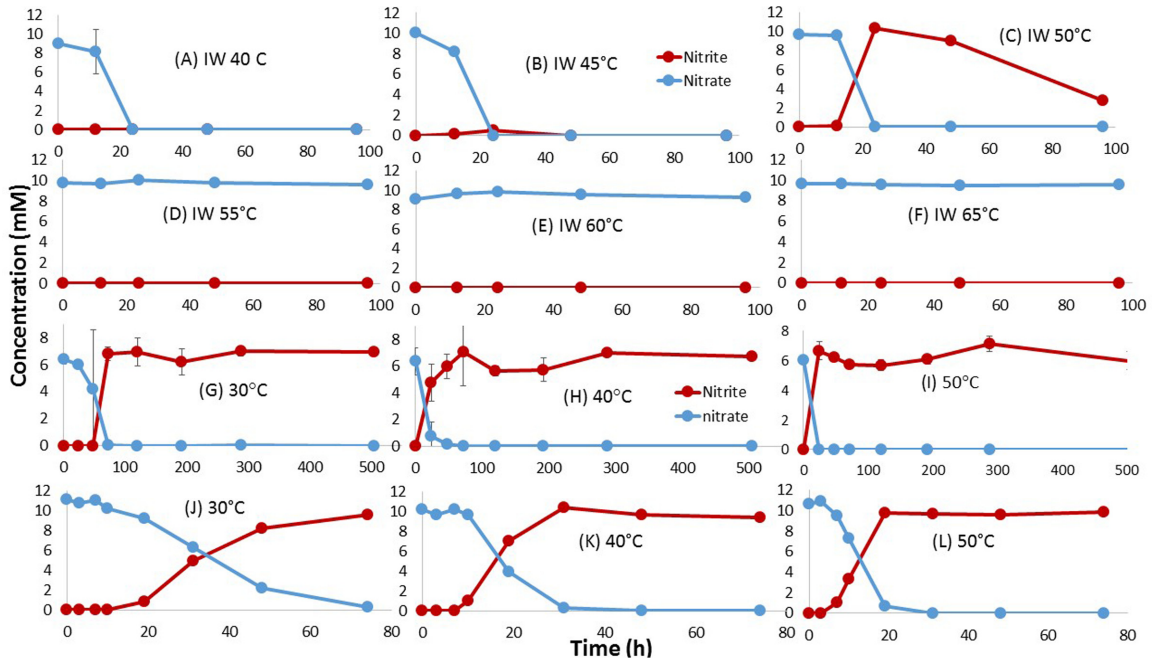

FIGURE 3 | Effect of incubation temperature on nitrate reduction in cultures derived from IW5_15. Data are for primary enrichments **(A–F)**, for secondary enrichments inoculated with primary enrichment **(C)** grown at 50°C **(G–I)** and for a pure culture isolate, identified as *Marinobacter* sp., obtained at 50°C **(J–L)**. No growth was observed for the cultures in **(G–L)** at 55°C or higher temperature. The CSBA medium contained 3 mM VFA and 10 mM nitrate.

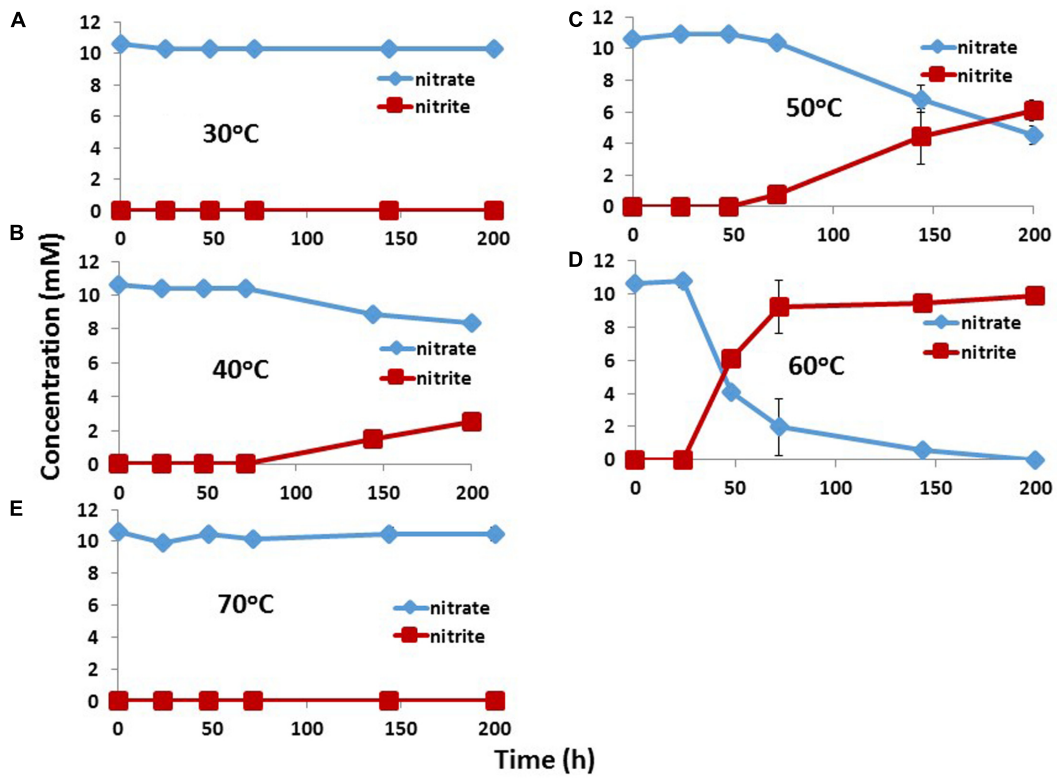

FIGURE 4 | Effect of incubation temperature on nitrate reduction by a pure culture isolate *Geobacillus* sp. TK004, obtained from IW1_14. Data are averages for duplicate incubations; standard deviations are shown. The medium contained 3 mM VFA and 10 mM nitrate. 30°C **(A)**, 40°C **(B)**, 50°C **(C)**, 60°C **(D)**, and 70°C **(E)**.

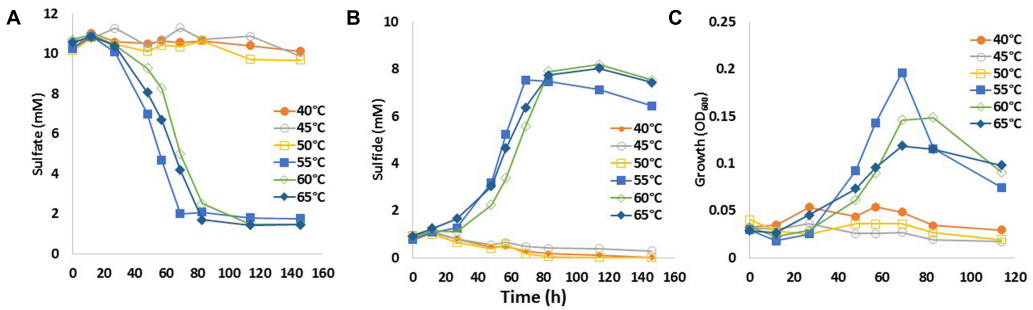

FIGURE 5 | Effect of incubation temperature on growth and sulfate reduction by tSRB consortia enriched from PW1_14. The concentration of sulfate **(A)** and of sulfide **(B)**, as well as the cell density as OD_{600} **(C)** are presented as a function of time. Data are averages for duplicate incubations. The medium contained 20 mM lactate and 10 mM sulfate.

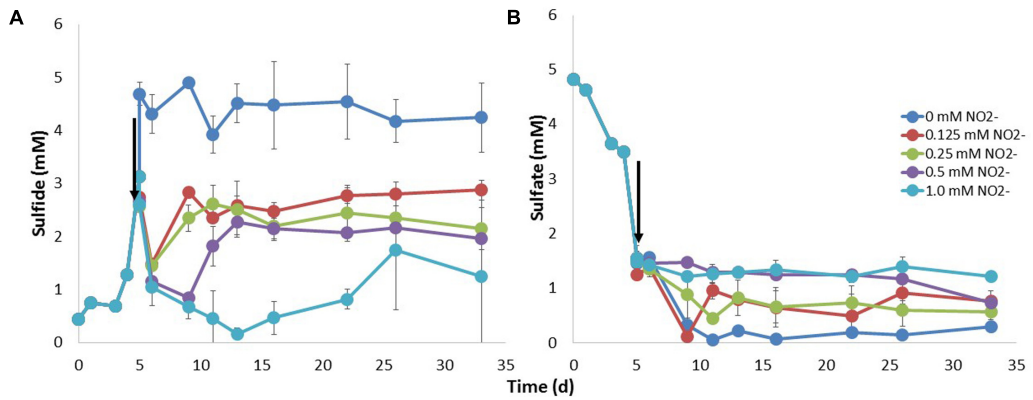

FIGURE 6 | Inhibition of sulfate reduction by tSRB with nitrite. A tSRB consortium enriched at 60°C (**Figure 5**) was grown at this same temperature in medium with 20 mM lactate and 10 mM sulfate. The concentrations of **(A)** sulfide and **(B)** sulfate are shown as a function of time. Nitrite was injected at midlog phase (↓) in concentrations as indicated.

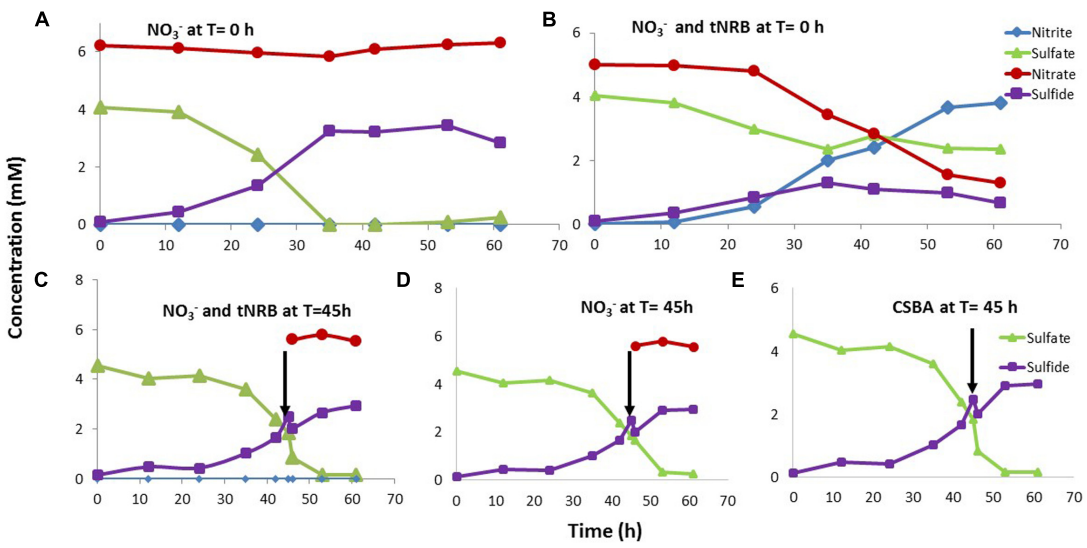

FIGURE 7 | Effect of addition of nitrate or of nitrate and tNRB on sulfate reduction by tSRB consortia grown at 60°C. Nitrate **(A)** or nitrate and tNRB **(B)** were added at T = 0 h **(A,B)** or at midlog phase of sulfate reduction at T = 45 h **(C,D)**; 100 μl of CSBA medium was added as a control at T = 45 h **(E)**. Data are averages for duplicate incubations.

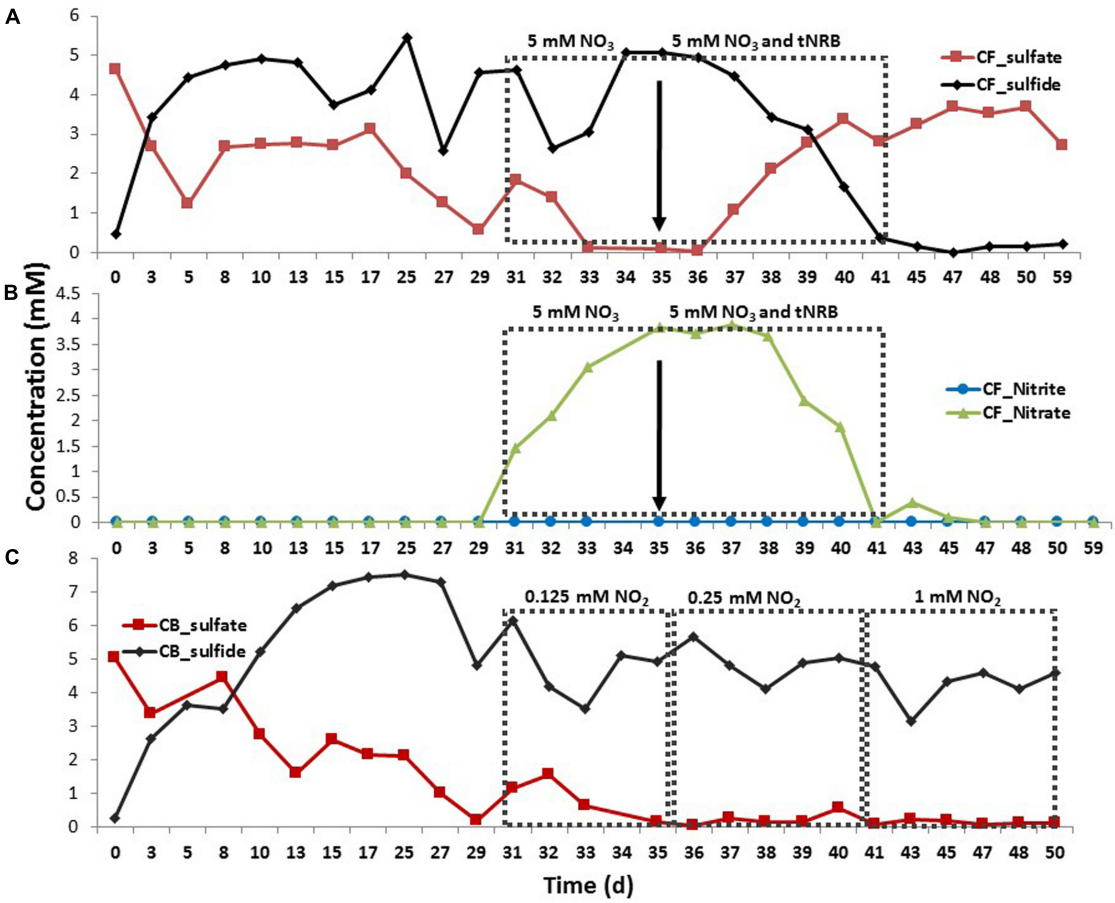

FIGURE 8 | Effect of addition of nitrate, of nitrate and tNRB, or of nitrite on tSRB activity during continuous culture conditions at 60°C. The concentrations (mM) are shown as a function of time (days) for **(A)** sulfate and sulfide in chemostat F (CF), **(B)** nitrate and nitrite in CF and **(C)** sulfate and sulfide in chemostat B (CB). CF was injected with medium containing lactate and sulfate. This was switched to medium with lactate, sulfate and nitrate as indicated; tNRB were added as indicated (↓). CB was injected with medium containing lactate and sulfate with addition of 0.125, 0.250, and 1.0 mM of nitrite as indicated. Note that the time scale is not linear.

Effect of Addition of Nitrite or Nitrate to tSRB Enrichments in Batch Culture

The effect of nitrite on sulfate reduction was tested at 60°C, using the 60°C tSRB enrichment of **Figure 5**, which contained mostly *Desulfotomaculum* (Supplementary Table S4). Addition of nitrite at mid-log phase caused an instant drop in sulfide concentration (**Figure 6A**), due to chemical reaction of nitrite with sulfide. Addition of the lowest concentrations of 0.125 and 0.25 mM nitrite inhibited sulfide production only transiently. However, the final concentration of sulfide produced remained below that of the untreated culture (**Figure 6A**). Sulfate concentrations remained constant following addition of 0.5 or 1 mM nitrite, while some sulfate reduction was observed at lower nitrite concentrations (**Figure 6B**).

When nitrate was added it was not reduced and reduction of sulfate to sulfide was complete in 35 h (**Figure 7A**). However, when both nitrate and tNRB (a mixture of *Geobacillus* sp. strains TK004 and TK005) were added at time zero reduction of nitrate to nitrite was observed from 24 h onward. This inhibited the reduction of sulfate, which remained constant from 35 h onward. Sulfide concentrations decreased from 35 h onward (**Figure 7B**); development of a yellow color indicated the formation of polysulfides from reaction of nitrite and sulfide. The addition of nitrate and actively growing tNRB or of nitrate only to a tSRB culture at mid-log phase did not give nitrate reduction and no inhibition of sulfate reduction was observed (**Figures 7C,D**). This was because the time necessary for tNRB to grow (**Figure 7B**: 24 h), exceeded the time needed for the tSRB culture to grow to completion (**Figures 7C–E**: 5 h). Overall the results indicated that addition of tNRB and nitrate at time zero resulted in inhibition of tSRB activity due to formation of nitrite. Inhibition was not observed when only nitrate was added or when tNRB and nitrate were added at midlog phase.

Addition of Nitrate, Nitrate and tNRB or Nitrite to Continuous Cultures of tSRB

A continuous culture (chemostat) of tSRB, inoculated with the 60°C enrichment of **Figure 5**, was fed with CSBA medium with lactate and 5 mM sulfate at a dilution rate of 0.33 day^{-1}; 5 mM nitrate was included in the inflowing medium from day

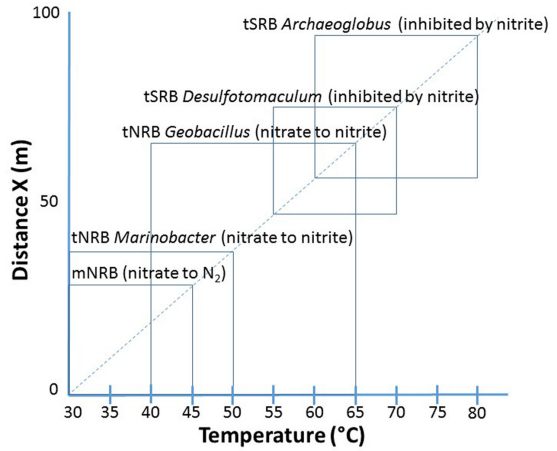

FIGURE 9 | Distribution of NRB and SRB from Terra Nova identified or cultivated in this study in the NIWR. These included mesophilic NRB, tNRB *Marinobacter*, tNRB *Geobacillus*, tSRB *Desulfotomaculum* and the thermophilic sulfate-reducing archaeon (tSRA) *Archaeoglobus*. The latter was not cultivated and its range of activity was inferred from the literature. The scale on the *Y* axis is an estimate of the size of the NIWR (from 0 to 100 m) and the approximate position of the taxa in this region

31 to day 41. This led to a gradual increase in the nitrate concentration in the chemostat to 4 mM from day 31–35 (**Figure 8B**). This indicated that nitrate was not reduced. Indeed, the reduction of sulfate to sulfide was not affected (**Figure 8A**: day 31–35). However, when a single dose of tNRB was added to the chemostat on day 36 (**Figures 8A,B**: ↓), the nitrate concentration decreased from 4 mM to zero from day 36 to day 41 (**Figure 8B**). The concentration of sulfide decreased from 5 to 0.2 mM, whereas the concentration of sulfate increased from 0 to 3 mM (**Figure 8A**). The development of turbidity and yellow color indicated formation of sulfur and polysulfide (S-PS), respectively. Nitrite was not detected, likely because it reacted with sulfide to form S-PS. When the medium was switched on day 41 to medium with sulfate only (no nitrate), the tSRB did not recover as indicated by zero sulfide and 3.7 mM sulfate from day 41–59 (**Figure 8A**). Addition of 0.125, 0.25, or 1 mM nitrite to the inflowing medium in another similarly run chemostat did not inhibit the reduction of sulfate of which the concentration remained at zero (**Figure 8C**). However, sulfide concentrations dropped. Nitrite was again not detected indicating reaction of nitrite and sulfide (**Figure 8C**). Note that the average concentration of added nitrite over the indicated time periods would be approximately half of that added to the inflowing medium (0.062, 0.125, and 0.5 mM). The gradual addition of nitrite appeared to affect tSRB in continuous culture less than the addition of a single dose in batch culture (**Figures 6A**, **8C**).

DISCUSSION

Oil production from Terra Nova started in 2002 with seawater injection being required soon after (Haugen et al., 2007). Souring became evident after about 8 years of seawater flooding (Sharpe et al., 2015) and nitrate and nitrite were injected as a souring control strategy from 2014 onward. Because of the high reservoir temperature of 95°C some regions will be abiotic and microbial growth is expected only in regions where the temperature is below 80°C (**Figure 1**). It is generally thought that most souring occurs in the NIWR, where sulfate-containing IW comes in contact with oil. Because injected sea water has a high sulfate concentration (**Table 1**) both mesophilic SRB and thermophilic SRM may contribute to souring (Thrasher and Vance, 2005; Torsvik and Sunde, 2005). The produced sulfide then travels through the reservoir. Its appearance in produced water can take a long time (i.e., 8 years in the case of Terra Nova) due to sulfide scavenging by reservoir rock (Thrasher and Vance, 2005).

Uncovering the microbiology of the NIWR is thus relevant, but is challenging because only samples of IW and of produced water are available in most cases. Reversing the flow of IW would allow a more direct collection of samples from the NIWR, but such samples are only rarely available (Bødtker et al., 2009). Microbial community data obtained for produced water samples cannot be pinpointed to a particular region. These samples may contain IW microbes, which passed through the reservoir and were heat killed along the way, as well as sessile bacteria growing on the walls of pipelines transporting produced water and oil to the FPSO (**Figure 1**). Low microbial counts and activities are commonly observed in produced waters from high temperature reservoirs (Bonch-Osmolovskaya et al., 2003; Birkeland, 2005; Kaster et al., 2007). Likewise, the seawater used as IW may contain thermophiles from the reservoir or pipeline walls, due to the continuous discharge of de-oiled, high temperature produced water (**Figure 1**). Therefore, a variety of approaches including community analysis, culturing and determination of temperature optima are needed to reconstruct the positioning of microbes and their activities in the NIWR.

Of the thermophiles detected in this study, *Thermoanaerobacter* spp. are fermentative bacteria, which have been frequently found in produced water samples from high temperature oil fields (Orphan et al., 2000; Pavlova-Kostryukova et al., 2014; Yeung et al., 2015). Other detected thermophiles were the fermentative bacterial taxon *Thermosipho* (Haridon et al., 2001; Dahle et al., 2008), the archaeal taxon *Thermococcus*, which is also a sulfur reducer (Zhang Y. et al., 2012; Liang et al., 2014; Lin et al., 2014; Gorlas et al., 2015) and the methanogen *Methanothermococcus*. These results indicate that regions in the NIWR and pipeline walls with the right temperature regime will harbor diverse metabolically active thermophilic and hyperthermophilic anaerobes (Slobodkin et al., 1999; Orphan et al., 2003) of which only a few have been cultured (Orphan et al., 2000). Gittel et al. (2009) reported that an enrichment of a sample, which had 56% *Archaeoglobus* sequences, had no sulfate-reducing activity. These authors were also unable to enrich tNRB from produced water samples from the Ekofisk oilfield. *Desulfotomaculum* spp. are the most documented culturable tSRB isolated from oil field environments (Nilsen et al., 1996a,b; Nazina et al., 2006; Aüllo et al., 2013), but are not often detected with next generation sequencing approaches (Müller et al., 2014; Wunderlin et al., 2014). *Thermodesulforhabdus norvegicus* and

Archaeoglobus fulgidus strains were among the dominant tSRM detected by Nilsen et al. (1996a) in North Sea oil reservoirs and Beeder et al. (1995) isolated a novel acetate-oxidizing *T. norvegicus,* which grew at temperature of up to 74°C. Li et al. (2007) detected *Thermodesulfovibrio*, a Gram-negative tSRB, as a major component of a 16S rRNA gene clone library from a North Sea field.

Fida et al. (2016) reported the isolation of the tNRB *Petrobacter* sp. TK002 (optimum growth at 50°C) and *Geobacillus* sp. TK003 (optimum growth at 65°C), which reduced nitrate to nitrite. Although some tNRB have been reported to reduce nitrate to N_2 or ammonium (Greene et al., 1997; Miranda-Tello et al., 2003), reduction of nitrate to nitrite appeared to be the norm for oil field tNRB (Fida et al., 2016). The addition of nitrate often does not inhibit tSRB consortia, because these lack tNRB. Such tSRB consortia are only inhibited by nitrite or by nitrate, if tNRB are also injected (**Figures 6B**, **7A,B**). The inhibition of the tSRB consortia used in this study and in other work by low concentrations of nitrite (Kaster et al., 2007) indicates absence of Nrf nitrite reductase, which reduces nitrite to ammonium. Nrf protects many mesophilic SRB from inhibition by nitrite (Greene et al., 2003; Haveman et al., 2004).

Although this would suggest that injection of nitrite, which directly inhibits SRM, is preferable to the injection of nitrate this may not apply at Terra Nova, where both mesophilic and tNRB are present. Mesophilic NRB grow closest to the injection wellbore at 30–45°C (**Figure 9**). These reduce nitrate to N_2 (**Figures 3A,B**), but have not been phylogenetically characterized. These are followed by moderately tNRB of the genus *Marinobacter* growing at 30–50°C (**Figures 3C,G-I**, **9**) and these are succeeded by tNRB of the genus *Geobacillus*, which grow from 40 to 65°C (**Figure 4**; Fida et al., 2016). There is no tNRB activity at 70°C or higher temperature. The activity of tSRB of the genus *Desulfotomaculum* extends from 55 to 70°C (**Figure 5** and Supplementary Figure S3). The observation of significant fractions of *Archaeoglobus* in some samples (Supplementary Table S1: entry #28) indicates that the temperature limit for sulfate reduction may be at even higher temperature (Beeder et al., 1994; Gittel et al., 2009). Because mesophilic SRB were not detected with cultivation or 16S rRNA gene sequencing, we assume that these were largely absent from Terra Nova, where nitrate injection may displace SRB from low temperature zones. Thus at Terra Nova sulfide may be mainly produced by tSRB living in a high temperature zone (65–80°C) from which tNRB are excluded. Preventing the temperature of the NIWR to drop below 50°C would increase the production of nitrite from injected nitrate in tNRB inhabited zones (50–65°C). Transfer of this produced nitrite into the adjacent higher temperature zone (65–80°C) will inhibit the resident tSRB, if the rate of transfer exceeds the rate of sulfide production by tSRB. These conditions were apparently not met in our continuous culture study (**Figure 8C**). Injection of hot recycled produced water to keep the temperature above 50°C will increase the transfer of nitrite into tSRB-inhabited zones and is therefore a promising strategy to control souring in high temperature oil reservoirs, as suggested previously (Fida et al., 2016).

AUTHOR CONTRIBUTIONS

GO, CC, and TF designed and carried out the study, collected data, performed the analysis. GO wrote the manuscript. GV contributed to data interpretation and preparation of the manuscript.

FUNDING

This work was supported by an NSERC Industrial Research Chair Award to Gerrit Voordouw, which was also supported by BP America Production Co., Baker Hughes Canada, Computer Modeling Group Limited, ConocoPhillips Company, Dow Microbial Control, Enbridge Inc., Enerplus Corporation, Intertek Commercial Microbiology, Oil Search (PNG) Limited, Shell Global Solutions International, Suncor Energy Inc., and Yara Norge AS, as well as by Alberta Innovates.

ACKNOWLEDGMENTS

We are thankful to Phil Stemler from Suncor for discussions of souring in the Terra Nova field and to Stephen Lear from Baker Hughes for sample collection and shipment. Yin Shen is thanked for administrative and technical support and Dongshan An for assistance with analysis of sequence data.

SUPPLEMENTARY MATERIAL

The Supplementary Material for this article can be found online at: http://journal.frontiersin.org/article/10.3389/fmicb.2017.01573/full#supplementary-material

REFERENCES

Agrawal, A., An, D., Cavallaro, A., and Voordouw, G. (2014). Souring in low-temperature surface facilities of two high-temperature Argentinian oil fields. *Appl. Microbiol. Biotechnol.* 98, 8017–8029. doi: 10.1007/s00253-014-5843-z

An, D., Caffrey, S. M., Soh, J., Agrawal, A., Brown, D., Budwill, K., et al. (2013). Metagenomics of hydrocarbon resource environments indicates aerobic taxa and genes to be unexpectedly common. *Environ. Sci. Technol.* 47, 10708–10717. doi: 10.1021/es4020184

Arahal, D. R., Lekunberri, I., Gonzá lez, J. M., Pascual, J., Pujalte, M. J., Pedró s-Alió, C., et al. (2007). *Neptuniibacter caesariensis* gen. nov., sp. nov., a novel marine genome-sequenced gammaproteobacterium. *Int. J. Syst. Evol. Microbiol.* 57, 1000–1006. doi: 10.1099/ijs.0.64524-0

Aüllo, T., Ranchou-Peyruse, A., Ollivier, B., and Magot, M. (2013). *Desulfotomaculum* spp. and related gram-positive sulfate-reducing

bacteria in deep subsurface environments. *Front. Microbiol.* 4:362. doi: 10.3389/fmicb.2013.00362

Beeder, J., Nilsen, R. K., Rosnes, J. T., Torsvik, T., and Lien, T. (1994). *Archaeoglobus fulgidus* isolated from hot North Sea oil field waters. *Appl. Environ. Microbiol.* 60, 1227–1231.

Beeder, J., Torsvik, T., and Lien, T. (1995). *Thermodesulforhabdus norvegicus* gen. nov., sp. nov., a novel thermophilic sulfate-reducing bacterium from oil field water. *Arch. Microbiol.* 164, 331–336. doi: 10.1007/BF02529979

Birkeland, N.-K. (2005). "Sulfate-reducing bacteria and archaea," in *Petroleum Microbiology*, eds B. Ollivier and M. Magot (Washington, DC: ASM Press), 35–54. doi: 10.1128/9781555817589.ch3

Bødtker, G., Lysnes, K., Torsvik, T., Bjørnestad, E., and Sunde, E. (2009). Microbial analysis of backflowed injection water from a nitrate-treated North Sea oil reservoir. *J. Ind. Microbiol. Biotechnol.* 36, 439–450. doi: 10.1007/s10295-008-0515-6

Bonch-Osmolovskaya, E. A., Margarita, L., Lebedinsky, A. V., Nikolai, A., Nazina, T. N., Ivoilov, V. S., et al. (2003). Oligonucleotide microchip analyses of thermophilic microbial communities in a continental high-temperature petroleum reservoir. *Appl. Environ. Microbiol.* 69, 6143–6151. doi: 10.1128/AEM.69.10.6143

Callbeck, C. M., Dong, X., Chatterjee, I., Agrawal, A., Caffrey, S. M., Sensen, C. W., et al. (2011). Microbial community succession in a bioreactor modeling a souring low-temperature oil reservoir subjected to nitrate injection. *Appl. Microbiol. Biotechnol.* 91, 799–810. doi: 10.1007/s00253-011-3287-2

Chen, C., Shen, Y., An, D., and Voordouw, G. (2017). Use of acetate, propionate, and butyrate for reduction of nitrate and sulfate and methanogenesis in microcosms and bioreactors simulating an oil reservoir. *Appl. Environ. Microbiol.* 83:e2983-16. doi: 10.1128/AEM.02983-16

Cline, J. D. (1969). Spectrophotometric determination of hydrogen sulfide in natural waters. *Limnol. Oceanogr.* 14, 454–458. doi: 10.4319/lo.1969.14.3.0454

Cornish Shartau, S. L., Yurkiw, M., Lin, S., Grigoryan, A. A., Lambo, A., Park, H.-S., et al. (2010). Ammonium concentrations in produced waters from a mesothermic oil field subjected to nitrate injection decrease through formation of denitrifying biomass and anammox activity. *Appl. Environ. Microbiol.* 76, 4977–4987. doi: 10.1128/AEM.00596-10

Dahle, H., Garshol, F., Madsen, M., and Birkeland, N.-K. (2008). Microbial community structure analysis of produced water from a high-temperature North Sea oil-field. *Antonie Van Leeuwenhoek* 93, 37–49. doi: 10.1007/s10482-007-9177-z

Eden, B., Laycock, P. J., and Fielder, M. (1993). Oilfield reservoir souring. *Health Saf. Exec.* 92, 385.

Fida, T. T., Chen, C., Okpala, G., and Voordouw, G. (2016). Implications of limited thermophilicity of nitrite reduction for control of sulfide production in oil reservoirs. *Appl. Environ. Microbiol.* 82, 4190–4199. doi: 10.1128/AEM.00599-16

Gittel, A., Kofoed, M. V. W., Sørensen, K. B., Ingvorsen, K., and Schramm, A. (2012). Succession of deferribacteres and epsilonproteobacteria through a nitrate-treated high-temperature oil production facility. *Syst. Appl. Microbiol.* 35, 165–174. doi: 10.1016/j.syapm.2012.01.003

Gittel, A., Sørensen, K. B., Skovhus, T. L., Ingvorsen, K., and Schramm, A. (2009). Prokaryotic community structure and sulfate reducer activity in water from high-temperature oil reservoirs with and without nitrate treatment. *Appl. Environ. Microbiol.* 75, 7086–7096. doi: 10.1128/AEM.01123-09

Gorlas, A., Marguet, E., Gill, S., Geslin, C., Guigner, J.-M., Guyot, F., et al. (2015). Sulfur vesicles from Thermococcales: a possible role in sulfur detoxifying mechanisms. *Biochimie* 118, 356–364. doi: 10.1016/j.biochi.2015.07.026

Greene, A. C., Patel, B. K. C., and Sheehy, A. J. (1997). *Deferribacter thermophilus* gen. nov., sp. nov., a novel thermophilic manganese- and iron-reducing bacterium isolated from a petroleum reservoir. *Int. J. Syst. Bacteriol.* 47, 505–509. doi: 10.1099/00207713-47-2-505

Greene, E. A., Hubert, C., Nemati, M., Jenneman, G. E., and Voordouw, G. (2003). Nitrite reductase activity of sulphate-reducing bacteria prevents their inhibition by nitrate-reducing, sulphide- oxidizing bacteria. *Environ. Microbiol.* 5, 607–617. doi: 10.1046/j.1462-2920.2003.00446.x

Gutierrez, T., Singleton, D. R., Berry, D., Yang, T., Aitken, M. D., and Teske, A. (2013). Hydrocarbon-degrading bacteria enriched by the Deepwater Horizon oil spill identified by cultivation and DNA-SIP. *ISME J.* 7, 2091–2104. doi: 10.1038/ismej.2013.98

Haridon, S., Miroshnichenko, M. L., Hippe, H., Fardeau, M.-L., Bonch-osmolovskaya, E. A., Stackebrandt, E., et al. (2001). *Thermosipho geolei* sp. nov., a thermophilic bacterium isolated from a continental. *Int. J. Syst. Evol. Microbiol.* 51, 1327–1334. doi: 10.1099/00207713-51-4-1327

Haugen, E., Hydro, N., Costello, J., Wilcox, L., Albrechtsons, E., and Kelly, I. (2007). *Reservoir Management Challenges of the Terra Nova Offshore Field?: Lessons Learned After Five Years of Production*. Richardson, TX: Society of Petroleum Engineers.

Haveman, S. A., Greene, E. A., Stilwell, C. P., Voordouw, J. K., and Voordouw, G. (2004). Physiological and gene expression analysis of inhibition of *Desulfovibrio vulgaris* hildenborough by nitrite. *J. Bacteriol.* 186, 7944–7950. doi: 10.1128/JB.186.23.7944-7950.2004

Howell, G. B., Duggal, A. S., and Lever, G. V. (2001). "The terra nova FPSO turret mooring system," in *Proceedings of the Offshore Technology Conference*, Houston, TX, doi: 10.4043/13020-MS

Hubert, C., Nemati, M., Jenneman, G., and Voordouw, G. (2003). Containment of biogenic sulfide production in continuous up-flow packed-bed bioreactors with nitrate or nitrite. *Biotechnol. Prog.* 19, 338–345. doi: 10.1021/bp020128f

Kaster, K. M., Grigoriyan, A., Jenneman, G., and Voordouw, G. (2007). Effect of nitrate and nitrite on sulfide production by two thermophilic, sulfate-reducing enrichments from an oil field in the North Sea. *Appl. Microbiol. Biotechnol.* 75, 195–203. doi: 10.1007/s00253-006-0796-5

Lambo, A. J., Noke, K., Larter, S. R., and Voordouw, G. (2008). Competitive, microbially-mediated reduction of nitrate with sulfide and aromatic oil components in a low-temperature, western Canadian oil reservoir. *Environ. Sci. Technol.* 42, 8941–8946. doi: 10.1021/es801832s

Lenchi, N., Inceoğlu, O., Kebbouche-Gana, S., Gana, M. L., Llirós, M., Servais, P., et al. (2013). Diversity of microbial communities in production and injection waters of algerian oilfields revealed by 16S rRNA gene amplicon 454 pyrosequencing. *PLoS ONE* 8:e66588. doi: 10.1371/journal.pone.0066588

Li, H., Yang, S. Z., and Mu, B. Z. (2007). Phylogenetic diversity of the archaeal community in a continental high-temperature, water-flooded petroleum reservoir. *Curr. Microbiol.* 55, 382–388. doi: 10.1007/s00284-007-9002-y

Li, R., Zi, X., Wang, X., Zhang, X., Gao, H., and Hu, N. (2013). *Marinobacter hydrocarbonoclasticus* NY-4, a novel denitrifying, moderately halophilic marine bacterium. *Springerplus* 2:346. doi: 10.1186/2193-1801-2-346

Liang, R., Grizzle, R. S., Duncan, K. E., McInerney, M. J., and Suflita, J. M. (2014). Roles of thermophilic thiosulfate-reducing bacteria and methanogenic archaea in the biocorrosion of oil pipelines. *Front. Microbiol.* 5:89. doi: 10.3389/fmicb.2014.00089

Liebensteiner, M. G., Tsesmetzis, N., Stams, A. J. M., and Lomans, B. P. (2014). Microbial redox processes in deep subsurface environments and the potential application of (per)chlorate in oil reservoirs. *Front. Microbiol.* 5:428. doi: 10.3389/fmicb.2014.00428

Lin, J., Hao, B., Cao, G., Wang, J., Feng, Y., Tan, X., et al. (2014). A study on the microbial community structure in oil reservoirs developed by water flooding. *J. Pet. Sci. Eng.* 122, 354–359. doi: 10.1016/j.petrol.2014.07.030

Magot, M. (2005). "Indigenous microbial communities in oil fields," in *Petroleum Microbiology*, eds B. Ollivier and M. Magot (Washington, DC: ASM Press), 21–34. doi: 10.1128/9781555817589.ch2

Mayumi, D., Mochimaru, H., Yoshioka, H., Sakata, S., Maeda, H., Miyagawa, Y., et al. (2011). Evidence for syntrophic acetate oxidation coupled to hydrogenotrophic methanogenesis in the high-temperature petroleum reservoir of Yabase oil field (Japan). *Environ. Microbiol.* 13, 1995–2006. doi: 10.1111/j.1462-2920.2010.02338.x

McGenity, T. J., Folwell, B. D., McKew, B. A., and Sanni, G. O. (2012). Marine crude-oil biodegradation: a central role for interspecies interactions. *Aquat. Biosyst.* 8:10. doi: 10.1186/2046-9063-8-10

Menon, P., and Voordouw, G. (2016). Impact of light oil toxicity on sulfide production by acetate-oxidizing, sulfate-reducing bacteria. *Int. Biodeterior. Biodegrad.* (in press). doi: 10.1016/j.ibiod.2016.11.021

Miranda-Tello, E., Fardeau, M.-L., Sepúlveda, J., Fernández, L., Cayol, J.-L., Thomas, P., et al. (2003). *Garciella nitratireducens* gen. nov., sp. nov., an anaerobic, thermophilic, nitrate- and thiosulfate-reducing bacterium isolated from an oilfield separator in the Gulf of Mexico. *Int. J. Syst. Evol. Microbiol.* 53, 1509–1514. doi: 10.1099/ijs.0.02662-0

Müller, A. L., de Rezende, J. R., Hubert, C. R. J., Kjeldsen, K. U., Lagkouvardos, I., Berry, D., et al. (2014). Endospores of thermophilic bacteria as tracers of microbial dispersal by ocean currents. *ISME J.* 8, 1153–1165. doi: 10.1038/ismej.2013.225

Nakano, M., Okunishi, S., Tanaka, R., and Maeda, H. (2009). Denitrifying activity and homologous enzyme analysis of alcanivorax dieselolei Strain N1203. *Biocontrol Sci.* 14, 97–105. doi: 10.4265/bio.14.97

Nazina, T. N., Shestakova, N. M., Grigor'yan, A. A., Mikhailova, E. M., Tourova, T. P., Poltaraus, A. B., et al. (2006). Phylogenetic diversity and activity of anaerobic microorganisms of high-temperature horizons of the Dagang oil field (P. R. China). *Microbiology* 75, 55–65. doi: 10.1134/S0026261706010115

Nilsen, R. K., Beeder, J., and Thorstenson, T. (1996a). Distribution of thermophilic marine sulfate reducers in north sea oil field waters and oil reservoirs. *Appl. Environ. Microbiol.* 62, 1793–1798.

Nilsen, R. K., Torsvik, T., and Lien, T. (1996b). *Desulfotomaculum thermocisternum* sp. nov., a sulfate reducer isolated from a hot north sea oil reservoir. *Int. J. Syst. Bacteriol.* 46, 397–402. doi: 10.1099/00207713-46-2-397

Orphan, V. J., Goffredi, S. K., Delong, E. F., and Boles, J. R. (2003). Geochemical influence on diversity and microbial processes in high temperature oil reservoirs geochemical influence on diversity and microbial processes in high temperature oil reservoirs. *Geomicrobiol. J.* 20, 295–311. doi: 10.1080/01490450390241017

Orphan, V. J., Taylor, L. T., Hafenbradl, D., and Delong, E. F. (2000). Culture-dependent and culture-independent characterization of microbial assemblages associated with high-temperature petroleum reservoirs. *Appl. Environ. Microbiol.* 66, 700–711. doi: 10.1128/AEM.66.2.700-711.2000. Updated

Pavlova-Kostryukova, N. K., Tourova, T. P., Poltaraus, A. B., Feng, Q., and Nazina, T. N. (2014). Microbial diversity in formation water and enrichment cultures from the Gangxi bed of the Dagang terrigenous oilfield (PRC). *Microbiology* 83, 616–633. doi: 10.1134/S0026261714050208

Piceno, Y. M., Reid, F. C., Tom, L. M., Conrad, M. E., Bill, M., Hubbard, C. G., et al. (2014). Microbial physiology and metabolism temperature and injection water source influence microbial community structure in four Alaskan North Slope hydrocarbon reservoirs. *Front. Microbiol.* 5:409. doi: 10.3389/fmicb.2014.00409

Reinsel, M. A., Sears, J. T., Stewart, P. S., McInerney, M. J., and Mclnerney, M. J. (1996). Control of microbial souring by nitrate, nitrite or glutaraldehyde injection in a sandstone column. *J. Ind. Microbiol.* 17, 128–136. doi: 10.1007/BF01570056

Sharpe, E., Barua, R., Brateteig, A., and Bath, Z. (2015). "Case study: laser-based gas detection technology and dispersion modeling used to eliminate false alarms and improve safety performance on Terra Nova FPSO," in *Proceedings of the 49th Annual Loss Prevention Symposium (LPS), AIChE Spring Meeting & 11th Global Congress on Process Safety,* Austin, TX.

Shen, Y., and Voordouw, G. (2015). "Primers for dsr genes and most probable number method for detection of sulfate-reducing bacteria in oil reservoirs," in *Hydrocarbon and Lipid Microbiology Protocols*, eds T. J. McGenity, K. N. Timmis, and B. Nogales (Berlin: Springer-Verlag), 35–43. doi: 10.1007/8623_2015_72

Singh, A. K., Sherry, A., Gray, N. D., Jones, D. M., Bowler, B. F. J., and Head, I. M. (2014). Kinetic parameters for nutrient enhanced crude oil biodegradation in intertidal marine sediments. *Front. Microbiol.* 5:160. doi: 10.3389/fmicb.2014.00160

Slobodkin, A., Zavarzina, D., and Sokolova, T. (1999). Dissimilatory reduction of inorganic electron acceptors by thermophilic anaerobic prokaryotes. *Mikrobiologiia* 68, 522–542.

Stepanov, V. G., Xiao, Y., Lopez, A. J., Roberts, D. J., and Fox, G. E. (2016). Draft genome sequence of *Marinobacter* sp. strain P4B1, an electrogenic perchlorate-reducing strain isolated from a long-term mixed enrichment culture of marine bacteria. *Genome Announc.* 4:e1617-15. doi: 10.1128/genomeA.01617-15

Thrasher, D. R., and Vance, I. (2005). "Reservoir souring: mechanisms and prevention," in *Petroleum Microbiology*, eds B. Ollivier and M. Magot (Washington, DC: ASM Press), 123–142. doi: 10.1128/9781555817589.ch7

Torsvik, T., and Sunde, E. (2005). "Microbial control of hydrogen sulfide production in oil reservoirs," in *Petroleum Microbiology*, eds B. Ollivier and M. Magot (Washington, DC: ASM Press), 201–213. doi: 10.1128/9781555817589.ch10

Voordouw, G., Grigoryan, A. A., Lambo, A., Lin, S., Park, H. S., Jack, T. R., et al. (2009). Sulfide remediation by pulsed injection of nitrate into a low temperature Canadian heavy oil reservoir. *Environ. Sci. Technol.* 43, 9512–9518. doi: 10.1021/es902211j

Wunderlin, T., Junier, T., Roussel-Delif, L., Jeanneret, N., and Junier, P. (2014). Endospore-enriched sequencing approach reveals unprecedented diversity of Firmicutes in sediments. *Environ. Microbiol. Rep.* 6, 631–639. doi: 10.1111/1758-2229.12179

Yeung, C. W., Lee, K., Cobanli, S., King, T., Bugden, J., Whyte, L. G., et al. (2015). Characterization of the microbial community structure and the physicochemical properties of produced water and seawater from the Hibernia oil production platform. *Environ. Sci. Pollut. Res.* 22, 17697–17715. doi: 10.1007/s11356-015-4947-z

Zhang, F., She, Y.-H., Chai, L.-J., Banat, I. M., Zhang, X.-T., Shu, F.-C., et al. (2012). Microbial diversity in long-term water-flooded oil reservoirs with different in situ temperatures in China. *Sci. Rep.* 2:760. doi: 10.1038/srep00760

Zhang, Y., Zhao, Z., Chen, C.-T. A., Tang, K., Su, J., and Jiao, N. (2012). Sulfur metabolizing microbes dominate microbial communities in andesite-hosted shallow-sea hydrothermal systems. *PLoS ONE* 7:e44593. doi: 10.1371/journal.pone.0044593

Conflict of Interest Statement: The authors declare that the research was conducted in the absence of any commercial or financial relationships that could be construed as a potential conflict of interest.

frontiers in Microbiology

ORIGINAL RESEARCH
published: 17 August 2017
doi: 10.3389/fmicb.2017.01564

Tetrathionate and Elemental Sulfur Shape the Isotope Composition of Sulfate in Acid Mine Drainage

Nurgul Balci[1]*, *Benjamin Brunner*[2,3] *and Alexandra V. Turchyn*[4]

[1] Geomicrobiolog-Biogeochemistry Lab, Department of Geological Engineering, Istanbul Technical University, Istanbul, Turkey, [2] Department of Biogeochemistry, Max Planck Institute for Marine Microbiology, Bremen, Germany, [3] Department of Geological Sciences, University of Texas at El Paso, El Paso, TX, United States, [4] Department of Earth Sciences, University of Cambridge, Cambridge, United Kingdom

Sulfur compounds in intermediate valence states, for example elemental sulfur, thiosulfate, and tetrathionate, are important players in the biogeochemical sulfur cycle. However, key understanding about the pathways of oxidation involving mixed-valance state sulfur species is still missing. Here we report the sulfur and oxygen isotope fractionation effects during the oxidation of tetrathionate ($S_4O_6^{2-}$) and elemental sulfur (S°) to sulfate in bacterial cultures in acidic conditions. Oxidation of tetrathionate by *Acidithiobacillus thiooxidans* produced thiosulfate, elemental sulfur and sulfate. Up to 34% of the tetrathionate consumed by the bacteria could not be accounted for in sulfate or other intermediate-valence state sulfur species over the experiments. The oxidation of tetrathionate yielded sulfate that was initially enriched in ^{34}S ($\varepsilon^{34}S_{SO4-S4O6}$) by +7.9‰, followed by a decrease to +1.4‰ over the experiment duration, with an average $\varepsilon^{34}S_{SO4-S4O6}$ of +3.5 ± 0.2‰ after a month of incubation. We attribute this significant sulfur isotope fractionation to enzymatic disproportionation reactions occurring during tetrathionate decomposition, and to the incomplete transformation of tetrathionate into sulfate. The oxygen isotope composition of sulfate ($\delta^{18}O_{SO4}$) from the tetrathionate oxidation experiments indicate that 62% of the oxygen in the formed sulfate was derived from water. The remaining 38% of the oxygen was either inherited from the supplied tetrathionate, or supplied from dissolved atmospheric oxygen (O_2). During the oxidation of elemental sulfur, the product sulfate became depleted in ^{34}S between −1.8 and 0‰ relative to the elemental sulfur with an average for $\varepsilon^{34}S_{SO4-S0}$ of −0.9 ± 0.2‰ and all the oxygen atoms in the sulfate derived from water with an average normal oxygen isotope fractionation ($\varepsilon^{18}O_{SO4-H2O}$) of −4.4‰. The differences observed in $\delta^{18}O_{SO4}$ and the sulfur isotope composition of sulfate ($\delta^{34}S_{SO4}$), acid production, and mixed valence state sulfur species generated by the oxidation of the two different substrates suggests a metabolic flexibility in response to sulfur substrate availability. Our results demonstrate that microbial processing of mixed-valence-state sulfur species generates a significant sulfur isotope fractionation in acidic environments and oxidation of mixed-valence state sulfur species may produce sulfate with characteristic sulfur and oxygen isotope signatures. Elemental sulfur and tetrathionate are not only intermediate-valence state sulfur compounds that play a central role in sulfur oxidation pathways, but also key factors in shaping these isotope patterns.

Keywords: tetrathionate, oxygen isotopes, sulfur isotopes, microbial oxidation, intermediate valence state sulfur

OPEN ACCESS

Edited by:
Colleen Hansel, Woods Hole Oceanographic Institution, United States

Reviewed by:
Mustafa Yucel, Middle East Technical University, Turkey
Andrew Laurence Masterson, Northwestern University, United States

***Correspondence:**
Nurgul Balci
ncelik@itu.edu.tr

Specialty section:
This article was submitted to Microbiological Chemistry and Geomicrobiology, a section of the journal Frontiers in Microbiology

Received: *02 April 2017*
Accepted: *02 August 2017*
Published: *17 August 2017*

Citation:
Balci N, Brunner B and Turchyn AV (2017) Tetrathionate and Elemental Sulfur Shape the Isotope Composition of Sulfate in Acid Mine Drainage. Front. Microbiol. 8:1564. doi: 10.3389/fmicb.2017.01564

INTRODUCTION

The oxidation of sulfide minerals in oxic or anoxic environments drives the formation, and subsequent oxidation or reduction of various sulfur compounds; these are often associated with the generation of protons, creating a serious global environmental problem known as acid mine drainage (AMD; Schippers et al., 1996; Ramírez et al., 2004; Gleisner et al., 2006; Balci et al., 2007, 2012). Since sulfur is found in valence states ranging from +6 (sulfate) to −2 (sulfide), its transformation operates via several complex redox reaction pathways, many of which are microbially-mediated (Ehrlich, 1982). Elemental sulfur (S°), and mixed-valence-state sulfur species—molecules that consist of more oxidized sulfonate ($-SO_3$) and more reduced sulfane ($-S$) components—including thiosulfate, ($S_2O_3^{2-}$), and tetrathionate, ($S_4O_6^{2-}$), have been observed during the microbially-mediated oxidation of monosulfides (e.g., galena, sphalerite) and disulfide (e.g., pyrite) minerals by both oxygen and ferric iron (Schippers et al., 1996; Schippers and Sand, 1999; Balci et al., 2007, 2012). Some mixed-valence-state sulfur species are stable at corrosive conditions (pH < 3; Williamson and Rimstidt, 1993; Xu and Schoonen, 1995; Schippers et al., 1996; Druschel et al., 2003; Bernier and Warren, 2007). For example, in acidic ferric iron (Fe^{3+})-rich solutions, the kinetics of abiotic trithionate and tetrathionate oxidation are several orders of magnitude slower than the formation of these polythionates from thiosulfate (Druschel et al., 2003).

The relative stability of these mixed-valence-state sulfur species in conditions found in acid-mine drainage raises the question of whether the production and oxidation state of different sulfur species is sulfide mineral–specific and how the fate of these mixed-valence-state sulfur species contributes to the overall corrosive conditions found in AMD (Druschel et al., 2003). For example, in contrast to the direct oxidation of pyrite, which lowers pH and contributes to the environmental acidity, the formation of aqueous hydrogen sulfide and its subsequent oxidation to elemental sulfur in acid conditions and in the presence of monosulfide minerals (e.g., sphalerite) consumes protons and may ameliorate acidic conditions (Schippers, 2004). Therefore, a variety of sulfur compounds may be important players in the overall redox reactions of sulfur in acid-mine drainage (Chambers and Trudinger, 1979; Steudel et al., 1987; Kelly, 1999; Schippers and Sand, 1999; Suzuki, 1999; Takano et al., 2000; Xu et al., 2000). Currently, our knowledge is incomplete regarding whether these sulfur species play a significant role in sulfur cycling since their oxidation involves multiple pathways and mixed-valence state species which have been difficult to quantify (Williamson and Rimstidt, 1993; Xu and Schoonen, 1995; Schippers et al., 1996; Schippers and Sand, 1999; Druschel et al., 2003).

A complicating factor is that microbial enzymatic reactions are faster than the kinetics of the abiotic reactions (Pronk et al., 1990; Hallberg et al., 1996; Friedrich et al., 2001), which not only leads to accelerated transformation of various sulfur compounds, but may also yield reaction products that differ from abiotic processes. The interplay between abiotic and microbially-catalyzed reactions plays a critical role in the biogeochemical sulfur cycle AMD conditions. However, particularly in acidic conditions it is difficult to distinguish reactions with mixed-valence state sulfur compounds carried out by microorganisms from purely abiotic reactions (Suzuki, 1974, 1999). Most of our knowledge about microbially-mediated sulfur redox chemistry in acidic conditions comes from studies carried out with *Acidithiobacillus ferrooxidans,* an acidophilic chemolithotrophic ferrous iron (Fe^{2+}) and elemental sulfur oxidizer (Hazeu et al., 1986, 1988; Suzuki et al., 1994; Schippers et al., 1996; Gleisner et al., 2006; Balci et al., 2007, 2012; Thurston et al., 2010). Although, most studies have been done with *A. ferrooxidans*, phylogenetically similar organisms also perform a number of different sulfur redox reactions involving intermediate and mixed-valence state sulfur species (Bernier and Warren, 2007; Poser et al., 2014). *Acidithiobacillus thiooxidans* is another common elemental sulfur oxidizer commonly found in acidic environments (Knickerbocker et al., 2000; Smith et al., 2012). In contrast to *A. ferrooxidans, A. thiooxidans* is not able to oxidize ferrous iron to ferric iron. In experimental studies, this difference can be advantageous, because the sulfur transformations catalyzed by *A. thiooxidans* are not overprinted by concomitant reactions of sulfur species with ferric iron. Oxidation of mixed-valence state sulfur compounds including thiosulfate and tetrathionate by *Acidithiobacillus* spp. suggests that the rate of acid generation and the type and concentration of mixed-valence state sulfur species produced were specific to both the substrate and microbial species (Bernier and Warren, 2005, 2007).

Since sulfur oxidation, reduction, and disproportionation reactions are often accompanied by sulfur and oxygen isotope fractionation, the sulfur and oxygen isotope composition of sulfate, may provide insight into the oxidation pathways of these sulfur compounds. A wide range of sulfur isotope fractionation has been reported under various experimental conditions during the microbial oxidation of various sulfur compounds. For example, phototrophic oxidation of sulfide to elemental sulfur and elemental sulfur to sulfate produced no sulfur isotope fractionation (Fry et al., 1984, 1988; Kelly, 2008); a similar lack of sulfur isotope fractionation was reported for phototrophic oxidation of sulfite and thiosulfate to sulfate (Fry et al., 1985) and chemotrophic oxidation of thiosulfate to sulfate (Fry et al., 1986). On the other hand, significant sulfur isotope fractionation during chemotrophic oxidation of sulfide to sulfate (−10.5 to −18.0‰, normal isotope effect) and of sulfide to polythionates (+0.6 to +19‰, inverse isotope effect) has also been shown (Kaplan and Rittenberg, 1964). Fry et al. (1988) reported a normal sulfur isotope fractionation of −5.2‰ during abiotic oxidation of sodium sulfide (Na_2S) by dissolved atmospheric oxygen (O_2) in aqueous solution at pH 11 such that the product sulfate has a lighter $\delta^{34}S_{SO4}$ signature than the sulfide from which it derives, which is in contrast to the inverse effect (reaction product is enriched in heavy isotope relative to reactant) associated with anaerobic oxidation of sulfide by photosynthetic bacteria. Apparent inverse (and normal) isotope effects can be caused by isotope exchange between co-existing species, such as between bisulfide (HS^-) and hydrogen sulfide (H_2S), between sulfur compounds with different redox state, such as sulfite and sulfide,

or within a compound that has mixed valence state sulfur atoms, such as between sulfonate and sulfane in thiosulfate. This suggests that sulfur isotope fractionation is possibly caused by the formation of mixed-valence state sulfur species—even abiotically (Kaplan and Rittenberg, 1964; Goldhaber, 1983). Generally, relatively little is known about sulfur isotope fractionation during the oxidation of polythionates (Fry et al., 1986; Kelly, 2008; Alam et al., 2013).

Oxygen isotope fractionation during oxidation of sulfur compounds can be even more intricate than the sulfur isotope fractionation, because in addition to kinetic isotope fractionation, it involves the incorporation of oxygen from different sources, particularly from water and O_2, and because some sulfur compounds, such as sulfite, rapidly exchange oxygen isotopes with water (e.g., Müller et al., 2013a,b; Wankel et al., 2014). For the best documented AMD process, pyrite oxidation, oxygen incorporation from O_2 into sulfate ranges from 0 to 36% (Taylor et al., 1984; Balci et al., 2007; Tichomirowa and Junghans, 2009), with an associated kinetic isotope fractionation with respect to O_2 ($\varepsilon^{18}O_{SO4-O2}$) between −11.4 to −4.3‰ (Taylor et al., 1984; Balci et al., 2007; Tichomirowa and Junghans, 2009), and an associated kinetic isotope fractionation with respect to water ($\varepsilon^{18}O_{SO4-H2O}$) between −4.4 to 4‰ (**Table 1**). The $\delta^{34}S_{SO4}$ and $\delta^{18}O_{SO4}$ thus hold potential as tracers for the oxidation pathways and microbial mediation of oxidative sulfur cycling. Furthermore, thanks to the incorporation of oxygen from O_2 during sulfur oxidation, the oxygen isotope signature of sulfate may help decipher the geologic history of atmospheric oxygen (Bao, 2015).

Given the complexity of abiotic and microbially-catalyzed sulfur transformations, and the large number of potentially involved sulfur compounds, it becomes essential to identify what shapes the $\delta^{34}S_{SO4}$ and $\delta^{18}O_{SO4}$ of sulfate produced in acid-mine drainage. We identified two sulfur compounds with these attributes: tetrathionate and elemental sulfur. The choice of tetrathionate is based on the observation that in presence of ferric iron, which is common in acid-mine drainage, thiosulfate is quickly transformed into tetrathionate:

$$2Fe^{3+} + 2S_2O_3^{2-} \rightarrow 2Fe^{2+} + S_4O_6^{2-} \quad (1)$$

Thiosulfate itself is the first reaction product in the oxidation of acid-insoluble metal sulfides such as pyrite, (FeS_2), molybdenite (MoS_2), or tungstenite (WS_2), the so-called thiosulfate mechanism (Schippers and Sand, 1999), while tetrathionate is much more stable in AMD conditions. Microorganisms are likely to take advantage of the relative kinetic stability of tetrathionate by catalyzing the degradation of this compound. Moreover, the abiotic decomposition of tetrathionate produces sulfate and disulfane/monosulfonic acid (Schippers et al., 1996). The latter can react with other sulfur species to yield a suite of sulfur compounds with intermediate oxidation state, including elemental sulfur, thiosulfate, tri- and pentathionate (Schippers et al., 1996). From the perspective of isotope fractionation, tetrathionate may preserve the isotope signature of thiosulfate, whereas the conversion of tetrathionate into various other sulfur compounds offers the potential to express a variety of diagnostic isotope fractionations. If oxygen from O_2 is incorporated during these processes, it may end up in the final oxidation product sulfate, leaving a unique isotopic fingerprint. Moreover, the expression of the oxygen and sulfur isotope fractionation in this process could strongly depend on the involved microorganisms, as well as acidity, and concentration of oxidants such as O_2 and ferric iron. Elemental sulfur, the second chosen key component is not only a product of the decomposition of tetrathionate, but also central in the oxidation of acid-soluble metal sulfides, such as sphalerite (ZnS), where the first oxidation reaction product are polysulfides, which under acid conditions quickly decompose to form elemental sulfur (polysulfide mechanism; Schippers and Sand, 1999). As for tetrathionate, the abiotic oxidation of elemental sulfur is kinetically slow relative to the processes that form this compound, providing microorganisms with the opportunity to catalyze this process.

To date, there have been no studies exploring sulfur or oxygen isotope fractionation during microbial oxidation of tetrathionate to sulfate under acidic conditions (pH < 4) where the accumulation and oxidation of tetrathionate occurs and influences the sulfur cycle (Druschel et al., 2003) and there are no data on the sulfur or oxygen isotope fractionation during microbial oxidation of elemental sulfur by *A. thiooxidans* under AMD conditions. In this pilot study, we assess if tetrathionate indeed holds the potential to be a key compound in shaping the $\delta^{34}S_{SO4}$ and $\delta^{18}O_{SO4}$ and we determine the sulfur and oxygen isotope fractionation during microbial oxidation of elemental sulfur by *A. thiooxidans*.

MATERIALS AND METHODS

Bacterial Strain, Media, and Growth Conditions

The acidophilic sulfur oxidizing bacterium *A. thiooxidans* (11,478; formerly, *Thiobacillus thiooxidans*) was used for all the experiments and was obtained from Deutsche Sammlung von Mikroorganismen und Zellkulturen (DSMZ) culture collection. Before use in the experiments, the strain was grown chemolithoautotrophically in batch culture in a medium containing the modified basal salts solution supplemented with either tetrathionate (20 mM $K_2S_4O_6$) or elemental sulfur (1 g/100 mL). The basal salts consist of 0.6 g/L NH_4Cl, 0.2 g/L $MgCl_2.6H_2O$, 0.1 g/L K_2HPO_4; 0.10 g/L KCI; 0.01 g/L $Ca(NO_3)_2$. The medium was prepared by adding these salts to 1 L of deionized water and the pH of the medium was adjusted to 4 with trace-metal grade HCl. Then the culture medium was autoclaved for 25 min for the experiments with elemental sulfur and, to prevent oxidation, filter sterilized for the experiments with tetrathionate. Bacteria were harvested in late exponential phase (at an optical density at 440 nm of between 0.27 and 0.28), centrifuged, and re-suspended in the medium and used in the biological oxidation experiments for 2 h. For the cultures grown on elemental sulfur, sequential centrifugation was applied to obtain sulfur-free cells: first the cultures were centrifuged at 1,800 rpm to remove elemental sulfur particles. Subsequently, the supernatant containing cells was further centrifuged at 10,000 rpm for 10 min. The cell pellet

TABLE 1 | Compilation of previous relevant studies.

Experimental condition	H_2O (%)	$\varepsilon^{18}O_{SO4\text{-}H2O}$ (‰)	$\varepsilon^{18}O_{SO4\text{-}O2}$ (‰)	$\varepsilon^{34}S_{SO4\text{-}S0}$ (‰)	$\varepsilon^{34}S_{S0\text{-}S2}$ (‰)	$\varepsilon^{34}S_{SO4\text{-metal Sulfide}}$ (‰)	$\varepsilon^{34}S_{SO4/SxOy\text{-}S2/SxOy}$ (‰)	References
Oxidation of H_2S to S^o by *A. thiooxidans*					−1.2 to +2.5	n.a		Kaplan and Rittenberg, 1964
Phototrophic oxidation of S^{2-} to S^o by *Chromatium* sp.					−3.6 to −10			Kaplan and Rittenberg, 1964
Phototrophic oxidation of S^{2-} to SO_4^{2-} by *Chromatium* sp.							+0.9 to −2.9	Kaplan and Rittenberg, 1964
Phototrophic oxidation of S^{2-} to $S_XO_6^{2-}$ by *Chromatium* sp.							+4.9 to +11.2	Kaplan and Rittenberg, 1964
Oxidation of S^{2-} to SO_4^{2-} [(a)] by *A. thiooxidans*							−18 to −10.5	Kaplan and Rittenberg, 1964
Oxidation of S^{2-} to S_xO_6 [(a)] by *A. thiooxidans*							+0.6 to +19	Kaplan and Rittenberg, 1964
Aerobic S^o oxidation with *T. Concretivorus*				−0.1 to +1.4				Kaplan and Rittenberg, 1964
Aerobic S^o (soil slurry)	100	0		< +2.3				Mizutani and Rafter, 1969
Pyrite oxidation with *A. ferrooxidans*	70	+3.5	−11.4					Taylor et al., 1984
Abiotic pyrite oxidation	n.d	n.d	−4.3					Taylor et al., 1984
Oxidation of $S_2O_3^{2-}$ to SO_4^{2-} by *Paracoccus versutus*	n.d	n.d	n.d				+0.4	Fry et al., 1986
Oxidation of $S_2O_3^{2-}$ to SO_4^{2-} by *Halothiobacillus neapolitanus*	n.d	n.d	n.d				+1.2 to +2.9	Kelly, 2008
Aerobic pyrite oxidation with *A. ferrooxidans*	85 to 92	−4.0 to +4.0	−10 to −11					Balci et al., 2007
Anaerobic pyrite oxidation by Fe^{3+}(aq) with/without by *A. ferrooxidans*	94 to 95	+3.6						Balci et al., 2007
Anaerobic pyrite oxidation	87 to 97	+3.3 to +4.0						Heidel et al., 2009
Abiotic/Submerged pyrite oxidation	72 to 85	n.d				−0.0 to +0.3		Tichomirowa and Junghans, 2009
Abiotic/Wet/Dry pyrite oxidation	64 to 81	n.d				−0.4 to +0.0		Tichomirowa and Junghans, 2009
Anoxygenic phototropic S oxidation with *Chlorobium tepidum*		n.d		1.9 ± 0.8				Zerkle et al., 2009
Abiotic pyrite oxidation	91	+4.1 to +4.8	−8.4	n.d				Heidel and Tichomirowa, 2010
Anaerobic chalcopyrite oxidation by Fe^{3+}(aq) with/without by *A. ferrooxidans*	92 to 94	+3.8		n.d	−3.0	−3.8		Thurston et al., 2010

(Continued)

TABLE 1 | Continued

Experimental condition	H_2O (%)	$\varepsilon^{18}O_{SO4\text{-}H2O}$ (‰)	$\varepsilon^{18}O_{SO4\text{-}O2}$ (‰)	$\varepsilon^{34}S_{SO4\text{-}S0}$ (‰)	$\varepsilon^{34}S_{S0\text{-}S2}$ (‰)	$\varepsilon^{34}S_{SO4\text{-metal Sulfide}}$ (‰)	$\varepsilon^{34}S_{SO4/SxOy\text{-}S2/SxOy}$ (‰)	References
Aerobic chalcopyrite oxidation by *A. ferrooxidans*	92 to 95	+6.4		n.d		−1.5		Thurston et al., 2010
Abiotic oxidation of chalcopyrite O_2(aq)	57	+5.2 to 7.4		n.d		−0.5		Thurston et al., 2010
Sphalerite oxidation by Fe(III)aq with/without *A. ferrooxidans*	96	+7.5 to +8.2		−2.8 to −2.9	+0.3 to +0.6	−2.6 to −2.4		Balci et al., 2012
Aerobic sphalerite oxidation with *A. ferrooxidans*	92 to 96	+9.5 to +8.1				0		Balci et al., 2012
Aerobic S° oxidation with *A. thiooxidans*	84 to 97	−6.2 to −0.9		0.4 ± 0.8				Smith et al., 2012
Aerobic S° oxidation by *A. ferrooxidans* (short term, 10 days)		n.d		−1.8				Balci et al., 2012
Aerobic S° oxidation by *A. ferrooxidans* (short term, 20 days)	100	8.3		−1.1				Balci et al., 2012
Aerobic oxidation of $S_2O_3^{2-}$ to SO_4^{2-} by *Thiomicrospria crunogena*							−1.9 to + 4.6	Alam et al., 2013
Aerobic oxidation of $S_2O_3^{2-}$ to SO_4^{2-} by *Tetrathiobacter kashmirensis*							−4.9 to −0.8	Alam et al., 2013
Aerobic oxidation of $S_2O_3^{2-}$ to SO_4^{2-} by *Paracoccus pantothrophus*							−5.8 to 1.8	Alam et al., 2013
Aerobic oxidation of elemental sulfur by *A. thioxidans*	58 to 87	−4.2		−1.8 to 0				Current study
Aerobic oxidation of tetrathionate by *A. thioxidans*	60 to 62						+2.9 to +3.5	Current study

[(a)]*Determined as a minor product.*

was then re-suspended in 5 ml medium and used for elemental sulfur oxidation experiments. The cell densities in the biological experiments were determined by phase contrast microscopy: 10^7 cell/ml (with S° as a substrate) or 10^6 cell/ml (with tetrathionate). *A. thiooxidans* was subcultured three times before being used in the biological experiments.

Biological and Abiotic Oxidation of S° and $S_4O_6^{2-}$ under Aerobic Conditions

A sulfate-free medium was used as an experimental solution with the same basal salt concentration as above to ensure that the sulfate recovered after chemolithotrophic growth was exclusively produced from the oxidation of elemental sulfur or tetrathionate. Two hundred and fifty milliliters of microbiological medium was placed into 500 ml Erlenmeyer flasks and autoclaved at 121°C for 20 min. The flasks were then kept in a sterile hood under UV light for 25 min to decontaminate their surfaces. Prior to use, the elemental sulfur was ground and sieved to a grain size of <63 μm. For sterilization, elemental sulfur was soaked with 70% ethanol and spread in a thin even layer under UV radiation (germicidal) in a sterile hood for 30 min. Then the elemental sulfur was immediately placed in sterile experimental containers. To initiate the experiments, 2.5 g of elemental sulfur and 5 ml (5×10^7 cell) of the *A. thiooxidans* cell suspension were added to each flask and subsequently adjusted to a pH of 4 with trace metal grade HCl. For the experiments with tetrathionate, 250 ml of medium containing 20 mM $K_2S_4O_6$ was placed into 500 ml Erlenmeyer flask and pH of the medium was adjusted to 4 with HCl at 25°C and filter-sterilized. The flasks used for elemental sulfur and tetrathionate oxidation experiments were loosely sealed with a sterilized thin aluminum film such that gas exchange between the headspace and ambient air could take place. The biological incubations were done with waters with different $\delta^{18}O$ values (−4.4‰; referred to as W1), +58.0‰ (W2) and +84.4‰ (W3). For each $\delta^{18}O$ of the water, 15 flasks were used. This experimental design serves to determine the relative contribution of water to the oxygen in the produced sulfate. All the biological experiments were incubated at 25°C for 30 days with continuous shaking (150 rpm) in a room where temperature and humidity were held constant. One abiotic-control experiment with a $\delta^{18}O$ of water of −4.4‰ was conducted with elemental sulfur, and two abiotic control experiments with different $\delta^{18}O$ of water (−4.4‰ and +84.4‰) were conducted with tetrathionate.

Sampling for Aqueous Sulfur Species and Analysis

Each flask from the experiments with different $\delta^{18}O$ of water was terminated at various time points and pH was directly measured in the flask with a pH meter (WTW model 340i) following a 4-point calibration using pH 1.0, 2.0, 4.0, and 7.0 buffers. A 5 ml of aliquot was collected at each time point and immediately filtered through a 0.2 μm syringe filter into a sterile 5 ml dark tube in the anaerobic chamber (Coylab) and kept at −20°C for determination of the concentrations of sulfur species including thiosulfate and sulfite. Another 5 ml aliquot was collected at each time point and was used for elemental sulfur quantification. Elemental sulfur was quantified by extraction with acetone/water (19:1) followed by the cyanolysis methods (Kelly and Wood, 1994, 1998; Beard et al., 2011). Thiosulfate concentrations were determined by applying the decoloration of methylene-blue method at 670 nm in acidic conditions (Kletzin, 1989). The bimane derivatization method was used to quantify sulfite concentrations (Zopfi et al., 2004). A cold-cyanolysis protocol was used to determine tetrathionate concentrations at the end of the incubation (Kelly et al., 1969). An additional 5 ml aliquot filtered through 0.2 μm syringe filter was analyzed for sulfate concentrations by ion exchange chromatography using a Dionex ion chromatograph. The following mass balance can be used to estimate the percentage of tetrathionate consumed (see **Table 2** for sulfur concentrations of the individual compounds):

$$[S_4O_6]_{consumed} = [S_4O_6]_{initial} - \left(4^*[S_4O_6]_{final} + [SO_4]_{final} + 2^*[S_2O_3]_{final} + [SO_3]_{final} + [S^0]_{final}\right)/4 \quad (2)$$

It must be noted that the calculated value for $[S_4O_6]_{consumed}$ represents a minimum estimate, as sulfur may be accumulated in the form intermediate-valence state species that are not measured, or lost from the experiment in gaseous form, such as SO_2.

Isotopic Analyses

Filtered samples (10 ml) from each experimental time point were kept tightly sealed and frozen until the $\delta^{18}O$ of water could be analyzed. The remaining reaction medium (∼200 ml) was filtered through a 0.2 μm Millipore filter and brought to a pH 3 using dilute NaOH. A 10% (wt/wt) $BaCl_2$ solution was added and the product barium sulfate ($BaSO_4$) allowed to settle overnight. The $BaSO_4$ precipitate was filtered and collected on a 0.2 μm Millipore filter, washed first with 100 ml of 1N HCl, then rinsed 3 times with a total of 500 ml of deionized water. The $BaSO_4$ samples were then dried. The sulfur isotope analysis of initial tetrathionate and elemental sulfur was performed without additional treatment on $K_2S_4O_6$ and S^0, respectively. No oxygen isotope analysis of $K_2S_4O_6$ was performed.

Sulfur and oxygen isotope ratios were determined by continuous flow isotope ratio mass spectrometry (CF-IRMS) using an elemental analyzer (for sulfur isotopes—at the Max Plank Institute for Marine Microbiology, Bremen) or a Thermo-Finnigan TC/EA at 1,450°C (for oxygen isotopes—in the Godwin Laboratory at the University of Cambridge). The oxygen and sulfur isotope composition is expressed relative to the Vienna Standard Mean Ocean Water (V-SMOW), and Vienna Canyon Diablo Troilite (V-CDT) standards, respectively, using the standard delta notation:

$$\delta^{18}O \text{ or } \delta^{34}S = (R_{sample}/R_{standard} - 1)^*1000‰, \quad (3)$$

where R is the ratio of the heavy to light isotope ($^{18}O/^{16}O$ or $^{34}S/^{32}S$) of sample and reference, respectively. For sulfur isotope measurements, IAEA S1 (−0.3‰), S_2 (+21.7‰), SO-5 (+0.49‰), and SO-6 (−34.05‰) were analyzed for calibration and normalization purposes, the error reported on the analyses is

TABLE 2 | Changes in solution chemistry during microbial oxidation of elemental sulfur.

Time (hours)	W1 Experiments				W2 Experiments				W3 Experiments			
	pH	SO_4 (mM)	S_2O_3 (mM)	SO_3 (μM)	pH	SO_4 (mM)	S_2O_3 (mM)	SO_3 (μM)	pH	SO_4 (mM)	S_2O_3 (mM)	SO_3 (μM)
0	3.15	0.02	0.0	n.d	3.09	0.02	0	n.d	3.15	0.02	n.d	n.d
4	3.09	0.02	0.0	n.d	3.01	0.04	0.000	n.d	3.08	0.02	0.000	n.d
24	2.60	5.7	0.029	n.d	2.81	3.5	0.024	n.d	2.81	4.1	0.022	n.d
33	2.55	10.5	0.048	0.05	2.52	14.2	0.051	n.d	2.55	9.6	0.040	n.d
48	2.20	16.2	0.107	n.d	2.39	15.3	0.073	n.d	2.28	13.4	0.073	n.d
60	2.09	23.5	0.099	n.d	2.17	16.3	0.086	n.d	1.99	26.3	0.016	n.d
72	1.70	38.4	0.063	n.d	1.89	29.1	0.095	n.d	1.74	31.2	0.024	n.d
84	1.42	49.3	n.d	n.d	1.71	28.4	n.d	n.d	1.56	36.3	n.d	n.d
96	1.52	52.6	0.007	0.24	1.68	48.7	0.001	0.16	1.5	51.2	0.005	0.14
124	1.42	63.2	n.d	n.d	1.52	52.3	n.d	n.d	1.38	58.6	n.d	n.d
146	1.31	68.3	n.d	n.d	1.47	64.3	n.d	n.d	1.3	62.7	n.d	n.d
168	1.26	76.2	n.d	n.d	1.34	n.d	n.d	n.d	1.18	96.4	n.d	n.d
264	0.83	131.3	n.d	n.d	1.09	98.4	n.d	n.d	0.81	115.2	n.d	n.d
336	0.80	133.2	0.001	n.d	1.13	101.63	n.d	n.d	0.77	151.7	n.d	n.d
504	0.74	155.7	n.d	n.d	0.92	120.33	n.d	n.d	0.72	148.6	n.d	n.d
720	0.72	158.2	0.001	n.d	0.74	154.98	0.001	n.d	0.68	161.6	n.d	n.d

n.d., not determined.

based on replicate analysis of these standards within each run and was generally better than 0.2‰. Oxygen isotope ratios of sulfate were normalized to NBS 127 ($\delta^{18}O = +8.6‰$) which was run at the beginning and end of each block of five samples. Samples for oxygen isotopes in sulfate were run in triplicate and the average and standard deviation of these triplicate analyses is reported (generally better than 0.5‰).

The $\delta^{18}O$ of water was determined by analyzing CO_2 gas that had equilibrated with 200 μl aliquots at 40°C in septum-capped vials. Raw data were corrected for the H_2O–CO_2 oxygen isotope fractionation, and then adjusted for small instrumental effects using results obtained for water standards that had been previously calibrated against VSMOW and SLAP. Replicate analyses agreed within less than ±0.1‰. The $\delta^{18}O$ of O_2 in the flasks was analyzed through injection into the TC/EA and the $\delta^{18}O$ value of O_2 was +23.5 ± 0.5‰ ($n = 4$) at the beginning of study and +24.3 ± 1.7‰ at the end of the experiments (30 days).

Calculation of the Source of Oxygen and Isotopic Fractionation during Elemental Sulfur Oxidation

The $\delta^{18}O_{SO4}$ of sulfate produced during elemental sulfur oxidation depends on: (1) the fraction of oxygen atoms coming from water (X), (2) the $\delta^{18}O$ of the water, (3) any oxygen isotope fractionation between water oxygen and sulfate oxygen during the incorporation of oxygen atoms from water during oxidation ($\varepsilon^{18}O_{SO4-H2O}$), (4) the fraction of oxygen atoms derived from molecular O_2 (1−X), (5) the $\delta^{18}O$ of atmospheric oxygen, and (6) any oxygen isotope fractionation between atmospheric oxygen and sulfate oxygen during the incorporation of oxygen atoms from atmospheric oxygen during oxidation ($\varepsilon^{18}O_{SO4-O2}$) (Mandernack et al., 1995; Balci et al., 2007; Thurston et al., 2010). The overall contributions of these factors is given in the following equation:

$$\delta^{18}O_{SO4} = X^*(\delta^{18}O_{H2O} + \varepsilon^{18}O_{SO4-H2O}) + (1 - X)^*(\delta^{18}O_{O2} + \varepsilon^{18}O_{SO4-O2}) \quad (4)$$

which can be simplified and rearranged to form:

$$\delta^{18}O_{SO4} = X^*\left(\delta^{18}O_{H2O} + \varepsilon^{18}O_{SO4-H2O} - \delta^{18}O_{O2} - \varepsilon^{18}O_{SO4-O2}\right) + (\delta^{18}O_{O2} + \varepsilon^{18}O_{SO4-O2}) \quad (5)$$

Because the $\delta^{18}O$ of atmospheric oxygen is constant and the experimental conditions are performed such that $\varepsilon_{SO4-H2O}$ and ε_{SO4-O2} are expected to be constant, the fraction of oxygen derived from water can be determined by replicate experiments with variable $\delta^{18}O$ for water. A linear least squares regression for $\delta^{18}O_{SO4}$ vs. $\delta^{18}O_{H2O}$ has a slope, X, equal to the fraction of oxygen derived from water, and (1 − X) is the remaining fraction from O_2. The average $\delta^{18}O_{H2O}$ from the initial and final time points were used for these graphs.

Equation (5) has two unknowns, the oxygen isotope fractionation for the incorporation of water into sulfate ($\varepsilon^{18}O_{SO4-H2O}$) and the oxygen isotope fractionation for the incorporation of atmospheric oxygen into sulfate ($\varepsilon^{18}O_{SO4-O2}$). If the produced sulfate is entirely derived from oxygen-atoms from water (slope, X = 1 or close to 1) equation 5 is simplified and $\varepsilon^{18}O_{SO4-H2O}$ can be estimated from the intercept with the y-axis:

$$\delta^{18}O_{SO4} = \delta^{18}O_{H2O} + \varepsilon^{18}O_{SO4-H2O} \quad (6)$$

Calculation of Contribution of Oxygen from Water during Tetrathionate Oxidation

In the case of tetrathionate oxidation, the $\delta^{18}O_{SO4}$ of sulfate generated depends also on the oxygen isotope composition of tetrathionate. If all oxygen from tetrathionate ends up in sulfate, i.e., no oxygen from tetrathionate is lost to water during the oxidation, the contribution of tetrathionate-oxygen to sulfate-oxygen can be assessed from the following chemical reaction:

$$S_4O_6^{2-} + 3.5O_2 + 3H_2O \rightarrow 4SO_4^{2-} + 6H^+ \quad (7)$$

This indicates that as much as 37.5% of oxygen in the resultant sulfate could be derived from the initial tetrathionate, 43.75% from O_2, and as little as 18.75% from water. Analogous to Equation (5), the approach with using water with different $\delta^{18}O$ allows us to determine the actual contribution of oxygen from water, however, does not permit us to differentiate between the contribution of oxygen from O_2 and tetrathionate. To achieve the latter, additional experiments would need to be carried out in which different $\delta^{18}O$ of O_2 are used.

Estimates of Error on Measured $\delta^{18}O_{SO4}$ Values from Contamination with Sulfate

In our biological sulfur oxidation experiments, a relatively large background concentration of sulfate was measured during the first 24 h after inoculation. This initial concentration of sulfate may be due to analytical error in the ion chromatograph or due to sulfate carried over with the inoculum. The impact on the $\delta^{18}O_{SO4}$ at the end of the experiments is low as this sulfate is insignificant relative to the total sulfate produced during the experiment. However, this initial sulfate corresponds to as much as 60% of the total sulfate in the first 24 h of the incubation. To determine the $\delta^{18}O_{SO4}$ of the produced sulfate in the early stage of oxidation a correction for the initially present sulfate in the culture medium was applied. We used the mass balance equation

$$\delta^{18}O_{SO4\_measured} = X^*(\delta^{18}O_{SO4\_initial}) + (1-X)^*(\delta^{18}O_{SO4\_product}), \quad (8)$$

where X is the percentage of sulfate derived from the initial sulfate; $\delta^{18}O_{SO4\_initial}$ corresponds to the $\delta^{18}O$ of initial sulfate; $(1 - X)$ refers to the percentage of sulfate derived from biological oxidation of elemental sulfur at a given point, and $\delta^{18}O_{SO4\_product}$ and $\delta^{18}O_{SO4\_measured}$ are the $\delta^{18}O$ of the measured sulfate in solution, and $\delta^{18}O$ of the produced sulfate at a given time point.

RESULTS

Changes in Solution Chemistry during Elemental Sulfur Oxidation

The initial sulfate concentration in all the biological experiments was ~20 μM. In all experiments, an initial lag phase delayed sulfate production (**Table 2**, **Figure 1**). An initial lag phase is commonly observed during batch culture experiments, particularly during elemental sulfur oxidation (Yu et al., 2001; Balci et al., 2012; Smith et al., 2012). The length of this lag phase may depend on the pH of the medium, substrate availability, chemical composition of the experimental vs. culture-growing medium in addition to the inoculation stage of culture (Yu et al., 2001; Swinnen et al., 2004). Since a direct contact between *A. thiooxidans* and sulfur grains is required to overcome the hydrophobic nature of elemental sulfur and to initiate the process of microbial oxidation, it may be required for bacteria to attach to the surface of elemental sulfur; this further contributes to a longer lag phase (Knickerbocker et al., 2000; Yu et al., 2001). The initial lag phase is characterized by a slow increase in sulfate concentrations and high rates production of thiosulfate (**Figure 1**). A small decrease in pH (to 2.8) occurred in each of the biological experiments during this initial lag phase. Following this lag phase, sulfate concentrations increased with decreasing thiosulfate concentration over the course of the experiment (**Figure 1**). In our experiments, the rate of pH change slowed when the pH reached 1.0 with no further changes after the pH of the solution measured at 0.7. In the abiotic control, the pH of experiment rose after 48 h from 3.6 to 4.1 and remained invariant at 4.2 over the experiment (**Figure 1D**). These abiotic control experiments produced minimal sulfate (7.2 μM), indicating that >95% of sulfate produced in the biotic experiments resulted from microbial activity.

Sulfite was only found in a few samples over the course of each experiment, indicating sulfite was rapidly transformed into other sulfur species (**Table 2**). Prior studies also have reported the formation of some mixed-valence-state sulfur species, like thiosulfate, during the oxidation of elemental sulfur (Rohwerder and Sand, 2003). In the abiotic control experiments, thiosulfate and sulfite were not found over the course of the experiments.

Changes in Solution Chemistry during Tetrathionate Oxidation

In the biological experiments with *A. thiooxidans* grown on tetrathionate (initial concentration 20 mM, corresponding to 80 mM sulfur), sulfate, thiosulfate and elemental sulfur were produced (**Figures 2A–C**, **Table 3**). At the end of the month-long incubation 78% of the initial tetrathionate was oxidized to sulfate (62.4 mM), 2.9% of the sulfur from tetrathionate was found in the form of elemental sulfur (2.3 mM), and 4.1% remained as tetrathionate (0.82 mM) for W1. For W2, 59% of the tetrathionate was oxidized to sulfate (47.5 mM), 4% was converted to elemental sulfur (3.2 mM), and 2.7% remained as tetrathionate (0.53 mM). For W3, 65% of the tetrathionate was oxidized to sulfate (52.1 mM), 2% was converted to 3.2 mM elemental sulfur (1.6 mM), and 3.6% remained as tetrathionate (0.72 mM). These findings mean that in all experiments, a substantial proportion of the sulfur supplied in the form of tetrathionate remain unaccounted for. This "missing sulfur" corresponds to 15% (12.02 mM), 34% (27.18 mM), and 29% (23.42 mM) for W1, W2 and W3, respectively.

During each biological experiment, the pH dropped from 3.2 to 2.0 by the end of the experiments. The production of thiosulfate decreased with higher generation of acid and the

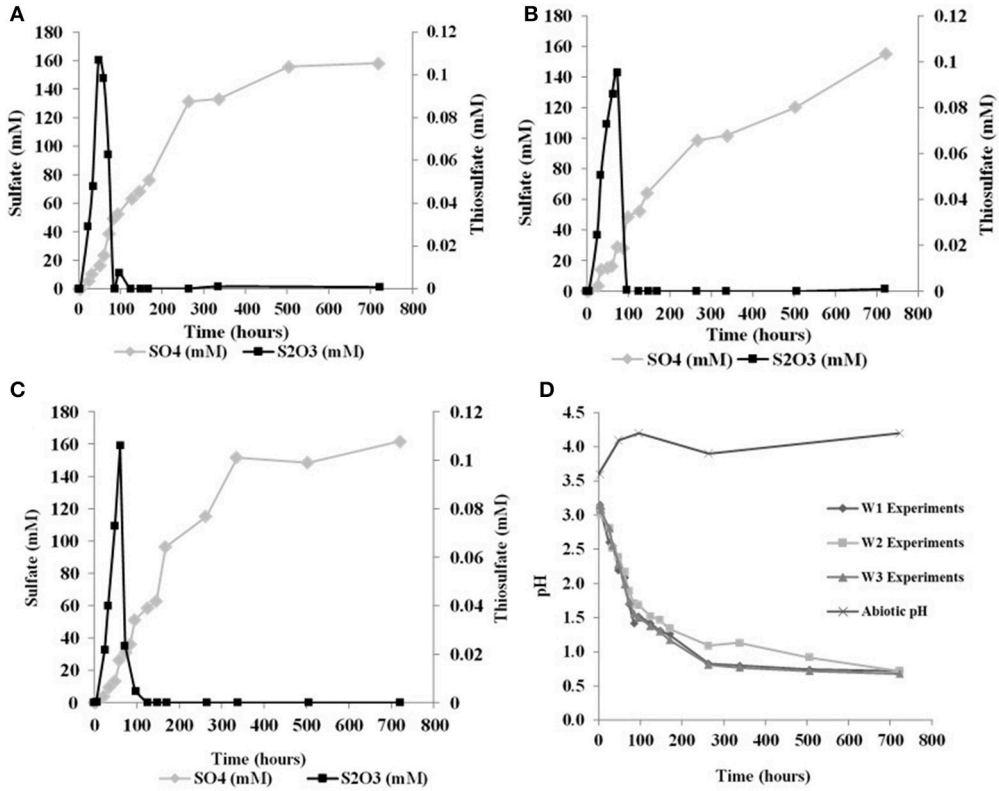

FIGURE 1 | Changes in solution chemistry during microbial oxidation of elemental sulfur **(A)**, W1 Experiments ($\delta^{18}O_{H2O}$ −5.5‰) **(B)** W2 Experiments ($\delta^{18}O_{H2O}$ +58.4‰) **(C)** W3 Experiments ($\delta^{18}O_{H2O}$ +84.4‰) **(D)** changes in pH vs. time.

TABLE 3 | Changes in solution chemistry during microbial oxidation of tetrathionate.

Time (hours)	W1 Experiments				W2 Experiments				W3 Experiments			
	pH	SO_4 (mM)	S_2O_3 (mM)	S° (mM)	pH	SO_4 (mM)	S_2O_3 (mM)	S° (mM)	pH	SO_4 (mM)	S_2O_3 (mM)	S° (mM)
0	3.14	0.21	n.d	n.d	3.2	0.16	n.d	n.d	3.15	0.20	n.d	n.d
48	3.17	0.38	5.20	4.70	3.07	0.38	2.35	2.2	3.04	0.00	1.20	4.60
144	2.95	1.60	n.d	n.d	3.16	1.67	n.d	n.d	3.10	0.42	n.d	n.d
192	2.74	7.50	10.29	n.d	3.08	12.41	8.94	n.d	2.98	0.81	10.87	13.10
240	2.47	9.70	12.44	11.00	2.85	14.02	11.71	11.50	2.82	11.60	18.31	n.d
288	2.45	14.80	12.44	n.d	2.54	14.22	11.28	n.d	2.54	14.00	16.68	n.d
360	2.44	11.07	9.80	7.20	2.57	16.27	11.05	8.10	2.52	14.34	16.74	9.2
408	2.13	12.76	11.53	5.60	2.52	n.d	8.20	n.d	2.48	14.77	16.21	n.d
480	2.03	15.63	10.50	9.30	2.25	18.80	6.72	7.50	2.13	14.72	19.43	6.4
600	2. 0	18.57	n.d	6.20	1.95	38.40	n.d	5.60	1.97	39.40	0.00	n.d
720	2.00	62.40	n.d	2.30	1.98	47.50	n.d	3.20	1.92	52.10	0.00	1.6

n.d., not determined.

lowest concentration of thiosulfate accompanied the highest concentration of sulfate in all the experiments (**Figures 2A–C**). We found that elemental sulfur formed in the experiments, and its concentration decreased with increasing incubation time (**Figure 2**, **Table 3**). The rate of sulfate, thiosulfate and elemental sulfur production differed slightly among the experiments. The abiotic control experiments run with tetrathionate as a substrate did not produce significant amounts of sulfate or thiosulfate over the course of the experiments (0.24 and 0.13 mM, respectively) and remained at nearly constant pH (**Figure 2D**). Neither elemental sulfur nor sulfite was found in these abiotic experiments.

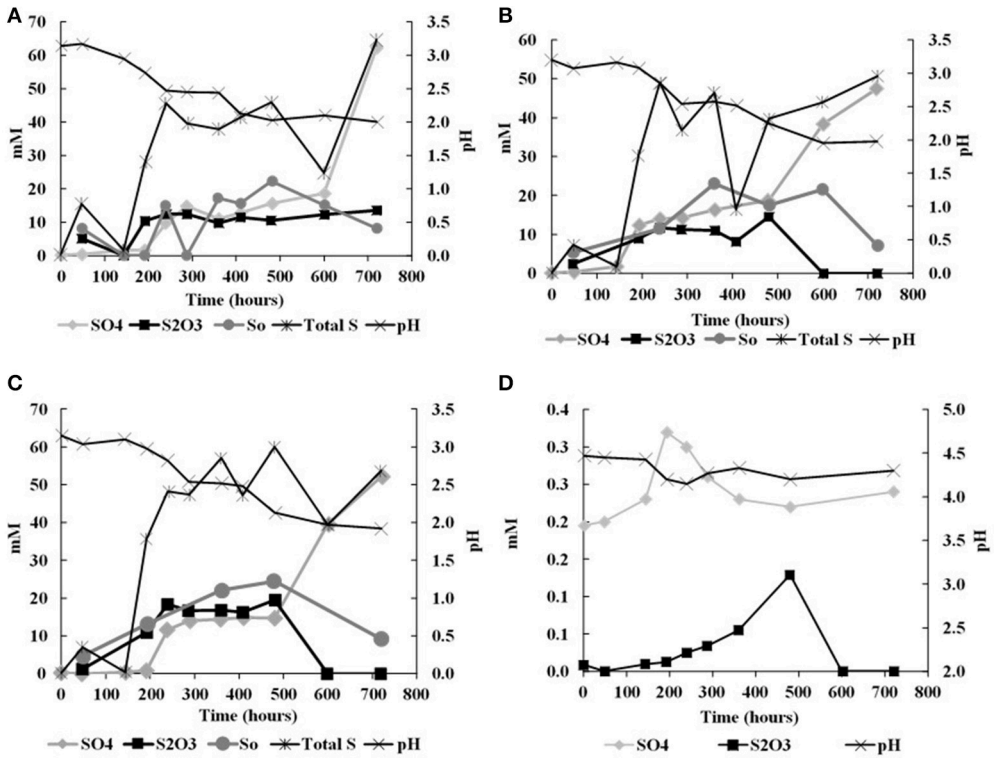

FIGURE 2 | Changes in solution chemistry during microbial oxidation of tetrathionate **(A)**, W1 Experiments ($\delta^{18}O_{H2O}$ −5.5‰) **(B)** W2 Experiments ($\delta^{18}O_{H2O}$ +58.4‰) **(C)** W3 Experiments ($\delta^{18}O_{H2O}$ +84.4‰) **(D)** abitoic oxidation of tetrathionate.

Oxygen and Sulfur Isotopic Composition of Sulfate in Experiments with Elemental Sulfur

A cross plot of $\delta^{18}O_{SO4}$ vs. $\delta^{18}O_{H2O}$ for the initial (lag phase) stage of the experiment shows a strong correlation ($r^2 > 0.99$). The slope (X) of this linear regression was used to estimate the contribution of water-derived oxygen into the product sulfate. During the prolonged lag phase where we observed low sulfate production coupled with high thiosulfate concentrations, the slope indicates that between 58 and 66% of the sulfate-oxygen was derived from water, with the remaining 34–42% derived from atmospheric oxygen (**Table 4**). During the main stage of the experiments (high sulfate production and low thiosulfate concentrations), the percentage of water–derived oxygen into the product sulfate significantly increased and essentially all oxygen atoms were sourced from water (**Table 4**, **Figure 3**). The average $\delta^{18}O_{SO4}$ vs. $\delta^{18}O_{H2O}$ for all the experiments including both the lag phase and exponential growth phase reveal a slope of 0.87 ± 0.07 suggesting between 80 and 94% of sulfate-oxygen was derived from water. This indicates that we can consider water the sole source of oxygen atoms in the product sulfate during elemental sulfur oxidation by *A. thiooxidans* (**Figure 3**). This is consistent with previous studies that suggest that oxygen atoms in sulfate produced during biological oxidation of elemental sulfur are derived from water (Mizutani and Rafter, 1969; Balci et al., 2012; **Table 4**, **Figure 3**). The incorporation of atmospheric O_2 into sulfate during the initial lag phase of the experiments might have resulted from the experimental design, which may have permitted chemisorption of O_2 on sulfur surfaces and its further incorporation into initial sulfate, which was previously suggested during pyrite oxidation experiments (Tichomirowa and Junghans, 2009). As the experiment progresses and enters exponential growth phase, the incorporation of this chemisorbed O_2 decreases and all oxygen atoms are derived from water.

The $\delta^{18}O$ of O_2 in the flasks was +23.5 ± 0.5‰ ($n = 4$) at the beginning of study and +24.3 ± 1.7‰ ($n = 4$) at the end of the study suggesting that the $\delta^{18}O$ of O_2 was constant within analytical error over the duration of the experiments. Since both water and atmospheric O_2 were incorporated into sulfate during the initial stage of elemental sulfur oxidation, determining $\varepsilon^{18}O_{SO4-H2O}$ and $\varepsilon^{18}O_{SO4-O2}$ and their relative contributions to the overall $\delta^{18}O_{SO4}$ was not possible. Since all oxygen atoms in the product sulfate were derived from water during the main stage of the experiment, the $\varepsilon^{18}O_{SO4-H2O}$ can be calculated from the y-intercepts of $\delta^{18}O_{H2O}$ vs. $\delta^{18}O_{SO4}$ plots (**Table 4**, **Figure 3**). In this case, $\varepsilon^{18}O_{SO4-H2O}$ ranged from −5.9 to −3.7‰ with an average of −4.8‰ during the main stage oxidation experiments (84–720 h). An average $\varepsilon^{18}O_{SO4-H2O}$ of −4.2 ± 4.4‰ can be calculated when the $\delta^{18}O_{SO4}$ values from all time points in the experiments are used (including those in the lag phase; **Figure 3**), meaning that ^{16}O from

TABLE 4 | Oxygen and sulfur isotope composition and isotopic enrichment factors for sulfate produced from microbial oxidation of elemental sulfur.

Time (hours)	W1 Experiments			W2 Experiments			W3 Experiments			% oxygen H_2O[a]	$\varepsilon^{18}O^{b}_{SO4-H2O}$
	$\delta^{18}O_{SO4}$ (‰)	$\delta^{34}S_{SO4}$ (‰)	$\varepsilon^{34}S_{SO4-S0}$ (‰)	$\delta^{18}O_{SO4}$ (‰)	$\delta^{34}S_{SO4}$ (‰)	$\varepsilon^{34}S_{SO4-S0}$ (‰)	$\delta^{18}O_{SO4}$ (‰)	$\delta^{34}S_{SO4}$ (‰)	$\varepsilon^{34}S_{SO4-S0}$ (‰)		(‰)
4	n.d	17.01	−1.19	n.d	n.d	n.d	n.d	n.d	n.d	n.d	n.d
24	−4.2	16.4	−1.79	12.7/51.2*	17.12	−1.08	15.4/40.41*	n.d	n.d	58 ± 0.3	n.a
33	−6.73	n.d	n.d	12.5/34.7*	n.d	n.d	23.4/51.7*	n.d	n.d	66 ± 0.0	n.a
48	−10.1	16.7	−1.49	20.1/29.2*	17.41	−0.79	30/42.5*	16.5	−1.75	60 ± 1.0	n.a
60	−9.1	n.d	n.d	25.3/33.6*	n.d	n.d	45.6	n.d	n.d	63 ± 4.0	n.a
72	−10.8	17.2	−0.97	48.32	17.43	−0.77	52.1	n.d	n.d	76 ± 0.17	n.a
84	−11.0	n.d	n.d	54.3	n.d	n.d	72.4	17.3	−0.9	96 ± 6.0	−5.2 ± 3.9
96	−9.3	16.9	−1.23	56.2	17.20	−1.00	76.7	17.2	−1	98 ± 4.0	−3.7 ± 2.7
124	−11.2	n.d	n.d	54.4	n.d	n.d	78.3	17.4	−0.82	1.02 ± 0.0	−5.9 ± 0.9
146	−10.9	16.9	−1.28	57.6	17.40	−0.80	77.2	n.d	n.d	1.01 ± 0.0	−4.8 ± 3.7
168	−9.9	n.d	n.d	57.4	n.d	n.d	76.2	n.d	n.d	1.00 ± 0.0	−4.0 ± 3.3
264	−10.6	17.1	−1.09	52.7	17.35	−0.85	77.4	n.d	n.d	99 ± 0.0	−5.5 ± 0.07
336	−10.9	17.6	−0.56	56.2	17.69	−0.51	75.1	17.6	−0.6	99 ± 0.0	−5.0 ± 3.8
504	n.d	n.d	n.d	59.2	17.60	−0.62	n.d	n.d	n.d	n.d	n.d
720	−10.6	18.0	−0.13	57.5	17.73	−0.47	79.3	17.9	−0.35	1.03 ± 0.0	−4.7 ± 2.6
Average	−9.6/−10.2 ($n = 13$)	17.1 ± 0.2	−1.1 ± 0.2	50.2/51.4 ($n = 14$)	17.4 ± 0.2	−0.8 ± 0.2	64.9/65 ($n = 13$)	17.3 ± 0.2	−0.9 ± 0.2	87 ± 7.0[c]	−4.2 ± 4.4[c]
$\delta^{18}O_{H2O\_initial}$ (‰)	−4.44			58.4			84.4				
$\delta^{18}O_{H2O\_final}$ (‰)	−5.60			58.04			81.70				
Avg. $\delta^{18}O_{H2O}$(‰)	−5.02			58.22			83.05				

$\delta^{34}S_{S0} = 18.2 \pm 0.2$‰ ($n = 5$);

**Calculated values based on the mass balance equation (see text);*

[a]*Estimated from linear regressions between $\delta^{18}O_{SO4}$ and $\delta^{18}O_{H2O}$ (Balci et al., 2012);*

[b]*$\varepsilon^{18}O_{SO4-H2O}$ was obtained from the intercept calculated from linear regressions between $\delta^{18}O_{SO4}$ and $\delta^{18}O_{H2O}$ (Balci et al., 2012);*

[c]*Estimated from linear regressions between average $\delta^{18}O_{SO4}$ ($n = 37$) and average $\delta^{18}O_{H2O}$ ($n = 3$) values (**Figure 3**);*

n.a, not applicable; n.d, not determined.

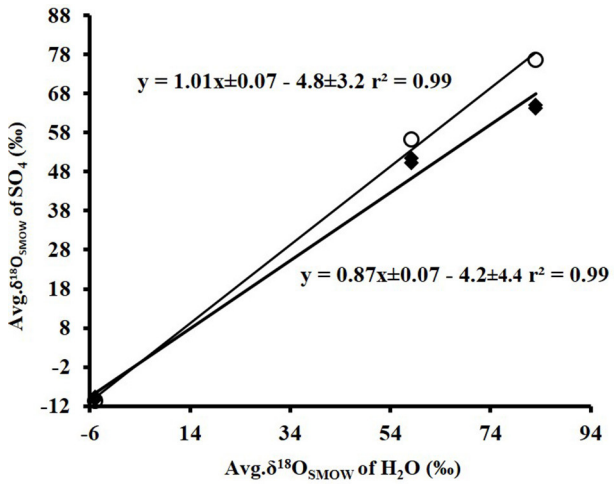

FIGURE 3 | Plot of the average $\delta^{18}O_{SO4}$ ($n = 37$)(•) produced from microbial oxidation of elemental sulfur and (○) produced from main stage oxidation vs. average $\delta^{18}O_{H2O}$ ($n = 3$) values and used in the experiments (see **Table 1**).

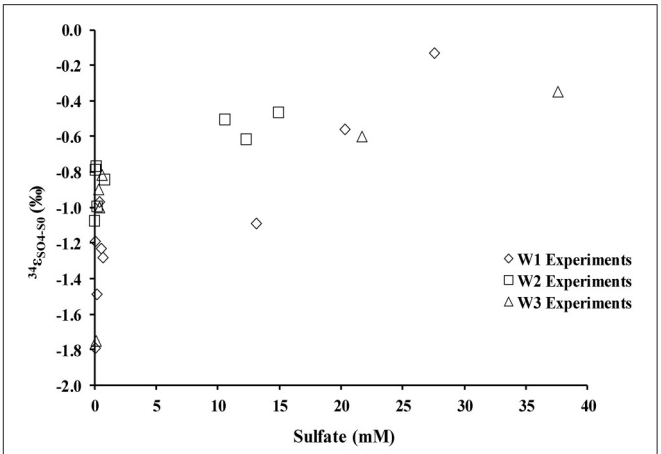

FIGURE 4 | Sulfur isotope enrichment during oxidation of elemental sulfur in the presence of *A. thiooxidans*.

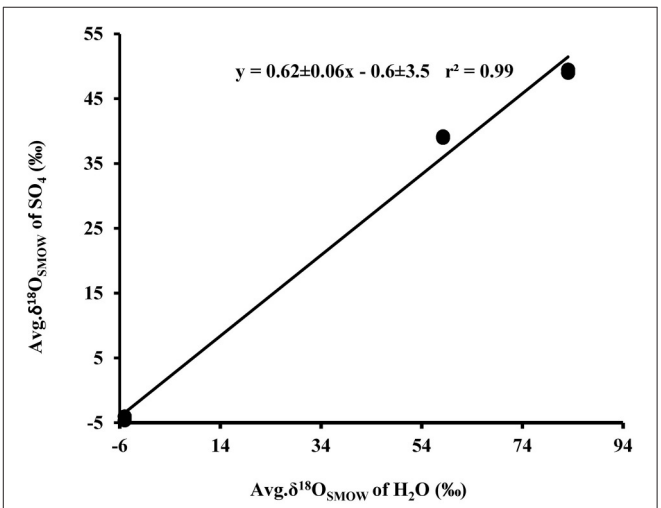

FIGURE 5 | Plot of the average $\delta^{18}O_{SO4}$ produced from biological (•) and abitoic (○) oxidation of tetrathionate vs. average $\delta^{18}O_{H2O}$ used in the experiments (see **Table 4**).

water is preferentially incorporated into sulfate (normal isotope effect).

During the oxidation of elemental sulfur, the $\delta^{34}S$ of the sulfate produced ranged from +16.4 to +18.0‰ with averages of 17.1, 17.4, and 17.3‰ for the W1, W2, and W3 experiments, respectively. Over the course of the experiments with elemental sulfur, the average difference between elemental sulfur and the sulfate formed ($\varepsilon^{34}S_{SO4-S0}$) was −1.1, −0.8, and −0.9‰ calculated from the W1, W2, and W3 experiments, respectively; the $\delta^{34}S$ of the product sulfate is almost the same as the elemental sulfur substrate (**Table 3**). During the lag stage of the oxidation of elemental sulfur, a slightly larger normal sulfur isotope fractionation between elemental sulfur and sulfate was found (approximately −1.8‰; **Table 4**, **Figure 4**).

Oxygen and Sulfur Isotopic Composition of Sulfate Produced from Oxidation of Tetrathionate

Plots of $\delta^{18}O_{SO4}$ vs. $\delta^{18}O_{H2O}$ for the experiments involving the oxidation of tetrathionate show a strong linear correlation ($r^2 > 0.99$) with a slope of 0.62 ± 0.06 suggesting the incorporation of 62% water-derived oxygen into the sulfate with the remainder derived from atmospheric O_2 or from tetrathionate (**Figure 5**). In contrast to the experiments with elemental sulfur, the percentage of water-derived oxygen into sulfate was lower and did not show significant change with the progressive oxidation from lag to exponential growth phase (**Table 5**).

During growth on tetrathionate, *A. thiooxidans* produced sulfate enriched in ^{34}S compared to the $\delta^{34}S$ of the tetrathionate substrate (which was 3.9‰). The calculated sulfur isotope fractionation ($\varepsilon^{34}S_{SO4-S4O6}$) was between +1.4 and +7.9‰ with an average of 2.9‰ ($n = 9$), 3.5‰ ($n = 7$), and 3.8‰ ($n = 5$) for the W1, W2, and W3 experiments, respectively (**Table 5**, **Figure 6**). The $\varepsilon^{34}S_{SO4-S4O6}$ was large during the initial stage of experiments, and became substantially smaller over time (**Table 5**, **Figure 6**), but remained inverse (^{34}S preferentially ended up in sulfate).

DISCUSSION

Microbial Oxidation of Tetrathionate and Elemental Sulfur

In all experiments with *A. thiooxidans*, the pH dropped from the initial pH to between 0.68 and 2.0 at the end of the month-long incubation, regardless if the substrate was elemental sulfur or tetrathionate (**Figures 1**, **2**, **Tables 2**, **3**). In the aseptic abiotic control experiments, the pH rose after 150 h from 4.1 to 4.2 with elemental sulfur, and remained invariant at 4.5 until 144 h

TABLE 5 | Oxygen and sulfur isotope composition and isotopic enrichment factors for sulfate produced from microbial oxidation of tetrathionate.

Time (hours)	W1 Experiments H_2O[a]			W2 Experiments			W3 Experiments			% oxygen
	$\delta^{18}O_{SO4}$ (‰)	$\delta^{34}S_{SO4}$ (‰)	$\varepsilon^{34}S_{SO4\text{-}S4O6}$ (‰)	$\delta^{18}O_{SO4}$ (‰)	$\delta^{34}S_{SO4}$ (‰)	$\varepsilon^{34}S_{SO4\text{-}S4O6}$ (‰)	$\delta^{18}O_{SO4}$ (‰)	$\delta^{34}S_{SO4}$ (‰)	$\varepsilon^{34}S_{SO4\text{-}S4O6}$ (‰)	
48	−5.7	n.d	n.d	n.d	n.d	n.d	n.d	n.d	n.d	n.d
144	−4.2	7.3	3.4	40.1	9.2	5.3	22.3/51.9*	n.d	n.d	64
192	−4.4	9.4	5.5	39.2	8.1	4.2	33.1/47.2*	11.8	7.9	60
240	−2.6	8.9	4.9	42.3	7.81	3.9	49.2	n.d	n.d	61
288	−3.8	7.2	3.2	37.2	n.d	n.d	40.1	7.8	3.9	53
360	−4.1	6.2	2.2	42.5	6.8	2.9	n.d	n.d	n.d	n.d
408	−4.5	5.8	1.9	38.7	7.2	3.3	49.2	6.7	2.8	62
480	−4.4	6.1	2.2	34.6	6.6	2.7	47.4	n.d	n.d	59
600	−3.5	5.4	1.4	35.4	n.d	n.d	51.2	5.9	2.0	61
720	−2.6	6.4	2.4	38.8	5.9	2.0	52.2	6.1	2.2	62
Average	−4.0, −4.6 ($n = 10$)	6.9 ± 0.2	2.9 ± 0.2	38.8/39.2 ($n = 9$)	7.4 ± 0.2	3.5 ± 0.2	49/49.5 ($n = 8$)	7.7 ± 0.2	3.8 ± 0.2	62 ± 0.06[b]
$\delta^{18}O_{H2Oinitial}$ (‰)	−4.44			58.4			84.4			
$\delta^{18}O_{H2Ofinal}$ (‰)	−5.60			58.04			81.70			
Avg. $\delta^{18}O_{H2O}$(‰)	−5.02			58.22			83.05			

$\delta^{34}S_{S4O6} = 3.9$‰ ($n = 4$);

[a]Estimated from linear regressions between $\delta^{18}O_{SO4}$ and $\delta^{18}O_{H2O}$ (Balci et al., 2012);

*[b]Estimated from linear regressions between average $\delta^{18}O_{SO4}$ ($n = 27$) and average $\delta^{18}O_{H2O}$ ($n = 3$) values (**Figure 4**);*

n.d, not determined.

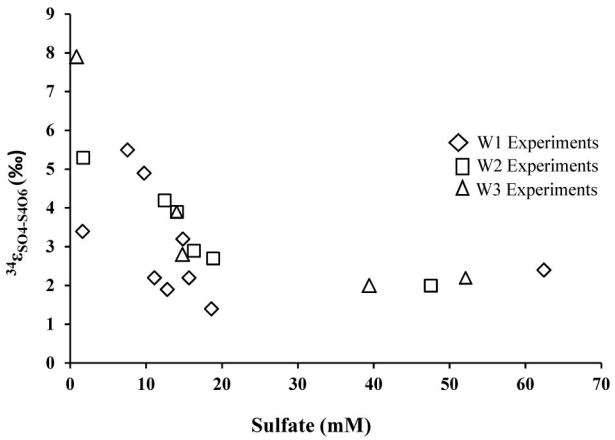

FIGURE 6 | Sulfur isotope enrichment during oxidation of tetrathionate in the presence of *A. thiooxidans*.

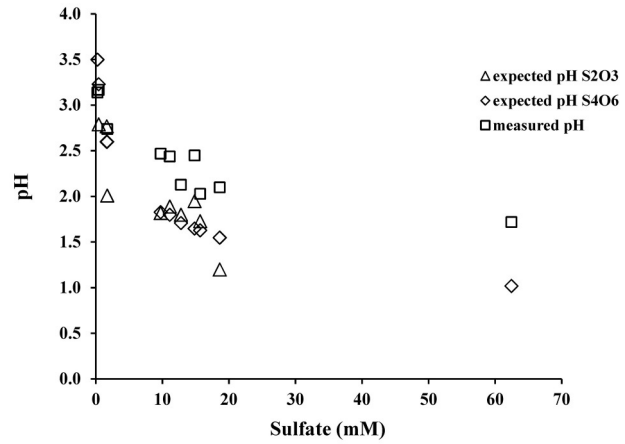

FIGURE 7 | Relationship between sulfate and pH as predicted from the oxidation stoichiometry of tetrathionate (reaction 9) and thiosulfate (reaction 13) or as measured from the experiments.

following a decrease to 4.15 in the experiments with tetrathionate (**Figures 1D**, **2D**). The amount of acid generation and sulfate produced are substrate dependent; the pH was lower and the amount of sulfate produced was higher in the experiments with elemental sulfur than for those with tetrathionate. The microbial disproportionation of tetrathionate caused a partial reduction of tetrathionate to thiosulfate and a fractional oxidation to sulfate and elemental sulfur via reaction (9) rather than a straight oxidation of tetrathionate to sulfate (reaction 7),

$$S_4O_6^{2-} + H_2O \rightarrow S_2O_3^{2-} + S^0 + SO_4^{2-} + 2H^+ \quad (9)$$

This is supported by the fact that when *A. thiooxidans* grew on tetrathionate, there is less acidity generated and less sulfate produced, confirming that complete oxidation of tetrathionate to sulfate (reaction 7) does not occur (**Figure 7**). Our data also suggest that during tetrathionate oxidation the rates of the subsequent thiosulfate and elemental sulfur oxidation are lower than the rate of production of both species, leading to an accumulation of thiosulfate and elemental sulfur in the media (**Figure 2**).

The product thiosulfate, initially produced during both elemental sulfur and tetrathionate oxidation, may further be converted to sulfite and elemental sulfur through the initial cleavage of thiosulfate (reaction 10) followed by the oxidation of elemental sulfur (reaction 11) and sulfite to sulfate (reaction 12) (Meulenberg et al., 1993; Beard et al., 2011). The net reaction (13) is the overall oxidation of thiosulfate to sulfate.

$$S_2O_3^{2-} + 2H^+ \rightarrow S^0 + H_2SO_3 \quad (10)$$

$$S^0 + O_2 + H_2O \rightarrow H_2SO_3 \quad (11)$$

$$2H_2SO_3 + O_2 \rightarrow 2SO_4^{2-} + 4H^+ \quad (12)$$

$$S_2O_3^{2-} + H_2O + 2O_2 \rightarrow 2SO_4^{2-} + 2H^+ \quad (13)$$

When the pH of the experimental solution reached 2.0, thiosulfate was almost completely exhausted but small amounts of elemental sulfur remained and sulfate became the major anion (**Figure 2**, **Table 3**). If we combine the initial oxidation of tetrathionate to thiosulfate, and tetrathionate disproportionation to sulfate and elemental sulfur (reaction 6) with the overall oxidation of thiosulfate with O_2 (reaction 11) we can predict the expected ratios of proton to sulfate generation during oxidation of tetrathionate as suggested by Bernier and Warren (2007). The predicted pH decrease from reactions (9) and (13) exceeds the observed pH decrease in our experiments indicating a substantial proton consumption occurred in parallel to the proton production during these oxidation reactions (**Figure 6**). Proton consumption during microbial oxidation of tetrathionate and thiosulfate has previously been reported under similar experimental conditions and attributed to microbial disproportionation reactions occurring during the oxidation of tetrathionate and thiosulfate (e.g., reaction 10, Bernier and Warren, 2007; Houghton et al., 2016). Reaction (14), which is microbially-mediated, has been suggested to consume protons under conditions similar to our laboratory experiments:

$$2S_2O_3{}^{2-} + 2H^+ + 0.5O_2 \rightarrow S_4O_6{}^{2-} + H_2O \quad (14)$$

Production of tetrathionate (up to 7.7 mM) from thiosulfate in experiments buffered at low pH has previously been reported (Houghton et al., 2016), which corroborates the hypothesis that reaction (14) plays an important role in buffering the pH. Bernier and Warren (2007) modeled the kinetics of the abiotic disproportionation of thiosulfate over a pH range of 1.5–4.0 according to the following reaction (reaction 15):

$$S_2O_3 + 2H^+ \rightarrow S^0 + H_2SO_3 \quad (15)$$

Their data indicated that this reaction was likely too slow to play a significant role; hence thiosulfate should not abiotically disproportionate to elemental sulfur and sulfite under experimental conditions similar to ours (Johnston and McAmish,

1973; Druschel et al., 2003). Lower concentrations of thiosulfate, sulfate and insignificant pH change measured in the abiotic experiments are consistent with these previous studies and further suggest that formation of thiosulfate and sulfate are due to microbial activity (Druschel et al., 2003; Bernier and Warren, 2007; **Figure 2D**).

Mass balance calculations demonstrate that up to 34% of the total sulfur is not accounted for by the sulfur species we measured (tetrathionate, thiosulfate, and elemental sulfur) during the experiment (**Table 3**). Sulfite is not expected to account for a significant fraction of the sulfur mass balance, since it should be rapidly oxidized under our experimental conditions (Pronk et al., 1990; Kappler and Dahl, 2001). This "missing sulfur" in the tetrathionate experiments may be linked to the formation of long-chain polythionates such as tri-, penta-, and hexa/thionate (Steudel et al., 1987; Pronk et al., 1990; Druschel et al., 2003; Bernier and Warren, 2007; Shiers et al., 2011). The production of long-chain polythionates has been also reported in aerated *A. ferrooxidans* suspensions, which is phylogenetically similar (at the genus level) to *A. thiooxidans*, incubated with tetrathionate (Steudel et al., 1987; Hazeu et al., 1988). Druschel et al. (2003) attributed the formation of trithi-and pentathionate to reactions involving polysulfane monosulfonic acids (Steudel et al., 1987, 1988; Pronk et al., 1990; Steudel, 2003). As suggested by Druschel et al. (2003) the chemical reactions involving polysulfane monosulfonic acids may have been altered the oxidation stoichiometry of tetrathionate and thiosulfate (reactions 9 and 13, respectively) resulting in a change in the expected stoichiometric ratio between sulfate and acid. Another possibility is that volatile sulfur species escape the experiments. Such a process has been considered for the initial stage of pyrite oxidation in acidic solutions, where it was showed that under highly acidic conditions, sulfite can form sulfur dioxide gas (SO_2), and degas into the headspace (Brunner et al., 2008). The conversion of sulfite into SO_2 consumes protons, i.e., which would slow down the drop to lower pH during tetrathionate oxidation.

When elemental sulfur is the sole substrate or is produced as a by-product of tetrathionate disproportionation (reactions 9 and 10), it needs to be activated before it is transferred into the periplasm of microorganisms for further chemical reaction (Bobadilla Fazzini et al., 2013). Following its activation, the first step of elemental sulfur oxidation is thought to be the transition of sulfur to thiosulfate catalyzed by sulfur dioxygenase (SDO), which generates sulfite (Meulenberg et al., 1993; Bobadilla Fazzini et al., 2013). The activation of elemental sulfur results in a slower growth and lower cell numbers represented by a long lag phase during the oxidation reactions, as discussed above (**Figure 1**). Trace amount of sulfite detected in the experiments suggest that sulfite may have been produced but was readily converted to sulfate (via reactions 9, 10, and 11). The formation and subsequent oxidation of sulfite to sulfate occurs during tetrathionate and elemental sulfur oxidation in the presence of various *Acidithiobacillus* spp., as has previously been suggested (Hallberg et al., 1996; Suzuki, 1999; Shiers et al., 2011).

Fractionation of Sulfur Isotopes between Sulfate, Elemental Sulfur, and Tetrathionate

There was a negligible sulfur isotope fractionation observed during the microbial oxidation of elemental sulfur (**Table 4**, **Figure 4**). However, a small but significant sulfur isotope fractionation ($\varepsilon^{34}S_{SO4-S0} \sim -2‰$) was observed during the initial 48 h of the experiment. This change in sulfur isotope fractionation over the course of the experiment has been previously reported for experiments with a phylogenetically similar microorganism, *A. ferrooxidans* (Balci et al., 2012) and in earlier studies exploring elemental sulfur oxidation (Kaplan and Rittenberg, 1964; Mizutani and Rafter, 1969; McCready and Krouse, 1982). This reported larger sulfur isotope fractionation in the initial stage of microbial growth might relate to sulfur isotope fractionation during the activation of elemental sulfur. This activation stage requires an opening of the S_8 ring and thus a bond-breaking processes between S–S atoms by the thiol groups of cysteine residues (Tichomirowa and Junghans, 2009). Overall, our results demonstrate that elemental sulfur is fully oxidized to sulfate under acidic conditions, resulting in an overall negligible sulfur isotope fractionation, a finding that is consistent with the fact that sulfur isotope fractionation associated with oxidation of solid phase sulfur is insignificant relative to the oxidation of aqueous hydrogen sulfide (Nakai and Jensen, 1964; McCready and Krouse, 1982; Taylor et al., 1984; Fry et al., 1986; Balci et al., 2007, 2012; Thurston et al., 2010; Smith et al., 2012).

In contrast to the elemental sulfur experiments, biological oxidation of tetrathionate produced sulfate that is enriched in ^{34}S relative to tetrathionate throughout the experiments. The average $\varepsilon^{34}S_{SO4-S4O6}$ of +2.9, +3.5, and +3.8‰ obtained from the experiments in this study falls with the range of other experimental results for the microbial oxidation of various sulfur compounds (**Table 1**). However, it must be noted the magnitude of this inverse sulfur isotope fractionation decreased over the course of the experiment, from approximately to +7.9 to +1.4‰ (**Table 5**, **Figure 6**). The oxidation of tetrathionate to sulfate involves a series of microbially-catalyzed reactions (given above, reactions 9–14). The sulfur isotope fractionation associated with multi-step microbial transformations have not been fully determined, and there is a large gap in knowledge for reactions taking place at low pH. Previous studies on microbially-catalyzed sulfur oxidation have produced vastly different results that may be difficult to reconcile. For example, a large inverse sulfur isotope fractionation ($\varepsilon^{34}S_{SxO6-S2} = +0.6$ to +19‰) was observed during the oxidation of sulfide to polythionates by *A. thiooxidans*, whereas, a large normal sulfur isotope fractionation (−18 to −10.5‰) was observed with *A. thiooxidans* oxidizing sulfide to sulfate (Kaplan and Rittenberg, 1964). It is likely that two mixed-valence state sulfur species, thiosulfate and tetrathionate, play a critical role in shaping the isotope composition of the product of the oxidation process. Thiosulfate and tetrathionate possess sulfur atoms with different valence states, whereby the sulfane (S−) sulfur atoms (connected by S–S bonds) have a lower valence state than the sulfonate ($-SO_3$) sulfur species, which have a S–S bonds and three S–O bonds (Druschel et al., 2003). The sulfur isotope difference between

the two sulfur atoms in thiosulfate is estimated to be between 6 and 14‰ with the sulfonate sulfur species enriched in ^{34}S relative to the sulfane species (Chambers and Trudinger, 1979; Fry et al., 1986; Smock et al., 1998). In analogy, it is likely that at chemical equilibrium, the sulfonate species of tetrathionate are substantially enriched in ^{34}S relative to the sulfane species. It can thus be argued that the shift from large inverse sulfur isotope fractionation (+7.9‰) to a smaller sulfur isotope fractionation of +1.4‰ is due to the initial disproportionation of tetrathionate into sulfate (reaction 9), followed by a delayed oxidation of other sulfur intermediates to sulfate. If the former sulfate is mainly supplied from isotopically heavy sulfonate-sulfur, and the latter from isotopically light sulfane-sulfur, one would expect to observe the described trend. We did not analyze the sulfur isotope composition of the sulfane and sulfonate moieties of the tetrathionate used in our experiments, and therefore, cannot further test this hypothesis, however, the oxygen isotope signature of formed sulfate provides additional insight.

Fractionation of Oxygen Isotopes between SO_4 and H_2O during Oxidation of Elemental Sulfur and Tetrathionate

The contribution of water-derived oxygen to sulfate during oxidation of elemental sulfur by *A. thiooxidans* ranged from 58% to 103% and the $\varepsilon^{18}O_{SO4-H2O}$ was estimated to be between −5.9 ± 0.9 to −3.7 ± 2.7‰ with a mean of −4.8 ± 3.2‰ (**Table 4**). The high percentage of sulfate-oxygen derived from water is consistent with previous studies on microbially-mediated elemental sulfur oxidation (Balci et al., 2012; Smith et al., 2012) indicating similar elemental sulfur processing pathways among *Acidithiobacillus* spp.

There are two reasons why oxygen from O_2 is negligible in sulfate formed from elemental sulfur oxidation. First, biological oxidation of solid elemental sulfur proceeds via stepwise enzymatic reactions where molecular oxygen acts as an electron acceptor (Kelly, 1982; Pronk et al., 1990). The first documented step in sulfur oxidation is the activation of extracellular elemental sulfur (S_8) to thiol-bound sulfane sulfur atoms (R-S-SH) and then it is transferred into the periplasm where it is oxidized by the sulfur dioxygenase (SDO) to produce sulfite which further combines chemically with sulfur atoms to produce thiosulfate (Pronk et al., 1990; Suzuki, 1999; Bobadilla Fazzini et al., 2013; Yin et al., 2014). The electron transport system for elemental sulfur oxidation is the likely cause for the complete incorporation of water oxygen into sulfate. *Acidithiobacillus* spp., derive energy from sulfur oxidation by coupling to reduction of oxygen from O_2, but the electrons from elemental sulfur pass through several steps of the electron transport system before they reduce O_2 to water in the final step. Consequently, the reduction of O_2 to water is physically separated from the final oxidation of sulfite to sulfate and the oxygen in sulfate then can derive wholly from water (Kelly, 1982). The transfer of electrons from sulfur to the electron acceptor (O_2) provides energy by cycling electrons through the electron transport system (Ehrlich, 1982). From this follows that if the bacteria produce sulfate through the electron transport system then the $\delta^{18}O_{SO4}$ of the produced sulfate should not be affected by $\delta^{18}O_{O2}$.

Secondly, oxygen isotope exchange between sulfite, a common intermediate valence state sulfur species, and water is likely to occur under the low pH of our experimental conditions and may be partially responsible for the large calculated water-oxygen incorporation into sulfate (reactions 10–12). It has been reported that oxygen isotope exchange between sulfite and water is on the order of nanoseconds under acidic conditions, which is in stark contrast to the multi-million year timescale for oxygen isotope exchange between sulfate and water at circum-neutral pH (Lloyd, 1968; Pearson and Rightmire, 1980; Holt et al., 1981). Chiba and Sakai (1985) reported that oxygen isotope exchange between sulfate and water should take $\sim 10^9$ year at 100–300°C and pH 2 to 7—based on laboratory experiments. Extrapolating the experimental data of Hoering and Kennedy (1957) and Chiba and Sakai (1985) to pH 0, 1, and 2, the respective half times required for oxygen isotopic exchange between sulfate and water could be as low as 1 year at pH 0 and 10^5 years at pH 2 (Rennie and Turchyn, 2014). Based on these results, it can be safely assumed that sulfate–water oxygen isotope exchange is unlikely to occur under our experimental conditions. Alternatively, Mizutani and Rafter (1969, 1973), and Fritz et al. (1973) demonstrated that oxygen isotope exchange between sulfate and water proceeds through enzyme-bound intermediates during the bacterial reduction of sulfate. Similar enzyme-mediated oxygen isotope exchange processes might occur during mixed-valence state sulfur species oxidation to sulfate.

The enrichment in ^{18}O in sulfite during oxygen isotope equilibration with water ($\varepsilon^{18}O_{SO3-H2O}$) has been addressed in several studies, but large uncertainties remain. Holt et al. (1981) reported that $\delta^{18}O_{SO3}$ was enriched by 24‰ with respect to $\delta^{18}O_{H2O}$ under equilibrium conditions. Consistent with Holt et al. (1981) and Brunner et al. (2006) reported that $\varepsilon^{18}O_{SO3-H2O}$ increased as pH decreased and reported $\varepsilon^{18}O_{SO3-H2O}$ of 11.5 and 7.9‰ for pH 7.2 and 8, respectively at 23°C. Since no experiments have been conducted for strongly acidic pH it is unsure if $\varepsilon^{18}O_{SO3-H2O}$ would continue to increase with decreasing pH (Müller et al., 2013a; Wankel et al., 2014). Several estimates for $\varepsilon^{18}O_{SO4-H2O}$ have been reported during oxidation of reduced sulfur compounds. For example, Smith et al. (2012) estimated the $\varepsilon^{18}O_{SO4-H2O}$ ranging −6.2 to −0.9‰ during elemental sulfur oxidation by *A. thiooxidans* under various temperature and nutrient regimes while Mizutani and Rafter (1969) found an oxygen isotope fractionation of 0‰. The range of −5.9 ± 0.9 to −3.7 ± 2.7‰ for $\varepsilon^{18}O_{SO4-H2O}$ from the current experiments appears to be consistent with the range reported by these studies.

In contrast to experiments with elemental sulfur, our data demonstrate that contribution of water-derived oxygen to sulfate ranged from 53 to 64% (average of 62%) during oxidation of tetrathionate (**Tables 3**, **5**, **Figure 5**), which is at the lower end of the percentage of water-derived oxygen ranging between 50 and 97% reported for biological and abiological sulfide oxidation to sulfate under aerobic and acidic conditions (Toran and Harris,

1989; van Stempvoort and Krouse, 1994; Balci et al., 2007, 2012; **Table 1**). It is interesting to note that 37.5% of oxygen in sulfate could be derived from tetrathionate (reaction 7), which leaves 62.5% to oxygen from water or O_2. In analogy to the findings for elemental sulfur oxidation, it could be inferred that no oxygen from O_2 is incorporated into sulfate during tetrathionate oxidation. Such an interpretation would demand that the entire oxygen inventory of tetrathionate ends up in sulfate, which requires that no oxygen-atoms from tetrathionate are exchanged with oxygen from water, i.e., no S–O bonds from the sulfonate moieties are broken. While this interpretation is appealing, it is difficult to reconcile it with the argument that the shift from large inverse sulfur isotope fractionation to a smaller sulfur isotope fractionation is due to the initial transformation of the sulfonate moiety of tetrathionate into sulfate followed by a delayed oxidation of other sulfur intermediates that originated from the sulfane moiety of tetrathionate. If this was the case, one would expect to initially observe a minimal contribution of water-oxygen (i.e., 25%, as fourth oxygen atom required to convert sulfonate into sulfate), followed by an increase toward 62.5% concomitant to the oxidation of increase in the oxidation of sulfur intermediates derived from the sulfane moiety of tetrathionate. This is not the case, as there is no trend that would indicate a consistent increase in the contribution of oxygen from water to sulfate over time (**Table 5**). This indicates that at least one of the two proposed explanations—either incorporation of oxygen from water and none from air, or a change in the observed sulfur isotope fractionation—is overly simplistic. Since oxygen isotopes are likely fractionated during the incorporation of oxygen from water, tetrathionate, and molecular O_2 into the product sulfate, it was not possible to directly determine the corresponding isotope fractionation factors $\varepsilon^{18}O_{SO4-H2O}$, $\varepsilon^{18}O_{SO4-S4O6}$, and $\varepsilon^{18}O_{SO4-O2}$ (Sessions and Hayes, 2005).

Implications for the Natural Environment

Recent experimental studies have shown the formation of mixed-valence-state sulfur species during metal sulfide oxidation in acid-mine drainage settings and suggested that these sulfur species play a significant role in redox sulfur cycling in these environments (Schippers et al., 1996; Druschel et al., 2003; Heidel and Tichomirowa, 2010). Therefore, while the occurrence of mixed-valence sulfur compounds has been reported in various environments (e.g., mine wastes, marine, and freshwater sediments), the role of these sulfur molecules and their contribution to the acidic redox cycling of sulfur remains unclear, particularly whether there may be a way to track the cycling of these species using stable isotopes. Most of our knowledge about how sulfur is reduced and re-oxidized derives from the sulfur and oxygen isotope composition of sulfate generated during sulfide mineral oxidation (biotic or abiotic; Taylor et al., 1984; Balci et al., 2007, 2012; Brunner et al., 2008; Balci, 2010; Heidel and Tichomirowa, 2010; Thurston et al., 2010; Sanliyuksel Yucel et al., 2016).

In general, a small sulfur isotope fractionation between metal sulfide and the product sulfate resulting from oxidation of sulfur under acid conditions by microorganisms has been reported (**Table 1**—Taylor et al., 1984; Rye et al., 1992; Seal, 2003; Balci et al., 2007; Heidel et al., 2009; Heidel and Tichomirowa, 2010; Thurston et al., 2010). Furthermore, only a small sulfur isotope fractionation generally accompanies the aerobic oxidation of H_2S, S^0, $S_2O_3^{2-}$, and SO_3^{2-} to either S^0 or SO_4^{2-} (Fry et al., 1986; **Table 1**). In contrast, larger sulfur isotope fractionation has been found during disproportionation of $S_2O_3^{2-}$, S^0, and SO_3^{2-} at more neutral conditions (Habicht et al., 1998; Poser et al., 2016). Consistent with previous studies, the sulfur isotope fractionation of elemental sulfur oxidation to sulfate under aerobic acidic conditions was characterized by a small sulfur isotope fractionation in this study (**Table 1**). In contrast, we found significantly ^{34}S-enriched sulfate during experiments involving tetrathionate oxidation under acid conditions, and observed that the incorporation of oxygen from water in this step is only 62%. Tetrathionate is accepted as a key intermediate in the oxidation of acid-insoluble sulfides, such as pyrite (e.g., Schippers and Sand, 1999; Druschel et al., 2003), a process that commonly displays little to no sulfur isotope fractionation, and often oxygen incorporation from water near to 100%, but with considerable scatter for both parameters (**Table 1**).

Our results suggest that if tetrathionate is produced in acidic conditions such as those found in acid-mine drainage, there is higher potential to observe such a scatter than under conditions where elemental sulfur or metal sulfide are directly oxidized to sulfate, with insignificant sulfur isotope fractionation (**Table 1**). The question becomes if there are conditions that would favor the expression of sulfur and oxygen isotope effects tied to the presence of tetrathionate. In the case of sulfur isotope fractionation, a prerequisite is that the sulfur from tetrathionate is not quantitatively converted to sulfate. Our microbial experiments show that tetrathionate oxidation is indeed not quantitative. According to Schippers (2004), the degradation of tetrathionate strongly depends on pH and the presence of catalysts such as pyrite. In acidic conditions, tetrathionate formed in the presence of pyrite is quickly hydrolyzed to disulfane-monosulfonic acid rather than oxidized to sulfate (Steudel et al., 1987; Schippers et al., 1996). Disulfate-monosulfonic acid is unstable and will react to form to various sulfur compounds (e.g., trithionate, pentathionate) before forming sulfate. The competition between microbial agents and mineral surfaces in the catalysis of tetrathionate oxidation may be decisive for fate of the sulfur moieties of tetrathionate, and control if the oxidation process is quantitative (no sulfur isotope fractionation) or incomplete (potential for sulfur isotope fractionation).

Microbes may also be key in catalyzing sulfur isotope exchange between sulfur moieties in tetrathionate or thiosulfate, or through reversibility of enzymatic steps, between different sulfur intermediates. For example, sulfur isotope exchange between the two sulfur atoms of thiosulfate leading to an enrichment of ^{34}S in sulfate up to 12‰ during disproportionation of thiosulfate has been previously suggested (Habicht et al., 1998). The initial steps during tetrathionate oxidation, such as the transport into the cell without a change in its oxidation state, do not involve the breaking of bonds

and should not generate sulfur isotope fractionation. However, in the periplasm the tetrathionate can be disproportionated to thiosulfate, elemental sulfur and sulfate by a tetrathionate hydrolase enzyme, such as the ones that have been isolated from acidophilic cells of *A. ferrooxidans* and *A. thiooxidans* (Meulenberg et al., 1992; De Jong et al., 1997; Yin et al., 2014). Tetrathionate disproportionation consists of multiple enzymatic steps that involve breaking of bonds and thus the sulfur isotopic fractionation measured between the final product sulfate and the reactant tetrathionate will reflect the sum of sulfur isotope fractionations associated with these enzymatic reactions. It is well documented that sulfur isotope fractionation during disproportionation may be controlled by the cell-specific rate of disproportionation in addition to various environmental and physicochemical factors (Habicht et al., 1998; Poser et al., 2016). During disproportionation of sulfur substrates such as elemental sulfur, thiosulfate, or tetrathionate, reversible reactions are involved that further modulate the sulfur isotope fractionation (Habicht et al., 1998; Kelly, 2008). Oxidation of thiosulfate from the reductive branch of tetrathionate disproportionation may also contribute to the larger overall sulfur isotope fractionation measured in our experiments. The co-occurrence of a larger sulfur isotope fractionation and the production of thiosulfate in this study suggests that there is a link between thiosulfate cycling and sulfur isotope partitioning (**Table 3**).

These considerations highlight that the formation of tetrathionate could be the reason why there is considerable scatter in the isotope data among various studies of the oxidation of pyrite and other reduced sulfur species. If the role of tetrathionate in these processes is understood, the scatter in the data sets could be used to decipher specific environmental conditions of different AMD systems based on sulfur and oxygen isotope signatures that are preserved in sulfate. Our pilot study demonstrates that tetrathionate clearly holds the potential to be a key compound in shaping the $\delta^{34}S_{SO4}$ and $\delta^{18}O_{SO4}$ of sulfate in AMD, and sets the stage for further investigations of the oxidation of this compound, such as the determination of the contribution of O_2 to the formed sulfate, and experiments that test if the presence of ferric or ferrous iron, in combination with microorganism that catalyze iron oxidation, has an impact on the quantity of "missing sulfur" during tetrathionate oxidation.

CONCLUSIONS

Sulfur isotope fractionation during the microbial oxidation of elemental sulfur to sulfate was negligible, while for the microbial oxidation of tetrathionate to sulfate the sulfur isotope fractionation was +3.5‰. Such a large sulfur isotope fractionation requires that ^{34}S-depleted sulfur compounds form, which we attribute to the up to 34% of "missing sulfur" that was noticed in the experiments involving tetrathionate oxidation, which we hypothesize comprised tri/pentathionates, but also loss of sulfur dioxide to the atmosphere may contribute to the observed isotope fractionation. The $\delta^{18}O$ of sulfate produced from the oxidation of elemental sulfur suggests that water-oxygen was the sole source of oxygen atoms for the sulfate ion, while the sulfate produced from tetrathionate oxidation derived oxygen from both water (62%). There are substantial differences in the sulfur and oxygen isotope signatures, acid generation and associated sulfur speciation between the oxidation of tetrathionate and elemental sulfur with the very same organism, an observation that likely can be generalized for other substrates in sulfur oxidation. Mixed-valence state sulfur species are microbially available and play substantial roles in sulfur cycle in acid-mine drainage systems. The analysis of both sulfur and oxygen isotopes in sulfate can be an important tool to detect and monitor the oxidation of such mixed-valence state sulfur species by *A. thiooxidans* in acidic environments.

AUTHOR CONTRIBUTIONS

All authors listed have made a substantial, direct and intellectual contribution to the work, and approved it for publication.

ACKNOWLEDGMENTS

We very much appreciate the comments and suggestions by our two reviewers, which greatly improved our manuscript. We would also like to thank Inigo Müller for carrying out sulfite concentration measurements. This work was supported by TUBITAK (the Scientific and Technological Research Council of Turkey)—GERMANY (DFG-German Research Foundation) European Scientific Exchange Programme, and TUBITAK Research Project (108Y177), grant to NB, and an ERC Starting Investigator Grant (307582) to AT.

REFERENCES

Alam, M., Pyne, P., Mazumdar, A., Peketi, A., and Ghosh, W. (2013). Kinetic enrichment of S-34 during proteobacterial thiosulfate oxidation and the conserved role of SoxB in S–S bond breaking. *Appl. Environ. Microbiol.* 79, 4455–4464. doi: 10.1128/AEM.00956-13

Balci, N. C. (2010). Effect of bacterial activity on trace metals release from oxidation of sphalerite at low pH (<3) and implications for AMD environment. *Earth Environ. Sci.* 60, 485–493. doi: 10.1007/s12665-009-0189-z

Balci, N., Mayer, B., Shanks, I. I. I., W. C., and Mandernack, K. W. (2012). Oxygen and sulfur isotope systematics of sulfate produced during abiotic and bacterial oxidation of sphalerite and elemental sulfur. *Geochim. Cosmochim. Acta* 77, 335–351. doi: 10.1016/j.gca.2011.10.022

Balci, N., Shanks, W. C. III., Mayer, B., and Mandernack, K. W. (2007). Oxygen and sulfur isotope systematics of sulfate produced by bacterial and abiotic oxidation of pyrite. *Geochim. Cosmochim. Acta* 71, 3796–3811. doi: 10.1016/j.gca.2007.04.017

Bao, H. (2015). Sulfate: a time capsule for Earth's O2, O3, and H2O. *Chem. Geol.* 395, 108–118. doi: 10.1016/j.chemgeo.2014.11.025

Beard, S., Paradela, A., Albar, J. P., and Jerez, C. A. (2011). Growth of Acidithiobacillus ferrooxidans ATCC 23270 in thiosulfate under oxygen-limiting conditions generates extracellular sulfur globules by means of a secreted tetrathionate hydrolase. *Front. Microbiol.* 2:79. doi: 10.3389/fmicb.2011.00079

Bernier, L., and Warren, L. A. (2005). Microbially driven acidity generation in a tailings lake. *Geobiology* 3, 115–133. doi: 10.1111/j.1472-4669.2005.00047.x

Bernier, L., and Warren, L. A. (2007). Geochemical diversity in S processes mediated by culture-adapted and environmental-enrichments of *Acidithiobacillus* spp. *Geochim. Cosmochim. Acta* 71, 5579–5584. doi: 10.1016/j.gca.2007.08.010

Bobadilla Fazzini, R. A., Cortés, M. P., Padilla, L., Maturana, D., Budinich, M., Maass, A., et al. (2013). Stoichiometric modeling of oxidation of reduced inorganic sulfur compounds (Riscs) in *Acidithiobacillus thiooxidans*. *Biotechnol. Bioeng.* 110, 2242–2251. doi: 10.1002/bit.24875

Brunner, B., Mielke, R. E., and Coleman, M. (2006). Abiotic oxygen isotope equilibrium fractionation between sulfite and water. *Eos Trans. AGU 87 (52) Fall Meet. Suppl., Abstract V11C-0601.*

Brunner, B., Yu, J.-Y., Mielke, R. E., MacAskill, J. A., Madzunkov, S., McGenity, T. J., et al. (2008). Different isotope and chemical patterns of pyrite oxidation related to lag and exponential growth phases of *Acidithiobacillus ferrooxidans* reveal a microbial growth strategy. *Earth Planet. Sci. Lett.* 270, 63–72. doi: 10.1016/j.epsl.2008.03.019

Chambers, L. A., and Trudinger, P. A. (1979). Microbiological fractionation of stable sulfur isotopes: a review and critique. *Geomicrobiol. J.* 1, 249–293. doi: 10.1080/01490457909377735

Chiba, H., and Sakai, H. (1985). Oxygen isotope exchange rate between dissolved sulfate and water at hydrothermal temperatures. *Geochim. Cosmochim. Acta* 49, 993–1000. doi: 10.1016/0016-7037(85)90314-X

De Jong, G. A., Hazeu, W., Bos, P., and Kuenen, J. G. (1997). Isolation of the tetrathionate hydrolase from *Thiobacillus acidophilus*. *Eur. J. Biochem.* 243, 678–683. doi: 10.1111/j.1432-1033.1997.00678.x

Druschel, G. K., Hamers, R. J., and Banfield, J. F. (2003). Kinetics and mechanism of polythionate oxidation to sulfate at low pH by O2 and Fe3+. *Geochim. Cosmochim. Acta* 67, 4457–4469. doi: 10.1016/S0016-7037(03)00388-0

Ehrlich, H. L. (1982). *Geomicrobiology*. New York, NY: Marcel Dekker Inc.

Friedrich, C. G., Rother, D., Bardischewsky, F., Quentmeier, A., and Fischer, J. (2001). Oxidation of reduced inorganic sulfur compounds by bacteria: emergence of a common mechanism? *Appl. Environ. Microbiol.* 67, 2873–2882. doi: 10.1128/AEM.67.7.2873-2882.2001

Fritz, P., Basharmal, G. M., Drimmie, R. J., Ibsen, J., and Qureshi, R. M. (1973). Oxygen isotope exchange between sulfate and water during bacterial reduction of sulfate. *Chem. Geol.* 79, 99–105.

Fry, B., Cox, J., Gest, H., and Hayes, J. M. (1986). Discrimination between 32-S and 34-S during bacterial metabolism of inorganic sulfur compounds. *J. Bacteriol.* 165, 328–330. doi: 10.1128/jb.165.1.328-330.1986

Fry, B., Gest, H., and Hayes, J. M. (1984). Isotope effects associated with the anaerobic oxidation of sulfide by the purple photosynthetic bacterium, *Chromatium vinosum*. *FEMS Microbiol. Lett.* 22, 283–287. doi: 10.1111/j.1574-6968.1984.tb00742.x

Fry, B., Gest, H., and Hayes, J. M. (1985). Isotope effects associated with the anaerobic oxidation of sulfite and thiosulfate by the photosynthetic bacterium, *Chromatium vinosum*. *FEMS Microbiol. Lett.* 27, 227–232. doi: 10.1111/j.1574-6968.1985.tb00672.x

Fry, B., Ruf, W., Gest, H., and Hayes, J. M. (1988). Sulfur isotope effects associated with the non-biological oxidation of sulfide in aqueous solution. *Chem. Geol.* 73, 205–210.

Gleisner, M., Herbert, R. B. Jr., and Frogner Kockum, P.C. (2006). Pyrite oxidation by *Acidithiobacillus ferrooxidans* at various concentrations of dissolved oxygen. *Chem. Geol.* 225, 16–29. doi: 10.1016/j.chemgeo.2005.07.020

Goldhaber, M. B. (1983). Experimental study of metastable sulfur oxyanion formation during pyrite oxidation at pH 6–9 and 30 _C. *Am. J. Sci.* 283, 193–217. doi: 10.2475/ajs.283.3.193

Habicht, K. S., Canfield, D. E., and Rethmeier, J. (1998). Sulfur isotope fractionation during bacterial reduction and disproportionation of thiosulfate and sulfite. *Geochim. Cosmochim. Acta* 62, 2585–2595. doi: 10.1016/S0016-7037(98)00167-7

Hallberg, K. B., Dopson, M., and Lindström, E. B. (1996). Reduced sulfur compound oxidation by *Thiobacillus caldus*. *J. Bacteriol.* 178, 6–11. doi: 10.1128/jb.178.1.6-11.1996

Hazeu, W., Batenburg-van der Vegte, W. H., Bos, P., van der Pas, R. K., and Kuenen, J. G. (1988). The production and utilization of intermediary elemental sulfur during the oxidation of reduced sulfur compounds by *Thiobacillus ferrooxidans*. *Arch. Microbiol.* 150, 574–579. doi: 10.1007/BF00408252

Hazeu, W., Bijleveld, W., Grotenhuis, J. T. C., Kakes, E., and Kuenen, J. G. (1986). Kinetics and energetics of reduced sulfur oxidation by chemostat cultures of *Thiobacillus ferrooxidans*. *Antonie Leeuwenhoek* 52, 507–518. doi: 10.1007/BF00423411

Heidel, C., Tichomirowa, M., and Junghans. M. (2009). The influence of pyrite grain size on the final oxygen isotope difference between sulfate and water in aerobic pyrite oxidation experiments. *Isotopes Environ. Health Stud.* 45, 321–342. doi: 10.1080/10256010903357001

Heidel, C., and Tichomirowa, M. (2010). The role of dissolved molecular oxygen in abiotic pyrite oxidation under acid pH conditions – experiments with 18O-enriched molecular oxygen. *Appl. Geochem.* 25, 1664–1675. doi: 10.1016/j.apgeochem.2010.08.014

Hoering, T. C., and Kennedy, J. W. (1957). The exchange of oxygen between sulfuric acid and water. *J. Am. Chem. Soc.* 79, 560–650. doi: 10.1021/ja01558a013

Holt, B. D., Kumar, R., and Cunningham, P. T. (1981). Oxygen-18 study of the aqueous phase oxidation of sulfur dioxide. *Atmos. Environ.* 17, 625–632. doi: 10.1016/0004-6981(83)90136-1

Houghton, J. L., Foustoukos, D., Flynn, T. M., Vetriani, C., Bradley, A. S., and Fike, D. A (2016). Thiosulfate oxidation by *Thiomicrospira thermophila*: metabolic flexibility in response to ambient geochemistry. *Environ. Microbiol.* 18, 3057–3072. doi: 10.1111/1462-2920.13232

Johnston, F., and McAmish, L. (1973). A study of the rates of sulfur production in acid thiosulfate solutions using S-35. *J. Colloid Interf. Sci.* 42, 112–119. doi: 10.1016/0021-9797(73)90013-1

Kaplan, I. R., and Rittenberg, S. C. (1964). Microbiological fractionation of sulfur isotopes. *J. Gen. Microbiol.* 34, 195–212. doi: 10.1099/00221287-34-2-195

Kappler, U., and Dahl, C. (2001). Enzymology and molecular biology of prokaryotic sulfite oxidation. *FEMS Microbiol. Lett.* 203, 1–9. doi: 10.1111/j.1574-6968.2001.tb10813.x

Kelly, D. (1982). Biochemistry of the chemolithotrophic oxidation of inorganic sulphur. *Philos. Trans. R. Soc. Lond. B* 298, 499–528. doi: 10.1098/rstb.1982.0094

Kelly, D. P. (1999). Thermodynamic aspects of energy conservation by chemolithotrophic sulfur bacteria in relation to the sulfur oxidation pathways. *Arch. Microbiol.* 171, 219–229. doi: 10.1007/s002030050703

Kelly, D. P. (2008). Stable sulfur isotope fractionation and discrimination between the sulfur atoms of thiosulfate during oxidation by *Halothiobacillus neapolitanus*. *FEMS Microbiol. Lett.* 282, 299–306. doi: 10.1111/j.1574-6968.2008.01146.x

Kelly, D. P., Chambers, L. A., and Trudinger, P. A. (1969). Cyanolysis and spectrophotometric estimation of trithionate in mixture with thiosulfate and tetrathionate. *Anal. Chem.* 41, 898–902. doi: 10.1021/ac60276a029

Kelly, D. P., and Wood, A. P. (1994). Synthesis and determination of thiosulfate and polythionates. *Methods Enzymol.* 243, 475–501. doi: 10.1016/0076-6879(94)43037-3

Kelly, D. P., and Wood, A. P. (1998). "Microbes of the sulfur cycle," in *Techniques in Microbial Ecology*, eds R. S. Burlage, R. Atlas, D. Stahl, G. Geesey, and G. Sayler (New York, NY:Oxford University Press), 31–57.

Kletzin, A. (1989). Coupled enzymatic production of sulfite, thiosulfate, and hydrogen sulfide from sulfur: purification and properties of a sulfur oxygenase reductase from the facultatively anaerobic archaebacterium *Desulfurolobus ambivalens*. *J. Bacteriol.* 171, 1638–1643. doi: 10.1128/jb.171.3.1638-1643.1989

Knickerbocker, C., Nordstrong, D., and Southam, G. (2000). The role of blebbing in overcoming the hydrophobic barrier during biooxidation of elemental sulfur by *Thiobacillus thiooxidans*. *Chem. Geol.* 169, 425–433. doi: 10.1016/S0009-2541(00)00221-7

Lloyd, R. M. (1968). Oxygen isotope behavior in the sulfate water system. *J. Geophys. Res.* 73, 6099–6110. doi: 10.1029/JB073i018p06099

Mandernack, K. W., Fogel, M. L., Tebo, B. M., and Usui, A. (1995). Oxygen isotope analyses of chemically and microbially produced manganese

oxides and manganates. *Geochim. Cosmochim. Acta* 59, 4409–4425. doi: 10.1016/0016-7037(95)00299-F

McCready, R. G. L., and Krouse, H. R. (1982). Sulfur isotope fractionation during the oxidation of elemental sulfur by Thiobacilli in a Solonetzic soil. *Can. J. Soil Sci.* 62, 105–110. doi: 10.4141/cjss82-012

Meulenberg, R., Pronk, J. T., Hazeu, W., Bos, P., and Kuenen, J. G. (1992). Oxidation of reduced sulphur compounds by intact cells of *Thiobacillus acidophilus*. *Arch. Microbiol.* 157, 161–168.

Meulenberg, R., Scheer, E. J., Pronk, T., Hazeu, W., Bos, P., and Kuenen, J. G. (1993). Metabolism of tetrathionate in *Thiobacillus acidophilus*. *FEMS Microbiol. Lett.* 112, 167–172. doi: 10.1111/j.1574-6968.1993.tb06443.x

Mizutani, Y., and Rafter, A. T. (1973). Isotopic behaviour of sulphate oxygen in the bacterial reduction of sulphate. *Geochem. J.* 6, 183–191. doi: 10.2343/geochemj.6.183

Mizutani, Y., and Rafter, T. (1969). Bacterial fractionation of oxygen isotopes in the reduction of sulfate and in the oxidation of sulfur. *New Zeal. J. Sci.* 12, 60–68.

Müller, I. A., Brunner, B., Breuer, C., Coleman, M., and Bach, W. (2013a). The oxygen isotope equilibrium fractionation between sulfite species and water. *Geochim. Cosmochim. Acta* 120, 562−581. doi: 10.1016/j.gca.2013.06.037

Müller, I. A., Brunner, B., and Coleman, M. (2013b). Isotopic evidence of the pivotal role of sulfite oxidation in shaping the oxygen isotope signature of sulfate. *Chem. Geol.* 354, 186–202. doi: 10.1016/j.chemgeo.2013.05.009

Nakai, N., and Jensen, M. L. (1964). The kinetic isotope effect in the bacterial reduction and oxidation of sulfur. *Geochim. Cosmochim. Acta* 28, 1893–1912. doi: 10.1016/0016-7037(64)90136-X

Pearson, F. J., and Rightmire, C. T. (1980). "Sulfur and oxygen isotopes in aqueous sulfur compounds," in *Handbook of Environmental Isotope,* eds P. Fritz and J. C. H. Fontes (Amsterdam: Elsevier), 226–258.

Poser, A., Vogt, C., Knöller, K., Ahlheim, J., Weiss, H., Kleinsteuber, S., et al. (2014). Stable sulfur and oxygen isotope fractionation of anoxic sulfide oxidation by two different enzymatic pathways. *Environ. Sci. Technol.* 48, 9094–9102. doi: 10.1021/es404808r

Poser, A., Vogt, C., Knöller, K., Sorokin, D. Y., Finster, K. W., and Richnow, H. H. (2016). Sulfur and oxygen isotope fractionation during bacterial sulfur disproportionation under anaerobic haloalkaline conditions. *Geomicrobiol. J.* 33, 934–941. doi: 10.1080/01490451.2015.1128993

Pronk, J. T., Meulenberg, R., Hazeu, W., Bos, P., and Kuenen, J. G. (1990). Oxidation of reduced inorganic sulphur compounds by acidophilic thiobacilli. *FEMS Microbiol Lett.* 75, 293–306. doi: 10.1111/j.1574-6968.1990.tb04103.x

Ramírez, P., Guiliani, N., Valenzuela, L., Beard, S., and Jerez, C. A. (2004). Differential protein expression during growth of *Acidithiobacillus ferrooxidans* on ferrous iron, sulfur compounds, or metal sulfides. *Appl. Environ. Microbiol.* 70, 4491–4498. doi: 10.1128/AEM.70.8.4491-4498.2004

Rennie, V. C. F., and Turchyn, A. V. (2014). The preservation of and in carbonate-associated sulfate during marine diagenesis: a 25 Myr test case using marine sediments. *Earth Planet. Sci. Lett.* 395, 13–23 doi: 10.1016/j.epsl.2014.03.025

Rohwerder, T., and Sand, W. (2003). The sulfane sulfur of persulfides is the actual substrate of the sulfur-oxidizing enzymes from *Acidithiobacillus* and *Acidiphilium* spp. *Microbiology* 149, 1699–1709. doi: 10.1099/mic.0.26212-0

Rye, R., Bethke, P., and Wasserman, M. (1992). The stable isotope geochemistry of acid sulfate alteration. *Econ. Geol.* 87, 225–262. doi: 10.2113/gsecongeo.87.2.225

Sanliyuksel Yucel, D., Balci, N., and Baba, A. (2016). Generation of acid mine lakes associated with abandoned coal mines in Northwest Turkey. *Arch. Environ. Contam. Toxicol.* 70, 757–782. doi: 10.1007/s00244-016-0270-z

Schippers, A. (2004). "Biogeochemistry of metal sulfide oxidation in mining environments, sediments, and soils," in *Sulfur Biogeochemistry –Past and Present. Special Paper 379,* eds J. P. Amend, K. J. Edwards, and T. W. Lyons (Boulder, CO: Geological Society of America), 49–62.

Schippers, A., Jozsa, P.-G., and Sand, W. (1996). Sulfur chemistry in bacterial leaching of pyrite. *Appl. Environ. Microbiol.* 62, 3424–3231.

Schippers, A., and Sand, W. (1999). Bacterial Leaching of metal sulfides proceeds by two indirect mechanisms via thiosulfate or via polysulfides and sulfur. *Appl. Environ. Microbiol.* 65, 319–321.

Seal, R. R. (2003). "Stable-isotope geochemistry of mine waters and related solids," in *Environmental Aspects of Mine Wastes,* Short Course Series, 31, eds J. L. Jambor, D. W. Blowes (Vancouver, BC: Mineralogical Association of Canada), 303–334.

Sessions, A. L., and Hayes, J. M. (2005). Calculation of hydrogen isotopic fractionations in biogeochemical systems. *Geochim. Cosmochim. Acta* 69, 593–597. doi: 10.1016/j.gca.2004.08.005

Shiers, D. W., Ralph, D. E., and Watling, H. R. (2011). Batch culture of *Acidithiobacillus caldus* on tetrathionate. *Biochem. Eng. J.* 54, 185–191 doi: 10.1016/j.bej.2011.02.018

Smith, L., Hendry, J. M., Wassenaar, L., and Lawrence, J. (2012). Rates of microbial elemental sulfur oxidation and ^{18}O and ^{34}S isotopic fractionation under varied nutrient and temperature regimes. *Appl. Geochem.* 27, 186–196. doi: 10.1016/j.apgeochem.2011.10.003

Smock, A. M., Böttcher, M. E., and Cypionka, H. (1998). Fractionation of sulfurisotopes during thiosulfate reduction by *Desulfovibrio desulfuricans*. *Arch. Microbiol.* 169, 460–463. doi: 10.1007/s002030050597

Steudel, R. (2003). Inorganic polysulfanes H2Sn with n > 1. *Top. Curr. Chem.* 231, 99–125. doi: 10.1007/b13182

Steudel, R., Göbel, T., and Holdt, G. (1988). The molecular decomposition of hydrophilic sulfur sols prepared by acid decomposition of thiosulfate. *Z. Naturforsch B* 43, 203–218. doi: 10.1515/znb-1988-0212

Steudel, R., Holdt, G., Göbel, T., and Hazeu, W. (1987). Chromatographic separation of higher polythionates SnO62 (n = 3... 22) and their detection in cultures of *Thiobacillus ferrooxidans;* molecular composition of bacterial sulfur secretions. *Angew. Chem. Int. Ed. Engl.* 26, 151–153. doi: 10.1002/anie.198701511

Suzuki, I. (1974). Mechanisms of inorganic oxidation and energy coupling. *Annu. Rev. Microbiol.* 28, 85–102. doi: 10.1146/annurev.mi.28.100174.000505

Suzuki, I. (1999). Oxidation of inorganic sulfur compounds: chemical and enzymatic reactions. *Can. J. Microbiol.* 45, 97–105. doi: 10.1139/w98-223

Suzuki, I., Chan, C. W., and Takeuchi, T. L. (1994). "Oxidation of inorganic sulfur compounds by thiobacilli," in *Environmental Geochemistry of Sulfide Oxidation*, eds C. N. Alpers and D. W. Blowes (Washington, DC: American Chemical Society), 61–67

Swinnen, I. A. M., Bernaerts, K., Dens, E. J. J., Geeraerd, A. H., and Van Impe, J. F. (2004). Predictive modeling of the microbial lag phase: a review. *Int. J. Food Microbiol.* 94, 137–159. doi: 10.1016/j.ijfoodmicro.2004.01.006

Takano, B., Zheng, Q., and Ohsawa, S. (2000). A telemetering system for monitoring aqueous polythionates in an active crater lake. *J. Volcanol. Geotherm. Res.* 97, 397–406. doi: 10.1016/S0377-0273(99)00163-8

Taylor, B., Wheeler, M., and Nordstrom, D. (1984). Stable isotope geochemistry of acid mine drainage: experimental oxidation of pyrite. *Geochim. Cosmochim. Acta* 48, 2669–2678. doi: 10.1016/0016-7037(84)90315-6

Thurston, R. S., Mandernack, K. W., and Shanks, I. I. I., W. C. (2010). Laboratory chalcopyrite oxidation by *Acidithiobacillus ferrooxidans*: oxygen and sulfur isotope fractionation. *Chem. Geol.* 269, 252–261. doi: 10.1016/j.chemgeo.2009.10.001

Tichomirowa, M., and Junghans, M. (2009). Oxygen isotope evidence for sorption of molecular oxygen to pyrite surface sites and incorporation into sulfate in oxidation experiments. *Appl. Geochem.* 24, 2072–2092. doi: 10.1016/j.apgeochem.2009.08.002

Toran, L., and Harris, R. F. (1989). Interpretation of sulphur and oxygen isotopes in biological and abiological sulphide oxidation. *Geochim. Cosmochim. Acta.* 53, 2341–2348. doi: 10.1016/0016-7037(89)90356-6

van Stempvoort, D., and Krouse, H. (1994). "Controls of d18O in Sulfate: a review of experimental data and application to specific environments," in *Environmental Geochemistry of Sulfide Oxidation,* eds C. N. Alpers and D. W. Blowes (Washington, DC: American Chemical Society), 446–480.

Wankel, S. D., Bradley, A. S., Eldridge, D. L., and Johnston, D. T. (2014). Determination and application of the equilibrium oxygen isotope effect between water and sulfite. *Geochim. Cosmochim. Acta* 125, 694–711. doi: 10.1016/j.gca.2013.08.039

Williamson, M. A., and Rimstidt, J. D. (1993). The rate of decomposition of the ferric-thiosulfate complex in acidic aqueous solutions. *Geochim. Cosmochim. Acta* 57, 3555–3561. doi: 10.1016/0016-7037(93)90138-M

Xu, Y., and Schoonen, M. A. A. (1995). The stability of thiosulfate in the presence of pyrite in low temperature aqueous solutions. *Geochim. Cosmochim. Acta* 59, 4605–4622. doi: 10.1016/0016-7037(95)00331-2

Xu, Y., Schoonen, M. A. A., Nordstrom, D. K., Cunningham, K. M., and Ball, J. W. (2000). Sulfur geochemistry of hydrothermal waters in Yellowstone National Park, Wyoming, U. S. A., II: F*ormation and decomposition of thiosulfate*

and polythionates in Cinder Pool. J. Volcanol. Geotherm. Res. 97, 407–423. doi: 10.1016/S0377-0273(99)00173-0

Yin, H., Zhang, X., Li, X., He, Z., Liang, Y., Guo, X., et al. (2014). Whole-genome sequencing reveals novel insights into sulfur oxidation in the extremophile *Acidithiobacillus thiooxidans*. *BMC Microbiol.* 14:179. doi: 10.1186/1471-2180-14-179

Yu, J. Y., McGenity, T., and Coleman, M. (2001). Solution chemistry during the lag phase and exponential phase of pyrite oxidation by *Thiobacillus ferrooxidans*. *Chem. Geol.* 175, 307–317. doi: 10.1016/S0009-2541(00)00332-6

Zerkle, A. L., Farquhar, J., Johnston, D. T., Cox, R. P., and Canfield, D. E. (2009). Fractionation of multiple sulfur isotopes during phototrophic oxidation of sulfide and elemental sulfur by a green sulfur bacterium. *Geochim. Cosmochim. Acta* 73, 291–306. doi: 10.1016/j.gca.2008.10.027

Zopfi, J., Ferdelman, T. G., and Fossing, H. (2004). Distribution and fate of sulfur intermediates – sulfite, tetrathionate, thiosulfate, and elemental sulfur – in marine sediments. *Geol. Soc. Am. Spec. Pap.* 379, 97–116. doi: 10.1130/0-8137-2379-5.97

Conflict of Interest Statement: The authors declare that the research was conducted in the absence of any commercial or financial relationships that could be construed as a potential conflict of interest.

frontiers in Earth Science

ORIGINAL RESEARCH
published: 02 August 2017
doi: 10.3389/feart.2017.00062

Rates and Cycles of Microbial Sulfate Reduction in the Hyper-Saline Dead Sea over the Last 200 kyrs from Sedimentary $\delta^{34}S$ and $\delta^{18}O_{(SO4)}$

Adi Torfstein[1,2]* *and Alexandra V. Turchyn*[3]

[1] Institute of Earth Sciences, Hebrew University of Jerusalem, Jerusalem, Israel, [2] Interuniversity Institute for Marine Sciences, Eilat, Israel, [3] Department of Earth Sciences, University of Cambridge, Cambridge, United Kingdom

We report the $\delta^{34}S$ and $\delta^{18}O_{(SO4)}$ measured in gypsum, pyrite, and elemental sulfur through a 456-m thick sediment core from the center of the Dead Sea, representing the last ~200 kyrs, as well as from the exposed glacial outcrops of the Masada M1 section located on the margins of the modern Dead Sea. The results are used to explore and quantify the evolution of sulfur microbial metabolism in the Dead Sea and to reconstruct the lake's water column configuration during the late Quaternary. Layers and laminae of primary gypsum, the main sulfur-bearing mineral in the sedimentary column, display the highest $\delta^{34}S$ and $\delta^{18}O_{(SO4)}$ in the range of 13–28 and 13–30‰, respectively. Within this group, gypsum layers deposited during interglacials display lower $\delta^{34}S$ and $\delta^{18}O_{(SO4)}$ relative to those associated with glacial or deglacial stages. The reduced sulfur phases, including chromium reducible sulfur, and secondary gypsum crystals are characterized by extremely low $\delta^{34}S$ in the range of −27 to +7‰. The $\delta^{18}O_{(SO4)}$ of the secondary gypsum in the M1 outcrop ranges from 8 to 14‰. The relationship between $\delta^{34}S$ and $\delta^{18}O_{(SO4)}$ of primary gypsum suggests that the *rate* of microbial sulfate reduction was lower during glacial relative to interglacial times. This suggests that the freshening of the lake during glacial wet intervals, and the subsequent rise in sulfate concentrations, slowed the rate of microbial metabolism. Alternatively, this could imply that sulfate-driven anaerobic methane oxidation, the dominant sulfur microbial metabolism today, is a feature of the hypersalinity in the modern Dead Sea. Sedimentary sulfides are quantitatively oxidized during epigenetic exposure, retaining the lower $\delta^{34}S$ signature; the $\delta^{18}O_{(SO4)}$ of this secondary gypsum is controlled by oxygen atoms derived equally from atmospheric oxygen and from water, which is likely a unique feature in this hyperarid environment.

Keywords: Dead Sea, microbial sulfate reduction, isotope fractionation, sulfates, sulfide oxidation, paleolimnology

OPEN ACCESS

Edited by:
Tanja Bosak, Massachusetts Institute of Technology, United States

Reviewed by:
Susan Childers, Colby College, United States
David T. Wang, Massachusetts Institute of Technology, United States

***Correspondence:**
Adi Torfstein
adi.torf@mail.huji.ac.il

Specialty section:
This article was submitted to Microbiological Chemistry and Geomicrobiology, a section of the journal Frontiers in Earth Science

Received: *26 March 2017*
Accepted: *11 July 2017*
Published: *02 August 2017*

Citation:
Torfstein A and Turchyn AV (2017) Rates and Cycles of Microbial Sulfate Reduction in the Hyper-Saline Dead Sea over the Last 200 kyrs from Sedimentary $\delta^{34}S$ and $\delta^{18}O_{(SO4)}$. Front. Earth Sci. 5:62. doi: 10.3389/feart.2017.00062

INTRODUCTION

Overview

The biological use of sulfur in its multiple valence states is a primary tracer of the redox dynamics in lacustrine environments both in the modern environment and over geological time (Claypool et al., 1980; Strauss, 1997; Canfield, 2004; Bottrell and Newton, 2006; and references therein). The microbially-mediated reduction of sulfate to sulfide, termed "microbial sulfate reduction," involves

a large sulfur isotopic fractionation where the lighter ^{32}S isotope is preferentially reduced relative to the heavier ^{34}S. The magnitude of this sulfur isotope fractionation can range between 2 and 70‰ and is largely a function of the rate of microbial sulfate reduction, which itself is a function of temperature, sulfate concentration, and organic carbon supply (Kaplan and Rittenberg, 1964; Chambers and Trudinger, 1979; Canfield, 1998; Habicht et al., 1998; Wortmann et al., 2007; Sim et al., 2011). Changes in the redox conditions of bottom waters or within sediments can impart measureable sulfur isotopic differences in sulfate and sulfide minerals preserved in the sedimentary record; these isotopic changes have been used to reconstruct past redox conditions and the behavior of the biogeochemical sulfur cycle. In particular, the sulfur isotope composition of sulfate minerals has been used to study the evolution of closed or semi-closed water bodies such as the Black Sea (e.g., Lyons, 1997; Neretin et al., 2003), Lake Baikal (Watanabe et al., 2004), the Messinian Mediterranean (e.g., Lu et al., 2001), Lake Eyre (e.g., Baas-Becking and Kaplan, 1956), Death Valley (Yang et al., 1997), the Estancia Basin in New Mexico (Szynkiewicz et al., 2009), and the lacustrine deposits of the Green River Formation (e.g., Tuttle and Goldhaber, 1993), among others. The isotopic signature of the sedimentary archive reflects past patterns of sulfur isotope composition of the lake, allowing for the reconstruction of water column configuration, water sources, and in turn, regional climatic-hydrologic trends (e.g., Claypool et al., 1980; Strauss, 1997).

Typically, arid continental basins are characterized by low precipitation-to-evaporation ratios which result in the development of hypersaline water bodies and high deposition rates of evaporate minerals such as carbonate and gypsum (e.g., Great Salt Lake of Utah, Lake Chad of Central Africa, the Caspian Sea, and the Dead Sea; Eugster, 1980). Under such conditions, climate perturbations can induce larger freshwater influx triggering density stratification of the water column that disconnects the lower body from the atmosphere, leading to the development of anoxic conditions. Because sulfur is a redox-sensitive element the study of the sulfur cycle in terminal lacustrine bodies can impart important information on regional and global hydrological patterns.

Of the above mentioned lacustrine bodies, the Dead Sea is the most saline deep lake in the world today [~300 m water depth, water level 430 m below mean sea level (mbmsl), salinity ~340 g/l], and its water levels and limnological history have been shown to reflect regional climate patterns, themselves controlled by northern hemisphere climate change during the Quaternary (e.g., Stein, 2001; Bartov et al., 2003; Enzel et al., 2003; Bookman Ken-Tor et al., 2004; Torfstein et al., 2013b). Due to its high salinity, any input of freshwater induces density stratification that can persist for several years. Long term lake stratification also developed in the geological past, when freshwater input was significantly higher than present, and was sustained for several thousands of years. Such a stratified water column can develop intense anoxic conditions in the lower layer (e.g., Froelich et al., 1979; Arndt et al., 2013). This deepwater anoxia drives changes in microbial communities and biogeochemical cycles of redox sensitive elements like iron, manganese, and sulfur.

In spite of the high salinity in the modern Dead Sea, evidence for microbial sulfate reduction, likely coupled to anaerobic methane oxidation, has been found in ground water and sedimentary deposits (Oldenburg et al., 2000a,b; Gavrieli et al., 2001; Avrahamov et al., 2014; Thomas et al., 2016). Microbial sulfate reduction has been inferred from the coexistence of aqueous sulfate and sulfide, as well as measurements of sulfur isotopes that suggest a sulfur isotope fractionation of about 30‰ in the modern Dead Sea (Gavrieli et al., 2001). As the lake was hypersaline over the course of the Quaternary (Torfstein et al., 2009), with a similar configuration to the modern lake, it is likely that microbial sulfate reduction dominated the oxidation of organic carbon in the past as well. There is further evidence for microbial sulfate reduction in late Quaternary deposits exposed along the lake margins, in the form of a sulfur isotope offset between gypsum and sulfur nodules found within gypsum. This offset has been interpreted to reflect microbial sulfate reduction under carbon-limited conditions (Torfstein et al., 2005, 2008; Bishop et al., 2013). Thus far, evidence of past microbial sulfate reduction has been limited to the marginal and exposed sites along the Dead Sea, precluding the direct reconstruction of the composition and history of the deep anoxic layer in the deep center of the lake.

Here, we focus on the isotopic composition of sulfur ($\delta^{34}S$) and sulfate-bound oxygen [$\delta^{18}O_{(SO4)}$] in primary and secondary gypsum, reduced sulfide minerals, and native sulfur. Samples are studied in the deep center of the Dead Sea and compared with an exposed marginal lacustrine sedimentary record (**Figure 1**). In particular, we report for the first time results from the recent Dead Sea Deep Drilling Project (DSDDP), which recovered a continuous 456 m thick core from the deep center of the modern lake spanning the last ~200,000 years (Neugebauer et al., 2014; Torfstein et al., 2015). We use the results to reconstruct

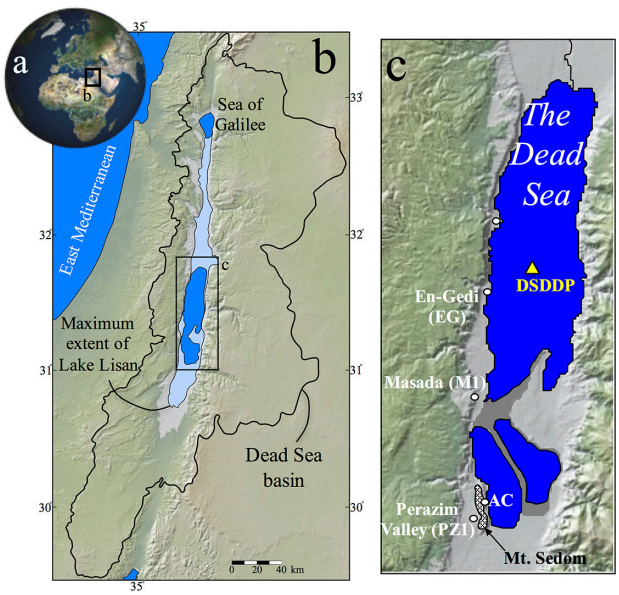

FIGURE 1 | Location map.

the evolution of redox conditions in the deep-water column, understand the rate of microbial sulfate reduction and how it links to the source of carbon, and explore the oxidation pathways of sulfide minerals in the Dead Sea Basin (DSB).

The Dead Sea

Limnology

The Quaternary Dead Sea lacustrine bodies evolved from the Pliocene Sedom Lagoon, which derived its chemical constituents from ingressing seawater and interaction with the carbonate wall-rock, and resulted in the development of the unique calcium-chloride composition of the DSB brines (Zak, 1967; Starinsky, 1974; Stein et al., 2000, 2002). After the disconnection of the Sedom lagoon from the open sea around 3 Ma (Torfstein et al., 2009; Belmaker et al., 2013; Matmon et al., 2014), the limnological and geochemical history of the closed and terminal water bodies that subsequently occupied the DSB (the early- to mid-Pleistocene Lake Amora, last glacial Lake Lisan, and the Holocene Dead Sea) was controlled by the interaction between the brine and freshwater input (Katz et al., 1977; Stein, 2001; Gavrieli and Stein, 2006; Katz and Starinsky, 2008).

The Dead Sea brines are characterized by a distinct enrichment in calcium and chloride (16,700 and 219,700 mg/l, respectively; Stein et al., 1997), while incoming freshwater runoff, which largely drains carbonate terrains, is enriched in bicarbonate (∼200 mg/l; Stein et al., 1997). The high calcium concentrations in the lake impose very low concentrations of bicarbonate and sulfate through the saturation of calcium carbonate and gypsum ($CaSO_4{\cdot}2H_2O$), respectively. Incoming freshwater, delivering bicarbonate, swiftly precipitates as calcium carbonate (dominantly aragonite), while dissolved sulfate (also introduced into the mixolimnion from freshwater sources) accumulates until gypsum saturation is eventually reached. At that point, gypsum crystals settle through the water column to the anoxic monimolimnion, where gypsum is under saturated due to the removal of sulfate through microbial sulfate reduction and dissolves (Torfstein et al., 2005).

Sedimentology

The Dead Sea lacustrine deposits include sequences of alternating aragonite and detrital laminae (*aad facies,* **Figure 2**), which represent annual deposition cycles of primary inorganic aragonite precipitated from the lake during summer evaporation and silt-size detritus washed into the lake during winters (Begin et al., 1974; Katz et al., 1977; Stein et al., 1997). The *aad facies* reflects a wet hydrological regime with high freshwater and thus bicarbonate input, and is associated with relatively higher lake levels. Increasing aridity is reflected by decreased amounts of aragonite relative to detritus, then precipitation of gypsum, followed by halite. Brown silt layers, a few cm thick or more, mark enhanced activity of freshwater floods during relatively low-level intervals.

These lithological types appear throughout the DSDDP core (**Figures 2–4**) as well as in sediment outcrops along the margins of the modern Dead Sea, such as the M1 sedimentary section located on the foothills of the Masada archeological site. The main interval that is exposed in the M1 sedimentary section is the last glacial Lisan Formation (70–14 ka; Kaufman, 1971; Haase-Schramm et al., 2004). Massive halite units that reflect major lake level drawdowns occur uniquely in the deep DSDDP core, and are synchronous with interglacial cycles (Torfstein et al., 2015).

Sulfur and Sulfate Bound Oxygen

The sulfur isotopic composition (measured as $^{34}S/^{32}S$ reported relative to the Vienna Canon Diablo Troilite standard in parts-per-thousand, or permil units) of sulfate or other sulfur species in sedimentary systems is often controlled by microbial reduction of sulfate that imposes a large sulfur isotope fractionation among the various sulfur species (Rees, 1973; Cypionka et al., 1998; Habicht et al., 1998). Microbial sulfate reduction coupled to organic carbon oxidation is described through the simplified equation:

$$2CH_2O + SO_4^{2-} \rightarrow 2HCO_3^- + H_2S \quad (1)$$

Specifically, sulfur isotopes in sulfate increase monotonically as the ^{32}S atom is slowly distilled into the product sulfide during microbial sulfate reduction; the rate at which the $^{34}S/^{32}S$ ratio in the residual sulfate increases is a function largely of the sulfate reduction rate as well as temperature, organic carbon source, microbial community, pressure, and other environmental factors. Microbial sulfate reduction also fractionates the sulfate-bound oxygen isotopes [$\delta^{18}O_{(SO4)}$ is the ratio of $^{18}O/^{16}O$ reported vs. Vienna-Standard Mean Ocean Water in permil units], whereby the residual sulfate is preferentially enriched in the heavy isotope (^{18}O).

In the microbial cell however, oxygen isotopes in intermediate valence state sulfur species such as sulfite, can equilibrate with water and these intermediate valence state species may return to the extracellular sulfate pool (Brunner et al., 2005; Brunner and Bernasconi, 2005; Antler et al., 2013). Thus, the relative change in the sulfur and oxygen isotope composition of sulfate over the onset of microbial sulfate reduction has been shown to reflect the degree of recycling of sulfur within cells (over the amount which is unidirectionally reduced). Because of this, the oxygen isotope ratio of sulfate has become a powerful tool for exploring sedimentary and aqueous sulfur redox dynamics (Brunner et al., 2005; Wortmann et al., 2007; Antler et al., 2013; Knossow et al., 2015). The oxygen isotope composition of sulfate is "fixed" the last time that any reduced valence state sulfur species is oxidized to sulfate (the oxygen atoms in sulfate do not subsequently readily equilibrate or exchange with water). Most sulfide oxidation pathways involve only small sulfur isotope fractionations, while the oxygen isotope composition of the resulting sulfate depends on the variable contribution of oxygen atoms from water and from atmospheric oxygen (Balci et al., 2007; Calmels et al., 2007). Thus, the $\delta^{18}O_{(SO4)}$ often reflects the pathway by which the reduced sulfur was last oxidized plus any equilibration with water along the oxidation or reduction pathway. Together, the measurement of sulfur and oxygen isotopes in sulfate provide a powerful tool for reconstructing the microbially-mediated redox cycling of sulfur in a range of marine, marginal marine, and lacustrine environments (e.g., Claypool et al., 1980; Aharon and Fu, 2000;

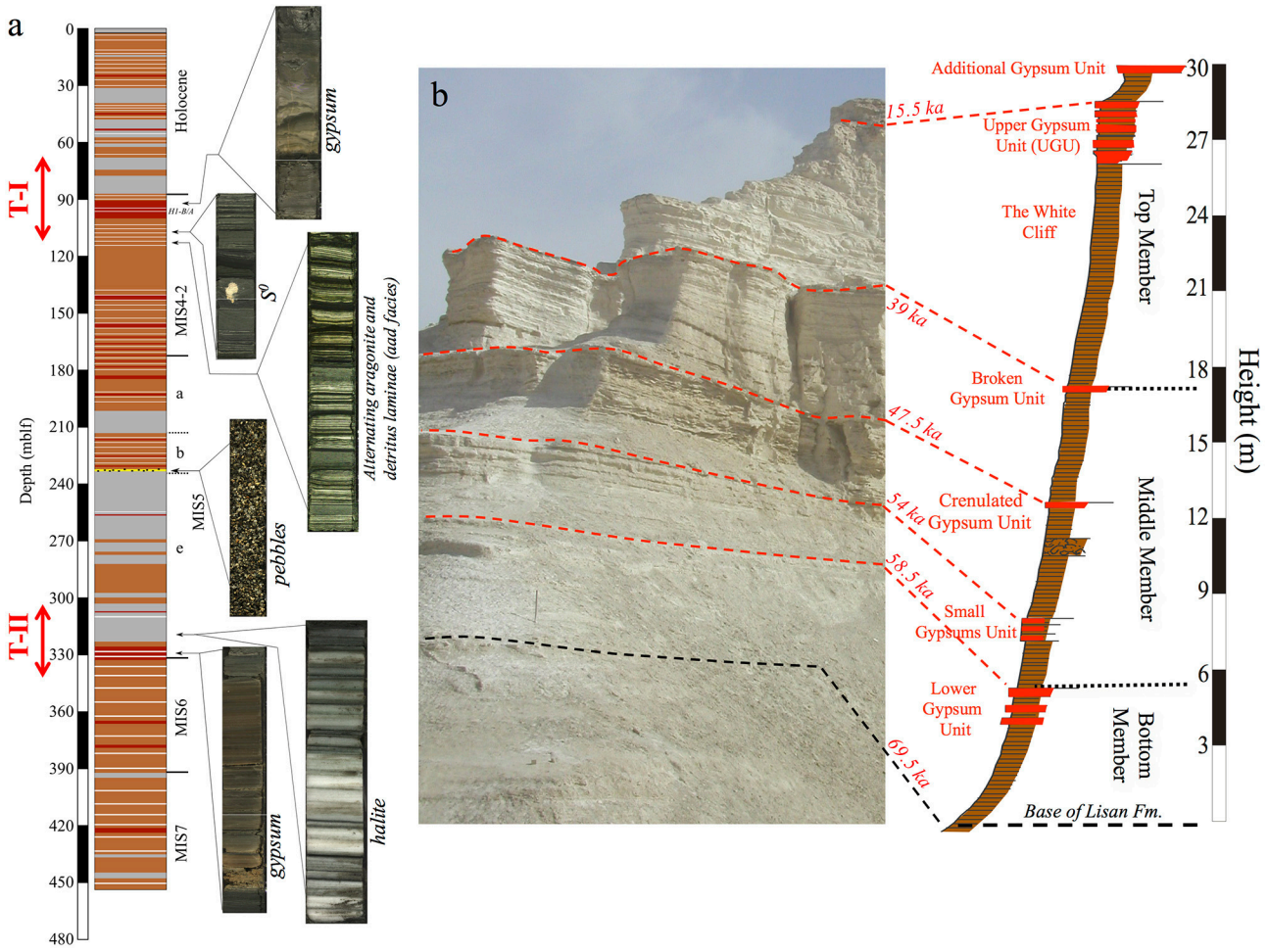

FIGURE 2 | (a) Generalized columnar section of the Dead Sea Deep Drilling Project (DSDDP) core, **(b)** Masada M1 section. Core photos of several sediment facies are presented in **(a)**. Legend for columnar section: gray, halite; red, gypsum; white stripes, aad facies; brown, marl; yellow layer (at 234 mblf), pebble layer. The timing of Termination –II and –I is marked by red arrow left of the columnar section. Ages of marker layers in **(b)** are from Torfstein et al. (2013a). Note that the Masada M1 section of the Lisan Formation, corresponds to depths of ~177–90 mblf in the DSDDP core.

Bottrell and Newton, 2006; Leavitt et al., 2013; Antler et al., 2015).

Previous studies have explored the sulfur cycle in the Dead Sea and its precursors over the late Quaternary but have been limited to the marginal outcrops of the Dead Sea. The density-driven stratification during increased freshwater influx to the Dead Sea partitioned aqueous sulfur into two distinct and separated reservoirs; ^{34}S depleted sedimentary sulfide minerals (resulting from water column microbial sulfate reduction) and ^{34}S-enriched sulfate that remains in the water column and is found in gypsum beds that precipitate during lake overturn. The longer and stronger the persistence of anoxic conditions in the stratified lake during wet periods, the thicker and more ^{34}S-enriched the gypsum that precipitates when conditions turn arid and the lake level declines resulting in water column mixing (Torfstein et al., 2008, 2005). This interpretation of the evolution of the biogeochemical sulfur cycle over hydrological changes in the Dead Sea derives entirely from measurements of ^{34}S-enriched gypsum (ranging between ~ −25 and +30‰) from the lake margin deposits; thus far no sedimentary sulfide minerals have been found in the marginal outcrops. By contrast, secondary gypsum, found in the Lisan Formation (Fm.) in the form of fine laminae or micro-concretions, displays ^{34}S-depleted compositions unlike the primary gypsum beds (Torfstein et al., 2005, 2008). These secondary gypsum crystals have been interpreted to derive from the oxidation of the (missing) reduced sulfur minerals initially formed by water column microbial sulfate reduction in the Dead Sea.

METHODS

Sample Collection

Most of the samples studied here were retrieved from the Dead Sea Deep Drilling Project (DSDDP) core, which was acquired by the International Continental Drilling Program (ICDP) campaign during 2010–2011 (Neugebauer et al., 2014; Torfstein

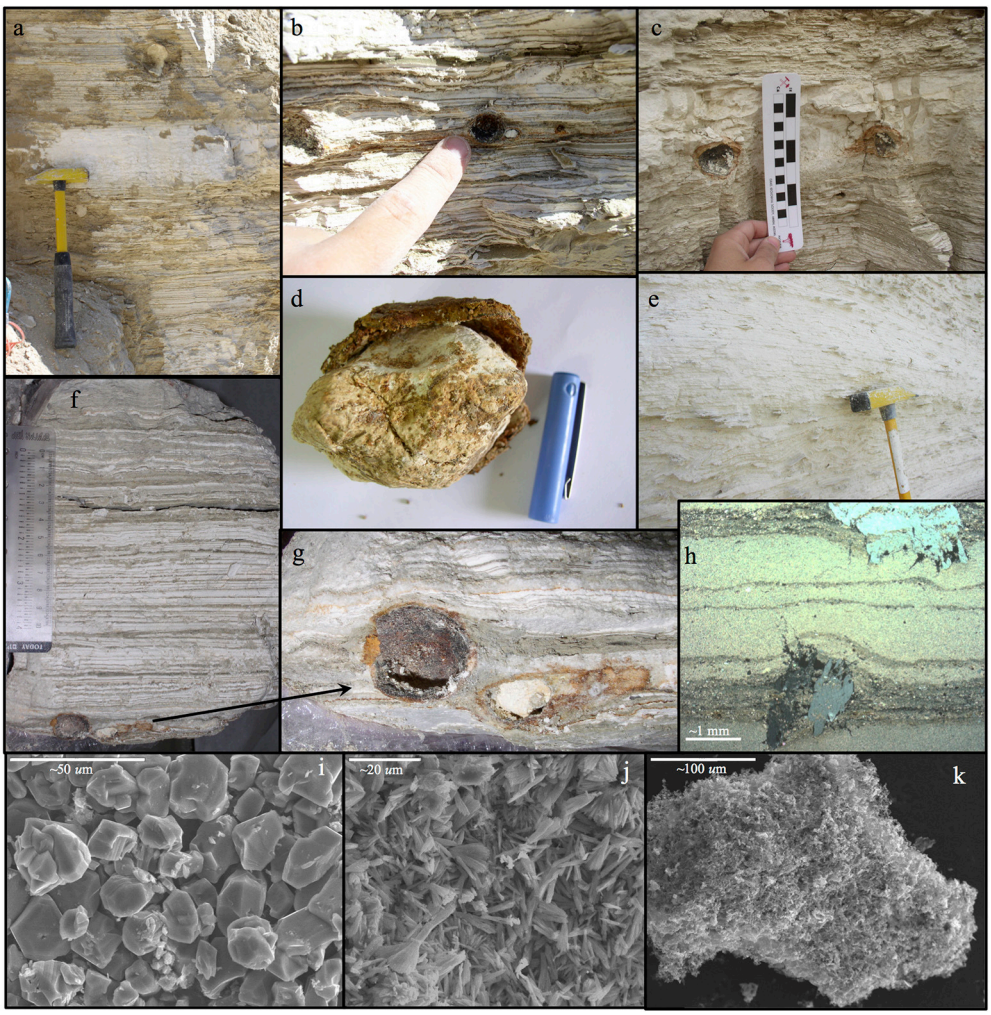

FIGURE 3 | (a) Native sulfur nodule in aragonite-detritus sequence ∼20 cm above the Lower Gypsum Unit (M1), **(b)** Nodules in aragonite-detritus outcrop. The black coating of the extracted nodules and the yellow native sulfur nodule on the right, **(c)** Native sulfur nodules in massive gypsum layer, **(d)** Native sulfur nodule in its crust, comprised of secondary gypsum and Fe-oxides, **(e)** Aragonite-detritus sequence of the Lisan Formation at M1. The abundant secondary gypsum concretions and bulges throughout the sequence, **(f,g)** Native sulfur nodules at the base of a field sample extracted from between the gypsum units comprising the Lower Gypsum Unit at M1, **(h)** Thin section under polarized light exhibiting micro secondary gypsum concretions offsetting surrounding aragonite laminae (from Haliva-Cohen et al., 2012). The concretion at the lower part of **(h)** is ∼1 mm thick from bottom to top, **(i)** SEM magnification of primary gypsum crystals, **(j)** SEM magnification of aragonite needles, **(k)** SEM magnification of a native sulfur particle.

et al., 2015). Additional samples are from the Masada (M1) section, Arubotaim Cave (AC) section, and En Gedi (EG) section exposed on the western margins of the Dead Sea (**Figure 1**), representing the last glacial Lisan Fm., mid-Pleistocene Amora Fm., and Holocene Ze'elim Fm., respectively. The samples consist of primary gypsum layers, secondary gypsum laminae and micro-concretions, soluble salts, and marly silt (mud) samples, from which sulfide phases were extracted (see below).

Sample Processing and Analysis

The primary and secondary gypsum minerals were dissolved in a sodium chloride saturated solution (∼50 g/L). A super-saturated barium chloride solution (∼30 g/L) was added to the effluent to precipitate the aqueous sulfate from gypsum dissolution as barite ($BaSO_4$). The barite was weighed into tin and silver capsules and analyzed for sulfur and oxygen isotopes, respectively, at the University of Cambridge in the Godwin Laboratory. For sulfur isotopes vanadium pentoxide was added as a combustion agent. Sulfur isotopes were analyzed through combustion to SO_2 in a Flash Element Analyzer coupled by continuous helium flow to a Delta Advantage mass spectrometer (CF-GS-IRMS – Thermo Finnegan). Samples for sulfur isotopes were bracketed by international standard NBS-127 (samples were corrected to NBS-127 $\delta^{34}S = 20.3‰$, stdev = 0.2‰ based on repeat analysis of the standards and blind replicates). Oxygen isotopes in sulfate were analyzed in triplicate through pyrolysis in a TC/EA coupled by continuous helium flow to a Delta Advantage mass spectrometer (GS-CF-IRMS – Thermo Finnegan). Samples were bracketed

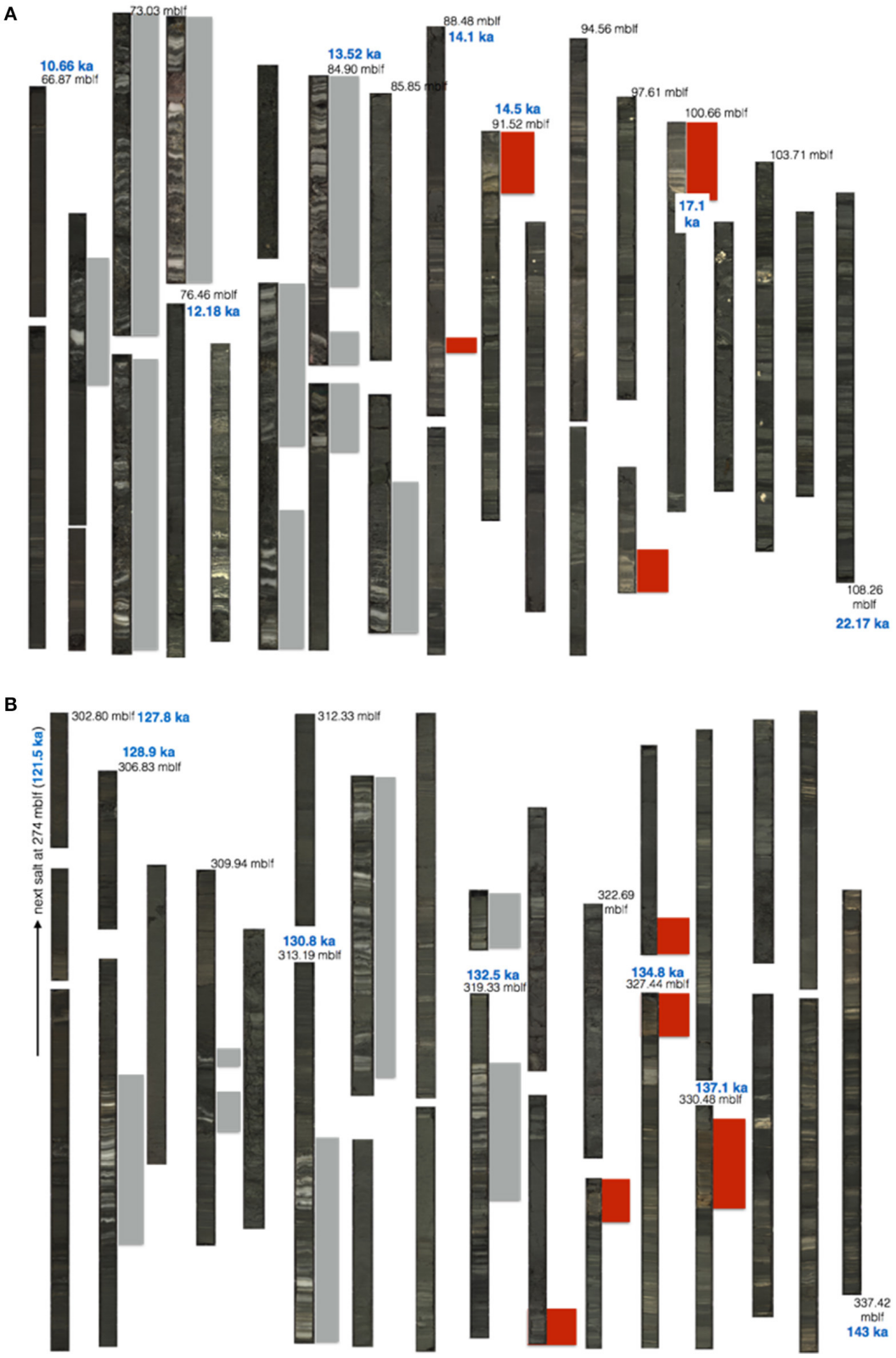

FIGURE 4 | DSDDP core photos of **(A)** Termination-I, and **(B)** Termination-II. Depth in meters below lake floor (mblf), and ages (ka) are marked in black and blue, respectively (ages after Torfstein et al., 2015). Red and gray rectangles highlight the location of gypsum and halite intervals, respectively.

by NBS-127 [$\delta^{18}O_{(SO4)}$ = 8.6‰], with reported uncertainties reflecting the average and standard deviation of triplicate analyses of each sample.

Acid Volatile Sulfide (AVS) and Chromium Reducible Sulfur (CRS) were extracted from silt mud samples throughout the DSDDP core. The acid volatile sulfides are largely understood to be iron monosulfides, while the chromium reduction targets the iron disulfide minerals, primarily pyrite. The samples had been pre-washed by submerging in deionised water and agitating for 24 h then dried prior to extraction. Approximately 2–3 g of sample material then was weighed and transferred to a reaction vessel which was placed upon a hotplate and flushed with nitrogen. The AVS fraction was extracted with the addition of 35 ml of 0.1 M stannous chloride in 6 M hydrochloric acid. The mixture was heated and kept at sub-boiling temperature for 35 min. The CRS fraction was extracted through 35 ml of 1 M chromous chloride in 0.5 M hydrochloric acid. Pyrite and elemental sulfur are both reduced to hydrogen sulfide by chromous chloride, which is oxidized to chromic chloride ($CrCl_3$) in the process. The mixture was heated for 2–3 h. The two chemical digestions done on the sample produced both hydrogen sulfide gas (from the sulfide minerals) as well as chlorine gas (from the presence of hydrochloric acid in the reagents). To remove the chlorine, an in-line nitric acid trap containing 0.1 M nitric acid in deionised water was used such that the gas stream was bubbled through the trap, dissolving the chlorine. The hydrogen sulfide gas was passed into a further trap containing a solution of 0.2 M silver nitrate in 10% ammonium hydroxide, forming silver sulfide. The silver sulfide from both the CRS and AVS extractions was then washed and vacuum filtered with 0.45 μm filter paper and left to dry.

The silver sulfide was prepared for sulfur isotope analysis in the same way as the barite. An additional standard (IAEA-S3 – $\delta^{34}S$ = −32.3‰) was also run. Following established protocol, the raw data from the mass spectrometer were adjusted relative to the difference between the measured and expected values of the standards, using a linear interpolation between the average of each set of standards.

Several bulk mud samples from the DSDDP core were exposed to long dissolution (several weeks while agitated) in NaCl to ascertain whether the overnight leaching and likely non-quantitative dissolution of gypsum imparted a sulfur or oxygen isotope fractionation on the gypsum. The isotope composition of both long and short dissolution was the same.

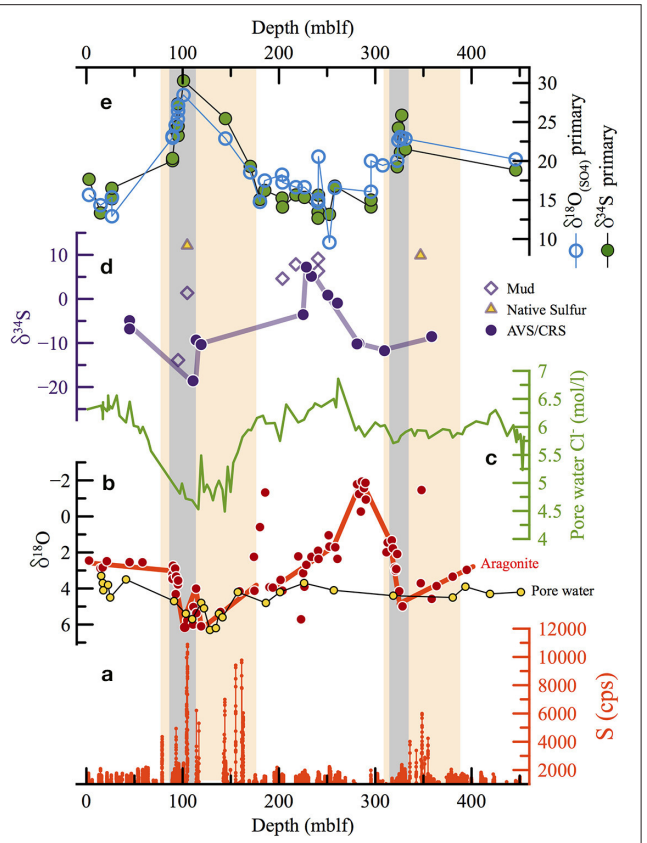

FIGURE 5 | The DSDDP core. **(a)** Abundance of sulfur from XRF scanning, **(b)** $\delta^{18}O$ of aragonite laminae (red, from Torfstein et al., 2015) and pore waters (yellow, from Lazar et al., 2014) (note the reverse *y* axis). **(c)** Chloride concentrations in pore waters (from Lazar et al., 2014), **(d)** $\delta^{34}S$ (‰) of reduced sulfur minerals. Full circles represent the AVS and CRS fractions, and empty diamonds mark sulfate extracted from in mud intervals. Yellow triangles mark native sulfur nodules. **(e)** $\delta^{34}S$ and $\delta^{18}O_{(SO4)}$ of primary gypsum. The similar trends of both isotopic systems, with a gradual rise toward maximum values in the two deglacial stages (marked by gray rectangles). Interglacial stages are characterized by consistently low values ca. 14–20‰. The orange rectangles mark the depth interval corresponding to two glacial cycles (MIS6 and last glacial). $\delta^{34}S$ of primary gypsum and AVS/CRS fractions displays decoupling, whereby the highest $\delta^{34}S$ of primary gypsum correspond to the interval of low $\delta^{34}S$ of AVS/CRM minerals, while during interglacial stages, characterized by relatively low primary gypsum $\delta^{34}S$, the AVS/CRS $\delta^{34}S$ is relatively high. This pattern supports the isotopic fractionation decoupling of sulfur phases in the high and stratified lake (during wet glacials) compared to a very weak decoupling during arid interglacials, when the lake is relatively low, mixed and the water column probably oxidized more frequently. High sulfur concentrations are observed during deglacials, representing the deposition of massive gypsum layers.

RESULTS

The isotopic composition of sulfur and oxygen in primary gypsum layers in the DSDDP core (Supplementary Table 1) and the M1 outcrop (Supplementary Table 2) reveal strong glacial—interglacial variability (**Figures 5–7**). Both the penultimate and last glacial terminations (T-II and T-I, respectively) are characterized by the precipitation of massive primary gypsum units (~137–134 and 17–14 ka; **Figure 4**) and both of these deglacial intervals display temporal $\delta^{34}S$ maxima of ~23‰ (MIS6/5) and 28‰ (last deglacial). During the subsequent interglacial stages, i.e., the last interglacial and the Holocene, the $\delta^{34}S$ of primary gypsum units dropped to ~12.9–15.7‰. Higher $\delta^{34}S$ is observed across the two glacial stages (MIS6 and 4-2), with a gradual rise with time toward the deglacial maxima. The ^{34}S-enrichment of primary gypsum during glacial maxima is most evident in the last glacial cycle, in agreement with previous observations from exposed-marginal outcrops (Torfstein et al., 2005, 2008). Primary gypsum units were not identified across the MIS6 interval in the DSDDP core. Overall, coeval samples

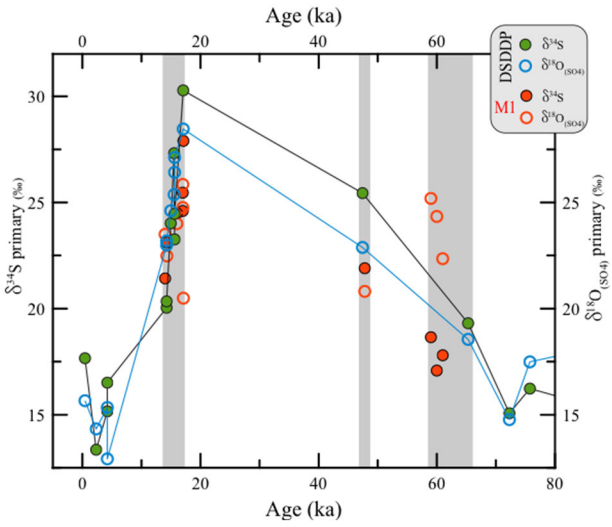

FIGURE 6 | Comparison between $\delta^{34}S$ vs. $\delta^{18}O_{(SO4)}$ in primary gypsum from the last glacial interval at the DSDDP core and the Masada M1 site. For reference, the displayed ages of different gypsum units pertain to the Lower Gypsum Unit (61–58.5 ka), Curled Gypsum Unit (49–47.5 ka), Upper Gypsum Unit (17.1–15.5 ka) and the Additional Gypsum Unit (14.5 ka) (see stratigraphic definitions of Torfstein et al., 2008).

from the DSDDP core and marginal outcrops display overlapping sulfur isotopic compositions (**Figure 6**).

The $\delta^{18}O_{(SO4)}$ of primary gypsum co-varies with $\delta^{34}S$ (i.e., low, rising and maximum values during interglacial stages, glacial stages and deglacial terminations, respectively) ranging between 12.7 and 30.3‰ in the DSDDP core and between 20.5 and 25.8‰ in the M1 outcrop (**Figures 6**, **7**). Although, the M1 site is exposed at 370–340 mbsl, approximately 400 m higher than the DSDDP site location, the $\delta^{34}S$ and $\delta^{18}O_{(SO4)}$ from gypsum measured at both locations are similar in magnitude and in pattern.

No secondary gypsum crystals were found in the DSDDP core, suggesting that this phase forms only after aerial exposure of the sedimentary section on the lake margins. The AVS and CRS sedimentary fraction from the DSDDP core (full circles in **Figure 5d**) are ^{34}S-depleted ranging between −18.6 and 7.2‰ (Supplementary Table 3). These fractions also vary temporally in opposite sign to the gypsum $\delta^{34}S$ and $\delta^{18}O_{(SO4)}$, with relatively higher $\delta^{34}S_{AVS}$ or $\delta^{34}S_{CRS}$ during interglacial stages [when gypsum $\delta^{34}S$ and $\delta^{18}O_{(SO4)}$ is relatively low] and lower $\delta^{34}S_{AVS}$ or $\delta^{34}S_{CRS}$ during glacial and deglacial stages [when gypsum $\delta^{34}S$ and $\delta^{18}O_{(SO4)}$ is relatively high]. Although, no sedimentary sulfide minerals are found in the marginal outcrop (M1), secondary gypsum from this site yields $\delta^{34}S$ between −27.5 and 1.0‰ and $\delta^{18}O_{(SO4)}$ between 8.4 and 13.6‰, which is distinctly lower than the primary gypsum beds.

The discrete primary gypsum layers are continuous across the lake area, and increase in thickness toward the geographic center of the lake (Torfstein et al., 2008). The main deglacial pulse of gypsum deposition, the "Upper Gypsum Unit" (UGU, 17.1–15.5 ka; Torfstein et al., 2013a), is observed at the Masada M1 outcrop (**Figure 2**) where it displays a thickness of 1.07 m and $\delta^{34}S$ in the range of 24.5–28‰ and $\delta^{18}O_{(SO4)}$ in the range of 20.5–26‰. By comparison, the same unit in the DSDDP core is 9.42 m thick (100.94–94.77 mblf), of which 1.35 m is comprised of primary gypsum (the rest are bracketing intervals of marl and aad, as well as a gap of 1.44 m between 100.66 and 99.22 mblf) and has a $\delta^{34}S$ and $\delta^{18}O_{(SO4)}$ in the range of 25.4–28.5‰ and 23.3–30.3‰, respectively (Supplementary Table 1). Thus, the Upper Gypsum Unit shows remarkable spatial and isotopic consistency, although slightly thicker and slightly ^{34}S- and $^{18}O_{(SO4)}$- enriched in the deep center of the lake. Similarly, the Holocene DSDDP interval yields $\delta^{34}S$ and $\delta^{18}O_{(SO4)}$ in the range of 12.9–15.7 and 13.3–17.7‰ in the primary gypsum, compared to 15.3 and 14.5‰, respectively, in the marginal Holocene Ze'elim Formation.

This correlation in isotopic composition between the DSDDP core and the marginal outcrop can also be observed in additional gypsum beds that have been previously correlated (Torfstein et al., 2015). For example, the two thin gypsum units between 89.72 and 89.47 mblf (equivalent to 14.40–14.26 ±0.5 ka) display $\delta^{34}S$ ≈23‰ and $\delta^{18}O_{(SO4)}$ ≈20.2‰, compared with the "Additional Gypsum Unit" at Masada [22–24‰; this study and Torfstein et al., 2008; and $\delta^{18}O_{(SO4)}$ ≈23‰].

The "Lower Gypsum Unit," marking the MIS4-3 transition (61–58.5 ka) is present in almost all marginal sites along the Dead Sea, yet its correlation to the DSDDP core is more challenging because the corresponding interval is characterized by the frequent occurrence of thinner gypsum laminae. An analysis of one of these gypsum laminae close to the base of the Lisan Fm. in the DSDDP core (170.17 mblf) yielded $\delta^{34}S$ and $\delta^{18}O_{(SO4)}$ of 18.5 and 19.3‰. In this case, the $\delta^{34}S$ is comparable with those of the Lower Gypsum Unit at M1 (17.1–18.7‰) but the $\delta^{18}O_{(SO4)}$ is much lower than those observed at M1 (22.4–25.2‰).

DISCUSSION

Source Water $\delta^{34}S$ and $\delta^{18}O_{(SO4)}$

The sulfur isotopic composition of aqueous sulfate in the Dead Sea lacustrine system, and therefore the gypsum that precipitates within this system, reflects the balance between the source composition (local runoff $\delta^{34}S$ ranges between 6 and 14‰; Gavrieli et al., 2001) and the amount of water column microbial sulfate reduction, which is controlled by the stability and length of water column stratification leading to the deep-lake anoxia. The oxygen isotopic composition of sulfate is controlled by the same processes, but is particularly sensitive to the incorporation of oxygen atoms during sulfide oxidation, and the degree of intracellular equilibration between intermediate valence state sulfur species and water. Avrahamov et al. (2014) reported one sample of marginal Dead Sea groundwaters with $\delta^{18}O_{(SO4)}$ = 13.6‰ (with $\delta^{34}S$ = 15.9‰), with saline spring waters along the modern Dead Sea displaying a range of typically higher $\delta^{18}O_{(SO4)}$ up to 19.3‰. Khayat et al. (2006) also studied groundwater north of the Dead Sea, around Jericho, and although these are possibly contaminated by anthropogenic sources, the reported $\delta^{18}O_{(SO4)}$ ranged between 1.4 and 17.3‰, similar to the range measured in the DSDDP core and M1 section. Until more

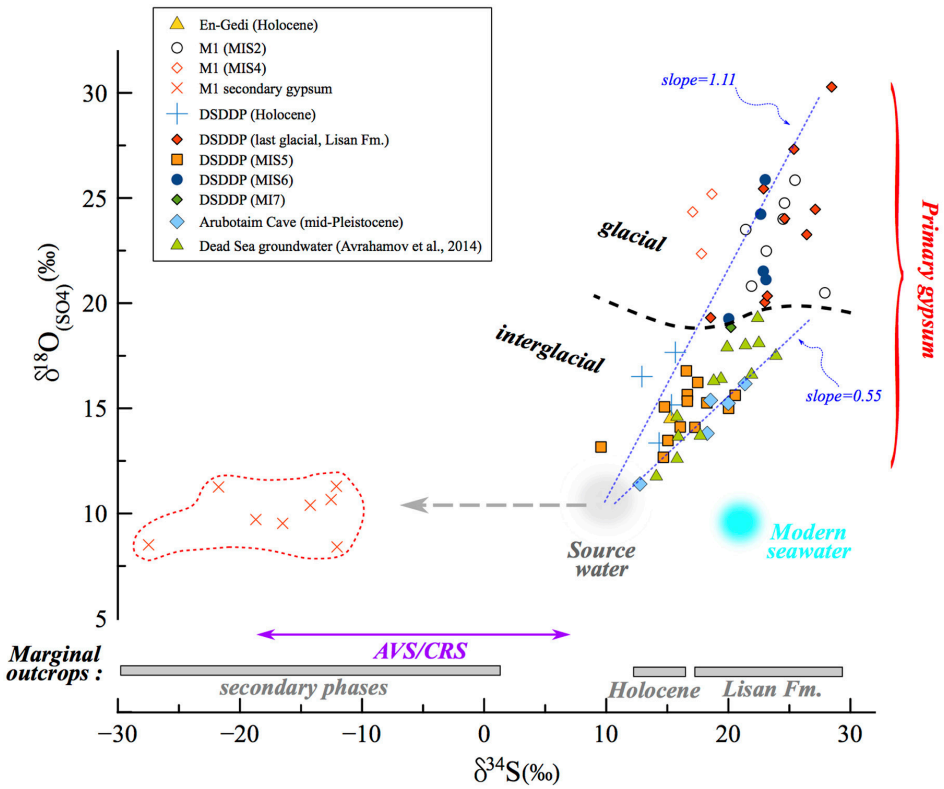

FIGURE 7 | $\delta^{34}S$ vs. $\delta^{18}O_{(SO4)}$ in the Dead Sea lacustrine environment. The compositions of primary and secondary minerals branch out from the same source sulfate composition, that of influxing freshwater (gray circle). The correlation reveals a clear difference (marked by dashed black curve) between interglacial deposits and those associated with full glacial and deglacial stages. In the land-locked Dead Sea basin, the distribution and evolution patterns of $\delta^{34}S$ and $\delta^{18}O_{(SO4)}$ are completely independent from the seawater composition (blue circle). In some samples only $\delta^{34}S$ was measured (gypsum from marginal outcrops from Torfstein et al., 2008 and AVS/CRS from the DSDDP core), and the range of these data are given in the bottom part of the diagram. The slope of the $\delta^{34}S$ vs. $\delta^{18}O_{(SO4)}$ has been shown to reflect the rate of microbial sulfate reduction, whereby the steeper the slope, the slower the rate. Accordingly, slopes calculated for interglacial periods (e.g., Amora Fm., Dead Sea groundwater) are systematically lower than those calculated for glacial period; two examples of linear regressions are presented (dashed blue curves): Amora Fm. with a slope of 0.55 and the glacial MIS2 samples yielding a higher slope of 1.11. This implies that the rate of microbial sulfate reduction processes was significantly slower during glacials relative to interglacials.

detailed characterization of the Dead Sea drainage is done, it is reasonable to assume an average freshwater $\delta^{18}O_{(SO4)}$ in the Dead Sea Basin of ~10‰ (gray circle in **Figure 7**) given the range of previously measured ground water, springs and other fluids in the area.

Coupling and Decoupling of $\delta^{34}S$ and $\delta^{18}O_{(SO4)}$

Our data is characterized by two primary features (**Figure 5**): 1. Temporal variations in the $\delta^{34}S$ and $\delta^{18}O_{(SO4)}$ of the gypsum which correlate with glacial–interglacial cycles, including a strong transient positive $\delta^{34}S$ and $\delta^{18}O_{(SO4)}$ perturbation during deglaciations, 2. Decoupling of the sign of $\delta^{34}S$ between sedimentary sulfate and sulfide minerals, with anticorrelated isotopic trends during different climatic stages. We will consider the former observation first.

Although, there is a clear temporal change in the $\delta^{34}S$ and $\delta^{18}O_{(SO4)}$ over glacial-interglacial cycles, before we can interpret changes in redox dynamics we need to determine whether there are changes in the oxygen isotope composition of the lake water over these intervals which may be reflected in the $\delta^{18}O_{(SO4)}$ of the sulfate, and thus recorded in the $\delta^{18}O_{(SO4)}$ of the primary gypsum. To a first order, changes in $\delta^{18}O$ measured in aragonite follow closely the patterns of $\delta^{18}O$ changes measured in the Soreq Cave and East Mediterranean surface water with higher $\delta^{18}O$ corresponding to glacial stages and lower $\delta^{18}O$ in interglacial, reflecting the control of temporal changes in the East Mediterranean source water composition on $\delta^{18}O$ compositions both in the cave and in the lake (see further discussion in Kolodny et al., 2005).

Figure 5 shows that the aragonite $\delta^{18}O$ is decoupled from both the $\delta^{34}S$ and $\delta^{18}O_{(SO4)}$ measured in the primary gypsum. The aragonite-derived $\delta^{18}O$ is also consistently lower than the $\delta^{18}O$ (of the water) measured in the sedimentary pore fluids (**Figure 5b**). Considering an observed coeval drop in chloride concentrations in interstitial waters (**Figure 5c**), Lazar et al. (2014) concluded that the lake bottom waters underwent significant freshening during the last glacial cycle with chloride concentrations in the monimolimnion decreasing to about 70% of their modern value, and the $\delta^{18}O$ of the lake water reached

~7‰, about 3‰ higher than present. Such a freshening of the lake would lower salinity and allow for higher sulfate concentrations to be maintained in the lake water (residence time of ~100–1,500 years) because they are controlled largely by gypsum saturation (Torfstein et al., 2005). Thus, the larger the lake volume during the glacial cycle, the bigger the pool of ^{34}S- and ^{18}O- enriched residual sulfate in the water column. When the lake destabilizes and declines during the glacial termination, the precipitating gypsum records the isotopic fingerprint and is characterized by higher $\delta^{34}S$ and $\delta^{18}O_{(SO4)}$. Accordingly, the thickness of the gypsum beds that precipitate during each glacial termination, and their sulfur and oxygen isotopic composition, are positively correlated and are a qualitative metric for the intensity of the stratification and the sulfate concentration in the lake during the glacial cycle.

The second observation pertains to an anticorrelation in the $\delta^{34}S$ between the gypsum phases and the sedimentary sulfide AVS and CRS fraction; in general, when the $\delta^{34}S$ of the gypsum is high, the sedimentary sulfide is low, and vice versa. One interpretation of this is that when the lake was less stratified (during interglacial lowstands) there is less water column microbial sulfate reduction and thus less opportunity to separate various phases chemically or isotopically. Another possibility is that during interglacials when there is less separation in the sulfur isotope composition of sulfate and sulfide, microbial sulfate reduction is limited to the surface sediment and behaves more like a "closed system" where the available sulfate is quantitatively converted to pyrite and thus retains a similar $\delta^{34}S$. The observation that sedimentary sulfides from glacial and deglacial periods display significantly lower $\delta^{34}S$, mirrors the ^{34}S-enrichment of coeval gypsum layers and likely reflects the strong water-column stratification and the separation of the two phases through more open-system microbial sulfate reduction.

Following lake level decline and exposure of the sedimentary column, percolation of meteoric freshwater ($\delta^{18}O_{H2O} = -6$ to -3‰) caused oxidation of reduced sulfur phases in the now-exposed sediments. This explains why sedimentary sulfide minerals are found in the DSDDP core but not in the exposed outcrop. The meteoric fluids percolated along the carbonate sediments, particularly along detrital laminae, which are more permeable than aragonite laminae, and became calcium-enriched. This in turn, favored secondary gypsum crystallization after oxidation of sedimentary sulfides. The $\delta^{34}S$ fingerprint of this gypsum is similar to that of the original sedimentary sulfide minerals (^{34}S-depleted). By contrast, the oxygen isotope composition of the sulfate would depend on where the sulfate derived its oxygen atoms from and any isotope fractionation associated with their incorporation into the sulfate molecule. Typically, during sulfide oxidation the canonical assumption is that one oxygen atom derives from the atmosphere (+23‰) and the other three from water; this has been shown in pure culture microbial studies and applied in a range of riverine environments to understand the pathway of pyrite oxidation (e.g., Balci et al., 2007; Calmels et al., 2007). However, it appears that the secondary gypsum in the M1 section derives oxygen atoms nearly perfectly as a 50/50 mix between water and atmospheric oxygen (**Figure 8**), hinting that during this oxidation, two of the oxygen atoms derive from percolating meteoric water and two from atmospheric oxygen. There is a possibility that this represents a mixture of sources of oxygen atoms and isotope fractionation on their incorporation, or isotope equilibration with water in an intermediate valence state. We suggest however, similar to the interpretation of the oxygen isotope composition of sulfate in river systems and in pure culture studies, that there is negligible oxygen isotope fractionation on sulfide oxidation and that intermediate valence state sulfur species, if created, are too short lived to isotopically equilibrate with water. If our suggestion is correct, it is the first observation of an equal contribution of oxygen atoms from the two sources. We postulate that in the hyperarid conditions under which the epigenetic oxidation occurred, the incorporation mechanism of oxygen into sulfate is different than previously reported.

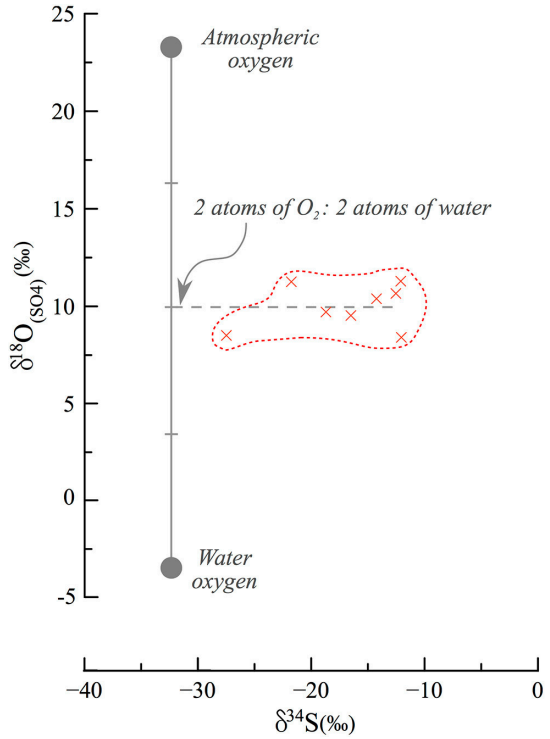

FIGURE 8 | End member mixing and oxidation pathways in secondary gypsum. Assuming that atmospheric oxygen (23‰) and local meteoric water (−6 to −3‰) are the source of oxygen to the oxidation process of sulfides, they each contribute an equal fraction of oxygen atoms. Previous studies have typically discussed the contribution of one O_2 atom from atmospheric oxygen and 3 atoms from water, and this is the first such observation of an implied equal contribution.

The Microbial Sulfur Cycle in Lake Lisan

The relative change in the sulfur and oxygen isotope composition of sulfate during microbial sulfate reduction reflects the degree of intracellular recycling of sulfur compounds and is related to the sulfate reduction rate (Brunner et al., 2005; Brunner and Bernasconi, 2005; Antler et al., 2014, 2013). Specifically, the slope between the sulfur and oxygen isotopes in sulfate over the course of sulfate reduction has been shown to correlate with the cell specific rate of sulfate reduction (Antler et al., 2013).

The faster the rate of sulfate reduction, the faster the sulfur isotope composition of the residual sulfate increases relative to the oxygen isotope composition of the residual sulfate and accordingly, the slope of the cross plot of $\delta^{34}S$ vs. $\delta^{18}O_{(SO4)}$ regression becomes less steep. The slope between sulfur and oxygen isotopes in sulfate has been shown to have a unique value when microbial sulfate reduction is coupled to anaerobic methane oxidation, ca. 0.39 (Antler et al., 2015). Anaerobic methane oxidation has been suggested to occur in the modern Dead Sea, but understanding the extent of methane production and oxidation during different climate intervals is a key question for understanding how the carbon budget in lakes may change with regional hydrological changes.

We take our measured $\delta^{18}O_{(SO4)}$ and $\delta^{34}S$ of gypsum as representing the sulfate in the lake during stratification, assuming minimal sulfur or oxygen isotope fractionation on gypsum precipitation. The slope for the full set of sulfur and oxygen isotope data measured in primary gypsum is 0.85, but when calculating the slope for specific time intervals at each site, a difference between glacial and interglacial periods is revealed. The calculated slope ranges between 0.55 for the Amora Fm. interglacial sequence at the Arubotaim Cave site, which is only slightly lower than the slope of modern Dead Sea groundwater (0.68) (**Figures 7**, **9**). By contrast, a much higher slope between 1.11 (MIS2) and 2.0 (MIS4) is identified at M1 during glacial intervals (for clarity, **Figure 7** displays only the Amora Fm. and MIS2 slopes).

This significant change in the slope between sulfur and oxygen isotopes in sulfate recorded in gypsum at different times implies that microbial sulfate reduction operates fundamentally differently between glacial and interglacial conditions, when water levels were high (fresher lake) and low (more saline lake), respectively. During interglacials, sulfate reduction is confined to the sediments (as it is today), and the rate derived from the $\delta^{18}O_{(SO4)}$ vs. $\delta^{34}S$ crossplot suggests the rate of microbial sulfate reduction is faster relative to glacial stages. This could be because of the presence of methane, and that sulfate may be dominantly reduced through anaerobic methane oxidation, associated with a low, unique slope (~0.39; Antler et al., 2015). This fast rate of microbial sulfate reduction will also contribute to the higher overall sulfur isotope composition of the sedimentary sulfide

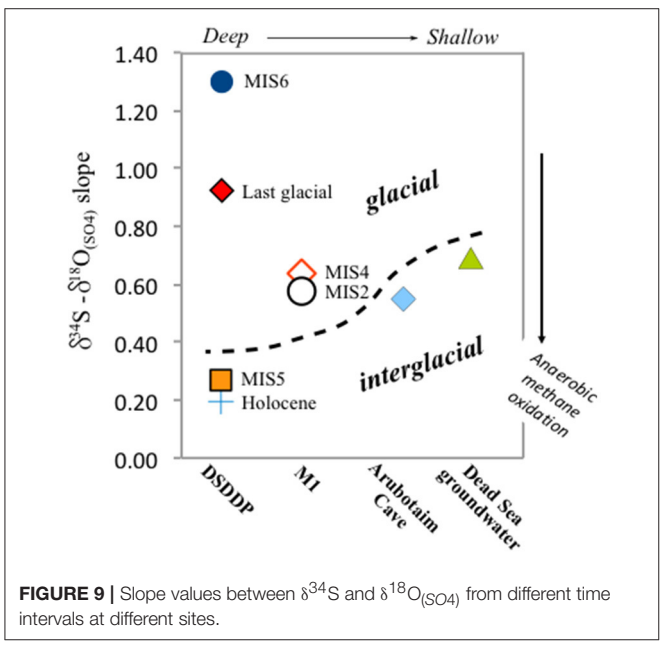

FIGURE 9 | Slope values between $\delta^{34}S$ and $\delta^{18}O_{(SO4)}$ from different time intervals at different sites.

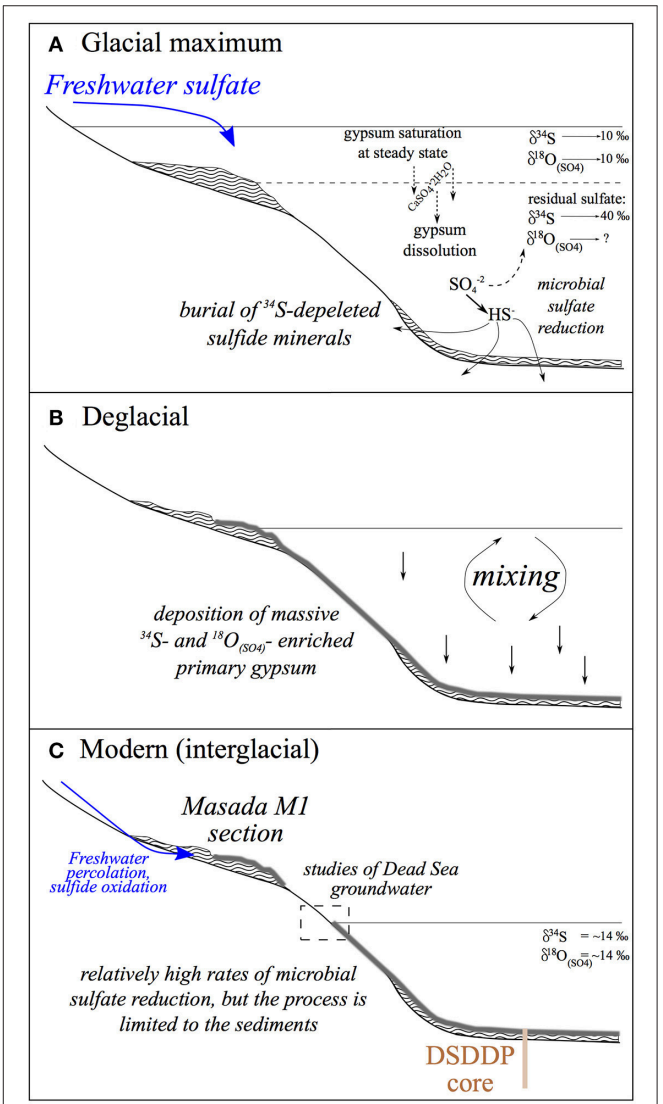

FIGURE 10 | Conceptual evolution patterns of the Dead Sea lacustrine system across Glacial—Interglacial cycles. **(A)** Glacial—large freshwater influx supports a high stand and density stratification. The overall reservoir of ^{34}S-enriched sulfate in the lake is highest during the glacial, **(B)** Deglacial—a regional shift from wet to dry conditions drives a lake level drop that causes water column mixing and massive precipitation of primary gypsum, **(C)** Modern (interglacial)—dry climatic conditions impose low water stands and a mixed water column. Microbial sulfate reduction is limited to the interstitial zone in the sediments but occurs at faster rates relative to glacial times. Marginal glacial deposits are exposed and occasional freshwater percolation through the sections results in oxidation of sedimentary sulfide to sulfate. These continue to crystalize and form secondary gypsum. This process is unique to the margins and is not recorded in the deep submerged sediments of the DSDDP.

minerals discussed above, in addition to the possible "closed system" behavior. In contrast, in glacial times when the lake was much larger, deeper, and stably stratified, microbial sulfate reduction occurred in the open water column. Although, this yields overall higher $\delta^{18}O_{(SO4)}$ and $\delta^{34}S$, the relative change in them is different relative to interglacial periods and corresponds to slower overall rates of microbial sulfate reduction. Our results suggest that the cell specific sulfate reduction rate is as much as two orders of magnitude faster in the modern basin (and more generally during interglacials) than it was during glacial periods when the lake was stratified and displayed significantly higher water level and higher lake sulfate concentrations.

These results have implications for interpreting the behavior of the microbial sulfur cycle during changes in lake salinity and regional hydrology. A conceptual summary of the evolution of these different lake parameters across Glacial—Interglacial cycles is given in **Figure 10**. Measuring the sulfur isotopes or oxygen isotopes in sulfate in isolation, they behave as we would have predicted; during lake stratification there is a stronger distillation of the isotopes between isotopically enriched oxidized phases in the lake and isotopically depleted reduced phases in the sediment. This is moderated during interglacials when sulfate reduction is limited to the sediments. However, the relative change in $\delta^{18}O_{(SO4)}$ vs. $\delta^{34}S$ suggests that the overall cell specific rate slows down when microbial sulfate reduction occurs in the stratified water column (primarily during glacial times), in spite of overall higher sulfate concentrations. We infer that this may be due to a change in the carbon source, where during the glacial fresher lake periods, an increase in primary production in the surface water (as suggested by $\delta^{13}C$ values in aragonite; Kolodny et al., 2005) supplies the primary carbon source for microbial sulfate reduction in the water column. In contrast, during interglacial periods, when the lake is low, mixed and more saline, primary production may be virtually absent, and the carbon source for microbial sulfate reduction is methane produced in the sediment from the reduction of previously deposited organic carbon. Microbial sulfate reduction also migrates from the water column to the sediment, and the overall rate increases. These results suggest that rates of microbial sulfate reduction may be independent of salinity even in hypersaline conditions.

SUMMARY

The temporal dynamics and rates of microbial sulfate reduction were studied in the terminal, hypersaline Dead Sea lacustrine system over the last 200 kyrs, based on $\delta^{34}S$ and $\delta^{18}O_{(SO4)}$ in the sedimentary record. The sulfur and oxygen isotopic composition of sulfate in the Dead Sea has evolved through multiple cycles of reduction and oxidation that are controlled by the regional hydrological regime. During wet glacial stages, influxing freshwater imposed stratified conditions, which resulted in the consumption of oxygen in the monimolimnion (lower brine) and development of anoxic conditions. These drove microbial sulfate reduction that impart the water column sulfate into reduced sulfide phases that are ^{34}S-depleted, and residual water ^{34}S- and ^{18}O- enriched sulfate. Our results suggest that despite the more favorable conditions, the rate of microbial sulfate reduction during glacials is actually slower than the rate during interglacials, when the lake level is lower and the lake is mixed and oxidized, confining microbial sulfate reduction to the sediments.

Analyses of secondary gypsum samples that evolved from the oxidation of sulfidic phases, reveals extremely ^{34}S-depleted compositions, but higher $\delta^{18}O_{(SO4)}$ suggesting that oxidation of sedimentary sulfide phases was facilitated by contact with meteoric surface water after the lake retreated. Thus, following their deposition, sedimentary sulfides was maintained in an oxygen-depleted environment until their recent exposure to the atmosphere. Moreover, the oxygen atoms in sulfate associated with secondary gypsum minerals are derived at a 1:1 ratio from the atmosphere and water. This ratio is globally unique to the Dead Sea basin, probably due to the hyperarid conditions that prevail in this area.

The coupling of $\delta^{34}S$ and $\delta^{18}O_{(SO4)}$ in the Dead Sea system has been shown to be highly sensitive to the regional hydrological budget, and can be used to reconstruct the limno-hydrology in older sequences of the Dead Sea record, as well as in other comparable environments elsewhere.

AUTHOR CONTRIBUTIONS

AT performed the field work and sampling. AVT processed the samples in the lab and analyzed them. Both AT and AVT performed data analyses and wrote the manuscript.

ACKNOWLEDGMENTS

Funding was provided by ERC Starting Investigator Grant 307582 to AVT and the Comer Science & Education Foundation grant CP69 to AT. The authors are grateful to Sam Johnson who extracted the sedimentary sulfides during a summer project. Constructive reviews by Susan Childers and David T. Wang helped to greatly improve this paper.

SUPPLEMENTARY MATERIAL

The Supplementary Material for this article can be found online at: http://journal.frontiersin.org/article/10.3389/feart.2017.00062/full#supplementary-material

REFERENCES

Aharon, P., and Fu, B. (2000). Microbial sulfate reduction rates and sulfur and oxygen isotope fractionations at oil and gas seeps in deepwater Gulf of Mexico. *Geochim. Cosmochim. Acta* 64, 233–246. doi: 10.1016/S0016-7037(99)00292-6

Antler, G., Turchyn, A. V., Herut, B., Davies, A., Rennie, V. C. F., and Sivan, O. (2014). Sulfur and oxygen isotope tracing of sulfate driven anaerobic methane oxidation in estuarine sediments. *Estuar. Coast. Shelf Sci.* 142, 4–11. doi: 10.1016/j.ecss.2014.03.001

Antler, G., Turchyn, A. V., Herut, B., and Sivan, O. (2015). A unique isotopic fingerprint of sulfate-driven anaerobic oxidation of methane. *Geology* 43, 619–622. doi: 10.1130/G36688.1

Antler, G., Turchyn, A. V., Rennie, V., Herut, B., and Sivan, O. (2013). Coupled sulfur and oxygen isotope insight into bacterial sulfate reduction

in the natural environment. *Geochim. Cosmochim. Acta* 118, 98–117. doi: 10.1016/j.gca.2013.05.005

Arndt, S., Jørgensen, B. B., LaRowe, D. E., Middelburg, J. J., Pancost, R. D., and Regnier, P. (2013). Quantifying the degradation of organic matter in marine sediments: a review and synthesis. *Earth Sci. Rev.* 123, 53–86. doi: 10.1016/j.earscirev.2013.02.008

Avrahamov, N., Antler, G., Yechieli, Y., Gavrieli, I., Joye, S. B., Saxton, M., et al. (2014). Anaerobic oxidation of methane by sulfate in hypersaline groundwater of the dead sea aquifer. *Geobiology* 12, 511–528. doi: 10.1111/gbi.12095

Baas-Becking, L., and Kaplan, I. (1956). The microbiological origin of the sulphur nodules of lake eyre. *Trans. R. Soc. South Aust.* 79, 52–65.

Balci, N., Shanks, W. C., Mayer, B., and Mandernack, K. W. (2007). Oxygen and sulfur isotope systematics of sulfate produced by bacterial and abiotic oxidation of pyrite. *Geochim. Cosmochim. Acta* 71, 3796–3811. doi: 10.1016/j.gca.2007.04.017

Bartov, Y., Goldstein, S. L., Stein, M., and Enzel, Y. (2003). Catastrophic arid episodes in the eastern mediterranean linked with the North Atlantic Heinrich events. *Geology* 31, 439–442. doi: 10.1130/0091-7613(2003)031<0439:CAEITE>2.0.CO;2

Begin, Z., Ehrlich, A., and Nathan, Y. (1974). Lake Lisan, the Pleistocene precursor of the dead sea. *Geol. Surv. Isr. Bull.* 63, 1–30.

Belmaker, R., Lazar, B., Beer, J., Christl, M., Tepelyakov, N., and Stein, M. (2013). 10Be dating of Neogene halite. *Geochim. Cosmochim. Acta* 122, 418–429. doi: 10.1016/j.gca.2013.08.033

Bishop, T., Turchyn, A., and Sivan, O. (2013). Fire and brimestone: the microbially mediated formation of elemental sulfur nodules from an isotope and major element study in the paleo-dead sea. *PLoS ONE* 8:e75883. doi: 10.1371/journal.pone.0075883

Bookman Ken-Tor, R., Enzel, Y., Agnon, A., and Stein, M. (2004). Late Holocene lake levels of the dead sea. *Geol. Soc. Am. Bull.* 116, 555–571. doi: 10.1130/B25286.1

Bottrell, S. H., and Newton, R. J. (2006). Reconstruction of changes in global sulfur cycling from marine sulfate isotopes. *Earth Sci. Rev.* 75, 59–83. doi: 10.1016/j.earscirev.2005.10.004

Brunner, B., Bernasconi, S., Kleikemper, J., and Schroth, M. (2005). A model for oxygen and sulfur isotope fractionation in sulfate during bacterial sulfate reduction processes. *Geochim. Cosmochim. Acta* 69, 4773–4785. doi: 10.1016/j.gca.2005.04.017

Brunner, B., and Bernasconi, S. M. (2005). A revised isotope fractionation model for dissimilatory sulfate reduction in sulfate reducing bacteria. *Geochim. Cosmochim. Acta* 69, 4759–4771. doi: 10.1016/j.gca.2005.04.015

Calmels, D., Gaillardet, J., Brenot, A., and France-Lanord, C. (2007). Sustained sulfide oxidation by physical erosion processes in the Mackenzie river basin: climatic perspectives. *Geology* 35, 1003–1006. doi: 10.1130/G24132A.1

Canfield, D. E. (1998). A new model for Proterozoic ocean chemistry. *Nature* 396, 450–453. doi: 10.1038/24839

Canfield, D. E. (2004). The evolution of the earth surface sulfur reservoir. *Am. J. Sci.* 304, 839–861. doi: 10.2475/ajs.304.10.839

Chambers, L. A., and Trudinger, P. A. (1979). Microbiological fractionation of stable sulfur isotopes: a review and critique. *Geomicrobiol. J.* 1, 249–293. doi: 10.1080/01490457909377735

Claypool, G., Holser, W., Kaplan, I., Sakai, H., and Zak, I. (1980). The age curves of sulfur and oxygen isotopes in marine sulfate and their mutual interpretation. *Chem. Geol.* 28, 199–260. doi: 10.1016/0009-2541(80)90047-9

Cypionka, H., Smock, A. M., and Boettcher, M. E. (1998). A combined pathway of sulfur compound disproportionation in desulfovibrio desulfuricans. *FEMS Microbiol. Lett.* 166, 181–186. doi: 10.1111/j.1574-6968.1998.tb13888.x

Enzel, Y., Bookman Ken Tor, R., Sharon, D., Gvirtzman, H., Dayan, U., Ziv, B., et al. (2003). Late holocene climates of the near east deduced from dead sea level variations and modern regional winter rainfall. *Quat. Res.* 60, 263–273. doi: 10.1016/j.yqres.2003.07.011

Eugster, H. (1980). Geochemistry of evaporitic lacustrine deposits. *Annu. Rev. Anthropol.* 8, 35–63. doi: 10.1146/annurev.ea.08.050180.000343

Froelich, P. N., Klinkhammer, G. P., Bender, M. L., Luedtke, N. A., Heath, G. R., Cullen, D., et al. (1979). Early oxidation of organic matter in pelagic sediments of the eastern equatorial Atlantic: suboxic diagenesis. *Geochim. Cosmochim. Acta* 43, 1075–1090. doi: 10.1016/0016-7037(79)90095-4

Gavrieli, I., and Stein, M. (2006). On the origin and fate of the brines in the dead sea basin. *Geol. Soc. Am. Spec. Pap.* 401, 183–194. doi: 10.1130/2006.2401(12)

Gavrieli, I., Yechieli, Y., Halicz, L., Spiro, B., Bein, A., and Efron, D. (2001). The sulfur system in anoxic subsurface brines and its implication in brine evolutionary pathways: the Ca-chloride brines in the Dead Sea area. *Earth Planet. Sci. Lett.* 186, 199–213. doi: 10.1016/S0012-821X(01)00247-3

Haase-Schramm, A., Goldstein, S. L., and Stein, M. (2004). U-Th dating of lake lisan (late Pleistocene dead sea) aragonite and implications for glacial east mediterranean climate change. *Geochim. Cosmochim. Acta* 68, 985–1005. doi: 10.1016/j.gca.2003.07.016

Habicht, K., Canfield, D., and Rethmeier, J. (1998). Sulfur isotope fractionation during bacterial reduction and disproportionation of thiosulfate and sulfite. *Geochim. Cosmochim. Acta* 62, 2585–2595. doi: 10.1016/S0016-7037(98)00167-7

Haliva-Cohen, A., Stein, M., Goldstein, S. L., Sandler, A., and Starinsky, A. (2012). Sources and transport routes of fine detritus material to the late quaternary dead sea basin. *Quat. Sci. Rev.* 50, 55–70. doi: 10.1016/j.quascirev.2012.06.014

Kaplan, I., and Rittenberg, S. (1964). Microbiological fractionation of sulphur isotopes. *J. Gen. Microbiol.* 34, 195–212. doi: 10.1099/00221287-34-2-195

Katz, A., Kolodny, Y., and Nissenbaum, A. (1977). The geochemical evolution of the pleistocene lake lisan-dead sea system. *Geochim. Cosmochim. Acta* 41, 1609–1626. doi: 10.1016/0016-7037(77)90172-7

Katz, A., and Starinsky, A. (2008). Geochemical history of the dead sea. *Aquat. Geochem.* 15, 159–194. doi: 10.1007/s10498-008-9045-0

Kaufman, A. (1971). U-Series dating of dead sea basin carbonates. *Geochim. Cosmochim. Acta* 35, 1269–1281. doi: 10.1016/0016-7037(71)90115-3

Khayat, S., Hötzl, H., Geyer, S., Ali, W., Knöller, K., and Strauch, G. (2006). Sulphur and oxygen isotopic characters of dissolved sulphate in groundwater from the pleistocene aquifer in the southern Jordan valley (Jericho area, Palestine). *Isotopes Environ. Health Stud.* 42, 289–302. doi: 10.1080/10256010600839780

Knossow, N., Blonder, B., Eckert, W., Turchyn, A. V., Antler, G., and Kamyshny, A. (2015). Annual sulfur cycle in a warm monomictic lake with sub-millimolar sulfate concentrations. *Geochem. Trans.* 16:7. doi: 10.1186/s12932-015-0021-5

Kolodny, Y., Stein, M., and Machlus, M. (2005). Sea-rain-lake relation in the last glacial east mediterranean revealed by δ18O-δ13C in lake lisan aragonites. *Geochim. Cosmochim. Acta* 69, 4045–4060. doi: 10.1016/j.gca.2004.11.022

Lazar, B., Sivan, O., Yechieli, Y., Levy, E. J., Antler, G., Gavrieli, I., et al. (2014). Long-term freshening of the dead sea brine revealed by porewater Cl- and d18O in ICDP dead Sea deep-drill. *Earth Planet. Sci. Lett.* 400, 94–101. doi: 10.1016/j.epsl.2014.03.019

Leavitt, W. D., Halevy, I., Bradley, A. S., and Johnston, D. T. (2013). Influence of sulfate reduction rates on the phanerozoic sulfur isotope record. *Proc. Natl. Acad. Sci. U.S.A.* 110, 11244–11249. doi: 10.1073/pnas.1218874110

Lu, F., Meyers, W., and Schoonen, M. (2001)., S and O (SO4) isotopes, simultaneous modeling, and environmental significance of the Nijar messinian gypsum, Spain. *Geochim. Cosmochim. Acta* 65, 3081–3092. doi: 10.1016/S0016-7037(01)00553-1

Lyons, T. (1997). Sulfur isotopic trends and pathways of iron sulfide formation in upper holocene sediments of the anoxic black sea. *Geochim. Cosmochim. Acta* 61, 3367–3382. doi: 10.1016/S0016-7037(97)00174-9

Matmon, A., Fink, D., Davis, M., Niedermann, S., Rood, D., and Frumkin, A. (2014). Unraveling rift margin evolution and escarpment development ages along the dead sea fault using cosmogenic burial ages. *Quat. Res.* 82, 281–295. doi: 10.1016/j.yqres.2014.04.008

Neretin, L. N., Böttcher, M. E., and Grinenko, V. A. (2003). Sulfur isotope geochemistry of the black sea water column. *Chem. Geol.* 200, 59–69. doi: 10.1016/S0009-2541(03)00129-3

Neugebauer, I., Brauer, A., Schwab, M. J., Waldmann, N., Enzel, Y., Kitagawa, H., et al. (2014). Lithology of the long sediment record recovered by the ICDP dead sea deep drilling project (DSDDP). *Quat. Sci. Rev.* 102, 149–165. doi: 10.1016/j.quascirev.2014.08.013

Oldenburg, T. B. P., Rullkotter, J., Bottcher, M. E., Nissenbaum, A. (2000a). Addendum to molecular and isotopic characterization of organic matter in recent and sub-recent sediments from the dead sea, [Organic, Geochemistry, 31 (2000). 251–265]. *Org. Geochem.* 31, 773–774. doi: 10.1016/S0146-6380(00)00079-6

Oldenburg, T. B. P., Rullkötter, J., Böttcher, M. E., and Nissenbaum, A. (2000b). Molecular and isotopic characterization of organic matter in recent and sub-recent sediments from the dead sea. *Org. Geochem.* 31, 251–265. doi: 10.1016/S0146-6380(00)00015-2

Rees, C. E. (1973). A steady-state model for sulphur isotope fractionation in bacterial reduction processes. *Geochim. Cosmochim. Acta* 37, 1141–1162. doi: 10.1016/0016-7037(73)90052-5

Sim, M. S., Bosak, T., and Ono, S. (2011). Large sulfur isotope fractionation does not require disproportionation. *Science* 333, 74–77. doi: 10.1126/science.1205103

Starinsky, A. (1974). *Relationship between Ca-chloride Brines and Sedimentary Rocks in Israel.* Ph.D. dissertation, The Hebrew University of Jerusalem.

Stein, M. (2001). The sedimentary and geochemical record of neogene-quaternary water bodies in the dead sea basin – inferences for the regional paleoclimatic history. *J. Paleolimnol.* 26, 271–282. doi: 10.1023/A:1017529228186

Stein, M., Agnon, A., Katz, A., and Starinsky, A. (2002). Strontium isotopes in discordant dolomite bodies of the Judea group, dead sea basin. *Isr. J. Earth Sci.* 51, 219–224. doi: 10.1560/61UM-UMQF-YU86-JNU0

Stein, M., Starinsky, A., Agnon, A., Katz, A., Raab, M., Spiro, B., et al. (2000). The impact of brine-rock interaction during marine evaporite formation on the isotopic Sr record in the oceans: evidence from Mt. Sedom, Israel. *Geochim. Cosmochim. Acta* 64, 2039–2053. doi: 10.1016/S0016-7037(00)00370-7

Stein, M., Starinsky, A., Katz, A., Goldstein, S. L., Machlus, M., and Schramm, A. (1997). Strontium isotopic, chemical, and sedimentological evidence for the evolution of lake lisan and the dead sea. *Geochim. Cosmochim. Acta* 61, 3875–3992. doi: 10.1016/S0016-7037(97)00191-9

Strauss, H. (1997). The isotopic composition of sedimentary sulfur through time. *Palaeogeogr. Palaeoclimatol. Palaeoecol.* 132, 97–118. doi: 10.1016/S0031-0182(97)00067-9

Szynkiewicz, A., Moore, C. H., Glamoclija, M., and Pratt, L. M. (2009) Sulfur isotope signatures in gypsiferous sediments of the Estancia and Tularosa basins as indicators of sulfate sources, hydrological processes, and microbial activity. *Geochim. Cosmochim. Acta* 73, 6162–6186. doi: 10.1016/j.gca.2009.07.009

Thomas, C., Ebert, Y., Kiro, Y., Stein, M., and Ariztegui, D. (2016). Microbial sedimentary imprint on the deep dead sea sediment. *Depos. Rec.* 118–138. doi: 10.1002/dep2.16

Torfstein, A., Gavrieli, I., Katz, A., Kolodny, Y., and Stein, M. (2008). Gypsum as a monitor of the paleo-limnological–hydrological conditions in lake lisan and the dead sea. *Geochim. Cosmochim. Acta* 72, 2491–2509. doi: 10.1016/j.gca.2008.02.015

Torfstein, A., Gavrieli, I., and Stein, M. (2005). The sources and evolution of sulfur in the hypersaline lake lisan (paleo-dead sea). earth planet. *Sci. Lett.* 236, 61–77. doi: 10.1016/j.epsl.2005.04.026

Torfstein, A., Goldstein, S., Kagan, E. J., and Stein, M. (2013a). Integrated multi-site U–Th chronology of the last glacial Lake Lisan. *Geochim. Cosmochim. Acta* 104, 210–231. doi: 10.1016/j.gca.2012.11.003

Torfstein, A., Goldstein, S. L., Kushnir, Y., Enzel, Y., Haug, G. H., and Stein, M. (2015). Dead sea drawdown and monsoonal impacts in the levant during the last interglacial. *Earth Planet. Sci. Lett.* 412, 235–244. doi: 10.1016/j.epsl.2014.12.013

Torfstein, A., Goldstein, S., Stein, M., and Enzel, Y. (2013b). Impacts of abrupt climate changes in the levant from last glacial dead sea levels. *Quat. Sci. Rev.* 69, 1–7. doi: 10.1016/j.quascirev.2013.02.015

Torfstein, A., Haase-Schramm, A., Waldmann, N., Kolodny, Y., and Stein, M. (2009). U-series and oxygen isotope chronology of the mid-pleistocene lake Amora (dead sea basin). *Geochim. Cosmochim. Acta* 73, 2603–2630. doi: 10.1016/j.gca.2009.02.010

Tuttle, M. L., and Goldhaber, M. B. (1993). Sedimentary sulfur geochemistry of the paleogene green river formation, western USA: implications for interpreting depositional and diagenetic processes in saline alkaline lakes. *Geochim. Cosmochim. Acta* 57, 3023–3039. doi: 10.1016/0016-7037(93)90291-4

Watanabe, T., Naraoka, H., Nishimura, M., and Kawai, T. (2004). Biological and environmental changes in lake Baikal during the late quaternary inferred from carbon, nitrogen and sulfur isotopes. *Earth Planet. Sci. Lett.* 222, 285–299. doi: 10.1016/j.epsl.2004.02.009

Wortmann, U., Chernyavsky, B., Bernasconi, S., Brunner, B., Böttcher, M., and Swart, P. (2007). Oxygen isotope biogeochemistry of pore water sulfate in the deep biosphere: dominance of isotope exchange reactions with ambient water during microbial sulfate reduction (ODP Site 1130). *Geochim. Cosmochim. Acta* 71, 4221–4232. doi: 10.1016/j.gca.2007.06.033

Yang, W., Spencer, R. J., and Roy Krouse, H. (1997). Stable isotope compositions of waters and sulfate species therein, death valley, California, USA: implications for inflow and sulfate sources, and arid basin climate. *Earth Planet. Sci. Lett.* 147, 69–82. doi: 10.1016/S0012-821X(97)00011-3

Zak, I. (1967). *The Geology of Mount Sedom.* Ph.D. dissertation, The Hebrew University of Jerusalem.

Conflict of Interest Statement: The authors declare that the research was conducted in the absence of any commercial or financial relationships that could be construed as a potential conflict of interest.

The reviewer DTW and handling Editor declared their shared affiliation, and the handling Editor states that the process nevertheless met the standards of a fair and objective review.

frontiers in Microbiology

ORIGINAL RESEARCH
published: 21 June 2017
doi: 10.3389/fmicb.2017.01164

Control of Sulfide Production in High Salinity Bakken Shale Oil Reservoirs by Halophilic Bacteria Reducing Nitrate to Nitrite

*Biwen A. An, Yin Shen and Gerrit Voordouw **

Petroleum Microbiology Research Group, Department of Biological Sciences, University of Calgary, Calgary, Alberta, AB, Canada

Microbial communities in shale oil fields are still poorly known. We obtained samples of injection, produced and facility waters from a Bakken shale oil field in Saskatchewan, Canada with a resident temperature of 60°C. The injection water had a lower salinity (0.7 Meq of NaCl) than produced or facility waters (0.6–3.6 Meq of NaCl). Salinities of the latter decreased with time, likely due to injection of low salinity water, which had 15–30 mM sulfate. Batch cultures of field samples showed sulfate-reducing and nitrate-reducing bacteria activities at different salinities (0, 0.5, 0.75, 1.0, 1.5, and 2.5 M NaCl). Notably, at high salinity nitrite accumulated, which was not observed at low salinity, indicating potential for nitrate-mediated souring control at high salinity. Continuous culture chemostats were established in media with volatile fatty acids (a mixture of acetate, propionate and butyrate) or lactate as electron donor and nitrate or sulfate as electron acceptor at 0.5 to 2.5 M NaCl. Microbial community analyses of these cultures indicated high proportions of *Halanaerobium*, *Desulfovermiculus, Halomonas,* and *Marinobacter* in cultures at 2.5 M NaCl, whereas *Desulfovibrio, Geoalkalibacter,* and *Dethiosulfatibacter* were dominant at 0.5 M NaCl. Use of bioreactors to study the effect of nitrate injection on sulfate reduction showed that accumulation of nitrite inhibited SRB activity at 2.5 M but not at 0.5 M NaCl. High proportions of *Halanaerobium* and *Desulfovermiculus* were found at 2.5 M NaCl in the absence of nitrate, whereas high proportions of *Halomonas* and no SRB were found in the presence of nitrate. A diverse microbial community dominated by the SRB *Desulfovibrio* was observed at 0.5 M NaCl both in the presence and absence of nitrate. Our results suggest that nitrate injection can prevent souring provided that the salinity is maintained at a high level. Thus, reinjection of high salinity produced water amended with nitrate maybe be a cost effective method for souring control.

Keywords: souring control, shale oil, Bakken, halophilic, nitrate, nitrite, sulfate-reducing bacteria, nitrate-reducing bacteria

OPEN ACCESS

Edited by:
Alexandra V. Turchyn, University of Cambridge, United Kingdom

Reviewed by:
Paula Mouser, The Ohio State University Columbus, United States
Hans Karl Carlson, University of California, Berkeley, United States

****Correspondence:***
Gerrit Voordouw
voordouw@ucalgary.ca

Specialty section:
This article was submitted to Microbiological Chemistry and Geomicrobiology, a section of the journal Frontiers in Microbiology

Received: *27 March 2017*
Accepted: *07 June 2017*
Published: *21 June 2017*

Citation:
An BA, Shen Y and Voordouw G (2017) Control of Sulfide Production in High Salinity Bakken Shale Oil Reservoirs by Halophilic Bacteria Reducing Nitrate to Nitrite. Front. Microbiol. 8:1164. doi: 10.3389/fmicb.2017.01164

INTRODUCTION

Hydraulic fracturing with subsequent production from horizontal wells is used both in shale gas and in shale oil fields (Caper, 2010; Daly et al., 2016; Shrestha et al., 2017). A key difference is that shale oil production can also require injection of water for continued oil recovery (Laurenzi et al., 2016). Flowback waters obtained from shale gas

fields are highly saline (Daly et al., 2016; Khan et al., 2016; Shrestha et al., 2017), as are produced waters obtained from shale oil fields (Strong et al., 2013). However, in the case of shale oil fields the salinity of produced water may change depending on the salinity of the injection water used (Shrestha et al., 2017).

The microbial communities in shale gas fields (Ivanova et al., 2011; Tucker et al., 2015; Daly et al., 2016; Ding et al., 2016) have been well characterized. These include the microorganisms introduced during hydraulic fracturing, as well as those indigenous to the formation (Cluff et al., 2014). Shale gas environments are typically rich in hydrocarbons and are at high pressure and temperature (Cluff et al., 2014; Daly et al., 2016; Liang et al., 2016). Previous studies on waters produced from hydraulic fracturing at different shale operations showed similar microbial community composition (Liang et al., 2016; Mouser et al., 2016). Aerobic freshwater microorganisms from the initial fracturing fluids dominated microbial communities in initial flowback waters. These changed to anaerobic halophilic communities with *Firmicutes (Halanaerobium), Bacteroidetes, Beta-, Gamma-, Delta-* and *Epsilonproteobacteria,* along with methanogenic taxa in subsequent flowback waters (Davis et al., 2012; Struchtemeyer et al., 2012; Murali Mohan et al., 2013; Strong et al., 2013; Cluff et al., 2014; Daly et al., 2016; Liang et al., 2016). These communities are capable of hydrocarbon degradation and fermentation at high salinity, including taxa such as *Marinobacter, Halomonas,* and *Halanaerobium* (Cluff et al., 2014; Daly et al., 2016; Liang et al., 2016). *Halanaerobium* in particularly has been linked to biofilm formation and corrosion by degrading the polysaccharide (guar gum) used in the fracturing process while reducing thiosulfate to sulfide (Daly et al., 2016; Liang et al., 2016). Archaeal taxa, are typically detected in later flow back samples, and many are methylotrophic methanogens such as *Methanohalophilus* and *Methanolobus* (Wuchter et al., 2013; Daly et al., 2016). Overall, the microbial communities in shale gas fields, introduced through well drilling or indigenous, have been studied extensively over the past decade.

Contrary to this wealth of knowledge on the microbial communities in shale gas fields, those in shale oil fields are much less well known. This is surprising given that shale oil production from the Bakken formation alone, which spans parts of Saskatchewan and Manitoba in Canada and of North Dakota in the US, is now a mature industry producing 1.2 million barrels of oil per day by 2015 (Laurenzi et al., 2016). In the Bakken formation 0.5 to 3 million gallons (1.9 to 11.4 million liters) of water are required per well (Wang et al., 2016). The oil from the Bakken formation is light (31° to 45° API) (Yevhen et al., 2011), but increasing concentrations of H_2S have been observed throughout the production process (Yevhen et al., 2011). Souring of Bakken wells can be attributed to geomechanical, thermochemical and biogenic factors (Yevhen et al., 2011). Biogenic souring in conventional oil fields is due to the reduction of sulfate, thiosulfate or sulfur to sulfide by microorganisms (Youssef et al., 2009; Gieg et al., 2011). Souring in oil reservoirs can lead to corrosion and environmental risks. It is not known whether biogenic souring is due to indigenous species or due to microorganisms introduced with the injection fluids. In addition, continuous injection of water to maintain reservoir pressure is not done in shale gas fields. The effect of this process on shale oil fields is currently unknown. High salinity and temperature can inhibit the presence and activity of microorganisms. However decreasing the salinity and temperature of the reservoir may increase biogenic souring potential (Youssef et al., 2009; Gieg et al., 2011). Nitrate injection is often used to control souring by sulfate-reducing bacteria (SRB) in both low temperature and high temperature fields (Reinsel et al., 1996; Gieg et al., 2011; Fida et al., 2016). During nitrate injection, nitrate-reducing bacteria (NRB) can reduce nitrate to nitrite, which can chemically react with sulfide and which inhibits the dissimilatory sulfite reductase (Dsr) in SRB preventing further formation of sulfide (Reinsel et al., 1996; Hubert et al., 2003; Hubert and Voordouw, 2007; Gieg et al., 2011; Fida et al., 2016). In extreme environments, such as at high temperature, nitrite can accumulate with nitrate injection, thus effectively inhibiting souring (Gieg et al., 2011; Fida et al., 2016). Compared to nitrate-mediated souring control at low salinity conditions, there is a lack of knowledge on its effectiveness at high salinity. In the past 4 years we have collected samples from a saline shale oil field in Saskatchewan and the results of our studies on the potential of the associated microbial communities in controlling souring with nitrate are reported here.

MATERIALS AND METHODS

Sample Collection

Samples were collected from points indicated in **Figure 1** in November 2013, January 2015 and August 2015 in 1 L autoclaved Nalgene bottles filled to the brim to exclude air and samples were shipped on ice. Shipping times for these three sets were 4, 3, and 4 days, respectively. The samples were stored in an anaerobic hood with 90% (v/v) N_2 and 10% CO_2 (N_2-CO_2) atmosphere upon arrival. Four types of samples were sent: source water (SW), injection water (IW), produced waters (PW) with emulsified oil, free-water knockout water (FW) and treatment water (TW). The aqueous layers of the PW samples were used for analyses and enrichments. Synthetic facility water, 300 mL per L of sample, was added to PW samples that had little water and were difficult to separate. Synthetic facility water contained per L: 146 g NaCl, 2.37 g KCl, 1.82 g $MgCl_2$, 6.48 g $CaCl_2$ and 0.34 g $NaHCO_3$.

Analytical Determinations and Most Probable Numbers

Water chemistry analyses for field samples were carried out using 50 mL of sample for pH, salinity, sulfate and ammonium concentration measurements. Sulfate concentrations were also measured for enrichments, continuous cultures and bioreactors. Analyses of the concentrations of sulfide, nitrate or nitrite were for enrichments, continuous cultures and bioreactors only. The pH was measured using an Orion pH meter (Model 370). Salinity in molar equivalent (Meq) of NaCl was analyzed with an Orion conductivity cell (model 013005MD). The concentration of dissolved sulfide was measured using the diamine method (Trüper and Schlegel, 1964). Samples were diluted to 1 Meq of NaCl before analyzing sulfate, nitrate and nitrite with the Waters 600E high performance liquid chromatography (HPLC)

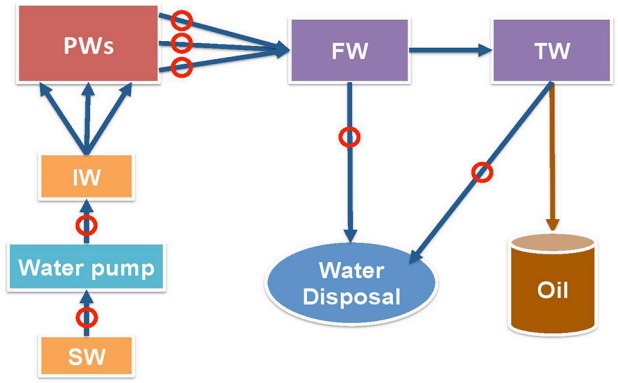

FIGURE 1 | Schematic diagram of shale oil production from a field in the Bakken formation. Mannville formation source water (SW) is injected at the injection well (IW) to pressurize multiple producing wells (PW). Oil-water emulsions from producing wells enter free water knockout (FW) facility first, then treater facility (TW) to separate oil from water. The produced water is not reinjected, but is disposed. Circles indicate the sampling points.

instrument. Sulfate was measured using a conductivity detector (Waters 423) and IC-PAK anion column (4 × 150 mm, Waters) with acetonitrile, borate/gluconate buffer at a flow rate of 2 ml/min. Nitrate and nitrite were eluted from the same column with the same buffer that were measured with an UV detector (UV/VIS-2489, Waters) at 220 nm. Ammonium concentrations were measured using spectrophotometry with the indophenol method (Aminot et al., 1997).

Viable SRB and acid-producing bacteria (APB) in field samples were enumerated by a miniaturized three well MPN method, using 48 well (6 × 8) plates. For the MPN of SRB, 0.1 ml of sample was inoculated into 0.9 ml of Postgate B medium (at 0.01 M and 2 M NaCl, per L: 0.5 g KH_2PO_4, 1.0 g NH_4Cl, 1.3 g $CaSO_4 \bullet 2H_2O$, 2.0 g $MgSO_4 \bullet 7H_2O$, 4.0 g 60% sodium lactate, 1.0 g yeast extract, 0.1 g ascorbic acid, 0.1 g thioglycolate, 0.5 g $FeSO_4 \bullet 7H_2O$, pH 7-7.5), containing lactate, sulfate and ferrous iron. These were then serially diluted 10-fold to 10^{-8} in the same medium in triplicate wells. The plate was immediately covered with a Titer-Tops membrane and incubated at 32°C inside the anaerobic hood. Wells were scored as positive when a black FeS precipitate was evident. For MPN of APB, the sample was serially diluted in Phenol Red Dextrose medium with 0.1 M or 2 M of NaCl (ZPRA-5, DALYNN Biologicals) using the same procedure as described for SRB. Growth of APB results in a decrease of pH detected as a change in color from orange to yellow. MPN values were calculated for triplicate dilution series by comparing the pattern of positive wells to a probability table for MPN tests (Shen and Voordouw, 2017).

Media and Growth Conditions of Enrichments and Continuous Cultures

Enrichments were grown in 120-mL serum bottles with 60 mL of anaerobic Coleville synthetic brine medium K (CSBK) containing the following in g/L: NaCl, 1.5, 29.2, 43.8, 58.4, 87.7, 116.9 or 146.1; KH_2PO_4, 0.05; NH_4Cl, 0.32; $CaCl_2 \bullet 2H_2O$, 0.21; $MgCl_2 \bullet 2H_2O$, 0.54; KCl, 0.1. After autoclaving 30 mL of 1 M $NaHCO_3$, 1 mL of vitamin solution and 1 mL of selenite-tungstate solution (Hubert et al., 2003) were added, 1 mM of Na_2S (as reductant) was also added and the pH was adjusted to 7.2 to 7.5 prior to dispensing medium into N_2-CO_2 flushed serum bottles. Autoclaved sulfate or nitrate (4 or 10 mM) was added as electron acceptors. Volatile fatty acids (VFA) (3 mM or 6 mM each of acetate, propionate, and butyrate) or lactate (20 mM) was added as the electron donors. Enrichments were incubated at 30°C in the dark shaking at 100 rpm. Enrichments were also used to inoculate continuous cultures (chemostats).

Aliquots (10% v/v) of 2013 and 2015 shale oil field samples were inoculated into 120 mL serum bottles containing 60 mL of reduced CSBK medium with different salinities (0.01, 0.5, 0.75, 1.0, 1.5, 2.0, or 2.5 M NaCl). Incubations received either lactate (20 mM) or VFA (3 or 6 mM) as electron donors and sulfate (10 mM) or nitrate (10 or 20 mM) as electron acceptors. All enrichments were done in duplicate and incubated at 30°C. Successful enrichments were transferred into medium with the same substrates.

Chemostats were inoculated using secondary enrichments of August 2015 field samples (08/15). High salinity (2.5 M NaCl) chemostats contained lactate and sulfate (LS_2.5), lactate and nitrate (LN_2.5), VFA and sulfate (VS_2.5) or VFA and nitrate (VN_2.5). These were inoculated with high salinity enrichments of TW_08/15. Low salinity (0.5 M NaCl) chemostats contained lactate and sulfate (LS_0.5) or lactate and nitrate (LN_0.5). Chemostats contained 100 mL of culture stirring at 400 rpm and were incubated at 37°C. The medium flow rate was generally 42 mL/day, corresponding to a dilution rate of 0.42 day^{-1}.

Bioreactor Setup and Start-Up

Bioreactors were set up to determine the effect of nitrate on sulfide production under flow conditions at high salt concentration using methods as described previously (Xue and Voordouw, 2015) (**Figure 2**) with plastic syringes (30 mL) without pistons as bioreactor columns. Glass wool and polymeric mesh were placed at the bottom of the bioreactors. The bioreactors were then tightly packed with sand (Sigma-Aldrich, 50–70 mesh particle size). The pore volume (PV) of the columns was calculated using the weight difference between medium-flooded columns and dry columns (PV = 12.47 ± 0.53 mL). The medium used was CSBK with 0.5 or 2.5 M NaCl and 10 mM sulfate, 10 mM nitrate, 20 mM lactate or 6 mM VFA, as indicated. After media flooding, the bioreactors were inoculated with 0.5 PV of an enrichment or a chemostat culture. Bioreactors were then incubated without flow for 2 weeks. Post incubation, medium with 4 mM sulfate and/or 4 mM nitrate was injected into the bioreactors at flow rates of 0.1 to 0.6 PV/day as indicated. Periodic measurements of anions and sulfide were taken for samples collected from the effluent port of the bioreactors (**Figure 2**). At the end of the experiment the microbial community compositions were analyzed by Illumina Miseq sequencing. Bioreactors were run at room temperature (22°C).

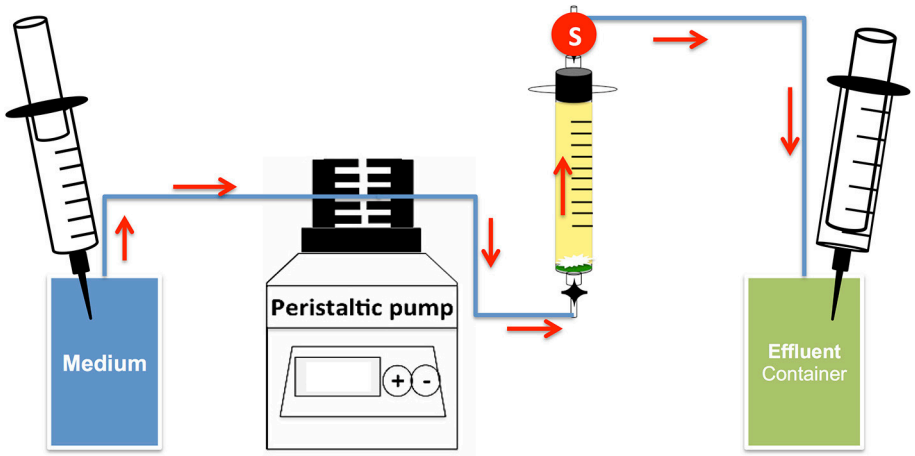

FIGURE 2 | Schematic of up-flow sand packed bioreactor system**.** The arrows indicate direction of media flow; circle S indicates the effluent sampling point. Pressure in both media and effluent containers was maintained using 30 mL plastic syringes of which the left one was filled with N_2-CO_2 gas.

DNA Extraction and Microbial Community Analyses

DNA was extracted from field samples and for samples from incubations or bioreactors. For field samples, 250 mL of the aqueous phase of each sample was centrifuged at 14,000x g for 20 min at 4°C to pellet the cells. For incubations, 5 mL of sample was centrifuged at 14,000x g for 10 min at 4°C. For the bioreactors, 5 mL of the effluent was collected on ice then centrifuged at 14,000x g for 10 min at 4°C. Following completion of the experiment, the bioreactors were dismantled and 5 mL of sterile water was added to 5 g of inlet sand fraction and shaken vigorously. The supernatant was then removed and centrifuged at 14,000x g for 10 min at 4°C to pellet cells. DNA was extracted from the cell pellets using the FastDNA extraction kit for soil (MP Biomedicals). DNA was quantified with a Qubit fluorimeter (Invitrogen) using the Quant-iT double-stranded DNA (dsDNA) HS assay kit (Invitrogen).

For the 2013 field samples 16S rRNA genes were amplified using a two step-PCR procedure. The first PCR (25 cycles) was done using non-barcoded universal 16S primers (926F: AAACTY AAAKGAATTGRCGG and 1392R: ACGGGCGGTGTGTRC) with conditions as described elsewhere (Park et al., 2011). PCR products were checked with gel electrophoresis and purified with a QIAquick PCR Purification Kit (Qiagen). The second PCR (10 cycles) was done using barcoded FLX titanium amplicon primers 454T_RA_X and 454T_FwB, which have the 16S primers (926F and 1392) as their 3'-ends (Park et al., 2011). The resulting PCR products were purified and quantified prior to pyrosequencing at the McGill University Genome Quebec Innovation Centre, Montreal, using a Genome Sequencer FLX instrument and a GS FLX titanium series XLR70 kit (Roche Diagnostic Corporation).

For 2015 field samples, incubation and bioreactor DNAs were amplified using the same two-step PCR process but with Illumina Miseq non-barcoded primers (926Fi5 TCGTCGGCA GCGTCAGATGTGTATAAGAGACAGAAACTYAAAKGA ATWGRCGG and 1392RiF GTCTCGTGGGCTCGGAGATGT GTATAAGAGACAGACGGGCGGTGWGTRC) for the first PCR (25 cycles). For the 2nd PCR (10 cycles), forward primer (P5-S50X-OHAF) with a 29-nt 5' Illumina sequencing adaptor (P5, AATGATACGGCGACCACCGAGATCTACAC), an 8-nt identifying index S50X and a 14-nt forward overhang adaptor (OHAF, TCGTCGGCAGCGTC), and reverse primer (P7-N7XX-OHAF) with a 24-nt 3' Illumina sequencing adaptor (P7, CAA GCAGAAGACGGCATACGAGAT), an 8-nt identifying index N7XX and a 14-nt reverse overhang adaptor (OHAF, GTC TCGTGGGCTCGG), were used. The final PCR product was purified and quantified using the same procedures as above and sent for Illumina Miseq sequencing at the University of Calgary.

Analyses of pyrosequencing and Illumina Miseq sequences were done with the MetaAmp software, (http://ebg.ucalgary.ca/metaamp/; developed by the University of Calgary Energy Bioengineering Group) and sequences were subjected to stringent quality control (QC). Merged reads using PEAR 0.9.8 were uploaded to MetaAmp, which used a cutoff quality score for each sequence of 50 and a minimum length of each sequence of 420 base pairs. The QC sequences were clustered into operational taxonomic units (OTUs) using average neighbor clustering at a distance of 3%. Each remaining OTU was assigned to a taxon by comparing with the latest version of the non-redundant 16S rRNA small subunit SILVA database. Samples were clustered into a dendrogram using the unweighted pair group method algorithm (UPGMA) and the distance between communities was calculated using the Bray-Curtis coefficient in the Mothur software. The dendrogram was visualized using the MEGA5.2.2. Program (Tamura et al., 2011). The entire sets of raw reads have been submitted to the NCBI Sequence Read Archive (SRA) under Bioproject accession number PRJNA181037, with Biosample numbers SAMN06624370 and SAMN06624665.

TABLE 1 | Water chemistry data for the Bakken field samples.

Sample type	Sample name	pH	Salinity (Meq NaCl)	Ion analysis (mM)	
				Sulfate	Ammonium
Source waters and injection water	8SW_11/13	6.4	0.7	27.5	1.3
	8SW_01/15	7.2	0.8	33.3	1.3
	8SW_08/15	6.9	0.6	30.2	2.3
	13IW_08/15	7.0	0.8	28.5	3.2
	Average ± Sd	6.9 ± 0.3	0.7 ± 0.1	29.9 ± 2.6	2.0 ± 0.9
Produced waters	5PW_11/13	5.8	2.3	5.1	22.8
	2PW_01/15	6.8	1.2	14.0	5.4
	4PW_01/15	6.5	2.2	15.1	19.0
	2PW_08/15	6.5	0.8	32.5	11.3
	11PW_08/15	6.2	0.6	27.8	33.0
	12PW_08/15	7.3	0.7	30.1	2.4
	14PW_08/15	6.4	3.7	30.3	33.2
	15PW_08/15	6.6	1.1	34.8	11.3
	Average ± Sd	6.5 ± 0.4	1.6 ± 1.0	23.7 ± 10.1	17.3 ± 11.0
Free water knockout and treater water	9FW_11/13	6.0	2.1	17.0	19.2
	10TW_11/13	6.0	2.2	19.2	20.1
	9FW_01/15	6.3	2.8	15.3	19.0
	10TW_01/15	6.3	2.7	17.1	24.3
	9FW_08/15	6.1	2.4	15.8	26.3
	10TW_08/15	6.2	2.3	18.8	26.1
	Average ± Sd	6.1 ± 0.1	2.4 ± 0.3	17.2 ± 1.6	22.5 ± 3.5

Data for source waters (SW), injection water (IW), produced waters (PW), free-water knockout (FW) and treater water (TW) samples from 2013 (11/13) and 2015 (01/15 or 08/15) are shown.

RESULTS

Water Chemistry and MPN

The water chemistry of the source water (SW), injection water (IW), produced water (PW), free water knockout water (FW) and treater water (TW) samples is summarized in **Table 1.** Samples that were mostly oil and required synthetic facility water for obtaining an aqueous extract are not included. SW and IW samples (SW-IWs) had an average salinity of 0.7 ± 0.1 Meq of NaCl, a high sulfate concentration of 29.9 ± 2.6 mM and a low ammonium concentration of 2.0 ± 0.9 mM. These values were similar for all samples reflecting those of the Mannville SW of which the water chemistry was apparently constant with time. In contrast the PWs had salinities ranging from 0.6 to 3.7 Meq of NaCl (average 1.6 ± 1.0 Meq of NaCl), sulfate concentrations from 5.1 to 34.8 mM (average 23.6 ± 10.1 mM) and ammonium concentrations from 2.4 to 33.2 mM (average 17.3 ± 11.0 mM). Three PWs had similar salinity and sulfate concentration as for the SW-IWs. However, only one of these (12PW_08/15) also had a low ammonium concentration of 2.4 mM (**Table 1**). The bivariate fit analysis of ammonium concentrations and salinity (JMP®, Version *13.1*. SAS Institute Inc., Cary, NC, 1989–2007), with the exception of sample 11PW_08/15, showed a linear relationship (Figure S1: $r^2 = 0.90$), indicating that the increased salinity and ammonium concentration of the PWs were likely contributed by the shale oil formation. However, salinity and sulfate concentration were not linearly correlated, indicating that the shale formation can either decrease or maintain the sulfate concentration of produced waters from the value of 30 mM (540 ppm) of the SW-IWs (**Table 1**). The ammonium concentration in flowback waters from shale gas fields was shown to correlate linearly with the chloride concentration in each geological formation with maximum values of 432 ppm (24 mM) of ammonium and 160,000 ppm (4.5 M) of chloride (Harkness et al., 2015). Produced waters from all producing wells are co-mingled in the FW and TW processing facilities. The PWs that were sampled were only a small subset of these. The average salinity of FW and TW (FW-TW) samples was 2.4 ± 0.3 Meq of NaCl. The average ammonium and sulfate concentrations were 22.5 ± 3.5 and 17.2 ± 1.6 mM, respectively. These averages were similar but not identical to those for the PWs, because the selected set of PWs may not represent the average.

MPNs for APB and SRB were determined both at 0.01 M and 2 M NaCl (Table S1). The MPNs were higher at higher salinity for APB in 6 of 7 and for SRB in 4 of 7 PW samples, indicating the presence of a halophilic microbial community.

Microbial Community Analysis of Field Samples

DNAs were isolated, subjected to PCR and either pyrosequencing (2013 samples) or Illumina sequencing (2015 samples).

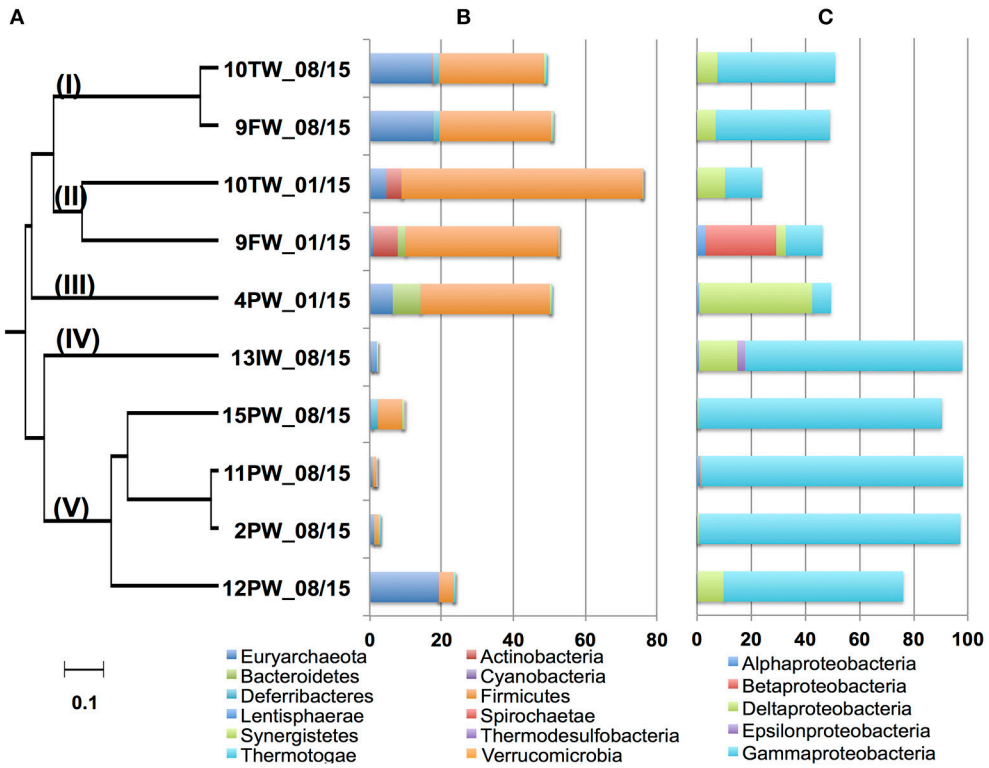

FIGURE 3 | Dendrogram of the 2015 Bakken field samples. The relational tree of microbial community compositions of 2015 samples indicates clades I to V **(A)**. Distribution of phyla other than *Proteobacteria* in the community compositions **(B)**. Distribution of classes from the phylum *Proteobacteria* in the community compositions **(C)**. The scale indicates 10% sequence divergence.

dendrogram for microbial community compositions of the 2015 samples (**Figure 3**) indicated five distinct clades (**Figure 3A**; I-V). Communities in FW-TW samples (clades I and II) were distinct from those in most produced water samples (clade V). Microbial community compositions for 4PW and 13IW were in clades III and IV, respectively.

Microorganisms can be described as being halophilic (requiring high salt for growth) or halotolerant (tolerating high salt, but growing better at low salt) (Oren, 2008). Because this property cannot be derived from most genus names, we will use the term halophilic/halotolerant to describe identified taxa. The microbial communities in clade I (FW-TW 08/15) were dominated by the halophilic/halotolerant genera *Halanaerobium*, *Modicisalibacter*, *Methanohalophilus,* and *Chromohalobacter*. Microbial communities from clade II (FW-TW 01/15), were dominated by *Halanaerobium, Desulfovermiculus, Methanohalophilus, Rhodococcus, Ralstonia, Marinobacterium,* and *Dethiosulfatibacter* (**Table 2**). The community compositions of PW samples in clade V had high fractions (45-95%) of *Marinobacter* with smaller fractions of *Halomonas, Thiomicrospira, Methanothermococcus,* and *Desulfotignum* (**Table 2**). The single IW sample in clade IV had a community dominated by *Thiomicrospira,* unidentified *Gammaproteobacteria* and *Desulfocella* (**Figure 3A**, **Table 2**), whereas the single PW sample in clade III had high fractions of *Halanaerobium* (36%) and *Desulfovermiculus* (41%) and smaller fractions of *Methanohalophilus, Chromohalobacter, Marinobacterium,* and *Sphingobacteriales*. Overall these results indicated dominance of halophilic/halotolerant taxa in the microbial communities of all samples, except 13IW.

The microbial communities in 2013 samples were also dominated by halophilic/halotolerant taxa. High fractions of *Methanohalophilus, Halanaerobium,* and *Desulfovermiculus*, as well as of *Flexistipes, Halomonas,* and *Desulfohalobium* were found (Table S2).

Reduction of Sulfate and Nitrate in Enrichment Cultures at Different Salinity

Media with 2.5 M NaCl, containing lactate and sulfate (LS_2.5), VFA and sulfate (VS_2.5) or VFA and nitrate (VN_2.5) were inoculated with 9 field samples collected in 2013. Incubations in LS_2.5 medium showed SRB activity for 5 of these with reduction of 9.5±0.03 mM sulfate to 5.2 ± 0.7 mM of aqueous sulfide in 20 to 60 days (**Figures 4A,B**), whereas incubations in VS_2.5 medium showed activity for 3 samples with reduction of 9.6 ± 0.2 mM sulfate to 3.8 ± 0.6 mM sulfide (**Figures 4C,D**). Five samples showed nitrate reduction (**Figure 4E**). Of these 4 accumulated up to 9.2 ± 0.6 mM nitrite (**Figure 4C**), whereas nitrite was transiently formed in 10TW_11/13 (**Figure 4F**).

TABLE 2 | Microbial community composition of the Bakken 2015 field samples.

#Taxonomy (Class; Order; Family; Genus)	I		II		III	IV	V			
	9FW 08/15	10TW 08/15	9FW 01/15	10TW 01/15	4PW 01/15	13IW 08/15	15PW 08/15	11PW 08/15	2PW 08/15	12PW 08/15
Gammaproteobacteria;Alteromonadales; Alteromonadaceae;Marinobacter;	**2.7**	**1.0**	**8.1**	**1.4**	**1.8**	0.0	**51.0**	**94.5**	**94.6**	**44.6**
Clostridia; Halanaerobiales; Halanaerobiaceae; Halanaerobium;	**31.1**	**29.3**	**31.1**	**66.5**	**36.0**	0.0	**6.6**	0.3	0.8	0.2
Gammaproteobacteria; Thiotrichales; Piscirickettsiaceae; Thiomicrospira;	0.1	0.2	0.0	0.0	0.0	**53.3**	0.0	0.0	0.0	**21.3**
Gammaproteobacteria; Oceanospirillales; Halomonadaceae; Modicisalibacter;	**28.0**	**35.8**	0.0	0.0	0.0	0.0	0.7	0.0	0.0	0.0
Deltaproteobacteria; Desulfovibrionales; Desulfohalobiaceae; Desulfovermiculus;	**1.0**	**1.2**	**1.0**	**6.4**	**40.5**	0.0	0.1	0.0	0.0	0.0
Gammaproteobacteria; Oceanospirillales; Halomonadaceae; Halomonas;	**1.4**	0.9	0.0	0.9	0.0	0.0	**38.2**	**2.1**	**2.0**	0.4
Methanomicrobia; Methanosarcinales; Methanosarcinaceae; Methanohalophilus;	**16.4**	**16.0**	**5.1**	**3.2**	**2.9**	0.0	0.3	0.1	0.1	0.0
Gammaproteobacteria;	0.0	0.0	0.4	0.3	0.0	**26.9**	0.0	0.0	0.0	0.0
Betaproteobacteria; Burkholderiales; Burkholderiaceae; Ralstonia;	0.0	0.0	**25.6**	0.1	0.0	0.0	0.0	0.0	0.0	0.0
Methanococci; Methanococcales; Methanococcaceae; Methanothermococcus;	**1.2**	**1.3**	0.0	**1.4**	**1.4**	0.0	0.1	0.0	**1.0**	**12.7**
Gammaproteobacteria; Oceanospirillales; Halomonadaceae; Chromohalobacter;	**9.8**	**5.5**	0.0	0.0	**1.3**	0.0	0.1	0.0	0.0	0.0
Deltaproteobacteria; Desulfobacterales; Desulfobacteraceae; Desulfocella;	0.0	0.0	0.0	0.1	0.0	**12.0**	0.0	0.0	0.0	0.1
Gammaproteobacteria; Oceanospirillales; Oceanospirillaceae; Marinobacterium;	0.2	0.1	0.0	**9.4**	**2.4**	0.0	0.0	0.0	0.0	0.1
Clostridia; Clostridiales; Clostridiales-Incertae-Sedis; Dethiosulfatibacter;	0.0	0.0	**10.9**	**3.1**	0.0	0.0	0.0	0.0	0.3	0.1
Actinobacteria; Corynebacteriales; Nocardiaceae; Rhodococcus;	0.0	0.0	**4.6**	**4.1**	0.0	0.0	0.0	0.0	0.0	0.0
Deltaproteobacteria; Desulfobacterales; Desulfobacteraceae; Desulfotignum;	0.0	0.0	0.9	0.0	0.0	0.0	0.0	0.0	0.0	**7.7**
Deltaproteobacteria; Desulfovibrionales; Desulfohalobiaceae; Desulfohalobium;	**1.7**	**1.7**	**1.2**	**2.7**	**1.0**	0.0	0.0	0.0	0.2	0.0
Methanobacteria; Methanobacteriales; Methanobacteriaceae; Methanothermobacter;	0.0	0.0	0.9	0.0	**5.2**	0.0	0.0	0.0	0.0	**6.3**
Deltaproteobacteria; Desulfovibrionales;	**3.2**	**3.8**	0.0	0.0	0.0	0.0	0.0	0.0	0.0	0.0
Sphingobacteriia; Sphingobacteriales; E6aC02;	0.0	0.0	0.0	0.0	**6.7**	0.0	0.0	0.0	0.0	0.0
Deferribacteres; Deferribacterales; Deferribacteraceae; Flexistipes;	**1.4**	**1.5**	0.9	0.0	0.0	0.0	**1.8**	0.0	0.1	0.1
Deltaproteobacteria; Desulfovibrionales; Desulfovibrionaceae; Desulfovibrio;	0.3	0.3	0.9	0.9	0.0	**1.2**	0.0	0.0	0.1	**1.6**

The fraction (%) of Illumina Miseq sequencing reads representing the indicated taxa for samples in 5 distinctive clades (I–V) is shown. Fractions in excess of 1% are indicated in bold.

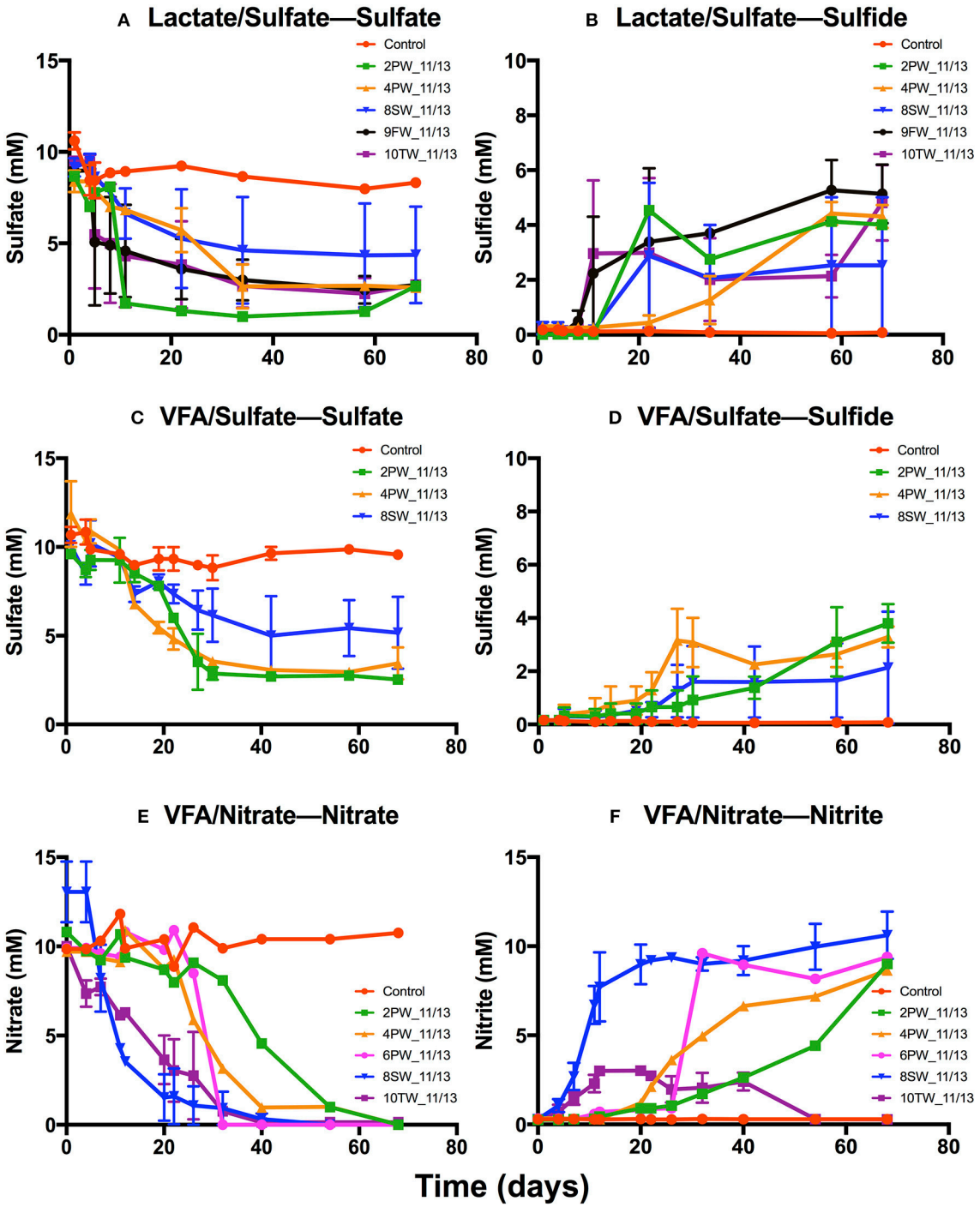

FIGURE 4 | Primary enrichments for November 2013 field samples in media with 2.5 M NaCl. Media contained 10 mM sulfate and 20 mM lactate **(A,B)**, 10 mM sulfate and 3 mM VFA **(C,D)** or 10 mM nitrate and 3 mM VFA **(E,F)**. Media were inoculated with 2PW_11/13, 4PW_11/13, 6PW_11/13, 8SW_11/13, 9FW_11/13, or 10TW_11/13, as indicated; the controls were not inoculated. The average concentrations of sulfide **(B,D)**, sulfate **(A,C)**, nitrate **(E)**, and nitrite **(F)** are shown as a function of time ± SD.

The enrichments in VS_2.5 medium were used to inoculate fresh cultures at 1.0 M or 2.5 M NaCl with or without 10 mM nitrate. With 4PW_11/13 enrichment sulfide was produced at 1.0 or 2.5 M NaCl, irrespective of the presence of nitrate (Figure S2B). Nitrate reduction was not observed (Figures S2C,D). Similar results were observed for 9FW_11/13 enrichment (Figure S3).

In incubations with 10TW_11/13 enrichment at 2.5 M NaCl sulfate was reduced to sulfide in the absence, but not in the presence of nitrate (Figures S4A,B). At 1 M NaCl nitrate was reduced first with little remaining at 15 days and little nitrite being formed (Figures S4C,D). Following the reduction of nitrate, sulfate was reduced with formation of 6.6 ± 0.01 mM sulfide (Figures S4A,B). These results suggest accumulation of nitrite at high salinity (2.5 M NaCl), which inhibits sulfate reduction. At low salinity no nitrite accumulated and no inhibition of sulfate reduction was observed. The results with enrichments of 4PW_11/13 (Figure S2) and 9FW_11/13 (Figure S3) indicated that NRB were absent. These were also absent from the primary enrichment of 9FW_11/13 in VN_2.5 medium (not shown). The primary enrichment of 4PW_11/13 did have NRB activity (**Figure 4F**).

Only 3 out of 6 samples collected in January 2015 showed SRB activity in LS_2.5 medium with 10.0 ± 0.2 mM sulfide being produced within 60 days (Figure S5). Both LS_0.75 and LS_2.5 were inoculated with 9 field samples collected in August 2015. SRB activity was observed in 6 of 9 samples with production of up to 9.3 and 10.7 mM sulfide at 0.75 and 2.5 M NaCl, respectively (Figures S6A,B). To test the effect of salinity on NRB activity, samples 2PW_08/15, 10TW_08/15, 13W_08/15, and 15PW_08/15 were inoculated into media with VFA and nitrate with 0, 0.5, 1.5 or 2.5 M NaCl (Figure S7). Nitrate reduction was slowest at 2.5 M NaCl with nitrite accumulating in incubations with 2PW_08/15, 10TW_08/15, and 15PW_08/15 (Figures S7A,B,D). Little nitrate reduction and no nitrite accumulation were observed at 2.5 M NaCl in the incubation of 13IW_08/15 (Figure S7C), indicating this sample to have few halophilic NRB. Nitrate reduction was faster at 1.5 M NaCl; nitrite accumulated only in the incubation with 10TW_08/15. Nitrate reduction was fastest at 0.5 and 0 M NaCl, with no nitrite accumulation in any of the incubations (Figure S7).

Thus, the results showed that samples from Bakken shale oil fields harbored halophilic SRB and NRB, capable of growth at 2.5 M NaCl. Halophilic NRB reduced nitrate mostly to nitrite under these conditions. At lower salinities nitrite accumulation was not observed, indicating reduction of nitrate to N_2. Production of N_2O was tested by headspace gas analyses, but was not found (results not shown).

Reduction of Sulfate and Nitrate in Continuous Cultures at Different Salinity

Chemostats at salinities of 0.5 and 2.5 M NaCl were established using secondary enrichments of 13IW_08/15 and 10TW_08/15, respectively. Steady state SRB activity was established within 2 days in LS_0.5-fed, within 50 days in LS_2.5-fed and within 60 days in VS_2.5-fed chemostats (Figures S8A–C). Likewise, steady state NRB activity was established more rapidly at low salinity in LN_0.5 medium (Figure S8F) than at high salinity in LN_2.5 and VN_2.5 media (Figures S8D,E). The average nitrite concentrations in these chemostats were 0.3±0.6, 2.0 ± 2.4 and 1.4 ± 1.5 mM, respectively. Although nitrate concentrations fluctuated significantly they were on average higher at high than at low salinity (Figures S8D–F).

The microbial community compositions in these six chemostats were very different (**Table 3**). Under sulfate-reducing conditions SRB of the genus *Desulfovibrio* dominated in LS_0.5, whereas *Halanaerobium* and the SRB *Desulfovermiculus* were most prominent at high salinity in LS_2.5 and VS_2.5 (**Table 3**). Under nitrate-reducing conditions *Geoalkalibacter, Mollicutes* and *Dethiosulfatibacter* dominated in LN_0.5, whereas *Halomonas*, *Marinobacter* and *Halanaerobium* dominated in LN_2.5 and VN_2.5 (**Table 3**).

Control of SRB-Mediated Souring in Bioreactors

SRB enrichments of 4PW_11/13, which had been transferred three times, were used to inoculate two bioreactors. These were then continuously injected with either VSN_2.5 or VS_2.5, as indicated (Figure S9). Injection of VS_2.5, containing 6 mM VFA, 4 mM sulfate and 2.5 M NaCl gave production of 2 mM sulfide after 120 days (Figure S9B), indicating the potential of souring at high salinity. The bioreactor injected with VSN_2.5, containing 6 mM VFA, 4 mM sulfate, 4 mM nitrate and 2.5 M NaCl gave reduction of 2 mM sulfate at day 75. Nitrate reduction did not start until day 110. No nitrate was observed in the bioreactor effluent from day 150 onwards. However, this did contain 2 mM nitrite. As a result sulfate reduction was no longer observed (Figure S9A). The slow start of nitrate reduction indicated that the halophilic SRB enrichment contained few residual NRB at the beginning of the experiment.

Reduction of nitrate and sulfate in bioreactors inoculated with the chemostat cultures of Figure S8 is shown in **Figure 5**. The duplicated bioreactors (I and II) were continuously injected with LS_0.5, LS_2.5, LSN_0.5, or LSN_2.5, containing 20 mM lactate and 4 mM sulfate without or with 4 mM nitrate. In the absence of nitrate after 30 days, steady concentrations of 3.2 ± 0.4 and 3.2 ± 0.2 mM sulfide were formed at 0.5 and 2.5 M NaCl, respectively (**Figure 5A**). In the presence of 4 mM sulfate and 4 mM nitrate at low salinity no nitrate or nitrite were detected in the effluent, and steady formation of 3.3 ± 0.2 mM sulfide was observed after 30 days. These results indicated sequential reduction of nitrate and sulfate, as observed elsewhere (Callbeck et al., 2011; Chen et al., 2017). In the presence of 4 mM sulfate and 4 mM nitrate at high salinity no reduction of sulfate to sulfide was detected, whereas all nitrate was reduced. On average 2.4 ± 1.0 mM nitrite persisted in the effluent of LSN_2.5 (**Figure 5B**). Thus, as in experiments with batch cultures and continuous cultures, nitrite also accumulated in bioreactors at high salinity preventing reduction of sulfate to sulfide (**Figure 5A**).

The microbial community in influent sand of the LS_2.5 bioreactors had high fractions of *Halanaerobium* and *Desulfovermiculus* (**Table 4**), while that of LSN_2.5 bioreactors had high fractions of *Halomonas* and *Halanaerobium*, but mostly lacked the halophilic SRB *Desulfovermiculus* (**Table 4**). At 0.5 M NaCl, with and without nitrate the dominant taxa were *Halanaerobium, Halomonas,* and *Desulfovibrio* (**Table 4**). A high fraction of *Pseudomonas* was also detected in influent sand of

TABLE 3 | Microbial community composition of the chemostat enrichments.

#Taxonomy (Phylum; Class; Order; Family; Genus)	Sulfate-reducing			Nitrate-reducing		
	0.5 M NaCl LS	2.5 M NaCl LS	2.5 M NaCl VS	0.5 M NaCl LN	2.5 M NaCl LN	2.5 M NaCl VN
Firmicutes; Clostridia; Halanaerobiales; Halanaerobiaceae; Halanaerobium;	0.1	**86.0**	**31.1**	0.0	**12.9**	**9.4**
Proteobacteria; Gammaproteobacteria; Oceanospirillales; Halomonadaceae; Halomonas;	0.9	0.2	0.4	0.5	**61.5**	**63.7**
Proteobacteria; Deltaproteobacteria; Desulfovibrionales; Desulfovibrionaceae; Desulfovibrio;	**89.3**	0.1	0.0	0.8	0.0	0.0
Proteobacteria; Deltaproteobacteria; Desulfuromonadales; Geobacteraceae; Geoalkalibacter;	0.0	0.0	0.0	**74.1**	0.3	0.1
Proteobacteria; Deltaproteobacteria; Desulfovibrionales; Desulfohalobiaceae; Desulfovermiculus;	0.0	**11.6**	**64.2**	0.0	0.0	0.0
Proteobacteria; Gammaproteobacteria; Alteromonadales; Alteromonadaceae; Marinobacter;	0.8	0.2	**2.2**	0.9	**24.6**	**26.5**
Tenericutes; Mollicutes; NA NB1-n;	**3.3**	0.0	0.0	**14.0**	0.0	0.0
Firmicutes; Clostridia; Clostridiales; no Clostridiales-Incertae-Sedis; Dethiosulfatibacter;	**1.5**	0.1	0.1	**8.8**	0.0	0.0
Proteobacteria; Epsilonproteobacteria; Campylobacterales; Campylobacteraceae; Arcobacter;	**2.5**	0.0	0.0	0.4	0.5	0.3
Firmicutes; Clostridia; Clostridiales; Peptococcaceae;	**1.1**	0.0	0.0	0.0	0.0	0.0

The fraction (%) of Illumina Miseq sequencing reads representing the indicated taxa is shown. Fractions in excess of 1% are indicated in bold.

the LSN_0.5 bioreactors, but not in that of LS_0.5 bioreactors (**Table 4**). Overall, the results from these bioreactors suggest that an accumulation of nitrite at high salinity inhibited growth of the SRB *Desulfovermiculus*. At 0.5 M NaCl *Desulfovibrio* was found as a major community component both in the absence and presence of nitrate. In the presence of nitrate this taxon likely grew in a zone, which was already depleted of nitrate, allowing sulfate reduction.

DISCUSSION

Our results on microbial activities and community compositions with Bakken shale oil field samples suggest a high potential for souring at both low and high salinities. However, high salinity souring can be effectively controlled by nitrate injection because nitrite accumulates. This is similar to the accumulation of nitrite found in samples from oil fields at or above 50°C (Fida et al., 2016). Thus, NRB limit reduction of nitrate to nitrite under extremophilic conditions, either high temperature or high salinity. Control of H_2S production by limited reduction of nitrate to nitrite at high salinity has not been previously demonstrated.

Assuming souring to be a problem in shale oil fields (Yevhen et al., 2011) and that nitrate injection is promising technology to remedy this problem, decreases in salinity should be avoided. The salinity of produced waters obtained in the present study varied from 0.6 to 3.7 Meq of NaCl. This was likely caused by continuous injection of SW-IW, which had 0.7 Meq of NaCl. Low salinity in produced waters may signal breakthrough of SW-IW, e.g., 12PW_08/15 had similar salinity, sulfate and ammonium concentrations as SW-IW (**Table 1**). This was also reflected in similarly high factions of *Thiomicrospira*, a moderately halophilic sulfur-oxidizing microorganism (Brinkhoff and Kuever, 1999) in the microbial communities of 13IW_08/15 (53%) and 12PW_08/15 (21%). This taxon was mostly absent from the communities in other samples (**Table 2**).

Community compositions of SW-IW samples were dominated by microorganisms, which grow optimally at moderate salinities (**Table 2**, Table S2) such as *Methanolobus* (optimum 0.35 M NaCl; Michimaru et al., 2009), *Thiomicrospira* (optimum 0.47 M NaCl; Brinkhoff and Kuever, 1999), *Desulfovibrio* (optimum 1.0 M NaCl for halophilic *Desulfovibrio*; Tardy-Jacquenod et al., 1998), *Methanobacterium* (optimum 0.1 M NaCl with tolerance of up to 1.7 M NaCl for some strains; Cadillo-Quiroz et al., 2014) and *Pelobacter* (minimally 0.2 M NaCl; Nasaringarao and Häggblom, 2007). Of these members of the genus *Desulfovibrio* are SRB known to be involved in reservoir souring and microbially influenced corrosion (Hubert et al., 2009; Kakooei et al., 2012; Guan et al., 2014) at low salinity and low temperature conditions. The presence of sulfur-reducers such as *Pelobacter* can further increase sulfide concentrations. Overall, the microbial communities in SW-IW samples had high potential to be involved in reservoir souring at low salinities.

Microbial community compositions of PWs were dependent on salinity. In samples from high salinity Bakken PWs, such as 2PW_11/13, 4PW_11/13 and 4PW_01/15 (2.2 Meq of NaCl), obligately anaerobic taxa, which are halophilic or halotolerant were detected, such as *Halanaerobium, Desulfovermiculus,* and *Desulfohalobium* (**Table 2**, Table S2). This suggests fermentative and souring potential at high salinity. Archaeal taxa such as *Methanohalophilus Methanothermococcus,* and *Methanothermobacter* were also detected in these high salinity PW samples (**Table 2**), suggesting potential methanogenic

activities. However, PW samples with low salinity, such as 2PW_08/15, 11PW_08/15, 12PW_08/15 (0.7 Meq of NaCl), had decreased fractions of *Halanaerobium* and increased fractions of *Marinobacter,* which grows optimally at lower salinities (Guo et al., 2007). Sample 15PW_08/15 with intermediate salinity (1.1 Meq of NaCl) had an intermediate fraction of *Halanaerobium* (**Table 2**: 6.6%). Hence, the decrease in PW salinities is reflected in the microbial community compositions.

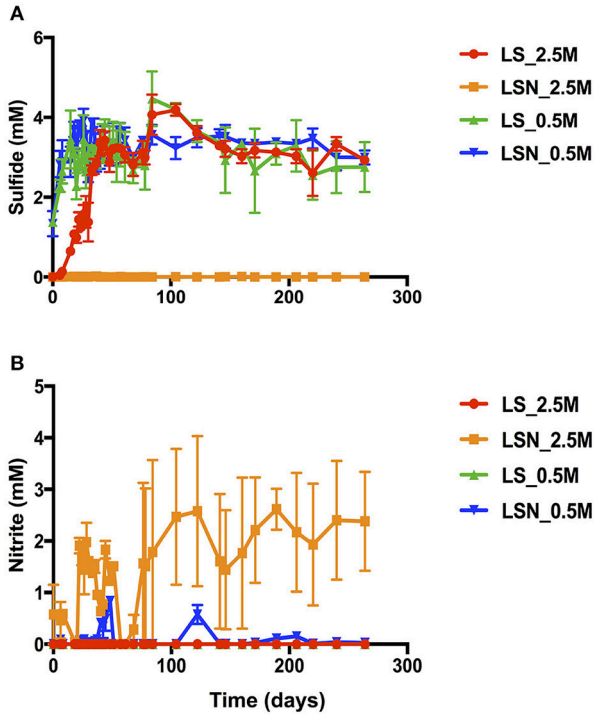

FIGURE 5 | Effect of nitrate on sulfide production in the effluent of bioreactors at low and high salinity**.** High salinity bioreactors were inoculated with high salinity chemostat cultures and were injected with LSN_2.5 or with LS_2.5. Low salinity bioreactors were inoculated with low salinity chemostat cultures and were injected with LSN_0.5 or with LS_0.5. The concentrations ± SD of sulfide **(A)** and nitrite **(B)** are shown as a function of time. Bioreactors were run at a flow rate of 0.6 PV/day.

Samples from the FW-TW facility, which processes oil-water emulsions from all (>100) producing wells, had high salinity throughout. These were dominated by the same obligately anaerobic, halophilic taxa as found in high salinity PWs (**Table 2**, Table S2: *Halanaerobium, Methanohalophilus, Desulfovermiculus,* and *Desulfohalobium*). The dominant SRB *Desulfovermiculus* and *Desulfohalobium* reduce sulfate using oil organics (butyrate and propionate) and H_2 (Belyakova et al., 2006; Jakobsen et al., 2006). The fermentative hydrogen producer *Halanaerobium* could enhance this sulfate reduction by providing H_2 and osmotic solutes (Daly et al., 2016). Other halophilic heterotrophic taxa such as *Modicisalibacter, Halomonas, Chromohalobacter,* and *Marinobacter* were found in FW-TW samples in more variable fractions (**Table 2**). These can grow fermentatively, but can also reduce nitrate (Vreeland et al., 1980; Gam et al., 2007).

Primary enrichments of SRB using 2013 or 2015 field samples produced sulfide at both low and high salinities (**Figure 4**, Figures S3,S4). The dominant taxa in these enrichments were *Halanaerobium, Desulfovibrio, Desulfovermiculus, Desulfohalobium,* and *Marispirillum* (data not shown). SRB enrichments at both 0.75 and 2.5 M NaCl were very similar in terms of sulfide formation and microbial community composition, suggesting the potential for souring at both SW-IW and FW-TW salinities (Figure S6). Nitrate reduction at high salinity gave nitrite accumulation (**Figures 4E,F**, Figure S7), which facilitated souring control (Figure S4), since nitrite prevents H_2S production by SRB (Callbeck et al., 2011; Gieg et al., 2011).

TABLE 4 | Microbial community compositions of the 2015 high and low salinity bioreactors.

#Taxonomy (Class; Order; Family; Genus)	High salinity (2.5 M NaCl)				Low salinity (0.5 M NaCl)			
	LS I	LS II	LSN I	LSN II	LS I	LS II	LSN I	LSN II
Clostridia; Halanaerobiales; Halanaerobiaceae; Halanaerobium;	**83.5**	**74.3**	**13.7**	**23.0**	**30.1**	**14.0**	**34.3**	**41.7**
Gammaproteobacteria; Oceanospirillales; Halomonadaceae; Halomonas;	**1.3**	**7.0**	**83.2**	**74.7**	**6.2**	**12.0**	**9.8**	**19.9**
Deltaproteobacteria; Desulfovibrionales; Desulfovibrionaceae; Desulfovibrio;	0.0	0.0	0.0	0.0	**54.5**	**68.0**	**31.2**	**29.8**
Gammaproteobacteria; Pseudomonadales; Pseudomonadaceae; Pseudomonas;	0.0	0.0	0.0	0.0	0.0	0.1	**18.1**	**6.8**
Deltaproteobacteria; Desulfovibrionales; Desulfohalobiaceae; Desulfovermiculus;	**10.1**	**9.4**	0.3	0.2	0.0	0.0	0.0	0.0
Clostridia; Clostridiales; Clostridiales-Incertae-Sedis; Dethiosulfatibacter;	0.2	0.2	0.0	0.0	**5.6**	**1.8**	**2.7**	0.5
Gammaproteobacteria; Chromatiales; Halothiobacillaceae; Halothiobacillus;	**1.5**	**3.2**	0.7	**1.4**	0.0	0.0	0.0	0.0
Kazan-3B-09;	**2.2**	**3.3**	0.0	0.0	0.0	0.00	0.0	0.0
Tenericutes; Mollicutes; NB1-n;	0.0	0.0	0.0	0.0	**1.6**	**1.5**	**2.4**	0.0
Clostridia; Clostridiales; Peptococcaceae;	0.0	0.0	0.0	0.0	**1.5**	**2.0**	0.8	**1.0**
Gammaproteobacteria; Alteromonadales; Alteromonadaceae; Marinobacter;	0.1	0.0	**2.0**	0.5	0.0	0.0	0.1	0.0
Deltaproteobacteria; Desulfobacterales; Desulfobacteraceae; Desulfosalsimonas;	0.2	**1.5**	0.0	0.0	0.0	0.0	0.0	0.0

The dendrogram for duplicated (I or II) bioreactors (0.5 M and 2.5 M NaCl) is shown on the top. The fraction (%) of Illumina Miseq sequencing reads representing the indicated taxa for duplicated (I or II) bioreactors (0.5 M and 2.5 M NaCl) is shown. Fractions in excess of 1% are indicated in bold.

At lower salinities (0, 0.5 and 1.0 M NaCl) nitrite did not accumulate (Figures S4,S7) and was likely reduced further to N_2, indicating that souring control through nitrate injection will be less effective under these conditions. Incomplete nitrate reduction with the accumulation of nitrite has also been observed at high temperature (Reinsel et al., 1996; Fida et al., 2016; 50°C or higher), indicating that this may generally occur at extreme salinity or temperature.

In contrast to the results with primary enrichments, continuous cultures showed distinct microbial community compositions at high and low salinity (**Table 3**). At high salinity under sulfate-reducing conditions the microbial community was dominated by *Halanaerobium* and *Desulfovermiculus*. The co-occurrence of these two taxa suggests a possible syntrophic relationship with *Desulfovermiculus* using H_2 produced by *Halanaerobium* for sulfate-reduction (Belyakova et al., 2006). At low salinity *Halanaerobium* and *Desulfovermiculus* were mostly absent in the LS_0.5 chemostat, where the dominant SRB was *Desulfovibrio*. The complete turnover of microbial compositions between high and low salinity reflects what might happen in the reservoir as low salinity SW-IW is continuously injected. The microbial community composition in nitrate-reducing chemostats at high salinity, LN_2.5 and VN_2.5, were nearly identical with *Halanaerobium, Halomonas,* and *Marinobacter* being dominant in both (**Table 3**). Of these *Halomonas* and *Marinobacter* are capable of reducing nitrate under saline conditions (Vreeland et al., 1980; Rani et al., 2017). At low salinity the continuous culture in LN_0.5 medium had a very different community (**Table 3**). This was dominated by *Geoalkalibacter*, an anaerobic nitrate-, sulfur- and iron-reducing microorganism, which grows optimally at 0.3 M NaCl (Greene et al., 2009). The distinctive separation of microbial communities in low salinity and high salinity chemostats correlates to field samples. The data also showed that repeated transferring of high salinity SRB enrichments causes a loss in nitrate-reducing taxa.

The bioreactor studies aimed to determine the feasibility of nitrate-mediated souring control at high salinity under flow conditions, as in the field. A problem with these studies was that halophilic NRB activity is lost from bioreactors, which are operated under sulfate-reducing conditions at high salinity for a prolonged period of time. E.g. in the bioreactor in Figure S9A, injected with nitrate and sulfate, NRB activity did not start until after more than 100 days of operation. Continuously injecting low concentrations of nitrate at high salinity led to nitrite accumulation and souring control (**Figure 5B**, Figure S9). The microbial communities in bioreactors injected with LS_2.5 continuously produced 3 mM sulfide and were dominated by *Halanaerobium* and *Desulfovermiculus*. In bioreactors injected with LS_0.5 a similar H_2S production was achieved by a different community dominated by *Desulfovibrio*. In the presence of nitrate LSN_2.5 bioreactors showed no sulfide production throughout the experiment, whereas sulfide was observed in the LSN_0.5 bioreactors. This was due to accumulation of nitrite in the LSN_2.5 bioreactors, which was not observed in the LSN_0.5 bioreactors (**Figure 5B**). *Halomonas*, which dominated the community in the LSN_2.5 injected bioreactors (**Table 3**: 75–83%), reduces nitrate only to nitrite (Vreeland et al., 1980). Excess concentrations of electron donors (VFA or lactate) were present throughout in these and other bioreactor studies (Callbeck et al., 2011). Thus, lack of sulfate reduction and incomplete reduction of nitrate to nitrite were not caused by a shortage of electron donor. The sulfide concentration in the LSN_0.5 injected bioreactors was comparable to that of the LS_0.5 injected bioreactors. These had similar communities with high fractions of *Desulfovibrio*, indicating the presence of a zone of sulfate reduction in the LSN_0.5 bioreactors with similar SRB as in the LS_0.5 bioreactors.

Overall, our results have demonstrated that souring in Bakken shale oil reservoirs is highly likely, especially with the ongoing injection of low salinity water with a high sulfate concentration. Reinjection of high salinity produced water amended with nitrate can decrease souring, while potentially improving water disposal issues. This is similar to high temperature oil fields, where reinjection of hot produced water is recommended to avoid lowering the reservoir temperatures to values below 50°C, where nitrite is reduced to N_2 (Fida et al., 2016).

AUTHOR CONTRIBUTIONS

BA: Experiment setup, data collection, interpretation, execution of the experiments, drafting and revision of the manuscript. YS: Conducted the experiments for Most Probable Numbers (MPN). GV: Provided funding, supervision, conception of the work and final approval of manuscript version to be published.

ACKNOWLEDGMENTS

This work was supported by an NSERC Industrial Research Chair Award to Dr. Gerrit Voordouw, which was also supported by BP America Production Co., Baker Hughes Canada, Computer Modeling Group Limited, ConocoPhillips Company, Dow Microbial Control, Enbridge Inc., Enerplus Corporation, Intertek Commercial Microbiology, Oil Search (PNG) Limited, Shell Global Solutions International, Suncor Energy Inc., and Yara Norge AS, as well as by Alberta Innovates-Energy and Environment Solutions. Special thanks to Priyesh Menon, who provided us with all the help and support to start this project. Thanks to Chris Farnden, Dominic Cote and Kirk Miner from Baker Hughes Canada for providing field information and sample collections.

SUPPLEMENTARY MATERIAL

The Supplementary Material for this article can be found online at: http://journal.frontiersin.org/article/10.3389/fmicb.2017.01164/full#supplementary-material

REFERENCES

Aminot, A., Kirkwood, D. S., and Kérouel, R. (1997). Determination of ammonia in seawater by the indolphenol-blue method: evaluation of the ICES NUTS I/C 5 questionnaire. *Mar. Chem.* 56, 59–75. doi: 10.1016/S0304-4203(96)00080-1

Belyakova, E. V., Rozanova, E. P., Borzenkov, I. A., Tourova, T. P., Pusheva, M. A., Lysenko, A. M., et al. (2006). The new facultatively chemolithoautotrophic, moderately halophilic, sulfate-reducing bacterium Desulfovermiculus halophilus gen. nov., sp. nov., isolated from an oil field. *Microbiology* 75, 161–171. doi: 10.1134/S0026261706020093

Brinkhoff, T., and Kuever, J. (1999). *Thiomicrospira chilensis* sp. nov., a mesophilic obligately chemolithoautotrophic sulfur- oxidizing bacterium isolated from a Thioploca mat. *Int. J. Syst. Bacteriol.* 49, 875–879.

Cadillo-Quiroz, H., Brauer, S. L., Goodson, N., Yavitt, J. B., and Zinder, S. H. (2014). *Methanobacterium paludis* sp. nov. and a novel strain of *Methanobacterium lacus* isolated from northern peatlands. *Int. J. Syst. Evol. Microbiol.* 64(Pt 5), 1473–1480. doi: 10.1099/ijs.0.059964-0

Callbeck, C. M., Dong, X., Chatterjee, I., Agrawal, A., Caffrey, S. M., Sensen, C. W., et al. (2011). Microbial community succession in a bioreactor modeling a souring low-temperature oil reservoir subjected to nitrate injection. *Appl. Microbiol. Biotechnol.* 91, 799–810. doi: 10.1007/s00253-011-3287-2

Caper, D. (2010). *Understanding Hydraulic Fracturing. Canadian Society for Unconventional Gas (CSUG), 23*. Available online at: http://www.csur.com/images/CSUG_publications/CSUG_HydraulicFrac_Brochure.pdf

Chen, C., Shen, Y., An, D., and Voordouw, G. (2017). Use of acetate, propionate and butyrate for reduction of nitrate and sulfate and methanogenesis in microcosms and bioreactors simulating an oil reservoir. *Appl. Environ. Microbiol.* 83:AEM.02983–16. doi: 10.1128/AEM.02983-16

Cluff, M. A., Hartsock, A., MacRae, J. D., Carter, K., and Mouser, P. J. (2014). Temporal changes in microbial ecology and geochemistry in produced water from hydraulically fractured Marcellus shale gas wells. *Environ. Sci. Technol.* 48, 6508–6517. doi: 10.1021/es501173p

Daly, R. A., Borton, M. A., Wilkins, M. J., Hoyt, D. W., Kountz, D. J., Wolfe, R. A., et al. (2016). Microbial metabolisms in a 2.5-km-deep ecosystem created by hydraulic fracturing in shales. *Nat. Microbiol.* 1:16146. doi: 10.1038/nmicrobiol.2016.146

Davis, J. P., Struchtemeyer, C. G., and Elshahed, M. S. (2012). Bacterial communities associated with production facilities of two newly drilled thermogenic natural gas wells in the barnett shale (Texas, USA). *Microb. Ecol.* 64, 942–954. doi: 10.1007/s00248-012-0073-3

Ding, J., Fu, L., Ding, Z.-W., Lu, Y.-Z., Cheng, S. H., and Zeng, R. J. (2016). Environmental evaluation of coexistence of denitrifying anaerobic methane-oxidizing archaea and bacteria in a paddy field. *Appl. Microbiol. Biotechnol.* 100, 439–446. doi: 10.1007/s00253-015-6986-2

Fida, T. T., Chen, C., Okpala, G., and Voordouw, G. (2016). Implications of limited thermophilicity of nitrite reduction for control of sulfide production in oil reservoirs. *Appl. Environ. Microbiol.* 82, 4190–4199. doi: 10.1128/AEM.00599-16

Gam, Z. B. A., Abdelkafi, S., Casalot, L., Tholozan, J. L., Oueslati, R., and Labat, M. (2007). *Modicisalibacter tunisiensis* gen. nov., sp. nov., an aerobic, moderately halophilic bacterium isolated from an oilfield-water injection sample, and emended description of the family Halomonadaceae Franzmann et al. 1989 emend. Ntougias et al. (2007). *Int. J. Syst. Evol. Microbiol.* 57, 2307–2313. doi: 10.1099/ijs.0.65088-0

Gieg, L. M., Jack, T. R., and Foght, J. M. (2011). Biological souring and mitigation in oil reservoirs. *Appl. Microbiol. Biotechnol.* 92, 263–282. doi: 10.1007/s00253-011-3542-6

Greene, A. C., Patel, B. K. C., and Yacob, S. (2009). Geoalkalibacter subterraneus sp. nov., an anaerobic Fe(III)- and Mn(IV)-reducing bacterium from a petroleum reservoir, and emended descriptions of the family Desulfuromonadaceae and the genus Geoalkalibacter. *Int. J. Syst. Evol. Microbiol.* 59, 781–785. doi: 10.1099/ijs.0.001537-0

Guan, J., Zhang, B. L., Mbadinga, S. M., Liu, J. F., Gu, J. D., and Mu, B. Z. (2014). Functional genes (dsr) approach reveals similar sulphidogenic prokaryotes diversity but different structure in saline waters from corroding high temperature petroleum reservoirs. *Appl. Microbiol. Biotechnol.* 98, 1871–1882. doi: 10.1007/s00253-013-5152-y

Guo, B., Gu, J., Ye, Y. G., Tan, Y. Q., Kida, K., and Wu, X. L. (2007). Marinobacter segnicrescens sp nov., a moderate halophile isolated from benthic sediment of the South China Sea. *Int. J. Syst. Evol. Microbiol.* 57, 1970–1974. doi: 10.1099/ijs.0.65030-0

Harkness, J. S., Dwyer, G. S., Warner, N. R., Parker, K. M., Mitch, W. A., and Vengosh, A. (2015). Iodide, bromide, and ammonium in hydraulic fracturing and oil and gas wastewaters: environmental implications. *Environ. Sci. Technol.* 49, 1955–1963. doi: 10.1021/es504654n

Hubert, C., Nemati, M., Jenneman, G., and Voordouw, G. (2003). Containment of biogenic sulfide production in continuous up-flow packed-bed bioreactors with nitrate or nitrite. *Biotechnol. Prog.* 19, 338–345. doi: 10.1021/bp020128f

Hubert, C., and Voordouw, G. (2007). Oil field souring control by nitrate-reducing *Sulfurospirillum* spp. that outcompete sulfate-reducing bacteria for organic electron donors. *Appl. Environ. Microbiol.* 73, 2644–2652. doi: 10.1128/AEM.02332-06

Hubert, C., Voordouw, G., and Mayer, B. (2009). Elucidating microbial processes in nitrate- and sulfate-reducing systems using sulfur and oxygen isotope ratios: the example of oil reservoir souring control. *Geochim. Cosmochim. Acta* 73, 3864–3879. doi: 10.1016/j.gca.2009.03.025

Ivanova, N., Sikorski, J., Chertkov, O., Nolan, M., Lucas, S., Hammon, N., et al. (2011). Complete genome sequence of the extremely halophilic *Halanaerobium praevalens* type strain (GSLT). *Stand. Genomic Sci.* 4, 312–321. doi: 10.4056/sigs.1824509

Jakobsen, T. F., Kjeldsen, K. U., and Ingvorsen, K. (2006). *Desulfohalobium utahense* sp. nov., a moderately halophilic, sulfate-reducing bacterium isolated from Great Salt Lake. *Internat. J. Syst. Evol. Microbiol.* 56(Pt 9), 2063–2069. doi: 10.1099/ijs.0.64323-0

Kakooei, S., Che Ismail, M., Ariwahjoedi, B., and Iskandar, B. S. (2012). Mechanisms of microbiologically influenced corrosion : a review. *World Appl. Sci. J.* 17, 524–531.

Khan, N. A., Engle, M., Dungan, B., Holguin, F. O., Xu, P., and Carroll, K. C. (2016). Volatile-organic molecular characterization of shale-oil produced water from the Permian Basin. *Chemosphere* 148, 126–136. doi: 10.1016/j.chemosphere.2015.12.116

Laurenzi, I. J., Bergerson, J. A., and Motazedi, K. (2016). Life cycle greenhouse gas emissions and freshwater consumption associated with Bakken tight oil. *Proc. Natl. Acad. Sci. U.S.A.* 113, 7672–7680. doi: 10.1073/pnas.1607475113

Liang, R., Davidova, I. A., Marks, C. R., Stamps, B. W., Harriman, B. H., Stevenson, B. S., et al. (2016). Metabolic capability of a predominant *Halanaerobium* sp. in hydraulically fractured gas wells and its implication in pipeline corrosion. *Front. Microbiol.* 7:988. doi: 10.3389/fmicb.2016.00988

Michimaru, H., Tamaki, H., Hanada, S., Imachi, H., Nakamura, K., Sakata, S., et al. (2009). *Methanolobus profundi* sp. nov., a methylotrophic methanogen isolated from deep subsurface sediments in a natural gas field. *Int. J. Syst. Evol. Microbiol.* 59, 714–718. doi: 10.1099/ijs.0.001677-0

Mouser, P. J., Borton, M., Darrah, T. H., Hartsock, A., and Wrighton, K. C. (2016). Hydraulic fracturing offers view of microbial life in the deep terrestrial subsurface. *FEMS Microbiol. Ecol.* 92, 1–18. doi: 10.1093/femsec/fiw166

Murali Mohan, A., Hartsock, A., Bibby, K. J., Hammack, R. W., Vidic, R. D., and Gregory, K. B. (2013). Microbial community changes in hydraulic fracturing fluids and produced water from shale gas extraction. *Environ. Sci. Technol.* 47, 13141–13150. doi: 10.1021/es402928b

Nasaringarao, P., and Häggblom, M. M. (2007). *Pelobacter seleniigenes* sp. nov., a selenaterespiring bacterium. *Int. J. Syst. Evol. Microbiol.* 57, 1937–1942. doi: 10.1099/ijs.0.64980-0

Oren, A. (2008). Microbial life at high salt concentrations: phylogenetic and metabolic diversity. *Saline Syst.* 4:2. doi: 10.1186/1746-1448-4-2

Park, H. S., Chatterjee, I., Dong, X., Wang, S. H., Sensen, C. W., Caffrey, S. M., et al. (2011). Effect of sodium bisulfite injection on the microbial community composition in a brackish-water-transporting pipeline. *Appl. Environ. Microbiol.* 77, 6908–6917. doi: 10.1128/AEM.05891-11

Rani, S., Koh, H., Kim, H., Rhee, S., and Park, S. (2017). *Marinobacter salinus* sp. nov., a moderately halophilic bacterium isolated from a tidal flat environment. *Int. J. Syst. Evol. Microbiol.* 67, 205–211. doi: 10.1099/ijsem.0.001587

Reinsel, M. A., Sears, J. T., Stewart, P. S., and Mclnerney, M. J. (1996). Control of microbial souring by nitrate, nitrite or glutaraldehyde injection in a sandstone column. *J. Ind. Microbiol.* 17, 128–136. doi: 10.1007/BF01570056

Shen, Y., and Voordouw, G. (2017). "Primers for dsr genes and most probable number method for detection of sulfate-reducing bacteria in oil reservoirs," in *Hydrocarbon and Lipid Microbiology Protocols: Microbial Quantitation, Community Profiling and Array Approaches,* eds T. J. McGenity, K. N. Timmis, and N. Balbina (Berlin; Heidelberg: Springer Berlin Heidelberg), 35–43.

Shrestha, N., Chilkoor, G., Wilder, J., Gadhamshetty, V., and Stone, J. J. (2017). Potential water resource impacts of hydraulic fracturing from unconventional oil production in the Bakken shale. *Water Res.* 108, 1–24. doi: 10.1016/j.watres.2016.11.006

Strong, L. C., Gould, T., Kasinkas, L., Sadowsky, M. J., Aksan, A., and Wackett, L. P. (2013). Biodegradation in waters from hydraulic fracturing: chemistry, microbiology, and engineering. *J. Environ. Eng.* 140, B4013001. doi: 10.1061/(ASCE)EE.1943-7870.0000792

Struchtemeyer, C. G., Morrison, M. D., and Elshahed, M. S. (2012). A critical assessment of the efficacy of biocides used during the hydraulic fracturing process in shale natural gas wells. *Int. Biodeterior. Biodegradation* 71, 15–21. doi: 10.1016/j.ibiod.2012.01.013

Tamura, K., Peterson, D., Peterson, N., Stecher, G., Nei, M., and Kumar, S. (2011). MEGA5: molecular evolutionary genetics analysis using maximum likelihood, evolutionary distance, and maximum parsimony methods. *Mol. Biol. Evol.* 28, 2731–2739. doi: 10.1093/molbev/msr121

Tardy-Jacquenod, C., Magot, M., Patel, B. K. C., Matheron, R., and Caumette, P. (1998). *Desulfotomaculum halophilum* sp. nov., a halophilic sulfate-reducing bacterium isolated form oil production facilities. *Int. J. Syst. Bacteriol.* 48, 333–338. doi: 10.1099/00207713-48-2-333

Trüper, H. G., and Schlegel, H. G. (1964). Sulphur metabolism in Thiorhodaceae, I. Quantitative measurements on growing cells of *Chromatium okenii. Antonie van Leeuwenhoek*, 30, 225–238. doi: 10.1007/BF02046728

Tucker, Y. T., Kotcon, J., and Mroz, T. (2015). Methanogenic archaea in marcellus shale: a possible mechanism for enhanced gas recovery in unconventional shale resources. *Environ. Sci. Technol.* 49, 7048–7055. doi: 10.1021/acs.est.5b00765

Vreeland, R. H., Litchfield, C. D., Martin, E. L., and Elliot, E. (1980). *Halomonas elongata*, a new genus and species of extremely salt-tolerant bacteria. *Int. J. Syst. Bacteriol.* 30, 485–495. doi: 10.1099/00207713-30-2-485

Wang, L., Burns, S., Giammar, D. E., and Fortner, J. D. (2016). Element mobilization from Bakken shales as a function of water chemistry. *Chemosphere* 149, 286–293. doi: 10.1016/j.chemosphere.2016.01.107

Wuchter, C., Banning, E., Mincer, T. J., Drenzek, N. J., and Coolen, M. J. L. (2013). Microbial diversity and methanogenic activity of antrim shale formation waters from recently fractured wells. *Front. Microbiol.* 4:367. doi: 10.3389/fmicb.2013.00367

Xue, Y., and Voordouw, G. (2015). Control of microbial sulfide production with biocides and nitrate in oil reservoir simulating bioreactors. *Front. Microbiol.* 6:1387. doi: 10.3389/fmicb.2015.01387

Yevhen, H., Jordan, M. B., John, A. H., Benjamin, L. H., Blaise, M., Ryan, J. K., et al. (2011). "Understanding the souring at Bakken oil reservoirs," in *SPE International Symposium on Oilfield Chemistry* (Woodlands, TX). doi: 10.2118/141434-MS

Youssef, N., Elshahed, M. S., and McInerney, M. J. (2009). Chapter 6 - microbial processes in oil fields: culprits, problems, and opportunities. *Advances Appl. Microbiol.* 66, 141–251. doi: 10.1016/S0065-2164(08)00806-X

Conflict of Interest Statement: The authors declare that the research was conducted in the absence of any commercial or financial relationships that could be construed as a potential conflict of interest.

frontiers in Microbiology

ORIGINAL RESEARCH
published: 20 June 2017
doi: 10.3389/fmicb.2017.01131

Impact of Aeolian Dry Deposition of Reactive Iron Minerals on Sulfur Cycling in Sediments of the Gulf of Aqaba

*Barak Blonder[1], Valeria Boyko[1], Alexandra V. Turchyn[2], Gilad Antler[2], Uriel Sinichkin[1], Nadav Knossow[1], Rotem Klein[1] and Alexey Kamyshny Jr.[1]**

[1] Department of Geological and Environmental Sciences, Faculty of Natural Sciences, Ben-Gurion University of the Negev, Beer Sheva, Israel, [2] Department of Earth Sciences, University of Cambridge, Cambridge, United Kingdom

The Gulf of Aqaba is an oligotrophic marine system with oxygen-rich water column and organic carbon-poor sediments (≤0.6% at sites that are not influenced by anthropogenic impact). Aeolian dust deposition from the Arabian, Sinai, and Sahara Deserts is an important source of sediment, especially at the deep-water sites of the Gulf, which are less affected by sediment transport from the Arava Desert during seasonal flash floods. Microbial sulfate reduction in sediments is inferred from the presence of pyrite (although at relatively low concentrations), the presence of sulfide oxidation intermediates, and by the sulfur isotopic composition of sulfate and solid-phase sulfides. Saharan dust is characterized by high amounts of iron minerals such as hematite and goethite. We demonstrated, that the resulting high sedimentary content of reactive iron(III) (hydr)oxides, originating from this aeolian dry deposition of desert dust, leads to fast re-oxidation of hydrogen sulfide produced during microbial sulfate reduction and limits preservation of reduced sulfur in the form of pyrite. We conclude that at these sites the sedimentary sulfur cycle may be defined as cryptic.

Keywords: Red Sea, Gulf of Aqaba, aeolian dust deposition, highly reactive iron, manganese, sulfide oxidation intermediates, cryptic sulfur cycle

OPEN ACCESS

Edited by:
Brian T. Glazer, Hawaii University, United States

Reviewed by:
Kai Waldemar Finster, Aarhus University, Denmark
Dirk De Beer, Max Planck Society (MPG), Germany

****Correspondence:***
Alexey Kamyshny Jr.
alexey93@gmail.com

Specialty section:
This article was submitted to Microbiological Chemistry and Geomicrobiology, a section of the journal Frontiers in Microbiology

Received: *23 March 2017*
Accepted: *02 June 2017*
Published: *20 June 2017*

Citation:
Blonder B, Boyko V, Turchyn AV, Antler G, Sinichkin U, Knossow N, Klein R and Kamyshny A Jr. (2017) Impact of Aeolian Dry Deposition of Reactive Iron Minerals on Sulfur Cycling in Sediments of the Gulf of Aqaba. Front. Microbiol. 8:1131. doi: 10.3389/fmicb.2017.01131

INTRODUCTION

Reduction–oxidation (redox) reactions in marine sediments are the only source of metabolic energy for microorganisms in the absence of light. The dominant electron donor in marine sediments is organic carbon due to its high metabolic energy yield and general availability in marine environments (Boudreau, 1992; Orcutt et al., 2011). Microbially mediated oxidation of this organic carbon utilizes electron acceptors according to the metabolic energy yield of the respective redox reaction. Electron acceptors are generally consumed according to the Gibbs free energy yield of respiratory pathways associated with organic matter oxidation (Froelich et al., 1979). Depending on the availability and lability of organic carbon in the sediment, and the concentration and speciation of electron acceptors, zones characterized by the reduction of various electron acceptors

may overlap (Canfield et al., 1993; Thamdrup, 2000; Hansel et al., 2015). In marine and marginal marine sediments, the oxidation of organic carbon coupled to iron reduction and microbial sulfate reduction are of key importance. Recent work has shown that the sedimentary iron and sulfur cycles may be coupled in interesting and complicated ways (Holmkvist et al., 2011; Mills et al., 2016).

There are three possible fates for hydrogen sulfide produced during microbial sulfate reduction. The first fate is removal through precipitation as iron monosulfide followed by conversion to pyrite (Burdige and Nealson, 1986). The second fate is possible in iron-limited environments: hydrogen sulfide can be incorporated into sedimentary organic matter through polysulfide formation (Werne et al., 2008; Amrani, 2014). The third fate is re-oxidation by chemical or microbially mediated processes to sulfide oxidation intermediates (S_n^{2-}, S^0, $S_2O_3^{2-}$, SO_3^{2-}, and $S_4O_6^{2-}$) and/or to the terminal oxidation product, sulfate (Chen and Morris, 1972; Yao and Millero, 1996; Lichtschlag et al., 2013; Holmkvist et al., 2014). Thus, if microbial sulfate reduction takes place in sediments rich in electron acceptors such as reactive Fe(III) (hydr)oxides and manganese oxides (MnO_2), hydrogen sulfide may be either totally reoxidized to sulfate or only partially preserved as trace amounts of pyrite in the sediment. If re-oxidation of hydrogen sulfide is fast enough, aqueous sulfide concentrations may remain low and no products of microbial sulfate reduction (e.g., iron sulfide, pyrite, organic sulfur) are preserved. In this case the sulfur cycle has been called "cryptic" (Turchyn et al., 2006; Holmkvist et al., 2011; Hansel et al., 2015; Mills et al., 2016).

Transformation of sulfate to hydrogen sulfide is associated with a large sulfur isotopic fractionation (Harrison and Thode, 1958); up to $\varepsilon \approx 70‰$ at ambient temperature has been suggested using models of microbial metabolism (Farquhar et al., 2003; Brunner and Bernasconi, 2005), sulfur isotopic fractionation up to $\varepsilon = 66‰$ has been measured in microbial pure cultures (Sim et al., 2011a), and sulfur isotope fractionation up to 77‰ has been measured in deep ocean sediments at elevated temperatures (Rudnicki et al., 2001). The extent of sulfur isotope fractionation depends on sulfate concentrations, microbial sulfate reduction rate, substrate type, and temperature (Habicht et al., 2002; Sim et al., 2011b). In the case of a cryptic sulfur cycle, where most hydrogen sulfide is re-oxidized to sulfate and neither free hydrogen sulfide nor pyrite are present, sulfur isotopes are less useful for study of the biogeochemical sulfur cycle because they are quantitatively conserved and do not necessarily exhibit a large sulfur isotope fractionation (Mills et al., 2016). In this case study, the oxygen isotope composition of sulfate has been shown to be a very powerful tool for studying the redox cycling of sulfur. Similar to sulfur isotopes, oxygen isotopes in dissolved sulfate ($\delta^{18}O_{SO4}$) also increase during microbial sulfate reduction as the light ^{16}O isotope is preferentially reduced, but at some stage stop increasing and reach a value that is in oxygen isotopic equilibrium with water (Fritz et al., 1989; Böttcher et al., 1999). As sulfate and water do not exchange oxygen isotopes easily, this observed oxygen isotope exchange is attributed to the intracellular exchange of oxygen atoms between sulfur intermediate species (such as sulfite) and water (Mizutani and Rafter, 1973; Fritz et al., 1989). The observed ^{18}O isotope enrichment over the isotopic composition of water (magnitude 22 - 30‰) reflects intracellular oxygen isotope exchange (Böttcher et al., 1998, 1999; Brunner et al., 2005, 2012; Turchyn et al., 2006, 2010; Antler et al., 2013). Therefore, if a significant fraction of sulfate is reduced and reoxidized to sulfate, exchange of oxygen isotopes between sulfate and water can be detected, and thus the oxygen isotopic composition of sulfate may be a proxy for any quantitative cycling of sulfur such as during a cryptic sulfur cycle (Bishop et al., 2013; Johnston et al., 2014).

Airborn dust is an important source of nutrients and essential metals to wide areas of the ocean (Duce et al., 1991). The input of mineral dust may affect seawater biogeochemistry and sedimentation processes (Jickells, 1995; Chen et al., 2008). Aeolian dust deposition is especially significant in marine systems that are situated in arid environments where fluvial input is limited. Wind-transported dust with high iron and manganese content, which mainly consists of minerals derived from arid and semi-arid mid-latitude regions in the Northern Hemisphere, has been suggested as a crucial factor that may control primary productivity in high nutrients - low chlorophyll marine ecosystems (Duce and Tindale, 1991; Street and Paytan, 2005). After deposition of dust at the ocean surface, only a small fraction of the aeolian iron flux becomes bioavailable due to the low solubility of the colloidal and particulate Fe(III) (mostly between 1 and 12%) that comprises the bulk of the aerosol iron pool (Mahowald et al., 2005). In the Red Sea, $\leq$2% of dry-deposited aerosol iron is dissolved during the transport of dust particles to the sediment (Chen et al., 2006).

High fluxes of aeolian dry deposition of dust from adjacent deserts makes the Gulf of Aqaba an ideal playground for the study of the impact of high concentrations of reactive iron and manganese on sulfur cycling in sediments in an oligotrophic marine system. In this work, we report on the concentrations of iron, manganese and sulfur (in various valence states) as well as the isotopic composition of sulfur in the sediments, across a range of water depths, including a site influenced by anthropogenic activity. We evaluate the importance of the reoxidative part of the sulfur cycle, and how this varies with changes in water depth, and identify a cryptic sulfur cycle at the deep-water sites.

STUDY SITE

The Gulf of Aqaba is 180 km long, 6 to 25 km wide and up to 1850 m deep (Ben-Avraham et al., 1979) (**Figure 1**). A transform fault located at the center of the Gulf of Aqaba causes steep-slope topography. The limited water influx from the Red Sea through the narrow (800 m wide) and shallow (80–250 m depth) Straits of Tiran results in high water column temperature (21–27°C) throughout the year, as warm surface waters flow from the Red Sea into the Gulf and deep waters flow out from the Gulf into the Red Sea (Ben-Avraham et al., 1979; Biton and Gildor, 2011). During the summer months, the water column is stratified and water mixing occurs only to a depth of 20 m. During winter, the water column typically mixes to a depth of 300-400 m but can be mixed down to 860 m depth during exceptionally cold winters (Genin et al., 1995). Nevertheless, the bottom waters of

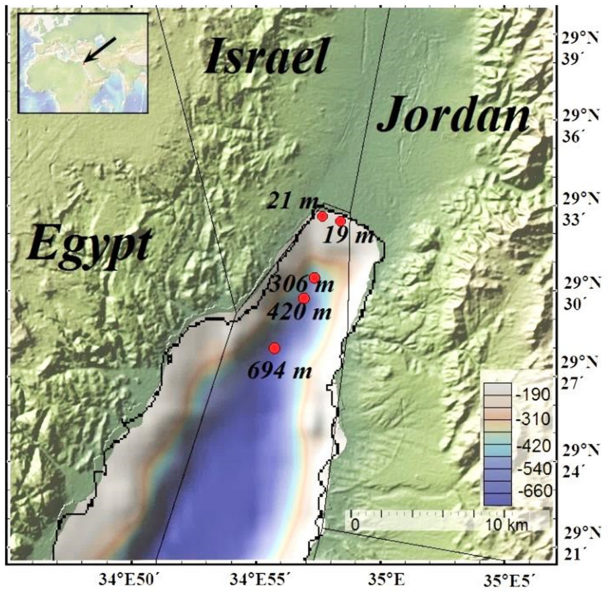

FIGURE 1 | Map of the Gulf of Aqaba. Red dots represent sampling sites (map was generated using GeoMapApp, http://www.geomapapp.org).

the Gulf of Aqaba are oxic throughout the year with a reported oxygen minimum of 168 μM at 800 m (Reiss and Hottinger, 1984; Badran, 2001). The Gulf of Aqaba is an oligotrophic marine system. Primary production in photic zone (upper 170 m) of the Gulf of Aqaba varies in the range of 0.05–3.38 mg C m^{-3} h^{-1} (Levanon-Spanier et al., 1979; Stambler, 2006). The productivity rates are limited due to the seasonal nutrient (N, P) depletion during summer stratification (Reiss and Hottinger, 1984; Li et al., 1998; Labiosa et al., 2003).

Particulate input is mostly of aeolian origin and other inputs are relatively low due to scarse local rainfall (22 mm y^{-1}). Recently, it was reported that possible sources of fluvial material to the Gulf are desert flash floods from the Arava desert after rare rainfall events (Katz et al., 2015), but deposition of this fluvial material would impact only sediments in the immediate vicinity of the shoreline. However, in the vicinity of coral reefs the coarse sediments are nearly all biogenic, as depositional rates of terrigenous material from wadies are equal to coral growth (Reiss and Hottinger, 1984). Reported iron content in suspended flashflood sediments is 41 mg g^{-1} with total inflow into the Gulf of 10 g Fe m^{-2} (179 mmol m^{-2}) (Katz et al., 2015). Sediments at the north shore of the Gulf, which is adjacent to Arava Valley, are fluvial silts and fine sands with a mean grain size of 257 μm and c.a. 20–23% silt (Katz et al., 2002). Sediments overlain by deep waters (825 m) are characterized by smaller grain size, with a mean grain size of 45 μm and total organic carbon of 0.4% (Rasheed et al., 2003).

Sedimentation rates in the deep waters (up to 826 m) near the Jordanian coast are 42–72 cm ky^{-1} (Al-Rousan et al., 2004). Lower rates, 4–10 cm ky^{-1} were reporetd by Reiss et al. (1980) at <900 m depth. Much higher rates, 220–330 cm ky^{-1}, were reported for shallow (10 m water depth, coral reef) sites by Larsen (1978). The strong variation in sedimentation rates in the Gulf of Aqaba may be caused by different degrees of resuspension, which depends on the textural properties of the sediments (e.g., finer sediments with low density are resuspended to larger areas) as well as on storm events (Schumacher et al., 1995; Al-Rousan, 1998).

TABLE 1 | Water depths and coordinates of sampling sites.

Sampling site	Water depth, *m*	Coordinates
RS-II-19	19	29°32′30.6″N/34°58′24″E
RS-V-21	21	29°32′41.4″N/34°57′45.6″E
RS-IV-306	306	29°30′58.2′N/34°57′30.6″E
RS-III-420	420	29°30′12.6′N/34°56′58.2′E
RS-I-694	694	29°28′3″N/34°55′41.4″E

The Gulf of Aqaba is strongly affected by dust storm events, which supply dust particles with iron, aluminum and manganese from adjacent (e.g., the Negev Desert, the Sinai, and Arabian Peninsulas) and distant (e.g., the Sahara) arid environments (Chase et al., 2006). The total deposition rate of aeolian mineral dust to the Gulf of Aqaba is 34.7 g m^{-2} $year^{-1}$ (Al-Taani et al., 2015), whereas the aerosol iron deposition flux varies in range of 1.5–116 μmol m^{-2} d^{-1} with a mean of 10 μmol m^{-2} d^{-1} (Chase et al., 2006). Inputs of terrigenous sedimentary material are restricted to seasonal hyperpycnal flows, which may reach reef sediments during rare rain events.

Along the northern shore of the Gulf of Aqaba near the Israel-Jordan border, a fish farm ('Ardag') operated from 1989 to 2008. The fish farm contributed large amounts of organic carbon to the previously organic matter-poor sediments. In 2002, total organic carbon content as high as 6.85% was detected in the sediments at the fish farm site (Black et al., 2012).

MATERIALS AND METHODS

Sampling

Five sampling campaigns were carried out between May 2012 and February 2013 at water depths of 19 m (site RS-II-19, ex-fish farm location), 21 m (site RS-V-21), 306 m (site RS-IV-306), 420 m (site RS-III-420), and 694 m (site RS-I-694) (**Figure 1** and **Table 1**). Sampling sites map was generated using GeoMapApp[1] (Ryan et al., 2009). At the deep-water sites, cores were retrieved by a multicorer from the IUI-Eilat research vessel. Near-shore sampling was performed manually by divers. The core liners were 50 cm long Perspex tubes with 9.5 cm internal diameter. Three cores were retrieved during each sampling. These cores were used for high resolution dissolved oxygen concentration measurements (Core 1), total sediment composition analysis (Core 2), pore-water extraction and chemical analyses (Core 3).

Pore-Water Extraction

The pore-waters were extracted at 4 cm intervals by Rhizon samplers (MacroRhizon, 9 cm long, 4.5 mm diameter,

[1]http://www.geomapapp.org

Rhizosphere Research Products, Netherlands) with a filter pore size of 150 ± 30 nm, under a nitrogen atmosphere in a glove box (Seeberg-Elverfeldt et al., 2005).

The first 1 mL of every sample was discarded to avoid sample contamination. The volume of pore-water extracted at each core depth was c.a. 50–80 ml. The extraction of large pore-water volumes was crucial in order to perform numerous geochemical analyses for a variety of dissolved species. The vertical overlap between pore fluid samples retrieved with the Rhizons was calculated according to Seeberg-Elverfeldt et al. (2005) and was found to be in the range of 0–14%.

Pore-Water Analysis

Ferrous (Fe^{2+}) iron was quantified spectrophotometrically by the ferrozine method according to Stookey (1970). The minimum detection limit (MDL) of this method is 1 μmol L^{-1}. Manganese in pore-waters was also measured spectrophotometerically (LaMotte, SMART Spectro) using the 1-(2-Pyridylazo)-2-naphthol (PAN) method (LaMotte test kit 3660-sc) according to Goto et al. (1977). Ascorbic acid was used to reduce total manganese to dissolved Mn^{2+}.

Hydrogen sulfide was measured by two methods. For samples with hydrogen sulfide concentration >1.5 μmol L^{-1} samples were pre-treated with 50 g L^{-1} zinc acetate at a ratio of at least 3:20 (V/V) immediately after sampling and the concentration was quantified by the methylene blue method according to Cline (1969). This method accounts for the following species: H_2S, HS^-, S^{2-}, S(II) in polysulfides, as well as nanoparticles of acid-soluble metal sulfides (e.g., MnS, FeS), which can pass through the pores of the Rhizon sampler. The MDL was 1.5 μmol L^{-1}. For samples with hydrogen sulfide concentration <1.5 μmol L^{-1}, quantification was performed by high-precision liquid chromatography (HPLC, Agilent Technologies 1260 Infinity) with fluorescence detection after derivatization with monobromobimane (Kosower et al., 1979; Fahey and Newton, 1987; Zopfi et al., 2004). The sulfur species measured by this method are: H_2S, HS^-, S^{2-} and, possibly, the S(II) of polysulfides. The MDL for the sum of these species was 2 nmol L^{-1}. Dissolved zero-valent sulfur (ZVS, includes dissolved and colloidal elemental sulfur and well as polysulfide zero-valent sulfur) was quanified by cyanolysis according to Kamyshny (2009a). The MDL was 60 nmol L^{-1}. The concentrations of polysulfides were below the detection limit of chromatographic quantification after derivatization to dimethylpolysulfanes with methyl trifluoromethanesulfonate (MDL = hundreds of nmol L^{-1} for individual polysulfides, Kamyshny et al. (2006)) in all samples. The analyses of thiosulfate and sulfite were carried out simultaneously by the same HPLC analysis procedure as for low hydrogen sulfide concentrations. The MDL was 2 nmol L^{-1}. Free thiocyanate (SCN^-) and tetrathionate ($S_4O_6^{2-}$) concentrations were below the detection limit (60 nmol L^{-1} and 500 nmol L^{-1}, respectively) of chromatographic analyses (Rong et al., 2005; Kamyshny, 2009a). Sulfate (SO_4^{2-}) was quantified by ion chromatography (DIONEX, DX500) with ASRS-300 suppressor. The eluent, which was composed of 1.8 mmol L^{-1} sodium carbonate and 1.7 mmol L^{-1} sodium bicarbonate, was pumped at a flow rate of 2 mL min^{-1} through a guard column (AG4A-SC), an anion exchange column (AS4A-SC). The MDL of this method was 10 μmol L^{-1}.

Solid Phase Analysis

Sediments were sliced in the field at 2 cm intervals using a core extruder and a spatula. For acid-volatile sulfur (hereafter AVS), non-S^0 chromium reducible sulfur (CRS) and elemental sulfur measurements, c.a. 15 mL of sediment were placed in a 50 mL volume falcon tube containing 25 mL zinc acetate in the field (50 g L^{-1}). Additionally, for metal speciation measurements, c.a. 25 mL of sediments were placed in a 50 mL falcon tube and frozen the same day on arrival to the laboratory. For porosity measurements, 10 mL of sediment were placed in a 15 mL volume falcon tube and stored at 4°C in the laboratory.

Elemental sulfur was extracted from the sediment that had been pre-treated with zinc acetate by shaking with methanol for 16 h on a rotary shaker (Zopfi et al., 2004). The sample-to-methanol ratio was c.a. 1/20 [w/v]. After separation of the sediment by centrifugation, elemental sulfur (S^0) in the methanol extract was quantified by HPLC. An Agilent Quaternary pump – G1311B, UV-VIS Detector (Agilent G1365D), and Prevail C18 Grace reverse phase column (250 mm × 4.6 mm × 5 μm) were used. Pure methanol (HPLC grade) was used as a mobile phase at a flow rate of 1 mL per minute. Elemental sulfur was detected at 230 nm wavelength with an MDL of 10 μmol kg^{-1} (wet sediment). In two samples of surface sediments at site RS-V-21, the elemental sulfur content was high enough to allow analysis of isotopic composition. Elemental sulfur was preconcentrated by partial evaporation of methanol on a rotary evaporator, extraction with dichloromethane from the residual methanol-water mixture and evaporation of dichloromethane under gentle flow of nitrogen. Elemental sulfur was reduced to hydrogen sulfide by Cr(II) reduction in the ethanol-water medium according to Gröger et al. (2009). Evolving hydrogen sulfide was trapped in $AgNO_3/HNO_3$ trapping solution.

Acid-volatile sulfur and CRS distillations were performed on the sediment sample after it had been subjected to methanol extraction, so that elemental sulfur was not accounted for in the CRS distillation. Although greigite (Fe_3S_4) is an important precursor for pyrite, its content in sediments is usually low (Morse and Cornwell, 1987). Thus, the main sulfur mineral recovered by CRS was pyrite sulfur, which will be referred to as pyrite-S (or Py-S) hereafter. The sediments were subjected to a two-step distillation. AVS was extracted over two hours by boiling in 5 M HCl, which was followed by 3 h boiling with 1 mol L^{-1} acidic $CrCl_2$ solution (extracting CRS) (Fossing and Jørgensen, 1989). The MDL was 10 μmol kg^{-1} wet sediment or 50 nmol total pyrite-S.

Total iron and manganese concentrations were measured according to Aller et al. (1986). For quantification of iron and manganese SpectrAA 300/400 Series Varian AAS was used. Results are presented in moles of metal per kilogram of wet sediment after correction based on sediment porosity. The MDL was 2 μmol kg^{-1} (wet sediment) for iron and 0.6 μmol kg^{-1}

(wet sediment) for manganese. For quantification of reactive iron species (Fe_{HR}) a sequential extraction scheme was used according to Poulton and Canfield (2005). Quantification was performed by AAS, and the MDL was 2 μmol kg^{-1} Fe (wet sediment). Pyritic iron was measured on a subsample by the CRS protocol.

For porosity analysis, the weight and volume of wet sediment and of sediment dried at 50°C for one week were measured. The porosity was calculated as the fraction of pore-water volume in the wet sediment. Total organic carbon (TOC) was quantified by an elemental analyzer (LECO SC632). The MDL was 0.005% TOC with precision of 1%.

Isotopic Analysis

For preparation for sulfur isotopic analysis of AVS and pyrite-S, zinc sulfide that was formed during hydrogen sulfide distillation was converted to silver sulfide by addition of an excess of silver nitrate solution. Each Ag_2S sample was aged for at least one week and cleaned with sequential washes of 4 × 50 mL Milli-Q water, rinsed in 50 mL of 1 M NH_4OH overnight, then washed with 3 × 50 mL Milli-Q water and dried at 55°C. For the isotopic analysis of sulfate, sediments were centrifuged, the supernatant was filtered, and an excess of barium chloride solution was added to the filtrate in order to precipitate $BaSO_4$. The precipitate was washed with 3 × 50 mL Milli-Q water and dried at 55°C.

For the analysis of $\delta^{18}O_{SO4}$, barium sulfate was pyrolyzed at 1450°C in a temperature conversion element analyzer (TC/EA), producing carbon monoxide. Carbon monoxide was measured by continuous helium flow in a GS-IRMS (Thermo Finnegan Delta V Plus, at the Godwin Laboratory, University of Cambridge). Analyses of $\delta^{18}O_{SO4}$ were performed in replicates (n = 3–5) and the standard deviation of the replicate analysis is reported (∼0.4‰ 1σ). To analyze the $\delta^{34}S_{SO4}$, $\delta^{34}S_{Py-S}$, $\delta^{34}S_{AVS}$, $\delta^{34}S_{S0}$ values, barite or silver sulfide with an excess of vanadium pentoxide were combusted at 1030°C in a flash element analyzer (EA), and the resulting sulfur dioxide (SO_2) was measured by continuous helium flow on a GS-IRMS (Thermo Finnegan Delta V Plus Godwin Laboratory, University of Cambridge). The analytical error for the $\delta^{34}S$ analysis was determined using the standard deviation of standards run at the beginning and the end of each run (long term reproducibility of our standards is ∼0.3‰ 1σ). $\delta^{18}O_{SO4}$ is reported relative to the Vienna Standard Mean Ocean Water (VSMOW) and $\delta^{34}S$ is reported with respect to Vienna Canyon Diablo Troilite (VCDT).

RESULTS

Sediment Description

In the vicinity of the north shore of the Gulf of Aqaba (sites RS-II-19 and RS-V-21), sediments contain grayish sandy particles, suggesting the source of the sediment is terrigenous material derived from adjacent rocks by erosion and/or weathering and transported by seasonal floods. The sediments from near the fish farm contained black fragments which are likely residual material from fish cages, consistent with the composition of sediment cores collected during the operation period of Ardag fish farm (Katz et al., 2002). The bulk composition of the north shore sediments is dominated by siliciclastic material with lower carbonate content (6.17%; Al-Rousan et al., 2006) compared to coral reef sediments (74.8%; Al-Rousan, 1998). The sediment from the intermediate and deep-water sites (RS-IV-306, RS-III-420, and RS-I-694) is characterized by a much finer grain size with a higher content of light brown clay and mud. These textural properties at the deeper-water sites reflect the aeolian source of particles derived from desert soils (Garrison et al., 2003).

Pore-Water Chemistry

Dissolved iron was present in the sediments of the deep-water sites (RS-IV-306, RS-III-420, and RS-I-694) at all depths below seafloor, while at the shallow water site that were not influenced by the fish farms (RS-V-21) no dissolved iron was detected below 3 cm below seafloor (**Figure 2A**). Dissolved manganese concentrations increase with overlying water column depth. Concentrations above 10 μmol L^{-1} were detectd only at the deepest site RS-I-694 (**Figure 2B**).

Sulfate concentrations were constant with depth at all the sampling sites, in the range of 32–35 mmol L^{-1} (data not shown). Hydrogen sulfide concentrations were below 0.34 μmol L^{-1} at the deep-water sites (RS-IV-306, RS-III-420 and RS-I-694), up to 1.3 μmol L^{-1} at former fish farm site RS-II-19, and up to 12 μmol L^{-1} at site RS-V-21 (**Figure 2C**). Zero valent sulfur (ZVS) was below detection limit at sites RS-II-19 and RS-IV-306, below 200 nmol L^{-1} at sites RS-III-420 and RS-I-694 and up to 301 nmol L^{-1} at site RS-V-21 (data not shown). The highest thiosulfate concentrations were detected at the shallow water sites (up to 4.05 μmol L^{-1} at site RS-V-21). At sites RS-IV-306 and RS-I-694, thiosulfate concentrations were <0.1 μmol L^{-1} (**Figure 2D**). Sulfite concentrations in the pore-waters were lower than thiosulfate concentrations. At the shallow sites (RS-II-19 and RS-V-21), sulfite concentrations were 78–972 nmol L^{-1}. Sulfite concentrations at the deeper sites were <150 nmol L^{-1} (**Figure 2E**).

Solid Phase Chemistry

The porosity of the sediments increased with increasing water depth as well as with depth below the sediment-water interface (**Figure 3A**). TOC content was in the range of 0.1-0.6 wt% at all sites. The AVS and pyrites sulfur contents of the sediment decreased with an increase in water column depth. At the shallow site not influenced by anthropogenic pollution (RS-V-21), AVS content decreased with depth below the seafloor and pyrite sulfur increased with depth below the seafloor. At site RS-II-19 (the site impacted by the fish farm) the lowest AVS concentration was detected in the upper 10 cm of sediments (**Figures 3B,C**). In the upper 10 cm of the sediment, elemental sulfur content was higher at the shallow water sites than at the deep-water sites (**Figure 3D**).

Sediments from the deep-water sites were enriched in total manganese in the upper two centimeters of the core. At RS-I-694 site total manganese content reached 26.0 mmol kg^{-1} of wet sediment. In cores taken from shallow-water sites (RS-II-19 and RS-V-21), the total manganese content was below 7 mmol kg^{-1} of wet sediment (**Figure 3E**). Sediments in the deep-water sites were enriched in iron compared to shallow-water sites, especially

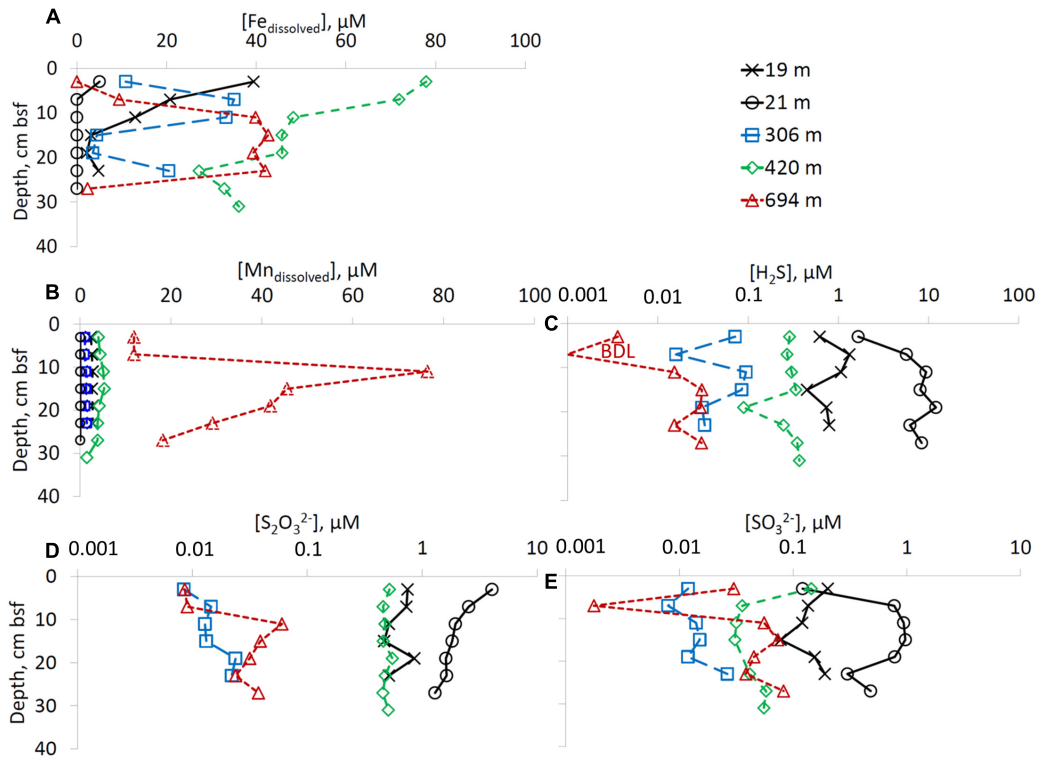

FIGURE 2 | Pore-water chemistry. Profiles of **(A)** dissolved iron, **(B)** dissolved manganese, **(C)** hydrogen sulfide (pay attention to logarithmic x-axis), **(D)** thiosulfate (pay attention to logarithmic x-axis), and **(E)** sulfite (pay attention to logarithmic x-axis). Right upper panel presnets a color codes for sampling sites.

in the upper 14 cm of the sediment. The highest total iron content was detected at site RS-II-420 (**Figure 3F**). Traditionally, highly reactive iron is defined as the sum of iron species which are reactive toward hydrogen sulfide and iron which has already reacted with sulfide (e.g., pyrite iron). The content of highly reactive iron, which in our study includes pyrite iron, acetate-, hydroxylamine-, dithionite-, and oxalate-extractable iron, increases with water depth (**Figure 3G**). As concentrations of pyrite are higher at the shallow-water sites (**Figure 3C**), concentrations of iron species which are still reactive toward hydrogen sulfide increase further with water depth. At the shallow-water sites (RS-II-19 and RS-V-21) concentrations of highly reactive iron slightly increased with depth (**Figure 3G**). Sodium acetate-extractable iron, which accounts for Fe(II) carbonate minerals such as siderite and ankerite represented less than 10% of the highly reactive iron at all water depths. Dithionite-extractable iron (goethite + hematite + akaganéite) represented the most abundant fraction of highly reactive iron in the sediments of the Gulf of Aqaba (data not shown).

Isotopic Composition of Sulfur Species

The isotopic composition of the Gulf of Aqaba seawater sulfate was measured in five samples. Three samples were taken at the surface at various locations and two samples were retrieved from 20 and 700 m depths. The isotope composition of sulfate at various locations and water depths within the Gulf of Aqaba is similar ($\delta^{34}S = 20.3 \pm 0.2‰$, $\delta^{18}O = 8.6 \pm 0.2‰$), and does not differ more than the error of the analytical method. At all sites, except at the former fish farm (site RS-II-19), the $\delta^{34}S$ of sulfate near the top of the sediment was similar to the overlying water (20.3–20.5‰). At these sites, the $\delta^{34}S$ increased with depth below the seafloor to 21.2–23.1‰. At the former fish farm site, sulfate sulfur was isotopically lower than seawater sulfate, possibly due to re-oxidation of isotopically light reduced sulfur minerals formed during fish farm operation (**Figure 4A**). At all depths bsf, the $\delta^{18}O$ of sulfate was higher than seawater sulfate (9.4–10.4‰ in the upper 2 cm of sediment vs. 8.6% in the water column). For the deep-water sites, a slight increase in $\delta^{18}O$ of sulfate was observed with depth (**Figure 4B**).

The sulfur isotopic composition of AVS is only reported for the shallow-water sites, as at the deep-water sites the AVS content was too low to perform sulfur isotopic analysis. The most ^{34}S-enriched AVS was detected at both shallow-water sites in the uppermost samples: $\delta^{34}S = -18.4‰$ to $-19.3‰$. At 17–29 cm bsf, the $\delta^{34}S$ of AVS was in the range of $-21.6‰$ to $-25.4‰$ (**Figure 4C**). Enough pyrite-S for sufur isotopic analysis was retrieved from all sediments at the two shallow-water sites, three samples from site RS-IV-306 from 14 to 20 cm, and one sample from site RS-I-694 at 18–20 cm (this point cannot be seen on the figure as it coincides with the point for RS-IV-306 profile). Pyrite sulfur was isotopically lower in $\delta^{34}S$ than AVS sulfur. At deepwater sites RS-IV-306 and RS-I-694, pyrite was isotopically lower in $\delta^{34}S$ than at the shallow-water sites (**Figure 4D**). The isotopic composition of elemental

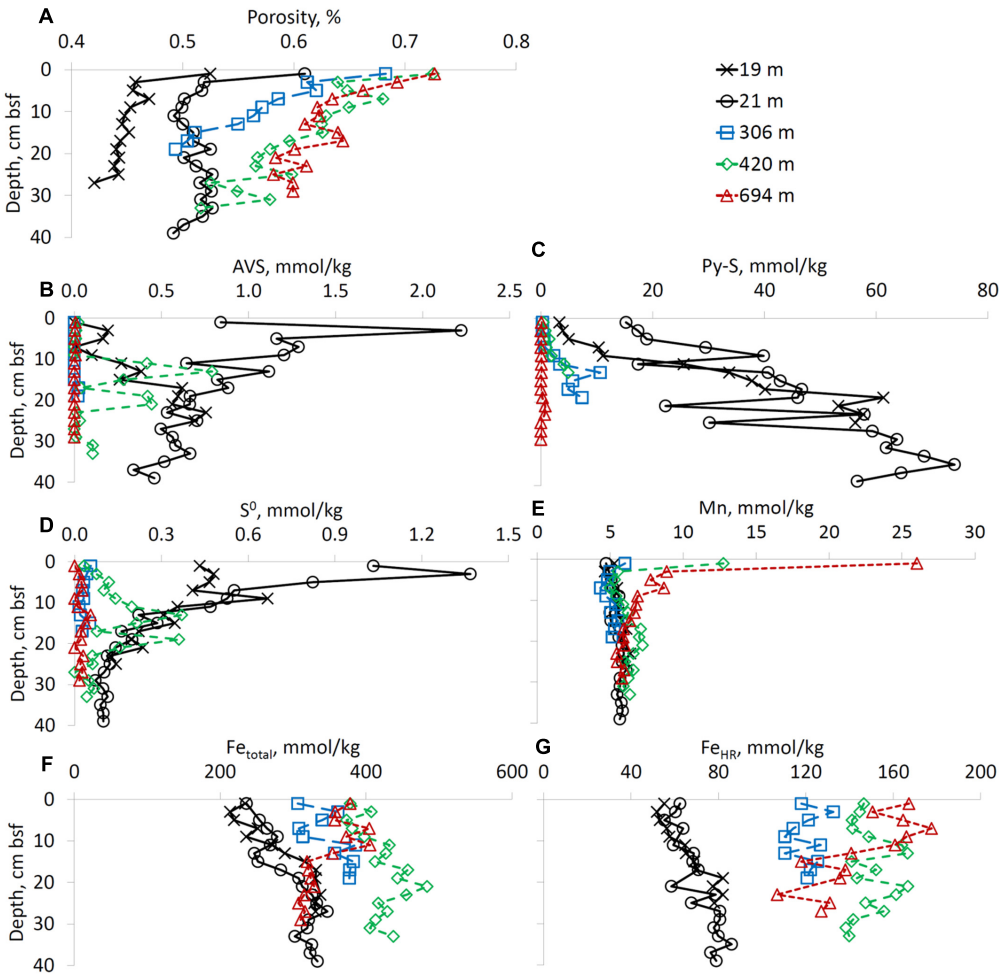

FIGURE 3 | Sediment porosity and solid-phase composition (except iron speciation). Profiles of **(A)** porosity, **(B)** AVS, **(C)** pyrite sulfur, **(D)** elemental sulfur, **(E)** manganese, **(F)** total iron, and **(G)** sum of "highly reactive" iron species. Right upper panel presnets a color codes for sampling sites. All concentrations are given in mmol kg^{-1} of wet sediment.

sulfur was measured in the 0–2 cm and 2–4 cm intervals in the sediments from site RS-V-21and the $\delta^{34}S$ was –20.9‰ and –22.4‰, respectively.

DISCUSSION

Manganese and Iron Cycles

The concentration of total manganese in the solid sediment increases with the depth of the overlying water column (**Figure 3E**). This increase is likely caused by greater contribution of aeolian dust to the sediment further from the shore. The atmospherically transported material from the Sahara and adjacent deserts has a high manganese content, as much as 880 ppm (16 mmol kg^{-1}) in Saharan dust (Mendez et al., 2010). In contrast, the shallow sediment has a dominance of fluvial input with lower manganese content. An enrichment in solid manganese in the upper 2 cm of the sediment was observed in the deep-water sites (**Figure 3E**). This solid manganese enrichment results from the oxidation of reduced aqueous manganese (Mn^{2+}), which is produced by microbial manganese reduction coupled to organic carbon oxidation. This reduced Mn^{2+} produced deeper in the sediment diffuses toward the water-sediment interface where it is oxidized to manganese oxides. The only site at which concentrations of dissolved manganese were higher than concentrations of dissolved iron was deepwater site RS-I-694 suggesting a dominance of the manganese cycle at this location.

The concentration of total sedimentary solid iron, similar to total manganese, increases as the depth of the overlying water column increases, except for the deepest site (RS-I-694) (**Figure 3F**). As with manganese, this increase may be explained by greater contribution of aeolian dust away from the shore. The fine-grain sediment that is transported from the Sahara and adjacent deserts by wind has a high iron content (Chase et al., 2006). The lack of a significant increase of solid total iron in the surface sediment layer is likely due to low iron sulfide solubility, which causes retention of iron in the sediment even

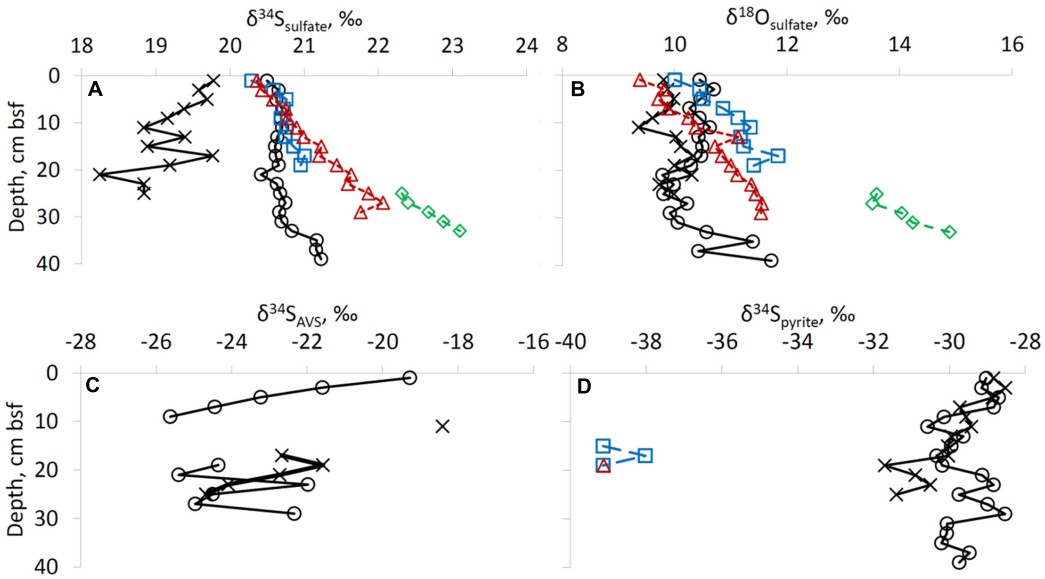

FIGURE 4 | Isotopic composition of sulfur species. Profiles of **(A)** $\delta^{34}S$ of sulfate, **(B)** $\delta^{18}O$ of sulfate, **(C)** $\delta^{34}S$ of AVS, **(D)** $\delta^{34}S$ of pyrite. For legend see right upper panel of **Figure 2**.

at low concentrations of hydrogen sulfide in the pore-waters (**Figures 2A,C**).

Highly reactive iron is traditionally defined as the fraction of iron in the sediment that can react with hydrogen sulfide to produce FeS or FeS_2 (Berner, 1970). There are different pools of iron that are defined based on their reactivity toward hydrogen sulfide. Ferrihydrite and lepidocrocite react with hydrogen sulfide within hours. The most abundant iron minerals in dust from the Saharan Desert, such as hematite and goethite, react with hydrogen sulfide on time scales of days (Poulton et al., 2004) and years (magnetite) (Canfield et al., 1992). For iron in sheet-silicate minerals it may take up to millions of years to react with hydrogen sulfide (Canfield et al., 1992; Raiswell and Canfield, 1996). Highly reactive iron concentrations are lower at the shallow water sites (RS-II-19 and RS-V-21) than at the sites overlain by deeper waters. We suggest that the difference in the reactive iron content could be due to the difference in the highly reactive iron content of dust (relatively high) and desert soil and rock material transported by flash floods (relatively low), which predominantly impact shallow-water sediments. Although detailed studies of reactive iron speciation of minerals and soils in the various locations in arid Arava valley are not yet published, total iron content in granite was recently reported for two locations near Eilat: Wadi Shelomo and Mt. Rehavam with 0.30–0.76% Fe_2O_3 and 0.12–1.60% Fe_2O_3, respectively (Eyal et al., 2010). The iron in these locations is mostly associated with biotite (Bogoch et al., 1997). The detailed study of iron speciation in the seasonal stream beds, which is out of scope of this study, should be performed in order to evaluate this hypothesis.

Sulfur Cycle

The concentration of hydrogen sulfide in the pore-water decreased with an increase in water column depth from 0.5 to 12 μmol L^{-1} at the shallow-water sites to ≤30 nmol L^{-1} at site RS-I-694. The latter concentration was detected by HPLC with a fluorescence detector and is a concentration we usually consider to be below the detection limit of standard spectrophotometric techniques (1 μmol L^{-1} – Cline, 1969). Despite extremely low concentrations of hydrogen sulfide in the deeper sediments, we use three lines of evidence to confirm the presence of a sedimentary sulfur cycle in the Gulf of Aqaba.

Pyrite Content

The first line of evidence for microbial sulfate reduction is the presence of pyrite. Pyrite is formed by two mechanisms, both involving hydrogen sulfide: the "polysulfide" mechanism (Eqs. 1–3) (Luther, 1991; Kamyshny et al., 2004) and the "sulfide" mechanism (Eqs. 1, 4) (Rickard and Luther, 1997; Gartman and Luther, 2013).

$$2FeOOH + 3H_2S \rightarrow 2FeS + S^0 + 4H_2O \quad (1)$$

$$H_2S + (n-1)S^0 \leftrightarrows 2H^+ + S_n^{2-} \quad (2)$$

$$FeS + S_n^{2-} \rightarrow FeS_2 + S_{n-1}^{2-} \quad (3)$$

$$FeS + H_2S \rightarrow FeS_2 + H_2 \quad (4)$$

In our case, circumneutral pH and the presence of elemental sulfur in the sediment (**Figure 3D**), suggest that the "polysulfide" mechanism is the most feasible pathway of pyrite formation. Although concentrations of polysulfides in the pore-waters were below the detection limit of our analytical technique (Kamyshny et al., 2006), it is likely that their concentration was low due to their fast reaction during pyrite precipitation. Oxidation of polysulfides by oxygen is known to be faster than oxidation of hydrogen sulfide by oxygen (Kleinjan et al., 2005). Thus, concentrations of polysulfides in various natural aquatic systems

are better explained by kinetics of their reaction rather than by thermodynamic considerations (Kamyshny and Ferdelman, 2010; Lichtschlag et al., 2013).

Sedimentary pyrite content decreases with increasing water column depth and with depth below the sediment-water interface (**Figure 3C**). Depth-based net pyrite formation rates were calculated from the linear approximation of the increase of pyrite concentrations with depth, and converted to time-based rates using the typical sedimentation rate for deep sites (0.054 cm year^{-1} – Al-Rousan et al., 2004). Net pyrite formation rates were estimated to be 0.68, 0.53, 0.11, 0.073, and 0.0063 nmol cm^{-3} wet sediment day^{-1} at sites RS-II-19, RS-V-21, RS-IV-306, RS-III-420, and RS-I-694, respectively. These rates of pyrite formation are lower than rates of microbial sulfate reduction in most marine sediments. One explanation of this observation is re-oxidation of a significant portion of hydrogen sulfide formed during microbial sulfate reduction. Reoxidation of hydrogen sulfide to sulfide oxidation intermeditates, which in turn may be microbially disproportionated to sulfate and hydrogen sulfide allows only trace amounts of pyrite to form. On the other hand, the higher highly reactive iron content at the deeper sites (**Figure 3G**) may give preference to iron reducing microorganisms, thus suppressing microbial sulfate reduction.

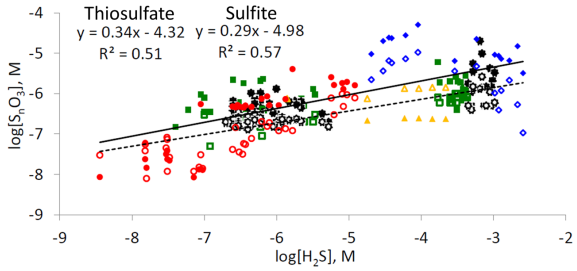

FIGURE 5 | Dependence of concentrations of thiosulfate (closed symbols) and sulfite (opened symbols) on concentrations of hydrogen sulfide in marine sediments (not including salt marshes and tidal flats). Red circles – this work from the Gulf of Aqaba, orange triangles – results from Thamdrup et al. (1994) from Aarhus Bay sediments, green rectangles – results from Zopfi et al. (2004) from the Black Sea, black stars – results from Zopfi et al. (2008) from the upwelling area off central Chile coast, blue diamonds – results from Lichtschlag et al. (2013) from Dvurechenskii mud volcano, Black Sea. Solid line represents a trendline for all thiosulfate vs. hydrogen sulide data points, dashed line represents a trendline for all sulfite vs. hydrogen sulfide datapoints. Only data which were obtained by chromatographic analysis after 2,2′-dithiobis(5-nitropyridine) derivatization (Valravamurthy and Mopper, 1990) and monobromobimane derivatization (see Materials and Methods section and references therein) for points where both hydrogen sulfide and sulfur oxoanion concentrations were above the detection limit are presented.

Sulfide Oxidation Intermediates

The second line of evidence for an active sulfur redox cycle in the sediments of the Gulf of Aqaba is the presence of intermediate-valence state sulfur species. Hydrogen sulfide is a precursor to sulfide oxidation intermediates such as zero-valent sulfur, thiosulfate and sulfite in sedimentary pore-waters (**Figures 2D,E**) as well as of zero-valent sulfur in the solid phase (**Figure 3D**). Thus, the presence of intermediate sulfur species in the sedimentary pore fluids may be interpreted as an argument for chemical or microbial oxidation of hydrogen sulfide.

Zopfi et al. (2004) suggested that concentrations of sulfide oxidation intermediates in marine sediments are controlled by their availability for microbial metabolism. Usually, the concentration of these intermediates decreases in the order $[S^0] > [S_2O_3^{2-}] > [SO_3^{2-}] > [S_4O_6^{2-}]$, as we observe in the sediments of the Gulf of Aqaba (**Figures 2D,E**, **3D**). As expected, the concentration of elemental sulfur in the sediments decreases with increasing water column depth, e.g., with the decrease in the rates of formation of its precursor, hydrogen sulfide. In the shallow-water sites, the concentration of elemental sulfur decreases with sediment depth as well, due to the formation of pyrite which will consume the available hydrogen sulfide. At the shallow-water sites, the concentration of elemental sulfur reaches 1 mmol kg^{-1} of wet sediment. Only colloidal sulfur with particles <150 nm, polysulfide sulfur, and dissolved elemental sulfur can pass the membrane of the Rhizon samplers. Sulfur is predominantly in the solid sediment, as zero-valent sulfur concentrations in pore-waters are <300 nmol L^{-1} at all sites and sediment depths. As the solubility of elemental sulfur in seawater at 25°C is 147 nmol L^{-1} (Kamyshny, 2009b), at some sites the presense of polysulfides is required to explain the observed results in the porewater, as colloidal sulfur equilibrates with hydrogen sulfide according to Eq. (2) in minutes to hours (Fossing and Jørgensen, 1990; Kamyshny and Ferdelman, 2010).

The concentration of thiosulfate in the pore-waters decreases with increasing water depth as is expected due to the corresponding decrease of hydrogen sulfide concentrations. A similar trend was observed for concentrations of sulfite. The concentrations of thiosulfate and sulfite are typical for marine sediments, although, it must be mentioned that in marine sediments, hydrogen sulfide concentrations are often much higher than our results for the Gulf of Aqaba (Thamdrup et al., 1994; Zopfi et al., 2004, 2008; Lichtschlag et al., 2013).

The co-dependences of the concentration of thiosulfate and sulfite on the concentration of their precursor - hydrogen sulfide - produces a rather unexpected relationship (**Figure 5**). The increase in the concentration of thiosulfate and sulfite in pore-waters is often more moderate than the increase in hydrogen sulfide concentrations: a 10-fold increase in hydrogen sulfide leads to only c.a. fivefold increase in concentration of intermediate sulfur oxyanions. The simultaneous presence of hydrogen sulfide and intermediate oxyanions in marine sediments is possible only if two conditions are fullfilled: (1) low or zero dissolved oxygen levels are present in pore-waters; (2) if oxygen is absent, other electron acceptors, capable of chemical or microbial oxidation of hydrogen sulfide (e.g., nitrate, MnO_2, Fe(III) (hydr)oxides)), are present in the sediment. As nitrate concentrations in seawater of the Northern Gulf of Aqaba are low (<6 μmol L^{-1}) (Al-Qutob et al., 2002) and it is depleted quickly in the pore-waters, manganese and iron oxides are the main electron acceptors responsible for hydrogen sulfide oxidation in these locations. Chemical oxidation of hydrogen sulfide by Mn(IV) leads to formation of zero-valence

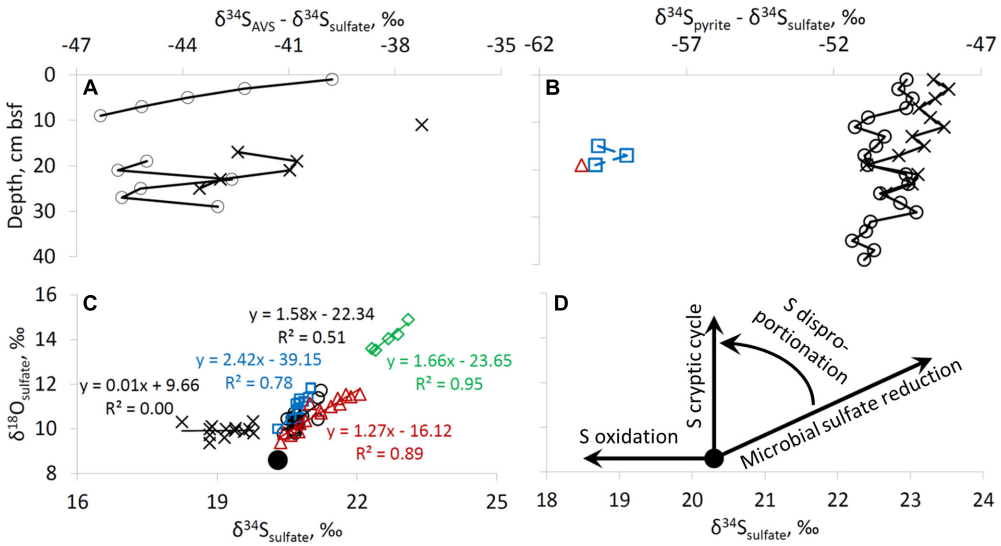

FIGURE 6 | Difference between $\delta^{34}S$ values of AVS and sulfate **(A)**, and of pyrite and sulfate **(B)**. Plot of $\delta^{18}O$ of sulfate vs. $\delta^{34}S$ of sulfate is presented in plate **(C)**. Schematic pathways of dependence of $\delta^{34}S$ and $\delta^{18}O$ values of sulfate on microbial sulfur transformation process is presented in the panel **(D)**. Large black circle in panels **(C,D)** represents isotopic composition of sulfate in the water column of the Red Sea. For legend see right upper panel of **Figure 2**.

sulfur, thiosulfate, sulfite, and sulfate (Burdige and Nealson, 1986), and chemical oxidation of hydrogen sulfide by Fe(III) forms mostly zero-valence sulfur, although the formation of other sulfide oxidation intermediates has been documented (Yao and Millero, 1996; Wan et al., 2014). Therefore, the distribution of sulfide oxidation intermediates depends on the ratio of hydrogen sulfide-to-electron acceptor, where at lower ratios more oxidized products are formed. These reactions are first order with respect to both hydrogen sulfide and the concentration of electron acceptor. Microbial disproportionation and oxidation of intermediate sulfur species may lead to the formation of other sulfide oxidation intermediates as well as of the terminal oxidation product, sulfate (Bak and Cypionka, 1987; Jørgensen, 1990a,b; Zopfi et al., 2004, and references therein).

We suggest the following explanation for the observed trends. The decrease in hydrogen sulfide concentration in pore-waters leads to a decrease in the ratio between hydrogen sulfide and the concentrations of reactive iron and manganese oxides in the sediment. This, in turn, leads to formation of more oxidized sulfide oxidation intermediates (e.g., more sulfite and thiosulfate and less zero-valent sulfur species). On the other hand, a decrease in the concentration of intermediate sulfur oxyanions, leads to a decrease in the rates of their chemical and microbial consumption. Thus, an increase in the fraction of hydrogen sulfide that is converted to sulfur oxyanions, combined with a decrease in their consumption rate, results in only a moderate decrease in their concentrations with a corresponding decrease in hydrogen sulfide concentrations. In the extreme case of the sediments of the Gulf of Aqaba, concentration ratios of up to 4 and 8 between thiosulfate and sulfite, respectively, to hydrogen sulfide were found at site RS-I-694.

Isotopic Composition of Sulfur Species

The third line of evidence for microbial sulfur cycling in the sediments is the isotopic composition of sulfur species. In this study, the sulfur isotopic fractionation between sulfate and AVS (which represents the sulfur isotopic composition of the most recently formed hydrogen sulfide) is 37–46‰ (**Figure 6A**). Usually, in marine sediments both AVS and pyrite become isotopically more enriched in ^{34}S with depth due to Rayleigh distillation of sulfur isotopes during microbial sulfate reduction and the diffusion of sulfate within pore-fluids. In our case, Rayleigh distillation cannot be invoked to explain the observed trends as (1) sulfate concentrations do not decrease significantly with depth, (2) AVS becomes lower in $\delta^{34}S$ with sediment depth, and (3) pyrite sulfur becomes isotopically lower in $\delta^{34}S$ with sediment depth and near the sediment surface it is isotopically lower in $\delta^{34}S$ than AVS by approximately 10‰. An increase in sulfur isotope fractionation with depth may be explained by a decrease in microbial sulfate reduction rates (Chambers et al., 1975; Canfield, 2001; Sim et al., 2011b), which results from preferential mineralization of more bioavailable organic matter in the uppermost sediments. The difference of approximately 10‰ in the sulfate-pyrite sulfur isotope fractionation between shallow-water and deep-water sites (**Figure 6B**) supports an increase in sulfur isotope fractionation with a decrease in the rate of formation of hydrogen sulfide. A possible explanation for the relatively constant $\delta^{34}S$ of pyrite in the surface sediments is the impact of bioturbation (**Figure 3C**). Rates of bioturbation in the shallow-water site near the fish farm (derived from chlorophyll profiles) were previously shown to be in the range of 0.013–0.069 $cm^2\ d^{-1}$ (Black et al., 2012). The sulfur isotopic composition and concentrations in the upper 6 cm of sediments at shallow-water sites are thus possibly homogenized by bioturbation

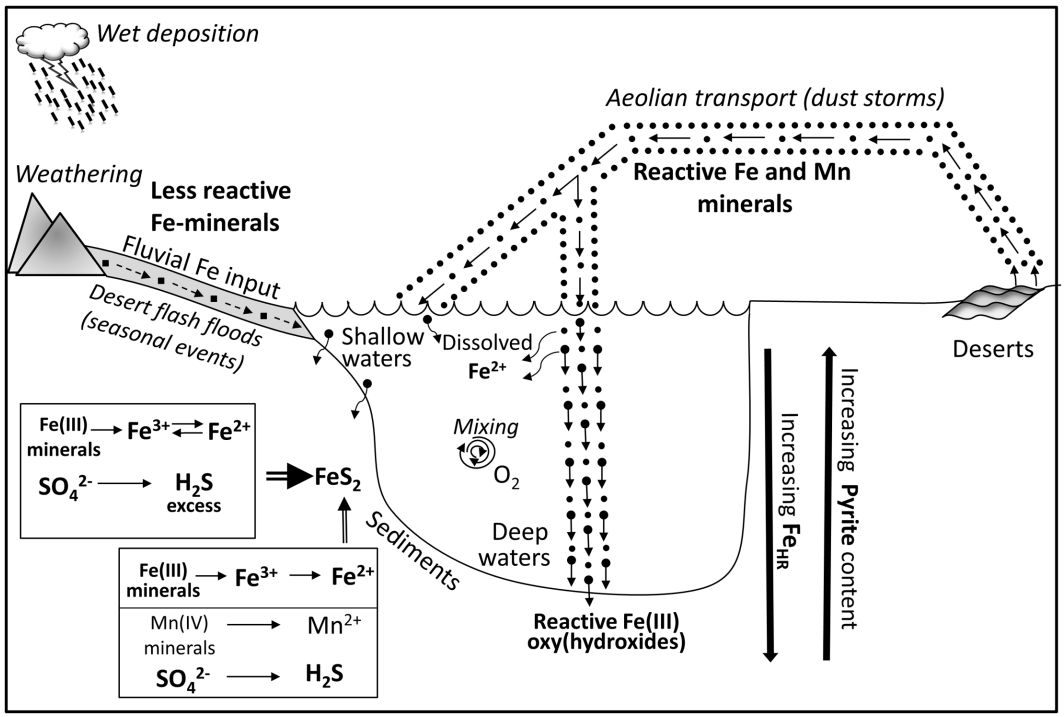

FIGURE 7 | Schematic illustration of impacts of aeolian and fluvial sedimentary inputs on biogeochemistry redox-sensitive elements in the sediments of the Gulf of Aqaba. Aeolian input of highly reactive iron minerals is presented as a sum of fluxes of mineral dust which is derived from adjacent areas (rock weathering, secondary airflow) and dust which is transported from deserts by long distance aeolian transport (dust events, dust storms). Fluvial iron input is presented as sediment transport from adjacent areas (mainly Arava desert) by seasonal flashfloods which take place during winter rainfall events. The majority of wind-blown iron particles rapidly settle throughout the water column to the sediment, while minor fraction of reactive iron (III) oxyhydroxides dissolves in the water column. See text for detailed explanation of biogeochemical processes in the sediments.

(**Figures 3C**, **4D**) which exponentially decreases with depth (Steiner et al., 2016).

In two analyzed samples (0–2 cm and 2–4 cm bsf at site RS-V-21) elemental sulfur was lower in $\delta^{34}S$ by 0.8–1.6‰ than AVS. These results suggest that equilibrium in the H_2S-polysulfide-S^0 system is not achieved, as at the equilibrium zero-valent sulfur is higher in $\delta^{34}S$ than hydrogen sulfide by up to 4‰ (Amrani et al., 2006; Kamyshny et al., 2014).

The relative change in the $\delta^{34}S$ and $\delta^{18}O$ of sulfate during microbial sulfate reduction has been shown to yield insight into the sulfur cycle in marine sediments and in laboratory cultures. At all the sites, except for RS-V-21, there is a coupled increase in $\delta^{18}O$ and $\delta^{34}S$ in sulfate as expected during microbial sulfate reduction. The relative change in $\delta^{18}O$ vs. $\delta^{34}S$ has been shown to correlate with the rate of microbial sulfate reduction (Böttcher et al., 1999; Aharon and Fu, 2003; Antler et al., 2013): the slower the sulfate reduction rate, the steeper the slope. The slopes in our sampling sites range between 1.2 ± 0.1 (at 694 m) to 2.4 ± 0.5 (at 306 m). It seems, however, that there is a discrepancy in the correlation between the slope and the sulfate reduction rates, as the most moderate slope is in the site where sulfate reduction rate is expected to be the lowest (694 m). We suggest that the disproportionation of intermediates of hydrogen sulfide oxidation increases the measured slope between $\delta^{18}O$ and $\delta^{34}S$ (Böttcher et al., 2005) (**Figures 6C,D**). At the former fish farm contaminated site (RS-II-19), a decrease in $\delta^{34}S$ was observed together with a scattered change in the $\delta^{18}O$ of sulfate (±0.6 ‰). This observation may be explained by more intense oxidation of reduced sulfur species at this site (**Figures 6C,D**). Combined with other evidence, the oxygen isotope composition of sulfate provides strong evidence for a presence of sulfur cycling in the sediments of the Gulf of Aqaba, including a near quantitative cycling of sulfur between oxidized and reduced or intermediate valence states with low net-consumption, which has been termed a 'cryptic' sulfur cycle.

Impact of Aeolian Deposition on the Sulfur Cycle in the Sediments of the Gulf of Aqaba

An integrated scheme of processes affecting cycling of redox-sensitive elements in the Gulf of Aqaba is presented in **Figure 7**. Sediments overlain by deep water receive predominantly input of aeolian dust, which has high manganese and reactive iron content. At these water depths, microbial iron and manganese reduction is preferred over sulfate reduction. In spite of a microbial cycle dominated by iron and manganese cycling, there is microbial sulfate reduction and trace amounts of pyrite accumulating. However, the vast majority of the hydrogen sulfide produced is reoxidized in the presence of the high concentration

of iron and manganese oxides to sulfide oxidation intermediates, which are further oxidized or disproportionated to form the terminal oxidation product, sulfate. These processes induce the high concentration of sulfide oxidation intermediates in pore waters and leave fingerprints in oxygen isotope composition of the sulfate. Thus, at these deep water sites the sulfur cycle is mostly cryptic.

Shallow water sites are influenced by a combination of aeolian dust input and fluvial iron and manganese inputs. At these sites, the manganese (especially close to the sediment-water interface) and reactive iron contents are lower than at the deep-water sites. Lower reactive iron content allows relatively high amounts of hyrdogen sulfide to be present in the pore-waters and to be further preserved in the form of pyrite.

In summary, this work shows that in arid environments, such as the Gulf of Aqaba, aeolian dry deposition from the surrounding deserts results in an increased flux of reactive iron and manganese to the sediments. Such increase leads to fast reoxidation of hydrogen sulfide and prevents pyrite formation in the sediments. Future work should concentrate on the detailed study of speciation of iron and manganese in the aeolian and fluvial sedimentary sources. Another direction of future research should include the study of impact of aeolian dry deposition on sedimentary sulfur cycle in other marine systems affected by aeolian dust deposition. Such research efforts are required in order to understand whether these considerations are unique to the Gulf of Aqaba or may be applied to other marine systems situated in arid regions.

AUTHOR CONTRIBUTIONS

BB and AK designed research; BB, VB, AT, GA, NK, RK and AK performed analyses; BB, VB, AT, GA, US, NK, RK and AK interpreted data, wrote the paper and approved the final version to be published.

FUNDING

This work was funded by Marie Curie Actions CIG Program, project number 303740. The isotope analyses were funded by ERC StG 307582 CARBONSINK to AT.

ACKNOWLEDGMENTS

We would like to thank Itamar Pelly, Jiwchar Ganor, Shimon Feinstein, and Orit Sivan (BGU) for an opportunity to use their analytical equipment. The sulfur isotope analyses were partially funded by ERC-StG 307582 (CARBONSINK) to AT. We are grateful to Sarit Melamed, Bibi Kerpel, Tamir Buchshtav, Peter Rendel, and Edna Danon (BGU) for assistance with sample analyses. Additionally, we would like to thank Timor Katz, Asaph Rivlin, Sefi Baruch and Moty Ohevia (IUI, Eilat) for assistance with the field work. We would like to thank Alyssa Findlay and Adi Torfstein for comments on the draft of the manuscript.

REFERENCES

Aharon, P., and Fu, B. (2003). Sulfur and oxygen isotopes of coeval sulfate–sulfide in pore fluids of cold seep sediments with sharp redox gradients. *Chem. Geol.* 195, 201–218. doi: 10.1016/S0009-2541(02)00395-9

Aller, R. C., Mackin, J. E., and Cox, R. T. Jr. (1986). Diagenesis of Fe and S in Amazon inner shelf muds: apparent dominance of Fe reduction and implications for the genesis of ironstones. *Cont. Shelf Res.* 6, 263–289. doi: 10.1016/0278-4343(86)90064-6

Al-Qutob, M., Häse, C., Tilzer, M. M., and Lazar, B. (2002). Phytoplankton drives nitrite dynamics in the Gulf of Aqaba. Red Sea. *Mar. Ecol. Prog. Ser.* 239, 233–239. doi: 10.3354/meps239233

Al-Rousan, S. (1998). *Sediment Role in Nutrient Cycle within Coral Reefs of the Gulf of Aqaba, Red Sea*. Master thesis, Yarmouk University, Irbid.

Al-Rousan, S., Patzold, J., Al-Moghrabi, S., and Wefer, G. (2004). Invasion of anthropogenic CO_2 recorded in planktonic foraminifera from the northern Gulf of Aqaba. *Int. J. Earth Sci.* 93, 1066–1076. doi: 10.1007/s00531-004-0433-4

Al-Rousan, S., Rasheed, M., Al-Horani, F., and Manasrah, R. (2006). Geochemical and textural properties of carbonate and terrigenous sediments along the Jordanian coast of the Gulf of Aqaba. *J. Oceanogr.* 62, 839–849. doi: 10.1007/s10872-006-0102-2

Al-Taani, A. A., Rashdan, M., and Khashashneh, S. (2015). Atmospheric dry deposition of mineral dust to the Gulf of Aqaba, Red Sea: rate and trace elements. *Mar. Pollut. Bull.* 92, 252–258. doi: 10.1016/j.marpolbul.2014.11.047

Amrani, A. (2014). Organosulfur compounds: molecular and isotopic evolution from biota to oil and gas. *Annu. Rev. Earth Planet. Sci.* 42, 733–768. doi: 10.1146/annurev-earth-050212-124126

Amrani, A., Kamyshny, A. Jr., Lev, O., and Aizenshtat, Z. (2006). Sulfur stable isotope distribution of polysulfide anions in $(NH_4)_2Sn$ aqueous solution. *Inorg. Chem.* 45, 1427–1429. doi: 10.1021/ic051748r

Antler, G., Turchyn, A., Rennie, V., Herut, B., and Sivan, O. (2013). Coupled sulfur and oxygen isotope insight into bacterial sulfate reduction in the natural environment. *Geochim. Cosmochim. Acta* 118, 98–117. doi: 10.1016/j.gca.2013.05.005

Badran, M. I. (2001). Dissolved oxygen, chlorophyll a and nutrient: seasonal cycles in waters of the Gulf of Aqaba, Red Sea. *Aquat. Ecosyst. Health Manag.* 4, 139–150. doi: 10.1080/14634980127711

Bak, F., and Cypionka, H. (1987). A novel type of energy metabolism involving fermentation of inorganic sulphur compounds. *Nature* 326, 891–892. doi: 10.1038/326891a0

Ben-Avraham, Z., Almagor, G., and Garfunkel, Z. (1979). Sediments and structure of the Gulf of Elat (Aqaba) – Northern Red Sea. *Sediment. Geol.* 23, 239–267. doi: 10.1016/0037-0738(79)90016-2

Berner, R. A. (1970). Sedimentary pyrite formation. *Am. J. Sci.* 268, 1–23. doi: 10.2475/ajs.268.1.1

Bishop, T., Turchyn, A. V., and Sivan, O. (2013). Fire and brimstone: the microbially mediated formation of elemental sulfur nodules from an isotope and major element study in the Paleo-Dead Sea. *PLoS ONE* 8:e75883. doi: 10.1371/journal.pone.0075883

Biton, E., and Gildor, H. (2011). The general circulation of the Gulf of Eilat/Aqaba revisited: the interplay between the exchange flow through the Straits of Tiran and surface fluxes. *J. Geophys. Res.* 116:C08020. doi: 10.1029/2010jc006860

Black, K. D., Calder, L. A., Nickell, T. D., Sayer, M. D. J., Orr, H., Brand, T., et al. (2012). Chlorophyll, lipid profiles and bioturbation in sediments around a fish cage farm in the Gulf of Eilat. Israel. *Aquaculture* 35, 317–327. doi: 10.1016/j.aquaculture.2012.04.049

Bogoch, R., Bourne, J., Shirav, M., and Harnois, L. (1997). Petrochemistry of a late Precambrian garnetiferous granite, pegmatite and aplite, southern Israel. *Mineral. Mag.* 61, 111–122. doi: 10.1180/minmag.1997.061.404.11

Böttcher, M., Thamdrup, B., Gehre, M., and Theune, A. (2005). 34S/ 32S and 18O/ 16O fractionation during sulfur disproportionation by *Desulfobulbus propionicus*. *Geomicrobiol. J.* 22, 219–226. doi: 10.1080/01490450590947751

Böttcher, M. E., Bernasconi, S. M., and Brumsack, H.-J. (1999). Carbon, sulfur, and oxygen isotope geochemistry of interstitial waters from the western Mediterranean. *Proc. Ocean Drill. Prog. Sci. Results* 161, 413–421.

Böttcher, M. E., Oelschläger, B., Höpner, T., Brumsack, H.-J., and Rullkötter, J. (1998). Sulfate reduction related to the early diagenetic degradation of organic matter and "black spot" formation in tidal sandflats of the German Wadden Sea (southern North Sea): stable isotope (13C, 34S, 18O) and other geochemical results. *Org. Geochem.* 29, 1517–1530. doi: 10.1016/S0146-6380(98)00124-7

Boudreau, B. P. (1992). A kinetic model for microbic organic-matter decomposition in marine sediments. *FEMS Microbiol. Ecol.* 102, 1–14. doi: 10.1111/j.1574-6968.1992.tb05789.x

Brunner, B., Bernasconi, S., Kleikemper, J., and Schroth, M. (2005). A model for oxygen and sulfur isotope fractionation in sulfate during bacterial sulfate reduction processes. *Geochim. Cosmochim. Acta* 69, 4773–4785. doi: 10.1186/1467-4866-15-7

Brunner, B., and Bernasconi, S. M. (2005). A revised isotope fractionation model for dissimilatory sulfate reduction in sulfate reducing bacteria. *Geochim. Cosmochim. Acta* 69, 4759–4771. doi: 10.1016/j.gca.2005.04.015

Brunner, B., Einsiedl, F., Arnold, G., Müller, I., Templer, S., and Bernasconi, S. (2012). The reversibility of dissimilatory sulphate reduction and the cell-internal multi-step reduction of sulphite to sulphide: insights from the oxygen isotope composition of sulphate. *Isotopes Environ. Health Stud.* 48, 33–54. doi: 10.1080/10256016.2011.608128

Burdige, D. J., and Nealson, K. H. (1986). Chemical and microbiological studies of sulfide-mediated manganese reduction. *Geochem. J.* 4, 361–387.

Canfield, D. (2001). Biogeochemistry of sulfur isotopes. *Rev. Mineral. Geochem.* 43, 607–636. doi: 10.2138/gsrmg.43.1.607

Canfield, D. E., Raiswell, R., and Bottrell, S. (1992). The reactivity of sedimentary iron minerals toward sulfide. *Am. J. Sci.* 292, 659–683. doi: 10.2475/ajs.292.9.659

Canfield, D. E., Thamdrup, B., and Hansen, J. W. (1993). The anaerobic degradation of organic-matter in Danish coastal sediments – iron reduction, manganese reduction, and sulfate reduction. *Geochim. Cosmochim. Acta* 57, 3867–3883. doi: 10.1016/0016-7037(93)90340-3

Chambers, L. A., Trudinger, P. A., Smith, J. W., and Burns, M. S. (1975). Fractionation of sulfur isotopes by continuous cultures of *Desulfovibrio desulfuricans*. *Can. J. Microbiol.* 21, 1602–1607. doi: 10.1139/m75-234

Chase, Z., Paytan, A., Johnson, K. S., Street, J., and Chen, Y. (2006). Input and cycling of iron in the Gulf of Aqaba. Red Sea. *Glob. Biogeochem. Cycles* 20:GB3017.

Chen, K. Y., and Morris, J. C. (1972). Kinetics of oxidation of aqueous sulfide by oxygen. *Environ. Sci. Technol.* 6, 529–537. doi: 10.1021/es60065a008

Chen, Y., Paytan, A., Chase, Z., Measures, C., Beck, A. J., Sañudo-Wilhelmy, S. A., et al. (2008). Sources and fluxes of atmospheric trace elements to the Gulf of Aqaba. Red Sea. *J. Geophys. Res.* 113:D5. doi: 10.1016/j.marpolbul.2014.11.047

Chen, Y., Street, J., and Paytan, A. (2006). Comparison between pure-water- and seawater-soluble nutrient concentrations of aerosols in the Gulf of Aqaba. *Mar. Chem.* 101, 141–152. doi: 10.1016/j.marchem.2006.02.002

Cline, J. (1969). Spectrophotometric determination of hydrogen sulfide in natural waters. *Limnol. Oceanogr.* 14, 454–458. doi: 10.4319/lo.1969.14.3.0454

Duce R. A., Liss P. S., Merrill J. T., Atlas E. L., Buat-Menard P., Hicks B. B.(1991). The atmospheric input of trace species to the world ocean. *Glob. Biogeochem. Cycles* 5:193–259. doi: 10.1029/91GB01778

Duce, R. A., and Tindale, N. W. (1991). Atmospheric transport of iron and its deposition in the ocean. *Limnol. Oceanogr.* 36, 1715–1726. doi: 10.4319/lo.1991.36.8.1715

Eyal, M., Litvinovsky, B., Jahn, B. M., Zanvilevich, A., and Katzir, Y. (2010). Origin and evolution of post-collisional magmatism: coeval neoproterozoic calc-alkaline and alkaline suites of the Sinai Peninsula. *Chem. Geol.* 269, 153–179. doi: 10.1016/j.chemgeo.2009.09.010

Fahey, R. C., and Newton, G. L. (1987). Determination of low-molecular-weight thiols using monobromobimane fluorescent labeling and high-performance liquid chromatography. *Methods Enzymol.* 143, 85–96. doi: 10.1016/0076-6879(87)43016-4

Farquhar, J., Johnston, D. T., Wing, B. A., Habicht, K. S., Canfield, D. E., Airieau, S., et al. (2003). Multiple sulphur isotopic interpretations of biosynthetic pathways: implications for biological signatures in the sulphur isotope record. *Geobiology* 1, 27–36. doi: 10.1046/j.1472-4669.2003.00007.x

Fossing, H., and Jørgensen, B. B. (1989). Measurement of bacterial sulfate reduction in sediments - evaluation of a single-step chromium reduction method. *Biogeochemistry* 8, 205–222. doi: 10.1007/BF00002889

Fossing, H., and Jørgensen, B. B. (1990). Oxidation and reduction of radiolabeled inorganic sulfur compounds in an estuarine sediment, Kysing Fjord, Denmark. *Geochim. Cosmochim. Acta* 54, 2731–2742. doi: 10.1016/0016-7037(90)90008-9

Fritz, P., Basharmal, G., Drimmie, R., Ibsen, J., and Qureshi, R. (1989). Oxygen isotope exchange between sulphate and water during bacterial reduction of sulphate. *Chem. Geol. Isot. Geosci.* 79, 99–105. doi: 10.1080/10256016.2011.622443

Froelich, P., Klinkhammer, G., Bender, M., Luedtke, N., Heath, G., Cullen, D., et al. (1979). Early oxidation of organic-matter in pelagic sediments of the eastern equatorial Atlantic: suboxic diagenesis. *Geochim. Cosmochim. Acta* 43, 1075–1090. doi: 10.1016/0016-7037(79)90095-4

Garrison, V. H., Shinn, E. A., Foreman, W. T., Griffin, D. W., Holmes, C. W., Kellogg, C. A., et al. (2003). African and Asian dust: from desert soils to coral reefs. *BioScience* 53, 469–480. doi: 10.1641/0006-3568(2003)053[0469:AAADFD]2.0.CO;2

Gartman, A., and Luther, G. W. (2013). Comparison of pyrite (FeS2) synthesis mechanism to reproduce natural FeS2 nanoparticles found at hydrothermal vents. *Geochim. Cosmochim. Acta* 120, 447–458. doi: 10.1016/j.gca.2013.06.016

Genin, A., Lazar, B., and Brenner, S. (1995). Atmospheric cooling, unusual vertical mixing and coral mortality following the eruption of Mt. Pinatubo. *Nature* 377, 507–510. doi: 10.1038/377507a0

Goto, K., Taguchi, S., Fukue, Y., Ohta, K., and Watanabe, H. (1977). Spectrophotometric determination of manganese with 1-(2-pyridylazo)-2-naphthol and a non-ionic surfactant. *Talanta* 24, 752–753. doi: 10.1016/0039-9140(77)80206-3

Gröger, J., Franke, J., Hamer, K., and Schulz, H. D. (2009). Quantitative recovery of elemental sulfur and improved selectivity in a chromium-reducible sulfur distillation. *Geostand. Geoanal. Res.* 33, 17–27. doi: 10.1111/j.1751-908X.2009.00922.x

Habicht, K. S., Gade, M., Thamdrup, B., Berg, P., and Canfield, D. E. (2002). Calibration of sulfate levels in the Archean Ocean. *Science* 298, 2372–2374. doi: 10.1126/science.1078265

Hansel, C. M., Ferdelman, T. G., and Tebo, B. M. (2015). Cryptic cross-linkages among biogeochemical cycles: novel insights from reactive intermediates. *Elements* 11, 409–414. doi: 10.2113/gselements.11.6.409

Harrison, A. G., and Thode, H. G. (1958). Mechanism of the bacterial reduction of sulphate from isotope fractionation studies. *Chem. Soc. Faraday Trans.* 54, 84–92. doi: 10.1039/tf9585400084

Holmkvist, L., Ferdelman, T. G., and Jørgensen, B. B. (2011). A cryptic sulfur cycle driven by iron in the methane zone of marine sediment (Aarhus Bay. Denmark). *Geochim. Cosmochim. Acta* 75, 3581–3599. doi: 10.1016/j.gca.2011.03.033

Holmkvist, L., Kamyshny, A. Jr., Brüchert, V., Ferdelman, T. G., and Jørgensen, B. B. (2014). Sulfidization of lacustrine glacial clay upon Holocene marine transgression (Arkona Basin. Baltic Sea). *Geochim. Cosmochim. Acta* 142, 75–94. doi: 10.1016/j.gca.2014.07.030

Jickells, T. D. (1995). Atmospheric inputs of metals and nutrients to the oceans: their magnitude and effects. *Mar. Chem.* 48, 199–214. doi: 10.1016/0304-4203(95)92784-P

Johnston, D. T., Gill, B. C., Masterson, A., Beirne, E., Casciotti, K. L., Knapp, A. N., et al. (2014). Placing an upper limit on cryptic marine sulphur cycling. *Nature* 513, 530–533. doi: 10.1038/nature13698

Jørgensen, B. B. (1990a). A thiosulfate shunt in the sulfur cycle of marine sediments. *Science* 249, 152–154.

Jørgensen, B. B. (1990b). The sulfur cycle of freshwater sediments: role of thiosulfate. *Limnol. Oceanogr.* 35, 1329–1342. doi: 10.1099/ijs.0.004986-0

Kamyshny, A. Jr. (2009a). Improved cyanolysis protocol for detection of zero-valent sulfur in natural aquatic systems. *Limnol. Oceanogr. Methods* 7, 442–448. doi: 10.4319/lom.2009.7.442

Kamyshny, A. Jr. (2009b). Solubility of cyclooctasulfur in pure water and sea water at different temperatures. *Geochim. Cosmochim. Acta* 73, 6022–6028. doi: 10.1016/j.gca.2009.07.003

Kamyshny, A. Jr., Druschel, G., Mansaray, Z. F., and Farquhar, J. (2014). Multiple sulfur isotopes fractionations associated with abiotic sulfur transformations in Yellowstone National Park geothermal springs. *Geochem. Trans.* 15:7. doi: 10.1186/1467-4866-15-7

Kamyshny, A. Jr., and Ferdelman, T. G. (2010). Dynamics of zero-valent sulfur species including polysulfides at seep sites on intertidal sand flats (Wadden Sea. North Sea). *Mar. Chem.* 121, 17–26. doi: 10.1016/j.marchem.2010.03.001

Kamyshny, A., Ekeltchik, I., Gun, J., and Lev, O. (2006). Method for the determination of inorganic polysulfide distribution in aquatic systems. *Anal. Chem.* 78, 2631–2639. doi: 10.1021/ac051854a

Kamyshny, A., Goifman, A., Gun, J., Rizkov, D., and Lev, O. (2004). Equilibrium distribution of polysulfide ions in aqueous solutions at 25 degrees C: a new approach for the study of polysulfides equilibria. *Environ. Sci. Technol.* 38, 6633–6644. doi: 10.1021/es049514e

Katz, T., Ginat, H., Eyal, G., Steiner, Z., Braun, Y., Shalev, S., et al. (2015). Desert flash floods form hyperpycnal flows in the coral-rich Gulf of Aqaba. Red Sea. *Earth Planet. Sci. Lett.* 417, 87–98. doi: 10.1016/j.epsl.2015.02.025

Katz, T., Herut, B., Genin, A., and Angel, D. L. (2002). Gray mullets ameliorate organically enriched sediments below a fish farm in the oligotrophic Gulf of Aqaba (Red Sea). *Mar. Ecol. Prog. Ser.* 234, 205–214. doi: 10.3354/meps234205

Kleinjan, W. E., de Keizer, A., and Janssen, A. J. H. (2005). Kinetics of chemical oxidation of polysulfide anions in aqueous solutions. *Water Res.* 39, 4093–4100. doi: 10.1016/j.watres.2005.08.006

Kosower, N., Kosower, E., Newton, G., and Ranney, H. (1979). Bimane fluorescent labels - labeling of normal human red-cells under physiological conditions. *Proc. Natl. Acad. Sci. U.S.A.* 76, 3382–3386. doi: 10.1073/pnas.76.7.3382

Labiosa, R. G., Arrigo, K. R., Genin, A., Monismith, S. G., and van Dijken, G. (2003). The interplay between upwelling and deep convective mixing in determining the seasonal phytoplankton dynamics in the Gulf of Aqaba: evidence from SeaWiFS and MODIS. *Limnol. Oceanogr.* 48, 2355–2368. doi: 10.4319/lo.2003.48.6.2355

Larsen, A. R. (1978). A note on the estimation of sedimentation rates in the Gulf of Elat (Aqaba), by use of Foraminifera. *Sedimentology* 25, 583–585. doi: 10.1111/j.1365-3091.1978.tb02082.x

Levanon-Spanier, I., Padan, E., and Reiss, Z. (1979). Primary production in a desert-enclosed sea: the Gulf of Elat (Aqaba). Red Sea. *Deep Sea Res.* 26, 673–686. doi: 10.1016/0198-0149(79)90040-2

Li, H., Veldhuis, M. J. W., and Post, A. F. (1998). Alkaline phosphatase activities among planktonic communities in the northern Red Sea. *Mar. Ecol. Prog. Ser.* 173, 107–115. doi: 10.3354/meps173107

Lichtschlag, A., Kamyshny, A. Jr., Ferdelman, T. G., and de Beer, D. (2013). Intermediate sulfur oxidation state compounds in the euxinic surface sediments of the Dvurechenskii mud volcano (Black Sea). *Geochim. Cosmochim. Acta* 105, 130–145. doi: 10.1016/j.gca.2012.11.025

Luther, G. W. III. (1991). Pyrite synthesis via polysulfide compounds. *Geochim. Cosmochim. Acta* 55, 2839–2849. doi: 10.1016/0016-7037(91)90449-F

Mahowald, N. M., Baker, A. R., Bergametti, G., Brooks, N., Duce, R. A., Jickells, T. D., et al. (2005). Atmospheric global dust cycle and iron inputs to the ocean. *Glob. Biogeochem. Cycles* 19, GB4025. doi: 10.1029/2004gb002402

Mendez, J., Guieu, C., and Adkins, J. (2010). Atmospheric input of manganese and iron to the ocean: seawater dissolution experiments with Saharan and North American dusts. *Mar. Chem.* 120, 34–43. doi: 10.1016/j.marchem.2008.08.006

Mills, J. V., Antler, G., and Turchyn, A. V. (2016). Geochemical evidence for cryptic sulfur cycling in salt marsh sediments. *Earth Planet. Sci. Lett.* 453, 23–32. doi: 10.1016/j.epsl.2016.08.001

Mizutani, Y., and Rafter, T. (1973). Isotopic behaviour of sulphate oxygen in the bacterial reduction of sulphate. *Geochem. J.* 6, 183–191. doi: 10.2343/geochemj.6.183

Morse, J., and Cornwell, J. C. (1987). Analysis and distribution of iron sulfide minerals in recent anoxic marine sediments. *Mar. Chem.* 22, 55–69. doi: 10.1016/0304-4203(87)90048-X

Orcutt, B. N., Sylvan, J. B., Knab, N. J., and Edwards, K. J. (2011). Microbial ecology of the dark ocean above at and below the seafloor. *Microbiol. Mol. Biol. Rev.* 75, 361–422. doi: 10.1128/MMBR.00039-10

Poulton, S. W., and Canfield, D. E. (2005). Development of a sequential extraction procedure for iron: implications for iron partitioning in continentally derived particulates. *Chem. Geol.* 214, 209–221. doi: 10.1016/j.chemgeo.2004.09.003

Poulton, S. W., Krom, M. D., and Raiswell, R. (2004). A revised scheme for the reactivity of iron (oxyhydr)oxide minerals towards dissolved sulfide. *Geochim. Cosmochim. Acta* 68, 3703–3715. doi: 10.1016/j.gca.2004.03.012

Raiswell, R., and Canfield, D. (1996). Rates of reaction between silicate iron and dissolved sulfide in Peru Margin sediments. *Geochim. Cosmochim. Acta* 60, 2777–2787. doi: 10.1016/0016-7037(96)00141-X

Rasheed, M., Badran, M. I., and Huettel, M. (2003). Influence of sediment permeability and mineral composition on organic matter degradation in three sediments from the Gulf of Aqaba. Red Sea. *Estuar. Coast. Shelf Sci.* 57, 369–384. doi: 10.1016/S0272-7714(02)00362-1

Reiss, Z., and Hottinger, L. (1984). *The Gulf of Aqaba: Ecological Micropaleontology: Ecological Studies*, Vol. 50. Berlin: Springer, 1–354. doi: 10.1007/978-3-642-69787-6

Reiss, Z., Luz, B., Almogi-Labin, A., Halicz, E., Winter, A., Wolf, M., et al. (1980). Late quaternary paleoceanography of the Gulf of Aqaba (Elat). Red Sea. *Quat. Res.* 14, 294–308. doi: 10.1016/0033-5894(80)90013-7

Rickard, D. T., and Luther, G. W. (1997). Kinetics of pyrite formation by H2S oxidation of iron(II) monosulfide in aqueous solutions between 25 and 125 degrees C: the mechanism. *Geochim. Cosmochim. Acta* 61, 135–147. doi: 10.1016/S0016-7037(96)00322-5

Rong, L., Lim, L., and Takeuchi, T. (2005). Determination of iodide and thiocyanate in seawater by liquid chromatography with poly(ethylene glycol) stationary phase. *Chromatographia* 61, 371–374. doi: 10.1365/s10337-005-0501-3

Rudnicki, M. D., Elderfield, H., and Spiro, B. (2001). Fractionation of sulfur isotopes during bacterial sulfate reduction in deep ocean sediments at elevated temperatures. *Geochim. Cosmochim. Acta* 65, 777–789. doi: 10.1016/S0016-7037(00)00579-2

Ryan, W. B. F., Carbotte, S. M., Coplan, J. O., O'Hara, S., Melkonian, A., Arko, R., et al. (2009). Global multi-resolution topography synthesis. *Geochem. Geophys. Geosyst.* 10:Q03014. doi: 10.1029/2008GC002332

Schumacher, H., Kiene, W., and Dullo, W. C. (1995). Factors controlling Holocene reef growth: an interdisciplinary approach. *Facies* 32, 145–188. doi: 10.1007/BF02536867

Seeberg-Elverfeldt, J., Schluter, M., Feseker, T., and Kolling, M. (2005). Rhizon sampling of porewaters near the sediment-water interface of aquatic systems. *Limnol. Oceanogr. Methods* 3, 361–371. doi: 10.4319/lom.2005.3.361

Sim, M. S., Bosak, T., and Ono, S. (2011a). Large sulfur isotope fractionation does not require disproportionation. *Science* 333, 74–77. doi: 10.1126/science.1205103

Sim, M. S., Ono, S., Donovan, K., Templer, S. P., and Bosak, T. (2011b). Effect of electron donors on the fractionation of sulfur isotopes by a marine *Desulfovibrio* sp. *Geochim. Cosmochim. Acta* 75, 4244–4259. doi: 10.1016/j.gca.2011.05.021

Stambler, N. (2006). Light and picophytoplankton in the Gulf of Eilat (Aqaba). *J. Geophys. Res.* 111:C11009. doi: 10.1029/2005jc003373

Steiner, Z., Lazar, B., Levi, S., Tsroya, S., Pelled, O., Bookman, R., et al. (2016). The effect of bioturbation in pelagic sediments: lessons from radioactive tracers and planktonic foraminifera in the Gulf of Aqaba (Eilat). Red Sea. *Geochim. Cosmochim. Acta* 194, 139–152. doi: 10.1016/j.gca.2016.08.037

Stookey, L. (1970). Ferrozine - a new spectrophotometric reagent for iron. *Anal. Chem.* 42, 779–781. doi: 10.1021/ac60289a016

Street, J., and Paytan, A. (2005). Iron, phytoplankton growth, and the carbon cycle. *Met. Ions Biol. Syst.* 43, 153–185.

Thamdrup, B. (2000). "Bacterial manganese and iron reduction in aquatic sediments," in *Advances in Microbial Ecology*, Vol. 16, ed. B. Schink (New York, NY: Springer), 41–84. doi: 10.1007/978-1-4615-4187-5_2

Thamdrup, B., Finster, K., Fossing, H., Hansen, J. W., and Jørgensen, B. B. (1994). Thiosulfate and sulfite distributions in porewater of marine sediments related to manganese, iron, and sulfur geochemistry. *Geochim. Cosmochim. Acta* 58, 67–73. doi: 10.1016/0016-7037(94)90446-4

Turchyn, A., Brüchert, V., Lyons, T., Engel, G., Balci, N., Schrag, D., et al. (2010). Kinetic oxygen isotope effects during dissimilatory sulfate reduction: a combined theoretical and experimental approach. *Geochim. Cosmochim. Acta* 74, 2011–2024. doi: 10.1016/j.gca.2010.01.004

Turchyn, A., Sivan, O., and Schrag, D. (2006). Oxygen isotopic composition of sulfate in deep sea pore fluid: evidence for rapid sulfur cycling. *Geobiology* 4, 191–201. doi: 10.1111/j.1472-4669.2006.00079.x

Valravamurthy, A., and Mopper, K. (1990). Determination of sulfite and thiosulfate in aqueous samples including anoxic seawater by liquid chromatography after derivatization with 2,2′-dithiobis(5-nitropyridine). *Environ. Sci. Technol.* 24, 333–337. doi: 10.1021/es00073a007

Wan, M., Shchukarev, A., Lohmayer, R., Planer-Friedrich, B., and Peiffer, S. (2014). Occurrence of surface polysulfides during the interaction between ferric (hydr)oxides and aqueous sulfide. *Environ. Sci. Technol.* 48, 5076–5084. doi: 10.1021/es405612f

Werne, J. P., Lyons, T. W., Hollander, D. J., Schouten, S., Hopmans, E. C., and Sinninghe Damsté, J. S. (2008). Investigating pathways of diagenetic organic matter sulfurization using compound-specific sulfur isotope analysis. *Geochim. Cosmochim. Acta* 72, 3489–3502. doi: 10.1016/j.gca.2008.04.033

Yao, W., and Millero, F. J. (1996). Oxidation of hydrogen sulfide by hydrous Fe(III) oxides in seawater. *Mar. Chem.* 52, 1–16. doi: 10.1016/0304-4203(95)00072-0

Zopfi, J., Böttcher, M. E., and Jørgensen, B. B. (2008). Biogeochemistry of sulfur and iron in *Thioploca*-colonized surface sediments in the upwelling area off central Chile. *Geochim. Cosmochim. Acta* 72, 827–843. doi: 10.1016/j.gca.2007.11.031

Zopfi, J., Ferdelman, T. G., and Fossing, H. (2004). "Distribution and fate of sulfur intermediates – sulfite, tetrathionate, thiosulfate, and elemental sulfur – in marine sediments," in *Sulfur Biogeochemistry – Past and Present*, eds J. P. Amend, K. J. Edwards, and T. W. Lyons (Denver, CO: The Geological Society of America), 97–116.

Conflict of Interest Statement: The authors declare that the research was conducted in the absence of any commercial or financial relationships that could be construed as a potential conflict of interest.

frontiers in Microbiology

ORIGINAL RESEARCH
published: 31 May 2017
doi: 10.3389/fmicb.2017.00956

The Effectiveness of Nitrate-Mediated Control of the Oil Field Sulfur Cycle Depends on the Toluene Content of the Oil

*Navreet Suri, Johanna Voordouw and Gerrit Voordouw**

Petroleum Microbiology Research Group, Department of Biological Sciences, University of Calgary, Calgary, AB, Canada

The injection of nitrate is one of the most commonly used technologies to impact the sulfur cycle in subsurface oil fields. Nitrate injection enhances the activity of nitrate-reducing bacteria, which produce nitrite inhibiting sulfate-reducing bacteria (SRB). Subsequent reduction of nitrate to di-nitrogen (N_2) alleviates the inhibition of SRB by nitrite. It has been shown for the Medicine Hat Glauconitic C (MHGC) field, that alkylbenzenes especially toluene are important electron donors for the reduction of nitrate to nitrite and N_2. However, the rate and extent of reduction of nitrate to nitrite and of nitrite to nitrogen have not been studied for multiple oil fields. Samples of light oil (PNG, CPM, and Tundra), light/heavy oil (Gryphon and Obigbo), and of heavy oil (MHGC) were collected from locations around the world. The maximum concentration of nitrate in the aqueous phase, which could be reduced in microcosms inoculated with MHGC produced water, increased with the toluene concentration in the oil phase. PNG, Gryphon, CPM, Obigbo, MHGC, and Tundra oils had 77, 17, 5.9, 4.0, 2.6, and 0.8 mM toluene, respectively. In incubations with 49 ml of aqueous phase and 1 ml of oil these were able to reduce 22.2, 12.3, 7.9, 4.6, 4.0, and 1.4 mM of nitrate, respectively. Nitrate reduced increased to 35 ± 4 mM upon amendment of all these oils with 570 mM toluene prior to incubation. Souring control by nitrate injection requires that the nitrate is directed toward oxidation of sulfide, not toluene. Hence, the success of nitrate injections will be inversely proportional to the toluene content of the oil. Oil composition is therefore an important determinant of the success of nitrate injection to control souring in a particular field.

Keywords: nitrate, nitrate-reducing bacteria, oil fields, toluene, souring control

OPEN ACCESS

Edited by:
Alexandra V. Turchyn, University of Cambridge, United Kingdom

Reviewed by:
Hans Karl Carlson, University of California, Berkeley, United States
Kai Waldemar Finster, Aarhus University, Denmark

****Correspondence:***
Gerrit Voordouw
voordouw@ucalgary.ca

Specialty section:
This article was submitted to Microbiological Chemistry and Geomicrobiology, a section of the journal Frontiers in Microbiology

Received: *24 March 2017*
Accepted: *12 May 2017*
Published: *31 May 2017*

Citation:
Suri N, Voordouw J and Voordouw G (2017) The Effectiveness of Nitrate-Mediated Control of the Oil Field Sulfur Cycle Depends on the Toluene Content of the Oil. Front. Microbiol. 8:956. doi: 10.3389/fmicb.2017.00956

INTRODUCTION

Sulfide accumulation in oil reservoirs through the reduction of sulfate in injection waters by sulfate-reducing bacteria (SRB) is referred to as souring and is highly undesirable. Addition of nitrate to these injection waters is a commonly used strategy to mitigate the negative impact of sulfide produced in oil fields. Nitrate promotes the growth of sulfide-oxidizing and heterotrophic nitrate-reducing bacteria (soNRB and hNRB). Among these, soNRB oxidize

sulfide directly while hNRB exclude SRB growth by competitive utilization of oil organics for nitrate reduction (Sunde and Torsvik, 2005; Youssef et al., 2009; Gieg et al., 2011; Voordouw, 2011). Volatile fatty acids (VFA, a mixture of acetate, butyrate, and propionate) and low molecular weight hydrocarbons such as alkylbenzenes are preferred oil organics for nitrate reduction by hNRB. Incomplete reduction of nitrate to nitrite is a key to the success of this approach to control souring. Nitrite accumulation in oil reservoirs is stimulated at high-temperatures (50–70°C). But nitrite is reduced further to dinitrogen (N_2) in low-temperature oil fields (below 50°C) in view of the excess of electron donors, which is usually present in oil fields (Reinsel et al., 1996; Agrawal et al., 2012, 2014; Fida et al., 2016).

Long-term injection of nitrate into the low-temperature (30°C) Medicine Hat Glauconitic C (MHGC) field gave nitrate breakthrough in some producing wells. The oil produced by these wells was found to be depleted in toluene and other alkylbenzenes suggesting that these were favored substrates for hNRB. Alkylbenzene-oxidizing NRB such as *Thauera* and *Azoarcus* were found to be members of the MHGC microbial communities (Agrawal et al., 2012). This suggested that the limited presence of alkylbenzenes prevented complete nitrate reduction.

Light oils may have higher proportions of alkylbenzenes as compared to heavy oils. More (51%) nitrate was reduced with light oil as compared to a heavy oil (15%) in laboratory microcosms. The remaining oils were most depleted in toluene (Lambo et al., 2008). Further incubations of oil field hNRB with 4 mM toluene indicated complete reduction of 8.9 mM nitrate (likely to N_2) while nitrate was only partially reduced to nitrite in the presence of 4 mM m-xylene. Other alkylbenzenes such as ethylbenzene, propylbenzene, m-ethyltoluene, o-ethyltoluene, or p-ethyltoluene did not support nitrate reduction during the incubation period (Lambo et al., 2008).

Several pure isolates have been reported to use alkylbenzenes for nitrate reduction. Among these, the utilization of toluene by hNRB isolates has been most studied (Spormann and Widdel, 2000; Weelink et al., 2010; Alain et al., 2012). Most of these isolates belong to the *Azoarcus/Thauera* cluster within the class *Betaproteobacteria* (Chakraborty and Coates, 2004). Bacterial strain ToN1, isolated on toluene was found to use crude oil for nitrate reduction. Oil analysis showed utilization of toluene only by this isolate among the oil components (Rabus and Widdel, 1996). Two other strains, mXyN1 and EbN1 isolated on m-xylene and ethylbenzene utilized toluene as well in addition to m-xylene and ethylbenzene, respectively. However, strain PbN1 isolated on n-propylbenzene did not reduce nitrate with crude oil (Rabus and Widdel, 1996; Spormann and Widdel, 2000).

All these studies indicate that not only the availability but also the type and fraction of alkylbenzenes in oil are factors in determining the extent of nitrate reduction by hNRB, which use oil as their substrate. Toluene appears to be a primary electron donor for the reduction of nitrate. The use of oil components to reduce nitrate to N_2 by hNRB prevents its desired application of sulfide oxidation by soNRB (Voordouw et al., 2009; Agrawal et al., 2012). For successful application of nitrate in limiting sulfide formation in oil reservoirs, it is thus very important to understand the effect of oil composition on nitrate reduction, which is the topic of the current contribution.

MATERIALS AND METHODS

Samples of Oil and Produced Water

Oils are classified as light, light/heavy or heavy depending on their American Petroleum Institute (API) gravity (American Petroleum Institute [API], 2011). These are in excess of 31°, from 21° to 31° and below 21°, respectively. Three light oils, two light/heavy oils as well as heavy MHGC oil were used (**Table 1**). Produced water from producing well 18PW in the MHGC field collected monthly was used to inoculate all cultures (Voordouw et al., 2009). Freshly collected samples of 18PW were stored in a Coy Anaerobic Hood in an atmosphere of 90% N_2 (v/v) and 10% CO_2 (N_2-CO_2).

Quantification of Alkylbenzenes in Oils by Gas Chromatography-Mass Spectrometry (GC-MS)

Oils (1 ml) were diluted with 9 ml of DCM. A 1 μl volume of the DCM extract was injected with an autoinjector (7683B series, Agilent Technologies, Santa Clara, CA, United States) into a gas chromatograph (7890N series, Agilent) equipped with an HP-1 fused silica capillary column (length 50 m, inner diameter 0.32 mm, film thickness 0.52 μm; J&W Scientific) with helium as the carrier gas and connected to a mass-selective detector (5975C inert XL MSD series, Agilent). Duplicate measurements were done on all the oil samples. Concentrations of toluene, ethylbenzene, o-xylene, and m/p-xylene in the oils were calculated based on the standard line obtained from the peak areas of pure individual standard alkylbenzenes (Sigma–Aldrich) analyzed by GC-MS.

Enrichment of hNRB in Microcosms

hNRB were enriched in 125 ml serum bottles, containing 44 ml of anoxic CSBK medium (Supplementary Table S1) amended with 0, 10, 20, 40, or 80 mM nitrate. To these 1 ml of the oils (2% of total volume of 50 ml), listed in **Table 1**, was added as electron donor and 5 ml of produced water from 18PW was used to inoculate the bottles. Bottles without hNRB inoculum were also prepared. The bottles had a headspace of N_2-CO_2, were sealed with sterile butyl rubber stoppers and crimped with aluminum seals. Duplicate serum bottles for all oils and all nitrate concentrations were incubated upside down at 30°C for 90 days, while shaking at 80 rpm.

To a second set of microcosms, additional toluene (71.2–570 mM) was added to 1 ml of oil phase in bottles that showed less than 5 mM reduction of nitrate after 90 days of incubation. These bottles were again incubated upside down at 30°C, while shaking at 80 rpm for an additional 85–90 days.

Enrichment of hNRB in Hungate Tubes

hNRB were also cultivated in 20 ml Hungate tubes, containing 12.5 ml of anoxic CSBK medium amended with 0, 10, 20, 40,

TABLE 1 | Physicochemical properties of oil samples used in this study.

Oil	Field information; location	API gravity	Viscosity (cP) at 20°C*	Designation
PNG	Conventional oil field; Papua New Guinea	46°	9.4	Light
CPM	Shale oil field in the Bakken formation; Saskatchewan, Canada	41°	10.8	Light
Tundra	Shale oil field in the Bakken formation; Manitoba, Canada	38°	11.8	Light
Gryphon	Shale oil field; Alberta, Canada	31°	16.6	Light/Heavy
Obigbo	Obigbo field; Nigeria	21°	50.9	Light/Heavy
MHGC	Conventional oil reservoir; Medicine Hat, Alberta, Canada	16°	2471	Heavy

Determined at a shear rate of 38/s except for MHGC oil, which was at 0.12/s.

or 80 mM nitrate. The tubes were inoculated with 1.5 ml of produced water from 18PW. As an electron donor, 1 ml of oils (**Table 1**; 6.7% of the total volume of 15 ml) was added to the tubes. Uninoculated tubes without nitrate were also prepared. Tubes were sealed with sterile butyl rubber stoppers, crimped with aluminum seals and contained a headspace of N_2-CO_2. Duplicates tubes were incubated upside down at 30°C while shaking at 80 rpm for 90 days.

Determination of Nitrate Utilization in hNRB Enrichments

The reduction of nitrate in microcosms was monitored as a function of time in serum bottles while nitrate was only measured at the end of incubation period in the Hungate tubes. Samples (200 μl) were transferred to 1.5 ml microfuge tubes using N_2-CO_2 flushed syringes and centrifuged at 14,000 rpm for 5 min throughout. Nitrate and nitrite concentrations were measured in the supernatant by High Performance Liquid Chromatography (HPLC) using a UV detector (Gilson, Lewis Center, OH, United States) and an IC-PAK anion column (4 mm × 150 mm, Waters) with borate/gluconate buffer at a flow rate of 2 ml/min (Agrawal et al., 2012). The reduction of nitrate (%) was calculated as: reduction (%) = (nitrite concentration/initial nitrate concentration)*40% + (initial nitrate concentration − residual nitrate concentration − nitrite concentration)/(initial nitrate concentration)*100%.

Determination of Alkylbenzene Utilization in hNRB Enrichments

To the first set of microcosms a known volume of mesitylene (1,3,5-trimethylbenzene) was added to the oil layer at the end of incubation period. A known volume of dichloromethane (DCM) was added to extract the oils. The oil-DCM layers settled at the bottom of the bottles were carefully taken into 2 ml GC-MS vials and were analyzed using GC-MS as described before. Utilization of a particular alkylbenzene for nitrate reduction was determined as the decrease in its peak area relative to that of mesitylene.

Biomass Formation in hNRB Enrichments

The contents of Hungate tubes were transferred to 15 ml Falcon tubes at the end of the incubation period and centrifuged at 12,000 rpm for 30 min at 4°C. Supernatants were separated and the cell pellets obtained were washed with 50 mM phosphate buffer (pH 7) twice and re-suspended in 14 ml of the same buffer. Biomass concentrations were determined by measuring the optical density of cell suspensions at 600 nm (OD_{600}) using phosphate buffer as a blank. Cell suspensions (100 μl) were also taken in 1.5 ml microfuge tubes, centrifuged at 17,000 × *g* for 5 min followed by re-suspension in 100 μl of 0.1 N NaOH and then mixed well by pipetting up and down. The tubes were incubated in a heating block at 90°C for 10 min and centrifuged again at 15,000 × *g* for 1 min. Protein concentrations were then measured in the supernatant with a Qubit fluorometer (Invitrogen) using a Qubit® protein assay kit (Life Technologies, United States).

Microbial Community Analysis of hNRB Enrichments

hNRB enrichments from microcosms with oils and the oils with added toluene were centrifuged at 12,000 rpm for 30 min to collect cell pellets at the end of incubation period of 171–180 days. Cell pellets from duplicate incubations were combined before DNA extraction. DNA was extracted using the Fast DNA® Spin Kit for Soil (MP Biomedicals) as per the manufacturer's instructions and quantified with a Qubit fluorometer (Invitrogen), using the Quant-iT™ dsDNA HS Assay Kit (Invitrogen). 16S rRNA genes of the extracted DNA were amplified using a two-step PCR procedure with each reaction of 50 μl volume containing premade reagents mixed in proportion as per manufacturer's instructions (Thermo-Scientific). The first PCR used 16S primers 926Fi5 (50-TCGTCGGCAGCGTCAGATGTGTATAAGAGACAGAAACT YAAAKGAATWGRCGG-30) and 1392Ri7 (50-GTCTCGTGG GCTCGGAGATGTGTATAAGAGACAGACGGGCGGTGWG TRC-30) as indicated elsewhere (Menon and Voordouw, 2016). The PCR was for 3 min at 95°C, followed by 25 cycles of 30 s at 95°C, 45 s at 55°C and 90 s incubation at 72°C, followed by a final step at 72°C for 10 min. The quality of the PCR product was evaluated by electrophoresis on a 1.5% (w/v) agarose gel. The PCR product obtained was purified using QIAquick PCR purification kit (Qiagen, Germany) and quantified. This was then used as the template for the second PCR reaction, which used primer P5-S50X-OHAF and P7-N7XX-OHAR for 10 cycles as described elsewhere (Menon and Voordouw, 2016). The resulting purified PCR product was sequenced using the 300PE (paired-end) MiSeq protocol on an Illumina Miseq system at the Department of Geosciences, University of

Calgary. The 300PE reads were merged into single reads using PEAR 0.9.6 with a 50 bp overlap and were further processed with a 420 bp cut-off of amplicon size using MetaAmp, a 16S rRNA data analysis pipeline, developed by the Energy Bioengineering Group, Department of Geosciences, University of Calgary. MetaAmp was also used for bioinformatic analysis (http://ebg.ucalgary.ca/metaamp). Raw read sequences have been submitted to NCBI Sequence Read Archive (SRA) under Bioproject accession number PRJNA181037, with biosample number SAMN06624307.

RESULTS

Physicochemical Properties and Concentrations of Alkylbenzenes

The physicochemical properties of the oils are listed in **Table 1**. PNG, CPM, and Tundra oils were light with API gravities from 38° to 46° and viscosities from 9.4 to 11.8 cP. The Gryphon and Obigbo oils were light/heavy with API gravities of 31° and 21° and viscosities of 16.6 and 50.9 cP, respectively, whereas the MHGC oil was heavy with an API gravity of 16° and a viscosity of 2471 cP. The concentrations of the alkylbenzenes toluene, ethylbenzene, o-xylene, and m/p-xylene differed for these oils (**Figure 1**). Of the light oils PNG oil had the highest concentrations of alkylbenzenes, whereas those of CPM oil and Tundra oil were much lower (**Figure 1**). The latter two are shale oils from the Bakken formation (**Table 1**), which have a low fraction of aromatics (Jiang and Li, 2002). Of the light/heavy oils Gryphon oil had a higher content of alkylbenzenes than Obigbo oil, whereas the alkylbenzene content of heavy MHGC oil was intermediate between that of Obigbo and Tundra oils (**Figure 1**). The toluene concentrations of PNG, CPM, Tundra, Gryphon, Obigbo, and MHGC oils were found to be 77, 5.9, 0.8, 17, 4.0, and 2.6 mM, respectively (**Figure 1**). Assuming toluene to be the most important substrate for nitrate reduction (Rabus and Widdel, 1996; Lambo et al., 2008; Agrawal et al., 2012) we expect nitrate reduction to be ranked as follows: PNG > Gryphon > CPM > Obigbo > MHGC > Tundra.

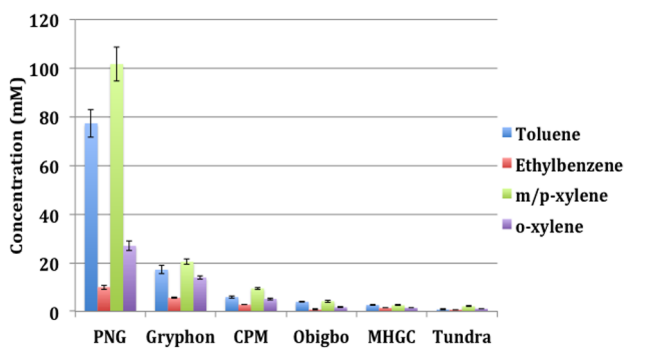

FIGURE 1 | Concentrations of alkylbenzenes determined by gas chromatography-mass spectrometry (GC-MS) analysis of oil samples used in this study. Error bars represent standard deviations for duplicate measurements.

Nitrate Reduction Using Oils as Electron Donors

Oils were incubated in microcosms with different concentrations of nitrate and the same inoculum from producing well 18PW in the MHGC field. Incubation of PNG oil with 80, 40, 20, and 10 mM nitrate gave reduction of 23.0 ± 2.4, 21.5 ± 2.8, 19.6 ± 0.4, and 10.0 ± 0.4 mM nitrate, respectively (**Figure 2A**). Hence, with nitrate in excess, the maximum concentration reduced was 22.2 ± 1.1 mM (**Table 2**). Reduction of nitrate led to transient formation of nitrite with maximum concentrations of 18.0 ± 0.5, 14.9 ± 1.4, 11.7 ± 2.1, and 6.6 ± 0.03 mM nitrite, respectively, and final concentrations of 9.7 ± 1.8, 8.3 ± 1.7, 3.3 ± 4.7, and 0 mM, respectively (**Figure 2B**). Incubation with Tundra oil gave reduction of only 1.4 ± 0.6 mM of nitrate (i.e., nitrate was in excess in all four incubations) with formation of maximally 0.4 ± 0.1 mM nitrite (**Figures 2C,D** and **Table 2**). Likewise incubations with Gryphon, CPM, Obigbo, and MHGC oils gave maximal reduction of 12.3 ± 1.6, 7.9 ± 0.6, 4.6 ± 0.7, and 4.0 ± 1.5 mM nitrate (**Table 2**) with transient formation of up to 8.7 ± 0.4, 3.9 ± 1.1, 2.1 ± 0.3, and 1.6 ± 0.3 mM nitrite (Supplementary Figure S1). Overall, we observed that nitrate reduction followed the order PNG > Gryphon > CPM > Obigbo > MHGC > Tundra, which was the same as that based on toluene concentrations in the oils.

Increasing the volume fraction of oil from 1 ml per 50 ml (2% v/v) in serum bottles to 1 ml per 15 ml (6.7% v/v) in Hungate tubes increased the reduction of nitrate to 80, 41.7 ± 5.2, 27.7 ± 0.8, 16.2 ± 3.4, 12.5 ± 2.1, and 6.9 ± 3.2 mM with PNG, Gryphon, CPM, Obigbo, MHGC, and Tundra oil, respectively (**Table 2** and Supplementary Figure S2). Hence, increasing the volume fraction of oils used as electron donor by 3.3-fold increased the reduction of nitrate on average by 3.5-fold (**Table 2**).

The maximum concentration of nitrate reduced with different oils as a function of their toluene concentrations is indicated in **Figure 3**. The maximum contribution which toluene in the oil can make to this reduction is also indicated in **Table 2**. These data indicate that components other than toluene also contributed to the observed reduction of nitrate. This contribution was least for high toluene PNG oil (32–34%) and most for low toluene Tundra oil (90–94%). The fraction of nitrate reduction to nitrite was on average 31% in serum bottles and 65% in Hungate tubes. Hence, increasing the ratio of oil to nitrate increased the concentration of nitrate reduced to nitrite, but nitrate reduction was less complete.

Biomass Concentration as a Function of Nitrate Reduction

The concentration of biomass formed in the Hungate tubes was measured as the OD_{600} (turbidity) of the aqueous phase or as the protein concentration of the aqueous phase, which showed similar trends (**Figure 4**). The biomass concentration

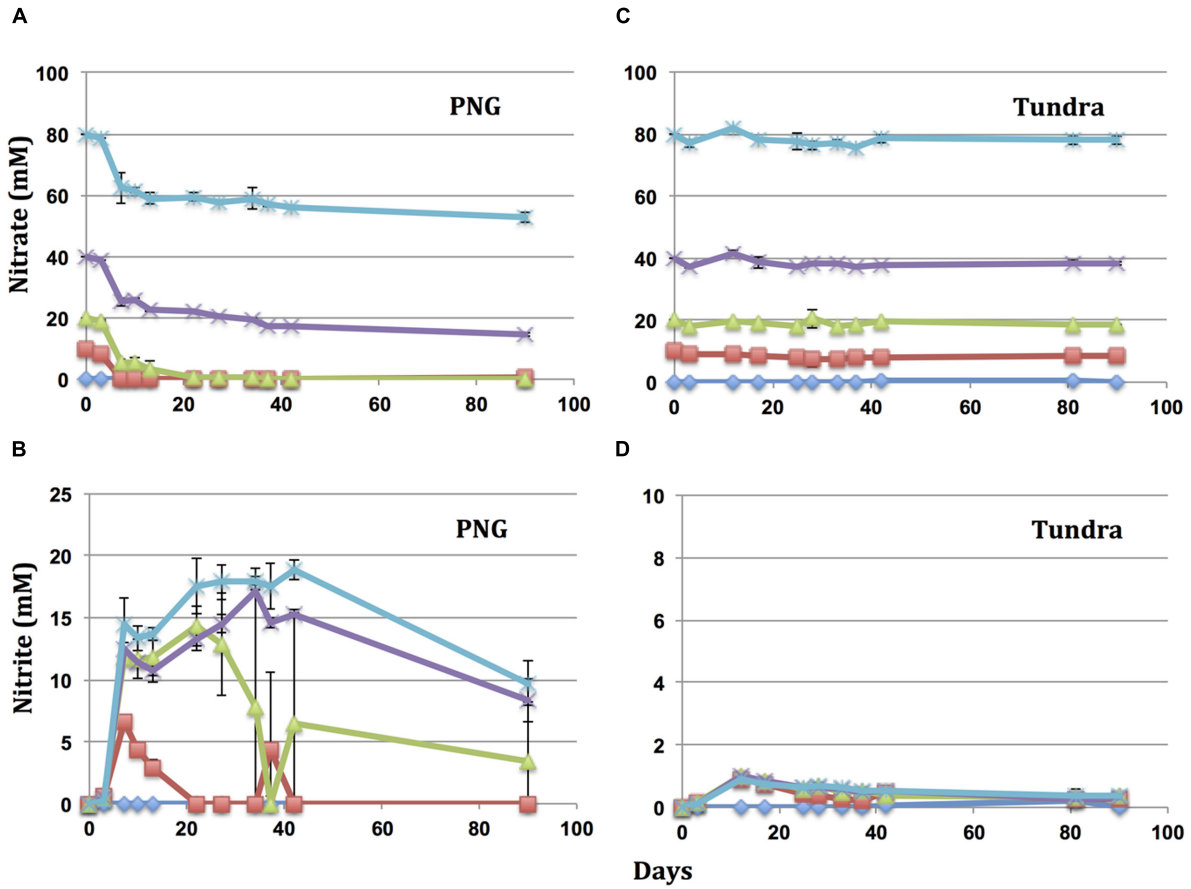

FIGURE 2 | Reduction of nitrate and formation of nitrite as a function of time in microcosms with PNG oil **(A,B)** and Tundra oil **(C,D)**. All microcosms were inoculated with a 10% (v/v) inoculum of produced water from 18PW in the MHGC field. The initial nitrate concentrations were 80 (*), 40 (×), 20 (▲), 10 (■), or 0 (♦) mM. Error bars represent the standard deviations for four measurements.

increased with increased reduction of nitrate and was, therefore highest with PNG oil and lowest with Tundra oil (**Figure 4** and **Table 2**). These observations indicate that increased nitrate reduction coupled to oil organics oxidation increased biomass formation.

Selective Utilization of Oil Components for Nitrate Reduction

Gas chromatography-mass spectrometry analysis of the oils incubated with nitrate and 18PW inoculum indicated use of alkylbenzenes for nitrate reduction (**Figure 5** and Supplementary Figure S3). Results showed that hNRB primarily used toluene as an electron donor for nitrate reduction. As compared to uninoculated enrichments without nitrate, toluene was completely utilized (0–1% remaining) in incubations of oils with 80 mM nitrate (**Figure 5** and Supplementary Figure S3). Oils incubated with lower concentrations of nitrate (10, 20, or 40 mM) were also depleted in toluene. Toluene was completely removed from oils with the lowest concentrations of toluene (e.g., from Tundra oil) even in incubations with 10 mM nitrate (**Figure 5** and Supplementary Figure S3).

Nitrate reduction was coupled to the utilization of other alkylbenzenes, including ethylbenzene and m/p-xylene, but not o-xylene. Oils extracted from serum bottles with 80 mM nitrate had 0–5% residual ethylbenzene and 25–93% of m/p-xylene at the end of the incubation period (**Figure 5** and Supplementary Figure S3). Hence, the use of alkylbenzenes may account for all of the nitrate reduction for PNG oil. However, nitrate reduction with the other oils must have involved oxidation of other oil components. This was clearly a slower process causing most nitrate to remain.

Increased Nitrate Reduction by Toluene Addition

The GC-MS analysis suggested that hNRB preferentially used toluene for nitrate reduction. Less nitrate was reduced in incubations of oils with less toluene. We tested, therefore, whether toluene addition to low toluene oils increased nitrate reduction. This was evaluated by adding 71, 142, 285, or 570 mM of toluene to 1 ml of oil in serum bottles with a 50 ml volume containing 10, 20, 40, or 80 mM nitrate, respectively, at day 90 of incubation (**Figure 6**). After 45 days of further incubation,

TABLE 2 | Maximum concentrations of nitrate reduced and nitrite produced at the end of incubations in serum bottles with 2% (v/v) of oil and in Hungate tubes with 6.7% (v/v) of oil.

Oil	2% (v/v) of oil				6.7% (v/v) of oil			Fold increase in nitrate reduced
	N	Nitrate reduced (mM)	Nitrite formed (mM)	Theoretical maximum toluene contribution (%)	N	Nitrate reduced (mM)	Nitrite formed (mM)	Theoretical maximum toluene contribution (%)	
PNG	6	22.2 ± 1.1	9.5 ± 7.3	68	2	80.0 ± 0*	39.7 ± 3.2	66	3.6
Gryphon	6	12.3 ± 1.6	3.9 ± 2.7	25	4	41.7 ± 5.2	32.3 ± 6.4	37	3.4
CPM	8	7.9 ± 0.6	2.6 ± 0.7	13	4	27.7 ± 0.8	23.2 ± 2.2	21	3.5
Obigbo	8	4.6 ± 0.7	1.4 ± 0.2	15	6	16.2 ± 3.4	14.8 ± 1.9	26	3.2
MHGC	8	4.0 ± 1.5	0.7 ± 0.2	11	6	12.5 ± 2.1	8.7 ± 1.3	17	2.2
Tundra	8	1.4 ± 0.6	0.4 ± 0.1	10	8	6.9 ± 3.2	1.2 ± 1.1	6	4.9

* *No nitrate remained in this incubation.*

Toluene contribution (%) = V_{oil}/V_{aq} [5($C_{nitrate\ reduced}$ − $C_{nitrite}$) + 2* $C_{nitrite}$)/36] * 100, where 36 is the number of electrons released for oxidation of toluene to 7CO_2.*

The average ± SD is for incubations with 10, 20, 40, or 80 mM nitrate in which some nitrate remained. The number of replicates (N) to which this applies is indicated.

microcosms containing toluene-amended Tundra oil and 10, 20, or 40 mM of nitrate showed complete reduction of nitrate without accumulation of nitrite indicating complete reduction of nitrate to N_2 (**Figure 6**). The microcosm with 570 mM toluene in the oil phase and 80 mM nitrate in the aqueous medium showed reduction of 32.3 ± 1.3 mM nitrate to nitrite, which was not reduced further even after continued incubation for an additional 36 days (**Figure 6** and Supplementary Figure S4). Similar results were obtained in incubations with other oils. Incubations with 10, 20, or 40 mM nitrate and oils with 71, 142, or 285 mM toluene, respectively, showed mostly complete reduction of nitrate (results not shown). Incubation of other oils with 570 mM of additional toluene in the oil phase and 80 mM nitrate in the aqueous phase gave on average reduction of 34.8 ± 4.2 mM nitrate ($N = 12$) with accumulation of 30.7 ± 4.7 mM nitrite ($N = 12$; Supplementary Figure S4). These observations confirmed that remediating toluene deficiency of an oil increases nitrate reduction, irrespective of whether the oil is light, light/heavy, or heavy.

Microbial Community Compositions of hNRB Enrichments

Microbial community compositions derived from 16S rRNA amplicons from the hNRB incubations with oils are compared in **Figure 7**. The dendrogram showed two main clusters I and II, representing incubations with and without nitrate, respectively (**Figure 7A**). The phylum *Proteobacteria,* class *Betaproteobacteria* dominated the community compositions in cluster I, whereas the phylum *Euryarchaeota* dominated the community compositions in cluster II (**Figures 7B,C**). Microbial community compositions in cluster I were dominated by *Betaproteobacteria* of the genus *Thauera* especially for incubations with nitrate and added toluene in which the communities consisted of 80–88% of this taxon (**Table 3**). *Thauera* is a known denitrifying hNRB, which oxidizes toluene (Spormann and Widdel, 2000; Chakraborty and Coates, 2004; Hubert and Voordouw, 2007; Fida et al., 2016). *Pseudomonas*, an extensively studied hNRB of the class *Gammaproteobacteria* (Altenschmidt and Fuchs, 1991; Grigoryan et al., 2008), was the second most dominant genus in this cluster. The proportions of *Thauera* were lower in cluster II (0.6–21%). Cluster II had high fractions of methanogens such as *Methanosaeta* (0.03–28%), *Methanocalculus* (3–7%), *Methanoculleus* (0.4–6%), and *Methanofollis* (0.2–2%). In cluster I, the fractions of these methanogens were less than 1.5% (**Table 3**).

DISCUSSION

The use of nitrate to control oil reservoir souring has been studied for the past 20 years (Youssef et al., 2009; Gieg et al., 2011). Its injection in a limited number of wells in the heavy-oil producing, low-temperature Coleville field in Saskatchewan, Canada, decreased sulfide concentrations in produced waters from connected producing wells, decreased numbers of SRB, while increasing those of NRB (Telang et al., 1997). Molecular biology analysis indicated large increases in the fraction of the

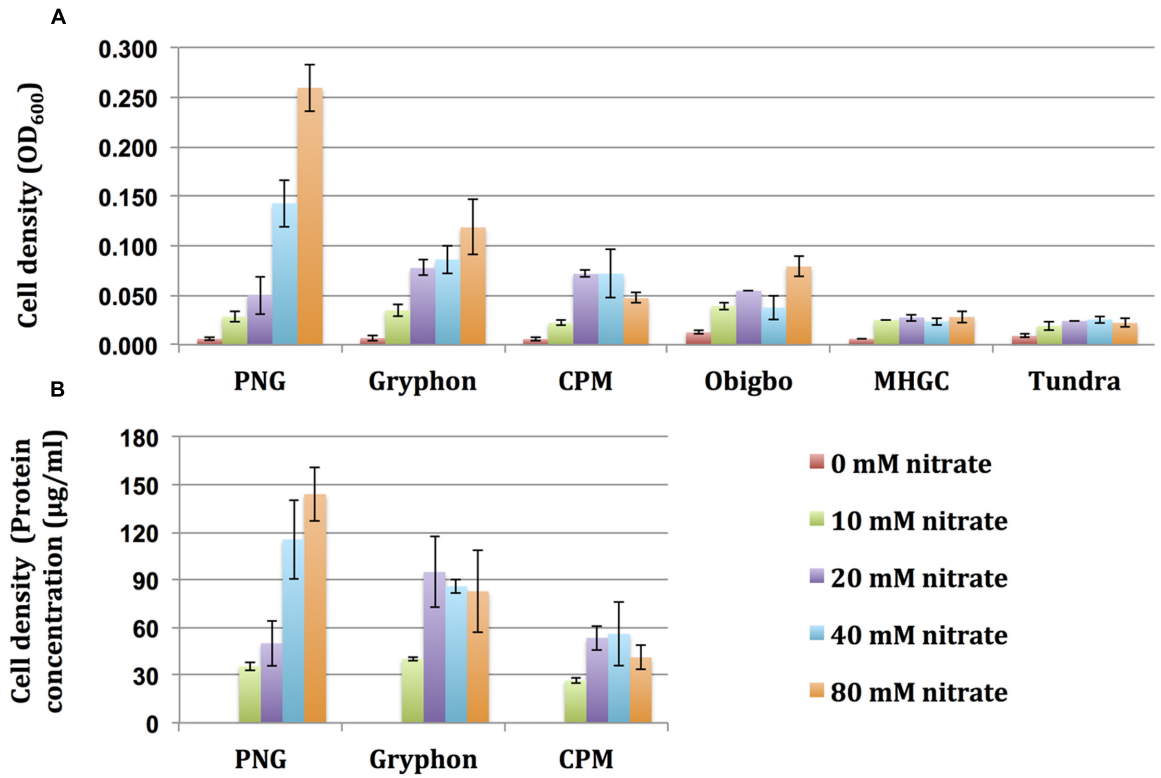

FIGURE 3 | Biomass concentration as a function of nitrate reduction in Hungate tube incubations with oils as electron donors. Cell density is represented by **(A)** Optical density measured at 600 nm and **(B)** Protein concentration (µg/ml). Error bars represent standard deviations of duplicate measurements.

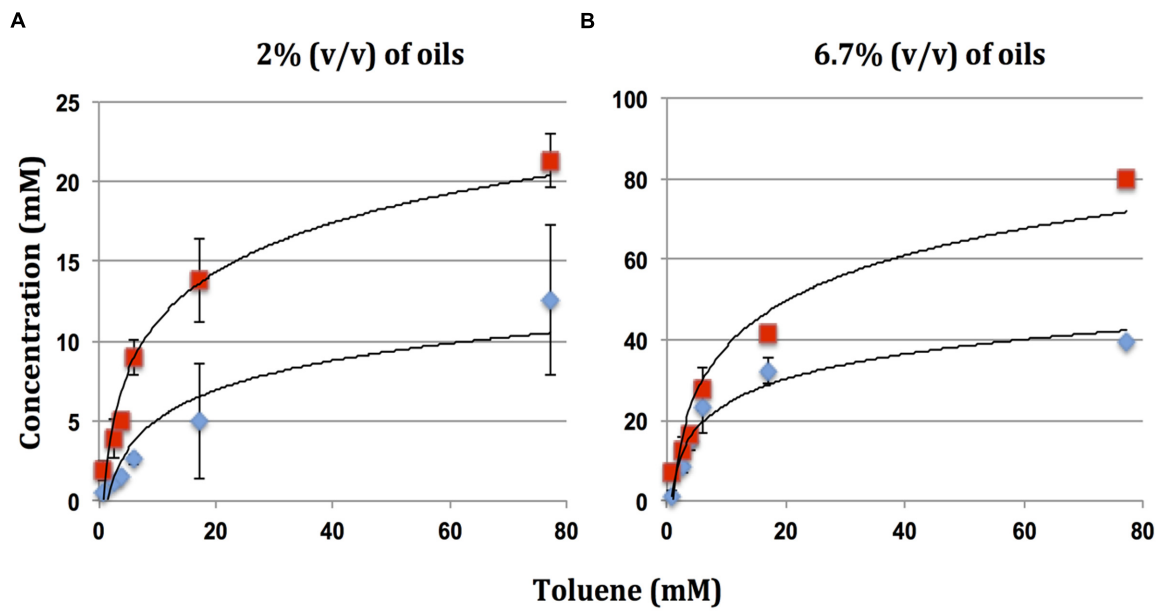

FIGURE 4 | Maximum reduction of nitrate (■) and formation of nitrite (♦) in microcosms incubated with oils with different toluene concentrations for 90 days. Data are for **(A)** serum bottles and **(B)** Hungate tubes. Error bars represent the standard deviations for eight replicate measurements.

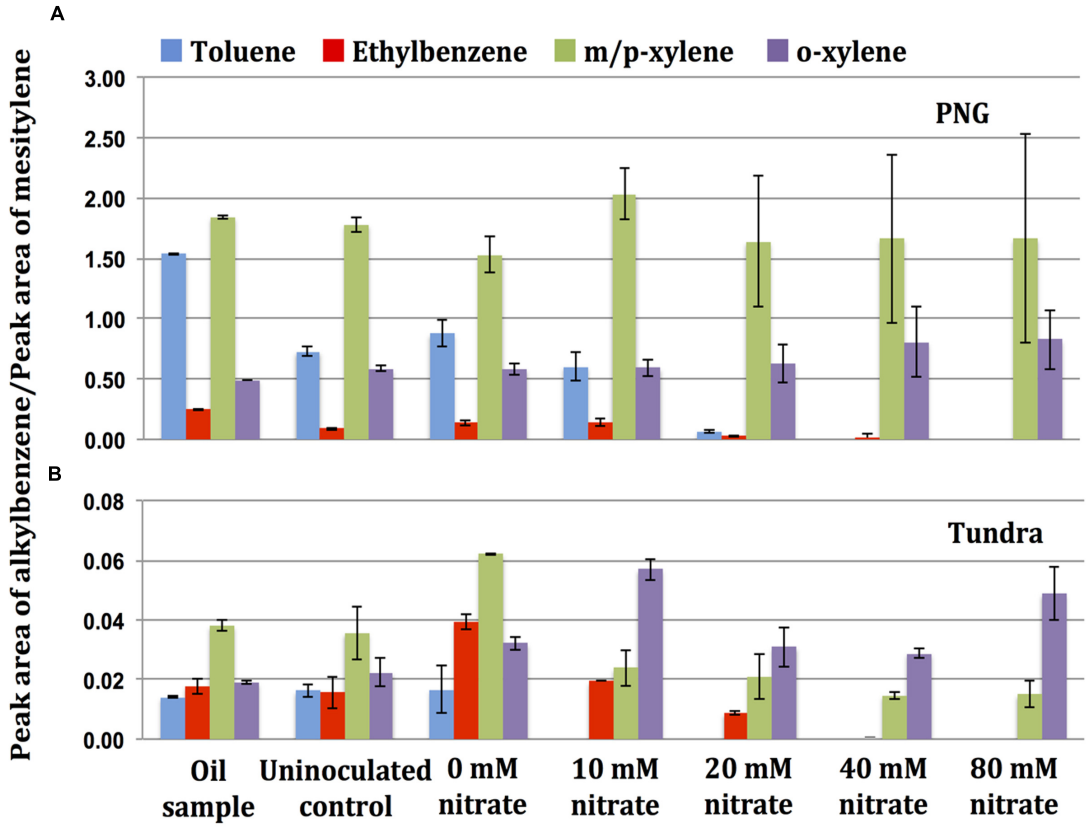

FIGURE 5 | Gas chromatography-mass spectrometry analysis of the oils, **(A)** PNG and **(B)** Tundra extracted from the incubations of oil field hNRB with nitrate and oils at the end of incubation period of 90 days. The presence of alkylbenzenes is represented as the ratio of peak areas of a particular alkylbenzene to mesitylene (1,3,5-trimethylbenzene). Note the difference in scale. Error bars represent standard deviations for duplicate measurements.

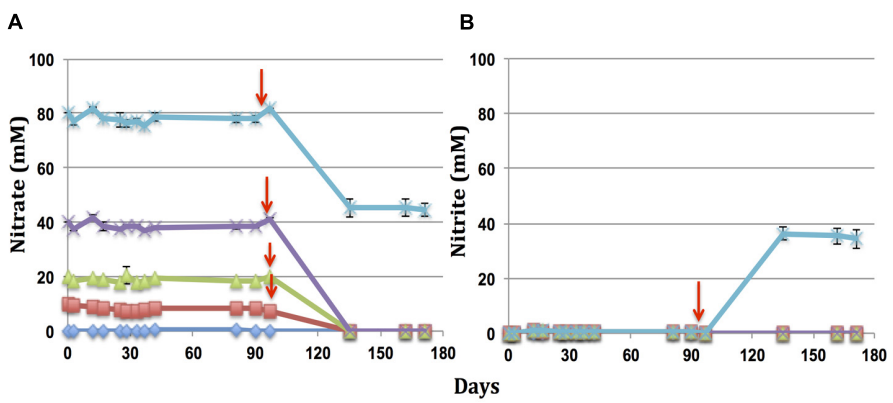

FIGURE 6 | Reduction of nitrate **(A)** and formation of nitrite **(B)** as a function of time in microcosms with Tundra oil amended with toluene at the indicated time (↓). Incubations contained 49 ml of inoculated medium with 80 (*), 40 (×), 20 (▲), 10 (■), or 0 (♦) mM nitrate and 1 ml of Tundra oil. The oil phase was amended with additional 570, 285, 142, and 71 mM of toluene, respectively. Error bars represent the standard deviations for duplicate measurements.

soNRB strain CVO (Coleville organism), now referred to as *Sulfurimonas* sp. strain CVO, in the microbial community in producing wells. Strain CVO oxidizes sulfide to sulfur or sulfate, while reducing nitrate to nitrite and nitrogen (Gevertz et al., 2000; Lin et al., 2008), explaining the success of this initial field test.

Since then successful control of the oil field sulfur cycle by continuous injection of 50–100 ppm (1–2 mM) of nitrate has been demonstrated, especially in deeper and therefore hotter fields in the North Sea (Sunde and Torsvik, 2005). The temperature limit of life in oil fields has been estimated to be at

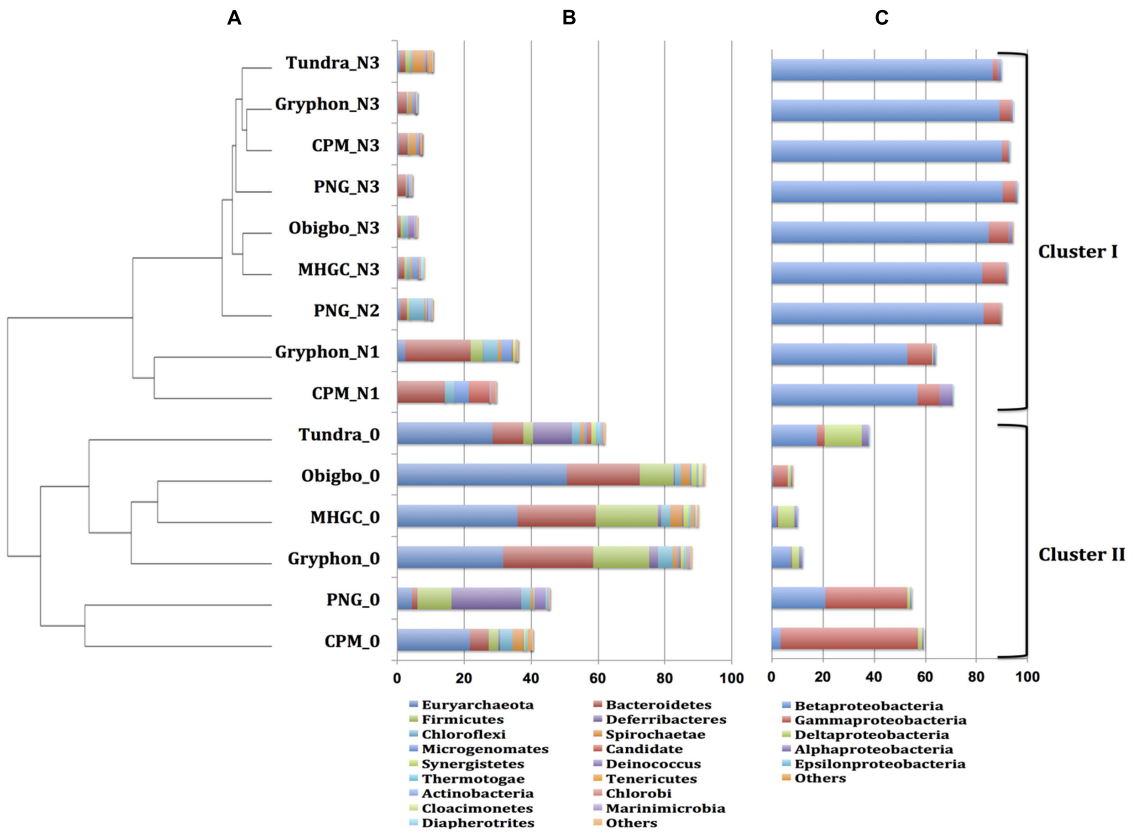

FIGURE 7 | Comparison of microbial community compositions derived from 16S rRNA amplicons of hNRB incubations with oils. **(A)** Relational tree generated using the UPGMA algorithm in MetaAmp. Microbial community compositions are represented at **(B)** at the phylum level excluding *Proteobacteria* and **(C)** at the class level for *Proteobacteria* only. Data are for incubations with the indicated oils without nitrate (0), with 10 mM nitrate (N1), with 10 and 20 mM nitrate (N2) or for incubations with additional toluene and 10, 20, 40, and 80 mM nitrate (N3), as in **Figure 5**; chromosomal DNA's for these latter incubations with a given oil were combined.

80–90°C (Magot, 2005). However, cooling of the near injection wellbore region (NIWR) by injected seawater creates a thermal viability shell in which microbes including SRB and sulfate-reducing *Archaea* can thrive. This region is limited in size with the bulk of the reservoir remaining too hot for microbial activity. Thus control of souring is required in a limited region only, which may explain the reported success of nitrate injection in high-temperature fields (Larsen, 2002; Larsen et al., 2004; Sunde and Torsvik, 2005). However, a more recent evaluation of souring control by nitrate injection in hot North Sea oil fields indicated only partial success over the longer term (Mitchell et al., 2010). Souring stabilized, decreased or kept on increasing gradually in fields injected with nitrate. Interestingly, nitrate reduction in oil fields appears to stop at nitrite at or above 50°C, causing nitrite accumulation and strong inhibition of SRB activity (Greene et al., 2003; Haveman et al., 2004; Fida et al., 2016). Thus souring control with nitrate in high-temperature fields may be improved if the temperature of the NIWR can be prevented from dropping below this temperature.

Monitoring of nitrate injection to control souring in the low-temperature MHGC field has indicated why nitrate injections may fail (Voordouw et al., 2009). Reduction of nitrate to nitrite by hNRB inhibits SRB, but the subsequent reduction of nitrite to N_2 or ammonium (90 and 10%, respectively; Cornish-Shartau et al., 2010) removes the inhibition. Unfortunately, continuous injection of water containing nitrate and sulfate will cause the reduction of nitrate, followed by reduction of sulfate and then oil-dependent methanogenesis in separate zones along the injection water flow path (Voordouw et al., 2009; Agrawal et al., 2012; Chen et al., 2017). The injected nitrate is reduced to N_2 by hNRB using oil components as electron donor under these conditions and does not reach the deeper adjacent zone in which sulfate is reduced to sulfide.

If hNRB were to use a wide variety of oil components then these observations would seem to preclude the successful use of nitrate in inhibiting reservoir souring. However, incubations of MHGC oil and produced water with nitrate and/or sulfate indicated that the hNRB were specific in the use of alkylbenzenes with a further preference for toluene (Lambo et al., 2008; Agrawal et al., 2012), whereas SRB used a broader suite of oil components (Agrawal et al., 2012). This hNRB specificity was expressed in the MHGC field by the fact that nitrate breakthrough in a producing well was associated with the production of toluene-free oil (Agrawal et al., 2012). In view

TABLE 3 | Microbial community compositions of hNRB enrichments.

		Cluster I									Cluster II					
#Taxonomy (Class; Order; Family; Genus)	**Average**	**Tundra_N3**	**Gryphon_N3**	**CPM_N3**	**PNG_N3**	**Obigbo_N3**	**MHGC_N3**	**PNG_N2**	**Gryphon_N1**	**CPM_N1**	**Tundra_0**	**Obigbo_0**	**MHGC_0**	**Gryphon_0**	**PNG_0**	**CPM_0**
Betaproteobacteria; Rhodocyclales; Rhodocyclaceae; Thauera	**48.5**	**84.2**	**85.0**	**88.2**	**83.7**	**82.7**	**80.1**	**75.7**	**45.2**	**51.2**	**17.0**	**0.6**	**1.9**	**7.5**	**20.5**	**3.5**
Gammaproteobacteria; Pseudomonadales; Pseudomonadaceae; Pseudomonas	**9.5**	**1.7**	**4.4**	**1.9**	**5.0**	**7.3**	**9.1**	**6.3**	**9.5**	**5.9**	**2.7**	**3.4**	0.4	0.3	**31.6**	**53.3**
Sphingobacteriia; Sphingobacteriales; WCHB1-69	**6.9**	0.7	**1.8**	**1.2**	0.5	0.6	**1.1**	0.4	**15.7**	**10.8**	**5.2**	**20.2**	**18.9**	**23.6**	0.3	**2.6**
Methanomicrobia; Methanosarcinales; Methanosaetaceae; Methanosaeta	**6.6**	0.0	0.0	0.0	0.0	0.0	0.0	0.0	0.1	0.0	**12.1**	**28.4**	**25.9**	**18.1**	0.0	**14.5**
Methanomicrobia; Methanomicrobiales; Methanomicrobiales-Incertae-Sedis; Methanocalculus	**2.6**	0.0	0.0	0.0	0.0	0.0	0.0	0.4	**1.3**	0.0	**12.8**	**6.2**	**4.3**	**6.9**	**3.4**	**3.8**
Deferribacteres; Deferribacterales; Deferribacteraceae	**2.5**	0.0	0.0	0.0	0.0	0.0	0.0	0.0	0.1	0.0	**11.5**	0.3	0.9	**2.6**	**20.8**	0.5
Bacteroidia; Bacteroidales; Porphyromonadaceae; Proteiniphilum	**1.8**	0.7	0.4	**1.2**	**1.7**	0.1	0.2	**1.4**	**3.1**	**3.2**	**3.5**	**1.2**	**3.0**	**2.9**	**1.2**	**3.0**
Anaerolineae; Anaerolineales; Anaerolineaceae	**1.7**	0.3	0.2	0.1	0.0	**1.3**	0.6	**3.3**	**3.5**	**2.6**	**2.0**	**1.3**	**2.3**	**3.2**	**1.9**	**2.8**
Clostridia; Clostridiales; Eubacteriaceae; Acetobacterium	**1.4**	0.0	0.0	0.0	0.0	0.0	0.0	0.0	0.0	0.0	0.0	**2.2**	**14.2**	0.0	**4.9**	0.1
Deltaproteobacteria; Syntrophobacterales; Syntrophaceae; Smithella	**1.3**	0.0	0.0	0.0	0.0	0.0	0.0	0.0	0.0	0.0	**13.4**	0.6	**3.8**	**1.8**	0.0	0.5
Methanomicrobia; Methanomicrobiales; Methanomicrobiaceae; Methanoculleus	**1.3**	0.4	0.1	0.5	0.0	0.0	0.2	0.3	0.7	0.1	**2.6**	**5.0**	**1.4**	**5.8**	0.4	**2.3**
Clostridia; Clostridiales; Peptococcaceae	**1.0**	0.0	0.0	0.0	0.0	0.1	0.0	0.0	0.1	0.0	0.8	**1.1**	**2.1**	**11.3**	0.2	0.0
Total reads	**414570**	**27365**	**27828**	**19220**	**33375**	**30297**	**29162**	**33228**	**27373**	**31623**	**31623**	**21499**	**28059**	**30608**	**24053**	**24436**

*These are presented in the same order as in the dendrogram (**Figure 7**). Taxa with an average fraction in excess of 1.0% of total Illumina reads are presented in decreasing order. N3, N2, N1 and 0 represent incubations of the indicated oils with 10–80 mM, 10–20 mM, 10 mM nitrate or without nitrate, respectively.*

of these observations it appears that oil composition, especially toluene content, could be a major determinant of the success of nitrate injections.

Selective use of alkylbenzenes in oil, especially toluene, ethylbenzene, and m-xylene, by strains ToN1, mXyN1, and EnN1 was shown by Rabus and Widdel (1996). Although the phylogeny of these strains was not identified these may have included *Thauera aromatica* and *Azoarcus tolulyticus* strains (Spormann and Widdel, 2000). Reviews have indicated that the majority of hNRB use toluene as electron donor (Spormann and Widdel, 2000; Chakraborty and Coates, 2004); hNRB using benzene are rare (Chakraborty and Coates, 2004). The metabolism of denitrifying *Betaproteobacteria* strain HxN1 using alkanes as electron donor for nitrate reduction has been characterized in detail (Grundmann et al., 2008) and an *Azoarcus* sp., capable of using heptane as electron donor for nitrate reduction has been enriched from the MHGC field (Kryachko and Voordouw, 2014). However, these are not major community components in enrichments with oil and nitrate and nitrate remained in these incubations, despite the presence of significant alkanes in light and heavy oil (Lambo et al., 2008; Agrawal et al., 2012; this study). Incubations of MHGC oil, toluene or VFA and nitrate with MHGC produced waters stimulated the growth of *Thauera* and *Pseudomonas* spp. (Lambo et al., 2008, Voordouw et al., 2009; Gassara et al., 2015; Fida et al., 2016; Chen et al., 2017). These were also found in high proportions in other low-temperature oil fields (Li et al., 2014) and the effect of nitrate to toluene ratio on nitrate reduction by *Pseudomonas* sp. has been studied (Kim et al., 2013). Incubation of MHGC produced water 18PW with toluene-amended oils and nitrate gave very high fractions of *Thauera* (45–88%) and lower fractions of *Pseudomonas* (1.7–9.5%) (**Table 3**).

Note that the high concentrations of nitrate of up to 80 mM which we added to microcosms, greatly exceed the 1–2 mM concentrations typically injected into oil fields to control souring. We added these to determine the maximum concentrations of nitrate that could be reduced per ml of oil. Using this approach, we have found that more nitrate was reduced in incubations of oils with higher concentrations of toluene (e.g., PNG oil), as compared to the oils with lower concentrations of toluene (e.g., Tundra oil) as electron donor (**Figure 1** and **Table 2**). PNG and Tundra are both light oils with a high API gravity and low viscosity (**Table 1**). However, the lightness of the Tundra oil is caused by high concentrations (9 mM) of low molecular weight alkanes, like pentane and heptane (Jiang and Li, 2002; Menon and Voordouw, 2016). Its toluene content is very low (**Figure 1**), as has been observed for many other shale oils (Jiang and Li, 2002). Thus, despite the presence of a heptane-utilizing *Azoarcus* sp. in MHGC produced water (Kryachko and Voordouw, 2014) and the presence of low molecular weight alkanes in Tundra oil (Menon and Voordouw, 2016), nitrate reduction was limited by its low toluene content. Amendment of Tundra oil with additional toluene increased the reduction of nitrate (**Figure 6A**) through the activity of *Thauera,* which increased from 17 to 84% (**Table 3**). Toluene limitation would not affect the reduction of sulfate to sulfide, because SRB use a much wider range of oil components, including alkanes, as substrates (Davidova et al., 2006; Savage et al., 2010; Agrawal et al., 2012; Sherry et al., 2013).

We may, therefore, expect that when nitrate is injected into a reservoir with low toluene oil such as Tundra, it will penetrate deeper and will be more available to soNRB like *Sulfurimonas* for oxidizing SRB-produced sulfide than when it is injected in a high-toluene reservoir such as PNG. When injecting nitrate in high-toluene reservoir such as PNG, we expect extensive nitrate reduction and formation of high hNRB biomass concentrations (**Table 2** and **Figure 3**). This biomass may be surface-active itself or may produce biosurfactant causing oil emulsification increasing oil recovery (Youssef et al., 2009; Kryachko and Voordouw, 2014; Li et al., 2014; Gassara et al., 2017). Increasing the toluene-content of oil can be done by injecting water-dissolved toluene, which transfers to the oil phase. Subsequent injection of water-dissolved nitrate gives toluene and nitrate-mediated microbially enhanced oil recovery (MEOR; Gassara et al., 2015).

Thus, the toluene content of the oil in a reservoir is an important determinant of the success of nitrate injection for souring control and MEOR. If the goal is to control souring, then the toluene content should be low. If the goal is MEOR, then it should be high either naturally or through injection.

AUTHOR CONTRIBUTIONS

NS: Experiments, data collection, data analysis and interpretation, drafting the manuscript, critical revision of the manuscript. JV: DNA work. GV: Idea of the work, supervision, final approval of the manuscript to be published.

FUNDING

This work was supported by an NSERC Industrial Research Chair award to Dr. Gerrit Voordouw, which was also supported by Baker Hughes, BP America Production Co., Computer Modeling Group Ltd, ConocoPhillips, Intertek, Dow Microbial Control, Enbridge Inc., Enerplus Corporation, Oil Search Limited, Shell Global Solutions International, Suncor Energy Inc., Yara Norge as well as by Alberta Innovates Energy and Environment Solutions (AIEES).

ACKNOWLEDGMENTS

We are grateful to Rhonda Clark and Yin Shen for administrative support provided, to Fatma Gassara for technical support and to Baker Hughes, Enerplus, Shell Global Solutions International and Oil Search Limited Corporation for providing the field samples.

SUPPLEMENTARY MATERIAL

The Supplementary Material for this article can be found online at: http://journal.frontiersin.org/article/10.3389/fmicb.2017.00956/full#supplementary-material

REFERENCES

Agrawal, A., An, D., Cavallaro, A., and Voordouw, G. (2014). Souring in low-temperature surface facilities of two high-temperature Argentinian oil fields. *Appl. Microbiol. Biotechnol.* 98, 8017–8029. doi: 10.1007/s00253-014-5843-z

Agrawal, A., Park, H. S., Nathoo, S., Gieg, L. M., Jack, T. R., Miner, K., et al. (2012). Toluene depletion in produced oil contributes to souring control in a field subjected to nitrate injection. *Environ. Sci. Technol.* 46, 1285–1292. doi: 10.1021/es203748b

Alain, K., Harder, J., Widdel, F., and Zengler, K. (2012). Anaerobic utilization of toluene by marine alpha- and gammaproteobacteria reducing nitrate. *Microbiology* 158, 2946–2957. doi: 10.1099/mic.0.061598-0

Altenschmidt, U., and Fuchs, G. (1991). Anaerobic degradation of toluene in denitrifying *Pseudomonas* sp.: indication for toluene methylhydroxylation and benzoyl-CoA as central aromatic intermediate. *Arch. Microbiol.* 156, 152–158. doi: 10.1007/BF00290990

American Petroleum Institute [API] (2011). *API Specification for Materials and Testing for Petroleum Products*, 11th Edn. Dallas, TX: API, 20–21.

Chakraborty, R., and Coates, J. D. (2004). Anaerobic degradation of monoaromatic hydrocarbons. *Appl. Microbiol. Biotechnol.* 64, 437–446. doi: 10.1007/s00253-003-1526-x

Chen, C., Shen, Y., An, D., and Voordouw, G. (2017). Use of acetate, propionate and butyrate for reduction of nitrate and sulfate and methanogenesis in microcosms and bioreactors simulating an oil reservoir. *Appl. Environ. Microbiol.* 83:e2983-16. doi: 10.1128/AEM.02983-16

Cornish-Shartau, S. L., Yurkiw, M., Lin, S., Grigoryan, A. A., Lambo, A., Park, H. S., et al. (2010). Ammonium concentrations in produced waters from a mesothermic oil field subjected to nitrate injection decrease through formation of denitrifying biomass and anammox activity. *Appl. Environ. Microbiol.* 76, 4977–4987. doi: 10.1128/AEM.00596-10

Davidova, I. A., Duncan, K. E., Choi, O. K., and Suflita, J. M. (2006). *Desulfoglaeba alkanexedens* gen. nov., sp. nov., an n-alkane-degrading, sulfate-reducing bacterium. *Int. J. Syst. Evol. Microbiol.* 56, 2737–2742. doi: 10.1099/ijs.0.64398-0

Fida, T. T., Chen, C., Okpala, G., and Voordouw, G. (2016). Implications of limited thermophilicity of nitrite reduction for control of sulfide. *Appl. Environ. Microbiol.* 82, 4190–4199. doi: 10.1128/AEM.00599-16

Gassara, F., Suri, N., Stanislav, P., and Voordouw, G. (2015). Microbially enhanced oil recovery by sequential injection of light hydrocarbon and nitrate in low- and high-pressure bioreactors. *Environ. Sci. Technol.* 49, 12594–12601. doi: 10.1021/acs.est.5b03879

Gassara, F., Suri, N., Stanislav, P., and Voordouw, G. (2017). Nitrate-mediated microbially enhanced oil recovery (N-MEOR) from model upflow bioreactors. *J. Hazard. Mater.* 324, 94–99. doi: 10.1016/j.jhazmat.2015.12.039

Gevertz, D., Telang, A. J., Voordouw, G., and Jenneman, G. E. (2000). Isolation and characterization of strains CVO and FWKO B, two novel nitrate-reducing, sulfide-oxidizing bacteria isolated from oil field brine. *Appl. Environ. Microbiol.* 66, 2491–2501. doi: 10.1128/AEM.66.6.2491-2501.2000

Gieg, L. M., Jack, T. R., and Foght, J. M. (2011). Biological souring and mitigation in oil reservoirs. *Appl. Microbiol. Biotechnol.* 92, 263–282. doi: 10.1007/s00253-011-3542-6

Greene, E. A., Hubert, C., Nemati, M., Jenneman, G. E., and Voordouw, G. (2003). Nitrite reductase activity of sulphate-reducing bacteria prevents their inhibition by nitrate-reducing, sulphide-oxidizing bacteria. *Environ. Microbiol.* 5, 607–617. doi: 10.1046/j.1462-2920.2003.00446.x

Grigoryan, A. A., Cornish, S. L., Buziak, B., Lin, S., Cavallaro, A., Arensdorf, J. J., et al. (2008). Competitive oxidation of volatile fatty acids by sulfate- and nitrate-reducing bacteria from an oil field in Argentina. *Appl. Environ. Microbiol.* 74, 4324–4335. doi: 10.1128/AEM.00419-08

Grundmann, O., Behrends, A., Rabus, R., Amann, J., Halder, T., Heider, J., et al. (2008). Genes encoding the candidate enzyme for anaerobic activation of n-alkanes in the denitrifying bacterium, strain HxN1. *Environ. Microbiol.* 10, 376–385. doi: 10.1111/j.1462-2920.2007.01458.x

Haveman, S. A., Greene, E. A., Stilwell, C. P., Voordouw, J. K., and Voordouw, G. (2004). Physiological and gene expression analysis of inhibition of *Desulfovibrio vulgaris* Hildenborough by nitrite. *J. Bacteriol.* 186, 7944–7950. doi: 10.1128/JB.186.23.7944-7950.2004

Hubert, C., and Voordouw, G. (2007). Oil field souring control by nitrate-reducing *Sulfurospirillum* spp. that outcompete sulfate-reducing bacteria for organic electron donors. *Appl. Environ. Microbiol.* 73, 2644–2652. doi: 10.1128/aem.02332-06

Jiang, C., and Li, M. (2002). Bakken/Madison petroleum systems in the Canadian Williston Basin. Part 3: geochemical evidence for significant Bakken-derived oils in Madison Group reservoirs. *Org. Geochem.* 33, 761–787. doi: 10.1016/S0146-6380(02)00037-2

Kim, D., Park, M., Lim, D., and Choi, J. (2013). Impact of nitrate dose on toluene degradation under denitrifying condition. *Appl. Biochem. Biotechnol.* 170, 248–256. doi: 10.1007/s12010-013-0176-4

Kryachko, Y., and Voordouw, G. (2014). Microbially enhanced oil recovery from miniature model columns through stimulation of indigenous microflora with nitrate. *Int. Biodeterior. Biodegrad.* 96, 135–143. doi: 10.1016/j.ibiod.2014.08.013

Lambo, A. J., Noke, K. I., Larter, S. R., and Voordouw, G. (2008). Competitive, microbially-mediated reduction of nitrate with sulfide and aromatic oil components in a low-temperature, Western Canadian oil reservoir. *Environ. Sci. Technol.* 42, 8941–8946. doi: 10.1021/es801832s

Larsen, J. (2002). "Downhole nitrate applications to control sulfate reducing bacteria activity and reservoir souring," in *Proceedings of the Corrosion Conference and Expo 2002*, (Houston, TX: NACE International).

Larsen, J., Rod, M. H., and Zwolle, S. (2004). "Prevention of reservoir souring in the Halfdan field by nitrate injection," in *Proceedings of the Corrosion Conference and Expo 2004*, (Houston, TX: NACE International).

Li, G., Gao, P., Wu, Y., Tian, H., Dai, X., Wang, Y., et al. (2014). Microbial abundance and community composition influence production performance in a low-temperature petroleum reservoir. *Environ. Sci. Technol.* 48, 5336–5344. doi: 10.1021/es500239w

Lin, S., Voordouw, G., and Coombe, D. (2008). "Sulfate production associated with souring control by nitrate injection: a potential corrosion risk?," in *Proceedings of NACE Expo 2008 Annual Conference and Exposition, New Orleans, LA, Paper 01712*, (Houston, TX: NACE).

Magot, M. (2005). "Indigenous microbial communities in oil fields, Petrol Microbiol," in *Petroleum Microbiology*, eds B. Ollivier and M. Magot (Washington, DC: ASM Press), 21–34.

Menon, P., and Voordouw, G. (2016). Impact of light oil toxicity on sulfide production by acetate-oxidizing, sulfate-reducing bacteria. *Int. Biodeterior. Biodegradation* (in press). doi: 10.1016/j.ibiod.2016.11.021

Mitchell, A. F., Bruras-Harvik, A. M., Andfinsen, A., and Hustad, B. M. (2010). "A review of reservoir souring for three North Sea fields," in *Proceedings of the Corrosion Conference and Expo 2010, Paper 10248*, (Houston, TX: NACE).

Rabus, R., and Widdel, F. (1996). Utilization of alkylbenzenes during anaerobic growth of pure cultures of denitrifying bacteria on crude oil. *Appl. Environ. Microbiol.* 62, 1238–1241.

Reinsel, M. A., Sears, J. T., Stewart, P. S., and McInerney, M. J. (1996). Control of microbial souring by nitrate, nitrite or glutaraldehyde injection in a sandstone column. *J. Ind. Microbiol.* 17, 128–136. doi: 10.1007/BF01570056

Savage, K. N., Krumholz, L. R., Gieg, L. M., Parisi, V. A., Suflita, J. M., Allen, J., et al. (2010). Biodegradation of low-molecular-weight alkanes under mesophilic, sulfate-reducing conditions: metabolic intermediates and community patterns. *FEMS Microbiol. Ecol.* 72, 485–495. doi: 10.1111/j.1574-6941.2010.00866.x

Sherry, A., Gray, N. D., Ditchfield, A. K., Aitken, C. M., Jones, D. M., Röling, W. F. M., et al. (2013). Anaerobic biodegradation of crude oil under sulphate-reducing conditions leads to only modest enrichment of recognized sulphate-reducing taxa. *Int. Biodeterior. Biodegrad.* 81, 105–113. doi: 10.1016/j.ibiod.2012.04.009

Spormann, A. M., and Widdel, F. (2000). Metabolism of alkylbenzenes, alkanes, and other hydrocarbons in anaerobic bacteria. *Biodegradation* 11, 85–105. doi: 10.1023/A:1011122631799

Sunde, E., and Torsvik, T. (2005). "Microbial control of hydrogen sulfide production in oil reservoirs," in *Petroleum Microbiology*, eds B. Ollivier and M. Magot (Washington, DC: ASM Press), 201–214. doi: 10.1128/9781555817589.ch10

Telang, A. J., Ebert, S., Foght, J. M., Westlake, D. W. S., Jenneman, G. E., Gevertz, D., et al. (1997). The effect of nitrate injection on the microbial community in an oil field as monitored by reverse sample genome probing. *Appl. Environ. Microbiol.* 63, 1785–1793.

Voordouw, G. (2011). Production-related petroleum microbiology: progress and prospects. *Curr. Opin. Biotechnol.* 22, 401–405. doi: 10.1016/j.copbio.2010.12.005

Voordouw, G., Grigoryan, A. A., Lambo, A., Lin, S., Park, H. S., Jack, T. R., et al. (2009). Sulfide remediation by pulsed injection of nitrate into a low temperature Canadian heavy oil reservoir. *Environ. Sci. Technol.* 43, 9512–9518. doi: 10.1021/es902211j

Weelink, S. A. B., van Eekert, M. H. A., and Stams, A. J. M. (2010). Degradation of BTEX by anaerobic bacteria: physiology and application. *Rev. Environ. Sci. Biotechnol.* 9, 359–385. doi: 10.1007/s11157-010-9219-2

Youssef, N., Elshahed, M. S., and McInerney, M. J. (2009). Microbial processes in oil fields: culprits, problems and opportunities. *Adv. Appl. Microbiol.* 66, 141–251. doi: 10.1016/S0065-2164(08)00806-X

Conflict of Interest Statement: The authors declare that the research was conducted in the absence of any commercial or financial relationships that could be construed as a potential conflict of interest.

frontiers in Microbiology

ORIGINAL RESEARCH
published: 29 May 2017
doi: 10.3389/fmicb.2017.00890

Influence of Phosphorus and Cell Geometry on the Fractionation of Sulfur Isotopes by Several Species of *Desulfovibrio* during Microbial Sulfate Reduction

*Shikma Zaarur *†‡, David T. Wang *‡, Shuhei Ono and Tanja Bosak*

Department of Earth, Atmospheric and Planetary Sciences, Massachusetts Institute of Technology, Cambridge, MA, United States

OPEN ACCESS

Edited by:
William Sunda, University of North Carolina at Chapel Hill, United States

Reviewed by:
Dirk De Beer, Max Planck Society (MPG), Germany
Gordon T. Taylor, Stony Brook University, United States

***Correspondence:**
Shikma Zaarur
shikma.zaarur@mail.huji.ac.il
David T. Wang
dtw@alum.mit.edu

†Present Address:
Shikma Zaarur, Institute of Earth Sciences, The Hebrew University of Jerusalem, Jerusalem, Israel

‡*These authors have contributed equally to this work.*

Specialty section:
This article was submitted to Microbiological Chemistry and Geomicrobiology, a section of the journal Frontiers in Microbiology

Received: *14 February 2017*
Accepted: *02 May 2017*
Published: *29 May 2017*

Citation:
Zaarur S, Wang DT, Ono S and Bosak T (2017) Influence of Phosphorus and Cell Geometry on the Fractionation of Sulfur Isotopes by Several Species of Desulfovibrio during Microbial Sulfate Reduction. Front. Microbiol. 8:890. doi: 10.3389/fmicb.2017.00890

We investigated the influence of organic substrates and phosphate concentration on the rates of dissimilatory microbial sulfate reduction and the $^{34}S/^{32}S$ isotopic fractionation produced by several *Desulfovibrio* species. Our experiments corroborate the previously reported species-specific correlation between sulfur isotope fractionation and cell-specific sulfate reduction rates. We also identify cell size as a key factor that contributes to the species-effect of this correlation. Phosphate limitation results in larger cells and contributes to a small decrease in sulfur isotope fractionation concomitant with an apparent increase in cell-specific sulfate reduction rates. Sulfur isotope fractionation in phosphate-limited cultures asymptotically approaches a lower limit of approximately 5‰ as cell-specific sulfate reduction rates increase to >100 fmol cell^{-1} day^{-1}. These experimental results test models that link the reversibilities of enzymatic steps in dissimilatory sulfate reduction to sulfur isotope fractionation and show that these models can provide consistent predictions across large variations in physiological states experienced by sulfate reducing bacteria.

Keywords: sulfate reducing bacteria, organic substrate, phosphate limitation, sulfur isotopes, sulfur cycle

INTRODUCTION

The oxidation of organic matter by sulfate reducing bacteria (SRB) is a globally distributed anaerobic process that influences the redox state of the Earth's surface and the preservation of organic matter in sediments (Jørgensen, 1982; Westrich and Berner, 1984; Widdel and Hansen, 1992; Shen and Buick, 2004). Microbial sulfate reduction (MSR) fractionates sulfur isotopes, producing sulfide depleted in heavier isotopes. The magnitude of this fractionation ($^{34}\varepsilon$, defined in Equation 6) is a critical parameter for reconstructions of the carbon and sulfur cycles through Earth history (Holland, 1973; Garrels and Lerman, 1981; Berner, 2001; Luo et al., 2016). For over half a century, many investigators have attempted to understand factors that affect sulfur isotope fractionation during MSR. Dozens of studies have reported fractionations produced in pure cultures of sulfate reducing organisms under controlled laboratory conditions (e.g., Harrison and Thode, 1958; Thode et al., 1961; Kaplan and Rittenberg, 1964; Chambers et al., 1975; Chambers and Trudinger, 1979), in experiments with natural microbial populations (e.g., Canfield, 2001; Canfield et al., 2010) and under *in situ* conditions (e.g., Jorgensen, 1979; Rudnicki et al., 2001; Wortmann et al., 2001).

Marine sulfides exhibit a wide range of sulfur isotope compositions, ranging up to a 70‰ depletion in the $^{34}S/^{32}S$ ratio relative to that of the sulfate from which they were formed (Thode et al., 1953; Kaplan et al., 1963; Canfield and Teske, 1996). Because early laboratory studies could not reproduce fractionations of this magnitude in pure culture, they established a limit of 47‰ for single-step microbially mediated sulfate reduction (Kaplan and Rittenberg, 1964). Thus, for many decades, large fractionations (>47‰) between sulfate and sulfide in rocks and natural environments were interpreted as evidence for oxidative recycling of sulfides or microbial disproportionation of intermediate sulfur species (e.g., Canfield and Thamdrup, 1994; Habicht and Canfield, 2001; Johnston et al., 2005). Recently, one bacterium (*Desulfovibrio* sp. DMSS-1), has been shown to produce fractionations that exceeded the 47‰ limit (Sim et al., 2011a). The largest fractionations (up to 66‰) are produced during slow growth with glucose as the electron donor. This approaches the theoretical limit of 70‰ proposed for microbial sulfate reduction by Brunner and Bernasconi (2005).

In pure cultures, factors reported to influence the isotopic fractionation include temperature (Canfield et al., 2006), sulfate concentration (Canfield et al., 2000; Habicht et al., 2002; Bradley et al., 2015), availability and chemical properties of the electron donor (Harrison and Thode, 1958; Kaplan and Rittenberg, 1964; Chambers et al., 1975; Kleikemper et al., 2004; Sim et al., 2011a,b; Leavitt et al., 2013; Bradley et al., 2015; Antler et al., 2017), nutrient limitation (Sim et al., 2012), sulfate reduction rate (e.g., Harrison and Thode, 1958), altered gene expression (Sim et al., 2013; Leavitt et al., 2016), and unspecified strain-specific effects (Brüchert et al., 2001; Detmers et al., 2001). These factors can be mutually dependent. For example, when the type and concentration of electron donor (hydrogen or organic carbon compounds) dictate the cell-specific sulfate reduction rate (csSRR; per-cell respiration rate) in pure culture experiments, $^{34}\varepsilon$ appears to be inversely proportional to csSRR (Chambers et al., 1975; Kleikemper et al., 2004; Hoek et al., 2006; Sim et al., 2011b; Leavitt et al., 2013). However, changes in bacterial species (Detmers et al., 2001) or growth temperature (Kaplan and Rittenberg, 1964; Canfield et al., 2006; Johnston et al., 2007) disrupt the correlation between $^{34}\varepsilon$ and csSRR. This led Detmers et al. (2001) to hypothesize that growth on different electron donors would result in distinct $^{34}\varepsilon$ vs. csSRR correlations for each species.

Here, we test this hypothesis by measuring sulfur isotope fractionations produced during dissimilatory sulfate reduction by several *Desulfovibrio* species (*D. fructosovorans*, *D. inopinatus*, and DMSS-1) grown in batch cultures on various substrates. We also examine the effect of phosphate limitation on sulfur isotope fractionation by SRB. Phosphate is an essential nutrient and a component of DNA, RNA, lipid membranes, and the energy carrier ATP that is used to activate sulfate during MSR (Peck, 1960; Cypionka, 1995; Muyzer and Stams, 2008). Its concentrations in oceanic and sedimentary environments may limit the growth of sulfate reducing bacteria in some natural environments (Bosak et al., 2016) and may have varied dramatically through Earth's history (Planavsky et al., 2010). Therefore, limitation by this essential nutrient may directly influence both the rates of sulfate reduction and the observed sulfur isotope fractionation.

Our results confirm a strong dependence of $^{34}\varepsilon$ on organic substrates. The data are generally consistent with an inverse correlation between $^{34}\varepsilon$ and csSRR. Offsets and deviations among SRB species appear to be rooted in morphological and physiological differences. Further offsets from the general inverse correlation may arise from intracellular responses to phosphorus starvation (Bosak et al., 2016). Comparisons of our data with predictions from recent efforts to numerically simulate isotopic signals produced via dissimilatory sulfate reduction (Wing and Halevy, 2014) test the predictions of these models over a range of conditions that sulfate reducing bacteria can experience in nature.

METHODS

Cultures

Three SRB species were used in this study: *Desulfovibrio inopinatus*, *Desulfovibrio fructosovorans*, and *Desulfovibrio* sp. DMSS-1. As is common in studies of isotope fractionation by SRB, experiments were conducted in batch cultures. Isotope fractionation trends that were first identified from batch cultures have been confirmed by chemostat experiments in which steady-state conditions can be maintained (Sim et al., 2011a,b; Antler et al., 2017). Therefore, we consider batch cultures suitable for this study. Experimental cultures were grown on different substrates (lactate, fructose, malate, and/or pyruvate) and/or in media with different initial phosphate concentrations (from <1 μM to >1 mM) and with excess sulfate as described below.

Desulfovibrio inopinatus

Desulfovibrio inopinatus (cat. no. 10711) was obtained from the German Collection of Microorganisms and Cell Cultures (DSMZ, Braunschweig, Germany: Catalogue of strains 1993). This microbe was isolated from marine sediments of Venice, Italy (Reichenbecher and Schink, 1997). Cultures were maintained anaerobically in glass serum bottles capped with butyl rubber septa under an atmosphere containing 80% N_2 and 20% CO_2. Culture medium was prepared according to DSMZ recipe #196-13871, with the exception of NaCl concentration because *D. inopinatus* grew better at 21 g/L than at the 7 g/L concentration suggested in the DSMZ recipe. The medium contains (per liter): $NaHCO_3$, 9.0 g; Na_2SO_4, 3.0 g; KH_2PO_4, 0.20 g; NH_4Cl, 0.30 g; NaCl, 21 g; KCl, 0.50 g, $MgCl_2{\cdot}6H_2O$, 3.1 g; $CaCl_2{\cdot}2H_2O$, 0.15 g; resazurin, 1 mg; a trace element solution (SL-10), 1 ml (Widdel and Pfennig, 1981; Imhoff-Stuckle and Pfennig, 1983), and a general vitamin mix (described in DSMZ recipe #141), 10 ml. Sodium ascorbate (1.5 g/L) was added to maintain anoxic conditions (Kligler and Guggenheim, 1938). The medium did not contain any yeast extract. The pH of the medium was adjusted to 7.5 by dropwise addition of 1 M NaOH or 1 M HCl prior to inoculation.

Culture medium was supplemented with lactate (28 mM), malate (28 mM), or fructose (14 mM) as organic substrate and sole electron donor. Initial concentrations of organic substrates were chosen such that sulfate would be in excess: sulfate

reduction with stoichiometric conversion of any substrate to acetate would produce only ∼14 mM of sulfide from the initial 21 mM sulfate, see **Table 1**. For each experiment, 7–15 bottles were inoculated with 5% (v/v) of a mid- to late-exponential phase pre-culture grown on the same organic substrate as that used in the experiment. Inoculums were pelleted via centrifugation and rinsed three times with clean medium in an anaerobic chamber (under an atmosphere of 80% N_2, 15% CO_2, and 5% H_2) to ensure the removal of all residual sulfide and organic substrate, and then transferred into 40 mL of fresh media. Bottles were incubated in the dark at room temperature. Microbial growth was monitored daily in one "master" bottle to minimize puncturing of septa of the experimental bottles. At each time point (**Tables 2, 3**), one experimental bottle was subsampled for cell counts and the colorimetric assay of sulfide concentration. The remaining culture volume was sacrificed by the addition of a 1 M zinc acetate solution (at a 10% v/v ratio) to terminate microbial activity and precipitate sulfide as ZnS for isotopic analyses.

To test the effect of phosphate limitation, additional batch cultures were grown with varying initial concentrations of phosphate in the medium. Serum bottles used for these cultures were autoclaved three times with deionized water (18.2 MΩ·cm, Barnstead Nanopure™ filtration system) to remove residual phosphate. Medium was prepared as described above, with lactate (28 mM) as organic substrate and without added phosphate. Phosphate (as KH_2PO_4) was then added from a concentrated stock solution, to final concentrations of 150, 15, and 3 μM. Another set of serum bottles did not receive any added phosphate. The concentration of phosphate in this nominally "0" phosphate medium was estimated to be <1 μM based on lot analyses provided with the chemicals used in the media (see also Experiments with Different Phosphate Concentrations). **Figure A2** shows that ∼3 to 5 μM of added phosphate is limiting, suggesting that the blank is likely <5 μM. Conclusions reached in this paper would be unaffected by a blank of 5 μM or less. Experimental bottles (containing 10 mL of fresh media) were inoculated with a 5% (v/v) sample of pre-cultures that were already conditioned to growth in the presence of lower or limiting concentrations of phosphate. Cell densities were low when phosphate was limiting, so inoculums were pelleted and rinsed only once to minimize the loss of biomass prior to inoculation. Cultures were monitored and sampled as described above.

Desulfovibrio fructosovorans

Desulfovibrio fructosovorans strain JJ (cat. no. 3604) was obtained from DSMZ. This strain was isolated from estuarine sediment (Jones et al., 1984; Cord-Ruwisch et al., 1986), and it incompletely oxidizes pyruvate, lactate, or fructose to acetate (Ollivier et al., 1988). The mineral medium (modified from DSMZ recipe #63) contained (per liter): $NaHCO_3$, 2.6 g; Na_2SO_4, 3.0 g; KH_2PO_4, 0.30 g; NH_4Cl, 0.50 g; KCl, 0.20 g; $CaCl_2$, 0.10 g; $MgCl_2$, 2.0 g; resazurin, 1 mg; SL-10 trace element solution (see above), 1 ml; vitamin solution #141 (see above), 10 ml; and sodium ascorbate, 1.5 g (see above). Media were supplemented with limiting concentrations of one of the following organic substrates: lactate, 20 mM; pyruvate, 40 mM; or fructose, 10 mM. The starting concentrations of lactate, fructose, and pyruvate were chosen such that 10 mM of sulfide would be produced by stoichiometric conversion of the substrate to acetate (**Table 1**). The pH of the medium was adjusted to 7.0 before inoculation. Bottles for all experiments with *D. fructosovorans* were inoculated with 5% (v/v) of a late-exponential phase pre-culture grown on lactate. Media and cultures were otherwise prepared and maintained as described for *Desulfovibrio inopinatus* above.

Desulfovibrio sp. strain DMSS-1

Desulfovibrio sp. DMSS-1 (henceforth "DMSS-1"), isolated from a salt marsh on Cape Cod, Massachusetts, USA and characterized by Sim et al. (2011b), was grown in batch cultures in the presence of varying concentrations of phosphate. Serum bottles were cleaned and prepared in the same manner as described above for *D. inopinatus*. Medium for DMSS-1 was prepared following Sim et al. (2011b), with the exception of phosphate, and contained (per liter): $NaHCO_3$, 9 g; Na_2SO_4, 3 g; NH_4Cl, 0.3 g; NaCl, 21 g; KCl, 0.5 g; $MgCl_2{\cdot}6H_2O$, 6 g; $CaCl_2{\cdot}2H_2O$ 0.3 g; resazurin, 1 mg; SL-10 trace element solution (see above), 1 ml; vitamin solution #141 (see above), 10 ml; 1 ml of selenium stock solution (0.4 mg of Na_2SeO_3 per 200 ml of 0.01 N NaOH); and sodium ascorbate,

TABLE 1 | Reaction stoichiometry of and Gibbs free energy change of reaction at biochemical standard state ($\Delta_rG°'$) and at $f = 0.90$ ($\Delta_rG'_{0.90}$) for dissimilatory sulfate reduction via incomplete oxidation of lactate, malate, pyruvate, or fructose to acetate.

Substrate	Reaction	$\Delta_rG°'$ (kJ mol^{-1})[a]	$\Delta_rG'_{0.90}$ (kJ mol^{-1})[b]
Lactate	$2\ CH_3CH(OH)COO^- + SO_4^{2-} \rightleftharpoons 2\ CH_3COO^- + 2\ HCO_3^- + HS^- + H^+$	−170.7	−193.5
Malate	$2\ CO(O^-)CH_2CH(OH)COO^- + SO_4^{2-} \rightleftharpoons 2\ CH_3COO^- + 4\ HCO_3^- + HS^- + H^+$	−209.3	−242.5
Pyruvate	$4\ CH_3COCOO^- + SO_4^{2-} \rightleftharpoons 4\ CH_3COO^- + 4\ HCO_3^- + HS^- + 3\ H^+$	−340.1	−379.8
Fructose	$C_6H_{12}O_6 + SO_4^{2-} \rightleftharpoons 2\ CH_3COO^- + 2\ HCO_3^- + HS^- + 3\ H^+$	−360.4	−391.7

Reaction stoichiometry from Cord-Ruwisch et al. (1986), Thauer et al. (1977), and Sim et al. (2011b). Values of $\Delta_rG°'$ are given at 298 K and 1 bar for a hypothetical ideal-dilute solution with unit activity of solutes at concentrations of 10^{-7} M for H^+ and 1 M for all other aqueous species.

[a]*Standard Gibbs energies were calculated using the CHNOSZ software package (Dick, 2008) from thermodynamic data (Shock and Helgeson, 1988; Shock, 1995; Amend and Plyasunov, 2001; Wagner and Pruß, 2002; Dalla-Betta and Schulte, 2009) compiled in database updates to the SUPCRT92 program developed by Johnson et al. (1992).*

[b]*Gibbs energies of reaction were calculated at 25°C for medium compositions resembling those used for D. fructosovorans (see Methods), assuming 10% conversion of initial SO_4^{2-} to HS^- with stoichiometric changes in concentrations of other reactants and products. Activity coefficients were assumed to be unity and pH was held constant at 7.0. All dissolved inorganic carbon was assumed to be as HCO_3^-, and all sulfide as HS^-.*

TABLE 2 | Physiological and isotopic data for batch cultures of *D. fructosovorans* and *D. inopinatus* grown on various substrates under non-phosphate-limited conditions.

Substrate	PO_4^{3-} (μM)	Time[a] (days)	OD[b]	*N* (10^6 cells/ml)[c]	ΣH_2S (mM)	*k* (day^{-1})	*Y* (10^6 cells/ μmol SO_4^{2-})	csSRR (fmol/cell/day)	*f*	$\delta^{34}S$ sulfate	$\delta^{34}S$ sulfide	$^{34}\varepsilon$ (‰)
D. fructosovorans												
Lactate	2,200	0.5	0.044	3.3	0.1				0.996	(−0.4)		
		3.4*	0.084	7.3	1.7				0.917			
		4.4	0.120	20.5	3.3	1.09 ± 0.22	8.5 ± 2.9	129 ± 34	0.843		−13.8	14.6 ± 0.8
		5.3	0.179	48.0	5.7	1.03 ± 0.12	10.2 ± 2.4	101 ± 19	0.727		−12.0	13.7 ± 0.9
		6.1	0.216	64.5	7.8	0.83 ± 0.08	9.5 ± 2.0	88 ± 15	0.629		−10.7	13.2 ± 1.0
		6.8[d]	0.212	96.0	7.6				0.636		−10.6	12.9 ± 1.0
Pyruvate	2,200	0.5	0.043	3.6	0.0				0.999	(−0.4)		
		3.4*	0.071	7.9	0.4				0.979		−21.0	20.9 ± 0.7
		4.4	0.141	15.3	0.9	0.69 ± 0.22	14.9 ± 6.1	46 ± 11	0.955			
		5.3	0.249	45.7	2.1	0.96 ± 0.12	23.0 ± 5.2	42 ± 7	0.901		−25.1	26.0 ± 0.8
		6.1	0.364	81.4	2.9	0.88 ± 0.08	29.7 ± 6.1	30 ± 5	0.861			
		6.9[d]	0.414	65.7	3.8				0.821		−24.9	27.1 ± 0.9
Fructose	2,200	0.5	0.043	1.4	0.0				0.998	(−0.4)		
		3.4*	0.071	5.5	0.4				0.983		−24.0	23.8 ± 0.7
		4.4	0.112	23.8	0.6	1.54 ± 0.22	76.3 ± 28.9	20 ± 7	0.972		−27.7	27.7 ± 0.7
		5.3	0.143	56.4	1.1	1.27 ± 0.12	72.6 ± 17.1	18 ± 4	0.950		−28.8	29.1 ± 0.7
		6.1	0.293	106.2	2.3	1.13 ± 0.08	50.5 ± 10.0	22 ± 4	0.888		−29.1	30.5 ± 0.8
		6.8[d]	0.413	60.0	4.1				0.805		−27.5	30.2 ± 0.9
D. inopinatus												
Fructose	1,500	0.0	0.002	0.5	0.1				0.995	(−0.9)		
(Expt. 1)		2.0*	0.021	0.3	0.4				0.981		−18.9	18.2 ± 0.7
		5.3	0.061		1.9				0.911			
		6.9	0.108		3.8				0.821			
		9.1	0.200		5.3				0.747			
		13.2	0.267	38.1	7.4	0.45 ± 0.02	5.4 ± 1.0	82 ± 14	0.647		−25.5	30.6 ± 1.3
		15.2	0.351	39.6	8.6	0.38 ± 0.02	4.8 ± 0.9	80 ± 13	0.590			
		19.1	0.410	46.0	8.2	0.30 ± 0.01	5.8 ± 1.1	52 ± 9	0.608		−23.1	28.6 ± 1.4
Fructose	1,500	0.0	0.002	0.1	0.1				0.997	(−0.9)		
(Expt. 2)		3.0	0.004		0.0				0.998			
		7.1	0.020		0.5				0.977			
		9.9*	0.017	1.4	0.8				0.964		−30.5	30.1 ± 0.7
		13.0	0.175		4.2				0.801			
		14.2	0.161		4.3				0.797			
		16.0	0.227	27.1	6.6	0.49 ± 0.03	4.4 ± 0.9	111 ± 18	0.686		−26.7	31.1 ± 1.2
		17.0	0.288		7.5				0.642			
		19.8	0.418	56.9	9.4	0.38 ± 0.02	6.4 ± 1.2	59 ± 10	0.553		−24.6	32.1 ± 1.7
Malate	1,500	0.0	0.003		0.0				1.000	(+1.0)		
		7.8	0.003	0.7	0.1				0.997			
		12.8*	0.009	1.0	1.6				0.924		−25.3	27.3 ± 0.8
		23.8	0.137	9.6	10.8	0.21 ± 0.02	0.9 ± 0.2	223 ± 36	0.485		−23.6	35.6 ± 2.3
		27.8	0.207	22.7	15.0	0.21 ± 0.01	1.6 ± 0.3	130 ± 21	0.284			
		32.8	0.263	(25.1)	15.8	0.16 ± 0.02	1.7 ± 0.6	96 ± 24	0.246		−17.8	40.0 ± 7.4
		35.7[d]	0.237	(22.6)	18.4				0.122			
		42.9[d]	0.278	25.0	18.4				0.124			
Lactate	1,500	0.0			0.6[e]				1.000	(−0.9)		
		1.0	0.012	0.8	0.8				0.992		−6.5	
		2.0	0.008		1.0				0.980			
		3.8	0.008		3.2				0.874			

(Continued)

TABLE 2 | Continued

Substrate	PO_4^{3-} (μM)	Time (days)	OD[b]	*N* (10^6 cells/ml)[c]	ΣH_2S (mM)	*k* (day^{-1})	*Y* (10^6 cells/ μmol SO_4^{2-})	csSRR (fmol/cell/day)	*f*	$\delta^{34}S$ sulfate	$\delta^{34}S$ sulfide	$^{34}\varepsilon$ (‰)
		4.9*	0.012	2.2	4.3				0.823		−9.4	10.0 ± 0.9
		5.9	0.028	(2.9)	5.9	0.29 ± 0.34	0.7 ± 1.1	397 ± 296	0.746			
		7.0	0.039	(5.3)	7.3	0.42 ± 0.16	1.3 ± 0.8	329 ± 131	0.679			
		7.9	0.085	(15.4)	8.8	0.64 ± 0.11	3.4 ± 1.5	191 ± 62	0.608			
		8.9	0.131	26.0	10.6	0.61 ± 0.05	4.2 ± 1.1	146 ± 34	0.525		−10.0	13.0 ± 1.2
		11.0	0.183	28.2	10.7	0.42 ± 0.03	4.5 ± 1.2	93 ± 21	0.520		−7.6	9.6 ± 1.2
		11.9	0.199	(40.0)	9.7	0.42 ± 0.05	7.8 ± 3.0	53 ± 17	0.565			
		12.9	0.256	55.9	13.8	0.40 ± 0.03	6.0 ± 1.4	67 ± 13	0.371		−6.8	10.1 ± 1.7
		13.9[d]	0.248	(50.5)	13.1				0.406			

Sulfur isotope values ($\delta^{34}S$) are reported with respect to V-CDT in permil (‰). The $\delta^{34}S$ values of initial sulfate are listed in parentheses. The initial concentration of sulfate was 21 ± 0.5 mM. Errors in k, Y, csSRR, and $^{34}\varepsilon$ were propagated from uncertainties (1σ) associated with measurements of sulfide concentration (ΣH_2S, ±10%), cell density (N, ±15%), and $\delta^{34}S$ (±0.5‰) by standard methods (Ku, 1969).

[a] Time points marked with an asterisk (*) were taken to be the beginning of exponential growth (t_1, see Calculations).

[b] Optical density measured at 630 nm for D. fructosovorans and 660 nm for D. inopinatus.

[c] Cell densities shown in parentheses are extrapolated from optical density data calibrated to microscopy-based cell counts.

[d] These time points represent cultures that have reached stationary phase, and as such, k, Y, and csSRR are not listed.

[e] Sulfide (0.6 mM) was carried over from the preculture of the D. inopinatus cultures grown on lactate with 1,500 μM PO_4^{3-}. The presence of this initial sulfide and its isotopic composition was accounted for in the calculation of f and $^{34}\varepsilon$ for this experiment.

1.5 g (see above). Phosphate was added to final concentrations of 360, 36, 5 μM, and "0" (<1 μM).

Analyses

Cell Counts and Sulfide Assays

Growth was monitored using optical density (OD) measurements and microscopic cell counts. OD was measured at 630 or 660 nm using a spectrophotometer (Synergy 2 microplate reader, BioTek, Winooski, Vermont, USA). For cell counts, subsamples of experimental cultures were preserved in 2.5% glutaraldehyde at 4°C. Preserved cells were stained with SYBR Green I nucleic acid stain (Invitrogen Molecular Probes, Eugene, Oregon, USA), and filtered onto Whatman 0.2 μm Nuclepore polycarbonate filters. Stained cells were visualized and imaged by epifluorescence microscopy using a Zeiss Axio Imager M1 microscope (Carl Zeiss Microscopy, LLC), and cell densities were determined by manual counting (Noble and Fuhrman, 1998). Cell lengths and widths were measured in the epifluorescence micrographs using measuring tools in Zeiss AxioVision software.

Sulfide from subsamples was precipitated as ZnS in a 50 mM zinc acetate solution, and stored at 4°C until analysis. Sulfide concentrations ($\Sigma H_2S = H_2S + HS^- + S^{2-}$) were determined by a modified methylene blue colorimetric method (Cline, 1969). Briefly, 200 μL samples of medium were reacted with 1 ml of 0.05 M zinc acetate and 10 μL of *N*,*N*-dimethyl-*p*-phenylenediamine sulfate solution. Optical density was read at 670 nm using a microplate reader (Sim et al., 2011b).

Sulfur Isotope Ratios

Sulfide was extracted for isotopic analysis by acidifying each ZnS sample with 3 to 6 M HCl, and gently boiling for 1 h under a stream of N_2 gas. Sulfate in samples were then converted to H_2S using a general reducing agent (HCl, HI, and H_3PO_2) (Thode et al., 1961; Forrest and Newman, 1977; Arnold et al., 2014). Volatiles were passed through a condenser and a distilled H_2O trap. H_2S produced in the reactions was precipitated as ZnS in zinc acetate, and then converted to Ag_2S via addition of silver nitrate, or precipitated as Ag_2S directly in a silver nitrate solution. The recovered Ag_2S was washed with deionized water, dried at 70°C, and converted to SF_6 by reaction with F_2 at 300°C overnight. The SF_6 product was purified by cryogenic trapping and preparative gas chromatography, and analyzed on a ThermoFinnigan MAT 253 isotope-ratio mass spectrometer operated in dual-inlet mode as described previously (Ono et al., 2006).

Sulfur isotope values are reported in the standard δ notation against Vienna Cañon Diablo Troilite (VCDT):

$$\delta^{34}S_{sulfide} = \frac{\left(^{34}S/^{32}S\right)_{sample}}{\left(^{34}S/^{32}S\right)_{VCDT}} - 1 \quad (1)$$

Following IUPAC recommendations (Coplen, 2011), we have omitted the factor of 1000‰ from the definition of δ in Equation 1.

Calculations

Specific growth rates (*k*) for the cultures were calculated using an exponential growth equation (Monod, 1949):

$$k_x = \frac{\ln\left(N_x/N_1\right)}{t_x - t_1} \quad (2)$$

where N_x and N_1 are the cell densities (number of cells per milliliter) at t_x and t_1, respectively (Sim et al., 2011b). Growth rates calculated in this manner represent an average of the cumulative growth of the organism over the time interval between the beginning of exponential growth (t_1) and the time at which the sample was taken (t_x).

Cellular growth yields (Y) were calculated with respect to amount of produced sulfide:[1]

$$Y_x = \frac{N_x - N_1}{[H_2S]_x - [H_2S]_1} \quad (3)$$

The cell-specific sulfate reduction rate (csSRR) is defined as the amount of sulfate reduced per cell per unit time, and can be described as:

$$\text{csSRR}_x = k_x / Y_x \quad (4)$$

In a batch culture, isotopic fractionation factors can be determined from a Rayleigh distillation equation for closed systems. Here, we use the measured isotopic composition of the produced sulfide ($\delta^{34}S_{sulfide}$) to calculate the fractionation factor α, assuming isotopic mass balance between sulfide and remaining sulfate:

$$\alpha = (\ln f)^{-1} \times \ln\left[1 - (1-f) \times \frac{\delta^{34}S_{sulfide} + 1}{\delta^{34}S_{initial} + 1}\right] \quad (5)$$

where $\delta^{34}S_{initial}$ and $\delta^{34}S_{sulfide}$ are the measured isotopic compositions of the initial sulfate in the media and the produced sulfide respectively, and f is the fraction of initial sulfate that remained at the time of sampling. The value of f is calculated from measured ΣH_2S concentrations and assuming that all consumed sulfate was reduced into sulfide.

The isotopic enrichment factor ($^{34}\varepsilon$) is defined as:

$$^{34}\varepsilon = 1 - {}^{34}\alpha \quad (6)$$

According to this definition, positive $^{34}\varepsilon$ values represent depletion of ^{34}S in sulfide with respect to sulfate.

[1]Cellular yield (Y) has units of cells per mole sulfate. It is a measure of the number of cells supported by a given amount of transferred electrons. Relating Y to biomass yield (i.e., g mol^{-1}) requires accounting for cell size differences.

RESULTS

Experiments with Different SRB Species and Substrates

Table 2 shows data from experiments that were designed to test the dependence of sulfur isotope fractionation on species (*D. fructosovorans* and *D. inopinatus*) and substrates (lactate, fructose, malate, or pyruvate). Batch cultures used in these experiments were typically grown to late exponential phase. Cultures of *D. fructosovorans* grew in media with fructose, pyruvate, or lactate as the organic substrate. Exponential growth was observed within 2 to 3 days, and experiments lasted for 7 days (**Figure A1**). Growth rates (k) on all three substrates ranged between 0.6 and 1.5 day^{-1}. Cultures of *D. inopinatus* grew in media that contained fructose, malate or lactate as the electron donors. Growth experiments with *D. inopinatus* lasted 14, 20, and 43 days, respectively, for cultures grown on lactate, fructose and malate, respectively, due to the longer lag phase (**Figure A1**). Growth rates of *D. inopinatus* in cultures grown on fructose and lactate were similar (0.40 and 0.44 day^{-1}, respectively), but were lower during growth on malate (0.17 day^{-1}). Sulfide concentrations in all cultures increased with the increasing cell densities (**Figure A1**). Cultures of *D. inopinatus* grown on malate produced more sulfide (up to 18 mM) than the 14 mM concentration predicted by incomplete malate oxidation (**Table 1**), perhaps indicating that some of the malate may have been oxidized completely to CO_2 or to small organic compounds.

D. inopinatus cells were both longer and wider than cells of *D. fructosovorans* and DMSS-1 (**Figure 1**). Cell morphology appeared to be mostly independent of organic substrate (**Table 4**), but small, measurable differences were observed in some cultures of *D. inopinatus*. Cells of *D. inopinatus* were on average ∼1 μm longer when grown on malate compared to fructose or lactate, and slightly wider (by ∼0.3 μm) when grown on fructose compared to malate or lactate. Cells of *D. fructosovorans* grown on different substrates did not exhibit measurable differences.

Calculated sulfur isotope enrichment factors ($^{34}\varepsilon$) ranged from 13 to 31‰ in *D. fructosovorans* cultures and from 10 to 40‰ in *D. inopinatus* cultures (**Table 2**). The smallest $^{34}\varepsilon$ values

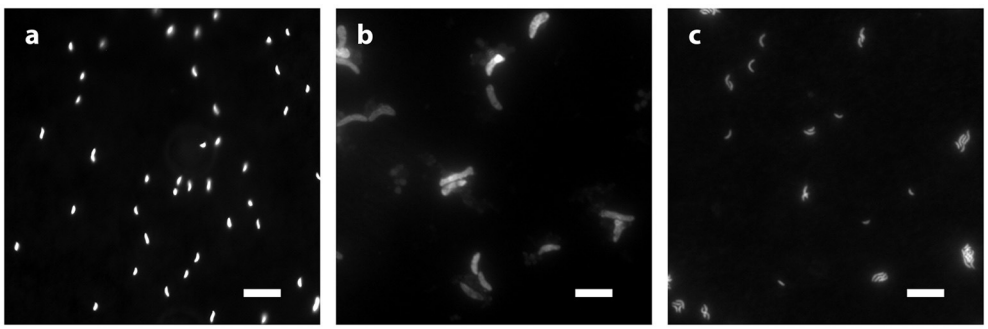

FIGURE 1 | Morphology of species growing in phosphate-rich media and visualized by epifluorescence microscopy: (a) *D. fructosovorans* (pyruvate, 2,200 μM PO_4^{3-}, 6.1 days); **(b)** *D. inopinatus* (malate, 1,500 μM PO_4^{3-}, 27.8 days); and **(c)** DMSS-1 (lactate, 360 μM PO_4^{3-}, 6.1 days). Scale bars in all panels represent 10 μm.

(averaging 13 and 11‰ for the two species, respectively) were observed in cultures grown on lactate. When grown on fructose, both bacteria exhibited 15–17‰ larger $^{34}S/^{32}S$ fractionations. The highest enrichment factors, up to 40‰, were observed in the cultures of *D. inopinatus* grown on malate (**Table 2**).

Experiments with Different Phosphate Concentrations

Data shown in **Table 3** are from experiments that test the effect of variable phosphate concentrations on *D. inopinatus* and DMSS-1. Cultures grown in media containing initial phosphate concentrations ≤15 and ≤5 μM for *D. inopinatus* and DMSS-1, respectively, had smaller growth rates and cell densities relative to cultures grown at higher phosphate levels (≥150 and ≥36 μM; **Figure A2**). At the lowest phosphate concentration (nominally <1 μM), the optical density of *D. inopinatus* increased slowly, but that of DMSS-1 did not increase over a period of 43 days. Sulfide was produced under all tested conditions, though *D. inopinatus* and DMSS-1, produced only up to 2.3 and 0.3 mM of sulfide, respectively, when no phosphate was added to the growth media (**Figure 4**). Growth rates and csSRR of *D. inopinatus* and DMSS-1 were the highest at 15 and 36 μM phosphate, respectively.

Low phosphate concentrations strongly influenced the cell morphology (**Table 4**). At the lowest phosphate condition (<1 μM), the average *D. inopinatus* cell was up to five times longer (**Figure 2**), whereas the average cell length of DMSS-1 increased up to three times relative to the phosphate-replete conditions. In addition, the variance (σ^2) in cell length (**Table 4**) was larger at lower phosphate concentrations: cell sizes at high concentrations of phosphate were rather uniform, but both "normal" single cells with typical lengths (∼7 μM) and extremely long chains (over 100 μm in *D. inopinatus* cultures, **Figure 2**) were present at low phosphate concentrations. The cell lengths were strongly correlated with the phosphate concentration in the cultures of both organisms (**Figure 3**), and cell lengths typically increased with time in each phosphate-limited experiment. Samples were vigorously vortexed prior to staining, filtration, and visualization. Because these procedures did not separate these long chain-looking cells and no cell wall was recognized, we counted them as single cells. However, microscopy-based cell counts were challenging because a single long chain-like cell (as long as 10 individual cells) can appear similar to a chain of several cells of shorter length located end-to-end (e.g., **Figure 2c**). These issues may cause some of the scatter in the growth rate and csSRR data, but should not affect the overall trends observed in this study.

The isotopic composition of sulfide was measured during mid-exponential growth phase in most of our experiments, with the exception of the culture of DMSS-1 grown with <1 μM initial phosphate, where $\delta^{34}S_{sulfide}$ was measured at 42.8 days, and growth was not detected at any point during the experiment. While measured $\delta^{34}S_{sulfide}$ values varied little, from −5.8 to −6.6‰ for *D. inopinatus* and from −3 to −4.7‰ for DMSS-1, the calculated enrichment factors ($^{34}\varepsilon$) decreased with decreasing phosphate concentrations (**Figure 4a**). The $^{34}\varepsilon$ values in *D. inopinatus* cultures grown with lactate decreased from 16‰ at 150 μM phosphate (similar to regular, phosphate-replete conditions) to 7‰ at <1 μM phosphate. The $^{34}\varepsilon$ values of DMSS-1 cultures decreased from 8 to 5‰ over a similar range of phosphate concentrations.

DISCUSSION

Variation of $^{34}\varepsilon$ with Substrates and Species

Differences among Species

Both *D. fructosovorans* and *D. inopinatus* discriminate against heavier isotopes of sulfur more when they grow on fructose ($^{34}\varepsilon \sim 30$‰) relative to the growth on lactate (10 to 15‰). Data from Sim et al. (2011b) for DMSS-1 growing on fructose (30 to 40‰) and lactate (∼6‰) in batch cultures exhibited the same trend and similar ranges of $^{34}\varepsilon$. Growth on pyruvate and malate yielded $^{34}\varepsilon$ values that were dissimilar among the studied species. While fractionations during the growth on pyruvate were larger than those during the growth on lactate and smaller than those during the growth on fructose for both *D. fructosovorans* and DMSS-1, $^{34}\varepsilon$ was ∼27‰ for the former species, but only 8‰ for the latter. The relatively high fractionation by pyruvate-grown *D. fructosovorans* contrasts with previous studies of sulfate reducing bacteria that oxidize organic substrates completely to CO_2. These microbes generally produce values of $^{34}\varepsilon$ smaller than 19‰ when oxidizing pyruvate to acetate in batch culture (Brüchert, 2004; Sim et al., 2011b). An increased fractionation may be a consequence of simultaneous fermentation and respiration of pyruvate, an effect that has been inferred in cultures of *D. vulgaris* Hildenborough and other species (Sass et al., 2002; Sim et al., 2013), and to which higher fractionations could be attributed (Sim et al., 2013). Another unexplained difference in fractionation is evident during the growth on malate by *D. inopinatus* (up to ∼40‰) and DMSS-1 (ca. 17‰). Such differences suggest that the magnitude of sulfur isotope fractionations is not a direct function of the organic substrate itself, but depends on the specific pathways by which organisms take up and oxidize organic compounds, transfer the reducing equivalents to sulfate (or instead to an organic compound via fermentation), and generate ATP.

$^{34}\varepsilon$ and csSRR

The trend in $^{34}\varepsilon$ vs. csSRR for *D. fructosovorans* generally resembles the inverse correlations reported by several previous studies (Harrison and Thode, 1958; Kaplan and Rittenberg, 1964; Chambers et al., 1975; Kleikemper et al., 2004; Hoek et al., 2006; Sim et al., 2011a,b; Leavitt et al., 2013). Data from several of these studies are shown in **Figure 5a**. *D. inopinatus* data fall within the range observed for other *Desulfovibrio* species, but there is no clear trend between $^{34}\varepsilon$ and csSRR; this may be in part due to the high fractionations observed during growth on malate. In general, trends for different species are subparallel in $^{34}\varepsilon$–$\log_{10}$(csSRR) space, have different slopes and intercepts, and may be offset by several orders of magnitude in csSRR. These observations are evidence of the complexity that depends on species-specific responses to substrates and growth conditions.

TABLE 3 | Physiological and isotopic data for batch cultures of *D. inopinatus* and DMSS-1 grown on lactate in the presence of varying concentrations of phosphate (PO_4^{3-}).

Substrate	PO_4^{3-} (μM)	Time[a] (days)	OD[b]	*N* (10^6 cells/ml)[c]	ΣH_2S (mM)	*k* (day^{-1})	*Y* (10^6 cells/ μmol SO_4^{2-})	csSRR (fmol/cell/day)	*f*	$\delta^{34}S$ sulfate	$\delta^{34}S$ sulfide	$^{34}\varepsilon$ (‰)
D. inopinatus												
Lactate	150	0.0		(2.0)	0.0				1.000	(+0.9)		
		7.0*	0.021	5.2	3.0				0.858			
		9.8	0.079	(13.5)	12.4	0.34 ± 0.12	0.9 ± 0.5	388 ± 89	0.408			
		10.9	0.105	(17.5)	16.4	0.31 ± 0.05	0.9 ± 0.2	339 ± 56	0.219			
		12.9	0.164	(25.2)	16.6	0.26 ± 0.06	1.5 ± 0.6	180 ± 42	0.210		−5.8	16.0 ± 4.1
		16.0	0.197	(29.7)	17.0	0.19 ± 0.04	1.7 ± 0.7	111 ± 26	0.188			
		17.8[d]	0.192	(29.0)	16.8				0.201			
		20.8[d]	0.183	27.5	17.5				0.167			
		21.8[d]	0.196	(29.6)	15.4				0.267			
	15	0.0		(0.4)	0.0				1.000	(+0.9)		
		6.0	0.016	(1.4)	0.5				0.977			
		9.9*	0.022	0.9	2.7				0.869			
		12.8	0.039	(2.9)	5.7	0.40 ± 0.11	0.7 ± 0.3	577 ± 165	0.729			
		16.8	0.099	8.4	15.4	0.33 ± 0.03	0.6 ± 0.1	547 ± 91	0.267		−6.2	14.8 ± 2.9
		19.8	0.115	(7.9)	17.6	0.22 ± 0.03	0.5 ± 0.2	463 ± 111	0.164			
		20.8	0.138	(9.4)	16.3	0.22 ± 0.03	0.6 ± 0.2	341 ± 83	0.224			
		26.8[d]	0.114	8.5	17.1				0.187			
		28.0[d]	0.226	14.0	17.3				0.178			
	3	0.0			0.0				1.000	(+0.9)		
		6.9	0.006		0.0				0.998			
		8.8*	0.008	0.7	0.1				0.996			
		12.8	0.020	0.8	1.1	0.03 ± 0.05	0.1 ± 0.2	311 ± 50	0.948			
		15.7	0.031	(4.5)	3.0	0.26 ± 0.05	1.3 ± 0.5	203 ± 46	0.857			
		20.8	0.026	(3.4)	3.3	0.13 ± 0.03	0.8 ± 0.3	155 ± 34	0.841		−6.6	8.2 ± 0.8
		22.7	0.033	(4.9)	3.9	0.14 ± 0.02	1.1 ± 0.4	125 ± 28	0.814			
		25.7[d]	0.028	3.8	4.9				0.768			
		26.9[d]	0.020	(2.2)	2.2				0.896			
	<1	0.0	0.001		0.0				1.000	(+0.9)		
		8.0*	0.010	0.3	0.3				0.984			
		9.9[e]	0.016	(0.4)	0.7	0.14 ± 0.18	0.2 ± 0.3		0.966			
		11.9[e]	0.012	(0.3)	1.0	0.02 ± 0.09	0.0 ± 0.2		0.953			
		16.0[e]	0.016	(0.3)	1.3	0.03 ± 0.04	0.1 ± 0.1		0.940		−6.1	7.3 ± 0.8
		19.8[e]	0.014	(0.3)	1.3	0.02 ± 0.03	0.1 ± 0.1		0.940			
		20.8[e]	0.014	0.3	1.0	0.01 ± 0.02	0.1 ± 0.1		0.954			
		26.8[e]	0.022	(0.4)	2.3	0.02 ± 0.02	0.1 ± 0.1		0.893			
***Desulfovibrio* sp. DMSS-1**												
Lactate	360	0.0			0.0				1.000	(+1.1)		
		3.1*	0.006	2.9	0.8				0.964			
		4.2	0.067	(12.2)	6.6	1.31 ± 0.28	1.6 ± 0.7	824 ± 180	0.684			
		5.0	0.072	(12.9)	9.7	0.76 ± 0.16	1.1 ± 0.5	676 ± 147	0.538		−4.8	8.2 ± 1.1
		6.1	0.111	18.8	10.7	0.61 ± 0.05	1.6 ± 0.3	379 ± 55	0.493			
	36	0.0			0.0				1.000	(+1.1)		
		3.1*	−0.004	1.3	0.8				0.962			
		4.2	0.060	(11.1)	5.2	1.91 ± 0.30	2.2 ± 0.8	862 ± 204	0.753		−3.0	4.8 ± 0.9
		5.0	0.095	(16.4)	12.0	1.26 ± 0.17	1.3 ± 0.5	939 ± 223	0.430			
		6.1[d]	0.095	(16.4)	11.3				0.461			
		7.0[d]	0.095	(16.4)	10.9				0.480			

(Continued)

TABLE 3 | Continued

Substrate	PO_4^{3-} (μM)	Time (days)	OD[b]	*N* (10^6 cells/ml)[c]	ΣH_2S (mM)	*k* (day^{-1})	*Y* (10^6 cells/ μmol SO_4^{2-})	csSRR (fmol/cell/day)	*f*	$\delta^{34}S$ sulfate	$\delta^{34}S$ sulfide	$^{34}\varepsilon$ (‰)
	5	0.0	0.001	(2.2)	0.0				1.000	(+1.1)		
		4.0*	0.006	(3.0)	1.0				0.950			
		6.0	0.016	(4.5)	2.2	0.21 ± 0.20	1.3 ± 1.3	165 ± 47	0.894		−3.9	5.3 ± 0.8
		13.0	0.038	(7.7)	7.7	0.11 ± 0.04	0.7 ± 0.4	149 ± 35	0.631			
		14.9[d]	0.036	(7.5)	8.2				0.612			
		20.8[d]	0.037	(7.6)	11.7				0.445			
	<1	0.0		(1.8)	0.0				1.000	(+1.1)		
		7.9	0.001	(2.2)	0.0				1.000			
		13.0	0.000	(1.8)								
		14.8*	0.000	(2.1)	0.0				0.999			
		21.7[e]	0.000	(1.6)	0.0	−0.04 ± 0.05	227 ± 7216		1.000			
		28.9[e]	0.000	(2.0)	0.0	0.00 ± 0.03	−1.6 ± 26.9		0.998			
		35.7[e]	0.002	(2.4)	0.3	0.01 ± 0.02	1.0 ± 3.3		0.986			
		42.8[e]	0.001	(2.2)	0.2	0.00 ± 0.01	0.6 ± 4.4		0.991		−4.7	5.9 ± 0.7

*See caption of **Table 2** for explanations of data columns.*

[a] *Time points marked with an asterisk (*) were taken to be the beginning of exponential growth (t_1, see Calculations).*

[b] *Optical density measured at 660 nm.*

[c] *Cell densities shown in parentheses are extrapolated from optical density data calibrated to microscopy-based cell counts.*

[d] *These time points represent cultures that have reached stationary phase, and as such, k, Y, and csSRR are not listed.*

[e] *No growth and/or sulfide production was detected. Uncertainties in k and/or Y exceed the values themselves; therefore, csSRRs calculated for these time points would be spurious and are not listed.*

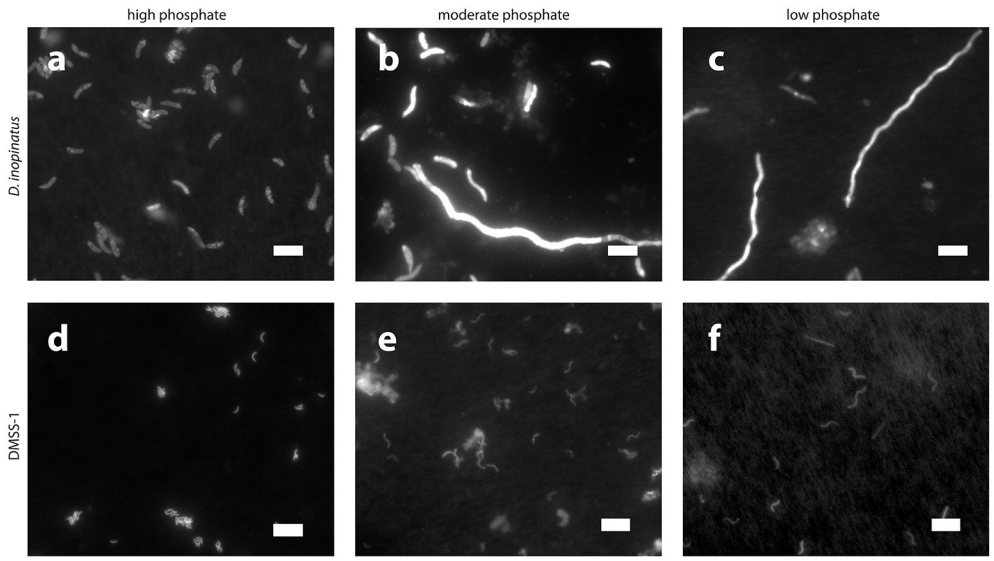

FIGURE 2 | Epifluorescence photomicrographs of cultures grown on lactate in the presence of different concentrations of phosphate. Top row, *D. inopinatus* in **(a)** 1,500 μM PO_4^{3-} (12.9 days); **(b)** 15 μM (14.7 days); and **(c)** <1 μM (8.0 days). Bottom row, DMSS-1 in **(d)** 360 μM PO_4^{3-} (6.1 days, see also **Figure 1c** for inset); **(e)** 5 μM (13.0 days); and **(f)** <1 μM (42.8 days). Scale bars represent 10 μm. Panels **(b,c,f)** show long chain-like single cells.

Cell Size and $^{34}\varepsilon$

The three *Desulfovibrio* species have very different cell sizes despite their grossly similar vibrioid morphology (**Figure 1**), and generally, higher sulfate reduction rates are observed in the larger cells. To test whether the surface areas or volumes of cells account for some of the observed differences in csSRR between species, we expressed $^{34}\varepsilon$–$\log_{10}$(sulfate reduction rate) relationships per unit of cell surface area or volume. To estimate the surface areas and volumes, we measured the cell dimensions of *D. inopinatus*, *D. fructosovorans* and DMSS-1 grown in this study and those of DvH previously grown in our laboratory (Sim et al., 2013; **Table 4**). The csSRR values were divided by either surface area or volume, and expressed as "cell area (or volume) normalized sulfate reduction rate" [canSRR or cvnSRR;

TABLE 4 | Cell sizes (values are mean ± 1σ measured on $n > 30$ cells).

Strain	Substrate	PO_4^{3-} (μM)	Time (days)	Length (μm)	Width (μm)	Surface area (μm^2)	Volume (μm^3)
D. fructosovorans	Lactate	2,200	6.1	2.7 ± 0.5	1.0 ± 0.2	10 ± 3	2.1 ± 1.0
	Pyruvate	2,200	6.1	2.5 ± 0.5	0.9 ± 0.1	8 ± 2	1.6 ± 0.7
	Fructose	2,200	6.1	2.7 ± 0.4	1.0 ± 0.1	10 ± 2	2.0 ± 0.7
D. inopinatus	Fructose	1,500	13.2	6.3 ± 1.1	2.1 ± 0.3	49 ± 11	22.3 ± 7.7
	(Expt. 1)		19.1	6.7 ± 1.4	2.1 ± 0.2	50 ± 12	22.7 ± 7.7
	Fructose	1,500	16.0	7.1 ± 1.4	2.3 ± 0.3	59 ± 14	29.4 ± 10.3
	(Expt. 2)		19.8	6.4 ± 1.1	1.8 ± 0.3	42 ± 11	17.2 ± 7.4
	Malate	1,500	12.8	8.1 ± 1.8	1.7 ± 0.3	48 ± 13	18.7 ± 7.6
			27.8	7.6 ± 1.3	1.7 ± 0.3	47 ± 13	18.8 ± 7.4
	Lactate	1,500	8.9	6.8 ± 1.6	1.7 ± 0.3	41 ± 8	16.2 ± 5.1
			12.9	7.0 ± 1.3	1.8 ± 0.3	45 ± 8	18.0 ± 5.5
		150	7.0	11.4 ± 4.5	1.9 ± 2.9	73 ± 102	32.1 ± 76.1
			10.9	10.0 ± 2.0	1.1 ± 0.2	38 ± 9	10.4 ± 3.5
		15	16.8	9.3 ± 2.6	1.9 ± 0.5	63 ± 23	28.7 ± 15.3
			28.0	12.4 ± 8.0	1.9 ± 0.4	79 ± 52	36.3 ± 31.5
		3	8.8	23.2 ± 13.9	1.9 ± 0.3	148 ± 96	71.1 ± 54.7
			25.7	18.8 ± 16.5	1.9 ± 0.4	125 ± 119	61.9 ± 69.6
		<1	8.0	18.8 ± 9.0	1.7 ± 0.3	106 ± 52	44.9 ± 25.7
			20.8	30.3 ± 22.3	2.0 ± 0.4	201 ± 152	102.6 ± 92.0
Desulfovibrio sp. DMSS-1	Lactate	3,600[a]	3	2.3 ± 0.5	–	–	–
			–	1.8 ± 0.2	–	–	–
			–	1.9 ± 0.3	–	–	–
			–	2.3 ± 0.4	–	–	–
		360	3.1	2.6 ± 1.0	0.7 ± 0.1	6 ± 2	0.9 ± 0.5
		36	5.0	3.1 ± 0.9	0.5 ± 0.1	6 ± 2	0.7 ± 0.3
		5	13.0	4.7 ± 1.4	0.7 ± 0.1	11 ± 4	1.9 ± 1.2
		<1	21.7	4.6 ± 1.5	0.7 ± 0.1	12 ± 4	2.1 ± 1.1
			42.8	6.8 ± 2.3	0.7 ± 0.1	17 ± 7	3.1 ± 1.6
D. vulgaris Hildenborough[b]	Pyruvate	–	–	2.9 ± 0.8	0.8 ± 0.1	9 ± 3	1.7 ± 0.7

Surface areas and volumes were calculated for individual cells by approximating each cell as a cylinder.

[a] *Data from Sim et al. (2011b) for batch and continuous cultures of DMSS-1.*

[b] *Data from microscopy images taken by Sim et al. (2013) of a continuous culture of D. vulgaris Hildenborough.*

units of fmol H_2S $(\mu m)^{-2}$ day^{-1} or fmol H_2S $(\mu m)^{-3}$ day^{-1}, respectively]. **Figures 5b,c** show the $^{34}\varepsilon$ data for these species plotted against sulfate reduction rates normalized in this manner. Non-linear least-squares regression of a modified Michaelis-Menten-type equation (see **Figure 5** legend) to plots of $^{34}\varepsilon$ against canSRR or cvnSRR has higher coefficients of determination (R^2) of 0.55 or 0.56 (respectively), compared to 0.43 for $^{34}\varepsilon$ against csSRR. Thus, normalizing sulfate reduction rates to either cell surface area or cell volume reduces the scatter of the data (**Figure 5**). The improved fits may arise from the distribution of membrane transport proteins across the cell surface, and from the constraints on the amounts of enzyme in a single cell by the cell volume (Pomeroy et al., 2007). This result underscores similarities in the isotopic signals produced per unit of membrane area or biomass of different cultured sulfate reducing microbes, in spite of their differing cell geometries, growth rates, and capacities to oxidize different electron donors. We hypothesize that the larger cells require more energy (electrons) per cell to synthesize cellular components, and therefore exhibit higher csSRR values. Normalizing the sulfate reduction rate to cell volume eliminates that inherent difference amongst microbial species. Alternatively or additionally, larger cells also have larger surface areas that allow larger fluxes of sulfate in to the cell through the cell membrane.

We recognize that cell sizes almost certainly cannot explain all of the variation between the subparallel $^{34}\varepsilon$–$\log_{10}$(csSRR) trends, and other factors such as the capacity for complete oxidation of organic substrates, growth temperature, and efficiency of sulfate transport may be important (Detmers et al., 2001; Canfield et al., 2006; Bradley et al., 2015). However, similarities amongst the normalized data for several *Desulfovibrio* species strongly indicate that biomass and cell sizes influence the observed $^{34}\varepsilon$ in experimental and environmental studies. Ideally, we would compare our results to more of the previously published $^{34}\varepsilon$

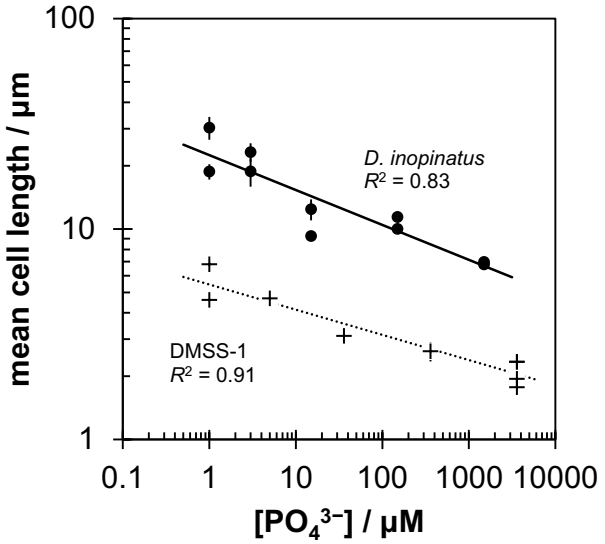

FIGURE 3 | Relationship between mean cell length and initial phosphate concentration in cultures of *D. inopinatus* (•) and DMSS-1 (+) grown on lactate. Data are from **Table 4**. Vertical error bars are 1 s.e.m. (standard error of the mean). For DMSS-1, error bars are smaller than the symbols.

values reported for SRB and archaea. However, neither the original descriptions of the SRBs, nor previous isotopic studies of MSR provide detailed cell size measurements that are required for this type of analysis. Rather, they report cell size ranges and do not examine the dependence of the cell size on the growth condition. The broad variations in these ranges translate into a large range of cell volumes and do not allow meaningful comparisons with our data. We encourage future studies of MSR in pure cultures to report cell sizes or biomass as functions of growth condition.

Fractionation of Sulfur Isotopes under Phosphorus Limitation

Morphological and Physiological Effects

Both *D. inopinatus* and DMSS-1 had slower growth rates (k) when limited by phosphate (**Figure 4b** and **Table 3**). The growth rate data for *D. inopinatus* are in good agreement with the Monod equation (Equation 7) (Monod, 1949) for a half-saturation constant (K_M) of ~10 µM phosphate (**Figure 4b**). Growth rates for DMSS-1 are more scattered but also decrease below ~10 µM phosphate.

$$k = k_{max}\frac{[PO_4^{3-}]}{K_M + [PO_4^{3-}]} \quad (7)$$

Phosphate limitation at ~10 µM for these species is similar to observations of phosphate limited growth at <12 µM for *D. desulfuricans* (Okabe and Characklis, 1992) and ~10 µM for *D. alaskensis* G20 (Bosak et al., 2016), suggesting that many *Desulfovibrio* species may use similar mechanisms to

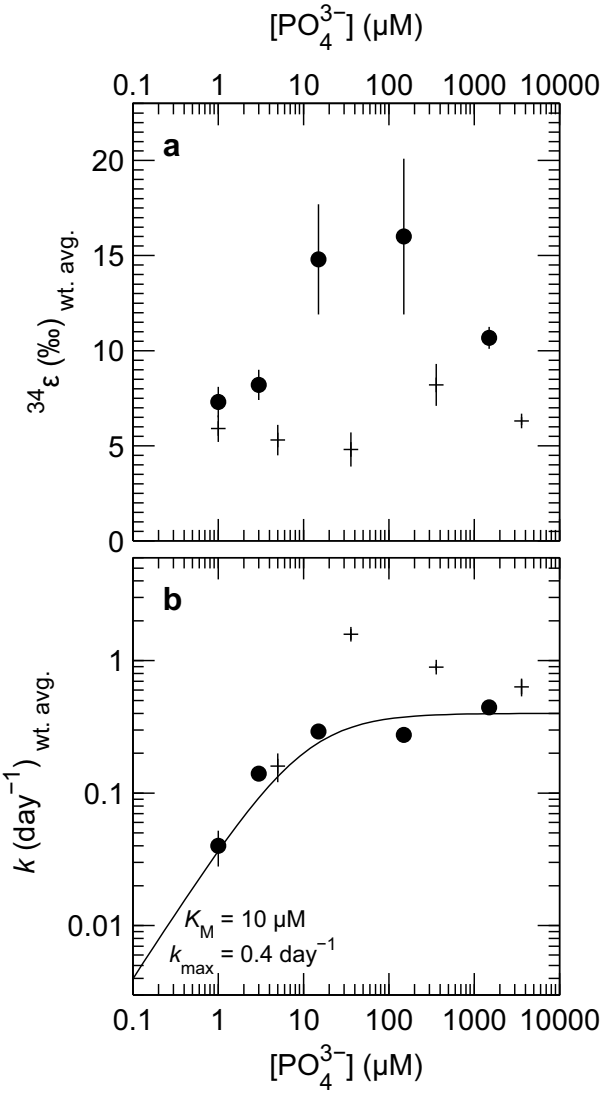

FIGURE 4 | Plot of weighted mean (a) isotope fractionation ($^{34}\varepsilon$) and **(b)** growth rate (k) for batch cultures of *D. inopinatus* (•) and DMSS-1 (+) grown on lactate at different initial concentrations of phosphate. Data from individual bottles were weighted by $1/\sigma^2$. Vertical error bars are 1σ for the weighted means, calculated following Bevington and Robinson (2002). Points corresponding to experiments in which phosphate was <1 µM are plotted at 1 µM. Data for DMSS-1 grown in 3,600 µM phosphate are from Sim et al. (2011b). The curve in **(b)** is a fit of the Monod equation (see Equation 7) (Monod, 1949), to the *D. inopinatus* data.

acquire phosphate during growth. Cellular yields (Y) decreased by several fold at lower phosphate concentrations (**Table 3**). Lower cell yields were also observed by Okabe and Characklis (1992) when the phosphate concentration was about 10 µM for *D. desulfuricans* grown in a chemostat; the C:P ratio of cells started to increase before the cell yield began to decrease. Thus, cells first adapted to moderately low phosphorus concentrations by reducing the cellular requirement for P. When the phosphorus availability decreased even further, cell yields

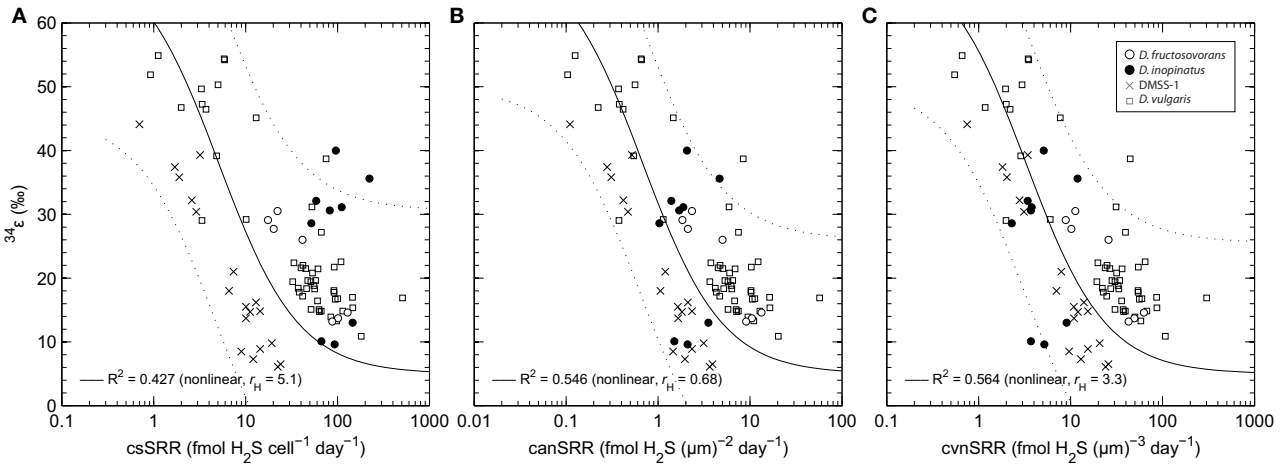

FIGURE 5 | Comparison of correlations between (a) $^{34}\varepsilon$ and cell-specific sulfate reduction rate (csSRR); **(b)** $^{34}\varepsilon$ and cell area-normalized sulfate reduction rate (canSRR); and **(c)** $^{34}\varepsilon$ and cell volume-normalized sulfate reduction rate (cvnSRR) for several *Desulfovibrio* spp. grown in culture under nutrient-replete conditions. In **(a)**, the DMSS-1 and *D. vulgaris* (Hildenborough) data are from Sim et al. (2011b) and Leavitt et al. (2013), respectively. In **(b,c)**, the sulfate reduction rates have been normalized using the cell size data shown in **Table 4**. The solid curve and coefficient of determination (R^2) represent non-linear least squares fits of a model function through all data in each panel. Equations describing the curves are of the form: $y = {}^{34}\varepsilon_{max} - x \cdot ({}^{34}\varepsilon_{max} - {}^{34}\varepsilon_{min})/(r_H + x)$, where $^{34}\varepsilon_{max} = 71‰$ (equilibrium at ~20°C and pH ~7.0; (Millero et al., 1988; Otake et al., 2008)), $^{34}\varepsilon_{min} = 5‰$ (high-rate asymptote, see Appendix), and r_H is a fitted parameter that has the same units as the *x*-axis (it represents the sulfate reduction rate at which $^{34}\varepsilon$ is halfway between its maximum and minimum limits). This equation was chosen because it can closely approximate model results of Wing and Halevy (2014) for the typical range of csSRR observed in experiments (see Appendix), and because R^2 for fits to this equation are uniformly higher than for linear least squares regressions of $^{34}\varepsilon$ against the log-transformed rates. Dotted envelope marks the non-simultaneous 95% prediction band.

began to decrease as well. Morphological changes observed in the two *Desulfovibrio* spp. we tested (see below), as well as structural adaptations to phosphate limitation and starvation observed in *D. desulfuricans* (Weimer et al., 1988) and *D. alaskensis* G20 (Bosak et al., 2016) are consistent with the higher bulk C:P ratio in phosphate-limited *D. desulfuricans* (Okabe and Characklis, 1992).

D. inopinatus and DMSS-1 cells elongated up to several hundred percent in the lowest phosphate conditions (**Table 4**). Cell elongation also occurs in phosphate limited cultures of *D. alaskensis* G20 (Bosak et al., 2016), albeit the overall effect in this microbe is smaller. Microscopic images of phosphate-limited *D. inopinatus* (**Figure 2**) revealed long chain-like cells as well as cells with more "typical" lengths. We attribute this cell morphology to incomplete cell division. Nucleic acids (particularly RNA, Elser et al., 2008; Yao et al., 2015) contain a very large fraction (up to tens of percent) of total cellular phosphorus; minimizing DNA and RNA synthesis and division may therefore enable survival in a competitive environment (see also Appendix). Growing phosphate-limited *D. alaskensis* G20 also replaces its membrane phospholipids by phosphorus-free lipids, synthesizes carbon-rich storage granules and metabolizes nucleic acids (Bosak et al., 2016). Cell elongation and the formation of intracellular carbon-rich granules may also aid in nutrient acquisition by increasing the surface area-to-volume ratio (Thingstad et al., 2005; Godwin and Cotner, 2015; Bosak et al., 2016). Also expected are decreases in the pools of phosphorus-containing metabolites dissolved in the cytoplasm: these metabolites should consist principally of inorganic phosphate, P_i. Below, we discuss how a diminished cytoplasmic phosphorus content can influence the kinetics of enzymatic processes and influence the correlation between $^{34}\varepsilon$ and csSRR.

Sulfur Isotope Fractionation

Phosphorus-limited *D. inopinatus* and DMSS-1 cultures grown on lactate did not fractionate sulfur isotopes very much (~5 to 8‰). These $^{34}\varepsilon$ values were generally lower in phosphate-limited than in phosphorus-replete cultures (**Figure 4a**) and we did not observe a distinct correlation with csSRR. In contrast, $^{34}\varepsilon$ values in DMSS-1 cultures grown in iron- and ammonium-limited media were ~5 and ~1‰ higher relative to the cultures grown in nutrient-replete media (Sim et al., 2012). The lower selectivity of the two phosphate-limited SRB species for sulfur isotopes may be related to any number of physiological changes experienced by cells at low phosphate concentrations: the composition and appearance of cell membranes and envelopes, the accumulation of storage polymers, transport of metals and others (Bosak et al., 2016). Some possibilities that directly influence the sulfate reducing pathway are discussed below.

The fitted half-saturation constant ($K_M = 10$ μM, **Figure 4**) appears to coincide with the phosphate concentration at which the isotopic fractionation changes from <10‰ to >10‰ for *D. inopinatus*. Phosphate-limited DMSS-1 cultures exhibit $^{34}\varepsilon$–$\log_{10}$(csSRR) values that fall off and plot to the right (higher csSRR) of the trend observed by Sim et al. (2011b) (**Figure 6**). The large heterogeneity in cell lengths of *D. inopinatus* at low phosphate concentrations (**Table 4** and **Figure 2**) complicates interpretations of csSRR, but assuming that per-cell enzyme activities scale linearly with either cell volume or surface area, the

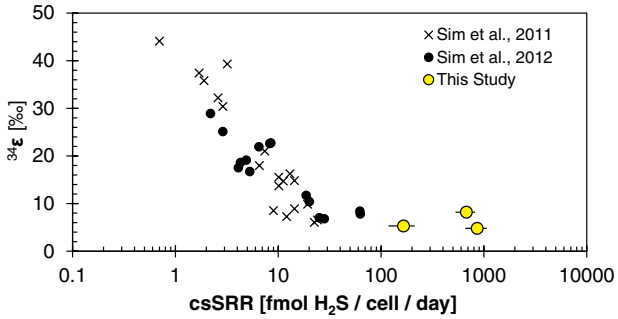

FIGURE 6 | Plot of $^{34}\varepsilon$ and cell-specific sulfate reduction rate (csSRR) observed for DMSS-1 grown on various substrates (Sim et al., 2011b), and under nutrient-limited conditions [(Sim et al., 2012) and this study].

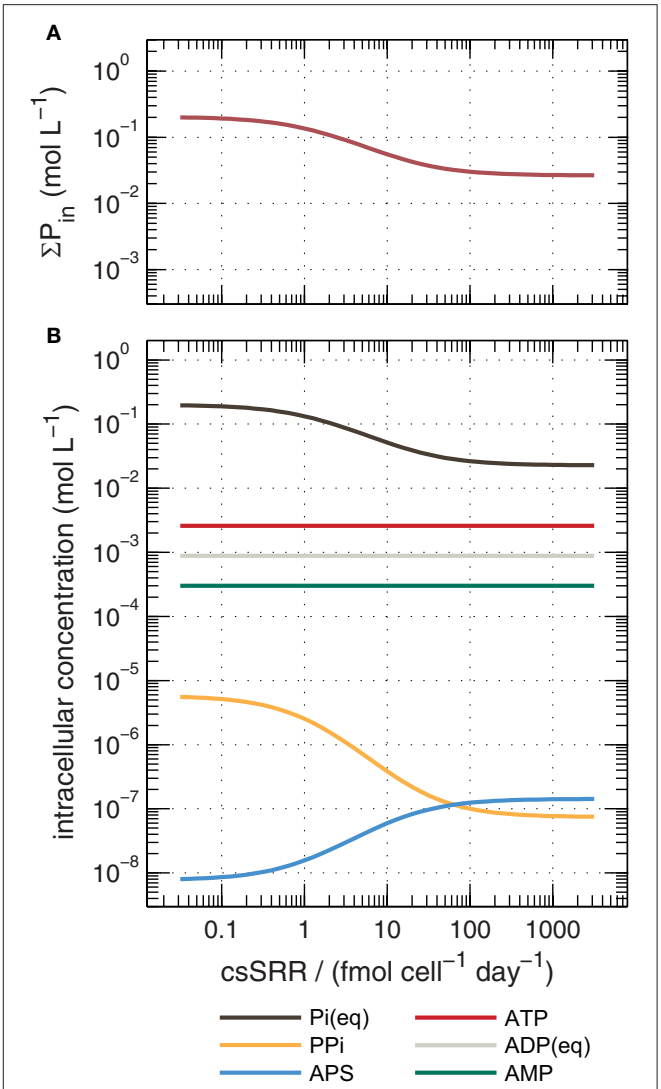

FIGURE 7 | Calculated concentrations of cytoplasmic phosphorus species during sulfate reduction by DMSS-1 predicted by an extended version of the model of Wing and Halevy (2014), described in the Appendix. Shown are **(a)** total intracellular phosphorus (ΣP_{in}, the sum of all species in panel, **b**), and **(b)** concentrations of individual species. Calculations assumed $\left[SO_4^{2-}\right]_{out} = 20$ mM and $[H_2S] = 1$ mM. P_i, inorganic orthophosphate; PP_i, pyrophosphate; APS, adenosine-5′-phosphosulfate; ATP, adenosine triphosphate; ADP, adenosine diphosphate; AMP, adenosine monophosphate.

increases in cell size (up to threefold for DMSS-1, **Table 4**) related to phosphate depletion cannot explain up to tenfold higher csSRRs. The elevated rates may additionally reflect changes in biochemical kinetics within the cell.

Rees (1973) introduced the reversibility of steps in the respiratory chain as a control on overall sulfur isotope fractionation, and this concept has been invoked or extended to explain features of many experimental datasets (Trudinger and Chambers, 1973; Eckert et al., 2011; Sim et al., 2011a,b; Brunner et al., 2012; Antler et al., 2017). More recently, Wing and Halevy (2014) proposed a quantitative model of dissimilatory sulfate reduction that uses enzyme kinetic and thermodynamic data to calculate $^{34}\varepsilon$ values as a function of csSRR. Their model explicitly calculates reversibilities, and thereby isotopic fractionations, for each enzymatic step in MSR. This approach offers insights into links between phosphorus, the sulfate reducing pathway and sulfur isotope fractionations. Phosphorus-containing metabolites (including the adenosine phosphates and inorganic pyrophosphate (PP_i)) influence the thermodynamic drive of reactions in the respiratory chain of sulfate reducers (Equations A1–A4), and their cytoplasmic concentrations are either assumed or explicitly predicted in their model (**Figure 7b**). The major conclusion of Wing and Halevy's study is that concentrations of intracellular metabolites dictate the energetic favorability and reversibility (ratio of backwards to forwards fluxes) at each step, and influence the overall sulfate reduction rate and the expression of kinetic and equilibrium isotope effects.

We reconstructed the numerical simulations of Wing and Halevy (2014), and extended them to simulate the changes in intracellular concentrations of orthophosphate (P_i) and other phosphorus-containing metabolites as a function of csSRR. The most salient features of the model are described in the Appendix. Our model results suggest that high csSRRs are associated with lower phosphorus contents within the cytoplasm (**Figure 7a**). This is a direct consequence of Wing and Halevy's finding that reduction of adenosine-5′-phosphosulfate (APS) to sulfite (Equation A3) is the primary rate-limiting step in MSR under conditions probed by most experiments. Because $[PP_i]$ depends on $[P_i]^2$ (according to Equation A6), and because P_i accounts for most phosphorus that is dissolved in the cytoplasm (see discussion in Appendix), a small decrease in total cytoplasmic phosphorus during phosphorus-limited growth and starvation induces a large decrease in the PP_i concentration. Lowered PP_i levels are counterbalanced by an increase in the concentration of APS (because Equation A2, sulfate activation to APS, is always near equilibrium; *Sat* in **Figure A3a**), as shown in **Figure 7b**. The buildup of [APS] associated with lowered $[P_i]$ increases the thermodynamic drive for APS reduction (Equation A3). Intuitively, APS reduction becomes less reversible (*Apr* in **Figure A3a**), and therefore isotope fractionation between APS

and the instantaneous sulfite product approaches the intrinsic kinetic isotope effect for this enzymatic step (22‰ in the default model of Wing and Halevy). Because the remaining step (sulfite reduction, Equation A4) is downstream of APS reduction and is almost fully reversible (*dSiR* in **Figure A3a**), the $\delta^{34}S$ value of H_2S is not sensitive to the kinetic isotope effect assumed for *dSiR* (in agreement with some experimental results, Leavitt et al., 2015, 2016) and is ∼22‰ lower than that of APS when csSRR is high (**Figure A3b**).

Modeled $^{34}\varepsilon$ values asymptote to a limit of ∼5 ± 2‰ at high csSRRs, in good agreement with our data from DMSS-1 cultures (**Figure A4**). Several assumptions built into the model require further examination to determine if they are applicable under nutrient-limited conditions. In particular, this includes the parameterization of the scaling factor $u_{vivo-vitro}$ (see Appendix). Although the agreement with our data may be circumstantial, the above treatment suggests a plausible mechanistic link between low extracellular phosphate concentrations and small $^{34}\varepsilon$ both in the laboratory and in the environment. How phosphate limitation affects the fractionation of sulfur isotopes during growth on substrates that typically produce large fractionations (e.g., fructose) is an open question. The above analysis predicts a decrease in $^{34}\varepsilon$ and increase in csSRR; a hypothesis that can be experimentally tested.

Studies of the sulfur cycle and the sulfur isotope record may benefit from consideration of the possible effects of phosphate limitation. While phosphorus is unlikely to limit growth of sulfate reducing bacteria in modern anoxic sediments where porewater phosphate concentrations are tens of micromolar or greater (Sundby et al., 1992), some studies hypothesize a more limited delivery flux of phosphate to Precambrian sediments (Bjerrum and Canfield, 2002; Reinhard et al., 2017). The very low sulfur isotope fractionation in sedimentary sulfates and sulfides during most of the Precambrian (Canfield, 1998) are consistent with this hypothesis. Overall, our data emphasize potential contributions of organic substrates and phosphate limitation to the persistently low sulfur isotope fractionations in the Archean and most of the Proterozoic.

CONCLUSIONS

The magnitudes of sulfur isotope fractionation by the three studied species of *Desulfovibrio* scale with the negative logarithm of the cell-specific sulfate reduction rate, and the trend does not appear to depend on the particular organic substrate. These findings are in agreement with previous observations from pure cultures of several other species of sulfate reducing microorganisms and support the idea that the quality of organic substrates and the availability of nutrients, particularly those involved in energy conservation, are key factors in regulating the intracellular fluxes of sulfur compounds and the expression of sulfur isotope effects during dissimilatory sulfate reduction. Clear trends appear to link sulfur isotopic fractionation and microbial sulfate reduction rates, but with large spread in the data. Normalizing the sulfate reduction rates to the cell surface area or cell volume can reduce the spread and improve the correlation between sulfur isotope fractionation and sulfate reduction rate for several *Desulfovibrio* spp.

The cells of two species of SRB grown on lactate elongate and form chain-like cells during phosphate limitation (<10 μM initial phosphate), their cell-specific sulfate reduction rates increase relative to the phosphate-replete cultures, and their sulfur isotope fractionations approach ∼5‰. Thus, sulfur isotope fractionation during microbial sulfate reduction in phosphorus-poor environments could deviate from predictions made under the assumption of unlimited phosphate supply. These experimental results are consistent with biochemical models that relate the kinetics and thermodynamics of enzyme-mediated reactions in the respiratory chain of SRB to expressed sulfur isotope effects.

AUTHOR CONTRIBUTIONS

SO, TB, SZ, and DW: Designed the study. SZ: Carried out the majority of the analytical work, analyzed the data and wrote the first draft of the manuscript. DW: Carried out analytical work and modeling. All authors contributed ideas in the interpretation of the data and wrote the final manuscript.

ACKNOWLEDGMENTS

The authors thank A. de Santiago Torio, W. Olszewski, M. S. Sim, H. Oduro, E. Molzberger, and A. Whitehill for assistance in the laboratory, and R. Summons, W. Leavitt, I. Halevy, and F. Schubotz for helpful discussions. This research was supported by the U.S. National Science Foundation (NSF EAR-1159318 to SO and TB.) and the NAI Complex Life (#NNA08CN84A). A Simons Foundation grant to R. Summons provided additional support. SO thanks the Kerr-McGee Professorship at MIT. TB thanks the Simons Foundation Collaboration on the Origins of Life, grant #327126. DW acknowledges support from an MIT Presidential Graduate Fellowship and the National Defense Science and Engineering Graduate (NDSEG) Fellowship.

REFERENCES

Amend, J. P., and Plyasunov, A. V. (2001). Carbohydrates in thermophile metabolism: calculation of the standard molal thermodynamic properties of aqueous pentoses and hexoses at elevated temperatures and pressures. *Geochim. Cosmochim. Acta* 65, 3901–3917. doi: 10.1016/S0016-7037(01)00707-4

Antler, G., Turchyn, A. V., Ono, S., Sivan, O., and Bosak, T. (2017). Combined ^{34}S, ^{33}S and ^{18}O isotope fractionations record different intracellular steps of microbial sulfate reduction. *Geochim. Cosmochim. Acta* 203, 364–380. doi: 10.1016/j.gca.2017.01.015

Arnold, G. L., Brunner, B., Müller, I. A., and Røy, H. (2014). Modern applications for a total sulfur reduction distillation method-what's old is new again. *Geochem. Trans.* 15:4. doi: 10.1186/1467-4866-15-4

Berner, R. A. (2001). Modeling atmospheric O_2 over Phanerozoic time. *Geochim. Cosmochim. Acta* 65, 685–694. doi: 10.1016/S0016-7037(00)00572-X

Bevington, P., and Robinson, D. K. (2002). *Data Reduction and Error Analysis for the Physical Sciences, 3rd Edn*. New York, NY: McGraw-Hill Education.

Bjerrum, C. J., and Canfield, D. E. (2002). Ocean productivity before about 1.9 Gyr ago limited by phosphorus adsorption onto iron oxides. *Nature* 417, 159–162. doi: 10.1038/417159a

Bosak, T., Schubotz, F., de Santiago Torio, A., Kuehl, J. V., Carlson, H. K., Watson, N., et al. (2016). System-wide adaptations of *Desulfovibrio alaskensis* G20 to phosphate-limited conditions. *PLoS ONE* 11:e0168719. doi: 10.1371/journal.pone.0168719

Bradley, A. S., Leavitt, W. D., Schmidt, M., Knoll, A. H., Girguis, P. R., and Johnston, D. T. (2015). Patterns of sulfur isotope fractionation during microbial sulfate reduction. *Geobiology* 14, 91–101. doi: 10.1111/gbi.12149

Bratbak, G., and Dundas, I. (1984). Bacterial dry matter content and biomass estimations. *Appl. Environ. Microbiol.* 48, 755–757.

Brüchert, V. (2004). "Physiological and ecological aspects of sulfur isotope fractionation during bacterial sulfate reduction," in *Sulfur Biogeochemistry: Past And Present Geological Society of America Special Papers*, eds J. P. Amend, K. J. Edwards, and T. W. Lyons (Geological Society of America), 1–16.

Brüchert, V., Knoblauch, C., and Jørgensen, B. B. (2001). Controls on stable sulfur isotope fractionation during bacterial sulfate reduction in Arctic sediments. *Geochim. Cosmochim. Acta* 65, 763–776. doi: 10.1016/S0016-7037(00)00557-3

Brunner, B., and Bernasconi, S. M. (2005). A revised isotope fractionation model for dissimilatory sulfate reduction in sulfate reducing bacteria. *Geochim. Cosmochim. Acta* 69, 4759–4771. doi: 10.1016/j.gca.2005.04.015

Brunner, B., Einsiedl, F., Arnold, G. L., Müller, I., Templer, S., and Bernasconi, S. M. (2012). The reversibility of dissimilatory sulphate reduction and the cell-internal multi-step reduction of sulphite to sulphide: insights from the oxygen isotope composition of sulphate. *Isotopes Environ. Health Stud.* 48, 33–54. doi: 10.1080/10256016.2011.608128

Canfield, D. (1998). A new model for Proterozoic ocean chemistry. *Nature* 396, 450–453. doi: 10.1038/24839

Canfield, D. E. (2001). Isotope fractionation by natural populations of sulfate-reducing bacteria. *Geochim. Cosmochim. Acta* 65, 1117–1124. doi: 10.1016/S0016-7037(00)00584-6

Canfield, D. E., Farquhar, J., and Zerkle, A. L. (2010). High isotope fractionations during sulfate reduction in a low-sulfate euxinic ocean analog. *Geology* 38, 415–418. doi: 10.1130/G30723.1

Canfield, D. E., Habicht, K. S., and Thamdrup, B. (2000). The Archean sulfur cycle and the early history of atmospheric oxygen. *Science* 288, 658–661. doi: 10.1126/science.288.5466.658

Canfield, D. E., Olesen, C. A., and Cox, R. P. (2006). Temperature and its control of isotope fractionation by a sulfate-reducing bacterium. *Geochim. Cosmochim. Acta* 70, 548–561. doi: 10.1016/j.gca.2005.10.028

Canfield, D. E., and Teske, A. (1996). Late Proterozoic rise in atmospheric oxygen concentration inferred from phylogenetic and sulphur-isotope studies. *Nature* 382:127. doi: 10.1038/382127a0

Canfield, D. E., and Thamdrup, B. (1994). The production of ^{34}S-depleted sulfide during bacterial disproportionation of elemental sulfur. *Science* 266, 1973. doi: 10.1126/science.11540246

Chambers, L. A., Trudinger, P. A., Smith, J. W., and Burns, M. S. (1975). Fractionation of sulfur isotopes by continuous cultures of *Desulfovibrio desulfuricans*. *Can. J. Microbiol.* 21, 1602–1607. doi: 10.1139/m75-234

Chambers, L., and Trudinger, P. (1979). Microbiological fractionation of stable sulfur isotopes: a review and critique. *Geomicrobiol. J.* 1, 249–293. doi: 10.1080/01490457909377735

Cline, J. D. (1969). Spectrophotometric determination of hydrogen sulfide in natural waters. *Limnol. Oceanogr.* 14, 454–458. doi: 10.4319/lo.1969.14.3.0454

Coplen, T. B. (2011). Guidelines and recommended terms for expression of stable-isotope-ratio and gas-ratio measurement results. *Rapid Commun. Mass Spectrom.* 25, 2538–2560. doi: 10.1002/rcm.5129

Cord-Ruwisch, R., Ollivier, B., and Garcia, J.-L. (1986). Fructose degradation by *Desulfovibrio* sp. in pure culture and in coculture with *Methanospirillum hungatei*. *Curr. Microbiol.* 13, 285–289. doi: 10.1007/BF01568654

Cypionka, H. (1995). "Solute transport and cell energetics," in *Sulfate-Reducing Bacteria*, ed L. L. Barton (New York, NY: Springer Nature), 151–184.

Dalla-Betta, P., and Schulte, M. (2009). Calculation of the aqueous thermodynamic properties of citric acid cycle intermediates and precursors and the estimation of high temperature and pressure equation of state parameters. *Int. J. Mol. Sci.* 10, 2809–2837. doi: 10.3390/ijms10062809

Detmers, J., Brüchert, V., Habicht, K. S., and Kuever, J. (2001). Diversity of sulfur isotope fractionations by sulfate-reducing prokaryotes. *Appl. Environ. Microbiol.* 67, 888–894. doi: 10.1128/AEM.67.2.888-894.2001

Dick, J. M. (2008). Calculation of the relative metastabilities of proteins using the CHNOSZ software package. *Geochem. Trans.* 9:10. doi: 10.1186/1467-4866-9-10

Eckert, T., Brunner, B., Edwards, E., and Wortmann, U. (2011). Microbially mediated re-oxidation of sulfide during dissimilatory sulfate reduction by *Desulfobacter latus*. *Geochim. Cosmochim. Acta* 75, 3469–3485. doi: 10.1016/j.gca.2011.03.034

Elser, J. J., Sterner, R. W., Gorokhova, E., Fagan, W. F., Markow, T. A., Cotner, J. B., et al. (2008). Biological stoichiometry from genes to ecosystems. *Ecol. Lett.* 3, 540–550. doi: 10.1111/j.1461-0248.2000.00185.x

Fagerbakke, K. M., Heldal, M., and Norland, S. (1996). Content of carbon, nitrogen, oxygen, sulfur and phosphorus in native aquatic and cultured bacteria. *Aquat. Microb. Ecol.* 10, 15–27. doi: 10.3354/ame010015

Forrest, J., and Newman, L. (1977). Silver-110 microgram sulfate analysis for the short time resolution of ambient levels of sulfur aerosol. *Anal. Chem.* 49, 1579–1584. doi: 10.1021/ac50019a030

Garrels, R. M., and Lerman, A. (1981). Phanerozoic cycles of sedimentary carbon and sulfur. *Proc. Natl. Acad. Sci. U.S.A.* 78, 4652–4656. doi: 10.1073/pnas.78.8.4652

Godwin, C. M., and Cotner, J. B. (2015). Stoichiometric flexibility in diverse aquatic heterotrophic bacteria is coupled to differences in cellular phosphorus quotas. *Front. Microbiol.* 6:159. doi: 10.3389/fmicb.2015.00159

Habicht, K. S., and Canfield, D. E. (2001). Isotope fractionation by sulfate-reducing natural populations and the isotopic composition of sulfide in marine sediments. *Geology* 29, 555–558. doi: 10.1130/0091-7613(2001)029<0555:IFBSRN>2.0.CO;2

Habicht, K. S., Gade, M., Thamdrup, B., Berg, P., and Canfield, D. E. (2002). Calibration of sulfate levels in the Archean ocean. *Science* 298, 2372–2374. doi: 10.1126/science.1078265

Harrison, A., and Thode, H. (1958). Mechanism of the bacterial reduction of sulphate from isotope fractionation studies. *Trans. Faraday Soc.* 54, 84–92. doi: 10.1039/tf9585400084

Hauser, L. J., Land, M. L., Brown, S. D., Larimer, F., Keller, K. L., Rapp-Giles, B. J., et al. (2011). Complete genome sequence and updated annotation of *Desulfovibrio alaskensis* G20. *J. Bacteriol.* 193, 4268–4269. doi: 10.1128/JB.05400-11

Heidelberg, J. F., Seshadri, R., Haveman, S. A., Hemme, C. L., Paulsen, I. T., Kolonay, J. F., et al. (2004). The genome sequence of the anaerobic, sulfate-reducing bacterium *Desulfovibrio vulgaris* Hildenborough. *Nat. Biotechnol.* 22, 554–559. doi: 10.1038/nbt959

Hoek, J., Reysenbach, A.-L., Habicht, K. S., and Canfield, D. E. (2006). Effect of hydrogen limitation and temperature on the fractionation of sulfur isotopes by a deep-sea hydrothermal vent sulfate-reducing bacterium. *Geochim. Cosmochim. Acta* 70, 5831–5841. doi: 10.1016/j.gca.2006.07.031

Holland, H. D. (1973). Systematics of the isotopic composition of sulfur in the oceans during the Phanerozoic and its implications for atmospheric oxygen. *Geochim. Cosmochim. Acta* 37, 2605–2616. doi: 10.1016/0016-7037(73)90268-8

Imhoff-Stuckle, D., and Pfennig, N. (1983). Isolation and characterization of a nicotinic acid-degrading sulfate-reducing bacterium, *Desulfococcus niacini* sp. nov. *Arch. Microbiol.* 136, 194–198. doi: 10.1007/BF00409843

Johnson, J. W., Oelkers, E. H., and Helgeson, H. C. (1992). SUPCRT92: a software package for calculating the standard molal thermodynamic properties of minerals, gases, aqueous species, and reactions from 1 to 5000 bar and 0 to 1000 C. *Comput. Geosci.* 18, 899–947. doi: 10.1016/0098-3004(92)90029-Q

Johnston, D. T., Farquhar, J., and Canfield, D. E. (2007). Sulfur isotope insights into microbial sulfate reduction: when microbes meet models. *Geochim. Cosmochim. Acta* 71, 3929–3947. doi: 10.1016/j.gca.2007.05.008

Johnston, D. T., Wing, B. A., Farquhar, J., Kaufman, A. J., Strauss, H., Lyons, T. W., et al. (2005). Active microbial sulfur disproportionation in the Mesoproterozoic. *Science* 310, 1477–1479. doi: 10.1126/science.1117824

Jones, W. J., Guyot, J.-P., and Wolfe, R. S. (1984). Methanogenesis from sucrose by defined immobilized consortia. *Appl. Environ. Microbiol.* 47, 1–6.

Jorgensen, B. B. (1979). A theoretical model of the stable sulfur isotope distribution in marine sediments. *Geochim. Cosmochim. Acta* 43, 363–374. doi: 10.1016/0016-7037(79)90201-1

Jørgensen, B. B. (1982). Mineralization of organic matter in the sea bed—the role of sulphate reduction. *Nature* 296, 643–645. doi: 10.1038/296643a0

Kaplan, I., Emery, K., and Rittenberg, S. (1963). The distribution and isotopic abundance of sulphur in recent marine sediments off southern California. *Geochim. Cosmochim. Acta* 27, 297–331. doi: 10.1016/0016-7037(63)90074-7

Kaplan, I., and Rittenberg, S. (1964). Microbiological fractionation of sulphur isotopes. *J. Gen. Microbiol.* 34, 195–212. doi: 10.1099/00221287-34-2-195

Kleikemper, J., Schroth, M. H., Bernasconi, S. M., Brunner, B., and Zeyer, J. (2004). Sulfur isotope fractionation during growth of sulfate-reducing bacteria on various carbon sources. *Geochim. Cosmochim. Acta* 68, 4891–4904. doi: 10.1016/j.gca.2004.05.034

Kligler, I., and Guggenheim, K. (1938). The influence of vitamin C on the growth of anaerobes in the presence of air, with special reference to the relative significance of E_h and O_2 in the growth of anaerobes. *J. Bacteriol.* 35, 141–156.

Ku, H. (1969). Notes on the use of propagation of error formulas. *J. Res. Nat. Bur. Stand. C* 70C, 263–273

Leavitt, W. D., Bradley, A. S., Santos, A. A., Pereira, I. A. C., and Johnston, D. T. (2015). Sulfur isotope effects of dissimilatory sulfite reductase. *Front. Microbiol.* 6:1392. doi: 10.3389/fmicb.2015.01392

Leavitt, W. D., Halevy, I., Bradley, A. S., and Johnston, D. T. (2013). Influence of sulfate reduction rates on the Phanerozoic sulfur isotope record. *Proc. Natl. Acad. Sci. U.S.A.* 110, 11244–11249. doi: 10.1073/pnas.1218874110

Leavitt, W. D., Venceslau, S. S., Pereira, I. A. C., Johnston, D. T., and Bradley, A. S. (2016). Fractionation of sulfur and hydrogen isotopes in *Desulfovibrio vulgaris* with perturbed DsrC expression. *FEMS Microbiol. Lett.* 363:fnw226. doi: 10.1093/femsle/fnw226

Luo, G., Ono, S., Beukes, N. J., Wang, D. T., Xie, S., and Summons, R. E. (2016). Rapid oxygenation of Earth's atmosphere 2.33 billion years ago. *Sci. Adv.* 2:e1600134. doi: 10.1126/sciadv.1600134

Millero, F. J., Plese, T., and Fernandez, M. (1988). The dissociation of hydrogen sulfide in seawater. *Limnol. Oceanogr.* 33, 269–274. doi: 10.4319/lo.1988.33.2.0269

Monod, J. (1949). The growth of bacterial cultures. *Ann. Rev. Microbiol.* 3, 371–394. doi: 10.1146/annurev.mi.03.100149.002103

Muyzer, G., and Stams, A. J. (2008). The ecology and biotechnology of sulphate-reducing bacteria. *Nat. Rev. Microbiol.* 6, 441–454. doi: 10.1038/nrmicro1892

Neretin, L. N., Schippers, A., Pernthaler, A., Hamann, K., Amann, R., and Jørgensen, B. B. (2003). Quantification of dissimilatory (bi)sulphite reductase gene expression in *Desulfobacterium autotrophicum* using real-time RT-PCR. *Environ. Microbiol.* 5, 660–671. doi: 10.1046/j.1462-2920.2003.00452.x

Noble, R. T., and Fuhrman, J. A. (1998). Use of SYBR Green I for rapid epifluorescence counts of marine viruses and bacteria. *Aquat. Microb. Ecol.* 14, 113–118. doi: 10.3354/ame014113

Okabe, S., and Characklis, W. G. (1992). Effects of temperature and phosphorous concentration on microbial sulfate reduction by *Desulfovibrio desulfuricans*. *Biotechnol. Bioeng.* 39, 1031–1042. doi: 10.1002/bit.260391007

Ollivier, B., Cord-Ruwisch, R., Hatchikian, E., and Garcia, J.-L. (1988). Characterization of *Desulfovibrio fructosovorans* sp. nov. *Arch. Microbiol.* 149, 447–450. doi: 10.1007/BF00425586

Ono, S., Wing, B., Johnston, D., Farquhar, J., and Rumble, D. (2006). Mass-dependent fractionation of quadruple stable sulfur isotope system as a new tracer of sulfur biogeochemical cycles. *Geochim. Cosmochim. Acta* 70, 2238–2252. doi: 10.1016/j.gca.2006.01.022

Otake, T., Lasaga, A. C., and Ohmoto, H. (2008). Ab initio calculations for equilibrium fractionations in multiple sulfur isotope systems. *Chem. Geol.* 249, 357–376. doi: 10.1016/j.chemgeo.2008.01.020

Peck, H. (1960). Evidence for oxidative phosphorylation during the reduction of sulfate with hydrogen by *Desulfovibrio desulfuricans*. *J. Biol. Chem.* 235, 2734–2738.

Planavsky, N. J., Rouxel, O. J., Bekker, A., Lalonde, S. V., Konhauser, K. O., Reinhard, C. T., et al. (2010). The evolution of the marine phosphate reservoir. *Nature* 467, 1088–1090. doi: 10.1038/nature09485

Pomeroy, L. R. B., Williams, P., le., Azam, F., and Hobbie, J. E. (2007). The microbial loop. *Oceanography* 20:28. doi: 10.5670/oceanog.2007.45

Postgate, J. R. (1979). *The Sulphate-Reducing Bacteria*. Cambridge, UK: CUP Archive.

Rees, C. E. (1973). A steady-state model for sulphur isotope fractionation in bacterial reduction processes. Geochim. *Cosmochim. Acta* 37, 1141–1162. doi: 10.1016/0016-7037(73)90052-5

Reichenbecher, W., and Schink, B. (1997). *Desulfovibrio inopinatus*, sp. nov., a new sulfate-reducing bacterium that degrades hydroxyhydroquinone (1, 2, 4-trihydroxybenzene). *Arch. Microbiol.* 168, 338–344. doi: 10.1007/s002030050507

Reinhard, C. T., Planavsky, N. J., Gill, B. C., Ozaki, K., Robbins, L. J., Lyons, T. W., et al. (2017). Evolution of the global phosphorus cycle. *Nature* 541, 386–389. doi: 10.1038/nature20772

Rudnicki, M. D., Elderfield, H., and Spiro, B. (2001). Fractionation of sulfur isotopes during bacterial sulfate reduction in deep ocean sediments at elevated temperatures. *Geochim. Cosmochim. Acta* 65, 777–789. doi: 10.1016/S0016-7037(00)00579-2

Sass, A., Rütters, H., Cypionka, H., and Sass, H. (2002). *Desulfobulbus mediterraneus* sp. nov., a sulfate-reducing bacterium growing on mono- and disaccharides. *Arch. Microbiol.* 177, 468–474. doi: 10.1007/s00203-002-0415-5

Shen, Y., and Buick, R. (2004). The antiquity of microbial sulfate reduction. *Earth Sci. Rev.* 64, 243–272. doi: 10.1016/S0012-8252(03)00054-0

Shock, E. L. (1995). Organic acids in hydrothermal solutions: standard molal thermodynamic properties of carboxylic acids and estimates of dissociation constants at high temperatures and pressures. *Am. J. Sci.* 295:496. doi: 10.2475/ajs.295.5.496

Shock, E. L., and Helgeson, H. C. (1988). Calculation of the thermodynamic and transport properties of aqueous species at high pressures and temperatures: correlation algorithms for ionic species and equation of state predictions to 5 kb and 1000 C. *Geochim. Cosmochim. Acta* 52, 2009–2036. doi: 10.1016/0016-7037(88)90181-0

Sim, M. S., Bosak, T., and Ono, S. (2011a). Large sulfur isotope fractionation does not require disproportionation. *Science* 333, 74–77. doi: 10.1126/science.1205103

Sim, M. S., Ono, S., and Bosak, T. (2012). Effects of iron and nitrogen limitation on sulfur isotope fractionation during microbial sulfate reduction. *Appl. Environ. Microbiol.* 78, 8368–8376. doi: 10.1128/AEM.01842-12

Sim, M. S., Ono, S., Donovan, K., Templer, S. P., and Bosak, T. (2011b). Effect of electron donors on the fractionation of sulfur isotopes by a marine Desulfovibrio sp. *Geochim. Cosmochim. Acta* 75, 4244–4259. doi: 10.1016/j.gca.2011.05.021

Sim, M. S., Wang, D. T., Zane, G. M., Wall, J. D., Bosak, T., and Ono, S. (2013). Fractionation of sulfur isotopes by *Desulfovibrio vulgaris* mutants lacking hydrogenases or type I tetraheme cytochrome c3. *Front. Microbiol.* 4:171. doi: 10.3389/fmicb.2013.00171

Sundby, B., Gobeil, C., Silverberg, N., and Alfonso, M. (1992). The phosphorus cycle in coastal marine sediments. *Limnol. Oceanogr.* 37, 1129–1145. doi: 10.4319/lo.1992.37.6.1129

Thauer, R. K., Jungermann, K., and Decker, K. (1977). Energy conservation in chemotrophic anaerobic bacteria. *Bacteriol. Rev.* 41:100.

Thingstad, T. F., Øvreås, L., Egge, J. K., Løvdal, T., and Heldal, M. (2005). Use of non-limiting substrates to increase size; a generic strategy to simultaneously optimize uptake and minimize predation in pelagic osmotrophs? *Ecol. Lett.* 8, 675–682. doi: 10.1111/j.1461-0248.2005.00768.x

Thode, H., Macnamara, J., and Fleming, W. (1953). Sulphur isotope fractionation in nature and geological and biological time scales. *Geochim. Cosmochim. Acta* 3, 235–243. doi: 10.1016/0016-7037(53)90042-8

Thode, H., Monster, J., and Dunford, H. (1961). Sulphur isotope geochemistry. *Geochim. Cosmochim. Acta* 25, 159–174. doi: 10.1016/0016-7037(61)90074-6

Trudinger, P. A., and Chambers, L. A. (1973). Reversibility of bacterial sulfate reduction and its relevance to isotope fractionation. *Geochim. Cosmochim. Acta* 37, 1775–1778. doi: 10.1016/0016-7037(73)90162-2

Tudge, A. P., and Thode, H. (1950). Thermodynamic properties of isotopic compounds of sulphur. *Can. J. Res.* 28, 567–578. doi: 10.1139/cjr50b-069

Van Mooy, B. A. S., Fredricks, H. F., Pedler, B. E., Dyhrman, S. T., Karl, D. M., Koblížek, M., et al. (2009). Phytoplankton in the ocean use

non-phosphorus lipids in response to phosphorus scarcity. *Nature* 458, 69–72. doi: 10.1038/nature07659

Wagner, W., and Pruß, A. (2002). The IAPWS formulation 1995 for the thermodynamic properties of ordinary water substance for general and scientific use. *J. Phys. Chem. Ref. Data* 31, 387–535. doi: 10.1063/1.1461829

Weimer, P. J., Van Kavelaar, M. J., Michel, C. B., and Ng, T. K. (1988). Effect of phosphate on the corrosion of carbon steel and on the composition of corrosion products in two-stage continuous cultures of *Desulfovibrio desulfuricans*. *Appl. Environ. Microbiol.* 54, 386–396.

Westrich, J. T., and Berner, R. A. (1984). The role of sedimentary organic matter in bacterial sulfate reduction: the G model tested. *Limnol. Oceanogr.* 29, 236–249. doi: 10.4319/lo.1984.29.2.0236

Widdel, F., and Hansen, T. (1992). "The dissimilatory sulfate-and sulfur-reducing bacteria," in *The Prokaryotes: A Handbook on the Biology of Bacteria: Ecophysiology, Isolation, Identification, Applications*, Vol. 1, eds A. Balows, H. Truper, M. Dworkin, W. Harder, and K. Schleifer (New York, NY: Springer-Verlag Inc.), 582–624.

Widdel, F., and Pfennig, N. (1981). Studies on dissimilatory sulfate-reducing bacteria that decompose fatty acids: I. Isolation of new sulfate-reducing bacteria enriched with acetate from saline environments. Description of *Desulfobacter postgatei* gen. nov., sp. nov. *Arch. Microbiol.* 129, 395–400. doi: 10.1007/BF00406470

Wing, B. A., and Halevy, I. (2014). Intracellular metabolite levels shape sulfur isotope fractionation during microbial sulfate respiration. *Proc. Natl. Acad. Sci. U.S.A.* 111, 18116–18125. doi: 10.1073/pnas.1407502111

Wortmann, U. G., Bernasconi, S. M., and Böttcher, M. E. (2001). Hypersulfidic deep biosphere indicates extreme sulfur isotope fractionation during single-step microbial sulfate reduction. *Geology* 29, 647–650. doi: 10.1130/0091-7613(2001)029<0647:HDBIES>2.0.CO;2

Yao, M., Elling, F. J., Jones, C., Nomosatryo, S., Long, C. P., Crowe, S. A., et al. (2015). Heterotrophic bacteria from an extremely phosphate-poor lake have conditionally reduced phosphorus demand and utilize diverse sources of phosphorus. *Environ. Microbiol.* 18, 656–667. doi: 10.1111/1462-2920.13063

Conflict of Interest Statement: The authors declare that the research was conducted in the absence of any commercial or financial relationships that could be construed as a potential conflict of interest.

APPENDIX

Cellular Distribution of Phosphorus in SRB

Using literature data, we can roughly estimate the amounts of phosphorus contained in (i) metabolites dissolved in cytoplasm (ΣP_{in}), (ii) in nucleic acids (DNA, RNA), and (iii) in lipid membranes of SRB cells. (i) Inorganic phosphate (P_i), calculated from a biochemical model of dissimilatory sulfate reduction (described below), ranges between ca. 10^{-2} and 10^{-1} M intracellularly and comprises the majority of ΣP_{in} (**Figure 7**). This range is consistent with limited experimental data for other bacteria (Thauer et al., 1977, and references therein). A $\sim$1 μm^3 cell ($= 1 \times 10^{-15}$ L), typical of healthy DMSS-1 cells, would therefore contain between 0.01 and 0.1 fmol of ΣP_{in}. Cells of other SRB we studied are typically 2–20 times larger (**Table 4**) and would contain proportionally more ΣP_{in}. (ii) The phosphorus in genomic DNA can be estimated from the size of the bacterial genome. A cell with a $\sim$3.6 Mbp genome, typical of *Desulfovibrio* spp. (Heidelberg et al., 2004; Hauser et al., 2011), would have 0.012 fmol P in its genomic DNA.[2] Additional phosphorus is found within the nucleic acids in plasmids and RNA. RNA, in particular, can contain up to 25 times more phosphorus than genomic DNA in SRB (Postgate, 1979). (iii) Phospholipids can contain as much cellular phosphorus as genomic DNA (Van Mooy et al., 2009). The lipid phosphorus inventory is highly flexible, as evidenced by near-total replacement of phospholipids by phosphorus-free lipids in phosphate-limited SRB cultures (Bosak et al., 2016).

Total phosphorus content is the sum of these fractions ($= \Sigma P_{in} + P_{nucleic\ acids} + P_{lipids}$) and can also be estimated independently from C:P ratios. For a $\sim$1 μm^3 cell, which is typical for healthy DMSS-1 cells (**Table 4**), and assuming a cellular carbon-to-volume ratio of 0.22 g C cm^{-3} (or 220 fg C μm^{-3}; Bratbak and Dundas, 1984) and atomic C:P ratio of 100:1 (Fagerbakke et al., 1996)[3] yields a total phosphorus content of 0.2 fmol P $cell^{-1}$. This is similar to the sum of the above components. Due to the wide variation in cell size and C:P ratios amongst species and growth conditions, estimated inventories are probably accurate to no better than a factor of 10. A population of 1×10^7 cells/ml would therefore require at least 2 μM phosphorus to synthesize all cellular components, a number that is of the same order of magnitude as phosphate concentrations ($\sim$10 μM) at which we and others have observed growth to be limiting in SRB cells.

Intracellular Phosphorus and Sulfur Isotope Fractionation

We calculated intracellular concentrations of phosphorus and the sulfur isotope fractionation factor ($^{34}\varepsilon$) as a function of csSRR, following the approach of Wing and Halevy (2014). Here, we briefly review key features of their numerical model, and then discuss some implications for phosphate metabolism in SRB.

Sulfate reduction is treated in four reversible enzymatically-mediated steps[4] in the model of Wing and Halevy:

$$SO_4^{2-}{}_{out} + nH^+{}_{out} \rightleftharpoons SO_4^{2-}{}_{in} + nH^+{}_{in} \quad (A1)$$

$$SO_4^{2-}{}_{in} + ATP \rightleftharpoons APS + PP_i \quad (A2)$$

$$APS + MK_{red} \rightleftharpoons SO_3^{2-} + MK_{ox} + AMP \quad (A3)$$

$$SO_3^{2-} + MK_{red} \rightleftharpoons H_2S + MK_{ox} \quad (A4)$$

Enzymes that mediate the reactions in Equations A1–A4 are (respectively), sulfate permeases/transporters (SulP family), sulfate adenylyltransferase (Sat), APS reductase (Apr), and dissimilatory sulfite reductase (dSiR).

For given values of csSRR, the model yields predictions of steady-state intracellular concentrations of pyrophosphate (PP_i), adenosine-5′-phosphosulfate (APS), and sulfite (SO_3^{2-}). Several variables have to be specified. Those most relevant to our study are $\left[SO_4^{2-}\right]_{out}$, the extracellular sulfate concentration; [H_2S], the sulfide concentration; concentrations of adenosine triphosphate (ATP) and adenosine monophosphate (AMP); and $u_{vivo-vitro}$, a scaling factor to account for differences in enzyme concentrations between intact cells and cell extracts studied in enzyme kinetic experiments. The first two parameters can be constrained by batch culture experiments. ATP and AMP concentrations are held constant (at 2.6 and 0.3 mM, respectively), as are concentrations of the reduced/oxidized forms of the electron carrier (menaquinone, MK in Equations A3, A4). The remaining parameter $u_{vivo-vitro}$ (intended as the ratio of enzyme activities in live SRB cells to enzyme activities in whole cell extracts) was calibrated by Wing and Halevy for DMSS-1 and several other species by fitting model results to isotopic data from pure cultures. We note that Wing and Halevy formulated $u_{vivo-vitro}$ as a linear function of csSRR (i.e., $u_{vivo-vitro} = m \times csSRR + b$, where m and b are constants chosen to fit $^{34}\varepsilon$–csSRR data for each species). Asymptotic behavior at high values of csSRR, where $b \ll m \times csSRR$, results from this parameterization. Although some evidence supports this scaling of gene expression with csSRR (Neretin et al., 2003; Wing and Halevy, 2014), it is unclear at present whether this relationship holds under phosphorus-limited conditions, as it would require high concentrations of enzymes under phosphorus stress. The biological reasons, if any, for this currently enforced asymptotic behavior requires further study.

Results of the model calculations are shown in **Figures 7B**, **A3**, **A4**. We noted several important features of the model results: (i) Most of the change in $^{34}\varepsilon$ [the linear portion of the 1 mM H_2S curve on the $^{34}\varepsilon$–$\log_{10}$(csSRR) plot in **Figure A4B**] occurs at csSRRs between 0.1 and 10 fmol $cell^{-1}$ day^{-1}; below this range, $^{34}\varepsilon$ approaches its thermodynamic value of $\sim$71‰; (Tudge and Thode, 1950), and above 10 fmol $cell^{-1}$ day^{-1}, $^{34}\varepsilon$ asymptotically approaches a range between 3 and 7‰;. (ii) Over the range of csSRRs from 0.1 to 100 fmol $cell^{-1}$ day^{-1}], concentrations of PP_i decrease by 100-fold, and [APS]

[2]Sequences from the DOE Joint Genome Institute (JGI) show that genomes of DMSS-1 (4.7 Mbp) and *D. inopinatus* (5.8 Mbp) are somewhat larger.

[3]Reported C:P ranges from 20:1 for *Desulfovibrio desulfuricans* (Okabe and Characklis, 1992) to 500:1 for *D. vulgaris* Hildenborough (Postgate, 1979).

[4]In these chemical equations, missing charges would be balanced by H^+ and H_2O, which do not appear in the reaction quotient when biochemical standard states are used and pH is assumed to be 7.0, as has been done here.

increases by 10-fold. (iii) Between 10 and 100 fmol cell^{-1} day^{-1}, concentrations of PP_i and APS are still sensitive to changes in csSRR, but $^{34}\varepsilon$ is not very sensitive (compare **Figures 7B**, **A4B**). This is because the reversibility of the process described by Equation A3 is insensitive to csSRR in this range (*Apr* in **Figure A3a**); the variation in $^{34}\varepsilon$ with csSRR here is driven mostly by the changes in the reversibility of sulfate uptake (Equation A1), which retains some sensitivity to csSRR in this range (*SulP* in **Figure A3a**).

We extended the Wing and Halevy model to calculate inorganic phosphate (P_i) and adenosine diphosphate (ADP) concentrations (**Figure 7B**). The model assumes that the concentrations of these species are governed by the following two equilibria (Thauer et al., 1977):

$$\mathrm{ATP} + \mathrm{AMP} \rightleftharpoons 2\mathrm{ADP}, \quad \Delta_r G^{\circ\prime} = 0\,\mathrm{kJ\,mol^{-1}} \tag{A5}$$

$$\mathrm{PP}_i + \mathrm{H_2O} \rightleftharpoons 2\mathrm{P}_i, \quad \Delta_r G^{\circ\prime} = -21.9\,\mathrm{kJ\,mol^{-1}} \tag{A6}$$

Because these reactions are catalyzed by efficient enzymes (adenylate kinase and pyrophosphatase, respectively; Cypionka, 1995), equilibrium is probably approached or attained under most growth conditions. Moderate deviations from the assumption of equilibrium do not influence the prediction of decreasing ΣP_{in} with higher csSRR shown in **Figure 7A**, because P_i makes up the majority of ΣP_{in} and exceeds the next most abundant species, ATP, by one or more orders of magnitude. In the model, decreased $[P_i]$ accommodates nearly the entirety of the decrease in ΣP_{in}, leaving the concentrations of adenosine phosphates unchanged (**Figure 7B**); this behavior is consistent with observations that the adenylate energy charge of cells remains nearly constant over a range of physiological states (Thauer et al., 1977). However, absolute concentrations of P_i, PP_i, and APS are sensitive to order-of-magnitude variations in $\left[SO_4^{2-}\right]_{out}$ and $[H_2S]$ (Wing and Halevy, 2014). Of particular note is that $[PP_i]$ is highly sensitive to $[P_i]$ (Equation A6), so PP_i concentrations will be suppressed to very low levels when phosphate levels inside the cell are low. Because PP_i is a product of the reaction for sulfate activation by ATP (Equation A2), low $[PP_i]$ increases the thermodynamic favorability of this reaction and pulls it toward the right (lower reversibility).

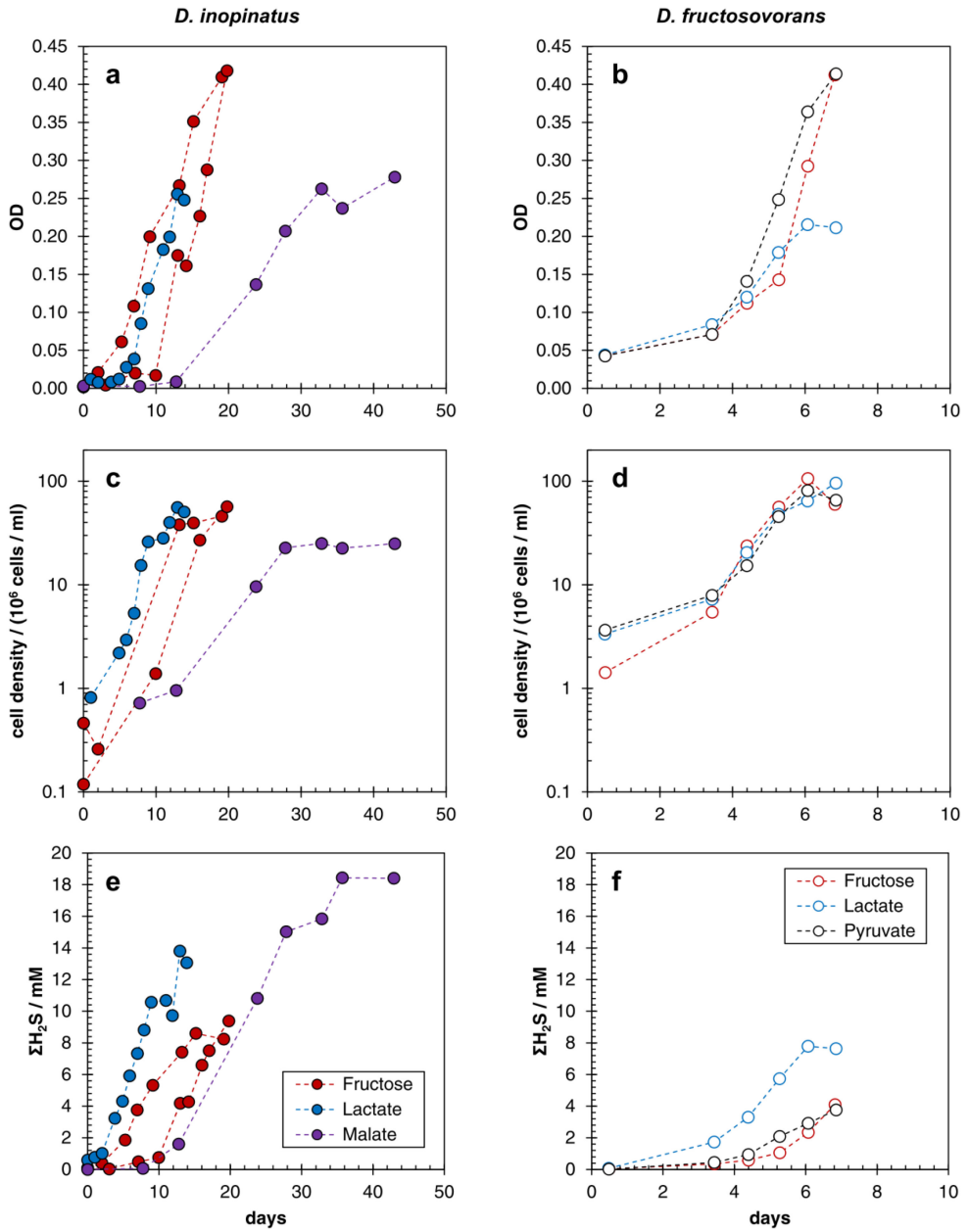

FIGURE A1 | Growth curves showing optical density of cultures (a,b), cell densities determined by epifluorescence microscopy **(c,d)**, and total sulfide (ΣH_2S) concentration **(e,f)** in batch cultures of *D. inopinatus* (left) and *D. fructosovorans* (right) grown on different organic substrates (see the legend for the explanation of color coding) in phosphate-replete (>1000 μM) media. Data are from **Table 2**. Note the difference in scales for the time axis between left and right panels. The uncertainties in cell density and sulfide concentration, respectively, were ±15% and ±10%, respectively.

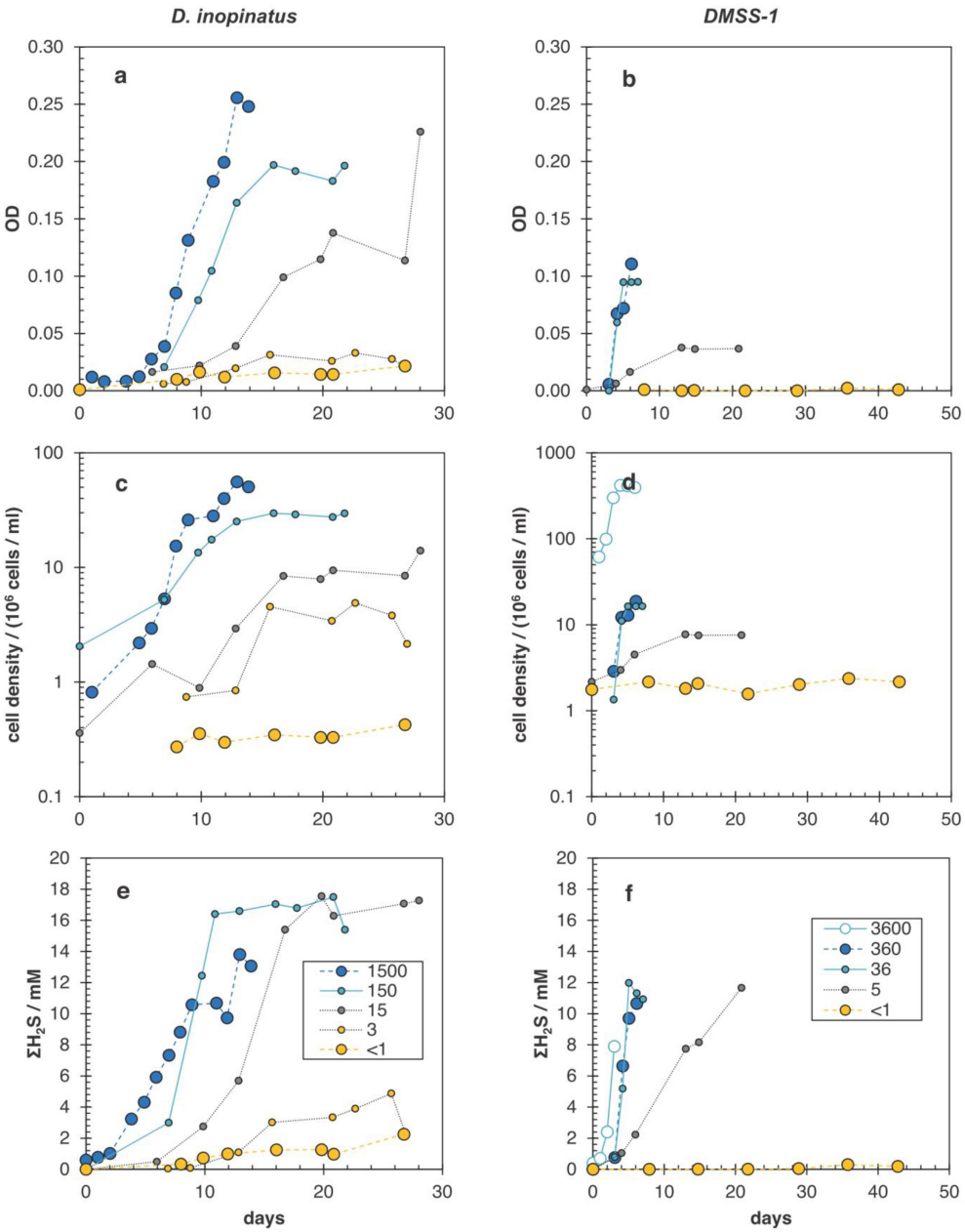

FIGURE A2 | Growth curves showing optical density of cultures (a,b), cell densities determined by epifluorescence microscopy **(c,d)**, and total sulfide (ΣH_2S) concentration **(e,f)** in batch cultures of *D. inopinatus* (left) and DMSS-1 (right) grown on lactate in the presence of different initial phosphate concentrations (in μM; legend shown in bottom panels). Data are from **Tables 2**, **3**, with the exception of the data for DMSS-1 cultures grown at 3600 μM phosphate (open circles in right panels), which are from Sim et al. (2011b). Note the difference in scales for the time axis between left and right panels. The uncertainties in cell density and sulfide concentration, respectively, were ±15% and ±10%, respectively.

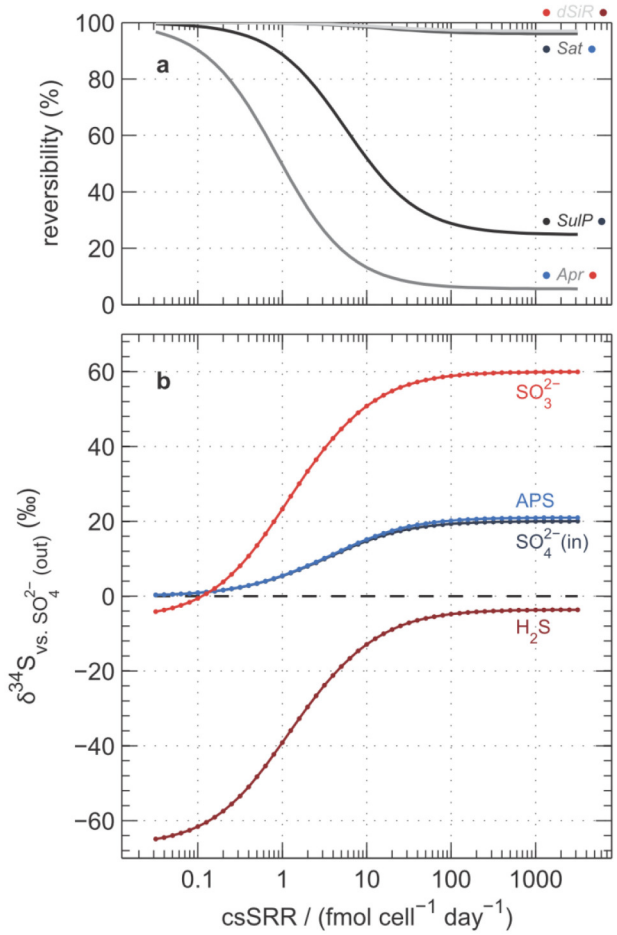

FIGURE A3 | Model predictions for (a) reversibility of key reactions and **(b)** isotopic composition of intracellular sulfur compounds. Calculations follow Wing and Halevy (2014) and assumptions are identical to those used in **Figure 7**. Labels in panel **(a)** indicate the enzyme responsible (see Equations A1–A4), and coloring of dots to the left and right correspond to colors in **(b)** of the sulfur-containing reactants and products, respectively. Predicted $\delta^{34}S$ values in **(b)** are expressed relative to extracellular sulfate at steady-state.

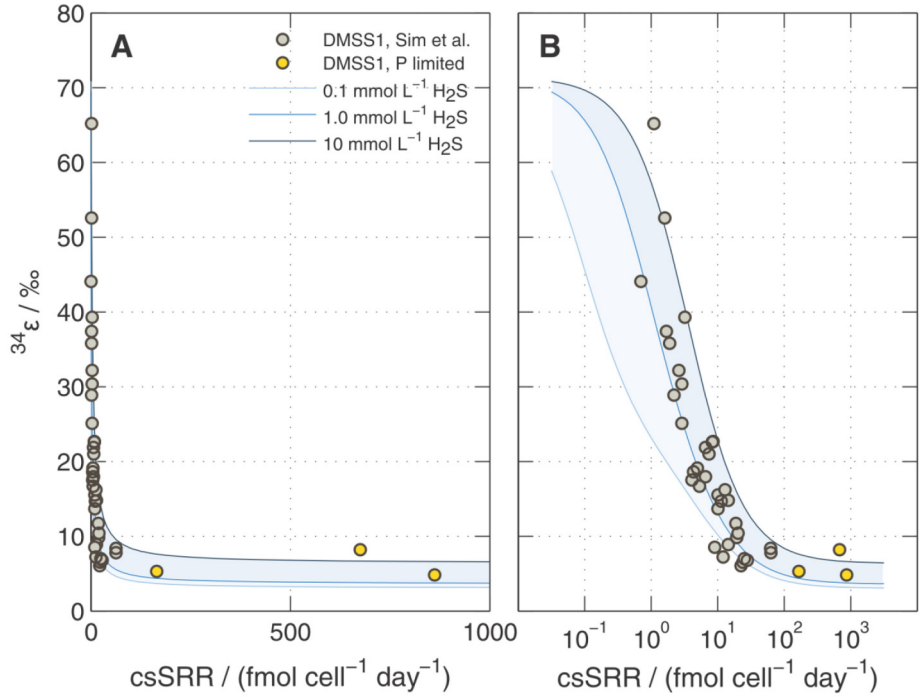

FIGURE A4 | Predicted $^{34}\varepsilon$ during sulfate reduction by DMSS-1 following Wing and Halevy (2014). Calculations are shown for three different H_2S concentrations (0.1, 1, and 10 mM) keeping $[SO_4^{2-}]_{out}$ constant at 20 mM. Overlaid on the model results are the data shown in **Figure 6**. Panels **(A)** and **(B)** show the same information but with linear and logarithmic x-axis scales (respectively).

frontiers in Microbiology

ORIGINAL RESEARCH
published: 05 May 2017
doi: 10.3389/fmicb.2017.00766

Co-existence of Methanogenesis and Sulfate Reduction with Common Substrates in Sulfate-Rich Estuarine Sediments

Michal Sela-Adler[1], Zeev Ronen[2], Barak Herut[3], Gilad Antler[4], Hanni Vigderovich[1], Werner Eckert[5] and Orit Sivan[1]*

[1] Department of Geological and Environmental Sciences, Ben Gurion University of the Negev, Beer-Sheva, Israel, [2] Zuckerberg Institute for Water Research, The Jacob Blaustein Institutes for Desert Research, Ben Gurion University of the Negev, Beer-Sheva, Israel, [3] Israel Oceanographic and Limnological Research, Haifa, Israel, [4] Department of Earth Sciences, University of Cambridge, Cambridge, UK, [5] The Yigal Allon Kinneret Limnological Laboratory, Israel Oceanographic and Limnological Research, Migdal, Israel

The competition between sulfate reducing bacteria and methanogens over common substrates has been proposed as a critical control for methane production. In this study, we examined the co-existence of methanogenesis and sulfate reduction with shared substrates over a large range of sulfate concentrations and rates of sulfate reduction in estuarine systems, where these processes are the key terminal sink for organic carbon. Incubation experiments were carried out with sediment samples from the sulfate-methane transition zone of the Yarqon (Israel) estuary with different substrates and inhibitors along a sulfate concentrations gradient from 1 to 10 mM. The results show that methanogenesis and sulfate reduction can co-exist while the microbes share substrates over the tested range of sulfate concentrations and at sulfate reduction rates up to 680 μmol L^{-1} day^{-1}. Rates of methanogenesis were two orders of magnitude lower than rates of sulfate reduction in incubations with acetate and lactate, suggesting a higher affinity of sulfate reducing bacteria for the available substrates. The co-existence of both processes was also confirmed by the isotopic signatures of $\delta^{34}S$ in the residual sulfate and that of $\delta^{13}C$ of methane and dissolved inorganic carbon. Copy numbers of *dsrA* and *mcrA* genes supported the dominance of sulfate reduction over methanogenesis, while showing also the ability of methanogens to grow under high sulfate concentration and in the presence of active sulfate reduction.

Keywords: sulfate reduction, methanogenesis, substrates, estuaries, co-existence

OPEN ACCESS

Edited by:
Kurt O. Konhauser, University of Alberta, Canada

Reviewed by:
Eric D. van Hullebusch, UNESCO-IHE Institute for Water Education, Netherlands
Matthias Egger, Aarhus University, Denmark

****Correspondence:***
Michal Sela-Adler
sela@post.bgu.ac.il

Specialty section:
This article was submitted to Microbiological Chemistry and Geomicrobiology, a section of the journal Frontiers in Microbiology

Received: *06 December 2016*
Accepted: *13 April 2017*
Published: *05 May 2017*

Citation:
Sela-Adler M, Ronen Z, Herut B, Antler G, Vigderovich H, Eckert W and Sivan O (2017) Co-existence of Methanogenesis and Sulfate Reduction with Common Substrates in Sulfate-Rich Estuarine Sediments. Front. Microbiol. 8:766. doi: 10.3389/fmicb.2017.00766

INTRODUCTION

Estuarine and shallow shelf sediments are often characterized by high fluxes of nutrients, high loads of organic carbon and marine salinity, thus containing high sulfate concentrations and housing intensive bacterial sulfate reduction and methanogenesis. Estuarine sediments account for 10% of oceanic carbon emission rates, despite its relatively small area (Bange et al., 1994; Abril and Iversen, 2002). Nevertheless, our knowledge of the competition and co-existence between sulfate reduction and methanogenesis in these sediments is limited, and specifically it has yet to be determined

whether they can co-exist while the active microbes sharing the same substrates. Furthermore, it is important to explore the conditions governing both the rates and initiation of methanogenesis in estuarine sediments. Here we examine the co-existence of methanogenesis and sulfate reduction while the microbes share the same substrates over a range of sulfate concentrations and rates of sulfate reduction through incubation experiments with sediment samples from the sulfate-methane transition zone of the Yarqon estuary (Israel).

The conventional paradigm states that thermodynamics govern biochemical depth profiles, and therefore in sedimentary environments, microbial processes that out-compete substrate uptake will suppress, or outcompete, other microbial processes, shifting the latter to greater depths in the sediment (Froelich et al., 1979; Stumm and Morgan, 1996). Despite this paradigm, a number of studies have shown that microbial processes can co-exist in complex sedimentary systems due to competition for electron donors rather than the difference in energy yield (Oremland and Taylor, 1978; Lovley et al., 1982). Examples of co-occurrence has been documented in the Black Sea sediments in which methane production was found within the sulfate reduction zone (Dale et al., 2008; Knab et al., 2008). Co-existence of sulfate reduction and methanogenesis characterizes also the coastal sediments of North Sea estuary. This co-existence was suggested to be controlled by the fast sediment accumulation combined with high organic carbon loading (Egger et al., 2016). These studies and others have emphasized that the various redox processes can co-exist in natural environments and may be coupled in a way that changes the rates of production or consumption of chemical species. These couplings would impact their distribution depth and their link to the subsurface carbon cycle. The co-existence between sulfate reduction and methanogenesis can occur at the interface between sulfate and methane, often termed the sulfate methane transition zone (SMTZ). Anaerobic oxidation of methane (AOM) coupled to sulfate reduction is typically found within this zone in marine sediments and has a large significance in controlling methane emission from marine sediment (Borowski et al., 2000; Archer, 2007; Knittel and Boetius, 2009). This process has been shown to consume up to 90% of the upward methane fluxes in marine sediments (Borowski et al., 1996; Valentine and Reeburgh, 2000).

Acetate and hydrogen are the preferred substrates for both sulfate reduction and methanogenesis (Schink, 1997; Conrad, 1999; Chidthaisong and Conrad, 2000a). From a thermodynamic perspective (Thauer et al., 1977; Schönheit et al., 1982; Ward and Winfrey, 1985; Lovley and Phillips, 1988) sulfate reducing bacteria can utilize hydrogen and acetate at lower concentrations than methanogens and therefore will likely outcompete them for substrate uptake, channeling the electron flow toward CO_2 production rather than methane (Lovley et al., 1982; Oremland and Polcin, 1982; Lovley and Klug, 1983; King, 1984; Lovley and Goodwin, 1988). Sulfate reduction is known to restrict methanogenesis through several paths. In complex environments such as natural sediments, in the presence of sulfate reducing bacteria and methanogens, sulfate supplementation or high sulfate concentrations will inhibit methanogenesis, diverting the electron flow toward sulfate reduction (Mountfort et al., 1980; Mountfort and Asher, 1981).

Nevertheless, methanogenesis has been detected in zones dominated by sulfate reduction in marine and salt marsh sediments (Oremland and Taylor, 1978; Dale et al., 2008; Treude et al., 2014). This methanogenesis is assumed to be the product of non-competitive substrate uptake, (i.e., substrates that are consumed only by methanogens) such as methanol, methane thiol and methylamines (Oremland and Polcin, 1982; Kiene et al., 1986). Another mechanism that can explain the coexistence of methanogenesis and sulfate reduction is a cooperation between acetoclastic sulfate reducing bacteria that produce hydrogen and hydrogenotrophic methanogens (Ozuolmez et al., 2015). It can be also be a coupling between methanogens and fermentative (hydrogen producing) *Clostridia* (Oremland and Taylor, 1978) that may also support methane production in sulfate-enriched environments. On the other hand, inhibition of methanogenesis by sulfate reduction can be the result of the toxicity of sulfide, the product of sulfate reduction (Koster et al., 1986), even though one study suggested that the methanogen *Methanosarcina barkeri* could tolerate sulfide concentrations as high as 20 mM (Mountfort et al., 1980). Therefore, the conditions under which sulfate reduction and methanogenesis can co-exist in natural sedimentary environments and specifically in estuaries, and the possibility of these processes to share ambient substrates are still unclear. The goal of this study was to define the terms in which the methanogenesis and sulfate reduction co-exist using the highly stratified sulfate-enriched Yarqon estuary as a case study.

MATERIALS AND METHODS

Study Site

The Yarqon (**Figure 1**) is the largest coastal river in Israel with length of 27.5 km and a drainage basin area of 1800 km^2. As other streams along the Mediterranean coast of Israel, the bottom bathymetry of the downstream lies below sea level, enabling the intrusion of seawater and the formation of highly stratified estuary up to a few kilometers inland. The estuary contains high organic carbon loads from upstream (20–60 mg L^{-1}; Arnon et al., 2015) and lower water mass close to seawater salinity (∼19000 mg Cl^-).

Sediment Core Sampling

Sediment cores (∼35 cm long, 5 cm in diameter) were collected during August and October 2013 at the Yarqon estuary, 3 km upstream (32° 06.0792′ N; 34° 48. 3633′ E), using a gravity corer as described in Antler et al. (2014). The cores were stored in the dark at 4°C and then sliced and treated within 48 h under anaerobic conditions.

Experimental Design

Three incubation Experiments (A, B, and C- described below) were carried out using 1–3 replicates of sediments cores. Treatments parameters are outlined in **Table 1**. Each of the

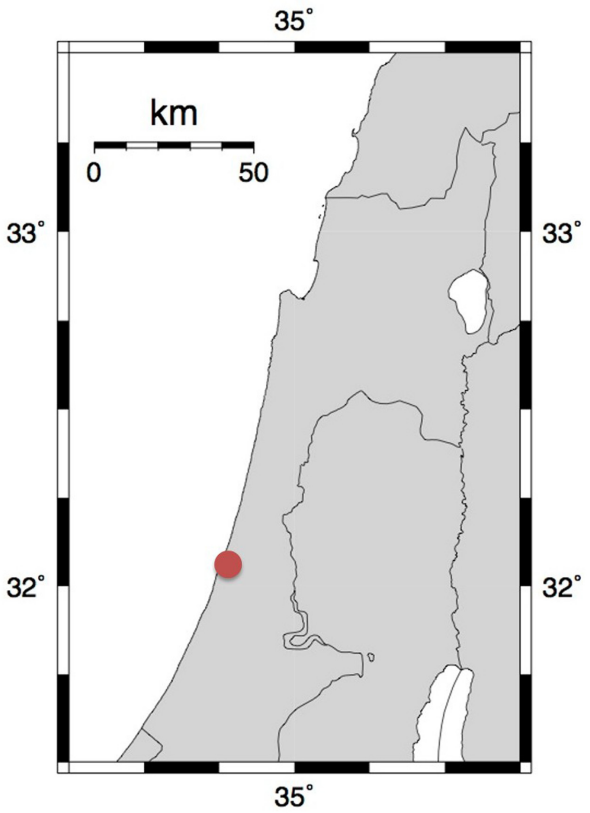

FIGURE 1 | Yarqon estuary location map at the Israeli coast of the Eastern Mediterranean.

cores was sliced in the 5–15 cm depth interval under N_2 flushing. Methane was measured from the head space using N_2 pre-flushed gas tight syringe. Porewater sub-samples for sulfate and dissolved inorganic carbon (DIC) concentrations and isotopic measurements were extruded using N_2 pre-flushed sterile 5 ml syringe (sub-sample of 2 ml).

Experiment A-(**Table 1**) was conducted on a sediment core from August 2013. The sub-sampled sediment was homogenized and approximately 30 gr of sediment was transferred to N_2 pre-flushed 300 ml sterile glass bottles. Sterile and anaerobic 3.5% NaCl omit solutions were pre-prepared with different sulfate concentrations (1, 2, or 9 mM), with or without molybdate (MoO_4^{2-}) as a sulfate reduction inhibitor (Oremland and Capone, 1988). The range of sulfate concentration and the layer isolated were chosen based on *in situ* sulfate and methane profiles that show that sulfate reduction and methanogenesis overlap in the Yarqon with sulfate concentration up to 10 mM (Antler et al., 2014). The sediment was mixed with the media at a 1:4 ratio to produce slurry and closed with black butyl rubber stoppers. Three times in sequence, bottles were shaken vigorously for 30 s followed by flushing with a N_2 + 300 ppm CO_2 mixture for 5 min at the beginning of the experiment. Labeled ^{13}C methane was added to all slurries at a concentration of 100 $\mu mol\ L_{slurry}^{-1}$. For each treatment duplicates were prepared. Killed control bottles were autoclaved after the bottles were sealed.

Experiment B and C-(**Table 1**) were conducted on three sediment cores retrieved on October 2013 that were sliced in the depth interval of 10–25 cm depth in an anaerobic hood (Coy Lab-Grass Lake, MI, USA). The sediment slices were homogenized and mixed with sterile and anaerobic medium solutions that were prepared in advance with 3.5% NaCl and 10 mM sulfate, in a 1:4 sediment: medium ratio. One hundred and twenty mililiter sub samples from each slurry were transferred into 300 ml sterile glass bottles and closed with black butyl rubber stoppers inside the anaerobic hood. Three times in sequence, bottles were shaken vigorously for 30 s followed by flushing with a N_2 + 300 ppm CO_2 mixture for 5 min at the beginning of the experiment. *Experiment B* was conducted on slurries treated with 10 mM

TABLE 1 | Description of Experiment A, B, and C with duplicate bottles for each treatment.

Experiment A	Sediment core collected during August 12th 2013; The goal of the experiment was to determine the effect of different sulfate concentrations on methane production rates, with and without sulfate reduction inhibitor				
Treatments	Sulfate concentration in slurry (mM)				
	100 µl of $^{13}CH_4$ (99.999%) was added to all slurries				
No inhibitor	9 mM	2 mM	1 mM	Killed control + 9 mM	
Sulfate reduction inhibitor	9 mM + Molybdate	2 mM + Molybdate	1 mM + Molybdate		
Experiment B	Sediment core collected during October 1st 2013; The goal of the experiment was to determine the effect of inhibitors addition on methane production and effect of sulfate reduction rates and isotopic signature				
	10 mM sulfate without substrate addition in all slurries Inhibition conditions				
Treatments	No inhibitor addition-control	20 mM BES	10 mM Molybdate		
Experiment C	Sediment core collected during October 1st 2013; The goal of the experiment was to determine the effect of substrate and the effect of inhibitors addition on methane production and sulfate reduction rates				
Treatment Substrate conditions	10 mM sulfate in all slurries Inhibition conditions				
40 mM acetate	No inhibitor	20 mM BES	Molybdate	Killed control with acetate addition	
10 mM lactate	No inhibitor				

molybdate as a sulfate reduction inhibitor or with 20 mM 2-bromoethanosulfonate (BES; Sigma–Aldrich, Rehovot, Israel) as a methanogenesis inhibitor (Chidthaisong and Conrad, 2000b) or without an inhibitor (as a control). All slurries in Experiment B were not amended with a substrate. *Experiment C* was conducted on slurries treated with substrate and inhibitors addition. The substrate additions were 7 mM acetate or 7 mM lactate. Killed control bottles were autoclaved after sealing and substrate was added. For each substrate, two bottles were treated with 20 mM of BES or 10 mM molybdate or with no inhibitor addition. Duplicate bottles were made for each treatment.

Analytical Methods

Chemical Analyses

Headspace methane concentrations were measured on a gas chromatograph equipped with a flammable ionization detector (FID) at a precision of 2 μmol CH_4 L^{-1}. Sulfate was measured after porewater were filtered with a 0.22 μm filter and diluted by a factor of ∼1:100 (by weight using a Dionex DX500 high pressure liquid chromatograph (HPLC) with an error of 3%. $\delta^{13}C_{DIC}$ was measured in ∼0.5 mL of each sample. The sample was transferred into a He-flushed vial containing 50 μl of concentrated H_3PO_4 that released all DIC to the headspace as CO_2. Measurements of the released CO_2 was done using a conventional isotopic ratio mass spectrometer (IRMS, DeltaV Advantage, Thermo) with a precision of ±0.1‰, and the results are reported versus the Vienna Pee Dee Belemnite (VPDB) standard. DIC concentration was calculated from the IRMS results according to peak height and to a calibration curve (by standard samples prepared from $NaHCO_3$) with an error of ±0.2 mM. The $\delta^{13}C_{CH4}$ values were measured using an IRMS equipped with a PreCon interface after oxidation to CO_2. The error between duplicates of this parameter was less than 0.5‰ and the results are reported versus the VPDB standard. For $\delta^{34}S_{SO4}$ analysis, sulfate was precipitated as barium sulfate (barite) using a saturated barium chloride solution (as described in Antler et al., 2014). The barite was then washed with 6N HCl and distilled water. The barite was combusted at 1030°C in a Flash Element Analyzer (EA), and the resulting sulfur dioxide (SO_2) was measured by continuous flow on a GS-IRMS (Thermo Finnegan Delta V Plus Godwin Laboratory, University of Cambridge). The error for $\delta^{34}S_{SO4}$ was determined using the standard deviation of the standard NBS 127 at the beginning and the end of each run (∼0.3‰ 1σ). Samples were corrected to NBS 127, IAEA-SO-5 and IAEA-SO-6 standards (20.3, 0.5, and −34.1‰, respectively). The $\delta^{34}S_{SO4}$ values are reported versus Vienna Canyon Diablo Troilite (VCDT). Data analysis of variance (single factor ANOVA) test was conducted on concentration measurements of methane and sulfate to test the variance between the treatments described above with $\alpha = 0.05$.

Quantitative Polymerase Chain Reaction (qPCR) Analyses

Reaction mix for qPCR included the following: 12.5 μl KAPA SYBR Fast Universal Ready mix (KAPA Biosystems, Woburn, MA, USA); 100 nM of each primer, 1 μl template (extracted DNA or plasmid) and DDW to complete to 25 μl. Thermocycling conditions included an initial denaturation step at 95°C, followed by 40 cycles of 95°C for 30 s; annealing temperatures as described in **Table 2** for 30 s; and 72°C for 30 s. Acquisition was performed at the completion of each cycle, following a short (2 s) step at 78°C to ensure primer dimer denaturation. Melting curves (72–95°C) showed only one peak for all qPCR reactions. PCR for *mcrA* (methanogens), *dsrA* (sulfate reducing bacteria), and 16S rRNA genes of archaea and bacteria were preformed based on Wilms et al. (2006) and Yu et al. (2008). Calibration curves for mcrA, dsrA, archaea and bacteria were created by conducting a 10-fold dilution series (∼10^3–10^9 copies) of plasmids (constructed as detailed below), containing environmental copies of the relevant genes. For calibration of 16s rRNA genes, genomic DNA from a pure culture of *Escherichia coli* was used, assuming that the 16S copy number in this genome is 6. Calibration curves had $R^2 > 0.975$, and the slope was between −3.0 and −3.9, corresponding to PCR efficacy of 90–111%. The copy number of *mcrA* was normalized to archaea copy number and the copy number of *dsrA* was normalized to bacteria copy number in the same sample. Amplification reactions were carried out in a Rotor-Gene™ 6000 thermocycler (Corbett Life Science, Concorde, NSW, Australia). Primer sequences are detailed in **Table 2**.

RESULTS

Experiment A

The first set of experiments (Experiment A) aimed to examine the effect of sulfate concentration on the rate of methanogenesis and the lag time for its initiation. Both, methanogenesis rates and the lag time of methanogenesis initiation were similar (40 days) regardless of sulfate concentrations (9, 2, and 1 mM sulfate; **Figure 2**). In this experiment the effect of sulfate reduction on methanogenesis was tested as well. This was done by molybdate addition, a sulfate reduction inhibitor. In all the non-inhibited slurries, methane concentrations reached ∼170 μmol L_{slurry}^{-1}, and even slightly higher values with 9 mM sulfate. As expected, when molybdate was added to the slurries, methanogenesis was stimulated and methane concentrations increased up to 250–300 μmol L_{slurry}^{-1} in all slurries. In the killed control (with 9 mM sulfate) methane concentrations did not increase throughout the experiment (**Figure 2**). A comparison between

TABLE 2 | Primers and annealing temperature based on *Wilms et al., 2006 and **Yu et al., 2008.

Primer name		Annealing temp	Length (bp)
dsrA*	5′-ACSCACTGGAAGCACG-3′ 5′-CGGTGMAGYTCRTCCTG-3′	58°C	450
mcrA*	5′-GCMATGCARATHGGWATGTC-3′ 5′-TGTGTGAASCCKACDCCACC-3′	54°C	350
Archaea**	5′-ACGGGGYGCAGCAGGCGCGA-3′ 3′-GTGCTCCCCCGCCAATTCCT-5′	48°C	320
Bacteria*	5′-CCTACGGGAGGCAGCAG-3′ 3′-ATTACCGCGGCTGCTGG-5′	60°C	270

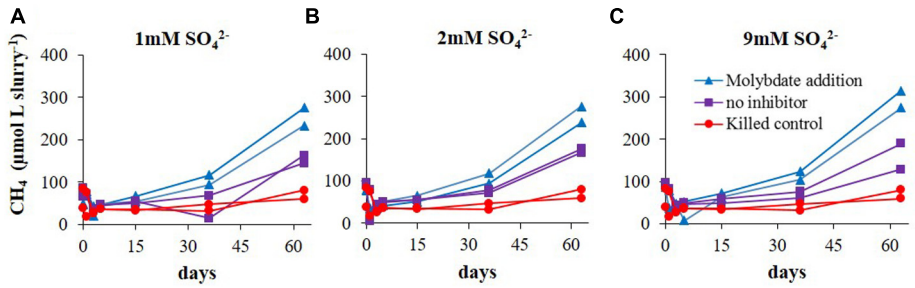

FIGURE 2 | Experiment A – Evolution of methane concentrations in slurries with (A) 1 mM SO_4^{2-} ; **(B)** 2 mM SO_4^{2-} ; and **(C)** 9 mM SO_4^{2-}.

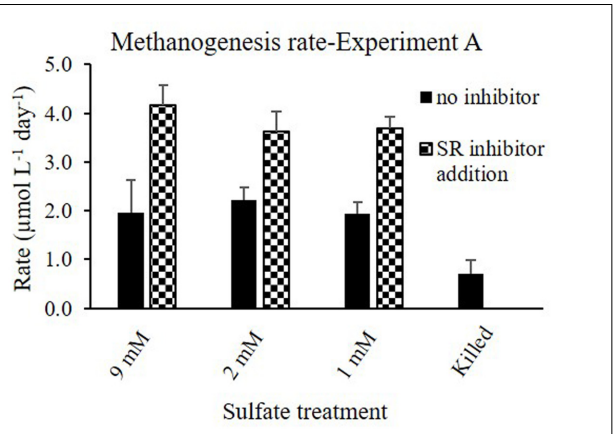

FIGURE 3 | Methanogenesis rates in Experiment A with and without sulfate reduction inhibitor (molybdate) under different sulfate concentrations.

methanogenesis rates in the range of sulfate concentrations with and without sulfate reduction inhibitor is presented in **Figure 3**.

During this experiment sulfate concentrations decreased by 0.1 – 0.3 mM, indicating low reduction rates. DIC concentrations increased by ∼0.9 mM when molybdate was added and by ∼1.0 mM in non-inhibited slurries. This difference is not significant as it is in the range of the standard error. The difference in the $\delta^{13}C_{DIC}$ values between the treatments was also not significant, and remained between −16‰ to −18‰. Although ^{13}C labeled methane was added to all slurries (initial concentration of 100 µmol L_{slurry}^{-1}), ^{13}C enriched DIC was not detected in slurries, indicating that AOM was insignificant in this short time scale experiments, as was shown in marine and lake sediments (Sivan et al., 2014; Bar-Or et al., 2015). Data of this experiment was not shown as it was similar to Experiment B, which was fuller and presented in **Figure 4**.

Experiment B

The effect of sulfate reduction on methanogenesis was examined by treatment with molybdate; and the effect of methanogenesis on sulfate reduction was examined by treatment with BES (a methanogen inhibitor) in slurries. The results of Experiment B without inhibitors supplementation (**Figure 4**) were similar to those of Experiment A. Sulfate concentrations in the non-inhibited and BES-treated slurries decreased by a factor of 5–10 relative to molybdate-treated slurries, demonstrating the efficiency of molybdate as an inhibitor of sulfate reduction (**Figure 4A**). The values of $\delta^{34}S_{SO4}$ increased by 2.3–5.1‰ in non-inhibited slurries and BES-treated slurries, and decreased in slurries treated with molybdate and in the killed controls by 0.4–0.9‰, (**Figure 4B**).

Methane concentrations increased in all treatments. As expected, the maximum increase was observed in slurries treated with molybdate and the minimum increase was observed in slurries treated with BES and in the non-inhibited slurries (**Figure 4C**). The initial value of $\delta^{13}C_{CH4}$ in all slurries was approximately −35‰, and decreased throughout the experiment. Maximum depletion was observed in BES-treated slurries (methane production in BES-treated slurries and non-inhibited slurries showed similar rates) and minimum depletion was observed in slurries treated with molybdate, corresponding to methanogenesis rates in the slurries (**Figure 4D**).

The DIC concentrations were similar in all slurries and increased only by approximately 3 mM (**Figure 4E**). The initial DIC concentrations were 4.6–5.4 mM in all slurries and the initial $\delta^{13}C_{DIC}$ value in all slurries was ∼ −12‰. This value slightly decreased during the experiment with a similar trend as $\delta^{13}C_{CH4}$ with maximum depletion in the BES-treated slurries, and minimum depletion in molybdate-treated slurries (**Figure 4F**).

Experiment C

The effect of acetate and lactate supplements on methane production and sulfate reduction rates was examined during Experiment C. These additions stimulated methane production in all slurries. The maximum increase in methane concentration was observed in slurries treated with lactate and in decreasing order with acetate addition, no substrate supplementation and finally killed control (**Figure 5A**). The most prominent decrease in sulfate during the experiment was in the slurries supplemented with lactate, where sulfate completely depleted within 5 days; followed by slurries supplemented with acetate, and those without substrate supplementation (**Figure 5B**). The effect of inhibitors and substrates addition on sulfate reduction and methanogenesis rates in Experiments B and C is shown in **Figure 6**.

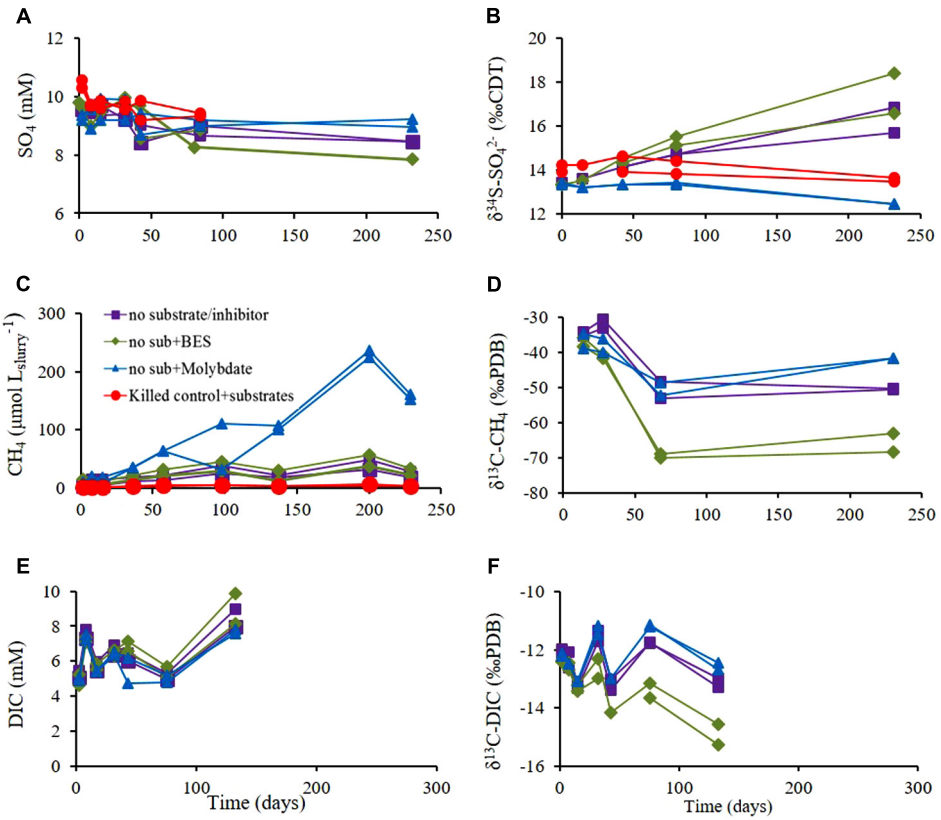

FIGURE 4 | Experiment B – Slurries with sediment amended with inhibitors of either sulfate reduction (molybdate) or methanogenesis (BES), control slurries (without inhibitor) and killed control (autoclaved). (A) Sulfate concentration; **(B)** $\delta^{34}S$ of residual SO_4^{2-} ; **(C)** CH_4 concentrations; **(D)** $\delta^{13}C$-CH_4; **(E)** DIC concentrations and **(F)** $\delta^{13}C$-DIC. Legend in panel **(A)** refers to all panels.

The qPCR results for the abundances of *mcrA* (normalized to copy number of archaea) and *dsrA* (normalized to the copy number of bacteria) functional genes at two time points in Experiment C (after 90 and 230 days) are presented in **Figure 7**. The results show that methanogens (based on *mcrA* gene) under natural conditions constituted approximately 10% of all archaea, and sulfate reducing bacteria (based on *dsrA* gene) were approximately 0.1% of all bacteria (**Figure 7** and **Table 3**). In general, sulfate reducing bacteria were more abundant during the first step of the experiment and methanogens became more abundant toward the end of the experiment (**Figure 7**).

DISCUSSION

Sulfate penetration into the methane production zone was already observed in diverse environments. For example, in continental margin sediments (Treude et al., 2014), in the gassy sediments of Eckernforde Bay in the German Baltic (Treude et al., 2005), in littoral Baltic Sea sediments (Thang et al., 2013), in the saline coastal sediments of Lake Grevelingen in the Netherlands (Egger et al., 2016), in the sediments of the Black Sea (Knab et al., 2009) and in salt marsh sediments (Parkes et al., 2012). However, couplings between sulfate concentrations, sulfate reduction rates and methanogenesis rates have not been fully examined in estuarine sediments. Previous porewater data from sediments of the Yarqon estuary documented a combination of a high organic matter loading and seawater sulfate concentrations, triggering relatively high rates of sulfate reduction (6.05×10^{-4} mol L^{-1} day^{-1}) with maximum values at the upper 5 cm sediment depth. These were relatively high rates compared to other marine or saline estuarine environments (Eliani-Russak et al., 2013). Methane accumulated to above 300 µmol L^{-1} in the sulfate reduction zone when sulfate concentrations were above 3 mM at sediment depth of ∼10 cm. In addition, sulfate was not completely exhausted until 20 cm below surface, penetrating into the methanogenesis zone. The isotopic signature of oxygen ($\delta^{18}O_{SO4}$) versus sulfur ($\delta^{34}S_{SO4}$) in dissolved sulfate profiles indicated that in the Yarqon estuary sediment (during May 2010), AOM is likely the main sulfate reduction process (Antler et al., 2014). In this study we used sediment cores from the saline Yarqon estuary at the zone identified as containing both processes.

Sulfate Concentration Effect

The experiments in this research were conducted under a sulfate concentration range of 1–10 mM. This specific concentration range was chosen for several reasons: (1) *In situ* evidences

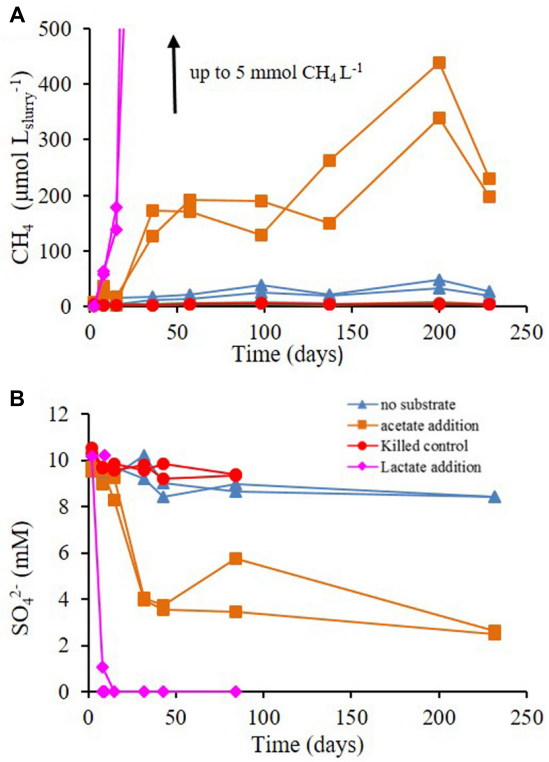

FIGURE 5 | Experiment C – (A) methane and **(B)** sulfate concentrations throughout the experiment with no substrate addition, acetate addition, lactate addition and killed control (autoclaved).

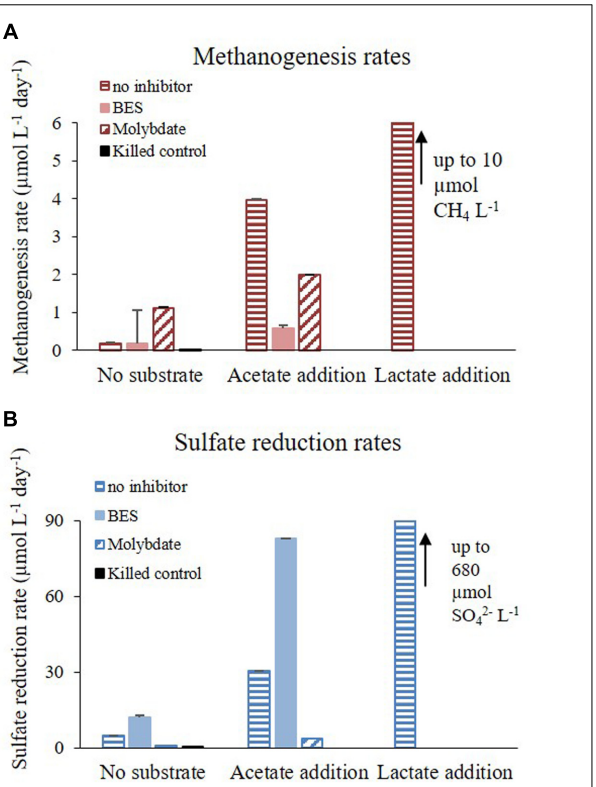

FIGURE 6 | Rates of (A) methanogenesis and **(B)** sulfate reduction during Experiments B and C treated with inhibitors (BES, molybdate or without inhibitor) and with substrate (acetate, lactate or without substrate addition).

show that sulfate reduction and methanogenesis overlap in the Yarqon and that sulfate concentrations in this depth can reach 10 mM (Antler et al., 2014); (2) Different sulfate and substrate concentrations cause different reduction rates in the sediment; (3) Flood events cause the salinity gradient to retreat toward seashore, which changes the sulfate concentration gradient.

Methanogens activity is not affected by sulfate concentrations, as was shown in pure cultures (King, 1984). Nevertheless, in different sedimentary systems, the competition with sulfate reducing bacteria for labile substrate controls methanogenesis, since sulfate reducing bacteria outcompete methanogens for substrate uptake. Elevated sulfate concentration will cause an enhancement in sulfate reduction rates and therefore a decrease in methanogenesis, and vise versa – low sulfate concentrations will decrease sulfate reduction rates and will enhance methanogenesis (Mountfort et al., 1980; Lovley et al., 1982; Lovley and Klug, 1983). Here we show that even at elevated sulfate concentrations in sedimentary systems, sulfate reduction and methanogenesis co-exist, and the rates of sulfate reduction control methanogenesis rates. The negligible effect of sulfate concentration on the methanogenesis rates in slurries indicates that the concentration itself is not the direct controlling factor of methanogenesis. The amendments of the slurries with sulfate at various concentrations (Experiment A; **Figure 2**) did not influence sulfate reduction rates either, indicating that this system is probably substrate depleted. Furthermore, supplementation of molybdate, which lowered the rates of sulfate reduction, enhanced methane production in all slurries (**Figure 3**). Therefore, we suggest that the competition between methanogens and sulfate reducing bacteria for a common substrate is the main factor controlling the rates and onset of methanogenesis.

Isotopic Effect

Microorganisms tend to discriminate against the heavy isotope, leaving the product isotopically enriched in the light isotope and the residual pool in the heavy isotope. Sulfate reduction and methanogenesis processes have large isotope fractionation effect, and thus related isotope measurements may be more distinct and sensitive than the measurement of concentration changes (e.g., Sivan et al., 2014). Dissimilatory sulfate reduction is characterized by large isotopic fractionation (up to 72‰) with the light isotope favored in the H_2S product (Kaplan and Rittenberg, 1964; Canfield, 2001; Wortmann et al., 2001; Sim et al., 2011). In experiment B there was a significant increase in $\delta^{34}S_{SO4}$ in the slurries without inhibitor and in the slurries with the BES addition. A small decrease was observed in the killed control and in the experiment with molybdate addition (**Figure 4B**). This indicates active sulfate reduction in the slurries without inhibitor and with the BES addition (the

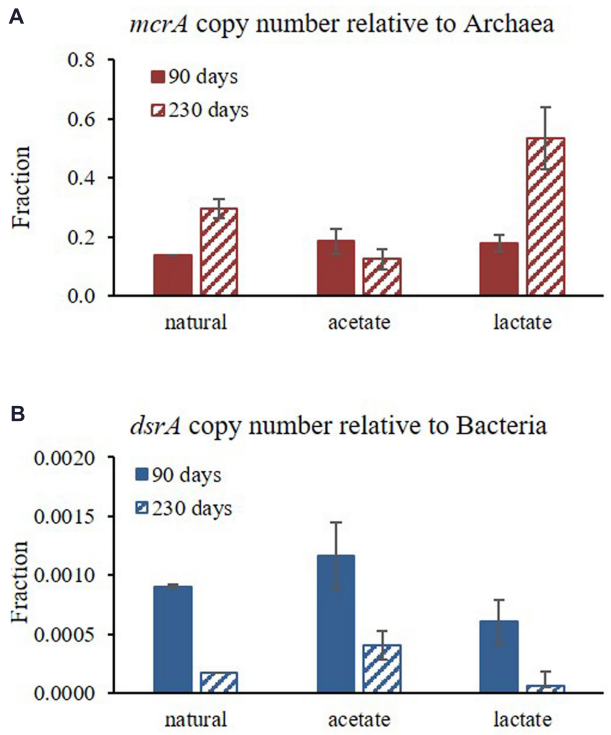

FIGURE 7 | Changes in the relative abundance of (A) *mcrA* functional gene relative to the copy number of Archaea; and **(B)** *dsrA* functional gene relative to the copy number of Bacteria over the course of the experiment at two time points (average of duplicate bottles (each samples in triplicates).

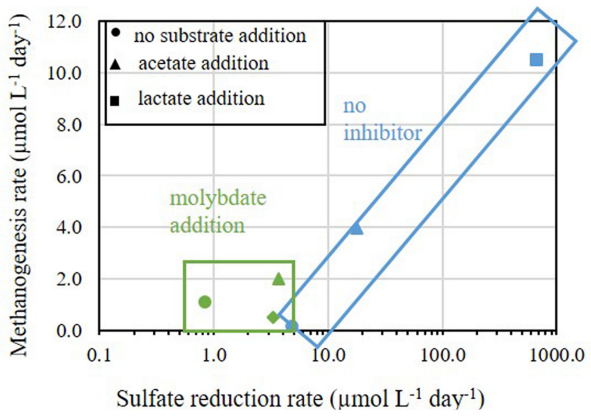

FIGURE 8 | Methanogenesis rates versus sulfate reduction rates in Experiments B and C. The rates of samples without addition of inhibitors are marked in blue symbols and rectangle and the rates of samples treated with molybdate are marked in green symbols and rectangle.

change in sulfate concentration is small during the course of the experiment as it is less sensitive). The decrease in $\delta^{34}S_{SO4}$ in the killed control and in the experiment with molybdate supplementation toward the end of experiment can be attributed to anaerobic abiotic oxidation of reduced sulfur compounds (Balci et al., 2007). Furthermore, sulfate reduction was enhanced when methanogenesis was inhibited (by BES) (**Figure 6B**) and methanogenesis rate was enhanced when sulfate reduction was inhibited (by molybdate) (**Figure 6A**). It seems therefore that the enrichment of ^{34}S of residual sulfate is correlated with the rate of sulfate reduction, as shown previously (Kaplan and Rittenberg, 1964; Habicht and Canfield, 1997; Sim et al., 2011).

During methanogenesis the carbon fractionation against ^{13}C is about 25–90‰, producing very light methane with $\delta^{13}C_{CH4}$ of −50 to −100‰ and enriched $\delta^{13}C_{DIC}$ (e.g., Ferry, 1992; Whiticar, 1999; Gelwicks et al., 1994). The fractionation varies among the different pathways of methanogenesis. In hydrogenotrophic methanogenesis, CO_2 is reduced by H_2, the fractionation is slightly larger than the fractionation of acetoclastic methanogenesis and can exceed 55‰. In acetoclastic methanogenesis methane is derived from the methyl group of acetate, the fractionation is slightly lower and ranges between 40 and 60‰ (Whiticar et al., 1986; Whiticar, 1999).

Slurries treated with BES and non-inhibited slurries showed similar methanogenesis rates, based on methane concentrations measurements. However, the isotope measurements, which are often more sensitive, showed significant stronger depletion of $\delta^{13}C_{CH4}$ in slurries treated with BES relative to non-inhibited slurries (**Figures 4D,F**). Valentine et al. (2004) and Penning et al. (2005) showed that during hydrogenotrophic methanogenesis high levels of H_2 were correlated with low fractionation in

TABLE 3 | Copies per gram dry sediment of specific genes for each of the duplicate bottles.

	Copies per gr dry sediment									
Natural sediment at t_0	**Archaea**		**Bacteria**		**Methanogens**		**Sulfate reducing bacteria**		**Archaea/Bacteria ratio**	
	2.4×10^8		1.0×10^{11}		3.4×10^7		7.6×10^7		2.4×10^{-3}	
Treatment	**90 days**	**230 days**	**90 days**	**230 days**	**90 days**	**230 days**	**90 days**	**230 days**	**90 days**	**230 days**
Natural	7.3×10^8	1.7×10^8	7.8×10^{11}	4.7×10^{11}	1.0×10^8	4.4×10^7	7.0×10^8	8.3×10^7	9.3×10^{-4}	3.6×10^{-4}
	6.0×10^8	1.5×10^8	4.9×10^{11}	4.2×10^{11}	8.3×10^7	4.9×10^7	4.5×10^8	7.2×10^7	1.2×10^{-3}	3.6×10^{-4}
Acetate	9.3×10^8	3.7×10^8	2.6×10^{12}	1.5×10^{12}	2.1×10^8	5.8×10^7	2.3×10^9	7.9×10^8	3.6×10^{-4}	2.5×10^{-4}
	4.8×10^8	1.8×10^8	6.8×10^{11}	8.6×10^{11}	6.8×10^7	1.6×10^7	9.9×10^8	2.4×10^8	7.1×10^{-4}	2.0×10^{-4}
Lactate	4.6×10^9	1.9×10^9	4.8×10^{12}	2.7×10^{12}	9.4×10^8	8.3×10^8	3.8×10^9	1.5×10^8	9.6×10^{-4}	7.2×10^{-4}
	8.1×10^9	2.7×10^9	7.0×10^{12}	4.7×10^{12}	1.2×10^9	1.8×10^9	2.9×10^9	3.1×10^8	1.2×10^{-3}	5.8×10^{-4}

carbon, and low levels of H_2 were correlated with higher fractionation. The authors hypothesized that this difference is controlled by the extent of the enzymatic reversibility which, is controlled by the Gibbs free energy of catabolism, similar to dissimilatory sulfate reduction (Kaplan and Rittenberg, 1964; Habicht and Canfield, 1997). BES is an analog of coenzyme M found in all methanogens and is a specific inhibitor for methanogens (Chidthaisong and Conrad, 2000b). Since coenzyme M is involved in the rate limiting step in methane production (Scheller et al., 2013), we propose that BES addition stops the reversibility of methanogenesis or acts similarly to low levels of H_2 or reduced Gibbs free energy (less negative) and therefore the fractionation is larger in the BES treated slurries.

Substrate Supplementation Effect

Methanogenesis and sulfate reduction rates calculated from Experiment C show that the supplementation of lactate and acetate had a significant effect on the rate of the processes (**Figure 6**). Similarly to Experiment A, when a sulfate reduction inhibitor (molybdate) was added methanogenesis was enhanced, with the exception of acetate supplementation (**Figure 6A**). The rates of sulfate reduction and methanogenesis increased by one order of magnitude as a result of acetate supplementation, and with lactate both rates increased by two orders of magnitude (**Figure 8**). Although the effect of a non-competitive substrate was not examined in this research, the results show that competitive labile organic matter had similar effects on the rates of sulfate reduction and methanogenesis. This indicates that at a high organic load, sulfate reduction and methanogenesis can co-exist and share ambient electron donors (Ozuolmez et al., 2015; Egger et al., 2016). The effect of labile organic matter on methanogenesis rate was shown also in a recent study from a shallow sediment in the Peruvian margins having co-existence of methanogenesis and sulfate reduction with 1–2 order of magnitudes difference in rates, which remain steady along the organic carbon concentration gradient (Maltby et al., 2015).

Nevertheless, when considering the absolute rates, sulfate reduction was the favorable process over methanogenesis in slurries with substrate supplementation. This advantage could be attributed to thermodynamic preference of sulfate reduction compared to methanogenesis (Lovley and Goodwin, 1988) and the population composition under natural conditions, in which sulfate reducing bacteria represented 10% of the total microbial community while methanogens represented less than 0.01% (**Table 3**). This is shown in **Figure 8**, which summarizes the effect of substrate addition on the rates of sulfate reduction and methanogenesis. When lactate and acetate were added both rates were enhanced by two and one orders of magnitude, respectively. Nevertheless, a two orders of magnitude difference between sulfate reduction and methanogenesis remained. Thus, it appears that the competition over substrate controls the intensity of methanogenesis in estuarine sediments (**Figure 8**).

According to the microbial population analysis, sulfate reducing bacteria were dominant at the beginning of Experiment B, whereas over the course of the experiment methanogen abundance increased, even though sulfate concentrations was still high with acetate supplementation (7 mM; **Figure 7**). In addition, lactate addition stimulated rapid sulfate reduction, which may have caused sulfate reducers to be sulfate-limited and enabled methanogens to strengthen. This suggests that sulfate reducing bacteria have an initial advantage for electron donor uptake; however, methanogens can also grow under elevated sulfate concentration and sulfate reduction rates. This observation strengthens our hypothesis that sulfate reduction and methanogenesis can co-exist and initial sulfate concentrations in the sediment do not control methane production initiation and intensity. The rate and initiation depth of methanogenesis is probably more strongly affected by the competition and the quantitative advantage of the sulfate reducing bacteria over the methanogens, as well as their stronger affinity for substrate uptake and the fact that sulfate reducing bacteria are not sulfate limited in these sediments (**Figure 7**).

Sulfate reducing bacteria have higher affinity to hydrogen and acetate than methanogens (Oremland and Polcin, 1982). However, co-existence of sulfate reduction and methanogenesis was shown under substrate limited conditions and following substrate supplementation, without dependence on sulfate concentration in the Yarqon sediments. The qPCR results show that acetate supplementation considerably enhanced the abundance of sulfate reducing bacteria and may indicate that the dominant electron donor in this process in the sediments is acetate. Lactate supplementation enhanced methanogens considerably, probably due to hydrogen production during lactate degradation and due to quick depletion in sulfate concentrations in the slurries treated with lactate.

SUMMARY

This study evaluated the regulatory effects of sulfate concentrations and microbial sulfate reduction on methanogenesis in the SMTZ of estuarine sediments using the Yarqon river estuary as a case study. The results show that: (a) Sulfate concentrations do not limit the onset and methanogenesis rates in the Yarqon estuarine sediments, even when sulfate concentrations are as high as 10 mM; (b) The main factors controlling methanogenesis initiation and intensity are sulfate reduction rate and substrate availability and; (c) Methanogenesis can co-exist with sulfate reduction in a large range of sulfate reduction rates (5–700 μmol L^{-1} day^{-1}) that are controlled by substrate and inhibitor additions. Sulfate reducing bacteria have a distinct favorable substrate utilization, as apparent by two orders of magnitude higher reduction rates compared to methanogenesis rates. The qPCR analysis results strengthen our geochemical data and show a shift in time from an initial dominance of sulfate reducing bacteria to a growth of the methanogen community toward the end of the experiment. Although estuarine sediments represent only 0.7% of the total marine sediments area, they contribute 7–10% of oceanic emissions of carbon to the atmosphere (Bange et al., 1994; Abril and Iversen, 2002). Thus, studying methane production controls and specifically the co-existence of the two main carbon sink processes in estuarine sediments is globally important. The results from the Yarqon estuary may be significant to

other estuarine environments that show co-existence of methanogenesis and sulfate reduction.

AUTHOR CONTRIBUTIONS

MS-A and OS designed the experiments, MS-A and HV performed the work, GA measured the sulfur isotopes. MS-A, ZR, BH, GA, WE, and OS analyzed the data and wrote the manuscript.

ACKNOWLEDGMENTS

We are grateful to Dr. D. Pargament and P. Rubinzaft from the Yarqon River Authority for their technical support in the field. We are thankful to E. Eliani-Russak for technical help in the lab. We are thankful to A. Turchyn for sulfur isotopes measurements, interpretation and for the internal review. We are thankful also to Prof. J. Ganor for the use in the HPLC. This research was supported by the Israel Science Foundation (#643/12).

REFERENCES

Abril, G., and Iversen, N. (2002). Methane dynamics in a shallow non-tidal estuary (Randers Fjord, Denmark). *Mar. Ecol. Prog. Ser.* 230, 171–181. doi: 10.3354/meps230171

Antler, G., Turchyn, A. V., Herut, B., Davies, A., Rennie, V. C., and Sivan, O. (2014). Sulfur and oxygen isotope tracing of sulfate driven anaerobic methane oxidation in estuarine sediments. *Estuar. Coast. Shelf Sci.* 142, 4–11. doi: 10.1016/j.ecss.2014.03.001

Archer, D. (2007). Methane hydrate stability and anthropogenic climate change. *Biogeosciences* 4, 993–1057. doi: 10.5194/bgd-4-993-2007

Arnon, S., Avni, N., and Gafny, S. (2015). Nutrient uptake and macroinvertebrate community structure in a highly regulated Mediterranean stream receiving treated wastewater. *Aquat. Sci.* 77, 623–637. doi: 10.1007/s00027-015-0407-6

Balci, N., Shanks, W. C., Mayer, B., and Mandernack, K. W. (2007). Oxygen and sulfur isotope systematics of sulfate produced by bacterial and abiotic oxidation of pyrite. *Geochim. Cosmochim. Acta* 71, 3796–3811. doi: 10.1016/j.gca.2007.04.017

Bange, H. W., Bartell, U., Rapsomanikis, S., and Andreae, M. O. (1994). Methane in the Baltic and North Seas and a reassessment of the marine emissions of methane. *Glob. Biogeochem. Cycles* 8, 465–480. doi: 10.1029/94GB02181

Bar-Or, I., Ben-Dov, E., Kushmaro, A., Eckert, W., and Sivan, O. (2015). Methane-related changes in prokaryotes along geochemical profiles in sediments of Lake Kinneret (Israel). *Biogeosciences* 12, 2847–2860. doi: 10.5194/bg-12-2847-2015

Borowski, W. S., Cagatay, N., Ternois, Y., and Paull, C. K. (2000). "Data report: carbon isotopic composition of dissolved CO2, CO2 gas, and methane, Blake-Bahama Ridge and northeast Bermuda Rise, ODP Leg 172," in *Proceedings of the Ocean Drilling Program, Scientific Results*, Vol. 172, eds L. D. Keigwin and D. Rio (College Station, TX: Ocean Drilling Program), 1–16. doi: 10.1021/es5006797

Borowski, W. S., Paull, C. K., and Ussler, W. (1996). Marine pore-water sulfate profiles indicate in situ methane flux from underlying gas hydrate. *Geology* 24, 655–658. doi: 10.1130/0091-7613(1996)024<0655:MPWSPI>2.3.CO;2

Canfield, D. E. (2001). Isotope fractionation by natural populations of sulfate-reducing bacteria. *Geochim. Cosmochim. Acta* 65, 1117–1124. doi: 10.1016/S0016-7037(00)00584-6

Chidthaisong, A., and Conrad, R. (2000a). Turnover of glucose and acetate coupled to reduction of nitrate, ferric iron and sulfate and to methanogenesis in anoxic rice field soil. *FEMS Microbiol. Ecol.* 31, 73–86.

Chidthaisong, A., and Conrad, R. (2000b). Specificity of chloroform, 2-bromoethanesulfonate and fluoroacetate to inhibit methanogenesis and other anaerobic processes in anoxic rice field soil. *Soil Biol. Biochem.* 32, 977–988. doi: 10.1016/S0038-0717(00)00006-7

Conrad, R. (1999). Contribution of hydrogen to methane production and control of hydrogen concentrations in methanogenic soils and sediments. *FEMS Microbiol. Ecol.* 28, 193–202. doi: 10.1111/j.1574-6941.1999.tb00575.x

Dale, A. W., Regnier, P., Knab, N., Jørgensen, B. B., and Van Cappellen, P. (2008). Anaerobic oxidation of methane (AOM) in marine sediments from the Skagerrak (Denmark): II. Reaction-transport modeling. *Geochim. Cosmochim. Acta* 72, 2880–2894. doi: 10.1111/j.1462-2920.2007.01526.x

Egger, M., Lenstra, W., Jong, D., Meysman, F. J. R., Sapart, C. J., van der Veen, C., et al. (2016). Rapid sediment accumulation results in high methane effluxes from coastal sediments. *PLoS ONE* 11:e0161609. doi: 10.1371/journal.pone.0161609

Eliani-Russak, E., Herut, B., and Sivan, O. (2013). The role of highly sratified nutrient-rich small estuaries as a source of dissolved inorganic nitrogen to coastal seawater, the Qishon (SE Mediterranean) case. *Mar. Pollut. Bull.* 71, 250–258. doi: 10.1016/j.marpolbul.2013.02.001

Ferry, J. G. (1992). Methane from acetate. *J. Bacteriol.* 174, 5489–5495. doi: 10.1128/jb.174.17.5489-5495.1992

Froelich, P., Klinkhammer, G., Bender, M. A. A., Luedtke, N., Heath, G. R., Cullen, D., et al. (1979). Early oxidation of organic matter in pelagic sediments of the eastern equatorial Atlantic: suboxic diagenesis. *Geochim. Cosmochim. Acta* 43, 1075–1090. doi: 10.1016/0016-7037(79)90095-4

Gelwicks, J. T., Risatti, J. B., and Hayes, J. M. (1994). Carbon isotope effects associated with aceticlastic methanogenesis. *Appl. Environ. Microbiol.* 60, 467–472.

Habicht, K. S., and Canfield, D. E. (1997). Sulfur isotope fractionation during bacterial sulfate reduction in organic-rich sediments. *Geochim. Cosmochim. Acta* 61, 5351–5361. doi: 10.1016/S0016-7037(97)00311-6

Kaplan, I. R., and Rittenberg, S. C. (1964). Microbiological fractionation of sulphur isotopes. *J. Gen. Microbiol.* 34, 195–212. doi: 10.1099/00221287-34-2-195

Kiene, R. P., Oremland, R. S., Catena, A., Miller, L. G., and Capone, D. G. (1986). Metabolism of reduced methylated sulfur compounds in anaerobic sediments and by a pure culture of an estuarine methanogen. *Appl. Environ. Microbiol.* 52, 1037–1045.

King, G. M. (1984). Utilization of hydrogen, acetate, and "noncompetitive"; substrates by methanogenic bacteria in marine sediments. *Geomicrobiol. J.* 3, 275–306. doi: 10.1080/01490458409377807

Knab, N. J., Cragg, B. A., Hornibrook, E. R. C., Holmkvist, L., Pancost, R. D., Borowski, C., et al. (2009). Regulation of anaerobic methane oxidation in sediments of the Black Sea. *Biogeosciences* 6, 1505–1518. doi: 10.5194/bg-6-1505-2009

Knab, N. J., Dale, A. W., Lettmann, K., Fossing, H., and Jørgensen, B. B. (2008). Thermodynamic and kinetic control on anaerobic oxidation of methane in marine sediments. *Geochim. Cosmochim. Acta* 72, 3746–3757. doi: 10.1016/j.gca.2008.05.039

Knittel, K., and Boetius, A. (2009). Anaerobic oxidation of methane: progress with an unknown process. *Annu. Rev. Microbiol.* 63, 311–334. doi: 10.1146/annurev.micro.61.080706.093130

Koster, I., Rinzema, A., De Vegt, A., and Lettinga, G. (1986). Sulfide inhibition of the methanogenic activity of granular sludge at various pH-levels. *Water Res.* 20, 1561–1567. doi: 10.1016/0043-1354(86)90121-1

Lovley, D. R., Dwyer, D. F., and Klug, M. J. (1982). Kinetic analysis of competition between sulfate reducers and methanogens for hydrogen in sediments. *Appl. Environ. Microbiol.* 43, 1373–1379.

Lovley, D. R., and Goodwin, S. (1988). Hydrogen concentrations as an indicator of the predominant terminal electron-accepting reactions in aquatic sediments. *Geochim. Cosmochim. Acta* 52, 2993–3003. doi: 10.1016/0016-7037(88)90163-9

Lovley, D. R., and Klug, M. J. (1983). Sulfate reducers can outcompete methanogens at freshwater sulfate concentrations. *Appl. Environ. Microbiol.* 45, 187–192.

Lovley, D. R., and Phillips, E. J. (1988). Novel mode of microbial energy metabolism: organic carbon oxidation coupled to dissimilatory reduction of iron or manganese. *Appl. Environ. Microbiol.* 54, 1472–1480.

Maltby, J., Sommer, S., Dale, A. W., and Treude, T. (2015). Microbial methanogenesis in the sulfate-reducing zone of surface sediments traversing the Peruvian margin. *Biogeosciences* 12, 14869–14910. doi: 10.5194/bgd-12-14869-2015

Mountfort, D. O., and Asher, R. A. (1981). Role of sulfate reduction versus methanogenesis in terminal carbon flow in polluted intertidal sediment of waimea inlet, Nelson, New Zealand. *Appl. Environ. Microbiol.* 42, 252–258.

Mountfort, D. O., Asher, R. A., Mays, E. L., and Tiedje, J. M. (1980). Carbon and electron flow in mud and sandflat intertidal sediments at delaware inlet, nelson, new zealand. *Appl. Environ. Microbiol.* 39, 686–694.

Oremland, R. S., and Capone, D. G. (1988). "Use of "specific" inhibitors in biogeochemistry and microbial ecology," in *Advances in Microbial Ecology (Anonymous)*, ed. K. C. Marshall (Berlin: Springer), 285–383.

Oremland, R. S., and Polcin, S. (1982). Methanogenesis and sulfate reduction: competitive and noncompetitive substrates in estuarine sediments. *Appl. Environ. Microbiol.* 44, 1270–1276.

Oremland, R. S., and Taylor, B. F. (1978). Sulfate reduction and methanogenesis in marine sediments. *Geochim. Cosmochim. Acta.* 42, 209–214. doi: 10.1016/0016-7037(78)90133-3

Ozuolmez, D., Na, H., Lever, M. A., Kjeldsen, K. U., Jørgensen, B. B., and Plugge, C. M. (2015). Methanogenic archaea and sulfate reducing bacteria co-cultured on acetate: teamwork or coexistence? *Front. Microbiol.* 6:492. doi: 10.3389/fmicb.2015.00492

Parkes, R. J., Brock, F., Banning, N., Hornibrook, E. R., Roussel, E. G., Weightman, A. J., et al. (2012). Changes in methanogenic substrate utilization and communities with depth in a salt-marsh, creek sediment in southern England. *Estuar. Coast. Shelf Sci.* 96, 170–178. doi: 10.1016/j.ecss.2011.10.025

Penning, H., Plugge, C. M., Galand, P. E., and Conrad, R. (2005). Variation of carbon isotope fractionation in hydrogenotrophic methanogenic microbial cultures and environmental samples at different energy status. *Glob. Change Biol.* 11, 2103–2113. doi: 10.1111/j.1365-2486.2005.01076.x

Scheller, S., Goenrich, M., Thauer, R. K., and Jaun, B. (2013). Methyl-coenzyme M reductase from methanogenic archaea: isotope effects on the formation and anaerobic oxidation of methane. *J. Am. Chem. Soc.* 135, 14975–14984. doi: 10.1021/ja406485z

Schink, B. (1997). Energetics of syntrophic cooperation in methanogenic degradation. *Microbiol. Mol. Biol. Rev.* 61, 262–280.

Schönheit, P., Kristjansson, J. K., and Thauer, R. K. (1982). Kinetic mechanism for the ability of sulfate reducers to out-compete methanogens for acetate. *Arch. Microbiol.* 132, 285–288. doi: 10.1007/BF00407967

Sim, M. S., Bosak, T., and Ono, S. (2011). Large sulfur isotope fractionation does not require disproportionation. *Science* 333, 74–77. doi: 10.1126/science.1205103

Sivan, O., Antler, G., Turchyn, A. V., Marlow, J. J., and Orphan, V. J. (2014). Iron oxides stimulate sulfate-driven anaerobic methane oxidation in seeps. *Proc. Natl. Acad. Sci. U.S.A.* 111, E4139–E4147. doi: 10.1073/pnas.1412269111

Stumm, W., and Morgan, J. J. (1996). *Aquatic Chemistry: Chemical Equilibria and Rates in Natural Waters*, 3rd Edn. Hoboken, NJ: John Wiley & Sons, Inc.

Thang, N. M., Brüchert, V., Formolo, M., Wegener, G., Ginters, L., Jørgensen, B. B., et al. (2013). The impact of sediment and carbon fluxes on the biogeochemistry of methane and sulfur in littoral Baltic Sea sediments (Himmerfjärden. Sweden). *Estuaries Coasts* 36, 98–115. doi: 10.1007/s12237-012-9557-0

Thauer, R. K., Jungermann, K., and Decker, K. (1977). Energy conservation in chemotrophic anaerobic bacteria. *Bacteriol. Rev.* 41, 100–180.

Treude, T., Krause, S., Maltby, J., Dale, A. W., Coffin, R., and Hamdan, L. J. (2014). Sulfate reduction and methane oxidation activity below the sulfate-methane transition zone in Alaskan Beaufort Sea continental margin sediments: implications for deep sulfur cycling. *Geochim. Cosmochim. Acta* 144, 217–237. doi: 10.1016/j.gca.2014.08.018

Treude, T., Krüger, M., Boetius, A., and Jørgensen, B. B. (2005). Environmental control on anaerobic oxidation of methane in the gassy sediments of Eckernförde Bay (German Baltic). *Limnol. Oceanogr.* 50, 1771–1786. doi: 10.4319/lo.2005.50.6.1771

Valentine, D. L., Chidthaisong, A., Rice, A., Reeburgh, W. S., and Tyler, S. C. (2004). Carbon and hydrogen isotope fractionation by moderately thermophilic methanogens. *Geochim. Cosmochim. Acta.* 68, 1571–1590. doi: 10.1016/j.gca.2003.10.012

Valentine, D. L., and Reeburgh, W. S. (2000). New perspectives on anaerobic methane oxidation. *Environ. Microbiol.* 2, 477–484. doi: 10.1046/j.1462-2920.2000.00135.x

Ward, D. M., and Winfrey, M. R. (1985). Interactions between methanogenic and sulfate-reducing bacteria in sediments. *Adv. Aquat. Microbiol.* 3, 141–179.

Whiticar, M. J. (1999). Carbon and hydrogen isotope systematics of bacterial formation and oxidation of methane. *Chem. Geol.* 161, 291–314. doi: 10.1016/S0009-2541(99)00092-3

Whiticar, M. J., Faber, E., and Schoell, M. (1986). Biogenic methane formation in marine and freshwater environments: CO_2 reduction vs. acetate fermentation—Isotope evidence. *Geochim. Cosmochim. Acta* 50, 693–709. doi: 10.1016/0016-7037(86)90346-7

Wilms, R., Sass, H., Kopke, B., Koster, J., Cypionka, H., and Engelen, B. (2006). Specific bacterial, archaeal, and eukaryotic communities in tidal-flat sediments along a vertical profile of several meters. *Appl. Environ. Microbiol.* 72, 2756–2764. doi: 10.1128/AEM.72.4.2756-2764.2006

Wortmann, U. G., Bernasconi, S. M., and Böttcher, M. E. (2001). Hypersulfidic deep biosphere indicates extreme sulfur isotope fractionation during single-step microbial sulfate reduction. *Geology* 29, 647–650. doi: 10.1130/0091-7613(2001)029<0647:HDBIES>2.0.CO;2

Yu, Z., Garcia-Gonzalez, R., Schanbacher, F. L., and Morrison, M. (2008). Evaluations of different hypervariable regions of archaeal 16S rRNA genes in profiling of methanogens by *Archaea*-specific PCR and denaturing gradient gel electrophoresis. *Appl. Environ. Microbiol.* 74, 889–893. doi: 10.1128/AEM.00684-07

Conflict of Interest Statement: The authors declare that the research was conducted in the absence of any commercial or financial relationships that could be construed as a potential conflict of interest.

frontiers in Earth Science

ORIGINAL RESEARCH
published: 22 July 2016
doi: 10.3389/feart.2016.00075

Off Limits: Sulfate below the Sulfate-Methane Transition

Benjamin Brunner[1], Gail L. Arnold[1], Hans Røy[2], Inigo A. Müller[3] and Bo B. Jørgensen[2]*

[1] Department of Geological Sciences, University of Texas at El Paso, El Paso, TX, USA, [2] Center for Geomicrobiology, Department of Bioscience, Aarhus University, Aarhus, Denmark, [3] Climate Geology, Geological Institute, ETH Zurich, Zürich, Switzerland

One of the most intriguing recent discoveries in biogeochemistry is the ubiquity of cryptic sulfur cycling. From subglacial lakes to marine oxygen minimum zones, and in marine sediments, cryptic sulfur cycling—the simultaneous consumption and production of sulfate—has been observed. Though this process does not leave an imprint in the sulfur budget of the ambient environment—thus the term cryptic—it may have a massive impact on other element cycles and fundamentally change our understanding of biogeochemical processes in the subsurface. Classically, the sulfate-methane transition (SMT) in marine sediments is considered to be the boundary that delimits sulfate reduction from methanogenesis as the predominant terminal pathway of organic matter mineralization. Two sediment cores from Aarhus Bay, Denmark reveal the constant presence of sulfate (generally 0.1–0.2 mM) below the SMT. The sulfur and oxygen isotope signature of this deep sulfate ($\delta^{34}S = 18.9‰$, $\delta^{18}O = 7.7‰$) was close to the isotope signature of bottom-seawater collected from the sampling site ($\delta^{34}S = 19.8‰$, $\delta^{18}O = 7.3‰$). In one of the cores, oxygen isotope values of sulfate at the transition from the base of the SMT to the deep sulfate pool ($\delta^{18}O = 4.5–6.8‰$) were distinctly lighter than the deep sulfate pool. Our findings are consistent with a scenario where sulfate enriched in ^{34}S and ^{18}O is removed at the base of the SMT and replaced with isotopically light sulfate below. Here, we explore scenarios that explain this observation, ranging from sampling artifacts, such as contamination with seawater or auto-oxidation of sulfide—to the potential of sulfate generation in a section of the sediment column where sulfate is expected to be absent which enables reductive sulfur cycling, creating the conditions under which sulfate respiration can persist in the methanic zone.

Keywords: cryptic sulfur cycle, biogeochemistry, sulfate reduction, sulfur isotopes, oxygen isotopes

OPEN ACCESS

Edited by:
Tanja Bosak, Massachusetts Institute of Technology, USA

Reviewed by:
David Fike, Washington University, USA
Boswell Wing, McGill University, Canada

****Correspondence:***
Benjamin Brunner
bbrunner@utep.edu

Specialty section:
This article was submitted to Microbiological Chemistry and Geomicrobiology, a section of the journal Frontiers in Earth Science

Received: *14 April 2016*
Accepted: *30 June 2016*
Published: *22 July 2016*

Citation:
Brunner B, Arnold GL, Røy H, Müller IA and Jørgensen BB (2016) Off Limits: Sulfate below the Sulfate-Methane Transition. Front. Earth Sci. 4:75. doi: 10.3389/feart.2016.00075

INTRODUCTION

In recent years, it has become evident that the classical view of sedimentary sulfur cycling is incomplete, and may in important aspects be incorrect. There is growing evidence that sulfur cycling occurs outside of the main sulfate reduction zone. In these environments, sulfur compounds are continuously reduced and re-oxidized, with the overall inventory of the sulfur constituents remaining constant. This sulfur cycle so far has eluded direct observation, and has been coined cryptic sulfur cycling.

For example, cryptic sulfur cycling is inferred to occur in the oxygen minimum zone off Peru where sulfide that is produced by microbial sulfate reduction in the oxygen-free core of

oxygen minimum zones is converted back to sulfate, presumably tied to reductive nitrogen cycling (Canfield et al., 2010b; Teske, 2010; Johnston et al., 2014). Another example for the potential of cryptic sulfur cycling comes from a sub-glacial lake in Antarctica (Mikucki et al., 2009), where sulfate-sulfur is apparently reduced and re-oxidized back to sulfate via coupling to reductive iron cycling. The finding of sulfate reducing microorganisms in in subsurface methanic sediments from Aarhus Bay (Baltic Sea) and Black Sea sediments (Leloup et al., 2007, 2009) that were traditionally considered to be sulfate-free and devoid of active sulfate reduction, and the presence of low, but detectable sulfate in subsurface methanic sediments from Aarhus Bay (Holmkvist et al., 2011) implies that cryptic sulfur cycling is an ongoing process throughout the anoxic sediment column.

The potential existence of a cryptic sulfur cycle beneath the main sulfate zone in marine sediments is particularly interesting. It challenges or at least transforms the paradigm that there is a sequential cascade of electron accepting processes in the environment across redox gradients, with the energetically most favorable electron acceptor being consumed first and the least attractive process being carried out last (i.e., in marine organic-rich sediments: oxygen respiration, nitrate, manganese, iron, and, sulfate reduction, methanogenesis). In the methanic zone, sulfate is assumed to have been completely consumed because microbial sulfate reduction occurs even at very low sulfate concentrations (Tarpgaard et al., 2011) and because sulfate reduction can be coupled to the anaerobic oxidation of methane. The finding of sulfate, and the persistence of sulfate reducing micororganisms in the methanic zone thus indicate that there is hidden, "cryptic" sulfate production in these sediments. Elucidating the mechanisms behind such sulfate production has the potential to gain new insights into the links between the biogeochemical cycles of different elements. For example, sulfide concentrations typically decrease below the sulfate-methane transition (SMT), presumably due to concomitant formation of pyrite (FeS_2), a process that necessitates sulfur oxidation. This demonstrates that in methanic sediments there is at least a potential for the availability of oxidants, such as reactive ferric iron, as invoked by Holmkvist et al. (2011) to explain the elevated concentrations of sulfate present below the SMT. Quantification of such a cryptic iron-sulfur cycle would shed light on how reactive such iron phases are, and to what extent microbial activity impacts the reactivity of the iron phases. An alternative avenue for the production of sulfate in methanic sediments could be the disproportionation of sulfur species with an intermediate oxidation state, which raises that question if, and under what circumstances, microbial sulfate reduction does not have sulfide as final metabolic product. This may be the case for in sulfate reduction coupled to the anaerobic oxidation of methane (Milucka et al., 2012) where zero-valent sulfur has been found to be an intermediate, but may even apply to classical microbial sulfate reduction (Bishop et al., 2013). As such, the exploration of cryptic sulfur cycling provides insight into how microbial processes under energy limitation work, and if/how specialized microorganisms share the already small amount of available energy to carry out different biochemical reactions.

The aim of this study was to investigate if sulfate production occurs below of the SMT in a setting that is typical for anaerobic marine sediments. This goal is pursued via the study of the sulfate concentration and the sulfate-sulfur and -oxygen isotope composition for two sediment cores retrieved from Aarhus Bay, Denmark.

METHODS

Sediment and Pore Water Sampling

Two sediment cores, one in May and one in October 2013 were taken at Station M1 in Aarhus Bay (56°07.0580′N and 10°20.8650′E, **Figure 1**) during sampling campaigns aboard the *RV Tyra*. Previous studies have identified elevated sulfate concentrations below the SMT at this station (Holmkvist et al., 2011). Sediment cores were taken with a gravity corer which was constructed with a steel barrel with a 12 cm diameter PVC core liner. A 220-cm long core was collected in May 2013 and a 320-cm long core in October 2013, hereafter referred to as the Spring and Fall cores. Immediately after coring the ship returned to harbor and the cores were transported to cold rooms at Aarhus University where they were stored and processed at ∼4°C.

In the Spring Campaign, all pore water samples were extracted using a Geotek® pore water squeezer and a manual hydraulic press. Whole round core sections, 10 cm in length were cut, starting from the deepest part of the sediment core and proceeding step-wise to the shallowest portion. All sub-SMT pore water samples were collected and processed within 24 h of core retrieval (core-on-deck) and the remainder of pore water samples processed within the subsequent 27 h. Sediment sections were extruded from the liner and 1–2 cm of sediment were removed from the top, bottom, and sides of the core to remove any potential surface contamination or oxidation products. After this, the remaining sediment was loaded into the pore water squeezer.

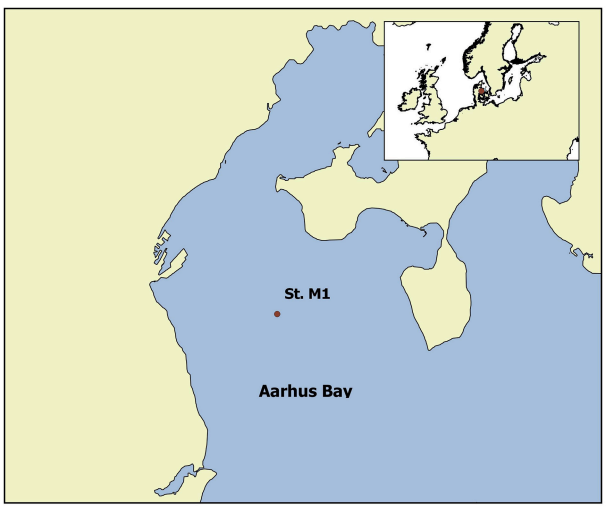

FIGURE 1 | Map of study site and location of Station M1 in Aarhus Bay, Denmark.

During loading, the pore water squeezer was continuously back-flushed with nitrogen gas. This procedure causes some loss of sulfide that is carried away in the nitrogen gas stream. After the squeezer was completely assembled, the nitrogen gas line was removed and pressure applied, expelling residual gas and starting the pore water extraction. The first 3–5 ml of pore water were discarded. Next a 10 ml plastic syringe was attached and ∼6 ml of pore water were collected for chemical concentration and $\delta^{18}O_{H2O}$ analyses. Finally, a length of plastic tubing with a needle tip on the end was attached to the pore water squeezer to enable the collection of a large volume of pore water for sulfur and oxygen isotope analysis of sulfur species. Pore water was allowed to fill the tubing and the first few drops let to waste before the needle tip was inserted into a 100 ml serum bottle with 2 ml of 20% zinc acetate, sealed, and flushed with nitrogen gas. It took on average 1 h to collect up to 50 ml of pore water for analysis.

Because our initial review of sampling artifact tests from the Spring Campaign indicated there was no threat of artifact effects during sediment core storage, we changed our pore water extraction protocol in the Fall Campaign. First, pore water samples above 170 cm were collected with a Rhizon® pore water sampler at a sampling resolution of 10 cm. Whole round cores were cut, the bottoms capped and the tops covered in plastic film to protect the exposed sediment surface from sulfide oxidation due to contact with air and secured with electric tape. Rhizon® samplers were inserted through the plastic film and pushed to a depth in the sediment to ensure pore water extraction from the center of the sediment core. As before, the first few milliliters of sample was discarded and then a total of 15–20 ml of pore water was collected for concentration and isotope analysis. Pore water sampling by Rhizon®, which was being processed concurrently with other sub-sectioning of the core for incubation experiments (not presented here) was completed within 48 h of core retrieval. Samples between 170 and 230 cm were collected with the pore water squeezer within the following 38 h (a total of 86 h after core retrieval, which could allow for contamination with sulfate from surface sediments of the core section, see Section Discussion) using the same procedure as was used in the Spring, with the exception that the serum bottles used to collect the large volume pore water samples were pre-flushed with N_2 but were not pre-loaded with zinc acetate.

Generally, pore water was split into sub-samples for (i) sulfate and chloride concentration, (ii) sulfide concentration, (iii) thiosulfate and sulfite concentration, (iv) $\delta^{18}O_{H2O}$, and (v) sulfate/sulfide sulfur and oxygen isotope composition as well as gravimetric determination of sulfate concentrations (**Table 1**). Weights and volumes were noted at every step. Sulfate, chloride, sulfide, and thiosulfate concentrations were analyzed by standard methods (ion chromatography, diamine/spectrophotometric methods, and bimane/HPLC, respectively). Sub-samples for sulfate/sulfide sulfur and oxygen isotope composition (sub-sample v) were treated sequentially to separate sulfate from sulfide. In the Spring, precipitated zinc sulfide (ZnS) was separated from the sample by vacuum filtration through a 0.2 μm filter. The ZnS was later converted to silver sulfide (Ag_2S) for sulfur isotope analysis. With a modified vacuum filtration system, the filtrate was directly collected in clean 50 ml serum vials that were subsequently acidified with 0.1 ml ultraclean hydrochloric acid (HCl), after which the filtrate was flushed with CO_2 gas for 1 h to ensure that no sulfide remained in the sample. Next, a sub-sample was transferred to a centrifuge tube and a saturated solution of barium chloride (∼1.3 M $BaCl_2$ in 0.05 M HCl) was added to precipitate sulfate as barium sulfate ($BaSO_4$). For samples above the SMT, the following day, the samples were centrifuged and the supernatant discarded. The $BaSO_4$ precipitate was washed several times, dried overnight in a 50°C oven and retained for sulfur and oxygen isotope analysis. For samples from below the SMT, the collection of the precipitate was modified to ensure quantitative recovery of the $BaSO_4$. Briefly, the $BaSO_4$ was collected on a filter. Filter and centrifuge tube (where $BaSO_4$ may remain adhered to the tube) were then washed with a chelator to re-dissolve the $BaSO_4$. Sample $BaSO_4$ was then recovered by the addition of hydrochloric acid according to the method of Bao (2006). In the Fall, no zinc acetate was added to the sub-samples for sulfate/sulfide sulfur and oxygen isotope composition (sub-sample v). Instead, directly after completion of pore water collection, the sample was acidified with 0.5 ml of concentrated ultra-clean HCl flushed with N_2 gas and the evolved H_2S was collected in a silver nitrate trap (10 ml of 1 M $AgNO_3$) as Ag_2S. The Ag_2S precipitate was washed several times, dried overnight in a 50°C oven and retained for sulfur isotope analysis of sulfide.

All isotope analyses were carried out at the stable isotope laboratory of the Department of Earth Sciences at ETH Zurich. All isotope values are reported according to the standard delta notation, relative to VSMOW for oxygen and VCDT for sulfur isotope measurements.

For the water-oxygen isotope analysis, 0.5 ml of sample was pipetted into a flat bottomed vial, the vial sealed and flushed with a CO_2/He mixture and allowed to equilibrate on a shaker at room temperature for at least 12 h. For every 10 samples, two in-house standards (WS2011, $\delta^{18}O = -0.59‰$; MW2011, $\delta^{18}O = 12.23‰$) were inserted. After equilibration between CO_2 headspace and the water sample, the samples and standards were transferred to a Thermo Scientific GasBench® equipped with an auto-sampler and connected to a ThermoFinnigan Delta V Plus® isotope ratio mass spectrometer (IRMS), with which the oxygen isotope composition of the CO_2 from the sample headspace was analyzed. The standard deviation (1σ) for replicate measurements of the two laboratory standards for water-oxygen isotope analysis was <0.1‰.

Oxygen isotope analysis of sulfate was done by continuous-flow isotope ratio mass spectrometry with a high temperature thermal conversion elemental analyzer, specifically a ThermoFinnigan TCEA®/Conflo IV®/Delta V Plus® IRMS combination. Approximately 0.3 mg of $BaSO_4$ samples and associated standards (NBS-127, IAEA-SO-5, and IAEA-SO-6) were weighed into silver capsules and carefully sealed. Samples and standards were then loaded into a Zero-Blank autosampler connected to the TCEA® and run. The standard deviation (1σ) for replicate measurements of a laboratory standard for oxygen isotope analysis of solid material was <0.5‰.

Sulfur isotope analysis was also done by continuous-flow isotope ratio mass spectrometry, but now coupled with a

TABLE 1 | Sampling protocol/distribution.

	Sample	Container type	Volume (ml)	Treatment
I	Sulfate and chloride concentration	Eppitube	0.5	Flushed with CO_2 to remove sulfide
ii	Sulfide concentration	Eppitube	1	0.20 ml 20% ZnAc
iii	Thiosulfate and sulfite concentration	Eppitube	0.5	Bimane
iv	Water-oxygen isotope ($\delta^{18}O_{H2O}$) composition	Eppitube	1.0	No treatment
v	Sulfate/sulfide isotope composition and gravimetric sulfate concentration	N_2 flushed 50 ml glass crimp top vial	12–50 ml	2 ml 20% ZnAc (Spring), acidification & N_2 flushing (Fall)

high temperature combustion elemental analyzer, specifically a Eurovector CNS analyzer® connected to a ThermoFinnigan Delta V® IRMS. For the determination of the sulfur isotope compositions of pure substances, i.e., $BaSO_4$ samples and standards, or Ag_2S samples and standards, 0.2–0.4 mg were weighed into tin capsules with an approximately equal amount of vanadium pentoxide (V_2O_5). The sulfur isotope measurements of $BaSO_4$ were calibrated with reference materials NBS-127 ($\delta^{34}S = +21.1‰$), IAEA-SO-5 ($\delta^{34}S = 0.49‰$), and IAEA-SO-6 ($\delta^{34}S = -34.1‰$). The standard deviation (1σ) for replicate measurements of a $BaSO_4$ laboratory standard was <0.5‰. The sulfur isotope measurements of Ag_2S were calibrated with reference materials IAEA-S-2 (previously called NZ2, $\delta^{34}S = 22.6‰$) and IAEA-S-3 ($\delta^{34}S = -32.5‰$). The standard deviation (1σ) for replicate measurements of a Ag_2S laboratory standard was <0.3‰.

RESULTS AND DISCUSSION

Sulfate Concentrations

The sulfate concentration profiles from sediment cores taken in Spring and Fall are very similar. There is good general agreement between the sulfate concentrations measured by ion chromatography and by gravimetric method based on the weight of barium sulfate precipitates, even at very low sulfate concentrations, such as for the deep sulfate pool in the Fall core (**Table 2**; **Figure 2**). Reproducibility of sulfate concentrations via gravimetric method based on multiple control samples is better than 0.02 mM (1 sd). In the absence of direct methane concentration measurements on the cores in this study, we consider the SMT to begin after sulfate concentrations drop below 1 mM and assign the base of the SMT to the depth directly above the deep sulfate pool. We define the deep sulfate pool as sulfate in the sediment column below the SMT where the sulfur and oxygen isotope composition of sulfate shows no clear depth trend and which begins at approximately a depth of 190 cm for both cores. For the Spring core, between a depth of 150 and 205 cm there is a discrepancy between sulfate concentrations determined by ion chromatography and the gravimetric method (**Figure 2B**). The good agreement between the gravimetric method and ion chromatography results from the Fall sampling campaign demonstrates that the gravimetric method does not systematically underestimate sulfate concentrations. The higher sulfate concentrations determined by ion chromatography in Spring could be due to incomplete sulfide removal during sampling and subsequent oxidation to sulfate. During the Spring campaign, sulfide was stripped by bubbling pure carbon dioxide gas through the sample. In the SMT, the sulfide peak concentrations can reach 5.5 mM (Holmkvist et al., 2011). Due to enhanced rates of sulfate reduction coupled to AOM, the pore-water pH is well buffered by the production of bicarbonate and carbonate ions. These circumstances may have led to incomplete sulfide removal by the carbon dioxide stripping in this portion of the sediment column. Irrespective of the reasons for the elevated sulfate concentrations determined by ion chromatography, we refer to the values determined by gravimetric method in the discussion of samples from the SMT and the deep sulfate zone, as the oxygen and sulfur isotope values were determined on the very same sub-samples.

Chloride Concentrations and Oxygen Isotope Composition of Water

Chloride concentrations decreased with depth, with a steeper gradient for the core taken in the Spring as compared to the core from the Fall (**Figure 3A**). A similar trend is observed for the oxygen isotope composition of water (**Table 2**). A cross plot of chloride vs. the oxygen isotope composition of water reveals nearly identical slopes for both the Spring and Fall (**Figure 3B**).

Linear extrapolation of the chloride gradients to zero concentration locates the depth of a potential freshwater interface to 441 cm depth for the core taken in Spring and 908 cm depth for the core taken in Fall. Both cores were taken at the approximately same position (i.e., within a distance of maximally 100 m). Beneath the Holocene marine sediments of Aarhus Bay is a buried landscape of till and sand that was formed by the glaciers toward the end of the last ice age, before the marine transgression took place some 9000 years ago. At site M1, where the cores were taken, a transition from terrestrial to marine sediments is observed at ca. 10 m depth, but the topography of this paleo-landscape can be highly variable over short lateral distances. Thus, the uppermost terrestrial sand layers may be the source of a freshwater intrusion to the overlaying marine deposits and the differences between the chloride and oxygen isotope profiles between the two sampling campaigns may be the result of a small deviation in coring location. A plot of the chloride vs. the oxygen isotope composition of pore water indicates that the fresh water source is likely the same for the Spring and Fall cores, with a tentative groundwater oxygen isotope composition of ∼ −7‰ (**Figure 3B**). This value is close to the oxygen isotope

TABLE 2 | Concentration and isotope data for the Spring campaign.

cm bsf Mean	$\delta^{18}O_{H2O}$ (VSMOW)	Cl^- (mM)	Sulfate mM—IC	Sulfate (mM—grav)	$\delta^{34}S_{SO_4}$ (VCDT)	$\delta^{18}O_{SO_4}$ (VSMOW)	Sulfide (mM)	$\delta^{34}S_{sulfide}$ (VCDT)	Thiosulfate (μM)
MAY 2013									
Bottom water			25		19.8	7.3			
6	−1.6	555	23.7		27.6	15.2	0.0	−38.9	117.4
21	−1.7	522	19.8		33.3	18.2	0.6	−34.8	15.1
31	−1.8	504	17.7		36.9	19.9	0.7	−31.3	9.9
41	−1.8	496	16.3		39.0	20.2	1.0	−28.4	6.8
51	−1.9	467	14.1		41.5	20.2	0.8	−24.6	6.9
61	−2.1	477	12.3		45.5	21.9	1.8	−20.1	10.1
71	−2.1	454	10.8		46.1	20.6	2.2	−17.0	15.0
81	−2.5	432	8.3		52.2	22.0	3.1	−12.6	13.4
91	−2.5	411	6.7		56.2	22.5	2.6	−8.3	16.1
101	−2.6	413	6.5		57.8	22.9	3.3	−6.3	7.3
111	−2.8	408	4.3		61.9	22.1	1.5	−0.1	92.4
121	−3.0	393	2.7	2.56	68.9	23.0	3.0	4.5	20.2
131	−3.1	379	1.8		75.1	21.7	2.7	8.1	23.4
141	−3.1	343	1.3		80.8	22.0	1.3	10.3	52.7
151	−3.4	357	0.6		81.4	23.6	2.2	14.6	167.8
161	−3.4	339	0.5	0.23	54.7	14.5	0.8	15.5	192.8
171	−3.5	334	0.5	0.17	36.4	9.8	1.0	15.8	170.3
181	−3.6	322	0.6	0.16	23.8	6.8	1.3	16.3	138.8
191	−3.7	332	0.8	0.13	19.8	4.5	1.6	16.7	56.7
201	−3.8	311	0.5	0.12	17.3	6.1	2.4	16.1	19.8
211	−3.9	298	1.0		21.2	5.6	2.0	15.3	28.9

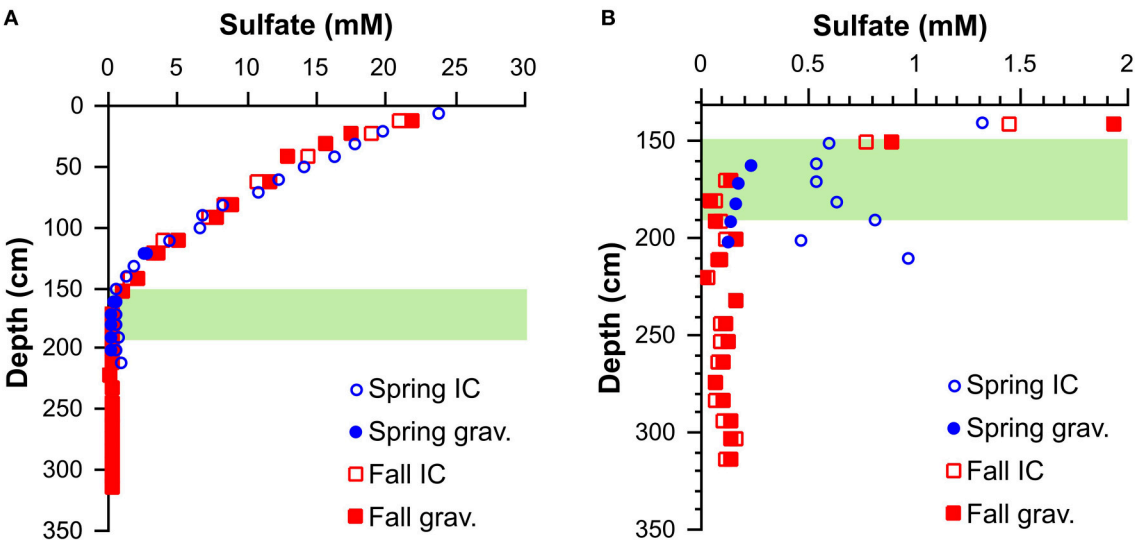

FIGURE 2 | (A) Sulfate concentration profiles for cores from Spring and Fall 2013 and **(B)** detailed profiles for the low sulfate concentration range. For the Spring core, there is a discrepancy between sulfate concentration measurements by ion chromatographic and gravimetric method. Error on the sulfate concentrations determined by ion chromatography is ±15% and better than ±0.02 mM by gravimetric method. The green band represents the SMT.

composition of meteoric water in Denmark (−8‰; Jørgensen and Holm, 1994) and to the isotope composition of water from two wells at Stautrup Waterworks near Aarhus (−7.95 to −8.65‰; Jørgensen and Holm, 2012).

Concentration of Sulfite and Thiosulfate

The concentrations of sulfite and thiosulfate were only determined for the Spring core. Sulfite could be detected, but was below the quantifiable level of 0.5 μM. Thiosulfate

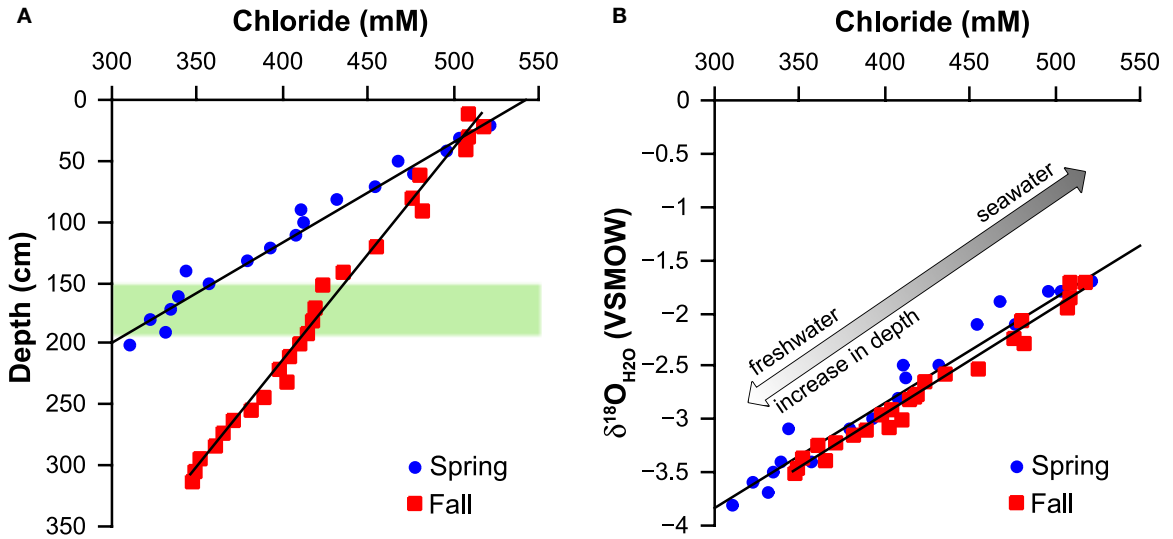

FIGURE 3 | (A) Chloride concentration vs. depth. Intercept at chloride = 0 indicates a freshwater source at 441 and 908 cm for Spring and Fall, respectively. **(B)** Chloride concentration vs. oxygen isotope composition of pore water intercept at chloride = 0 yields an oxygen isotope composition of the underlying freshwater source of ~ −7‰ (−6.78‰ Spring and −6.96‰ Fall). The green band represents the SMT.

concentrations fall in a range from 7 to 16 μM for most of the top 100 cm of the core, and show a peak of 193 μM between 150 and 185 cm, below which they drop to 29 μM at the bottom of the core at 211 cm (**Table 2**).

Concentration and Sulfur Isotope Composition of Sulfide

The concentration of sulfide scatters strongly for both the Spring and Fall core samples (**Tables 2**, **3**). We attribute this to the degassing of sulfide during sample processing, particularly to the loss of sulfide when the sediment is placed in the pore water press that is being vigorously flushed with N_2 to minimize potential sulfide oxidation. The sulfur isotope composition of sulfide does not appear to be affected by this loss. Values increase from the top of the cores (−38.9‰, Spring and −31.2‰, Fall) to heaviest values at 190 cm depth (16.7‰ for the Spring and 17.7‰ for the Fall core). Sulfide-sulfur isotope compositions then show a slight drop to lower values toward the bottom the cores (15.3, 15.5‰ for Spring and Fall, respectively). Notably, the sulfur isotope composition of sulfide below the SMT is fairly close to the isotope composition of bottom water sulfate at station M1 (19.8‰).

Sulfur and Oxygen Isotope Composition of Sulfate

In the top 150 cm of the sediment, the sulfur isotope values of sulfate show gradual relative enrichment of the heavy isotopes with depth. The $\delta^{34}S$ increased from 20‰ at the sediment surface to >80‰ where sulfate dropped to <1 mM in the SMT (**Tables 2**, **3**; **Figure 4A**). The sulfur isotope offset between sulfate and sulfide was remarkably constant, with an average value of 66 ± 2‰ for the Spring core and 65 ± 4‰ for the Fall core. The $\delta^{18}O$ of sulfate increased from 7.3‰ in the bottom water to about 15‰ in the top 0–10 cm and approached a plateau below 30 cm that is close to the oxygen isotope equilibrium fractionation between water and sulfate (**Figure 4B**; Fritz et al., 1989; Zeebe, 2010).

Just beneath the maximum values reached in the SMT, the $\delta^{34}S$ and $\delta^{18}O$ of sulfate dropped steeply to values that are remarkably close to the isotope composition of seawater sulfate at the sampling site ($\delta^{34}S = 19.8$‰ and $\delta^{18}O = 7.3$‰). For the samples obtained in the Spring, the oxygen isotope values fell slightly below the values for seawater sulfate. Sulfate concentrations below the SMT remained in a narrow range of 0.04–0.18 mM (**Figure 2B**) and showed a rather uniform sulfur and oxygen isotope composition. We designate this pool as the "deep sulfate pool," starting at approximately 190 cm depth and expanding down through the methanic zone. It is interesting to note that while the oxygen isotope values of the pore water decreased with depth (**Figure 4B**), there was no corresponding pattern in the $\delta^{18}O$ of sulfate.

POTENTIAL SAMPLING ARTIFACTS

With regards to potential artifacts during sampling of pore water from the methanic zone, there are two major concerns. First, a minor contamination with seawater sulfate can have detrimental consequences for the interpretation of the data, and second, sulfide can oxidize to sulfate if exposed to oxygen once the core is retrieved, also adversely affecting data quality (for an example see Raven et al., 2016). During the sampling campaign in Spring 2013, four whole-round core samples were taken from a well aligned core retrieved in parallel with the core used for all pore water concentration and isotope data. Two whole-round core samples were taken from within the main sulfate reduction zone (S44: 110–120 cm and S43: 140–150 cm depth) and two from below the SMT (S42: 170–180 cm and S41: 195–205 cm depth) to

TABLE 3 | Concentration and isotope data for the Fall campaign.

cm bsf Mean	$\delta^{18}O_{H2O}$ (VSMOW)	Cl^- (mM)	Sulfate mM—IC	Sulfate (mM—grav)	$\delta^{34}S_{SO_4}$ (VCDT)	$\delta^{18}O_{SO_4}$ (VSMOW)	Sulfide (mM)	$\delta^{34}S_{sulfide}$ (VCDT)	Thiosulfate (μM)
OCTOBER 2013									
10	−1.7	508	20.8	21.6	25.7	14.4	0.49	−31.2	*nm
20	−1.7	517	18.9	17.3	33.1	19.6	1.20	−31.1	*nm
30	−1.9	508	15.6	15.5	41.0	23.3	1.79	−26.0	*nm
40	−1.9	507	14.3	12.8	44.7	24.3	2.41	−23.7	*nm
50			14.6	*incubation experiment, not reported here*				−18.7	*nm
60	−2.1	480	10.5	11.5	50.6	24.3	2.79	−15.8	*nm
70			11.9	*incubation experiment, not reported here*				−11.8	*nm
80	−2.2	476	8.2	8.6	54.7	24.2	3.53	−9.3	*nm
90	−2.3	481	7.1	7.6	57.2	24.4	2.99	−5.0	*nm
100			7.2	*incubation experiment, not reported here*				−2.5	*nm
110	−2.4		3.8	4.9	63.3	25.5	3.08	0.9	*nm
120	−2.5	454	3.1	3.3	67.5	24.7	3.07	5.3	*nm
130			2.4	*incubation experiment, not reported here*				8.9	*nm
140	−2.6	435	1.4	1.9	77.5	25.6	3.84	10.4	*nm
150	−2.6	423	0.8	0.9	84.3	25.9	3.99	12.8	*nm
160			0.5	*incubation experiment, not reported here*				16.1	*nm
170	−2.8	418	0.1	0.1	28.9	9.7	3.18	17.7	*nm
180	−2.8	417	0.1	0.0		20.0	3.60	17.5	*nm
190	−2.8	413	0.1	0.1	18.9	7.7	3.08	17.7	*nm
200	−3.0	410	0.1	0.2	19.5	7.2	3.41	17.5	*nm
210	−2.9	403	0.1	0.1	18.5	7.7	3.30	17.3	*nm
220	−2.9	397	0.0	0.0		7.1	3.24	17.2	*nm
231.5	−3.1	401		0.2	18.1	6.9	0.78	17.5	*nm
243	−3.1	388	0.1	0.1	18.3	7.9	1.56	17.4	*nm
253	−3.1	381	0.1	0.1	17.7	7.7	2.03	17.2	*nm
263	−3.2	370	0.1	0.1	18.8	7.8	2.91	16.1	*nm
273	−3.4	364	0.1	0.1	18.8	7.6	2.87	15.5	*nm
283	−3.2	359	0.1	0.1	19.5	8.7	2.64	16.4	*nm
293	−3.3	351	0.1	0.1	19.6	7.8	2.50	16.1	*nm
303	−3.4	348	0.2	0.1	19.3	8.2	2.23	15.5	*nm
313	−3.5	346	0.1	0.1	19.5	8.4	2.40	15.5	*nm

**nm, not measured.*

test 1) the potential contamination with seawater sulfate and 2) the potential auto-oxidation of sulfide to sulfate during pore-water extraction. The following protocol documents the various steps:

1) The 10-cm long whole-round core samples were cut with the sediment remaining in the core liner. The exposed sediment at the top and bottom was then generously sprayed with ^{18}O-labeled deionized water with an oxygen isotope composition of 4800‰. The whole-round core samples were then tightly wrapped in plastic film, secured with tape, and remained for at least 48 h in the cold room.
2) After a minimum of 48 h, a Rhizon® sampler was inserted through the film and pushed into the center of the sample segment. A volume of ∼1.5 ml was then removed for sulfate concentration measurements and oxygen isotope analysis of water.
3) Immediately after Rhizon® sampling, the sediment was prepared for pore-water extraction. First, the top film cover was removed, and the sediment partially extruded by pushing on the still film-sealed bottom of the whole round section. Approximately 2 cm sediment was extruded, sliced off with a clean knife, and set aside for further processing. The same procedure was used to extract sediment from the bottom of the core. A clean section of plastic film was used to push the remaining sample down and partially out of the bottom of the section where again, 2 cm of sediment was sliced off with a clean knife, and added to the "top" sediment. The combined top and bottom 2 cm sub-samples were kept in a plastic container vigorously flushed with N_2 gas until pore-water extraction with a pore-water press at a later stage.
4) Without any delay, the remaining sediment core was extruded onto a clean surface, and the sides of the core (∼2 cm)

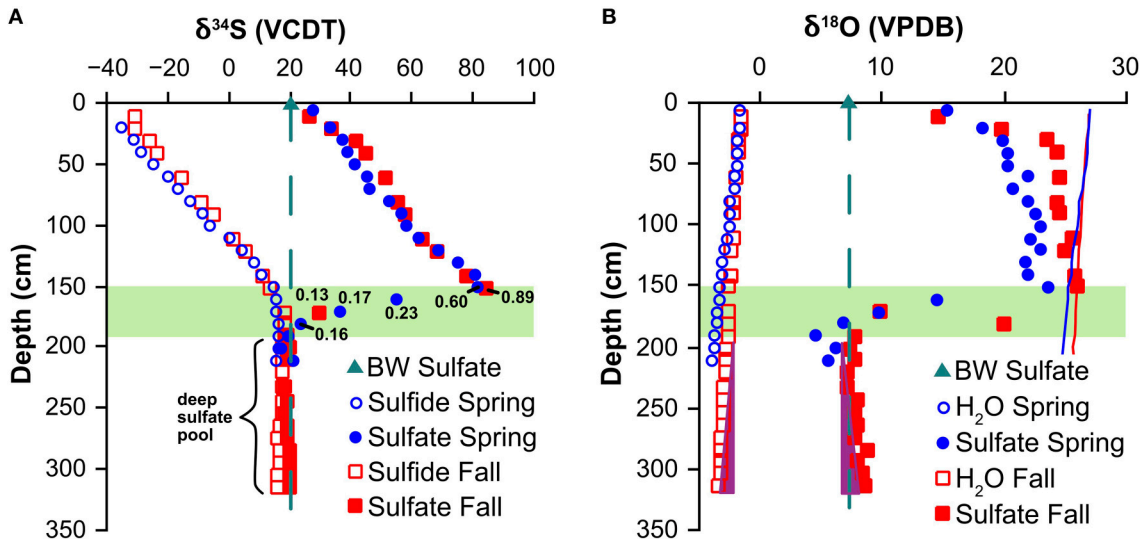

FIGURE 4 | (A) Sulfur and **(B)** oxygen isotope trends for sulfate, sulfide, and pore-water. The samples below a depth of 190 cm are designated as "deep sulfate pool," whereas samples in between a sediment depth of 150 and 190 cm are considered to belong to the lower part of the SMT. The dark green triangle and dashed line represent the seawater sulfate isotope composition. The solid blue and red line **(B)** are the predicted sulfate-oxygen isotope composition at equilibrium with water calculated from Fritz et al. (1989). Purple triangles **(B)** indicate oxygen isotope trends for water and sulfate do not correlate. The green band represents the SMT.

were scraped off and placed in a plastic container that was vigorously flushed with N_2 gas before pore-water extraction with a pore-water press at a later stage. Typically, the outside of the sediment core that was previously in contact with the core liner, showed a discoloration, presumably a result of oxidation.

5) Next, the freshly exposed center of the sediment core was generously sprayed with the ^{18}O-labeled deionized water ($\delta^{18}O = 4800‰$) so that the entire surface was wet. The core sample was then immediately placed into a pore-water press flushed with N_2 gas. The first 3–5 ml of pore water was discarded, followed by collection of ∼25 ml into a capped serum bottle (previously amended with 2 ml 20% zinc acetate and flushed with N_2), followed by collection of ∼8 ml of pore-water in a plastic syringe for sulfate concentration and other analyses, and finally the remaining pore water (typically another ∼25 ml) into the capped serum bottle. This back-and-forth procedure was chosen to avoid collecting predominantly ^{18}O labeled water, which is likely to be more quickly extruded by the press than interstitial pore water in the initial phase of extraction.
6) Subsequent to processing the center sample, pore-water was extracted from the "Bottom & Top" and "Side" samples with the pore-water press. The first 3–5 ml of pore water was discarded, followed by collecting ∼8 ml of pore water in a separate container for sulfate concentration and other analyses. The remaining pore-water (typically <20 ml due to small amount of sediment) was transferred into a capped serum bottle that was previously amended with 2 ml 20% zinc acetate and flushed with N_2.

It is important to note that placing samples in a plastic container that is vigorously flushed with N_2 gas will remove some H_2S, which is easily detectable as sulfide smell. Further loss of H_2S occurs when the sample is placed into the pore water press, which is also flushed with N_2. Consequently, severe underestimation of sulfide concentrations has to be expected when this method is employed. The sulfur isotope composition of collected sulfide, however, is not expected to be significantly altered by this loss.

Two objectives were pursued with the experiments with the heavily isotopically labeled water ($\delta^{18}O = 4800‰$). The first objective was to obtain a quantitative estimate of potential contamination with sulfate when a core segment was for more than 48 h in contact with a thin layer of seawater with a concentration of 28 mM sulfate. Such a scenario may occur if the diameter of the sediment core is smaller than the inner diameter of the core liner, leaving a thin gap which would allow for a contact of seawater with the exterior of the sediment core (**Figure 5**). As pore water squeezing is a time consuming process, sulfate from this thin film of seawater would have time to diffuse into the samples. The samples obtained with a Rhizon® inserted into the center of the sediment core segments and the samples obtained from the sides of the cores can provide an estimate of the extent of such a contamination with sulfate because they reveal how much ^{18}O-labeled water penetrated deeply into the sediment from the top and bottom of the core segment within a time frame of over 48 h. These estimates represent a worst-case scenario because the molecular diffusion of sulfate ions is slower than self-diffusion of $H_{2}{}^{18}O$ ($D_{sulfate} = 0.56 * 10^{-5}$ cm^2 s^{-1} in seawater at 4°C; Iversen and Jørgensen, 1985); $D_{water:\ self\text{-}diffusion} = 1.26 * 10^{-5}$ cm^2 s^{-1} in water at 4°C; Holz et al., 2000). Moreover, isotopically labeled water might be entrained from the top of the core when the Rhizon® is stuck into the center of the core. Finally, sediment from the side of the core is prone to exposure to isotopically labeled water that seeps down- and upward along the

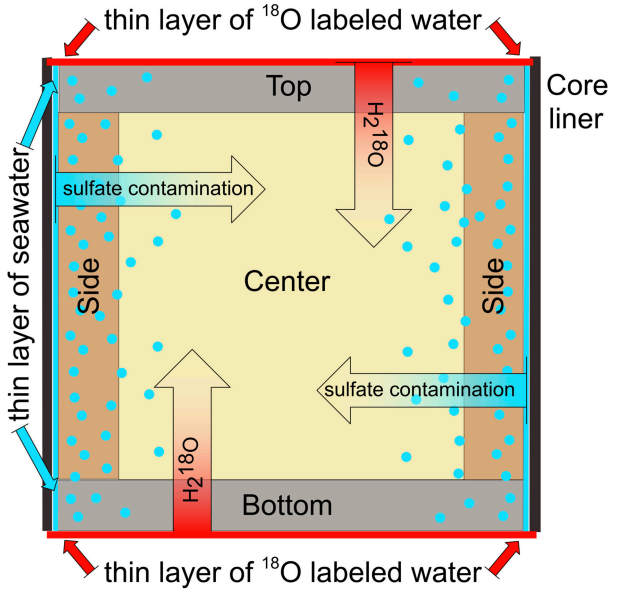

FIGURE 5 | Cross-section of whole-round core segment depicting potential contamination with sulfate from seawater and the experimental procedure with ^{18}O labeled water to quantify potential sulfate penetration.

core liner. The approximate mixing contribution of pristine water (1 − x) relative to isotopically labeled water (x) can be calculated as follows:

$$x = 1 - (\delta^{18}O_{mixture} - \delta^{18}O_{label})/(\delta^{18}O_{pristine} - \delta^{18}O_{label}). \quad (1)$$

If we now assume that pristine pore water was sulfate-free, the found value of x can be multiplied with the assumed concentration of sulfate contaminant (i.e., 28 mM), which yields the hypothetical concentration in the contaminated sample (**Table 4**). Our calculated "worst-case" potential contamination with sulfate from seawater falls in a range of 0.03–0.11 mM, with an average of 0.07 mM. Such a contamination could constitute a major portion of sulfate in the deep sulfate pool, i.e., it could reach 50% of the total sulfate concentration within 48 h. Initially, the results from our Spring studies where we focused on the effects of auto-oxidation indicated that an extended pore water extraction protocol would not adversely affect our results. However, in light of the fact that the deep sulfate samples for the Fall core were extracted between 48 and 86 h after core retrieval, the potential for contamination with sulfate by diffusion is high.

The second objective was to explore if auto-oxidation of sulfide to sulfate after core retrieval may have affected the sulfate concentration and the isotope data. Oxidation of sulfide by atmospheric oxygen would occur along the same diffusion path as the introduced ^{18}O labeled water. The oxygen isotope composition of water leaves a strong imprint on the isotope composition of sulfate generated by sulfide oxidation even if atmospheric oxygen (O_2) is the oxidant (e.g., see Müller et al., 2013 for role of sulfite as an intermediate in sulfide oxidation, and Taylor et al., 1984 for minimum oxygen incorporation from water into produced sulfate during wet/dry pyrite weathering). Because sulfide is also depleted in ^{34}S relative to the sulfate, one would further expect negative shifts in the sulfur isotope composition of sulfate. The experiments with core segment S43, which was stored in the cold room for more than 48 h demonstrates the effects of sulfide oxidation (**Table 4**). The sulfur and oxygen isotope composition of sulfate from the center of the sample shows similar values as for the sample from the adjacent core, which was fully processed in <48 h after coring. However, the measurements from the top and bottom, as well as the side of core segment S43 are different from its center. Particularly, the side of the core shows a higher sulfate concentration (3.0 mM) than the center (2.6 mM), and a lower oxygen and sulfur isotope composition of sulfate ($\delta^{18}O$ = 18.9‰, $\delta^{34}S$ = 64.8‰) than the sulfate from the center ($\delta^{18}O$ = 23.1‰, $\delta^{34}S$ = 67.3‰). This observation indicates that sulfide from the side, top and bottom of the core segment was oxidized, resulting in the addition of isotopically light sulfate. However, it appears the center of the core remained unaffected by this oxidation. Pore water squeezing of the core center of core segment S43, which was preceded by spraying of the freshly exposed center of the sediment with the ^{18}O-labeled deionized water ($\delta^{18}O$ = 4800‰) resulting in an oxygen isotope composition of the extracted water of 66.4‰, did not yield sulfate enriched in ^{18}O, indicating that sulfide oxidation to sulfate during pore water squeezing is negligible. This finding is corroborated by the results from the experiment with core segment S42 which was also stored for more than 48 h, where the isotope composition of sulfate from the center of the core ($\delta^{18}O$ = 19.6‰, $\delta^{34}S$ = 81.9‰) is close to the isotope composition of an adjacent core ($\delta^{18}O$ = 23.6‰, $\delta^{34}S$ = 81.9‰) which was processed in less than 24 h (**Table 4**).

In conclusion, the experiments with ^{18}O-isotopically labeled water show that auto-oxidation of sulfide during core storage and pore water squeezing is unlikely to impact our measurements. However, these experiments do not shed light on the potential for sulfide oxidation in subsequent sample preparation steps, as exemplified by the discrepancy between sulfate concentrations determined by ion chromatography and gravimetric method in Spring. Obviously, potential contamination with seawater sulfate is a concern. A contamination with 4 µl of bottom water per 1 ml of sulfate-free pore water would be sufficient to result in an apparent sulfate concentration of 0.1 mM with an isotopic composition of seawater.

INTERPRETATION

A simple explanation of our data could therefore be that *in situ* there is no deep sulfate pool but that the observed sulfate is the result of an artifact caused by contamination with seawater sulfate. In this scenario, one could assume that sulfate is entirely consumed by sulfate reduction within the SMT, and that the steep drop in sulfate-sulfur and -oxygen isotope composition from the center of the SMT to the lower limit of the SMT is the result of mixing of contaminant seawater sulfate and the very last remainder of original sulfate (**Table 5**; **Figure 4**). We can quantitatively explore this scenario in more detail for the samples

TABLE 4 | Results of sampling artifact experiments.

	Sulfate (mM)	$\delta^{18}O_{water}$ (VSMOW)	$\delta^{18}O_{sulfate}$ (VSMOW)	$\delta^{34}S_{sulfate}$ (VCDT)	$\delta^{34}S_{sulfide}$ (VCDT)	Cont. Pot. (mM)
CORE SEGMENT S44—EQUIV. DEPTH 90 cm						
Values from adjacent core	6.7	−2.5	22.5	56.2	−8.3	
Center	5.8	75.9	22.6	56.9	−6.6	
Bottom and Top	6.1	47.6	22.3	56.2	−6.1	
Side	6.0	16.8	20.2	56.0	−5.6	0.11
Center—Rhizon	5.6	15.1	No sample	No sample	No sample	0.10
CORE SEGMENT S43—EQUIV. DEPTH 120 cm						
Values from adjacent core	2.7	−3.0	23.0	68.9	4.5	
Center	2.6	66.4	23.1	67.3	3.7	
Bottom and Top	2.8	16.7	21.9	67.2	3.9	
Side	3.0	5.1	18.9	64.8	3.9	0.05
Center—Rhizon	2.3	2.5	No sample	No sample	No sample	0.03
CORE SEGMENT S42—EQUIV. DEPTH 150 cm						
Values from adjacent core	0.6	-3.4	23.6	81.4	14.6	
Center	0.7	43.9	19.6	81.9	12.4	
Bottom and Top	0.7	13.2	No sample	No sample	13.3	
Side	0.7	5.2	No sample	No sample	13.2	0.05
Center—Rhizon	0.7	6.0	No sample	No sample	No sample	0.05
CORE SEGMENT S41—EQUIV. DEPTH 175 cm						
Values averaged from adjacent core	0.2	−3.7	8.3	30.1	16.1	
Center	0.2	42.5	No sample	No sample	16.8	
Bottom and Top	1.5	29.9	No sample	No sample	16.4	
Side	0.6	9.6	No sample	No sample	No sample	0.08
Center—Rhizon	0.3	8.4	No sample	No sample	No sample	0.07

TABLE 5 | Contaminant mixing table.

Campaign	Depth (cm)	Sulfate (mM)	$\delta^{34}S_{SO_4}$ (‰ VCDT)	$\delta^{18}O_{SO_4}$ (‰ VSMOW)	Equilibrium* $\delta^{18}O_{SO_4}$ (‰ VSMOW)	Contaminant Sulfate (mM)	Calculated	
							Original Sulfate (mM)	Original $\delta^{34}S_{SO_4}$ (‰ VCDT)
March 2013	161	0.23	54.7	14.5	25.2	0.14	0.09	106.5
March 2013	171	0.17	36.4	9.8	25.1	0.14	0.02	137.7
October 2013	170	0.13	28.9	9.7	25.8	0.11	0.02	90.2
					Average	0.13		
					Stdev	0.02		

**Calculated after Fritz et al. (1989), $\delta^{18}O$ contaminant, 7.3; $\delta^{34}S$ contaminant, 19.8.*

at a depth of 161, 171 (Spring core), and 170 cm (Fall core). The very last remainder of original sulfate is likely to have an oxygen isotope composition close to the oxygen isotope equilibrium between sulfate and water (isotopic difference ∼25‰), whereas the sulfur isotope composition of sulfate is unknown. The isotope composition of contaminant sulfate from seawater is known ($\delta^{34}S_{cont} = 19.8$‰ and $\delta^{18}O_{cont} = 7.3$‰). Using these values and the sulfate concentration and isotope composition of the mixture between original sulfate and contaminant, one can quantify the hypothetical amount of contaminant sulfate, and determine the sulfur isotope composition of original sulfate (**Table 5**, for derivations of equations, see Appendix). On the average, the concentration of contaminant present is 0.13 mM sulfate, which is a good match to the sulfate concentrations in the deep sulfate pool (0.14 mM for the Spring core and 0.10 mM for the Fall core). The inferred sulfur isotope composition of the original sulfate for the investigated samples falls in a range of 90–138‰. Such strong enrichments in ^{34}S are not outside of the realm of possibilities, considering that the estimated amounts of residual sulfate can be as low as 0.02 mM and that the sulfur isotope composition might display a Rayleigh distillation trend. The implication of attributing the observed signatures to a mixture of residual sulfate

and contamination would be that sulfate reduction coupled to the anaerobic oxidation of methane strongly fractionates sulfur isotopes even at very low sulfate concentrations, consistent with recent modeling results for sulfur isotope fractionation during microbial sulfate respiration (Wing and Halevy, 2014).

The explanation that the observed sulfate concentration and isotope patterns from sediments below of the SMT are the result of contamination with seawater is compelling, and in our point of view at this stage, the most prudent interpretation of the data. However, there are inconsistencies in this scenario that must be addressed. A major inconsistency is that the oxygen isotope composition of sulfate for the four deepest samples for the Spring core are distinctly lighter than the oxygen isotope composition of seawater sulfate (average for $\delta^{18}O_{sulfate}$ of 5.7 vs. 7.3‰) and that one of these four sample shows a sulfate-sulfur isotope composition that is lighter than the isotope composition of seawater sulfate (17.3 vs. 19.8‰; **Figure 4**). These values cannot be the result of contamination with seawater sulfate and the clustering of the sulfur and oxygen isotope data make it unlikely that they could be the result of analytical error, i.e., we do not observe such variation in values for the entire deep sulfate pool for the Fall core. Hence, one would have to postulate that they are the result of auto-oxidation of sulfide—but there is no evidence that would support that this process is of importance for the time between coring and pore water extraction. Essentially, one would have to argue that auto-oxidation of sulfide after pore water extraction was the cause for the observed concentration and isotope patterns for sulfate obtained from the deepest part of the Spring core, whereas the contamination with sulfate was the cause of the patterns observed for the Fall core. As the sampling campaigns are not fully identical, one cannot rule out this possibility. In the Spring, sulfide was captured using a zinc acetate solution to precipitate zinc sulfide, separated from sulfate by vacuum filtration, followed by the acidification of the filtrate and removal of any residual sulfide with a CO_2 gas stream. The earliest extracted samples from at and below of the SMT that were fixed with zinc acetate remained in the cold room for up to 100 h within the sealed, nitrogen-flushed serum bottles before filtration. In the Fall, sulfide was immediately removed directly after pore water collection by acidification of the filtrate and flushing with a CO_2 gas stream. It would be curious and interesting find that one of the standard techniques to prevent sulfide oxidation—the fixation as zinc sulfide—yields artifacts, whereas immediate removal of sulfide by acidification is more reliable.

Another fact for consideration is that there is no increase in sulfate concentration observable for samples that were extracted toward the end of the pore water extraction process in Fall (**Figure 6**). Sulfate concentrations from deep in the sediment core are low, but variable indicating no relationship with regards to the time of sample processing or the potential for vertical diffusion and mixing. If there was contamination with seawater sulfate it would have had to occur early in the sampling campaign and then remain fixed throughout sample processing.

IF IT IS NOT AN ARTIFACT, THEN WHAT?

Being aware of these provisos, it is worth searching for an explanation of the persistent presence of sulfate and the sulfate-sulfur and -oxygen isotope composition below the SMT for the case where the observance of low concentrations of sulfate is not a result of an artifact. The concentration and isotope gradients between sulfate present in the SMT and the sulfate at the base of the SMT demonstrates that this pool does not represent "left over" sulfate that was not consumed during anaerobic oxidation of methane coupled to sulfate reduction. This isotopic shift can be achieved if the sulfate removed by sulfate reduction coupled to the anaerobic oxidation of methane is simultaneously replenished by either (i) an oxidative process, (ii) admixture of brackish water, or (iii) release of sulfate from a solid phase.

It is conceivable that the availability and reactivity of sulfide oxidants, as well as availability of substrates for microbial sulfate reduction, is uniform in the sediments that host the deep sulfate pool. This would explain why sulfate concentrations and sulfur isotope signatures in this closed oxidative-reductive sulfur turnover tend to be uniform as well. The remarkable similarity between the sulfur isotope composition of deep sulfate ($\delta^{34}S$ =

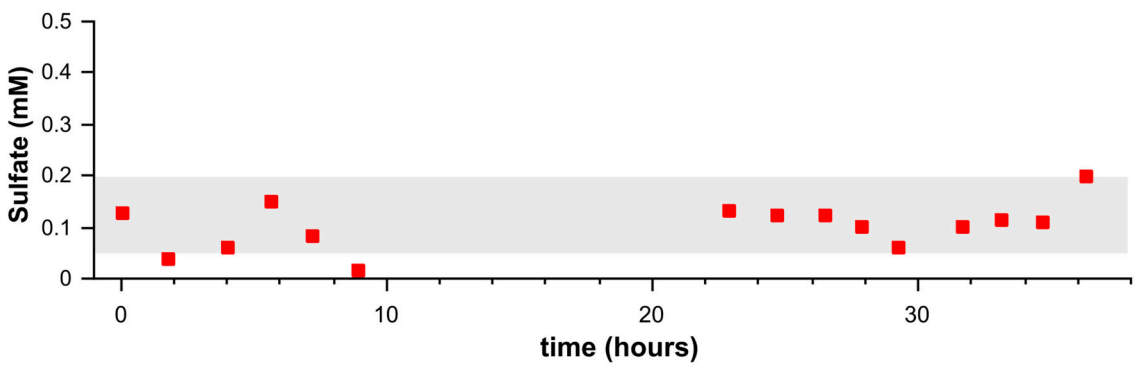

FIGURE 6 | Sulfate concentrations (red squares) from samples extracted by pore water press during a time frame of 36 h. They gray band represents ±1 sd of the average sulfate concentration for all sub-SMT samples in the Fall core. The sediment core (Fall 2013) was retrieved 2 days prior to when pore water pressing started ($t = 0$).

18.9‰) and seawater ($\delta^{34}S = 19.8‰$) may be rooted in the fact that sulfide produced at the SMT approaches the sulfur isotope composition of seawater sulfate ($\delta^{34}S$ of up to 17.5‰). As this sulfide diffuses downward into the deep sulfate pool, it can be oxidized to sulfate, a process that causes only a slight enrichment in the sulfur isotope composition (e.g., Fry et al., 1988; Balci et al., 2007; Brabec et al., 2012). Alternatively, it could be speculated that production of isotopically light sulfate at the base of the SMT is the result of polysulfide disproportionation. Polysulfides occur in direct proportion to the free sulfide concentration (Holmkvist et al., 2014) and may be produced by the activity of ANME archaea during sulfate reduction coupled to the anaerobic oxidation of methane at the SMT (Milucka et al., 2012). These polysulfides may be disproportionated throughout the sediment column (Fossing and Jørgensen, 1990). The presence of thiosulfate at and below the SMT highlights that sulfur species that can be disproportionated into sulfate and sulfide are indeed available (**Table 2**). One observation casts doubt on a scenario where newly formed sulfate in the methanic zone coincidentally yields the same oxygen isotope composition as seawater sulfate from Aarhus Bay. The water-oxygen isotope composition of the pore water continuously decreases within the methanic zone, from −2.8‰ at 170 cm depth to −3.5‰ at 313 cm depth. No such trend is observable for the oxygen isotope composition of sulfate over the same depth interval (**Figure 4**).

An appealing alternative scenario is an admixture of seawater and groundwater from a permeable sediment layer beneath the SMT, because it presents an explanation for the similarity in the isotope composition of deep sulfate and the bottom water collected from the sampling site ($\delta^{34}S = 19.8‰$, $\delta^{18}O = 7.3‰$) and for the decoupling of the oxygen isotope composition of deep sulfate from the oxygen isotope composition of water which continues to decrease with depth (**Figure 4**). The homogeneous, muddy sediments found in the cores indicate that it is unlikely that a permeable layer exists in close proximity to the base of the SMT. However, it could be speculated that a slight change in the slope in the chloride profile at depth (ca. 160 cm in the Spring core and 190 cm in the Fall core) may indicate local admixture of brackish water with low sulfate and chloride content. Lateral advection of sulfate through a broad sediment zone below the base of the SMT (that coincides with the location of the deep sulfate pool) with slightly enhanced permeability can be excluded based on the continuous gradient in the chloride concentration and oxygen isotope composition of water. This leaves the option of an admixture of seawater from a source below the sampled sediment profile. The decrease in both the chloride concentration and oxygen isotope composition of water with increasing depth are testimony of the existence of such an aquifer and agrees with descriptions of the sediment in Aarhus Bay (e.g., sandy sediments—previous topography at around 10 m depth; Jensen and Bennike, 2009). It is possible that the water in such an aquifer is brackish due to mixing of seawater with freshwater. In this scenario, the near-constant sulfate concentration and isotope profile from the bottom of the cores to the base of the SMT would be explained as the result of diffusive mixing in absence of any sulfate production or consumption.

Finally, dissolution of marine barite due to low sulfate concentrations (e.g., Riedinger et al., 2006) or release of carbonate-associated sulfate due to carbonate recrystallization catalyzed by the production of CO_2 associated with methanogenesis (Meister et al., 2011) could contribute to the stability of sulfate concentrations and isotope signatures in the deep sulfate pool (**Figure 4**). However, it must be noted that barite dissolution in sulfate-free seawater would yield a sulfate concentration $<20\,\mu M$, which is 5–10 fold smaller than the observed sulfate concentrations in the deep sulfate pool. With regards to the release of carbonate-associated sulfate in the Aarhus Bay sediments, carbonate is present in the form of mollusk shells throughout the sediment column (Holmkvist et al., 2011). Sulfate release from carbonates during recrystallization is difficult to assess, as this process involves simultaneous carbonate dissolution and re-precipitation, which may not be detected in concentration profiles of dissolved inorganic carbon, calcium, or magnesium. Nevertheless, it is evident that sulfate loss from carbonates occurs during this process (Staudt and Schoonen, 1995).

Curiously, all of the above arguments demand that in the deep sulfate zone sulfate reduction does not fractionate sulfur and oxygen isotopes, because the latter would drive the isotope values of sulfate heavy. This is problematic, as it is known that sulfate concentrations between 0.1 and 0.2 mM do not preclude microbial sulfate reduction (Holmkvist et al., 2011; Tarpgaard et al., 2011). Sulfur isotope fractionation during classical microbial sulfate reduction at low sulfate concentrations can be low (Habicht et al., 2002), for an alternative view see Canfield et al. (2010a). Recently, a modeling-based argument convincingly demonstrated that sulfur isotope fractionation by microbial sulfate reduction can be large (up to equilibrium isotope fractionation) at low sulfate concentration and low sulfate reduction rates (Wing and Halevy, 2014). If the argument that sulfur isotope fractionation by sulfate reduction is negligible in the deep sulfate zone holds, the oxygen isotope effects should be negligible as well, because both processes are linked by the reversibility of the sulfate reduction pathway (Brunner et al., 2005, 2012). Alternatively, sulfate consuming organisms in the methanic zone may employ sulfate reduction pathways that do not fractionate sulfur isotopes, for example pathways that are similar to sulfate assimilation or yet to-be elucidated sulfate reduction pathways inferred for ANME (Milucka et al., 2012), however, it needs to be noted that the phylogenetic diversity of sulfate reducers in the methanic zone are rather similar to those in the lower part of the sulfate zone (Leloup et al., 2009).

CONCLUSIONS

Avoiding artifacts in the extraction of sulfate from sulfidic low-sulfate pore water remains a challenge. Our sampling strategy overcomes the challenges related to sulfate production from sulfide auto-oxidation, but did not resolve all issues with regards to contamination with seawater sulfate. Consequently, it may be prudent to first assume that the sulfate detected in Aarhus Bay sediments retrieved below the SMT is a result of contamination

with sea water sulfate. Isotope mass balance calculations indicate that in this scenario, the sulfur isotope compositions in the bottom part of the SMT could be as high as 138‰ at residual sulfate concentrations as low as 0.02 mM. The implication of this finding is that sulfate reduction coupled to the anaerobic oxidation of methane strongly fractionates sulfur isotopes also at very low sulfate concentrations.

However, not all of the data for sulfate retrieved from the base or below of the SMT can be satisfactorily explained as result of contamination with seawater sulfate. The sulfate-oxygen isotope composition of the four deepest samples for the Spring campaign is lighter than the oxygen isotope composition of seawater sulfate, which is indicative for an oxidative process that either occurs *in situ* or as sampling artifact (i.e., auto-oxidation of reduced sulfur species). Our experiments indicate that auto-oxidation of reduced sulfur species does not pose a major issue for the stage between storage of the core in the cold room and pore water extraction. The main difference in sampling procedures between Spring and Fall is that the pore water in the Spring samples was amended with zinc acetate as to fix sulfide as zinc sulfide, a step that was omitted in Fall. For future studies of low-sulfate/high-sulfide environments this observation implies that the classic approach to fix sulfide as zinc sulfide may not be advisable.

Casting aside prudence, it is worthwhile to consider the implications if the data from the base and from below the SMT are not the result of artifacts. For the Spring core one would have to conclude that new sulfate is generated at the base of the SMT. Potential processes could be oxidative sulfur cycling with ferric iron (Riedinger et al., 2014; Sivan et al., 2014) or a yet unknown oxidant. For the Fall core one would need to find an answer to the question of how sulfate at depth can have a sulfur and oxygen isotope signature that is remarkably similar to seawater sulfate. Release of carbonate associated sulfate during carbonate recrystallization and dissolution of marine barite could provide such a signature, however, there is no quantitative assessment of the importance of these processes at this point. With regards to the elucidation of sulfur cycling at the base and below of the SMT much remains to be explored. It is known that organisms with the capability to reduce sulfate exist and thrive in methanic sediments (Leloup et al., 2007). At least, our data hint that oxidative sulfur cycling occurs at the base of the SMT providing encouragement to the further investigation of this process.

A lesson learned from our sampling campaigns is that contamination with seawater sulfate remains a major challenge whereas auto-oxidation of reduced sulfur species can be kept to a minimum using appropriate sampling protocols. Core-processing takes time and additional steps should be taken to prevent contamination with seawater during processing. One option to overcome contamination with seawater sulfate would be to take two parallel cores from the same site. One core could then be immediately sampled with Rhizon® samplers that are stuck in the center of the core segments. At the least, the pore water obtained in this way can be analyzed for sulfate concentrations. With a combination of elaborate sulfur extraction techniques (Arnold et al., 2014) and high sensitivity isotope analysis by multi-collector ICPMS (Paris et al., 2013; Lin et al., 2014) it might even be possible to measure the sulfur isotope composition of sulfate. However, in light that barite dissolution in sulfate-free seawater would yield a sulfate concentration $<20\,\mu M$ researchers must brace themselves for extremely low sulfate concentrations for sulfur and oxygen isotope analyses. Another lesson learned is that the concentration of sulfate and the sulfur isotope composition of sulfate are valuable tools for the interpretation of the data, but the most revealing information comes from the oxygen isotope composition of sulfate and water. This is in so far critical as high sensitivity oxygen isotope analysis by multi-collector ICPMS is not available. Unfortunately, for gas source isotope ratio mass spectrometry, much larger sulfate samples are needed, and this is where a second, parallel core would be helpful. The outer sediment of such a core would need to be removed as soon as possible after core retrieval to avoid contamination with seawater. More sophisticated alternatives such as freezing of core segments or freeze coring could be employed.

There are also new avenues in the exploration of cryptic sulfur cycling in marine sediments. The measurement of barite dissolution and carbonate recrystallization rates could help quantifying sulfate input from these sources, quantitative modeling of oxygen isotope exchange between sulfate and water in the main sulfate zone based on sulfur and oxygen isotope profiles (Wortmann et al., 2007) could provide insight if sulfur oxidation may also be important in this zone, and long-term studies with stable isotope tracers (*in* or *ex situ*) could provide direct evidence for the presence or absence of cryptic sulfur cycling.

AUTHOR CONTRIBUTIONS

All authors listed, have made substantial, direct and intellectual contribution to the work, and approved it for publication.

ACKNOWLEDGMENTS

We thank Stefano Bernasconi, Stewart Bishop, and Madalina Jaggi (ETH Zurich) for assistance with isotope analyses. We also thank Jeanette Pedersen and Karina Bomholt Henriksen (Aarhus University), for analytical work and technical support. We thank the Max Planck Institute for Marine Microbiology in Bremen for assistance with the concentration analysis of thiosulfate and sulfite and for lending us the pore water press. We are especially grateful to Captain Torben Vang and the crew of the RV Tyra of Aarhus University for outstanding support during the Aarhus Bay sampling campaigns. We thank our two reviewers for their encouraging and insightful comments. The research was funded by the Danish National Research Foundation and the European Research Council (ERC) Advanced Grant, MICROENERGY (grant n° 294200), awarded to BJ under the EU 7th FP. This work was supported by start-up funds for BB by the University of Texas at El Paso.

REFERENCES

Arnold, G. L., Brunner, B., Müller, I. A., and Røy, H. (2014). Modern applications for a total sulfur reduction distillation method - what's old is new again. *Geochem. Trans.* 15:4. doi: 10.1186/1467-4866-15-4

Balci, N., Shanks, I. I. I., Mayer, B., and Mandernack, K. W. (2007). Oxygen and sulfur isotope systematics of sulfate produced by bacterial and abiotic oxidation of pyrite. *Geochim. Cosmochim. Acta* 71, 3796–3811. doi: 10.1016/j.gca.2007.04.017

Bao, H. (2006). Purifying barite for oxygen isotope measurement by dissolution and reprecipitation in a chelating solution. *Anal. Chem.* 78, 304–309. doi: 10.1021/ac051568z

Bishop, T., Turchyn, A. V., and Sivan, O. (2013). Fire and brimstone: the microbially mediated formation of elemental sulfur nodules from an isotope and major element study in the Paleo-Dead Sea. *PLoS ONE* 8:e75883. doi: 10.1371/journal.pone.0075883

Brabec, M. Y., Lyons, T. W., and Mandernack, K. W. (2012). Oxygen and sulfur isotope fractionation during sulfide oxidation by anoxygenic phototrophic bacteria. *Geochim. Cosmochim. Acta* 83, 234–251. doi: 10.1016/j.gca.2011.12.008

Brunner, B., Bernasconi, S. M., Kleikemper, J., and Schroth, M. H. (2005). A model for oxygen and sulfur isotope fractionation in sulfate during bacterial sulfate reduction processes. *Geochim. Cosmochim. Acta* 69, 4773–4785. doi: 10.1016/j.gca.2005.04.017

Brunner, B., Einsiedl, F., Arnold, G. L., Müller, I., Templer, S., and Bernasconi, S. M. (2012). The reversibility of dissimilatory sulphate reduction and the cell-internal multi-step reduction of sulphite to sulphide: insights from the oxygen isotope composition of sulphate. *Isotopes Environ. Health Stud.* 48, 33–54. doi: 10.1080/10256016.2011.608128

Canfield, D. E., Farquhar, J., and Zerkle, A. L. (2010a). High isotope fractionations during sulfate reduction in a low-sulfate euxinic ocean analog. *Geology* 38, 415–418. doi: 10.1130/G30723.1

Canfield, D. E., Stewart, F. J., Thamdrup, B., Brabandere, L. D., Dalsgaard, T., Delong, E. F., et al. (2010b). A cryptic sulfur cycle in oxygen-minimum–zone waters off the chilean Coast. *Science* 330, 1375–1378. doi: 10.1126/science.1196889

Fossing, H., and Jørgensen, B. B. (1990). Oxidation and reduction of radiolabeled inorganic sulfur compounds in an estuarine sediment, Kysing Fjord, Denmark. *Geochim. Cosmochim. Acta* 54, 2731–2742. doi: 10.1016/0016-7037(90)90008-9

Fritz, P., Basharmal, G. M., Drimmie, R. J., Ibsen, J., and Qureshi, R. M. (1989). Oxygen isotope exchange between sulphate and water during bacterial reduction of sulphate. *Chem. Geol.* 79, 99–105. doi: 10.1016/0168-9622(89)90012-2

Fry, B., Ruf, W., Gest, H., and Hayes, J. M. (1988). Sulfur isotope effects associated with oxidation of sulfide by O2 in aqueous solution. *Chem. Geol.* 73, 205–210. doi: 10.1016/0168-9622(88)90001-2

Habicht, K. S., Gade, M., Thamdrup, B., Berg, P., and Canfield, D. E. (2002). Calibration of sulfate levels in the Archean Ocean. *Science* 298, 2372–2374. doi: 10.1126/science.1078265

Holmkvist, L., Ferdelman, T. G., and Jørgensen, B. B. (2011). A cryptic sulfur cycle driven by iron in the methane zone of marine sediment (Aarhus Bay, Denmark). *Geochim. Cosmochim. Acta* 75, 3581–3599. doi: 10.1016/j.gca.2011.03.033

Holmkvist, L., Kamyshny, A. Jr., Brüchert, V., Ferdelman, T. G., and Jørgensen, B. B. (2014). Sulfidization of lacustrine glacial clay upon Holocene marine transgression (Arkona Basin, Baltic Sea). *Geochim. Cosmochim. Acta* 142, 75–94. doi: 10.1016/j.gca.2014.07.030

Holz, M., Heil, S. R., and Sacco, A. (2000). Temperature-dependent self-diffusion coefficients of water and six selected molecular liquids for calibration in accurate 1H NMR PFG measurements. *Phys. Chem. Chem. Phys.* 2, 4740–4742. doi: 10.1039/B005319H

Iversen, N., and Jørgensen, B. B. (1985). Anaerobic methane oxidation rates at the sulfate-methane transition in marine sediments from Kattegat and Skagerrak (Denmark). *Limnol. Oceanogr.* 30, 944–955. doi: 10.4319/lo.1985.30.5.0944

Jensen, J. B., and Bennike, O. (2009). Geological setting as background for methane distribution in Holocene mud deposits, Århus Bay, Denmark. *Cont. Shelf Res.* 29, 775–784. doi: 10.1016/j.csr.2008.08.007

Johnston, D. T., Gill, B. C., Masterson, A., Beirne, E., Casciotti, K. L., Knapp, A. N., et al. (2014). Placing an upper limit on cryptic marine sulphur cycling. *Nature* 513, 530–533. doi: 10.1038/nature13698

Jørgensen, N. O., and Holm, P. M. (1994). "Isotope studies (18O/16O, D/H and 87Sr/86Sr) of saline groundwater in Denmark," in *Future Groundwater Resources at Risk (Helsinki Conference, FGR 94)*, (Helsinki: IAHS).

Jørgensen, N. O., and Holm, P. M. (2012). Strontium-isotope studies of chloride-contaminated groundwater, Denmark. *Hydrogeol. J.* 3, 52–57. doi: 10.1007/s100400050066

Leloup, J., Fossing, H., Kohls, K., Holmkvist, L., Borowski, C., and Jørgensen, B. B. (2009). Sulfate-reducing bacteria in marine sediment (Aarhus Bay, Denmark): abundance and diversity related to geochemical zonation. *Environ. Microbiol.* 11, 1278–1291. doi: 10.1111/j.1462-2920.2008.01855.x

Leloup, J., Loy, A., Knab, N. J., Borowski, C., Wagner, M., and Jørgensen, B. B. (2007). Diversity and abundance of sulfate-reducing microorganisms in the sulfate and methane zones of a marine sediment, Black Sea. *Environ. Microbiol.* 9, 131–142. doi: 10.1111/j.1462-2920.2006.01122.x

Lin, A.-J., Yang, T., and Jiang, S.-Y. (2014). A rapid and high-precision method for sulfur isotope δ34S determination with a multiple-collector inductively coupled plasma mass spectrometer: matrix effect correction and applications for water samples without chemical purification. *Rapid Commun. Mass Spectrom.* 28, 750–756. doi: 10.1002/rcm.6838

Meister, P., Gutjahr, M., Frank, M., Bernasconi, S. M., Vasconcelos, C., and McKenzie, J. A. (2011). Dolomite formation within the methanogenic zone induced by tectonically driven fluids in the Peru accretionary prism. *Geology* 39, 563–566. doi: 10.1130/G31810.1

Mikucki, J. A., Pearson, A., Johnston, D. T., Turchyn, A. V., Farquhar, J., Schrag, D. P., et al. (2009). A contemporary microbially maintained subglacial ferrous "Ocean." *Science* 324, 397–400. doi: 10.1126/science.1167350

Milucka, J., Ferdelman, T. G., Polerecky, L., Franzke, D., Wegener, G., Schmid, M., et al. (2012). Zero-valent sulphur is a key intermediate in marine methane oxidation. *Nature* 491, 541–546. doi: 10.1038/nature11656

Müller, I. A., Brunner, B., and Coleman, M. (2013). Isotopic evidence of the pivotal role of sulfite oxidation in shaping the oxygen isotope signature of sulfate. *Chem. Geol.* 354, 186–202. doi: 10.1016/j.chemgeo.2013.05.009

Paris, G., Sessions, A. L., Subhas, A. V., and Adkins, J. F. (2013). MC-ICP-MS measurement of δ34S and Δ33S in small amounts of dissolved sulfate. *Chem. Geol.* 345, 50–61. doi: 10.1016/j.chemgeo.2013.02.022

Raven, M. R., Sessions, A. L., Fischer, W. W., and Adkins, J. F. (2016). Sedimentary pyrite δ34S differs from porewater sulfide in Santa Barbara Basin: proposed role of organic sulfur. *Geochim. Cosmochim. Acta* 186, 120–134. doi: 10.1016/j.gca.2016.04.037

Riedinger, N., Formolo, M. J., Lyons, T. W., Henkel, S., Beck, A., and Kasten, S. (2014). An inorganic geochemical argument for coupled anaerobic oxidation of methane and iron reduction in marine sediments. *Geobiology* 12, 172–181. doi: 10.1111/gbi.12077

Riedinger, N., Kasten, S., Gröger, J., Franke, C., and Pfeifer, K. (2006). Active and buried authigenic barite fronts in sediments from the Eastern Cape Basin. *Earth Planet. Sci. Lett.* 241, 876–887. doi: 10.1016/j.epsl.2005.10.032

Sivan, O., Antler, G., Turchyn, A. V., Marlow, J. J., and Orphan, V. J. (2014). Iron oxides stimulate sulfate-driven anaerobic methane oxidation in seeps. *Proc. Natl. Acad. Sci. U.S.A.* 111, E4139–E4147. doi: 10.1073/pnas.1412269111

Staudt, W. J., and Schoonen, M. A. A. (1995). "Sulfate incorporation into sedimentary carbonates," in *Geochemical Transformations of Sedimentary Sulfur* ACS Symposium Series (American Chemical Society), 332–345. doi: 10.1021/bk-1995-0612.ch018

Tarpgaard, I. H., Røy, H., and Jørgensen, B. B. (2011). Concurrent low- and high-affinity sulfate reduction kinetics in marine sediment. *Geochim. Cosmochim. Acta* 75, 2997–3010. doi: 10.1016/j.gca.2011.03.028

Taylor, B. E., Wheeler, M. C., and Nordstrom, D. K. (1984). Stable isotope geochemistry of acid mine drainage: experimental oxidation of pyrite. *Geochim. Cosmochim. Acta* 48, 2669–2678. doi: 10.1016/0016-7037(84)90315-6

Teske, A. (2010). Cryptic links in the Ocean. *Science* 330, 1326–1327. doi: 10.1126/science.1198400

Wing, B. A., and Halevy, I. (2014). Intracellular metabolite levels shape sulfur isotope fractionation during microbial sulfate respiration. *Proc. Natl. Acad. Sci. U.S.A.* 111, 18116–18125. doi: 10.1073/pnas.1407502111

Wortmann, U. G., Chernyavsky, B., Bernasconi, S. M., Brunner, B., Böttcher, M. E., and Swart, P. K. (2007). Oxygen isotope biogeochemistry of pore water sulfate in the deep biosphere: dominance of isotope exchange reactions with ambient water during microbial sulfate reduction (ODP Site 1130). *Geochim. Cosmochim. Acta* 71, 4221–4232. doi: 10.1016/j.gca.2007.06.033

Zeebe, R. E. (2010). A new value for the stable oxygen isotope fractionation between dissolved sulfate ion and water. *Geochim. Cosmochim. Acta* 74, 818–828. doi: 10.1016/j.gca.2009.10.034

Conflict of Interest Statement: The authors declare that the research was conducted in the absence of any commercial or financial relationships that could be construed as a potential conflict of interest.

APPENDIX

The oxygen isotope mass balance,

$$\delta^{18}O_{mix} = x \bullet \delta^{18}O_{cont} + (1 - x) \bullet \delta^{18}O_{eq}$$

is rearranged to yield the value for the relative contribution of the contaminant (x), according to

$$x = (\delta^{18}O_{mix} - \delta^{18}O_{eq})/(\delta^{18}O_{cont} - \delta^{18}O_{eq}).$$

The absolute amount of contaminant equals x•conc$_{mix}$, and the amount of original sulfate equals $(1 - x)\bullet$ conc$_{mix}$. The sulfur isotope mass balance,

$$\delta^{34}S_{mix} = x \bullet \delta^{34}S_{cont} + (1 - x) \bullet \delta^{34}S_{orig}$$

is then rearranged to yield the sulfur isotope composition of original sulfate,

$$\delta^{34}S_{orig} = (\delta^{34}S_{mix} - x \bullet \delta^{34}S_{cont})/(1 - x).$$

frontiers in Earth Science

ORIGINAL RESEARCH
published: 01 June 2016
doi: 10.3389/feart.2016.00061

High Sulfur Isotope Fractionation Associated with Anaerobic Oxidation of Methane in a Low-Sulfate, Iron-Rich Environment

*Hannah S. Weber *, Bo Thamdrup and Kirsten S. Habicht †*

Nordic Center for Earth Evolution and Department of Biology, University of Southern Denmark, Odense, Denmark

Sulfur isotope signatures provide key information for the study of microbial activity in modern systems and the evolution of the Earth surface redox system. Microbial sulfate reducers shift sulfur isotope distributions by discriminating against heavier isotopes. This discrimination is strain-specific and often suppressed at sulfate concentrations in the lower micromolar range that are typical to freshwater systems and inferred for ancient oceans. Anaerobic oxidation of methane (AOM) is a sulfate-reducing microbial process with a strong impact on global sulfur cycling in modern habitats and potentially in the geological past, but its impact on sulfur isotope signatures is poorly understood, especially in low-sulfate environments. We investigated sulfur cycling and ^{34}S fractionation in a low-sulfate freshwater sediment with biogeochemical conditions analogous to early Earth environments. The zone of highest AOM activity was associated *in situ* with a zone of strong ^{34}S depletions in the pool of reduced sulfur species, indicating a coupling of sulfate reduction (SR) and AOM at sulfate concentrations <50 μmol L^{-1}. In slurry incubations of AOM-active sediment, the addition of methane stimulated SR and induced a bulk sulfur isotope effect of ~29‰. Our results imply that sulfur isotope signatures may be strongly impacted by AOM even at sulfate concentrations two orders of magnitude lower than at present oceanic levels. Therefore, we suggest that sulfur isotope fractionation during AOM must be considered when interpreting ^{34}S signatures in modern and ancient environments.

Keywords: anaerobic oxidation of methane, sulfur isotope fractionation, freshwater sediment, iron, early Earth analog

OPEN ACCESS

Edited by:
Orit Sivan,
Ben-Gurion University of the Negev, Israel

Reviewed by:
Aubrey L. Zerkle,
University of St. Andrews, UK
Gilad R. Antler,
Aarhus University, Denmark

****Correspondence:***
Hannah S. Weber
hannah@biology.sdu.dk

†Present Address:
Kirsten S. Habicht,
Unisense A/S, Aarhus, Denmark

Specialty section:
This article was submitted to Microbiological Chemistry and Geomicrobiology, a section of the journal Frontiers in Earth Science

Received: *06 January 2016*
Accepted: *09 May 2016*
Published: *01 June 2016*

Citation:
Weber HS, Thamdrup B and Habicht KS (2016) High Sulfur Isotope Fractionation Associated with Anaerobic Oxidation of Methane in a Low-Sulfate, Iron-Rich Environment. Front. Earth Sci. 4:61. doi: 10.3389/feart.2016.00061

INTRODUCTION

Microbial sulfur transformations play an important role in the biogeochemistry of the modern Earth surface and have done so during most of Earth's history, while the interactions of the sulfur, oxygen, and carbon cycles have undergone dramatic changes (Canfield and Teske, 1996; Canfield and Raiswell, 1999; Canfield et al., 2006). Stable isotope signatures archived in the geological record have been pivotal for reconstructing milestones of Earth's biogeochemical history and, consequently, the evolution of life, and they are useful for studies of modern sulfur cycling (Canfield and Raiswell, 1999; Canfield et al., 2000; Canfield, 2001).

Accurate interpretation of isotope signatures depends on a detailed understanding of the isotopic fractionation associated with different sulfur transformations. Fractionation of sulfur isotopes at low temperature is primarily controlled by microbes mediating dissimilatory SR and sulfur disproportionation. Microbial sulfate reducers are observed to discriminate kinetically against $^{34}SO_4^{2-}$ with enrichment factors, ε_{SRR}, in the range of –3 to –70‰ ($\varepsilon_{SRR} = [^{34}S/^{32}S_{sulfide} - {}^{34}S/^{32}S_{sulfate}] \times [^{34}S/^{32}S_{sulfate}]^{-1}$) in both natural settings and pure cultures (Canfield, 2001; Wortmann et al., 2001; Canfield et al., 2010; Sim et al., 2011). The magnitude of fractionation is impacted by environmental parameters such as, e.g., availability of sulfate and electron donors, and is highly dependent on the physiology and growth of the sulfate-reducing microorganisms (Bradley et al., 2016). Bradley et al. (2016) showed that sulfate reducers suppress the discrimination against heavier sulfate isotopes when sulfate concentrations in their environment fall below strain-specific concentration thresholds. A sulfate threshold of ∼200 μmol L^{-1} was suggested for natural communities of bacterial sulfate reducers (Habicht et al., 2002), but has recently been challenged by the report of substantial isotope fractionation between sulfate and sulfide at sulfate concentrations in the range of 5–10 μmol L^{-1} in the chemocline of ferruginous Lake Matano (Crowe et al., 2014). Isotope fractionation between sulfate and sulfide in natural environments may, however, also result from disproportionation processes. Disproportionation of intermediate sulfur species such as elemental sulfur, S^0, producing sulfide and sulfate, is associated with fractionations of up to ∼40‰ between the products (isotopically heavier sulfate and lighter sulfide; Canfield et al., 1998, 2005). Thus, in iron-rich environments where S^0 forms from abiotic sulfide reoxidation by ferric iron, repeated cycles of disproportionation and sulfide oxidation may increase the isotopic fractionation between sulfate and sulfide substantially above that caused by SR alone (Canfield and Thamdrup, 1994; Pellerin et al., 2015).

The global sulfur cycle is further impacted by anaerobic oxidation of methane (AOM), a microbial process controlling recent atmospheric levels of the powerful greenhouse gas methane (Reeburgh, 2007). For the interpretation of both modern and ancient stable sulfur isotope signatures, information is scarce about sulfur isotope fractionation during the process both on the biochemical and the biogeochemical level. In marine sediments, AOM is associated with a consortium of anaerobic methane-oxidizing archaea (ANME) and sulfate-reducing bacteria (SRB; Boetius et al., 2000). It was hypothesized that sulfate-AOM functions by syntrophic coupling, where ANME oxidize methane and produce a soluble interspecies electron carrier that is used by the sulfate-reducing partner (e.g., Meulepas et al., 2010). As an alternative, recent studies of ANME-SRB consortia suggest direct electron transfer between the microbial partners by nanowires and/or outer membrane cytochromes providing cell-to-cell-contact (McGlynn et al., 2015; Wegener et al., 2015). Another model suggested two novel unidentified enzymatic pathways where the ANME carries out SR and produces zero-valent sulfur as key intermediate that is further disproportionated by the associated bacterial partner (Milucka et al., 2012).

Sulfur isotope fractionation associated with SR coupled to AOM, and its impact on sulfur isotope signatures in the environment, has gained limited scientific attention so far. A few studies demonstrated that sulfur-cycling AOM influences $\delta^{34}S$ signatures in the environment (Jørgensen et al., 2004; Borowski et al., 2013) and concurrently alters the oxygen isotopic value in sulfate (Antler et al., 2014, 2015; Avrahamov et al., 2014; Deusner et al., 2014; Sivan et al., 2014). Two studies investigated sulfate-dependent AOM in slurry incubations fed with Black Sea microbial mats and seep sediments and suggested that AOM-driven sulfur isotope fractionation factors fall in the range of ∼20 to 40‰ in gas seeps (Deusner et al., 2014; Sivan et al., 2014) and may exceed 60‰ in marine sulfate-methane-transition zones (SMTZs; Deusner et al., 2014) .

So far, however, studies of sulfur isotope fractionation associated with AOM have focused mainly on sulfate concentrations in the millimolar range, whereas, from a geological perspective, sulfur cycling, and isotope fractionation at low sulfate concentrations is also of great relevance. Seawater sulfate levels in the Archaean Eon (before 2.5 billion years ago) are estimated to <0.01% of modern seawater, probably restricting biological productivity (Crowe et al., 2014), while estimated atmospheric methane levels were two to three orders of magnitudes higher than at present (Catling et al., 2001). As iron dominated oceanic chemistry during this time and through much of Earth's history, a coupling of AOM to iron instead of sulfate has been proposed as a globally important process on early Earth (Konhauser et al., 2005; Beal et al., 2009). Such a process was suggested to occur in modern sediment (Konhauser et al., 2005; Beal et al., 2009; Sivan et al., 2011), but has not been conclusively proven at the cellular level. In contrast, it has been demonstrated that cryptic sulfur cycling involving the generation and consumption of sulfur intermediates can catalyse large-scale iron turnover even at micromolar levels of sulfate (Hansel et al., 2015). Consequently, an apparent coupling of AOM and Fe reduction could possibly result from sulfate-dependent AOM fueled by rapid reoxidation of sulfide (Beal et al., 2011; Norði et al., 2013).

Freshwater systems low in sulfate are frequently used as early Earth analogs to study components of early ocean biogeochemistry (Canfield et al., 2010; Crowe et al., 2011; Knossow et al., 2015). One such site is the anoxic sediment of Lake Ørn, with sulfate concentrations <200 μmol L^{-1}, maximum methane concentrations of 1.4 mmol L^{-1} and reactive iron oxide concentrations of up to 65 μmol cm^{-3} (Norði et al., 2013). Here, 90% of the methane was found to be consumed by AOM before it reached the sediments surface, and AOM was active even at sulfate concentrations as low as 3 μmol L^{-1} (Norði et al., 2013). However, it was not clear from this study whether AOM was coupled to iron reduction or to SR supported by a cryptic sulfur cycle.

In the present study, we hypothesized that AOM in Lake Ørn sediment can be directly coupled to sulfur turnover at very low sulfate concentrations and even has the potential to induce fractionation of stable sulfur isotope species under these conditions. We demonstrate that sulfur cycling in the AOM zone in Lake Ørn sediment is associated with substantial

isotope fractionation and, based on experimental incubations, we infer a direct coupling of sulfur cycling and AOM at sulfate concentrations below 50 μmol L^{-1}.

MATERIALS AND METHODS

Sediment Sampling

Sediment was sampled in April and November 2012 at the center of Lake Ørn (water depth: 4 m), using a hand-operated Kajak sampler. In both April and November, three sediment cores were collected, each, for triplicate depth profiles of biogeochemical parameters. In April, samples were taken for depth profiles of stable sulfur isotopes ($\delta^{34}S$ of reduced sulfur) and in November samples were taken to obtain concentrations of HCl-extractable iron (Fe), sulfate, sulfide, methane, zero-valent sulfur, stable sulfur isotopes ($\delta^{34}S$ of reduced sulfur), porosity, rates of sulfate reduction (SR), and anaerobic oxidation of methane (AOM). Moreover, in November, we sampled (1) four additional cores and pooled the porewater from the corresponding horizons of all seven cores for measurement of $\delta^{34}S$ of sulfate and (2) 24 additional cores for a sediment slurry incubation experiment. At sampling days, the bottom water temperature was 7 and 8°C, in November and April, respectively and the overlying water column was oxygenated. The biogeochemistry of the sediment was described previously (Norði et al., 2013).

Slurry Incubation Experiment

Twenty-four cores (diameter = 5.2 cm) were dissected under a constant nitrogen flow into an upper (0–7 cm; "sulfide reoxidation zone") and a lower (7–21 cm, "AOM zone") depth interval, transferred into two and three Schott glass bottles, respectively, and mixed 1:1 with medium (anoxic water, 3 mmol L^{-1} $NaHCO_3$; pH = 6.6; 200 μmol L^{-1} and 50 μmol L^{-1} Na_2SO_4, respectively). For the lower depth interval, one slurry bottle was amended with S^0 to a final concentration of ∼100 μmol cm^{-3}. Slurries were then split and transferred into 0.5 L (sulfide reoxidation zone) and 1 L (AOM zone) Schott bottles, sealed with butyl rubber stoppers (anoxic as flushed and stored under helium atmosphere before usage) and the headspace was flushed with N_2:CO_2 (90:10; 0.5 bar) for 15 min. Afterwards, half of the bottles of the sulfide reoxidation zone slurries and two-thirds (including the elemental sulfur amended ones) of the AOM zone slurries were flushed with methane for 15 min. The bottles were individually packed into anaerobic plastic bags, which were flushed with helium. The bottles were stored at 5°C in darkness and carefully inverted for mixing every few days until further processing.

One bottle from each treatment was processed after 1, 6, 19, 43, 70 days, respectively, and for sulfide reoxidation zone, additionally after 103 days, as follows: the bottles were inverted, transferred into an anaerobic glove bag (filled with nitrogen) and samples were taken through the rubber stopper via a syringe and needle (flushed with helium prior to usage) for concentration determination of porewater parameters (sulfide, iron, sulfate), and filtered through a nylon syringe filter (Q-Max; pore size = 0.2 μm) directly into the corresponding vials. The bottles were then removed from the anaerobic glove bag and opened under constant nitrogen flow for concentration determination of solid and gaseous parameters (methane, iron, porosity, zero-valent sulfur, $\delta^{34}S$ signatures) and SR measurements in triplicates.

Solid, Porewater, and Gaseous Parameters

The cores obtained for depth profile characterization were all dissected in 2 cm intervals (April) or 2 cm (0–6 cm) and 3 cm (6–21 cm) intervals (November) within 2 days after sampling under constant nitrogen flow at 5°C. From each interval, one sample was taken per parameter, which resulted in triplicate depth profiles for each sampling point (April and November).

For porewater analysis, centrifugation vials were filled completely, centrifuged at 4000 g for 10 min (precooled, Centrifuge 5810; Eppendorf) and the supernatant was filtered anoxically (glove bag filled with nitrogen) through a syringe filter (pore size = 0.2 μm; syringe, needle, and filter flushed and stored in helium prior to usage). For dissolved Fe, 1 mL porewater was mixed with 20 μL 6 N hydrochloric acid (HCl), stored at −20°C, and Fe^{2+} concentrations were determined using the Ferrozine reagent (Stookey, 1970; Thamdrup et al., 1994). For analysis of sulfate and sulfide concentrations, 1 ml porewater was mixed with 20 μL of 20% zinc acetate and stored at −20°C. Sulfate concentrations were quantified via ion chromatography (Dionex ICS-1500) with a detection limit of 1 μmol L^{-1} and sulfide concentrations were quantified by the methylene blue method (detection limit = 0.5 μmol L^{-1}; Cline, 1969).

For analysing methane concentrations, 2 mL of sediment was subsampled in triplicates via a cut-off syringe directly into a 20 mL serum vial, prefilled with 5 mL 2.5% sodium hydroxide (NaOH), closed, and shaken immediately and stored upside down for at least 24 h to equilibrate the methane into the headspace. Methane was quantified by injecting 100 μL of the headspace into a gas chromatograph with an FID detector (Perkin Elmer).

The density was analyzed by subsampling 1 mL of sediment with a cut-off syringe into a pre-weight centrifugation vial and the water content/porosity as the weight loss from after drying at 90°C for 48 h. Solid-phase Fe was extracted by transferring 0.5 mL sediment into 5 ml 1 N HCl and shaking the samples on a rotary shaker for 24 h in darkness (Raiswell et al., 1994). The method quantitatively dissolves ferrihydrite ($Fe_2O_3 0.5(H_2O)$), and ferrous phases such as siderite ($FeCO_3$), vivianite ($Fe_3(PO_4)_2 8H_2O$) and iron monosulfides (FeS), but not crystalline iron oxides or pyrite (Raiswell et al., 1994). After extraction, we centrifuged the samples at 4000 g for 10 min (Centrifuge 5810; Eppendorf), filtered the supernatant through a nylon syringe filter (pore size = 0.2 μm) and quantified the concentration using the Ferrozine method (Stookey, 1970; Thamdrup et al., 1994). A previous study reported a total iron content of ∼3000 μmol g^{-1} in Lake Ørn sediment (O'Connell et al., 2015), suggesting that the 1 N HCl-extractable iron corresponds to <20% of the total iron pool. For quantification of zero-valent sulfur, sediment was mixed with 20% zinc acetate and stored at −20°C until further processing (Ferdelmann et al., 1997). For analysis, 0.2–0.5 g sediment of each sample was mixed with 10 mL methanol and shaken on a rotary shaker for 24 h. Thereafter, the methanol-extract was centrifuged

at 4000 g for 10 min (Centrifuge 5810; Eppendorf) and 1 mL of the supernatant was used for concentration measurements by HPLC-analysis (Agilent 1100 series, Hewlett Packard). For the incubations with S^0 addition, methanol treatment showed insufficient extraction of S^0 and data are therefore unreliable and not shown. For $\delta^{34}S$ and concentration analysis of reduced sulfur species (acid volatile sulfur, AVS, and chromium reducible sulfur, CRS) and $\delta^{34}S$ analysis of zero-valent sulfur and sulfate, sediment was mixed with 20% zinc acetate and stored at −20°C. After thawing, sediment was centrifuged immediately at 4000 g for 10 min (Centrifuge 5810; Eppendorf) to separate the supernatant from the sediment. For the $\delta^{34}S$ sulfate depth profiles, supernatant was pooled from seven cores. Thereafter, the supernatant was filtered through a polycarbonate filter (pore size = 0.45 μm), acidified with 6 N HCl to a pH = 1 and barium chloride ($BaCl_2$, 1 M) was added in surplus to form barium sulfate ($BaSO_4$). The sample was then heated up to 80°C to slowly evaporate water and finally the remaining $BaSO_4$ was boiled with 25 mL of a reducing mixture of hydriodic acid (HI), concentrated hydrochloric acid (HCl), and 50% hyphosphorous acid (H_3PO_4; Thode et al., 1961) for 6 h in a distillation flask connected to a reflux condenser. Liberated hydrogen sulfides were driven out by a constant N_2 flow through a water trap into 0.5 mol L^{-1} cadmium acetate dihydrate ($Cd(CH_3COO)_2{\cdot}2H_2O$) to produce cadmium sulfide (CdS). CdS was converted with 1 M silver nitrate ($AgNO_3$) into silver sulfide (Ag_2S), warmed up to 50°C for 24 h (facilitates coagulation), filtered onto a cellulose ester filter (pore size = 0.45 μm) and dried at room temperature. The reduced sulfur compounds AVS and CRS were obtained using the hot two-steps chromium distillation (Canfield et al., 1986; Fossing and Jørgensen, 1989), where AVS and CRS were reduced via HCl and hot chromium (Cr(II)) solution and liberated hydrogen sulfides were trapped as Ag_2S. To obtain $\delta^{34}S$ values from zero-valent sulfur, a Soxhlet extraction was carried out from samples at incubation start, using 5–10 g sediment and acetone as extractant. In brief, over an extraction period of 24 h, dissolved zero-valent sulfur was reduced and precipitated on copper wires (Cu) as copper sulfide (CuS; Allen and Parkes, 1995). Thereafter, CuS wires were distilled using the hot chromium distillation (Canfield et al., 1986; Fossing and Jørgensen, 1989) and liberated hydrogen sulfides were trapped as Ag_2S. A Soxhlet extraction was also carried out with zero-valent sulfur that was added to the incubations of the AOM zone. The sulfur isotope compositions of AVS, CRS, zero-valent sulfur, and sulfate were quantified with a gas-source Isotope Ratio Mass spectrometer (Delta V ADVANTAGE), where SO_2 gas was produced from combustion of the samples in a FlashEA 1112 Element Analyser and data were reported in Isodat Workspace 3.0 as per mill difference relative to the VCDT and three in-house (Ag_2S) standards (S.D. 0.5‰). The $\delta^{34}S$ value of zero-valent sulfur "off the shelf" was 16.7‰.

Subsampling for SR and AOM Rates

For SR and AOM rates, 5 mL sediment/slurry was filled into glass tubes in triplicates, closed with plunger and septum (stored under helium prior to sampling) and pre-incubated for 1 h before injection of radiotracers (Jørgensen, 1978).

For SR rates, per sample 20 μl carrier-free $^{35}SO_4^{2-}$ tracer (100 kBq) was injected through the septum and the samples incubated at 5°C in darkness for 6 h. The incubations were stopped by transfer to zinc acetate (20%; 10 mL) and freezing at −20°C. Killed controls were taken in parallel by transferring sediment/slurry to zinc acetate after incubation and then adding tracer. Radiolabeled sulfur species (sulfate and AVS + CRS) were determined via the cold chromium distillation (Kallmeyer et al., 2004; Røy et al., 2014).

For AOM rates, $^{14}CH_4$ (dissolved in water; 20 μl; 0.5 kBq; supplied from American Radiolabeled Chemicals, cleaned with hopcalite and sodium hydroxide) was injected through the septum into the sediment/slurry and samples incubated at 5°C in darkness for 20 h. To stop incubations the samples were transferred into glass vials prefilled with 15 ml sodium hydroxide (2.5% w/v) and immediately closed with butyl rubber stoppers, shaken, and stored upside down. Methane concentrations were determined as described above and activities of $^{14}CH_4$ and $^{14}CO_2$ were quantified (Treude et al., 2005), using phenylethylamine and sodium hydroxide (1:1) as CO_2 trap. Killed controls were taken with each time point, where tracer was injected after determining the microbial activity.

Radioactivity was measured on a QuantaSmart-4.00 Scintillation counter (count time: 10 min; coincidence time: 18 ns; delay before burst: 75 ns). For determining the detection limits for the SR and AOM rate measurements, the mean plus three times the standard deviation of the killed controls were subtracted from the product pools, ^{35}S sulfides, and $^{14}CO_2$, respectively.

Model

A curve-fitting model to obtain ε_{AOM} was built for the AOM zone incubations based on the assumption that the total sulfate consumption rate of AOM was the sum of the net sulfate production from the unamended incubations and the net sulfate consumption of the methane-amended incubations. We used T_0 values of the sulfate concentration and $\delta^{34}S$ sulfate from the AOM zone incubation amended with methane and calculated theoretical enrichments of $\delta^{34}S$ sulfate over a course of 80 one-day time steps for different values of ε_{AOM} between 20 and 40‰ at 1‰ increments. The model assumes no isotope fractionation associated with sulfate production from sulfide oxidation and approximates the rate of $^{32}SO_4^{2-}$ production and consumption by the measured bulk rates. In more detail, for time step T_0, we first calculated the ratio $^{34/32}R$ between $^{34}SO_4^{2-}$ and $^{32}SO_4^{2-}$ by $^{34/32}R = ((\delta^{34}S_{T0}/1000) + 1) \times {}^{34/32}R_{standard}$ with $\delta^{34}S_{T0}$ = 22.2‰ and $^{34/32}R_{standard}$ = 0.0045005 (VCDT). Thereafter, we obtained the $^{32}SO_4^{2-}$ and $^{34}SO_4^{2-}$ concentrations by $[^{32}SO_4^{2-}]_{T0} = [SO_4^{2-}]_{T0}/(^{34/32}R + 1)$ with $[SO_4^{2-}]_{T0}$ = 39 μmol L^{-1} and $[^{34}SO_4^{2-}]_{T0} = [SO_4^{2-}]_{T0} - [^{32}SO_4^{2-}]_{T0}$. For each following time step T_n, $[^{32}SO_4^{2-}]_{Tn}$ was calculated by $[^{32}SO_4^{2-}]_{Tn} = [^{32}SO_4^{2-}]_{Tn-1} + ((T_n - T_{n-1}) \times Prod_{SO42-}) - ((T_n - T_{n-1}) \times Con_{SO42-})$, where $Prod_{SO42-}$ = 3.5 nmol cm^{-3} day^{-1} is the net sulfate production rate in the slurry incubation without methane amendment and Con_{SO42-} = 4 nmol cm^{-3} day^{-1} is the net sulfate consumption in the slurry incubation

with methane addition. Furthermore, we calculated $[^{34}SO_4^{2-}]$ for the same time steps using $[^{34}SO_4^{2-}]_{Tn} = [^{34}SO_4^{2-}]_{Tn-1} + ((T_n - T_{n-1}) \times Prod_{SO42-} \times {}^{34/32}R_{sulfides}) - ((T_n - T_{n-1}) \times {}^{34}Prod_{Tn-1})$, where ${}^{34/32}R_{sulfides} = 0.0044856$ ($\delta^{34}S = 3.0‰$), which corresponds to the value of the sulfide pool of AOM zone slurry incubations. ${}^{34}Prod_{Tn-1}$ was calculated for each time step by ${}^{34}Prod_{Tn-1} = (Con_{SO42-}/\alpha) \times ([^{34}SO_4^{2-}]/[^{32}SO_4^{2-}])$. For α, we used values in the range of 1.020 and 1.040, which corresponds to ε_{AOM} values between 20 and 40‰. After calculating α-dependent $[^{34}SO_4^{2-}]$, and $[^{32}SO_4^{2-}]$ for all time steps, we calculated $\delta^{34}SO_4^{2-}$ using $\delta^{34}SO_4^{2-} = ((([^{34}SO_4^{2-}]/[^{32}SO_4^{2-}])/{}^{34/32}R_{standard}) - 1) \times 1000$ and matched the resulting $\delta^{34}S$ values with the $\delta^{34}S$ sulfate enrichment measured in the methane-amended incubations to determine the value of α yielding the best fit (least sum of squares). The ε_{AOM} value was determined from the best fit α.

TABLE 1 | Porewater and solid-phase parameters of triplicate depth profiles in November 2012, summarized for the AOM zone (7–21 cm) and the sulfide reoxidation zone (0–7 cm).

	AOM zone (7–21 cm)	Sulfide reox. zone (0–7 cm)
Sulfate [μmol L^{-1}]	<100	200–100
Methane [μmol L^{-1}]	max. 600	<20
Fe(III) [μmol cm^{-3}]	<80	200–80
Fe(II) [μmol cm^{-3}]	330–540	100–330
SR [nmol cm^{-3} day^{-1}]	max. 130	max. 105
AOM [nmol cm^{-3} day^{-1}]	max. 33	max. 2
S^0 [μmol cm^{-3}]	max. 9	<0.6
red. sulf. comp. [μmol cm^{-3}]	max. 53	<8
$\delta^{34}S$ sulfate [‰]	max. 19	3–17
$\delta^{34}S$ red sulf. comp. [‰]	min. −27 (April) and −15 (Nov)	min. −5 (April) and −6 (Nov)

RESULTS AND DISCUSSION

Large AOM Zone in Lake Ørn Sediment

The biogeochemical zonation of Lake Ørn sediment showed a well-developed AOM zone similar to a previous report (Norði et al., 2013). Thus, methane diffusing upwards from the methanogenic zone below 20 cm depth was largely consumed well below the oxic realm (upper 4 mm; Norði et al., 2013), as indicated by the concave trend of methane concentrations over depth and low μmolar levels above 7 cm (**Figure 1A**, **Table 1**). Characteristic of this sediment is a very high iron content and a deep penetration of poorly crystalline, HCl-extractable ferric iron, which reached down to 20 cm, while concentrations of HCl-extractable ferrous iron increased with depth (**Figure 1B**, **Table 1**). Sulfate depth profiles resembled each other in five of seven cores with surface concentrations of ∼200 μmol L^{-1} and a detection depth of 17 cm (**Figure 1A**, **Table 1**). In two of the cores, the sulfate profile deviated and one of them had a sulfate concentration of ∼70 μmol L^{-1} at maximal sampling depth (18–21 cm). Sulfate and methane coexisted in a broad SMTZ at 7–17 cm. Rates of dissimilatory SR were highest in the depth intervals 2–4 cm and 12–15 cm, and AOM rates increased steeply until 12–15 cm, locating the AOM zone to 8–21 cm (**Figure 1C**, **Table 1**), in good agreement with the SMTZ (**Figure 1A**). The rates ratio of SR to AOM in the AOM zone was ∼2:1. Thus, the measured SR rate exceeded the potential sulfate demand of AOM suggesting that at least some SR was coupled to organotrophy.

Microbially produced hydrogen sulfide did not accumulate to detectable levels in the porewater, which implies a rapid turnover time (10 min or less relative to the measured SR) in combination with ferric iron reduction and iron sulfide precipitation. The distributions of reduced sulfur species S^0, acid volatile sulfides (AVS, here: FeS) and chromium reducible sulfides (CRS), differed markedly between the two zones of highest SR rates and divided the sediment column into two distinct horizons: an upper layer (0–7 cm) with low concentrations and shallow gradients of these compounds, and a deeper layer at 7–21 cm, coincident with the AOM zone, where all three phases accumulated, reaching highest concentrations at the base of the SMTZ at 15–18 cm depth (**Figures 1D,E**, **Table 1**). The lack of accumulation of reduced sulfur species in the upper layer, despite active SR, indicated an extremely close coupling of SR, and sulfide reoxidation processes with ferric iron as the most likely electron acceptor (Schippers and Jørgensen, 2002; Holmkvist et al., 2011). Potential reactions include the abiotic oxidation of sulfide to zero-valent sulfur with iron (hydr)oxides (Pyzik and Sommer, 1981; Yao and Millero, 1996), followed by disproportionation to sulfide and sulfate (Thamdrup et al., 1993). Alternatively, sulfate may have been generated through direct oxidation of reduced sulfur compounds coupled to iron reduction without involvement of S^0 disproportionation, as discussed below. In the AOM zone, the availability of reactive ferric iron was lower and the pool of ferrous iron was larger than in the upper layer, and reduced sulfur compounds accumulated (**Figures 1B,E**, **Table 1**). Zero-valent sulfur concentrations increased steeply below 7 cm, resulting in a peak of 7 μmol cm^{-3}, corresponding to almost half of the AVS concentration (**Figures 1D,E**, **Table 1**), in the zone of highest AOM activity. A transient accumulation of S^0 is frequently observed during early diagenesis, where it is assumed to result from the reoxidation of H_2S with ferric iron (Thamdrup et al., 1994; Hansel et al., 2015). The large fraction of S^0 in Lake Ørn sediment is unusual, however, as S^0 is typically an order of magnitude less abundant than FeS in sulfate-reducing sediments (e.g., Thamdrup et al., 1994).

In summary, the geochemical profiles and rate measurements demonstrate active sulfur cycling throughout the sulfate-containing zone of the sediment, with highly efficient recycling of sulfide in the upper layer, where the ferric iron content is highest, and precipitation of reduced sulfur compounds in the AOM zone, although the accumulation of S^0 indicates some recycling there as well. The enhanced rate of SR in the AOM zone could suggest a coupling of the two processes, but the profiles alone do not allow us to discern between such a coupling and, e.g., a direct coupling of AOM to iron reduction.

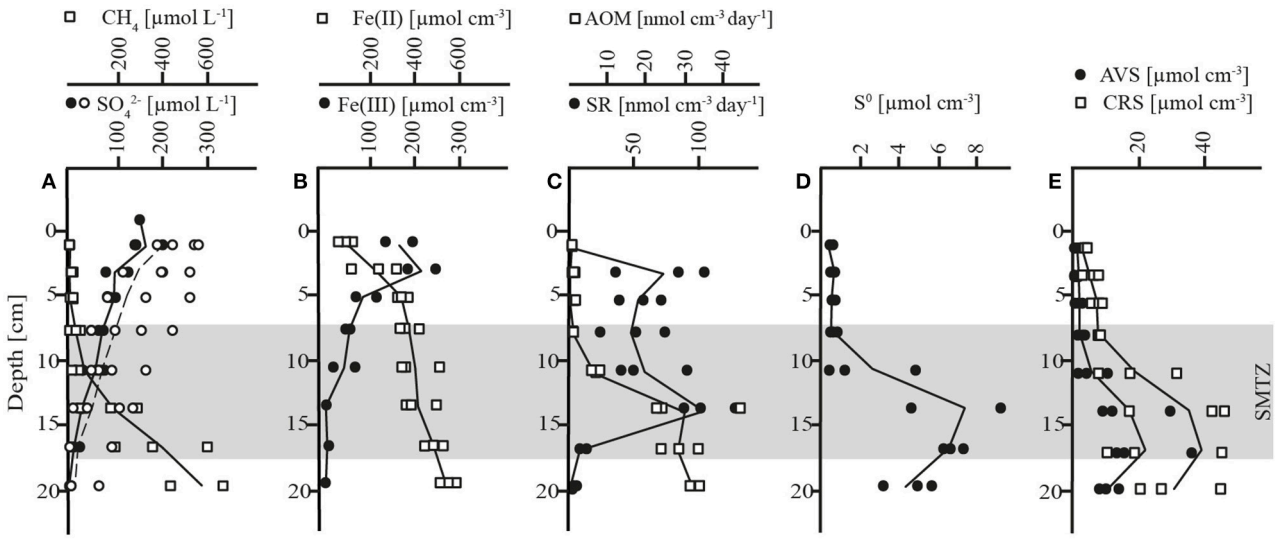

FIGURE 1 | Concentration depth profiles and microbial rates from November. (A) methane (CH_4) and sulfate (SO_4^{2-}), whereas closed circles represent sulfate data from triplicate cores and open circles represent sulfate data from four additional cores **(B)** HCl-extractable iron (Fe(II) and Fe(III)) **(C)** rates of sulfate reduction (SR) and anaerobic oxidation of methane (AOM) **(D)** zero-valent sulfur (S^0) **(E)** acid volatile sulfur (AVS); chromium reducible sulfur (CRS); shadowed area: sulfate-methane-transition-zone (SMTZ).

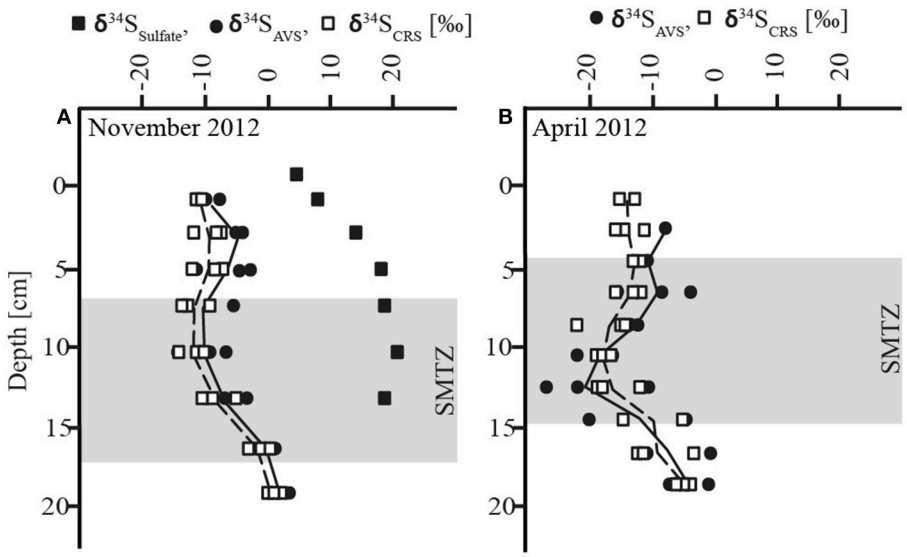

FIGURE 2 | (A) Depth profiles of $\delta^{34}S$ of sulfate, acid volatile sulfur (AVS) and chromium reducible sulfur (CRS) in November **(B)** Depth profiles of acid volatile sulfur (AVS) and chromium reducible sulfur (CRS) in April; shadowed area: sulfate-methane-transition-zone (SMTZ).

Depletion of ^{34}S in Sulfides in AOM Zone

The AOM zone coincided with a distinct zone of strong ^{34}S depletion in the reduced sulfur compounds with lowest $\delta^{34}S$ values of −27‰ in April and −15‰ in November (**Figure 2**, **Table 1**). In April, $\delta^{34}S$ values were up to 21 and 29‰ higher above and below the AOM zone, respectively, than within it. In November, the SMTZ was shifted a few cm downwards in comparison to April and coincided with a distinct, but less pronounced pool in ^{34}S-depleted sulfides. Here, $\delta^{34}S$ values above and below the AOM zone were up to 9 and 16‰ higher than within the zone, respectively. The shift of the ^{34}S depletion zone was likely dynamically related to microbial activity and therefore rather a result of seasonal dynamics than of historical origin. The $\delta^{34}S$ profile for sulfate, determined in November (**Figure 2A**) showed increasing enrichment of ^{34}S in the sulfate pool from ∼3 to ∼17‰ from the bottom water to 7 cm depth and a small further enrichment to ∼19‰ in the AOM zone. Accordingly, the isotopic shift between sulfate and reduced sulfur compounds,

in the following abbreviated as $\Delta^{34}S$ (SO_4^{2-} − HS^-), increased with depth: In the upper zone of sulfide reoxidation, where sulfate concentrations were >100 μmol L^{-1}, $\Delta^{34}S$ (SO_4^{2-} − HS^-) was between ∼15 and 29‰. In the AOM zone where sulfate concentrations decreased from 100 μmol L^{-1} to the detection limit, isotope differences between the two pools were between 21 and 34‰ While the $\Delta^{34}S$ (SO_4^{2-} − HS^-) values thus indicate substantial fractionation associated with the accumulation of reduced sulfur species in the AOM zone, this was not reflected in a concomitant increase in $\delta^{34}S$ of sulfate with depth in this zone, as should be expected (**Figure 2A**). We attribute this discrepancy to the procedure used to obtain sufficient material for the sulfate isotope measurements, which involved the combination of pore water from seven parallel cores for a single measurement, whereas $\delta^{34}S$ of reduced sulfur, as well as all other geochemical parameters, were measured in triplicates in the same three of the seven cores. Unfortunately, two of the additional cores used for $\delta^{34}S$ of sulfate had strongly deviating sulfate distribution with no evidence of sulfate consumption below 10 cm depth. As sulfate from these cores completely dominated the combined sulfate sample in the two deepest depth intervals, we speculate that it also caused the leveling off of the $\delta^{34}S$ sulfate profile. Thus, the $\Delta^{34}S$ (SO_4^{2-} − HS^-) values provide more robust evidence of isotope fractionation than the sulfate $\delta^{34}S$ gradient.

The $\delta^{34}S$ signatures and the distinct offset between the oxidized and reduced sulfur pools must be understood as a "bulk" signal and as a result of a concert of different metabolic pathways of the sulfur cycling community. The primary control of sulfur isotope fractionation is generally organotrophic SR and the process was likely to be active in both the sulfide reoxidation and in the AOM zone. An earlier study showed that microbial sulfate reducers, including Danish lake sediment communities, limit ^{34}S isotope fractionation at sulfate concentrations <200 μmol L^{-1}, reaching ≤5‰ below 100 μmol L^{-1} (Habicht et al., 2002). Based on this finding and due to decreasing sulfate concentrations, the impact of bacterial SR on sulfur isotope fractionation in Lake Ørn sediment was expected to be low in general, greatest in the sulfide reoxidation zone, and decreasing with increasing depth, which contrasts with our observations. However, the distinct ^{34}S depletion in the reduced sulfur compounds in Lake Ørn was not only associated with the zone of very low-sulfate concentrations, but also with the highest AOM activities (**Figures 1C**, **2**). This finding suggests that the observed sulfur isotope fractionation may arise specifically through AOM-dependent sulfur cycling. A recent study showed that the sulfate concentration dependence of sulfur isotope fractionation varies markedly between bacterial species (Bradley et al., 2016). Thus, AOM-dependent sulfate reducers could potentially be capable of ^{34}S fractionation at sulfate levels where fractionation is suppressed in organotrophic sulfate reducers. The potential for a distinct fractionation pattern associated with SR during AOM is further emphasized by the recent hypothesis that AOM-dependent SR occurs through a unique S^0-producing pathway, as hypothesized (Milucka et al., 2012). Antler et al. (2015) recently suggested that AOM-dependent SR imparts a unique $\delta^{18}O/\delta^{34}S$ ratio to the residual sulfate in estuarine and marine sediments, but this was based on sulfate at millimolar concentrations, and a fractionation factor relative to the reduced products was not determined.

In addition to microbial organiclastic and methanoclastic SR, the oxidative cycling of intermediate sulfur species may have affected the stable sulfur isotope signatures in Lake Ørn. In particular, S^0 was unusually abundant in the AOM zone (**Figure 1D**). The source S^0 may have been sulfate-dependent AOM either by a direct intracellular archaeal production (Milucka et al., 2012) or indirectly via a sulfide reoxidation process with ferric iron (**Figure 5**). Therefore, microbial disproportionation fueled by methanoclastic and organiclastic SR was potentially an active process contributing to the ^{34}S enrichment in the sulfate pool and ^{34}S depletion in the reduced sulfur compounds (Canfield and Thamdrup, 1994), both in the sulfide reoxidation zone and in the AOM zone.

To further investigate which sulfur cycling microbial processes were active and altering the $\delta^{34}S$ signatures in Lake Ørn sediment, we set up a series of anoxic slurry incubations from the zones of sulfide reoxidation and AOM. We studied sulfur turnover and $\delta^{34}S$ signatures in incubations of both zones where methane was removed at incubation start in comparison with incubations where methane was added to enable sulfate-dependent AOM. The potential for S^0 disproportionation was investigated in the AOM zone by addition of zero-valent sulfur to methane-amended incubations.

An Iron-Fueled Cryptic Sulfur Cycle

In slurries where methane was removed at incubation start, a net accumulation of sulfate was measured in both the sulfide reoxidation zone (0–7 cm) and the AOM zone (7–21 cm) with rates of 3.6 ± 0.9 and 3.3 ± 0.3 nmol cm^{-3} day^{-1}, respectively (**Figures 3A**, **4A**, Table S1). In both zones, there were no significant changes in S^0 concentrations over time (**Figures 3B**, **4B**, Table S1) and soluble hydrogen sulfide remained around the detection limit. At the same time, extractable ferrous iron concentrations increased and ferric iron decreased. Methane did not build up over the course of the experiment (Figures S1A, S2A). Despite net sulfate accumulation, SR as measured with the ^{35}S assay was active at rates averaging 1 nmol cm^{-3} day^{-1} in the sulfide reoxidation zone and 10 nmol cm^{-3} day^{-1} in the AOM zone, and was hence substantially lower in the slurries than in the depth profiles (**Figures 1C**, **3C**, **4C**, **Table 1**, Table S1). The $\delta^{34}S$ signatures showed depletion of ^{34}S in the growing sulfate pool from 3 to −2‰ in the sulfide reoxidation zone and from 21 to 8‰ in the AOM zone (**Figures 3D**, **4D**). At the same time, $\delta^{34}S$ values of reduced sulfur compounds remained around −9‰ (AVS) and −12‰ (CRS) in the top zone and around −4‰ (AVS) and −6‰ (CRS) in the AOM zone with no significant change over time (**Figures 3E,F**, **4E,F**).

The net production of sulfate with parallel reduction of ferric iron and increase of ferrous iron concentrations in the slurries indicated an iron-driven sulfate production mechanism. Sulfate production caused by oxidation of reduced sulfur compounds due to oxygen contamination can be excluded due to anoxic conditions. Therefore, by analogy to our interpretation of the lacking accumulation of reduced sulfur compounds at 0–7 cm (see above), we propose that anaerobic sulfide oxidation

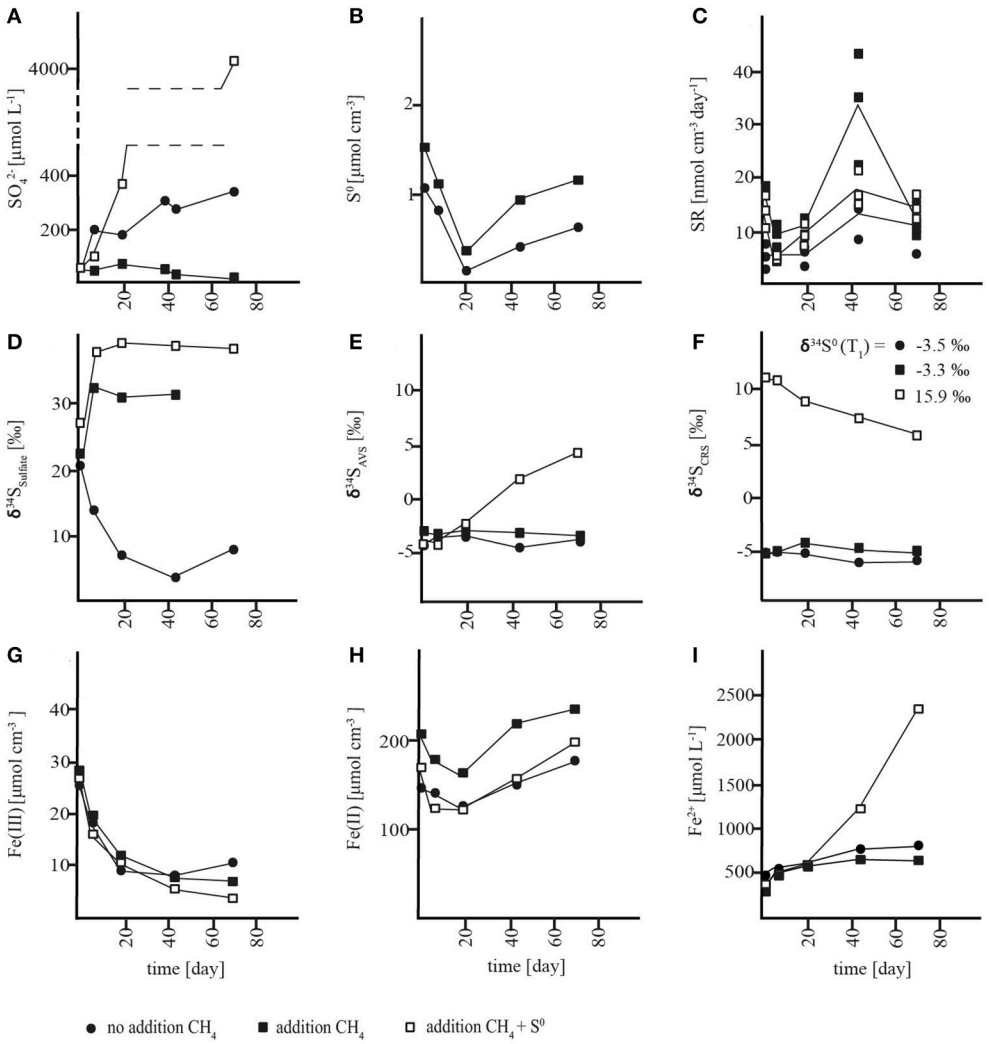

FIGURE 3 | Concentration changes over time in AOM zone slurry incubations. (A) sulfate (SO_4^{2-}), **(B)** zero-valent sulfur (S^0), **(C)** sulfate reduction rates (SR), **(D)** $\delta^{34}S$ values of sulfate, **(E)** $\delta^{34}S$ values of acid volatile sulfur (AVS) **(F)** $\delta^{34}S$ values of chromium reducible sulfur (CRS), **(G)** solid-phase HCl-extractable iron (Fe(III)), **(H)** solid-phase HCl-extractable iron (Fe(II)), and **(I)** porewater iron (Fe^{2+}).

was the source of sulfate through either (1) coupled partial oxidation and disproportionation or (2) a direct oxidation to sulfate. In the first scenario, abiotic oxidation of sulfide to S^0 would be coupled to iron reduction followed by microbial disproportionation of S^0. Subsequently, S^0 disproportionation would lead to the production of sulfate and sulfide (Thamdrup et al., 1993). As mentioned above, S^0 disproportionation leads to enrichment of sulfate and depletion of reduced sulfur compounds in ^{34}S (Canfield and Thamdrup, 1994), which is contrary to the observed ^{34}S depletion in sulfate and rather constant $\delta^{34}S$ values of the reduced sulfur compounds (**Figures 3E,F**, **4E,F**). Furthermore, a change in the $\delta^{34}S$ of the reduced sulfur compounds should have been evident especially in the sulfide oxidation zone incubations, where initial concentrations of reduced sulfur species were very low. By contrast, direct abiotic or microbial sulfide oxidation to sulfate is generally associated with negligible isotope fractionation (Habicht et al., 1998 and references therein). Thus, a direct oxidation of reduced sulfur compounds to sulfate is a likely explanation for the decreasing $\delta^{34}S$ of sulfate with no change in $\delta^{34}S$ of the reduced species. Indeed, a mixing plot of $\delta^{34}S$ versus sulfate concentration from the sulfide reoxidation zone showed that the sulfate produced corresponded to an end-member source with a $\delta^{34}S$ value of -11.2 ± 1.4‰ (Figure S3A), which equates to the $\delta^{34}S$ value of reduced sulfur compounds (-11‰). This result indicated that sulfate is supplied by direct sulfide oxidation to the sulfide oxidation zone, and that this oxidation included sulfide produced during SR, the activity of which was documented with the ^{35}S assay (**Figure 4C**), such that SR did not impact the $\delta^{34}S$ fingerprint. The AOM zone, on the other hand, showed an end-member value of $+3.9 \pm 3.0$‰ (Figure S3B), which was well-above the $\delta^{34}S$ value of reduced sulfur compounds of -5‰. This

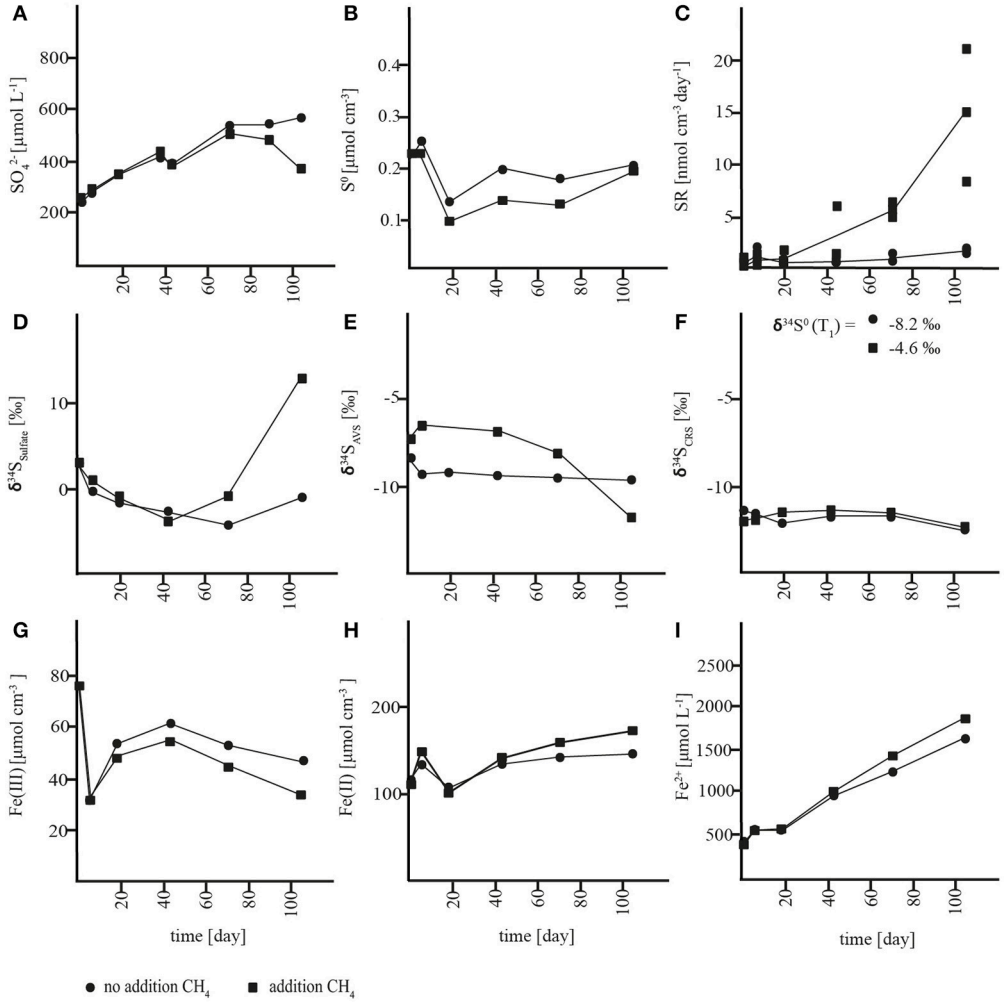

FIGURE 4 | Concentration changes over time in sulfide reoxidation zone slurry incubations. (A) sulfate (SO_4^{2-}), **(B)** zero-valent sulfur (S^0), **(C)**: sulfate reduction rates (SR), **(D)** $\delta^{34}S$ values of sulfate, **(E)** $\delta^{34}S$ values of acid volatile sulfur (AVS) **(F)** $\delta^{34}S$ values of chromium reducible sulfur (CRS), **(G)** solid-phase HCl-extractable iron (Fe(III)), **(H)** solid-phase HCl-extractable iron (Fe(II)), and **(I)** porewater iron (Fe^{2+}).

offset points to the involvement of additional processes in sulfur cycling, and the trend may be explained by S^0 disproportionation acting as an additional source of sulfate concomitantly with sulfur oxidation, or by incomplete reoxidation of sulfide formed during SR.

To further investigate the potential for S^0 disproportionation and to elucidate its effect on stable sulfur isotope signatures in Lake Ørn sediment, we added zero-valent sulfur (∼100 µmol cm^{-3}) to parallel methane-containing slurries of the AOM zone. As expected for S^0 disproportionation, sulfate concentrations increased (Thamdrup et al., 1993) dramatically at a rate of 61 ± 7 nmol cm^{-3} day^{-1}. Ferrous iron also accumulated while ferric iron concentrations decreased (**Figures 3G–I**). After depletion of ferric iron, soluble hydrogen sulfide started to build up (Figure S1D) as expected during disproportionation (Thamdrup et al., 1993) and in further support of our conclusion that porewater sulfide levels in Lake Ørn are controlled by iron with a large buffer capacity. SR rates, measured with the ^{35}S assay, averaged 13 nmol cm^{-3} day^{-1}, which was comparable to the rate in the previously described incubations of the AOM zone (**Figure 3C**, Table S1). With increasing sulfate concentrations in the S^0-amended slurry incubations, sulfate was enriched in ^{34}S from 27 to 38‰, corresponding to an isotopic shift of ∼22‰ between added S^0 and sulfate, while the CRS pool, including S^0, was depleted in ^{34}S (**Figures 3A,D,F**). The isotopic shift between S^0 and sulfate is within the range previously observed for sulfur disproportionation in freshwater cultures (Canfield et al., 1998). The results indicate that S^0 disproportionation was the dominant microbial pathway of sulfur transformation in the incubation with additional zero-valent sulfur and therefore had a general potential to occur *in situ*.

In conclusion, sulfide in Lake Ørn sediment was efficiently recycled to sulfate by direct, iron-driven anoxic sulfide oxidation, as well as by S^0 disproportionation. This indicates that the deep

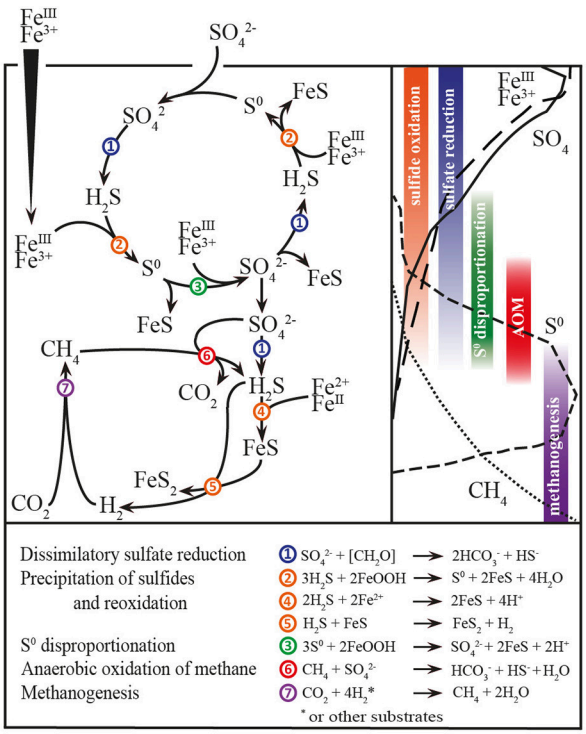

FIGURE 5 | Scheme of abiotical and microbial processes in Lake Ørn sediment. Left up: Sulfur, carbon, and iron cycling; numbers indicate processes; right up: depth distribution of porewater and solid parameters and depth distributions of processes; down: stoichiometric balanced microbial and abiotical process reactions.

sulfate-containing zone and the thick SMTZ in the sediment were maintained by this internal cryptic sulfur cycle, thus setting the scene for sulfur-cycling AOM (**Figure 5**).

Impact of Methane on Sulfur Turnover and $\delta^{34}S$ Signatures

In order to investigate the impact of methane on sulfur cycling and $\delta^{34}S$ signatures, methane was added to slurries from the sulfide reoxidation and the AOM zone (1.4 mmol L^{-1}). In the AOM zone, this resulted in substantial changes in sulfur turnover and $\delta^{34}S$ biogeochemistry relative to the incubations without methane addition. Instead of accumulating, sulfate was consumed at ~0.5 ± 0.3 nmol cm^{-3} day^{-1} until depletion at day 73, which corresponds to a gross consumption of ~4 nmol cm^{-3} day^{-1} (**Figure 3A**, Table S1), assuming that the sulfate production observed in the absence of methane was not affected by methane addition. In the sulfide reoxidation zone, sulfate was produced at the same rate as without methane addition during the first 43 days, but this was followed by less intense net sulfate production and eventually a net sulfate consumption of ~4 nmol cm^{-3} day^{-1} after day 73 (**Figure 4A**; Table S1). Changes of methane concentrations could not be determined in the methane-amended slurries due to the large methane pool of the headspace. SR rates measured by the ^{35}S assay increased over time and were substantially higher than SR rates from the unamended incubations, with mean rates of 11 nmol cm^{-3} day^{-1} in the top zone and 23 nmol cm^{-3} day^{-1} in the AOM zone (**Figures 3C**, **4C**, Table S1). In the latter, SR decreased abruptly at the last time point, as sulfate was depleted. The surplus sulfate consumption in comparison to the unamended incubations was similar for the two zones, 10–13 nmol cm^{-3} day^{-1}. Neither in the AOM zone nor the sulfide reoxidation zone significant changes in S^0 concentrations or accumulation of soluble H_2S were detected (**Figures 3B**, **4B**). Iron consumption and production rates were comparable to incubations without addition of methane in the AOM zone, but were enhanced in the sulfide reoxidation zone (**Figures 3G–I**, **4G–I**).

The addition of methane to the Lake Ørn slurries could have influenced the sulfur and iron cycles in three possible scenarios. In the first scenario, methane addition may have stimulated iron reduction that resulted in depletion of bioreducible Fe(III). Thereafter, organotrophic iron reducers may have been limited and their competitive suppression of organotrophic SR was overturned. Thus, in this scenario, methane addition would have resulted in enhanced organotrophic SR, which caused a net consumption of sulfate and a concurrent ^{34}S enrichment of the sulfate pool. We consider this explanation as rather unlikely, as methane addition did not affect Fe(III) concentrations in the AOM zone, and although an effect was observed in the sulfide reoxidation zone, Fe(III) was not depleted to an extent that would typically limit the process in sediments (**Figures 3G–I**, **4G–I**; Thamdrup, 2000).

In the second scenario, methanogens may have been active and competing with sulfate reducers for organic carbon, potentially in both investigated zones, but to a higher extent in the AOM zone. The addition of methane may have suppressed the methanogens, and therefore the activity of organiclastic SR increased, explaining the higher SR rates in the methane-amended slurries in comparison with the non-amended ones. In this scenario, the impact of methane on the sulfate concentrations and ^{34}S signatures would be explained solely by the activity of organotrophic SR and does not require any involvement of sulfur-cycling AOM. We argue against this scenario by highlighting (1) that methanogenesis was not detected in the incubations without methane amendment and (2) that organotrophic iron reduction was a dominant process in Lake Ørn sediment as shown by Norði et al. (2013) and by the apparently methane-independent rapid decrease in ferric iron and increase of ferrous iron in our incubations (**Figures 3G–I**, **4G–I**). Therefore, it is more likely that methanogens were inhibited by competition with iron reducers for common substrates (Lovley and Phillips, 1986; Roden and Wetzel, 1996) than that they were outcompeting organotrophic sulfate reducers for the same reason. Even if methanogenesis was occurring, an inhibition of the process at the methane levels used in our incubations has to our knowledge never been reported.

We therefore propose a third scenario in which methane addition stimulated the activity of sulfate-dependent AOM that caused net sulfate consumption and a significant alteration in the $\delta^{34}S$ fingerprint. We propose that the enhanced ^{35}SR rates in the methane-amended slurries reflect sulfate-dependent AOM activity. In the sulfide reoxidation zone, we interpret the first 43

incubation days as a lag phase and the rest of the incubation as an AOM phase although an earlier stimulation of SR may have been masked by complete reoxidation. We consider scenario three, the stimulation of sulfate-dependent AOM by methane addition, as the most likely and therefore propose that sulfate-dependent AOM results in substantial stable sulfur isotope fractionation at low micromolar sulfate levels. In comparison to the $\delta^{34}S$ depletion of sulfate in methane-unamended sediment, $\delta^{34}S$ values of sulfate showed ^{34}S enrichment of up to 17‰ in the top zone and 9‰ in the AOM zone relative to initial values in the methane-amended incubations. At the same time, reduced sulfur compounds became depleted in ^{34}S in the top zone, but did not change substantially in the AOM zone, where changes would have been masked by the high initial concentrations (**Figures 3E,F**, **4E,F**, **S1B,C**, **S2B,C**).

In conclusion, organotrophic SR probably took place in all slurry incubations and did apparently limit ^{34}S fractionation under incubation conditions. Microbial S^0 disproportionation showed potential to occur and caused an isotopic effect in S^0 amended incubations. A substantial difference in sulfur cycling and $\delta^{34}S$ signatures resulted due to the addition of methane, which we interpret as a direct effect of sulfate-dependent AOM. We applied a curve-fitting model for the AOM zone incubation with methane, in order to estimate a bulk fractionation factor for the sulfur fractionating microbial processes (**Figure S4**). The model was based on the sum of net sulfate production from the unamended incubations and the net sulfate consumption of the methane-amended incubations and yielded an isotope effect of 29‰ (Figure S4).

CONCLUSIONS AND IMPLICATIONS

AOM strongly regulates sulfur and methane dynamics in modern marine systems and probably did so in the geological past (Reeburgh, 2007; Knittel and Boetius, 2009; Norði et al., 2013). In the low-sulfate freshwater system Lake Ørn, we showed that the iron and sulfur cycles are tightly interconnected and sulfide reoxidation processes generate cryptic sulfur cycling that supplies sulfate internally to the microbial community. Slurry incubations complementing the biogeochemical depth profiles showed that organotrophic SR and S^0 disproportionation apparently co-occur with AOM in the broad SMTZ. In the slurry incubations, the availability of methane caused a dramatic change in sulfate concentration trends and resulted in an offset between sulfate and reduced sulfur compounds (29‰) comparable to the offset between these two pools in the AOM zone of the depth profiles (21–34‰).

Studies addressing ^{34}S isotope fractionation during AOM are rare and the physiology of sulfur cycling during AOM and the involved enzymes are not well-understood. Previous studies reported that sulfur-cycling AOM can induce sulfur isotope fractionation in marine environments and at sulfate concentrations in the millimolar range (Jørgensen et al., 2004; Antler et al., 2014, 2015; Avrahamov et al., 2014; Deusner et al., 2014; Sivan et al., 2014). A few of these studies assigned ε_{AOM} values of 20–30‰ for AOM in gas seeps (Deusner et al., 2014; Sivan et al., 2014) and suggested that AOM may cause fractionations of up to 60‰ in marine SMTZs (Jørgensen et al., 2004; Deusner et al., 2014).

However, the present study is, to our knowledge, the first report of substantial isotope fractionation during SR coupled to AOM at low micromolar sulfate levels in aquatic sediments ($\leq$50 μmol L^{-1} in the AOM zone incubation and *in situ*). A previous study with natural communities of organotrophic sulfate reducers stated a suppression of ^{34}S fractionation at sulfate concentrations <200 μmol L^{-1} (Habicht et al., 2002), which contradicts our findings at first glance. In that study, however, the Danish lake sediment microbial communities were fueled directly by the degradation of organic matter detritus and were not associated to anaerobic methane oxidation as in Lake Ørn, which suggests a specific association of fractionation to AOM at low sulfate concentrations. In line with this, a sulfur isotope difference of up to 23‰ between sulfate and sulfide was also demonstrated recently in the water column of ferruginous Lake Matano in Indonesia, where sulfate concentrations were in the range of 5–10 μmol L^{-1}, and the authors assigned the isotope effect to microbial SR (Crowe et al., 2014). Organic carbon mineralization rates are expectedly low in this extremely oligotrophic lake, and an earlier study suggested AOM to be active at the water depth of ^{34}S fractionation (Crowe et al., 2011). Hence, the sulfur isotope fractionation in Lake Matano might potentially be also a result of sulfur cycling associated with AOM. These results, and the recent finding of high variability of fractionation between different sulfate reducers (Bradley et al., 2016), highlight the importance of interpreting ^{34}S isotope fractionation during SR on a cellular and enzymatic level.

Sulfate-dependent AOM is mainly known from marine environments and associated with a consortium of archaea and bacteria (e.g., Hinrichs et al., 1999; Boetius et al., 2000). So far, it has not been possible to obtain a pure culture of the consortium or its partners and therefore, involved sulfur-cycling enzymatic pathways and their behavior towards ^{34}S fractionation could not be identified. Until recently, it was hypothesized that sulfur cycling and ^{34}S fractionation is restricted to the bacterial partner and follows enzymatic pathways known from bacterial sulfate reducers. However, Milucka et al. (2012) found that the archaeal ANME-2 partner of a marine AOM consortium was able to reduce sulfate and produce and accumulate zero-valent sulfur, which was subsequently disproportionated as disulfide by the bacterial *Desulfosarcina/Desulfococcus* partner. In Lake Ørn, a large accumulation of zero-valent sulfur, unusual to sediments with organotrophic SR, occurred in the zone of highest AOM activity. If zero-valent sulfur in Lake Ørn was provided by sulfur-cycling AOM following the model of Milucka et al. (2012), the methane-induced isotopic effect could have been shaped both by archaeal SR and by bacterial S^0 disproportionation.

The iron-rich and low-sulfate SMTZ of Lake Ørn sediment can serve as a model system for the study of ancient sulfur and methane turnover. In the Archaean Eon, atmospheric oxygen concentrations were low (Bekker et al., 2004), sulfate was probably only a trace constituent (Crowe et al., 2014) and there is geological evidence for microbial production

of methane (Canfield et al., 2005). Large-scale deposition of iron-rich sediments (banded iron formations, BIFs) during the Archaean Eon (>2.5 billion years ago) and parts of the Proterozoic (2.5–0.54 billion years ago) are evidence for the global importance of iron in Earth history (Canfield et al., 2005). Due to suggested high iron contents, AOM coupled to iron reduction has been suggested previously as an important methane sink during low-sulfate conditions in the Archaean Eon (Beal et al., 2009) but evidence for direct coupling of AOM and iron reduction is still pending. However, our findings suggest that sulfate-dependent AOM coupled indirectly to iron via a cryptic sulfur cycle could have been a possible metabolic pathway in the geological past and that this process is likely to have impacted $\delta^{34}S$ signatures of sedimentary sulfides.

To create a clearer picture of $\delta^{34}S$ signatures in modern and ancient environments, further investigations concerning ^{34}S fractionation during AOM, especially in low-sulfate environments are crucial. Previous studies showed that sulfur-cycling AOM impacts not only sulfur ($\delta^{34}S_{SO4}$), but also oxygen isotopes ($\delta^{18}O_{SO4}$) in the dissolved sulfate pool and apparently creates an unique pattern among them that can help to distinguish between organotrophic and methanotrophic SR to be the main drivers of the footprints (e.g., Antler et al., 2014, 2015; Avrahamov et al., 2014; Deusner et al., 2014). Therefore, future studies may probably be best approached by combined investigations of oxygen and sulfur isotopes.

AUTHOR CONTRIBUTION

HW, BT and KH designed research, analyzed and interpreted the data, and wrote the paper. HW performed field and laboratory based research.

ACKNOWLEDGMENTS

We acknowledge Michael Forth and Laura Bristow for their help sampling the sediment and Heidi Grøn Jensen, Susanne Møller, and Dina Holmgaard Skov for technical assistance in the laboratory. This study was supported by the National Danish Research Foundation.

SUPPLEMENTARY MATERIAL

The Supplementary Material for this article can be found online at: http://journal.frontiersin.org/article/10.3389/feart.2016.00061

REFERENCES

Allen, R. E., and Parkes, R. J. (1995). Digestion procedures for determining reduced sulfur species in bacterial cultures and in ancienct and recent sediments. *Geochem. Transform. Sediment. Sulfur* 612, 243–257. doi: 10.1021/bk-1995-0612.ch013

Antler, G., Turchyn, A. V., Herut, B., Davies, A., Rennie, V. C. F., and Sivan, O. (2014). Sulfur and oxygen isotope tracing of sulfate driven anaerobic methane oxidation in estuarine sediments. *Estuar. Coast. Shelf Sci.* 142, 4–11. doi: 10.1016/j.ecss.2014.03.001

Antler, G., Turchyn, A. V., Herut, B., and Sivan, O. (2015). A unique isotopic fingerprint of sulfate-driven anaerobic oxidation of methane. *Geology* 43, 619–622. doi: 10.1130/G36688.1

Avrahamov, N., Antler, G., Yechieli, Y., Gavrieli, I., Joye, S. B., Saxton, M., et al. (2014). Anaerobic oxidation of methane by sulfate in hypersaline groundwater of the Dead Sea aquifer. *Geobiology* 12, 511–528. doi: 10.1111/gbi.12095

Beal, E. J., Claire, M. W., and House, C. H. (2011). High rates of anaerobic methanotrophy at low sulfate concentrations with implications for past and present methane levels. *Geobiology* 9, 131–139. doi: 10.1111/j.1472-4669.2010.00267.x

Beal, E. J., House, C. H., and Orphan, V. J. (2009). Manganese- and iron-dependent marine methane oxidation. *Science* 325, 184–187. doi: 10.1126/science.1169984

Bekker, A., Holland, H. D., Wang, P.-L., Rumble, I. I. I., D., Stein, H. J., Hannah, J. L., et al. (2004). Dating the rise of atmospheric oxygen. *Nature* 427, 117–120. doi: 10.1038/nature02260

Boetius, A., Ravenschlag, K., Schubert, C. J., Rickert, D., Widdel, F., Gieseke, A., et al. (2000). A marine microbial consortium apparently mediating anaerobic oxidation of methane. *Nature* 407, 623–626. doi: 10.1038/35036572

Borowski, W. S., Rodriguez, N. M., Paull, C. K., and Ussler, W. I. (2013). Are ^{34}S-enriched authigenic sulfide minerals a proxy for elevated methane flux and gas hydrates in the geologic record? *Mar. Pet. Geol.* 43, 381–395. doi: 10.1016/j.marpetgeo.2012.12.009

Bradley, A. S., Leavitt, W. D., Schmidt, M., Knoll, A. H., Girguis, P. R., and Johnston, D. T. (2016). Patterns of sulfur isotope fractionation during microbial sulfate reduction. *Geobiology* 14, 91–101. doi: 10.1111/gbi.12149

Canfield, D. E., Raiswell, R., Westrich, J. T., Reaves, C. M., and Berner, R. A. (1986). The use of chromium reduction in the analysis of reduced inorganic sulfur in sediments and shales. *Chem. Geol.* 54, 149–155. doi: 10.1016/0009-2541(86)90078-1

Canfield, D. E., and Thamdrup, B. (1994). The production of ^{34}S-depleted sulfide during bacterial disproportionation of elemental sulfur. *Science* 266, 1973–1975.

Canfield, D. E., and Teske, A. (1996). Late Proterozoic rise in atmospheric oxygen concentration inferred from phylogenetic and sulphur-isotope studies. *Nature* 382, 127–132. doi: 10.1038/382127a0

Canfield, D. E., Thamdrup, B., and Fleischer, S. (1998). Isotope fractionation and sulfur metabolism by pure and enrichment cultures of elemental sulfur-disproportionating bacteria. *Limnol. Oceanogr.* 43, 253–264. doi: 10.4319/lo.1998.43.2.0253

Canfield, D. E., and Raiswell, R. (1999). The evolution of the sulfur cycle. *Am. J. Sci.* 299, 697–723. doi: 10.2475/ajs.299.7-9.697

Canfield, D. E., Habicht, K. S., and Thamdrup, B. (2000). The archean sulfur cycle and the early history of atmospheric oxygen. *Science* 288, 658–661. doi: 10.1126/science.288.5466.658

Canfield, D. E. (2001). Biogeochemistry of sulfur isotopes. *Rev. Mineral. Geochem.* 43, 607–636. doi: 10.2138/gsrmg.43.1.607

Canfield, D. E., Thamdrup, B., and Kristensen, E. (2005). "*Advances,*" *in Marine Biology Aquatic Geomicrobiology,* Vol. 48, eds A. J. Southward, P. A Tyler, C. M, Young, and L. A. Fuiman (San Diego, CA: Elsevier), 314–374.

Canfield, D. E., Rosing, M. T., and Bjerrum, C. (2006). Early anaerobic metabolisms. *Philos. Trans. R. Soc. Lond. Ser. B* 361, 1819–1836. doi: 10.1098/rstb.2006.1906

Canfield, D. E., Farquhar, J., and Zerkle, A. L. (2010). High isotope fractionations during sulfate reduction in a low-sulfate euxinic ocean analog. *Geology* 38, 415–418. doi: 10.1130/G30723.1

Catling, D. C., Zahnle, K. J., and McKay, C. P. (2001). Biogenic methane, hydrogen escape, and the irreversible oxidation of Early Earth. *Science* 293, 839–842. doi: 10.1126/science.1061976

Cline, J. D. (1969). Spectrophotometric determination of hydrogen sulfide in natural waters. *Limnol. Oceanogr. Methods* 14, 454–458. doi: 10.4319/lo.1969.14.3.0454

Crowe, S., A., Paris, G., Katsev, S., Jones, C., Kim, S.-T., Zerkle, A. L., et al. (2014). Sulfate was a trace constituent of Archean seawater. *Science* 346, 735–739. doi: 10.1126/science.1258966

Crowe, S. A., Katsev, S., Leslie, K., Sturm, A., Magen, C., Nomosatryo, S., et al. (2011). The methane cycle in ferruginous Lake Matano. *Geobiology* 9, 61–78. doi: 10.1111/j.1472-4669.2010.00257.x

Deusner, C., Holler, T., Arnold, G. L., Bernasconi, S. M., Formolo, M. J., and Brunner, B. (2014). Sulfur and oxygen isotope fractionation during sulfate reduction coupled to anaerobic oxidation of methane is dependent on methane concentration. *Earth Planet. Sci. Lett.* 399, 61–73. doi: 10.1016/j.epsl.2014.04.047

Ferdelmann, T. G., Lee, C., Pantoja, S., HArder, J., Bebout, B. M., and Fossing, H. (1997). Sulfate reduction and methanogenesis in a *Thioploca*-dominated sediment off the coast of Chile. *Gechim. Cosmochim. Acta* 61, 3065–3079. doi: 10.1016/S0016-7037(97)00158-0

Fossing, H., and Jørgensen, B. B. (1989). Measurement of bacterial sulfate reduction in sediments: evaluation of a single-step chromium reduction method. *Biogeochemistry* 8, 205–222. doi: 10.1007/BF00002889

Habicht, K. S., Canfield, D. E., and Rethmeier, J. (1998). Sulfur isotope fractionation during bacterial reduction and disproportionation of thiosulfate and sulfite. *Geochim. Cosmochim. Acta* 62, 2585–2595. doi: 10.1016/S0016-7037(98)00167-7

Habicht, K. S., Gade, M., Thamdrup, B., Berg, P., and Canfield, D. E. (2002). Calibration of sulfate levels in the Archean Ocean. *Science* 298, 2372–2374. doi: 10.1126/science.1078265

Hansel, C. M., Lentini, C. J., Tang, Y., Johnston, D. T., Wankel, S. D., and Jardine, P. M. (2015). Dominance of sulfur-fueled iron oxide reduction in low-sulfate freshwater sediments. *ISME J.* 9, 2400–2412. doi: 10.1038/ismej.2015.50

Hinrichs, K. U., Hayes, J. M., Sylva, S. P., Brewer, P. G., and DeLong, E. F. (1999). Methane-consuming archaebacteria in marine sediments. *Nature* 398, 802–805. doi: 10.1038/19751

Holmkvist, L., Ferdelman, T. G., and Jørgensen, B. B. (2011). A cryptic sulfur cycle driven by iron in the methane zone of marine sediment (Aarhus Bay, Denmark). *Geochim. Cosmochim. Acta* 75, 3581–3599. doi: 10.1016/j.gca.2011.03.033

Jørgensen, B. B. (1978). Comparison of methods for quantification of bacterial sulfate reduction in coastal marine sediments. 1. Measurement with radiotracer techniques. *Geomicrobiol. J.* 1, 11–27. doi: 10.1080/01490457809377721

Jørgensen, B. B., Böttcher, M. E., Lüschen, H., Neretin, L. N., and Volkov, I. I. (2004). Anaerobic methane oxidation and a deep H_2S sink generate isotopically heavy sulfides in Black Sea sediments. *Geochim. Cosmochim. Acta* 68, 2095–2118. doi: 10.1016/j.gca.2003.07.017

Kallmeyer, J., Ferdelman, T. G., Weber, A., Fossing, H., and Jørgensen, B. B. (2004). A cold chromium distillation procedure for radiolabeled sulfide applied to sulfate reduction measurements. *Limnol. Oceanogr. Methods* 2, 171–180. doi: 10.4319/lom.2004.2.171

Knittel, K., and Boetius, A. (2009). Anaerobic oxidation of methane: progress with an unknown process. *Annu. Rev. Microbiol.* 63, 311–334. doi: 10.1146/annurev.micro.61.080706.093130

Knossow, N., Blonder, B., Eckert, W., Turchyn, A. V., Antler, G., and Kamyshny, A. Jr. (2015). Annual sulfur cycle in a warm monomictic lake with sub-millimolar sulfate concentrations. *Geochem. Trans.* 16, 1–24. doi: 10.1186/s12932-015-0021-5

Konhauser, K. O., Newman, D. K., and Kappler, A. (2005). The potential significance of microbial Fe(III) reduction during deposition of Precambrian banded iron formations. *Geobiology* 3, 167–177. doi: 10.1111/j.1472-4669.2005.00055.x

Lovley, D. R., and Phillips, E. J. P. (1986). Organic matter mineralization with reduction of ferric iron in anaerobic sediments. *Appl. Environ. Microbiol.* 51, 683–689.

McGlynn, S. E., Chadwick, G. L., Kempes, C. P., and Orphan, V. J. (2015). Single cell activity reveals direct electron transfer in methanotrophic consortia. *Nature* 526, 531–535. doi: 10.1038/nature15512

Meulepas, R. J. W., Jagersma, C. G., Khadem, A. F., Stams, A. J. M., and Lens, P. N. L. (2010). Effect of methanogenic substrates on anaerobic oxidation of methane and sulfate reduction by an anaerobic methanotrophic enrichment. *Appl. Microbiol. Biotechnol.* 87, 1499–1506. doi: 10.1007/s00253-010-2597-0

Milucka, J., Ferdelman, T. G., Polerecky, L., Franzke, D., Wegener, G., Schmid, M., et al. (2012). Zero-valent sulphur is a key intermediate in marine methane oxidation. *Nature* 491, 541–546. doi: 10.1038/nature11656

Norði, K. Á., Thamdrup, B., and Schubert, C. J. (2013). Anaerobic oxidation of methane in an iron-rich Danish freshwater lake sediment. *Limnol. Oceanogr.* 58, 546–554. doi: 10.4319/lo.2013.58.2.0546

O'Connell, D. W., Mark Jensen, M., Jakobsen, R., Thamdrup, B., Joest Andersen, T., Kovacs, A., et al. (2015). Vivianite formation and its role in phosphorus retention in Lake Ørn, Denmark. *Chem. Geol.* 409, 42–53. doi: 10.1016/j.chemgeo.2015.05.002

Pellerin, A., Hao Bui, T., Rough, M., Mucci, A., Canfield, D. E., and Wing, B. A. (2015). Mass-dependent sulfur isotope fractionation during reoxidative sulfur cycling: a case study from Mangrove Lake, Bermuda. *Geochim. Cosmochim. Acta* 149, 152–164. doi: 10.1016/j.gca.2014.11.007

Pyzik, A., and Sommer, S. E. (1981). Sedimentary iron monosulfides: kinetics and mechanism of formation. *Geochim. Cosmochim. Acta* 45, 687–698. doi: 10.1016/0016-7037(81)90042-9

Raiswell, R., Canfield, D. E., and Berner, R. A. (1994). A comparison of iron extraction methods for the determination of degree of pyritisation and the recognition of iron-limited pyrite formation. *Chem. Geol.* 111, 101–110. doi: 10.1016/0009-2541(94)90084-1

Reeburgh, W. S. (2007). Oceanic methane biogeochemistry. *Chem. Rev.* 107, 486–513. doi: 10.1021/cr050362v

Roden, E. E., and Wetzel, R. G. (1996). Organic carbon oxidation and suppression of methane production by microbial Fe(III) oxide reduction in vegetated and unvegetated freshwater wetland sediments. *Limnol. Oceanogr.* 41, 1733–1748. doi: 10.4319/lo.1996.41.8.1733

Røy, H., Weber, H. S., Tarpgaard, I. H., Ferdelman, T. G., and Jørgensen, B. B. (2014). Determination of dissimilatory sulfate reduction rates in marine sediment via radioactive ^{35}S tracer. *Limnol. Oceanogr. Methods* 12, 196–211. doi: 10.4319/lom.2014.12.196

Schippers, A., and Jørgensen, B. B. (2002). Biogeochemistry of pyrite and iron sulfide oxidation in marine sediments. *Geochim. Cosmochim. Acta* 66, 85–92. doi: 10.1016/S0016-7037(01)00745-1

Sim, M. S., Bosak, T., and Ono, S. (2011). Large sulfur isotope fractionation does not require disproportionation. *Science* 333, 74–77. doi: 10.1126/science.1205103

Sivan, O., Adler, M., Pearson, A., Gelman, F., Bar-Or, I., John, S. G., et al. (2011). Geochemical evidence for iron-mediated anaerobic oxidation of methane. *Limnol. Oceanogr.* 56, 1536–1544. doi: 10.4319/lo.2011.56.4.1536

Sivan, O., Antler, G., Turchyn, A. V., Marlow, J. J., and Orphan, V. J. (2014). Iron oxides stimulate sulfate-driven anaerobic methane oxidation in seeps. *Proc. Natl. Acad. Sci. U.S.A.* 111, E4139–E4147. doi: 10.1073/pnas.1412269111

Stookey, L. L. (1970). Ferrozine-a new spectrophotometric reagent for iron. *Anal. Chem.* 42, 779–781. doi: 10.1021/ac60289a016

Thamdrup, B. (2000). "Bacterial manganese and iron reduction in aquatic sediments," *in Advances in Microbial Ecology,* ed B Schink (New York, NY: Kluwer Academic/Plenum Publishers), 41–84.

Thamdrup, B., Finster, K., Hansen, J. W., and Bak, F. (1993). Bacterial disproportionation of elemental sulfur coupled to chemical reduction of iron or manganese. *Appl. Environ. Microbiol.* 59, 101–108.

Thamdrup, B., Fossing, H., and Jørgensen, B. B. (1994). Manganese, iron and sulfur cycling in a coastal marine sediment, Aarhus Bay, Denmark. *Geochim. Cosmochim. Acta* 58, 5115–5129. doi: 10.1016/0016-7037(94)90298-4

Thode, H. G., Monster, J., and Dunford, H. B. (1961). Sulphur isotope geochemistry. *Geochim. Cosmochim. Acta* 25, 150–174. doi: 10.1016/0016-7037(61)90074-6

Treude, T., Krüger, M., Boetius, A., and Jørgensen, B. B. (2005). Environmental control on anaerobic oxidation of methane in the gassy sediments of Eckernförde Bay (German Baltic). *Limnol. Oceanogr.* 50, 1771–1786. doi: 10.4319/lo.2005.50.6.1771

Wegener, G., Krukenberg, V., Riedel, D., Tegetmeyer, H. E., and Boetius, A. (2015). Intercellular wiring enables electron transfer between methanotrophic archaea and bacteria. *Nature* 526, 587–589. doi: 10.1038/nature 15733

Wortmann, U. G., Bernasconi, S., and Böttcher, M. E. (2001). Hypersulfidic deep biosphere indicates extreme sulfur isotope fractionation during single-step microbial sulfate reduction. *Geology* 29, 647–650. doi: 10.1130/0091-7613(2001)029<0647:HDBIES>2.0.CO

Yao, W., and Millero, F. J. (1996). Oxidation of hydrogen sulfide by hydrous Fe(III) oxides in seawater. *Mar. Chem.* 52, 1–16. doi: 10.1016/0304-4203(95)00072-0

Conflict of Interest Statement: The authors declare that the research was conducted in the absence of any commercial or financial relationships that could be construed as a potential conflict of interest.

frontiers in Microbiology

METHODS
published: 26 May 2016
doi: 10.3389/fmicb.2016.00774

Stable Isotope Phenotyping via Cluster Analysis of NanoSIMS Data As a Method for Characterizing Distinct Microbial Ecophysiologies and Sulfur-Cycling in the Environment

Katherine S. Dawson[1], Silvan Scheller[1], Jesse G. Dillon[2] and Victoria J. Orphan[1]**

[1] Division of Geological and Planetary Sciences, California Institute of Technology, Pasadena, CA, USA, [2] Department of Biological Sciences, California State University Long Beach, Long Beach, CA, USA

OPEN ACCESS

Edited by:
Shuhei Ono,
Massachusetts Institute of Technology, USA

Reviewed by:
Nathan Yee,
Rutgers University, USA
Mark Alexander Lever,
ETH Zürich, Switzerland

***Correspondence:**
Katherine S. Dawson
kdawson@caltech.edu;
Victoria J. Orphan
vorphan@gps.caltech.edu

Specialty section:
This article was submitted to Microbiological Chemistry and Geomicrobiology, a section of the journal Frontiers in Microbiology

Received: 11 January 2016
Accepted: 09 May 2016
Published: 26 May 2016

Citation:
Dawson KS, Scheller S, Dillon JG and Orphan VJ (2016) Stable Isotope Phenotyping via Cluster Analysis of NanoSIMS Data As a Method for Characterizing Distinct Microbial Ecophysiologies and Sulfur-Cycling in the Environment. Front. Microbiol. 7:774. doi: 10.3389/fmicb.2016.00774

Stable isotope probing (SIP) is a valuable tool for gaining insights into ecophysiology and biogeochemical cycling of environmental microbial communities by tracking isotopically labeled compounds into cellular macromolecules as well as into byproducts of respiration. SIP, in conjunction with nanoscale secondary ion mass spectrometry (NanoSIMS), allows for the visualization of isotope incorporation at the single cell level. In this manner, both active cells within a diverse population as well as heterogeneity in metabolism within a homogeneous population can be observed. The ecophysiological implications of these single cell stable isotope measurements are often limited to the taxonomic resolution of paired fluorescence *in situ* hybridization (FISH) microscopy. Here we introduce a taxonomy-independent method using multi-isotope SIP and NanoSIMS for identifying and grouping phenotypically similar microbial cells by their chemical and isotopic fingerprint. This method was applied to SIP experiments in a sulfur-cycling biofilm collected from sulfidic intertidal vents amended with ^{13}C-acetate, ^{15}N-ammonium, and ^{33}S-sulfate. Using a cluster analysis technique based on fuzzy c-means to group cells according to their isotope (^{13}C/^{12}C, ^{15}N/^{14}N, and ^{33}S/^{32}S) and elemental ratio (C/CN and S/CN) profiles, our analysis partitioned ∼2200 cellular regions of interest (ROIs) into five distinct groups. These isotope phenotype groupings are reflective of the variation in labeled substrate uptake by cells in a multispecies metabolic network dominated by Gamma- and Deltaproteobacteria. Populations independently grouped by isotope phenotype were subsequently compared with paired FISH data, demonstrating a single coherent deltaproteobacterial cluster and multiple gammaproteobacterial groups, highlighting the distinct ecophysiologies of spatially-associated microbes within the sulfur-cycling biofilm from White Point Beach, CA.

Keywords: NanoSIMS, sulfur-cycling, stable isotope probing, ecophysiology, cluster analysis

INTRODUCTION

The application of stable isotope probing (SIP) to environmental microbial communities provides links between ecophysiology and phylogenetic identity without the need for pure or enrichment cultures (Radajewski et al., 2000; Dumont and Murrell, 2005). In SIP experiments, a substrate that is enriched in a particular stable isotope (e.g., D, ^{13}C, ^{15}N, ^{34}S) is added to an environmental sample incubation and the uptake of that substrate by members of the microbial community is tracked by the incorporation of the enriched isotope into cellular components. SIP, in combination with fluorescence *in situ* hybridization coupled to secondary ion mass spectrometry (FISH-SIMS or FISH-NanoSIMS; Orphan et al., 2001), can resolve substrate uptake and metabolic activity at the single-cell level within complex communities (Orphan et al., 2009; Wagner, 2009; Musat et al., 2012; Pett-Ridge and Weber, 2012).

SIP combined with FISH-NanoSIMS analysis offers a direct method for assessing the metabolic potential of microorganisms in the environment, where microbial communities are often supported through complex interspecies interactions on the micrometer scale and frequently consist of uncultured and poorly characterized microorganisms. Prior FISH-NanoSIMS studies have focused on single-cell measurements of anabolic activity, metabolic potential, and microbial metabolic interactions particularly with respect to the assimilation of ^{13}C-, ^{15}N-labeled substrates e.g., (Popa et al., 2007; Musat et al., 2008; Green-Saxena et al., 2014) and recently deuterated water (Berry et al., 2015; Kopf et al., 2015). Very few ecological studies have conducted cell specific SIP experiments with sulfur, despite the fact that sulfur is one of the abundant elements in biomolecules and plays a central role in redox biogeochemistry in many environments. NanoSIMS analyses have previously been applied to measure naturally occurring micron-scale variations in δ^{34}S of sulfide resulting from microbial sulfur metabolism in environmental samples (Fike et al., 2008, 2009), and ^{34}S-enriched sulfate SIP experiments combined with NanoSIMS have demonstrated the assimilation of ^{34}S into cell biomass (Milucka et al., 2012; Wilbanks et al., 2014). These studies focused on the variation in the ratio of ^{34}S/^{32}S. However, the existence of four stable isotopes of sulfur (^{32}S, ^{33}S, ^{34}S, and ^{36}S) and the ability of the CAMECA NanoSIMS 50L instrument to measure seven masses in parallel offers the potential for concurrent SIP NanoSIMS experiments with multiple sulfur species and isotope labels, as well as the potential to conduct mixed substrate incubation experiments that expand beyond ^{13}C- and ^{15}N-labeled substrate amendment to include multiple isotopes of sulfur.

Inter- and intra-species variation in labeled substrate metabolism associated with differences in growth rates, as well as the transfer of enriched isotope through microbial metabolic networks via cross-feeding of labeled metabolites results in heterogeneity of the isotope ratios measured for different populations (Pelz et al., 1999; Orphan et al., 2001; DeRito et al., 2005; Musat et al., 2008; House et al., 2009; Abraham, 2014; Kopf et al., 2015; Zimmermann et al., 2015). While cross-feeding during SIP incubations is generally considered to be a complicating factor in these experiments (Neufeld et al., 2007; Chen and Murrell, 2010), exploiting the resulting isotopic heterogeneity can move the interpretation of SIP experiments beyond the binary of enriched or not enriched. Using gradients in anabolic activity associated with multiple labeled substrates in combination with cluster analysis has the potential to distinguish metabolic niches, interspecies substrate transfer, and variation due to spatial distribution of microorganisms (DeRito et al., 2005; Chen and Murrell, 2010).

For complex environmental samples, distilling large datasets into manageable groups through clustering techniques supports the generation of hypotheses based on average group properties. Cluster analysis is an exploratory technique that utilizes discontinuities and gradients in multivariate datasets to identify and visualize relationships between subgroups of samples. These groupings can proceed by hierarchical clustering, agglomerating, or dividing samples into clusters and sub-clusters, or partitional methods, where an initial partitioning of the samples is optimized for intra-cluster homogeneity. Both hierarchical and partitional clustering has been applied extensively for identifying relationships within ecological datasets (McCune et al., 2002a,b; Legendre and Legendre, 2012). These techniques have a long history of development and application in macro and meiofaunal community ecology (Green, 1980; James and McCulloch, 1990; Legendre et al., 2005), and have become increasingly common in microbial ecology as applied to DNA or RNA-based diversity data (Ramette, 2007), with an effort toward identifying underlying trends in diversity and links between diversity and function in microbial communities (Fuhrman, 2009). A primary goal of both multivariate and SIP analysis in microbial ecology is identifying connections between identity and functional roles in biogeochemical cycles.

Here we expand upon the use of cluster analysis as a method to deconvolve multi-isotope NanoSIMS datasets (**Figure 1**) for microorganisms in environmental samples and describe a case study from a intertidal sulfur cycling, microbial biofilm at White Point Beach, CA after SIP time course incubation with ^{13}C, ^{15}N, and ^{33}S-labeled substrates. Using the high lateral spatial resolution of the NanoSIMS and cluster analysis of ^{13}C, ^{15}N, and ^{33}S enrichment in single cells, we resolved distinct microbial isotopic phenotypes occurring at close spatial scales within a microbial biofilm. Independently, these isotopic phenotypes were found to correlate with distinct delta- and gammaproteobacterial cell types identified by FISH and suggest a microbial, metabolic network for the cycling of carbon and sulfur in chemoautrophic microbial mats associated with sulfidic hydrothermal vents at White Point Beach in San Pedro, CA. The combination of NanoSIMS and cluster analysis in multiple isotope SIP experiments has the potential to provide insights into ecophysiology and element cycling in spatially proximal microorganisms in environmental and laboratory settings.

MATERIALS AND METHODS

Case Study Site Description

Chemoautrophic microbial mats form in shallow intertidal pools adjacent to sulfidic hydrothermal vents at White Point

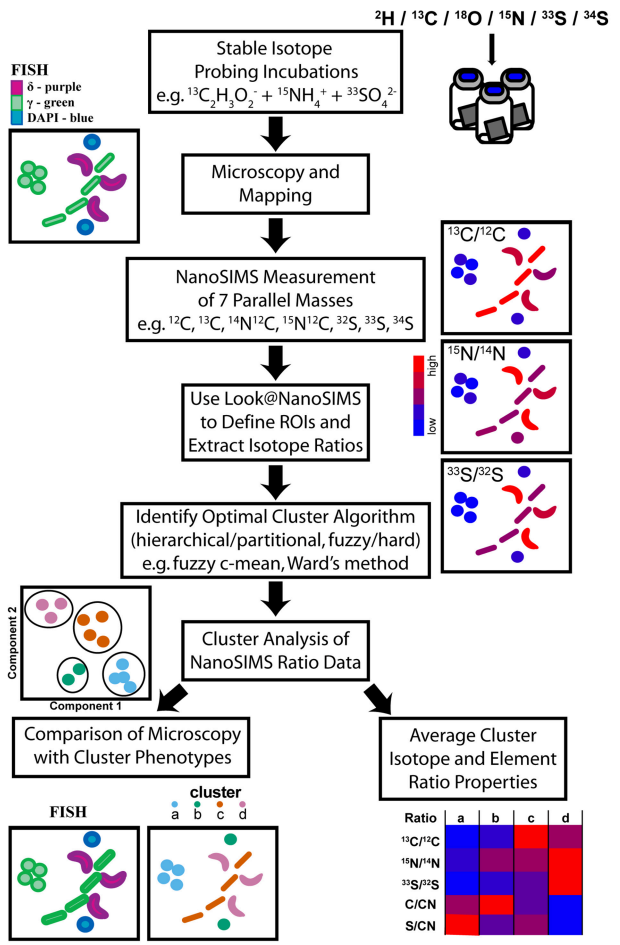

FIGURE 1 | Illustration of the workflow from multiple-isotope SIP incubations through to the identification of stable isotope phenotypes and their properties via cluster analysis of NanoSIMS data. After colonization with microbial biomass, NanoSIMS compatible Si-wafers were incubated with multiple stable isotope labeled substrates. Microscopy, using FISH probes, identified regions that were mapped for subsequent NanoSIMS analysis of up to seven parallel masses. NanoSIMS data was processed using Look@NanoSIMS to define single cell regions of interest (ROIs) and extract associated isotope and elemental composition ratios. Several cluster analysis algorithms were evaluated to determine the best method, which was then applied to partition the NanoSIMS ratio data. The properties of the stable isotope phenotype clusters were examined and compared to independent FISH images to investigate label uptake in a multispecies metabolic network.

Beach in San Pedro, CA (33.7159°N, 118.319°W; Stein, 1984; **Figure 2**). Sulfide is primarily geologically derived from the interaction of hydrothermal fluids with the sulfur containing Altamira shale unit of the Monterrey Formation (Woodring et al., 1946). The location of active venting was identified by enhanced localized colonization of white, filamentous microbial mats on the surface of rocks, sediments, and invertebrates. Illumina tag sequencing of rocks visibly colonized by microbial mat was performed as described previously in Case et al. (2015). Sequencing confirmed prior descriptions of *Thiothrix* spp. as the dominant sulfur-oxidizing bacteria in the microbial mats (Stein, 1984; Jacq et al., 1989; Kalanetra et al., 2004). Additional gammaproteobacterial groups belonging to the Thiotrichaceae and Oceanospirillaceae families accounted for 95% of the Gammaproteobacteria (35.8 and 4.1% relative abundance, respectively). Sequencing additionally identified putative sulfur- and sulfate-reducing deltaproteobacterial lineages belonging to the Desulfuromonadaceae, Desulfobacteraceae, and Desulfobulbaceae families (1.75, 0.51, and 0.22% relative abundance, respectively). The raw sequences from the *in situ* White Point mats were generated on an Illumina MiSeq platform at Laragen, Inc (Los Angeles, CA, USA) and have been deposited in the Sequence Read Archive (accession # PRJNA304767).

Triple Isotope Probing Experiments

Microbial mat biomass for the SIP experiments was collected by *in situ* colonization of NanoSIMS compatible contact slides. Specifically, 7 × 7 mm conductive Si-wafers (P-type/boron doped, 0.028 Ω cm^{-1}, 725 μm thick, Active Business Company Gmbh, Munich, Germany) were secured to a slide holder and incubated for 1 week in the intertidal pool adjacent to locations of active sulfide venting (**Figure 2**). The microbial mat colonized wafers were then transferred into 10 ml serum bottles containing 5 ml of filter-sterilized, N_2-sparged, sulfate-free artificial sea water that contained (g l^{-1}): 24 g NaCl; 5 g $MgCl_2 6H_2O$; 1.31 g $CaCl_2 2H_2O$; 0.67 g KCl; 0.2 g $NaHCO_3$; 0.1 g KBr; 0.027 g H_3BO_3; 0.027 g $SrCl_2 6H_2O$; 0.003 g NaF. Incubations were then amended with ^{13}C-acetate, $^{15}NH_4^+$, $^{33}SO_4^{2-}$, 20% air/80% N_2 headspace, with each treatment consisting of three parallel bottles with two replicate Si-wafers per bottle. After 2, 7, and 10 days one bottle per treatment was sacrificed and sampled for geochemistry, microscopy, and NanoSIMS analyses.

Additional incubations included an unlabeled control (NL) and a formaldehyde killed control (K), which were supplemented as follows: NL—acetate, NH_4^+, SO_4^{2-}, 20% air/80% N_2 headspace; K—^{13}C-acetate, $^{15}NH_4^+$, $^{15}NO_3^-$, $^{33}SO_4^{2-}$, 10% w/v formaldehyde, 20% air/80% N_2 headspace. Final concentrations and atom percent (at.%) enrichment for the supplements added to all additional incubations were as follows: sodium acetate—100 μM, 2-^{13}C, 99 at.% ^{13}C (Cambridge Isotope Laboratories, Tewksbury, MA, USA); NH_4Cl—100 μM, ~10 at.% ^{15}N (Cambridge Isotope Laboratories, Tewksbury, MA, USA); $NaNO_3$—100 μM, 98% ^{15}N (Cambridge Isotope Laboratories, Tewksbury, MA, USA); Na_2SO_4—28 mM, ~15 at.% ^{33}S (see below for synthesis details). The at.% ^{15}N and ^{33}S added to incubations was calculated by isotope mass balance as follows: $^{n}F_{final} = [(^{n}F_{unlabeled} \times m_{unlabeled}) + (^{n}F_{labeled} \times m_{labeled})]/m_{final}$, where mass (m) was the amount of NH_4Cl or $NaSO_4$ added to the mixture and at.% = $100 \times {}^{n}F$.

Synthesis of ^{33}S-Sulfate from ^{33}S-Elemental Sulfur

Na_2SO_4 enriched in ^{33}S was prepared in house by the oxidation of $^{33}S^0$ (99.8%, Trace Sciences International Inc., Wilmington, DE, USA). The oxidation reaction was conducted in a custom

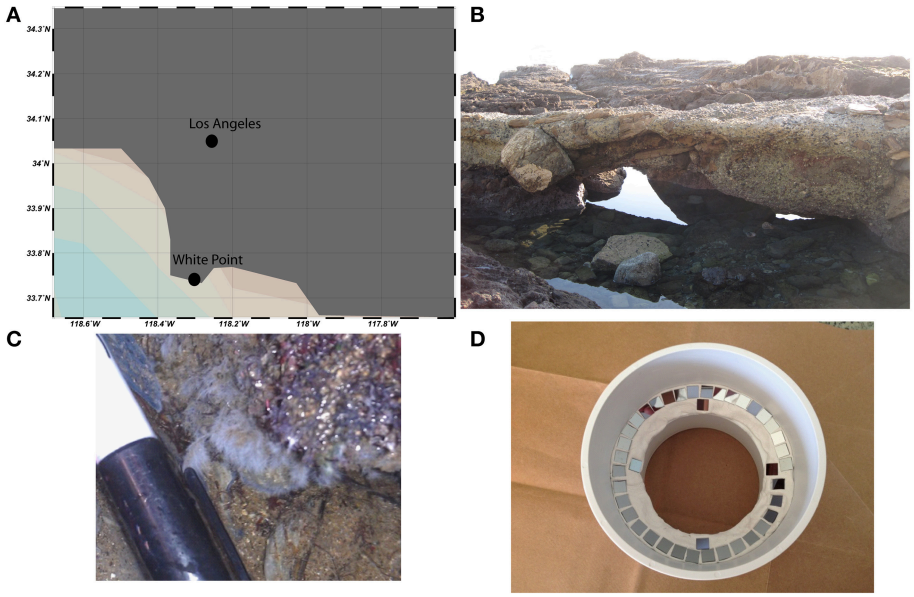

FIGURE 2 | White Point is located south of Los Angeles, CA on the Palos Verdes Peninsula (A). Conspicuous white, filamentous microbial mats form in intertidal pools adjacent to sulfidic hydrothermal vents **(B,C)**. Si-wafers (7 × 7 mm) were colonized *in situ* for 1 week before laboratory incubations with ^{13}C-acetate, $^{15}NH_4^+$, and $^{34}SO_4^{2-}$ **(D)**.

apparatus constructed from 6 mm glass tubing (Figure S-1). $^{33}S^0$ powder (170 mg) was placed into the glass tube and briefly melted to adhere to the glass with a bunsen burner. A gentle stream of pure O_2 (Air Liquide, USA) was passed through the glass tube (ca. 20 ml min^{-1}) and the other side was immersed into a 0.4 M NaOH solution (10 ml). After passing several volumes of O_2 through the apparatus, the sulfur was ignited in the tube by heating the outside with an ethanol-flame. The liquid sulfur burned with a blue flame and the resulting SO_2 was quantitatively absorbed in the NaOH solution. Glass wool had been placed behind the burning sulfur to prevent S^0 vapors from reaching the NaOH solution. Once reacted the solution of $Na_2^{33}SO_3$ (10 ml) was oxidized with an excess of 10 M H_2O_2 (500 µl) and vortexed. This reaction occurred within 5 min and complete oxidation was assumed by the presence of residual H_2O_2 using MQuant peroxide-test strips (EMD Millipore, Temecula, CA, USA). The excess H_2O_2 was decomposed by incubating the solution at 90°C for 20 h. Decomposition of all H_2O_2 was again confirmed with peroxide-test strips. The pH of the solution was adjusted to 4.0 by titration with 6 M HCl in 100 µl increments. The acidic solution was then filtered through a 0.22 µm filter, and neutralized with 1 M NaOH. Conversion to SO_4^{2-} was verified and quantified by ion chromatography using a Dionex ICS-2000 system with an IonPac AS18 anion exchange column (Dionex, Sunnyvale, CA, USA). Yields were typically >90% and SO_3^{2-} was not detected.

Fluorescence *in situ* Hybridization

At 2, 7, and 10 days the microbially colonized Si-wafers from one bottle of each experimental condition were gently washed with 3X phosphate buffered saline (PBS; g l^{-1}: 24 g NaCl, 0.6 g KH_2PO_4, 0.6 g KCl, 4.32 g Na_2HPO_4) to remove residual labeled media and fixed for microscopy by adding 4% fresh paraformaldehyde and 3x PBS in a 3:1 ratio and incubating at 4°C for 12 h. Fixed samples were subsequently washed with 3x PBS and stored in 3x PBS at 4°C. Ethanol was avoided to prevent the dissolution of internal sulfur granules.

Prior to FISH, the Si-wafers were etched with a series of grid lines using a LMD7000 laser microdissection system (Leica, Wetzlar, Germany) to provide a map for identifying sample locations on the NanoSIMS. FISH was performed as described previously (Glöckner et al., 1996), using fluorescently labeled oligonucleotide probes targeting Gammaproteobacteria (Gam42a; Manz et al., 1992) and Deltaproteobacteria (Delta495a + cDelta495a; Loy et al., 2002; Macalady et al., 2006). Oligonucleotide probes were labeled at the 5′ end with either a FAM or CY3 dye (IDT, Coralville, IA USA) and used at a final concentration of 5 ng μl^{-1} in hybridization buffer containing 45% formamide. Following the FISH hybridization, the cells were counterstained with 4′,6-diamidino-2-phenylindole (DAPI) at a final concentration of 2.5 ng μl^{-1} and coverslips were mounted with the anti-fade reagent, Vectashield (Vector Laboratories, USA). Regions positively hybridized with the FISH probes near the etched grid lines were mapped and imaged on a BX51 epifluorescence microscope (Olympus, Shinjuku, Japan) using 20x (UPlanFL N) dry, 60x (PlanApo N) and 100x (UPlanFL N) oil immersion objectives. After FISH analysis, coverslips were gently removed from the Si-wafers to minimize dislodging the cells and the water-soluble Vectashield was washed away with MQ water in a petri dish as described in Dekas and Orphan (2011).

^{13}C, ^{15}N, and ^{33}S Analysis of Single Cells Using FISH-NanoSIMS

Carbon, nitrogen, and sulfur isotopic compositions of microbial cells from mapped regions were measured using a NanoSIMS 50L (CAMECA, Gennevilliers, France) housed in the Center for Microanalysis in the Division of Geological and Planetary Sciences at the California Institute of Technology. All measurements included in this study were made in one continuous 10-day session on the instrument. Cells were analyzed on Si-wafers using a ∼4 pA primary Cs^+ beam current and were pre-sputtered with a ∼16 pA primary Cs^+ beam current for 10–15 min. Seven masses were collected in parallel ($^{12}C^-$, $^{13}C^-$, $^{14}N^{12}C^-$, $^{15}N^{12}C^-$, $^{32}S^-$, $^{33}S^-$, and $^{34}S^-$). Secondary ion images were collected for 30 × 30 μm raster areas at 512 × 512 pixel resolution with a dwell time of 15 ms/pixel for 20–40 cycles. *Clostridia* spores of a known isotopic composition (measured by EA-IRMS, $\delta^{13}C = -21.86‰$; $^{13}R = 0.01099$ and $\delta^{15}N = 7.94‰$; $^{15}R = 0.00371$) were analyzed daily to correct for instrumental isotope fractionation in the $^{13}C/^{12}C$ and $^{15}N/^{14}N$ ratios and to assess any instrument drift over the course of the run (Dekas and Orphan, 2011). No drift was detected over the 10-day period. To determine the instrumental isotope fractionation by the NanoSIMS instrument, the average NanoSIMS acquired $^{13}C/^{12}C$ and $^{15}N/^{14}N$ ratios were compared with the EA-IRMS acquired values for the *Clostridia* spores. A correction for $^{33}S/^{32}S$ was not possible due to the low sulfur content in the spores. However, it is unlikely that this relatively minor correction (permil) would alter the results of this analysis given the large atom percent enrichments observed in the cells after incubation with the labeled substrates. Raw data from all secondary ion images were processed using Look@NanoSIMS in MATLAB (Polerecky et al., 2012). Ion images were corrected for dead time, planes were accumulated and aligned, and discrete regions of interest (ROIs, $n = 3115$) were drawn by hand using the $^{14}N^{12}C^-$ ion image to identify and outline individual cells.

Cluster Analysis

Accumulated secondary ion counts, exported from Look@NanoSIMS, were used to calculate isotopic ratios for $^{13}C/^{12}C$, $^{15}N/^{14}N$ ($^{15}N^{12}C/^{14}N^{12}C$), $^{33}S/^{32}S$, and $^{34}S/^{32}S$. Additionally, ratios of C/CN and S/CN were calculated from the sum of accumulated secondary ion counts for C ($^{12}C + {}^{13}C$), CN ($^{14}N^{12}C + {}^{15}N^{12}C$), and S ($^{32}S + {}^{33}S + {}^{34}S$). The isotope and element composition ratios were compiled for individual raster areas as well as all raster areas corresponding to a given incubation time point. Cluster analysis was performed in the R environment (RStudio v.0.99.451, R v.3.2.1; R Core Team, 2015; R Studio Team, 2015) using clustering algorithms from the "cluster" package (Maechler et al., 2015), cluster method and number validation from the "clusterSim" (Walesiak et al., 2008) and "clusterCrit" (Desgraupes, 2015) packages, respectively, and graphical output from the "ggplot2" package (Wickham, 2009). Using "clusterSim" and "clusterCrit," 10 cluster analysis methods [single-linkage, median-linkage, average-linkage, complete-linkage, centroid-linkage, Ward's method, McQuitty's method, partitioning around medoids (pam), k-means and fuzzy c-means] were compared using the Calinski-Harabasz (CH) validity index (Caliński and Harabasz, 1974) for solutions where the number of clusters ranged between 2 and 10. Scripts written for processing data associated with this project can be found at https://github.com/katdawson/NanoSIMS-cluster-analysis.

The two main cluster analysis methods used to interpret the NanoSIMS isotope and elemental ratio datasets were k-means and fuzzy c-means. K-means cluster analysis starts with a fixed number of clusters (k) and starting configuration of cluster centers. The analysis proceeds by assigning objects, in this case ROIs, to clusters and iteratively optimizing the object memberships such that the sum of square distance is minimized between objects and the cluster center (Lance and Williams, 1967; MacQueen, 1967). Fuzzy c-means cluster analysis similarly requires an initial number of clusters to which objects are assigned, but allows objects to belong to more than one cluster. Fuzzy c-means iteratively optimizes both the cluster center and memberships (Bezdek et al., 1984; Equihua, 1990).

RESULTS

Fish-NanoSIMS Analysis of Cellular C, N, and S

FISH analyses of Si-wafers for the labeled incubation time series (2, 7, and 10 days) as well as unlabeled (7 day) and killed (10 day) control incubations were carried out using oligonucleotide probes targeting Gammaproteobacteria (Gam42a) and Deltaproteobacteria (Delta495a + cDelta495a; **Figure 3**). The relative abundance of Deltaproteobacteria increased over the course of the experiment: 2 days—3.0%; 7 days—6.8%; 10 days—44.7%. Deltaproteobacteria represented 3.6% of imaged cells in the unlabeled control and 11.9% of imaged cells in the killed control. These differences highlight the inherent heterogeneity of microbial assemblage composition during the *in situ* colonization in the intertidal vents at White Point.

A total of 21 FISH mapped regions (30 × 30 μm) on five incubated Si-wafers were examined by NanoSIMS and subsequently processed using Look@NanoSIMS resulting in 3115 cellular ROIs (**Table 1**, Figure S-4). These mapped areas included three regions from the 2-day labeled incubation (665 ROIs), four regions from the 7-day labeled incubation (777 ROIs), six regions from the 7-day labeled incubation (760 ROIs), three regions from the unlabeled control (645 ROIs), and three regions from the killed control (268 ROIs). Isotope ratios for ROIs from the different time points of the ^{13}C, ^{15}N, and ^{33}S-labeled substrate incubations had a broad distribution, with the standard deviations of similar magnitude to the mean ratios (**Table 1**). Over the 10-day incubation period with $^{15}NH_4^+$, the mean $^{15}N/^{14}N$ for ROIs identified as Deltaproteobacteria by FISH increased from 0.0447 ± 0.0169 at day 2 to 0.0628 ± 0.0203 by day 10 (ROIs in unlabeled control = 0.00347 ± 0.00019). In incubations amended with $^{33}SO_4^{2-}$, the mean $^{33}S/^{32}S$ for deltaproteobacterial cells increased from 0.0187 ± 0.0065 (day 2) to 0.1292 ± 0.1224 (day 7), followed by a decrease to 0.0578 ± 0.0430 at day 10. Gammaproteobacterial ROIs in those same incubations had an average $^{15}N/^{14}N$ ratio of 0.0354

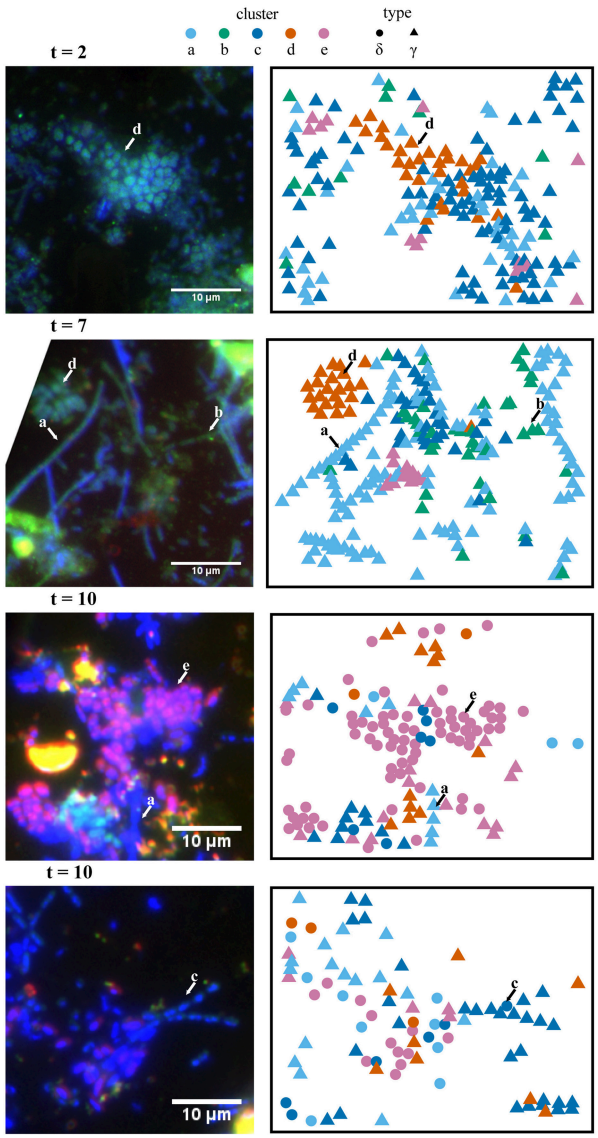

FIGURE 3 | Spatial (x,y) projections of isotope phenotype clusters determined from NanoSIMS data and corresponding FISH images. Independent analysis of these two data sets showed consistent correspondence between the isotope phenotypes (clusters a–e) and the morphologies and phylogenetic affiliation of cells determined in the FISH experiments. For example, cluster "e" primarily corresponds with putative sulfate-reducing bacteria hybridized with a deltaproteobacterial probe (purple). FISH (left panels) was performed with probe Delta495a targeting Deltaproteobacteria (purple) and Gam42a targeting Gammaproteobacteria (green). Representative cells for isotope phenotype clusters a–e, determined from fuzzy c-means cluster analysis of NanoSIMS data, are indicated with arrows in the FISH images. Clusters "a," "b," and "c" are primarily affiliated with filamentous Gammaproteobacteria. Cluster "d" is primarily affiliated with clusters of coccoidal Gammaproteobacteria, andcluster "e" is primarily affiliated with Deltaproteobacteria. FISH images were rotated to match the NanoSIMS image orientation, which resulted in the cropping of some images.

± 0.0125 which did not change appreciably during the 10 day incubation. However, FISH-identified gammaproteobacterial cells did show an increase in $^{33}S/^{32}S$ from 0.0138 ± 0.0106 at day 2 to 0.0302 ± 0.0270 by day 10. Amendments with ^{13}C-acetate produced similar trends in $^{13}C/^{12}C$ for both delta- and gammaproteobacterial cells with the peak in ^{13}C enrichment observed early in the incubation series at day 2 (0.1432 ± 0.0915) followed by a decrease to 0.0984 ± 0.0335 at day 7, with cells in the final incubation bottle (day 10) showing slightly a slightly higher $^{13}C/^{12}C$ ratio (0.1040 ± 0.0649). Cells recovered from the unlabeled control incubation did not show any isotope enrichment ($^{13}C/^{12}C$—0.0109 ± 0.00051; $^{15}N/^{14}N$—0.00347 ± 0.00019; $^{33}S/^{32}S$—0.00720 ± 0.00076) and only minor enrichment was detected for $^{13}C/^{12}C$ and $^{15}N/^{14}N$ in cells from the killed control amended with the same suite of isotopically enriched substrates ($^{13}C/^{12}C$—0.0123 ± 0.0032; $^{15}N/^{14}N$—0.0045 ± 0.00066; $^{33}S/^{32}S$—0.00568 ± 0.0011). Previous SIMS studies have reported similar levels of isotopic enrichment in cells above natural abundance from killed control experiments amended with isotopically labeled substrates (e.g., $^{15}NH_4^+$; Orphan et al., 2009; Kopf et al., 2015).

Cluster Method and Number Validation

A comparison of hierarchical (single-linkage, median-linkage, average-linkage, complete-linkage, centroid-linkage, Ward's method, and McQuitty's method) and partitional (pam, k-means and fuzzy c-means) cluster analysis methods using the CH validity index revealed that partitional algorithms better optimized groups of ROIs by isotope phenotype. These methods rely on cluster ellipsoids drawn to minimize the variance between the member ROIs and the mean cluster value, resulting in the best representation of normal distributions anticipated from biological activity (**Figure 4**; Legendre and Legendre, 2012). Higher CH index values represent better intra-cluster cohesion and inter-cluster separation (Caliński and Harabasz, 1974). With the exception of the single-linkage method, five to eight clusters maximized the CH index. The highest CH index values were determined for the following partitional methods, fuzzy c-means (5 clusters, CH = 509.2), k-means (5 clusters, CH = 509.4), pam (6 clusters, CH = 502.8), and Ward's method (5 clusters, CH = 457.3; **Figure 4**).

Based on these findings (**Figure 4**), k-means and fuzzy c-means clustering with five clusters appear to be equally valid methods for clustering NanoSIMS isotope ratio data and were used for all subsequent data analysis. Further comparison of k-means and fuzzy c-means, showed less visual overlap in the fuzzy c-means clusters projected into vector space (**Figure 5B**). Greater cluster differentiation with fuzzy c-means was confirmed by increased average and overall cluster silhouette width (**Figure 5D**). Silhouette plots provide a graphical assessment of cluster solutions, by combining the inter-cluster separation and the intra-cluster cohesion into a width for each object that increases with improvement in both parameters (Rousseeuw, 1987). The average silhouette widths indicated that clustering by fuzzy c-means improved partitioning of the data compared to the k-means method. However, there was still substantial overlap in the clusters defined by fuzzy c-means, particularly between clusters 1, 2, and 4. This overlap (**Figure 5**) was visible in both the projection of the clusters in bivariate plots and by the presence of negative silhouette widths.

TABLE 1 | Average isotope and elemental ratio properties for all cellular ROIs, the FISH-identified Delta- and Gammaproteobacteria, and the five cluster, fuzzy c-means solutions for all incubation and control experiments.

	All	Delta	Gamma	a	b	c	d	e
2 DAYS: ^{13}C-ACETATE + $^{15}NH_4^+$ + $^{33}SO_4^{2-}$								
Number of ROIs	665	20	645	253	107	257	30	18
$^{13}C/^{12}C$	0.1432	0.1817	0.1421	0.0625	0.2284	0.1889	0.1086	0.1757
sd	0.0915	0.1098	0.0915	0.0363	0.1024	0.0580	0.0486	0.0974
$^{12}C^{15}N/^{12}C^{14}N$	0.0394	0.0447	0.0393	0.0187	0.0569	0.0508	0.0370	0.0704
sd	0.0216	0.0169	0.0216	0.0112	0.0158	0.0123	0.0167	0.0259
$^{33}S/^{32}S$	0.0139	0.0187	0.0138	0.0094	0.0164	0.0141	0.0122	0.0622
sd	0.0106	0.0065	0.0106	0.0028	0.0070	0.0056	0.0051	0.0245
C/CN	0.4080	0.4286	0.4073	0.4239	0.5943	0.3383	0.2667	0.3066
sd	0.1405	0.1219	0.1405	0.1159	0.1267	0.0830	0.0842	0.1191
S/CN	0.1187	0.1032	0.1192	0.1084	0.1415	0.1028	0.2554	0.1281
sd	0.0452	0.0222	0.0452	0.0219	0.0213	0.0206	0.1106	0.0268
7 DAYS: ^{13}C-ACETATE + $^{15}NH_4^+$ + $^{33}SO_4^{2-}$								
Number of ROIs	777	53	724	443	136	106	32	60
$^{13}C/^{12}C$	0.0984	0.0727	0.0760	0.0304	0.0499	0.2687	0.0694	0.1323
sd	0.0335	0.0506	0.1009	0.0298	0.0385	0.1112	0.0397	0.0850
$^{12}C^{15}N/^{12}C^{14}N$	0.0283	0.0688	0.0214	0.0105	0.0157	0.0532	0.0217	0.1001
sd	0.0309	0.0471	0.0235	0.0105	0.0100	0.0125	0.0103	0.0162
$^{33}S/^{32}S$	0.0620	0.1292	0.0259	0.0151	0.0150	0.0306	0.0078	0.2229
sd	0.4579	0.1224	0.0481	0.0109	0.0102	0.0249	0.0016	0.0899
C/CN	0.2067	0.2726	0.4715	0.3736	0.7612	0.5187	0.4769	0.2759
sd	0.1113	0.1608	0.2032	0.1042	0.1953	0.1529	0.2435	0.1203
S/CN	0.0564	0.0880	0.1130	0.0886	0.1509	0.1188	0.3125	0.0690
sd	0.0593	0.0873	0.0531	0.0193	0.0326	0.0275	0.0815	0.0193
10 DAYS: ^{13}C-ACETATE + $^{15}NH_4^+$ + $^{33}SO_4^{2-}$								
Number of ROIs	760	340	420	306	0	158	66	230
$^{13}C/^{12}C$	0.1040	0.0938	0.1123	0.0655	n.d.	0.1943	0.0910	0.0968
sd	0.0649	0.0487	0.0746	0.0385	n.d	0.0638	0.0452	0.0307
$^{12}C^{15}N/^{12}C^{14}N$	0.0531	0.0628	0.0454	0.0379	n.d.	0.0561	0.0448	0.0739
sd	0.0222	0.0203	0.0207	0.0207	n.d	0.0104	0.0196	0.0106
$^{33}S/^{32}S$	0.0425	0.0578	0.0302	0.0146	n.d.	0.0285	0.0446	0.0887
sd	0.0377	0.0430	0.0270	0.0169	n.d.	0.0233	0.0283	0.0199
C/CN	0.4303	0.3493	0.4960	0.3113	n.d.	0.5350	0.8700	0.3907
sd	0.2528	0.1787	0.2832	0.1853	n.d.	0.1987	0.3895	0.1100
S/CN	0.0792	0.0804	0.0783	0.0648	n.d.	0.0650	0.1660	0.0833
sd	0.0436	0.0370	0.0482	0.0243	n.d.	0.0134	0.0905	0.0213
UNLABELED CONTROL (7 DAYS): ACETATE + NH_4^+ + SO_4^{2-}								
Number of ROIs	645	23	622	155	133	39	193	125
$^{13}C/^{12}C$	0.0109	0.0109	0.0109	0.0109	0.0105	0.0106	0.0109	0.0112
sd	0.0005	0.0004	0.0005	0.0003	0.0003	0.0004	0.0003	0.0003
$^{12}C^{15}N/^{12}C^{14}N$	0.0035	0.0035	0.0035	0.0036	0.0034	0.0034	0.0034	0.0034
sd	0.0002	0.0001	0.0002	0.0001	0.0001	0.0001	0.0001	0.0001
$^{33}S/^{32}S$	0.0072	0.0074	0.0072	0.0074	0.0074	0.0092	0.0068	0.0067
sd	0.0008	0.0005	0.0008	0.0004	0.0004	0.0009	0.0003	0.0002
C/CN	0.3362	0.4385	0.3324	0.3687	0.4739	0.4149	0.1868	0.3557
sd	0.1507	0.1484	0.1507	0.0891	0.1442	0.1209	0.0701	0.1202
S/CN	0.1101	0.1167	0.1099	0.0656	0.0697	0.0652	0.1103	0.2220
sd	0.0691	0.0847	0.0691	0.0168	0.0274	0.0213	0.0387	0.0607

(Continued)

TABLE 1 | Continued

	All	Delta	Gamma	a	b	c	d	e
KILLED CONTROL (10 DAYS): ^{13}C-ACETATE + $^{15}NH_4^+$ + $^{15}NO_3^-$ + $^{33}SO_4^{2-}$								
Number of ROIs	268	32	236	110	79	55	13	11
$^{13}C/^{12}C$	0.0123	0.0143	0.0120	0.0115	0.0123	0.0116	0.0120	0.0241
sd	0.0032	0.0027	0.0032	0.0015	0.0015	0.0010	0.0009	0.0060
$^{12}C^{15}N/^{12}C^{14}N$	0.0045	0.0046	0.0045	0.0046	0.0041	0.0044	0.0064	0.0048
sd	0.0007	0.0004	0.0007	0.0004	0.0003	0.0003	0.0008	0.0005
$^{33}S/^{32}S$	0.0057	0.0056	0.0057	0.0049	0.0063	0.0061	0.0066	0.0061
sd	0.0011	0.0011	0.0011	0.0009	0.0007	0.0008	0.0015	0.0003
C/CN	0.3114	0.3128	0.3112	0.3165	0.1999	0.4473	0.2845	0.4123
sd	0.1325	0.0370	0.1325	0.0729	0.0935	0.1433	0.0504	0.0903
S/CN	0.0917	0.0800	0.0933	0.0738	0.0855	0.1433	0.0684	0.0841
sd	0.0429	0.0373	0.0429	0.0137	0.0255	0.0618	0.0287	0.0225

Gamma, Gammaproteobacteria; Delta, Deltaproteobacteria; sd, standard deviation; n.d., not detected.

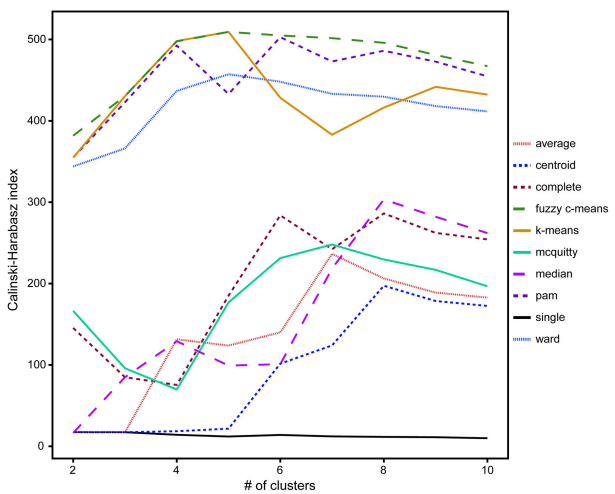

FIGURE 4 | A comparison of the 10 clustering algorithms with the Calinski-Harabasz validity index (CH index) for solutions containing between 2 and 10 clusters, where higher index values indicated better intra-cluster cohesion and inter-cluster separation. Of these clustering methods, the partitional methods fuzzy c-means (dashed green) and k-means (solid orange) with five clusters were found to be the optimal algorithms for the isotope and elemental ratio NanoSIMS data.

Test of Isotope Phenotyping with 1, 2, or 3 Isotope Ratios

In order to determine the benefit of additional ratio data for determining isotope phenotypes, we compared the five cluster fuzzy c-means assignments resulting from isotope and elemental ratio data derived from one ($^{15}N/^{14}N$), two ($^{15}N/^{14}N$, $^{13}C/^{12}C$, C/CN), or three ($^{15}N/^{14}N$, $^{13}C/^{12}C$, $^{33}S/^{32}S$, C/CN, S/CN) labeled substrates. These assignments were examined by projecting ROIs into x,y coordinate space alongside the corresponding FISH image (**Figure 4**, **Table 2**). In this comparative analysis, some ROI assignments remained consistent across all cluster analysis solutions (n = 171, 22.0%), and the addition of the $^{13}C/^{12}C$ and $^{33}S/^{32}S$ ratios improved the differentiation of non-filamentous cell types. The incorporation of all three isotope ratios ($^{15}N/^{14}N$,$^{13}C/^{12}C$, and $^{33}S/^{32}S$) resulted in the best correspondence between the NanoSIMS acquired cellular data and FISH image, revealing potential discrepancies in phylogenetic assignment of some ROIs identified by FISH. For these cells, the FISH-based assignment tended to be less clear, compromised by inherent autofluorescence in the sample, variability in fluorescence intensity between the larger filamentous microorganisms and co-occurring single cells, or weak hybridization possibly due to poor specificity of the oligonucleotide probe.

Cluster Assignment Consistency and Properties

Projection of the ROI x,y coordinate data for various raster areas and incubation time points (**Figure 3**) showed consistency between the cluster assignment and the independent taxon identification by FISH microscopy. Filamentous Gammaproteobacteria (putative *Thiothrix* spp.) were primarily associated with clusters "a," "b," and "c"; 86, 98, and 92% of the ROIs were FISH identified as Gammaproteobacteria, respectively. Cluster "d" was associated with non-filamentous cells consisting of both FISH-identified Gammaproteobacteria (85% of ROIs), as well as cells stained by DAPI with an undetermined phylogenetic affiliation (15% of ROIs). Deltaproteobacteria were primarily associated with cluster "e," with 68% of ROIs hybridizing with the deltaproteobacterial specific FISH probe, Delta495a.

Cross-plots of the ROI isotope and elemental ratios (**Figure 5**) demonstrated that clusters are associated with specific properties (**Table 1**). For example, cluster "a" ROIs had the lowest ratios of $^{13}C/^{12}C$, $^{15}N/^{14}N$, and $^{33}S/^{32}S$, while the cluster "b" ROIs were also characterized by low $^{13}C/^{12}C$, $^{15}N/^{14}N$, and $^{33}S/^{32}S$, but had higher elemental C/CN and S/CN ratios compared to other groups. ROIs in cluster "c" had the

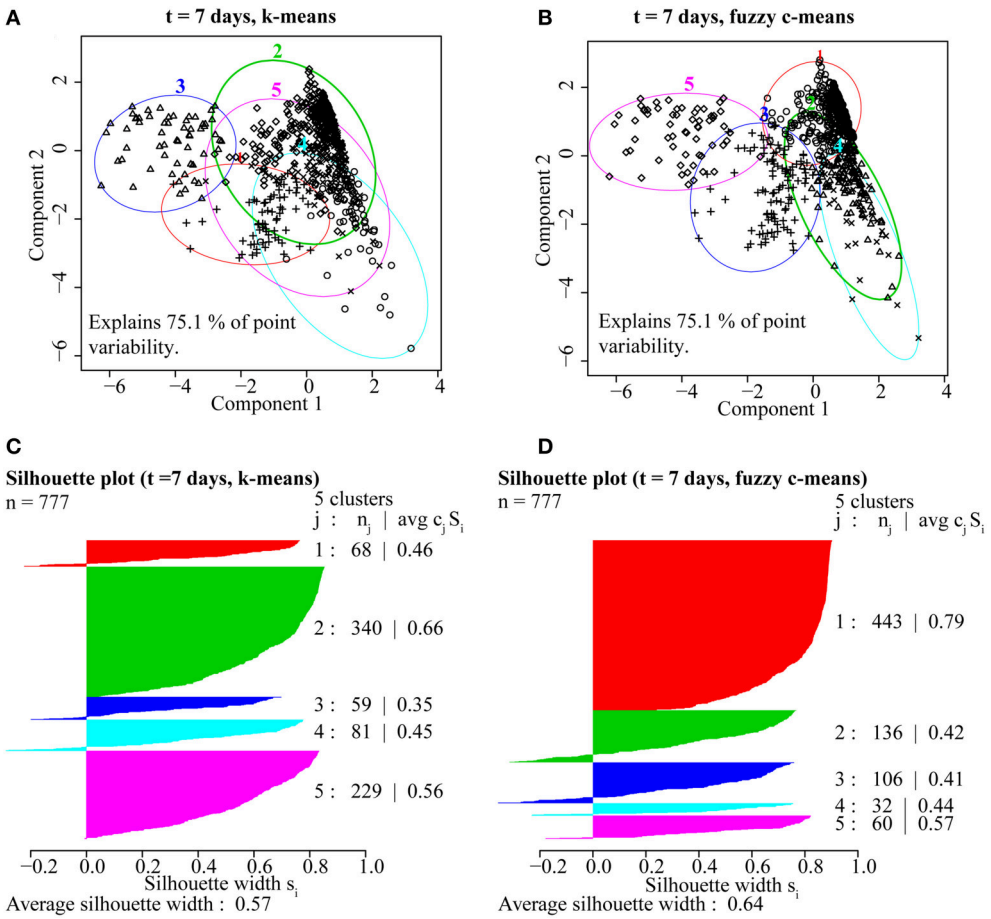

FIGURE 5 | A comparison of partitioning by (A) k-means and (B) fuzzy c-means for ROIs from the *t* = 7 day NanoSIMS isotope and elemental ratio data showed that fuzzy c-means resulted in better cluster resolution. The fuzzy c-means clustering solution minimized overlap **(A,B)** and resulted in higher average silhouette width (avg $c_j S_j$), a measure of intra-cluster cohesion and inter-cluster separation, for ROIs (n_j) distributed into the five clusters (j; **C,D)**.

highest $^{13}C/^{12}C$, with moderate $^{15}N/^{14}N$, and low $^{33}S/^{32}S$. Cluster "d" ROIs were similar to cluster "a" and "b" in terms of low isotopic ratios, but had the greatest (S/CN)/(C/CN) ratio. ROIs in cluster "e" were characterized by the highest $^{15}N/^{14}N$ and $^{33}S/^{32}S$, with low to moderate $^{13}C/^{12}C$ and low C/CN.

Natural variation in the stable isotope and elemental ratios recorded for cells in the unlabeled and killed control samples did not contain large enough gradients for the cluster algorithm to differentiate different cell types, despite the inherent variation in elemental ratios observed for some cell populations (Figures S-2, S-3). Cross-plots of isotope ratios showed minimal uptake of the ^{13}C and ^{15}N label in the killed control and a distribution of ROIs within one standard deviation of the calculated natural abundance value for all ratios in the unlabeled control. In both killed and unlabeled control samples, cross-plots of elemental ratios identified a subset of cell ROIs with higher S/CN consistent with the elevated ratios observed from a subset of the ROIs in the SIP experiments (**Figure 5**, cluster "d").

DISCUSSION

Since the development of FISH-SIMS and FISH-NanoSIMS for directly measuring the metabolic activity of taxonomically identified single microbial cells in environmental samples (Orphan et al., 2001; Wagner, 2009) this methodological approach has gained widespread use in the field of microbial ecology, illuminating within and between population differences in anabolic activity and ecophysiology of environmental microorganisms (House et al., 2009; Musat et al., 2012; Green-Saxena et al., 2014; Zimmermann et al., 2015). To extend the utility of this approach, we developed a taxonomy independent method that combines cluster analysis with multi-isotope SIP and NanoSIMS for identifying and grouping microbial cells with phenotypically similar isotopic ratios and chemical compositions reflective of distinct ecophysiologies (**Figure 1**). Cluster analysis utilizes discontinuities and gradients in multivariate datasets to identify and visualize relationships between groupings, here represented by combinations of isotopic enrichment or elemental ratios for environmental microorganisms after SIP.

TABLE 2 | Cluster assignments for a subset of ROIs ($n = 777$) using isotope and elemental ratios resulting from 1, 2, or 3 stable isotope labeled substrates.

Ratios used	FISH identification	Distribution of ROIs per cluster				
		a	b	c	d	e
$^{13}C/^{12}C$	Gamma	416	142	77	52	38
	Delta	13	27	12	1	0
$^{15}N/^{14}N$	Gamma	385	125	96	120	32
	Delta	13	2	6	5	27
$^{33}S/^{32}S$	Gamma	579	81	24	33	7
	Delta	18	5	1	17	12
$^{13}C/^{12}C$, $^{15}N/^{14}N$, C/CN	Gamma	309	77	207	82	51
	Delta	16	1	4	0	32
$^{13}C/^{12}C$, $^{33}S/^{32}S$, C/S	Gamma	483	100	29	84	29
	Delta	10	21	2	1	19
$^{15}N/^{14}N$, $^{33}S/^{32}S$, S/CN	Gamma	428	226	35	27	8
	Delta	14	8	2	16	13
$^{13}C/^{12}C$, $^{15}N/^{14}N$, $^{33}S/^{32}S$, C/CN, C/SN	Gamma	427	134	101	30	32
	Delta	16	2	5	2	28

Gamma, Gammaproteobacteria; Delta, Deltaproteobacteria.

The distillation of complex datasets into defined groupings facilitates data interpretation and new hypothesis development based on average group properties and composition. Similar clustering approaches, including the fuzzy–c-means algorithm, have been applied in the field of environmental metagenomics, enabling the binning of sequence reads within complex data sets (e.g., Nasser et al., 2008; Liu et al., 2015; Lu et al., 2016).

Here we show that clustering algorithms can be applied to NanoSIMS-acquired isotopic and elemental ratio data sets of single cells recovered from SIP experiments, enabling the identification of ecophysiological characteristics and trends for co-existing microorganisms and microbial populations in environmental samples. There are a number of different clustering algorithms available for characterizing multivariate datasets. Comparison of 10 different clustering algorithms, generally divided into either partitional or hierarchical-based clustering methods, revealed that partitional methods yielded more robust cluster solutions for our NanoSIMS isotope and element ratio data set, identifying five clusters (**Figure 4**). The success of partitional methods here is likely related to the underlying structure of our data, which consisted of gradients in isotopic enrichment resulting from anabolic activity and cross-feeding within the microbial community.

This methodological approach was then tested in a low complexity, sulfur cycling microbial mat community recovered from a hydrothermally influenced intertidal area at White Point beach, CA. NanoSIMS analysis of multi-isotope SIP experiments yielded ∼2200 single cell measurements of $^{13}C/^{12}C$, $^{15}N/^{14}N$, and $^{33}S/^{32}S$, as well as the associated cellular elemental ratios C/CN and S/CN. Fuzzy c-means cluster analysis partitioned data into five isotope phenotypes that were reflective of differences in the anabolism of acetate, sulfate, and ammonium. Comparison of these isotope phenotypes, which were determined solely by multivariate analysis of quantitative isotope and elemental ratio data, to corresponding FISH images supported the efficacy of cluster assignments to particular phylogenetic groups, and demonstrated the variability in general anabolic activity and the metabolism of carbon and sulfur within taxonomically related cells.

While many SIP and isotope tracer experiments utilize one or two isotope labels (Radajewski et al., 2000; Dumont and Murrell, 2005; Wegener et al., 2012), the Cameca NanoSIMS 50L instrument has the capability of measuring seven masses in parallel, providing a means for tracing the flow of three or four independently labeled substrates in an experiment. The incubations reported here used $^{15}NH_4^+$, ^{13}C-acetate, and $^{33}SO_4^{2-}$ to investigate N, C, and S cycling. The benefit of multiple stable isotope amendments for identifying metabolic niches in incubation samples was explored by applying the different clustering algorithms with data from one, two, or three different isotope labels (**Figure 6**). In all cases, clusters of cells were identified on the basis of trends in isotope ratios derived from metabolism of the labeled substrates. The use of a single ratio, in this case $^{15}N/^{14}N$, served as a general activity-based proxy, providing one dimension of information related to $^{15}NH_4^+$ assimilation and protein synthesis (e.g., Orphan et al., 2009; McGlynn et al., 2015). The addition of $^{13}C/^{12}C$ from ^{13}C-acetate and the elemental ratio C/CN added additional dimensions to the cluster analysis, potentially related to differences in intracellular carbon storage and the metabolism of ^{13}C-labeled acetate or ^{13}C-labeled dissolved inorganic carbon derived from acetate catabolism. A third dimension for discrimination of phenotypic cell types was gained through the addition of $^{33}S/^{32}S$ and S/CN. The sulfur isotope and elemental ratios partitioned cells based on ^{33}S-sulfate reduction, subsequent oxidation of ^{33}S-sulfide, and intracellular sulfur storage. Gradients in the $^{13}C/^{12}C$, $^{15}N/^{14}N$, and $^{33}S/^{32}S$ ratios emphasized variation in carbon, nitrogen, and sulfur metabolism within the mat microbial community and

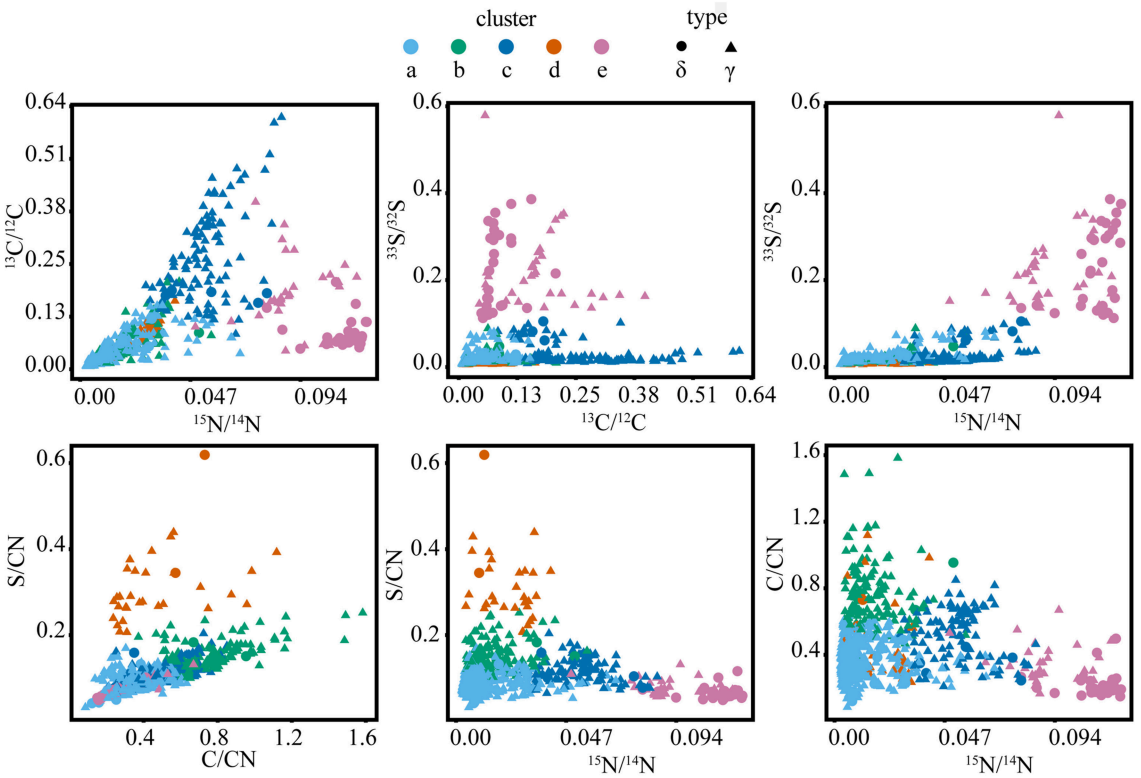

FIGURE 6 | Isotope and elemental ratio properties of the five clusters from the full SIP dataset (t = 2, 7, and 10 days), containing a total of 2202 cellular ROIs, which were used to determine isotope phenotypes from the sulfur cycling White Point microbial assemblage. Clusters "a," "b," and "c" are primarily affiliated with filamentous Gammaproteobacteria ("γ"). Cluster "d" is primarily affiliated with clusters of coccoid Gammaproteobacteria. Cluster "e" is primarily affiliated with Deltaproteobacteria ("δ").

resulted in better resolution of different phenotypic cell types (**Figures 3**, **7**; Figure S-4).

Cluster analysis partitioned ∼2200 ROIs from a total of 13 raster areas, distributed across three independent Si-wafers representing different SIP incubation time points (2, 7, and 10 days). Cluster assignment and cell type determined by FISH for the corresponding epifluorescence images was consistent for multiple mapped regions on the same Si-wafer and for mapped regions on independent Si-wafers at all-time points (**Figures 3A**, **7**; Figure S-4). The observed correlation between cluster and cell type across these different samples suggest that the isotope and element ratios of ROIs are coherent and likely reflective of distinct ecophysiologies or metabolic niches in this system. Filamentous, sulfide-oxidizing Gammaproteobacteria ("a," "b," and "c") and sulfate-reducing Deltaproteobacteria ("e"), which represented the metabolic endmembers of sulfur cycling in this system, stood out for their robustness. Additionally, two clusters ("a" and "e"), showed the lowest intra-cluster variance and greatest inter-cluster separation (**Figure 5**) indicating that the combined isotope and elemental ratios better differentiated these ROIs (**Figure 6**).

The defining features of the five microbial phenotypes were captured in a series of isotope and element ratio biplots (**Figure 6**). Three of these phenotypes emerged as particularly distinct both in their isotope and elemental ratios ("c," "d," and "e"). Cluster "c" consisted of the primary acetate metabolizers (highest $^{13}C/^{12}C$) and included a subset of cells that may be the principal sulfide oxidizers (second highest $^{33}S/^{32}S$). These phenotypic properties were consistent with FISH analysis, which indicated that cluster "c" was primarily composed of filamentous, sulfide-oxidizing Gammaproteobacteria. These Gammaproteobacteria are likely *Thiothrix* spp., identified by iTAG sequencing and previously reported to incorporate acetate (Nielsen et al., 2000). Based on comparison to FISH images, clusters "a," "b," and "c" were morphologically similar filamentous Gammaproteobacteria, which likely reflected a gradient of low ("a" and "b") to high ("c") anabolic activity ($^{15}N/^{14}N$) and acetate utilization. An activity gradient is further supported by a predominance of filaments with the less active "a" and "b" phenotypes in earlier time points (2 and 7 days), while later time point filaments showed an increase in the more active "c" phenotype and the absence of the "b" phenotype in the 10-day incubation (**Figures 3**, **6**). Cluster "b" is differentiated further by high ratios of C/CN, which may indicate the presence of carbon storage granules (Larkin and Strohl, 1983; Rossetti et al., 2003). In cultured *Thiothrix* relatives, intracellular carbon storage compounds were found to increase during acetate metabolism (Rossetti et al., 2003). However, none of these groups

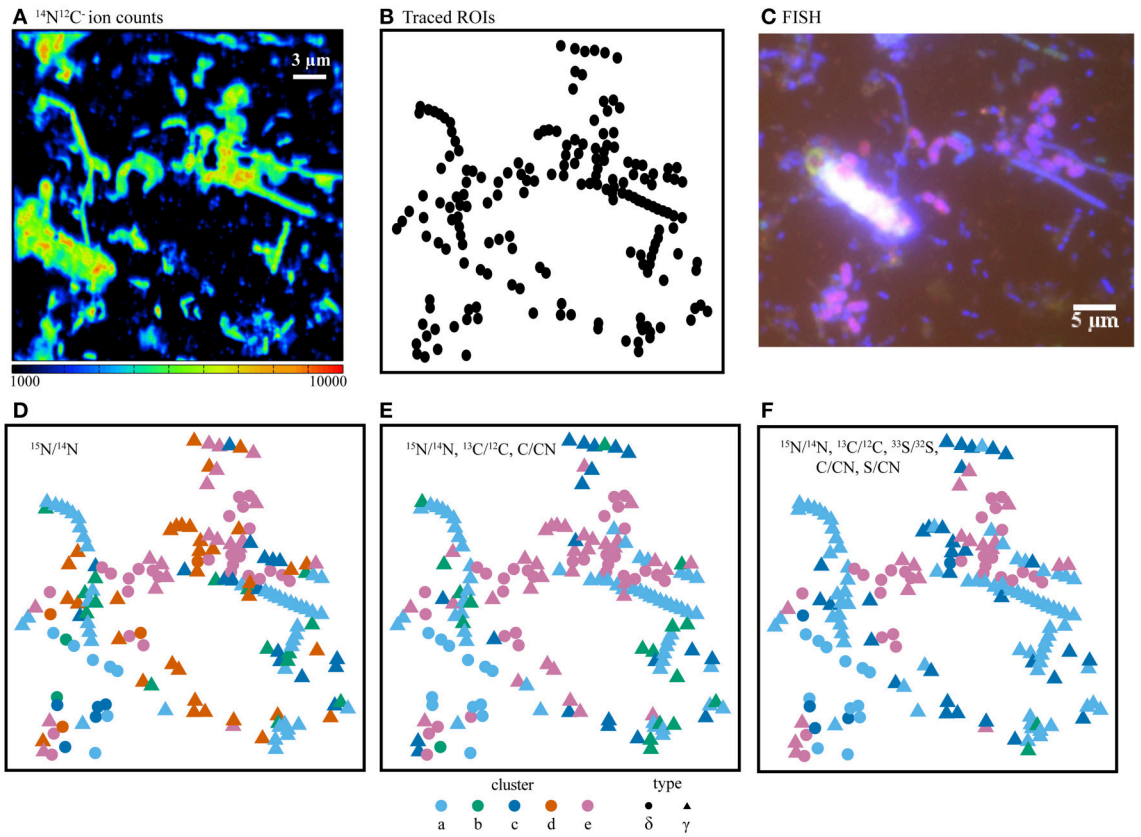

FIGURE 7 | (A) NanoSIMS ion counts from $^{14}N^{12}C^-$ as a proxy for biomass, **(B)** cell outlines (ROIs), and **(C)** the corresponding FISH image. Comparison of isotope and elemental ratio data resulting from SIP experiments using $^{15}NH_4^+$ + ^{13}C-acetate + $^{33}SO_4^{2-}$ where fuzzy c-means cluster determination was based on **(D)** one ratio, **(E)** three ratios, or **(F)** five ratios. Here, the use of five ratios provided the best differentiation of cell types as compared with the independent FISH data. In panels **D–F**, ROI colors were determined by cluster assignment (a–e). Phylogenetic assignments to "δ" (Deltaproteobacteria) or "γ" (Gammaproteobacteria) were determined by overlaying ROI positions in the NanoSIMS and FISH images prior to cluster analysis. FISH experiments **(C)** were performed with probes for Deltaproteobacteria (purple), Gammaproteobacteria (blue-green), and counter-stained with DAPI (blue).

displayed high S/CN ratios, suggesting an absence of sulfur storage globules in the incubated cells despite their observation in samples analyzed immediately after field collection. The lack of sulfur storage granules in the cells analyzed from the SIP time course experiments may be attributed to the low concentrations of sulfide, thiosulfate, and nitrate measured in incubations (data not shown), as well as the transition from aerobic to anaerobic conditions by the end of the incubation period. These conditions may have prompted these bacteria to oxidize sulfur stores generated during non-limiting conditions associated with colonization in the White Point intertidal pools (Nielsen et al., 2000; Okabe et al., 2005; Dahl and Prange, 2006).

Similar to cluster "a," the ROIs of cluster "d" showed lower $^{15}NH_4^+$ incorporation and ^{13}C-acetate derived carbon assimilation when compared to cluster "c." In contrast to the FISH-identified filamentous Gammaproteobacteria associated with clusters "a," "b," and "c," the non-filamentous Gammaproteobacteria associated with cluster "d" exclusively included ROIs with high amounts of sulfur to biomass (high S/CN ratio), possibly indicative of the presence of sulfur storage globules (**Figure 6**). A portion of the cluster "d" phenotype also showed high amounts of carbon to biomass (high C/CN), which may additionally indicate carbon storage granules. Comparison to FISH images showed that cluster "d" was associated with aggregates of coccoid Gammaproteobacteria, as well as other gammaproteobacterial cells and unidentified (DAPI-stained) single rods (**Figure 3**). Given the elevated S/CN ratio for this cluster, it is possible that these cells may also be sulfur-metabolizing microorganisms not targeted by our FISH probes (e.g., sulfur-oxidizing, Epsilonproteobacteria affiliated with *Sulfurovum* recovered in the White Point iTAG sequencing data).

Cluster "e" ROIs contained the primary sulfate reducers (highest $^{33}S/^{32}S$), which were also the most anabolically active cells (highest $^{15}N/^{14}N$; **Figure 6**). While 68% of cells within cluster "e" were FISH-identified as Deltaproteobacteria, an additional 32% of cells were only stained by DAPI and were not hybridized by either the Delta495a or GAM42a FISH probes (**Figure 3**, Figure S-4). The latter group may represent another sulfate-reducing bacterial group not targeted by the Delta495a

probe, or perhaps are due to suboptimal FISH hybridization. The unidentified members of cluster "e" showed greater acetate-derived carbon assimilation (high $^{13}C/^{12}C$), but lower $^{15}NH_4^+$ uptake than their FISH-hybridized, deltaproteobacterial counterparts. Neither subset of cluster "e" displayed high ratios of S/CN or C/CN, which indicated that these cells did not contain sulfur or carbon storage granules. The co-occurrence of more than one group of sulfate- or sulfur-reducing bacteria within cluster "e" is further supported by the presence of multiple families of Deltaproteobacteria (Desulfuromonadaceae, Desulfobacteraceae, and Desulfobulbaceae), as well as a putative thiosulfate- and sulfur-reducing *Fusibacter* spp. also identified in the iTAG data. These findings correspond with a companion study that reported low, but detectable rates of sulfate-reduction and identified members of the sulfur-reducing genus *Desulfuromusa* in the White Point mats (Miranda et al., in review).

Resolution of different cell types in these experiments relied on the combined metabolism of C, N, and S stable isotope labeled substrates to emphasize interspecies variation in three different element cycling pathways. Using the seven different collectors on the NanoSIMS 50L instrument additionally enables expansion of this method to include up to three distinct isotopically labeled sulfur substrates, including ^{33}S, ^{34}S, and/or ^{36}S. The ability to label independently both oxidized and reduced sulfur pools in the same incubation may offer additional insights into the sulfur cycling processes occurring within the White Point microbial mat community, as well as in other sulfur-based ecosystems. Alternatively, triple isotope SIP experiments utilizing $H_2^{18}O$ or D_2O as tracers for cellular growth and activity (Schwartz, 2007; Berry et al., 2015; Kopf et al., 2015) may also be directly combined with various ^{13}C and ^{15}N labeled substrates to expand the scope of the methods demonstrated here with sulfur metabolizing systems to ones where carbon and nitrogen metabolism drive the ecological dynamics. In this sulfur-cycling case study, we identified fuzzy c-means as the optimal clustering algorithm. While fuzzy c-means is likely to work well in other biological systems, testing and comparison of multiple clustering techniques is recommended as this technique is expanded to other environments and different multiple-isotope SIP combinations.

The major benefits of the triple isotope SIP experiments coupled to cluster analysis method described here are the microscopy-independent classification of microbial cells based on their phenotypic properties. Variability in the signal intensity of FISH probes, competing background autofluorescence, and taxonomic specificity are inherent problems for epifluorescence microscopy investigations of microorganisms in complex environmental systems, often complicating data interpretation and limiting the identification of subpopulations. This method offers a unique approach to quantitatively identify subpopulations of cells based on multivariate analysis of gradients in the assimilation of multiple isotopically labeled substrates and, if applicable, differences in elemental stoichiometry. These gradients in labeled substrate metabolism and anabolic activity may reflect ecophysiological niches, and thus the isotope phenotype groupings provide a taxonomically independent means of assessing metabolic networks within environmental microbial communities.

AUTHOR CONTRIBUTIONS

KD designed and carried out experiments and wrote the manuscript. VO designed experiments and wrote the manuscript. SS developed the labeled sulfur oxidation protocol and provided feedback on the manuscript. JD provided valuable contextual information for experimental design and feedback on the manuscript.

ACKNOWLEDGMENTS

We thank Y. Guan in Caltech's Center for Microanalysis for technical assistance with the NanoSIMS 50L measurements, P. Miranda for the introduction and assistance with field work at White Point, and A. Saxena-Green, A. Pasulka, and R. Hatzenpichler for helpful discussions. This research is funded by the Gordon and Betty Moore Foundation through Grant GBMF 3306, a grant from the National Science Foundation (EAR-1123391), as well as the NASA Astrobiology Institute (Award # NNA13AA92A; to VO). This is NAI-Life Underground Publication Number 80.

SUPPLEMENTARY MATERIAL

The Supplementary Material for this article can be found online at: http://journal.frontiersin.org/article/10.3389/fmicb.2016.00774

REFERENCES

Abraham, W.-R. (2014). Applications and impacts of stable isotope probing for analysis of microbial interactions. *Appl. Microbiol. Biotechnol.* 98, 4817–4828. doi: 10.1007/s00253-014-5705-8

Berry, D., Mader, E., Lee, T. K., Woebken, D., Wang, Y., Zhu, D., et al. (2015). Tracking heavy water (D_2O) incorporation for identifying and sorting active microbial cells. *Proc. Natl. Acad. Sci. U.S.A.* 112, E194–E203. doi: 10.1073/pnas.1420406112

Bezdek, J. C., Ehrlich, R., and Full, W. (1984). FCM: the fuzzy c-means clustering algorithm. *Comput. Geosci.* 10, 191–203. doi: 10.1016/0098-3004(84)90020-7

Caliński, T., and Harabasz, J. (1974). A dendrite method for cluster analysis. *Commun. Stat. Theory Methods* 3, 1–27. doi: 10.1080/03610927408827101

Case, D. H., Pasulka, A. L., Marlow, J. J., Grupe, B. M., Levin, L. A., and Orphan, V. J. (2015). Methane seep carbonates host distinct, diverse, and dynamic microbial assemblages. *MBio* 6, 1–12. doi: 10.1128/mBio.01348-15

Chen, Y., and Murrell, J. C. (2010). When metagenomics meets stable-isotope probing: progress and perspectives. *Trends Microbiol.* 18, 157–163. doi: 10.1016/j.tim.2010.02.002

Dahl, C., and Prange, A. (2006). "Bacterial sulfur globules: occurrence, structure and metabolism," in *Inclusions in Prokaryotes*, ed J. M. Shively (New York, NY: Springer), 21–51.

Dekas, A. E., and Orphan, V. J. (2011). "Identification of diazotrophic microorganisms in marine sediment via fluorescence *in situ* hybridization coupled to nanoscale secondary ion mass spectrometry (FISH-NanoSIMS)," in *Methods in Enzymology,* ed G. K. Martin (San Diego, CA: Academic Press), 281–305.

DeRito, C. M., Pumphrey, G. M., and Madsen, E. L. (2005). Use of field-based stable isotope probing to identify adapted populations and track carbon flow through a phenol-degrading soil microbial community. *Appl. Environ. Microbiol.* 71, 7858–7865. doi: 10.1128/aem.71.12.7858-7865.2005

Desgraupes, B. (2015). *ClusterCrit: Clustering Indices. R Package Version 1.2.5.* Available online at: http://CRAN.R-project.org/package=clusterCrit

Dumont, M. G., and Murrell, J. C. (2005). Stable isotope probing - linking microbial identity to function. *Nat. Rev. Microbiol.* 3, 499–504. doi: 10.1038/nrmicro1162

Equihua, M. (1990). Fuzzy clustering of ecological data. *J. Ecol.* 78, 519–534. doi: 10.2307/2261127

Fike, D. A., Gammon, C. L., Ziebis, W., and Orphan, V. J. (2008). Micron-scale mapping of sulfur cycling across the oxycline of a cyanobacterial mat: a paired nanoSIMS and CARD-FISH approach. *ISME J.* 2, 749–759. doi: 10.1038/ismej.2008.39

Fike, D. A., Finke, N., Zha, J., Blake, G., Hoehler, T. M., and Orphan, V. J. (2009). The effect of sulfate concentration on (sub)millimeter-scale sulfide $\delta^{34}S$ in hypersaline cyanobacterial mats over the diurnal cycle. *Geochim. Cosmochim. Acta* 73, 6187–6204. doi: 10.1016/j.gca.2009.07.006

Fuhrman, J. A. (2009). Microbial community structure and its functional implications. *Nature* 459, 193–199. doi: 10.1038/nature08058

Glöckner, F. O., Amann, R., Alfreider, A., Pernthaler, J., Psenner, R., Trebesius, K., et al. (1996). An *in situ* hybridization protocol for detection and identification of planktonic bacteria. *Syst. Appl. Microbiol.* 19, 403–406. doi: 10.1016/S0723-2020(96)80069-5

Green, R. H. (1980). Multivariate approaches in ecology: the assessment of ecologic similarity. *Annu. Rev. Ecol. Syst.* 11, 1–14. doi: 10.1146/annurev.es.11.110180.000245

Green-Saxena, A., Dekas, A. E., Dalleska, N. F., and Orphan, V. J. (2014). Nitrate-based niche differentiation by distinct sulfate-reducing bacteria involved in the anaerobic oxidation of methane. *ISME J.* 8, 150–163. doi: 10.1038/ismej.2013.147

House, C. H., Orphan, V. J., Turk, K. A., Thomas, B., Pernthaler, A., Vrentas, J. M., et al. (2009). Extensive carbon isotopic heterogeneity among methane seep microbiota. *Environ. Microbiol.* 11, 2207–2215. doi: 10.1111/j.1462-2920.2009.01934.x

Jacq, E., Prieur, D., Nichols, P., White, D. C., Porter, T., and Geesey, G. G. (1989). Microscopic examination and fatty acid characterization of filamentous bacteria colonizing substrata around subtidal hydrothermal vents. *Arch. Microbiol.* 152, 64–71. doi: 10.1007/BF00447013

James, F. C., and McCulloch, C. E. (1990). Multivariate analysis in ecology and systematics: panacea or pandora's box? *Annu. Rev. Ecol. Syst.* 21, 129–166. doi: 10.1146/annurev.es.21.110190.001021

Kalanetra, K. M., Huston, S. L., and Nelson, D. C. (2004). Novel, attached, sulfur-oxidizing Bacteria at shallow hydrothermal vents possess vacuoles not involved in respiratory nitrate accumulation. *Appl. Environ. Microbiol.* 70, 7487–7496. doi: 10.1128/AEM.70.12.7487-7496.2004

Kopf, S. H., McGlynn, S. E., Green-Saxena, A., Guan, Y., Newman, D. K., and Orphan, V. J. (2015). Heavy water and ^{15}N labelling with NanoSIMS analysis reveals growth rate-dependent metabolic heterogeneity in chemostats. *Environ. Microbiol.* 17, 2542–2556. doi: 10.1111/1462-2920.12752

Lance, G. N., and Williams, W. T. (1967). A general theory of classificatory sorting strategies II. Clustering systems. *Comput. J.* 10, 271–277. doi: 10.1093/comjnl/10.3.271

Larkin, J. M., and Strohl, W. R. (1983). Beggiatoa, thiothrix, and thioploca. *Ann. Rev. Microbiol.* 37, 341–367. doi: 10.1146/annurev.mi.37.100183.002013

Legendre, P., and Legendre, L. (2012). "Cluster analysis," in *Developments in Environmental Modelling: Numerical Ecology*, *3rd Edn.* (Amsterdam: Elsevier).

Legendre, P., Borcard, D., and Peres-Neto, P. R. (2005). Analyzing beta diversity: partitioning the spatial variation of community composition data. *Ecol. Monogr.* 75, 435–450. doi: 10.1890/05-0549

Liu, Y., Hou, T., and Fu, L. (2015). A new unsupervised binning method for metagenomic dataset with automated estimation of number of species. *PeerJ PrePrints* 3, e839ve831. doi: 10.7287/peerj.preprints.839v1

Loy, A., Lehner, A., Lee, N., Adamczyk, J., Meier, H., Ernst, J., et al. (2002). Oligonucleotide microarray for 16S rRNA gene-based detection of all recognized lineages of sulfate-reducing prokaryotes in the environment. *Appl. Environ. Microbiol.* 68, 5064–5081. doi: 10.1128/aem.68.10.5064-5081.2002

Lu, Y. Y., Chen, T., Fuhrman, J. A., and Sun, F. (2016). COCACOLA: binning metagenomic contigs using sequence COmposition, read CoverAge, CO-alignment, and paired-end read LinkAge. arXiv:1604.02512.

Macalady, J. L., Lyon, E. H., Koffman, B., Albertson, L. K., Meyer, K., Galdenzi, S., et al. (2006). Dominant microbial populations in limestone-corroding stream biofilms, Frasassi Cave System, Italy. *Appl. Environ. Microbiol.* 72, 5596–5609. doi: 10.1128/aem.00715-06

MacQueen, J. (1967). "Some methods for classification and analysis of multivariate observations," in *Proceedings of the fifth Berkeley Symposium on Mathematical Statistics and Probability* (Oakland, CA), 281–297.

Maechler, M., Rousseeuw, P., Struyf, A., Hubert, M., and Hornik, K. (2015). *Cluster: Cluster Analysis Basics and Extensions. R Package Version 2.0.* 2.

Manz, W., Amann, R., Ludwig, W., Wagner, M., and Schleifer, K.-H. (1992). Phylogenetic oligodeoxynucleotide probes for the major subclasses of Proteobacteria: problems and solutions. *Syst. Appl. Microbiol.* 15, 593–600. doi: 10.1016/S0723-2020(11)80121-9

McCune, B., Grace, J. B., and Urban, D. L. (2002a). "Hierarchical clustering," in *Analysis of Ecological Communities* (Gleneden Beach, OR: MjM Software Design).

McCune, B., Grace, J. B., and Urban, D. L. (2002b). "Overview of methods for finding groups," in *Analysis of Ecological Communities*. (Gleneden Beach, OR: MjM Software Design).

McGlynn, S. E., Chadwick, G. L., Kempes, C. P., and Orphan, V. J. (2015). Single cell activity reveals direct electron transfer in methanotrophic consortia. *Nature* 526, 531–535. doi: 10.1038/nature15512

Milucka, J., Ferdelman, T. G., Polerecky, L., Franzke, D., Wegener, G., Schmid, M., et al. (2012). Zero-valent sulphur is a key intermediate in marine methane oxidation. *Nature* 491, 541–546. doi: 10.1038/nature11656

Musat, N., Halm, H., Winterholler, B., Hoppe, P., Peduzzi, S., Hillion, F., et al. (2008). A single-cell view on the ecophysiology of anaerobic phototrophic bacteria. *Proc. Natl. Acad. Sci. U.S.A.* 105, 17861–17866. doi: 10.1073/pnas.0809329105

Musat, N., Foster, R., Vagner, T., Adam, B., and Kuypers, M. M. M. (2012). Detecting metabolic activities in single cells, with emphasis on nanoSIMS. *FEMS Microbiol. Rev.* 36, 486–511. doi: 10.1111/j.1574-6976.2011.00303.x

Nasser, S., Breland, A., Harris, F. C. Jr., and Nicolescu, M. (2008). "A fuzzy classifier to taxonomically group DNA fragments within a metagenome," in *Fuzzy Information Processing Society, 2008. NAFIPS 2008. Annual Meeting of the North American.* (New York, NY: IEEE), 1–6.

Neufeld, J. D., Vohra, J., Dumont, M. G., Lueders, T., Manefield, M., Friedrich, M. W., et al. (2007). DNA stable-isotope probing. *Nat. Protocols* 2, 860–866. doi: 10.1038/nprot.2007.109

Nielsen, P. H., De Muro, M. A., and Nielsen, J. L. (2000). Studies on the *in situ* physiology of *Thiothrix* spp. present in activated sludge. *Environ. Microbiol.* 2, 389–398. doi: 10.1046/j.1462-2920.2000.00120.x

Okabe, S., Ito, T., Sugita, K., and Satoh, H. (2005). Succession of internal sulfur cycles and sulfur-oxidizing bacterial communities in microaerophilic wastewater biofilms. *Appl. Environ. Microbiol.* 71, 2520–2529. doi: 10.1128/aem.71.5.2520-2529.2005

Orphan, V. J., House, C. H., Hinrichs, K.-U., McKeegan, K. D., and DeLong, E. F. (2001). Methane-consuming archaea revealed by directly coupled isotopic and phylogenetic analysis. *Science* 293, 484–487. doi: 10.1126/science.1061338

Orphan, V. J., Turk, K. A., Green, A. M., and House, C. H. (2009). Patterns of ^{15}N assimilation and growth of methanotrophic ANME-2 archaea and sulfate-reducing bacteria within structured syntrophic consortia revealed by FISH-SIMS. *Environ. Microbiol.* 11, 1777–1791. doi: 10.1111/j.1462-2920.2009.01903.x

Pelz, O., Tesar, M., Wittich, R.-M., Moore, E. R. B., Timmis, K. N., and Abraham, W.-R. (1999). Towards elucidation of microbial community metabolic pathways: unravelling the network of carbon sharing in a pollutant-degrading

bacterial consortium by immunocapture and isotopic ratio mass spectrometry. *Environ. Microbiol.* 1, 167–174. doi: 10.1046/j.1462-2920.1999.00023.x

Pett-Ridge, J., and Weber, P. K. (2012). "NanoSIP: NanoSIMS applications for microbial biology," in *Microbial Systems Biology*, Vol. 881, ed A. Navid (New York, NY: Springer), 375–408.

Polerecky, L., Adam, B., Milucka, J., Musat, N., Vagner, T., and Kuypers, M. M. M. (2012). Look@NanoSIMS – a tool for the analysis of nanoSIMS data in environmental microbiology. *Environ. Microbiol.* 14, 1009–1023. doi: 10.1111/j.1462-2920.2011.02681.x

Popa, R., Weber, P. K., Pett-Ridge, J., Finzi, J. A., Fallon, S. J., Hutcheon, I. D., et al. (2007). Carbon and nitrogen fixation and metabolite exchange in and between individual cells of *Anabaena oscillarioides*. *ISME J.* 1, 354–360. doi: 10.1038/ismej.2007.44

R Core Team (2015). *R: A Language and Environment for Statistical Computing*. v. 3.2.1. Available online at: http://www.R-project.org/

R Studio Team (2015). *R Studio: Integrated Development Environment for R*. v. 0.99.451. Available online at: http://www.rstudio.com/

Radajewski, S., Ineson, P., Parekh, N. R., and Murrell, J. C. (2000). Stable-isotope probing as a tool in microbial ecology. *Nature* 403, 646–649. doi: 10.1038/35001054

Ramette, A. (2007). Multivariate analyses in microbial ecology. *FEMS Microbiol. Ecol.* 62, 142–160. doi: 10.1111/j.1574-6941.2007.00375.x

Rossetti, S., Blackall, L. L., Levantesi, C., Uccelletti, D., and Tandoi, V. (2003). Phylogenetic and physiological characterization of a heterotrophic, chemolithoautotrophic *Thiothrix* strain isolated from activated sludge. *Int. J. Syst. Evol. Microbiol.* 53, 1271–1276. doi: 10.1099/ijs.0.02647-0

Rousseeuw, P. J. (1987). Silhouettes: a graphical aid to the interpretation and validation of cluster analysis. *J. Comput. Appl. Math.* 20, 53–65. doi: 10.1016/0377-0427(87)90125-7

Schwartz, E. (2007). Characterization of growing microorganisms in soil by stable isotope probing with $H_2^{18}O$. *Appl. Environ. Microbiol.* 73, 2541–2546. doi: 10.1128/aem.02021-06

Stein, J. L. (1984). Subtidal gastropods consume sulfur-oxidizing Bacteria: evidence from coastal hydrothermal vents. *Science* 223, 696–698. doi: 10.1126/science.223.4637.696

Wagner, M. (2009). Single-cell ecophysiology of microbes as revealed by raman microspectroscopy or secondary ion mass spectrometry imaging. *Annu. Rev. Microbiol.* 63, 411–429. doi: 10.1146/annurev.micro.091208.073233

Walesiak, M., Dudek, A., and Dudek, M. (2008). *Clustersim: Searching for Optimal Clustering Procedure for a Data Set. R Package Version 0.36-1*. Available online at: http://keii.ue.wroc.pl/clusterSim

Wegener, G., Bausch, M., Holler, T., Thang, N. M., Prieto Mollar, X., Kellermann, M. Y., et al. (2012). Assessing sub-seafloor microbial activity by combined stable isotope probing with deuterated water and ^{13}C-bicarbonate. *Environ. Microbiol.* 14, 1517–1527. doi: 10.1111/j.1462-2920.2012.02739.x

Wickham, H. (2009). *ggplot2: Elegant Graphics for Data Analysis*. New York, NY: Springer Science & Business Media.

Wilbanks, E. G., Jaekel, U., Salman, V., Humphrey, P. T., Eisen, J. A., Facciotti, M. T., et al. (2014). Microscale sulfur cycling in the phototrophic pink berry consortia of the Sippewissett Salt Marsh. *Environ. Microbiol.* 16, 3398–3415. doi: 10.1111/1462-2920.12388

Woodring, W. P., Bramlette, M. N., and Kew, W. S. W. (1946). *Geology and Paleontology of Palos Verdes Hills, California. U.S. Geological Survey Professional Paper* 207.

Zimmermann, M., Escrig, S., Hübschmann, T., Kirf, M. K., Brand, A., Inglis, R. F., et al. (2015). Phenotypic heterogeneity in metabolic traits among single cells of a rare bacterial species in its natural environment quantified with a combination of flow cell sorting and NanoSIMS. *Front. Microbiol.* 6:243. doi: 10.3389/fmicb.2015.00243

Conflict of Interest Statement: The authors declare that the research was conducted in the absence of any commercial or financial relationships that could be construed as a potential conflict of interest.

frontiers in Microbiology

ORIGINAL RESEARCH
published: 24 December 2015
doi: 10.3389/fmicb.2015.01392

Sulfur Isotope Effects of Dissimilatory Sulfite Reductase

William D. Leavitt[1,2†], Alexander S. Bradley[2†], André A. Santos[3], Inês A. C. Pereira[3] and David T. Johnston[1]*

[1] Department of Earth and Planetary Sciences, Harvard University, Cambridge, MA, USA, [2] Department of Earth and Planetary Sciences, Washington University in St. Louis, St. Louis, MO, USA, [3] Bacterial Energy Metabolism Laboratory, Instituto de Tecnologia Química e Biológica António Xavier, Universidade Nova de Lisboa, Oeiras, Portugal

The precise interpretation of environmental sulfur isotope records requires a quantitative understanding of the biochemical controls on sulfur isotope fractionation by the principle isotope-fractionating process within the S cycle, microbial sulfate reduction (MSR). Here we provide the only direct observation of the major ($^{34}S/^{32}S$) and minor ($^{33}S/^{32}S$, $^{36}S/^{32}S$) sulfur isotope fractionations imparted by a central enzyme in the energy metabolism of sulfate reducers, dissimilatory sulfite reductase (DsrAB). Results from *in vitro* sulfite reduction experiments allow us to calculate the *in vitro* DsrAB isotope effect in $^{34}S/^{32}S$ (hereafter, $^{34}\varepsilon_{DsrAB}$) to be 15.3 ± 2‰, 2σ. The accompanying minor isotope effect in ^{33}S, described as $^{33}\lambda_{DsrAB}$, is calculated to be 0.5150 ± 0.0012, 2σ. These observations facilitate a rigorous evaluation of the isotopic fractionation associated with the dissimilatory MSR pathway, as well as of the environmental variables that govern the overall magnitude of fractionation by natural communities of sulfate reducers. The isotope effect induced by DsrAB upon sulfite reduction is a factor of 0.3–0.6 times prior indirect estimates, which have ranged from 25 to 53‰ in $^{34}\varepsilon_{DsrAB}$. The minor isotope fractionation observed from DsrAB is consistent with a kinetic or equilibrium effect. Our *in vitro* constraints on the magnitude of $^{34}\varepsilon_{DsrAB}$ is similar to the median value of experimental observations compiled from all known published work, where $^{34}\varepsilon_{r-p}$ = 16.1‰ (*r–p* indicates reactant vs. product, $n = 648$). This value closely matches those of MSR operating at high sulfate reduction rates in both laboratory chemostat experiments ($^{34}\varepsilon_{SO4-H2S}$ = 17.3 ± 1.5‰, 2σ) and in modern marine sediments ($^{34}\varepsilon_{SO4-H2S}$ = 17.3 ± 3.8‰). Targeting the direct isotopic consequences of a specific enzymatic processes is a fundamental step toward a biochemical foundation for reinterpreting the biogeochemical and geobiological sulfur isotope records in modern and ancient environments.

Keywords: microbial sulfate reduction, enzyme-specific isotope fractionation, minor sulfur isotopes, global sulfur cycle, dissimilatory sulfite reductase

OPEN ACCESS

Edited by:
Orit Sivan,
Ben Gurion University of the Negev, Israel

Reviewed by:
Mustafa Yucel,
Middle East Technical University, Turkey
Timothy Ferdelman,
Max Planck Institute for Marine Microbiology, Germany
Florian Einsiedl,
Technische Universität München, Germany

***Correspondence:**
William D. Leavitt
wleavitt@eps.wustl.edu

† These authors have contributed equally to this work.

Specialty section:
This article was submitted to Microbiological Chemistry and Geomicrobiology, a section of the journal Frontiers in Microbiology

Received: *06 July 2015*
Accepted: *23 November 2015*
Published: *24 December 2015*

Citation:
Leavitt WD, Bradley AS, Santos AA, Pereira IAC and Johnston DT (2015) Sulfur Isotope Effects of Dissimilatory Sulfite Reductase. Front. Microbiol. 6:1392. doi: 10.3389/fmicb.2015.01392

INTRODUCTION

Microbial sulfate reduction provides a critical link between Earth's surface sulfur, carbon, iron, and oxygen cycles (Thode et al., 1961; Holland, 1973; Garrels and Lerman, 1981; Canfield, 2001a). This metabolism is comprised of a set of enzymes working in concert to reduce sulfate (SO_4^{2-}) to sulfide (H_2S) (Peck, 1961; Pereira et al., 2011; **Figure 1**). During this transformation, MSR generates $^{34}S/^{32}S$, $^{33}S/^{32}S$, $^{36}S/^{32}S$, $^{18}O/^{16}O$, and $^{17}O/^{16}O$ stable isotope fractionations

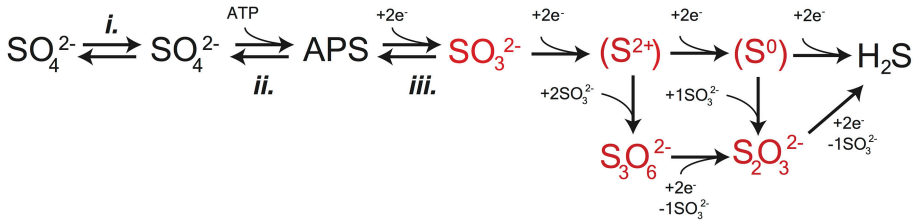

FIGURE 1 | A schematic capturing the central role of DsrAB in MSR. The *in vivo* dissimilatory sulfate reduction pathway, where red highlighted steps represent sulfite reduction by DsrAB in the absence of DsrC, as targeted here *in vitro*. The constituent steps of MSR relevant to S isotope fractionation are likely APS reduction to sulfite by APSr, sulfite reduction (the subject of this study) by DsrAB, and the terminal production of sulfide by DsrC/DsrMKJOP. The pathway is described in detail in the text.

(Harrison and Thode, 1958; Kaplan and Rittenberg, 1964; Kemp and Thode, 1968; Chambers et al., 1975; Goldhaber and Kaplan, 1975; Fritz et al., 1989; Canfield, 2001b; Sim et al., 2011b; Leavitt et al., 2013), the biochemical source of which is unclear (Chambers and Trudinger, 1979). To construct a biochemically constrained perspective of sulfur isotope fractionations during MSR requires we quantify how material moves through the metabolic network, and gain an understanding of the isotope effect(s) associated with each constituent enzymatic step (Hayes, 2001).

The enzyme catalyzed reaction network of MSR is represented in **Figure 1**. Sulfate is first imported into the cytoplasm by a variety of transporters (Cypionka, 1994; Piłsyk and Paszewski, 2009; **Figure 1**), and subsequently activated to a high-energy intermediate, adenosine 5′-phosphosulfate (APS). The latter reaction generates pyrophosphate (PPi) at the expense of ATP by the enzyme sulfate-adenylyl transferase (Sat) (Peck, 1962). APS is reduced to sulfite (SO_3^{2-}) through a two-electron transfer by the soluble cytoplasmic enzyme APS oxidoreductase (ApsR) (Peck, 1959), which is linked to energy conservation by the membrane-bound complex QmoABC (Pires et al., 2003). APS reduction is highly reversible, depending on the *in vivo* or *in vitro* conditions (Peck, 1960). Sulfite has several potential fates. Sulfite can either be re-oxidized to sulfate (directly or via APS) or further reduced to sulfide by DsrAB with the involvement of DsrC (Oliveira et al., 2008b). A critical step is during the reduction of sulfite when it binds the iron of the siroheme in the DsrAB active site. The subsequent reduction occurs via electron transfer from an adjacent Fe-S cluster (Oliveira et al., 2008a,b; Parey et al., 2010). *In vivo*, DsrAB has been proposed to generate intermediate valence sulfur, which is then bound to DsrC and converted to sulfide via DsrC/MK (Oliveira et al., 2008b; Venceslau et al., 2013, 2014; Santos et al., 2015). Sulfide then leaves the cell by diffusion (as H_2S) (Mathai et al., 2009) or through anion transport (as HS^- or S^{2-}) (Czyzewski and Wang, 2012), though the mechanism of sulfide exit in MSR is still not well known. In instances when DsrC is unavailable (e.g., when DsrAB is pure *in vitro*) or limiting (e.g., intracellular sulfite is in excess of reduced DsrC), intermediates such as thiosulfate ($S_2O_3^{2-}$) may become important, likely due to the reaction of sulfite with sulfide (*in vivo*) or the partially reduced sulfur from DsrAB (*in vitro*) (Chambers and Trudinger, 1975; Drake and Akagi, 1976, 1977, 1978; Kim and Akagi, 1985). A few examples exist where thiosulfate is a key component in closing S mass balance during *in vivo* MSR (Sass et al., 1992; Leavitt et al., 2014; Price et al., 2014), and in one instance trithionate is observed ($S_3O_6^{2-}$) (Sass et al., 1992), though it is not clear in this case it is a physiological product. Under these conditions, accumulation and excretion of such compounds as thiosulfate may be important (Bradley et al., 2011). It is within this broader biochemical and physiological context that we examine the isotopic consequences of sulfite reduction by DsrAB, which as outlined above, is central to the biochemistry of dissimilatory sulfate reduction.

Reduction of sulfite by DsrAB breaks three of the four S-O bonds in the original sulfate (Venceslau et al., 2014). As such, the isotope effect of DsrAB likely plays a significant role in setting the overall fractionations observed from MSR (Harrison and Thode, 1958; Rees, 1973; Farquhar et al., 2003; Brunner and Bernasconi, 2005). Measured enzyme-specific isotope effects are lacking for MSR and the S cycle in general. Such information has been transformative for the study of other biogeochemical elements like carbon. For example, experimental work quantifying the $^{13}C/^{12}C$ effect of RuBisCO (Park and Epstein, 1960; Farquhar et al., 1982; Tcherkez et al., 2006), the core enzyme in carbon fixation, has greatly advanced the applicability of carbon isotope biogeochemistry. More specifically, understanding the fractionation associated with RuBisCO allowed greater insight into modern (Hayes, 1993) and ancient (Hayes et al., 1999) carbon cycling, and facilitated a better understanding of primary productivity in the both modern (Laws et al., 1995) and ancient (Pagani et al., 2009) oceans. Similar enzyme-specific approaches have also proven greatly informative in studies of methanogenesis (Scheller et al., 2013), nitrate assimilation (Karsh et al., 2012) and nitrogen fixation (Sra et al., 2004). With these studies as a guide, we look to further unlock the sulfur cycle through targeting a key microbial sulfate reduction enzyme, DsrAB.

To close the knowledge gap between whole-cell observations and enzyme-catalyzed reactions, as well as to turn natural isotope records into catalogs of environmental information, we conduct the first enzyme-specific sulfur isotope experiments. Here we report the sulfur isotope fractionation factors associated with *in vitro* sulfite reduction by the dissimilatory sulfite

reductase enzyme (DsrAB). Using these results and a new multi-component isotope distillation model, we are able to place improved constraints on the root of sulfur isotope fractionation during MSR. This refines our understanding of the predominant biological process responsible for generating environmental S isotope records throughout geological history.

EXPERIMENTAL METHODS SUMMARY

We conducted a series of closed system *in vitro* sulfite reduction experiments with purified DsrAB from *Desulfovibrio vulgaris* str. Hildenborough (DSM 644) and *Archaeoglobus fulgidus*. These enzymes are structurally similar and evolutionarily related (Parey et al., 2013), and we chose them to attempt to determine conservation of isotope fractionation in *D. vulgaris* and *A. fulgidus* DsrAB. The complete isolation and purification details are available in the Supplementary Material.

DsrAB experiments were conducted *in vitro* under strictly anoxic conditions with H_2, [NiFe] hydrogenase, and methyl viologen as the electron donation system. Key considerations in experimental design are: (i) to provide enough sulfur at each time point for isotopic characterization of residual reactant and products; (ii) to provide the proper reaction conditions to allow for optimal DsrAB activity (pH = 7.1, $T = 20^\circ$ or 31°C for *D. vulgaris* and 65°C for *A. fulgidus*); (iii) to ensure hydrogenase activity is not inhibited by the experimental pH (optimum at pH 7.5, activity significantly depleted below pH 6.5, so we chose pH 7.1, to account for optima of both DsrAB and [NiFe]-hydrogenase); and finally (iv) to ensure the sulfite to hydrogen ratio strongly favors sulfite reduction. Experiments setup is detailed in the Supplementary Material.

Each experiment was performed in duplicate and sampled as sulfite was consumed (reaction progress tracked as f_{SO3}, equivalent to the fraction of remaining sulfite). The reaction consumed sulfite to form products thiosulfate and trithionate, with no detectable sulfide. Thiosulfate and trithionate concentrations were quantified following published cyanolysis protocols (Kelly and Wood, 1994), where we used a modified "Fuschin" method (Grant, 1947) to quantify sulfite and a modified Cline method (Cline, 1969) to measure sulfide. All quantification and experimental methods are fully detailed in the Supplementary Material. In addition to concentrations, we measured the major and minor sulfur isotopic compositions of three operationally defined and precipitated pools: sulfite (both initial and residual reactant), product sulfonate (from trithionate or thiosulfate) and the "reduced sulfur" products (central and terminal sulfurs in trithionate and thiosulfate, respectively). Complete IUPAC definitions of each S reservoir, along with all isotopic measurement methods and error propagation calculations are fully articulated in the Supplementary Material.

ISOTOPE NOTATION

The variability in ^{34}S of a measured pool is reported in standard delta notation (for instance $\delta^{34}S$, in ‰ units), where $^{34}S/^{32}S$ of the sample is the relative difference from a standard (Hayes, 1983), and is reported as the isotopic offset between two measured pools of sulfur, $^{34}\varepsilon$ ($=10^3 x(^{34}\alpha\text{-}1)$), still in ‰ units. Fractionation factors (α's and associated ε's) are annotated with a subscript to denote the process of interest or pools being related, such as $^{34}\varepsilon_{DsrAB}$, $^{34}\varepsilon_{MSR}$, $^{34}\varepsilon_{r-p}$, or $^{34}\varepsilon_{SO4-H2S}$. The same nomenclature convention is followed when a minor isotope, ^{33}S, is included. The only exception is the addition of one new term, $^{33}\lambda$, which is approximately the slope of a line on a plot of $\delta^{33}S$ vs. $\delta^{34}S$ (Miller, 2002; Farquhar et al., 2003), but can be simply interpreted as a measure of mass-dependent minor isotope fractionation. Mathematical definitions are provided below.

FRACTIONATION MODELING

Calculation of the isotopic fractionation imposed by the reduction of sulfite through DsrAB requires tracking the concentration of the reactant, accumulation of the products, and determining the isotopic composition of all as the reaction progressed. This necessitates the application of a closed-system model in order to calculate fractionation factors. Determining the intrinsic isotope effect associated with a closed system reaction can be approached in a number of ways. Normally, in a system where one reactant is consumed in order to generate a single product, a Rayleigh model is employed (Nakai and Jensen, 1964; Mariotti et al., 1981). This approach assumes that the reaction of interest is unidirectional, generates only one product, and that the fractionation factor is invariant throughout the reaction. In this case, the isotope effect is calculated as a function of the isotope ratio, R, of the starting composition (R_{ao}) and evolving product pool (R_p, defined below), equal to the mass balance on sulfite:

$$\alpha_{total} = \frac{\ln\left(\frac{R_p}{R_{a0}}(f-1)+1\right)}{\ln(f)}. \quad (1)$$

In this solution, f tracks the fractional amount of reactant remaining (SO_3^{2-}). For our experiments, we define f_{SO3}:

$$f_{SO_3} = \frac{\left[SO_3^{2-}\right]_t}{\left[SO_3^{2-}\right]_0}. \quad (2)$$

In the specific case of our experiments and the reduction of sulfite by DsrAB, however, the standard closed-system isotope distillation models (Equation 1) requires expansion. Recall that the *in vitro* reaction involves the accumulation of two products (trithionate and thiosulfate). Each of these products further contains sulfur moieties in more than one oxidation state (Suh and Akagi, 1969; Kobayashi et al., 1974; Drake and Akagi, 1976, 1977, 1978). This means that, rather than R_p being the isotope composition of a single product pool, we define it as the mass-weighted sum of the oxidized (R_{ox}) and reduced (R_{red}) products in trithionate and thiosulfate:

$$R_p = \left[\frac{1}{2}j + \frac{1}{3}(1-j)\right]R_{red} + \left[\frac{1}{2}j + \frac{2}{3}(1-j)\right]R_{ox}. \quad (3)$$

Here the reduced and oxidized pools are the operationally defined reservoirs discussed above. In the mass balance

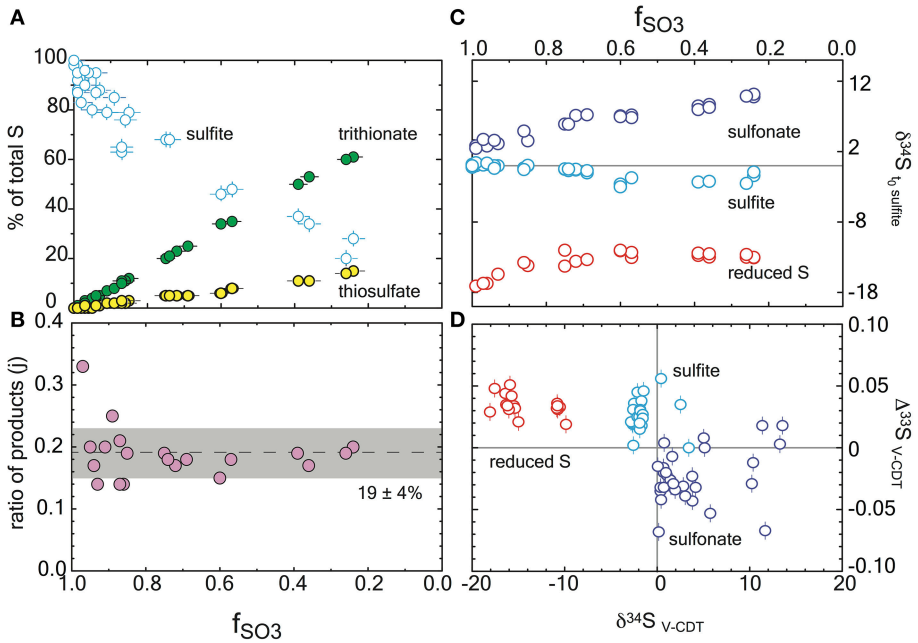

FIGURE 2 | Reaction progress during sulfite reduction with *D. vulgaris* DsrAB *in vitro*. Errors are included in all measurements (2σ) and are smaller than the symbol if not seen. **(A)** The mol fraction of sulfur in each sulfur product pool as a function of reaction progress, f_{SO3}. Mass balance conservation is discussed in the text. **(B)** The ratio of products at each time point, demonstrating the constancy of the reaction scheme (denoted as *j* in the model). This is the ratio of the slopes of the products from **(A)**. **(C)** Major isotope data for each operationally defined sulfur pool as a function of reaction progress, and normalized to the initial sulfite composition. **(D)** A triple isotope cross plot of the data presented in frame C, normalized to V-CDT.

accounting equation we introduce a term to quantify the ratio of products, *j* (**Figure 2**). The concentrations of sulfite, trithionate, and thiosulfate were measured at each time-point, ensuring the closure of mass balance and validating the use of a relative mass term. The *j* term is thus the fraction of products residing in thiosulfate:

$$j = \frac{2\left[S_2O_3^{2-}\right]_t}{2\left[S_2O_3^{2-}\right]_t + 3\left[S_3O_6^{2-}\right]_t}. \quad (4)$$

For isotopic measurements we quantitatively separated the oxidized moieties from trithionate and thiosulfate from the partially reduced moieties of both products. There were no available methods to separate trithionate and thiosulfate and isolate each S site within those products (a target for future work). We then measured the isotopic compositions of the pooled oxidized and pooled reduced products. As the goal is to identify the fractionation between the residual sulfite and either the oxidized ($^{3x}\alpha_{ox}$) or reduced ($^{3x}\alpha_{red}$) moieties in trithionate and thiosulfate, we present the general equation, ($^{3x}\alpha_z$):

$$\alpha_z = \frac{R_z}{R_{a0}} \frac{\alpha_{total}}{\left(f^{\alpha_{total}} - 1\right)} (f - 1), \quad (5)$$

where *z* is either *ox* or *red*. This solution is then translated into standard $^{3x}\varepsilon$ notation. Fractionation factors are then related in triple isotope space with:

$$^{3x}\lambda = \frac{ln\left(^{3x}\alpha\right)}{ln\left(^{34}\alpha\right)}, \quad (6)$$

a term which finds common application in mass-dependent studies (Young et al., 2002; Farquhar et al., 2003). Finally, we note the models assumptions: (1) sulfite and its isomers carry the same isotopic composition as each other, (2) the isotopic composition of the sulfonate groups (in trithionate and thiosulfate) are isotopically identical, and (3) similar to 2, the isotopic composition of reduced sulfur in trithionate and thiosulfate are isotopically identical.

The complexity added above in equation 6 allows for numerous products for a given reaction, but still assumes that the fractionation factors involved are static over the time series of the experiment (f_{SO3}) and that there is only one reaction present. If this is true, then the model prediction will match the observation over all values of f_{SO3}. Although, we observed a statistically invariant ratio of thiosulfate to trithionate production throughout the reaction (*j* in **Figure 2**), suggesting a static set of reactions through the entire experiment, it appears that the net fractionation factor was indeed time-dependent. In the event of an evolving α, the fractionation factor early in the experiment, where the concentration of products remains low, most closely approximates the isotope effect of DsrAB solely reducing sulfite. We explore this time-dependence further in the

Supplementary Material for all sampled points on the reaction progress coordinate (f_{SO3}). Thus, for extracting the intrinsic isotope effect associated with enzymatic reduction of sulfite, we focused on data where $f_{SO3} > 0.85$. To do so, we have used our modified Rayleigh-type isotope distillation model in which we account for the production of reduced and oxidized sulfur within aqueous products trithionate and thiosulfate. Procedures for error propagation associated with these calculations are described in the Supplementary Material.

RESULTS

We tracked all S pools at each time point. Mass balance was satisfied within ±10% of the initially provided sulfite in every experiment, and within ±5% in 27 of 33 experiments (**Figure 2A**). The majority of this variance is due to analytical error in the sulfite quantifications. In experiments with the *D. vulgaris* DsrAB, the products were generated with a mean of 19% of the product sulfur forming thiosulfate and the remainder accumulating as trithionate (**Figure 2B**). This is consistent with previous reports (Drake and Akagi, 1976, 1978), and expected given the absence of active DsrC in these experiments. Some inactive DsrC does accompany the *D. vulgaris* DsrAB during isolation and purification (Oliveira et al., 2008a,b, 2011), however there is no means to recycle this component, and as such, it is not a functional part of the experiment. Therefore, the *in vitro* sulfite reduction reactions produce thionates rather than sulfide. In our experiments, sulfite was always in excess of H_2, and therefore was not limiting at any point.

To extend our studies to a different taxonomic form of the enzyme, we also experimented on the DsrAB from the thermophilic archaeon *A. fulgidus*. This enzyme operates at higher temperature and lacks DsrC in the complex (Schiffer et al., 2008). *A. fulgidus* experiments showed consistent loss of sulfite and accumulation of products between replicates at each time point. Unlike *D. vulgaris* DsrAB experiments, however, only small quantities of product were generated. From these experiments we were able to resolve a complete sample set (i.e., sulfite, sulfonate, and reduced S) from one time-point and partial sets from another (i.e., sulfite and sulfonate). Special efforts were made to correct data available on *A. fulgidus* experiments (see the Supplementary Material). The results using DsrAB from *A. fulgidus* are consistent with those of *D. vulgaris*, but with a large calculated uncertainty. We therefore focus our interpretations on the results from the *D. vulgaris* experiments.

We use the concentrations of sulfite, trithionate, and thiosulfate, as well as the isotopic compositions of each operationally defined product to solve for the fractionations associated with DsrAB. The calculated $^{34}\varepsilon_{DsrAB}$ for sulfite reduction by the *D. vulgaris* DsrAB is 15.3 ± 2.0‰ (2σ, **Figure 3**), where the concurrent fractionation associated with the generation of the sulfonate is −3.2 ± 0.8‰ (2σ). The $^{34}\varepsilon_{DsrAB}$ from *A. fulgidus* is generally consistent with the *D. vulgaris* experiments, yielding a reductive fractionation of 16‰ (2σ from 22 to 12‰) at 65°C. Large and asymmetric errors on the *A. fulgidus* data are the result of exceptionally small sample sizes, which also precluded the collection of ^{33}S data

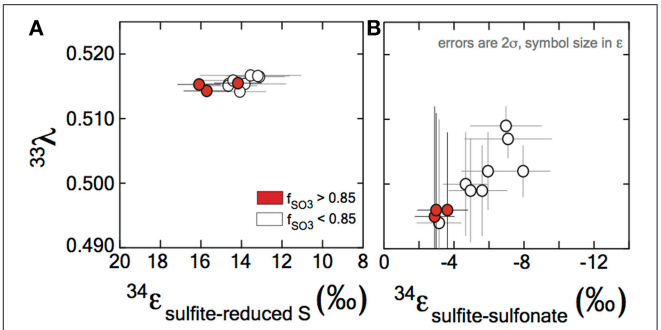

FIGURE 3 | Sulfur isotope fractionation during sulfite reduction by DsrAB. (A) The fractionation between sulfite and reduced sulfur (within trithionate and thiosulfate) facilitated by *in vivo* DsrAB. Initial values of $^{34}\varepsilon_{DsrAB}$ when f_{SO3} is >0.85 are near 15‰. A small amount of variability accompanies changes in f_{SO3} to <0.85. Data from *A. fulgidus* overlap *D. vulgaris* DsrAB data (see Figure A2 in the Supplementary Material). The minor sulfur isotope fractionation, $^{33}\lambda_{DsrAB}$, is stable near 0.515. **(B)** Fractionation factors for sulfonate generation are much smaller in $^{34}\varepsilon$ and carry the opposite sign. **(A,B)** Both the $^{34}\varepsilon$ and $^{33}\lambda$ evolve over the time course of the experiment, only after f_{SO3} < 0.85. Data and application to calculations are further discussed in the text.

(see the Supplementary Material). Together, these experiments demonstrate a broad consistency in fractionation by DsrAB over a wide range of temperatures (20 and 30°C for *D. vulgaris*, and 65°C for *A. fulgidis*) and across two Domains of life.

Fractionation of ^{33}S between sulfite and reduced sulfur by *D. vulgaris* DsrAB is reported as $^{33}\lambda_{DsrAB}$, with a calculated result of 0.5150 ± 0.0012 (2σ) over the initial range of f_{SO3}. The conversion of sulfite to sulfonate yielded a calculated $^{33}\lambda_{DsrAB}$ that changes as the reaction progressed, from 0.495 ± 0.017 (2σ) at $f_{SO3} > 0.85$, toward 0.510 at $f_{SO3} < 0.85$. The experimental error on $^{33}\lambda_{DsrAB}$ is inversely related to the magnitude of $^{33}\varepsilon_{DsrAB}$ (Johnston et al., 2007), thus is larger for sulfonate generation. We interpret the observed fractionation factors between sulfite and reduced S as representing the binding and reduction of sulfite by DsrAB. The fractionation associated with sulfonate production is more difficult to uniquely diagnose given the wide array of potential biotic and abiotic reactions.

DISCUSSION

Microbial sulfate reduction is a major process in the sulfur cycle and generates characteristic isotopic fractionations. These fractionations are critical in tracing the movement of sulfur within natural settings (marine and lacustrine). Determining the isotope effects associated with key enzymes in this pathway is critical to disentangling biological and physical controls on the distribution of sulfur isotopes among environmental pools of sulfur. In this study we provide the first constraints ($^{34}\varepsilon$ and $^{33}\lambda$) on the isotope effects associated with one such enzyme: DsrAB, the central redox enzyme in dissimilatory sulfate reduction. This experimental constraints generated herein provides insight and critical boundary conditions for understanding sulfur isotope fractionation by sulfate reducers. Fortunately, half a century of

research on sulfur isotope fractionation by MSR *in vivo* puts in place a series of useful observations that help to guide our interpretation as to the role of DsrAB. This in turn allows significantly greater access to the information locked in sulfur isotope records.

Fractionation at the Cellular Scale

The rich literature of whole cell isotope fractionation data associated with MSR lacks information about kinetic isotope effects associated with specific enzymes within the metabolism. Cellular-level observations include secular and spatial trends in sulfur isotope records attributed to changes in the environmental conditions at the site of MSR, and degree to which biogenic sulfide is preserved in marine sediments (Holland, 1973; Canfield and Farquhar, 2009; Leavitt et al., 2013). The environmental variables most commonly invoked to explain isotopic variability are aqueous sulfate and organic carbon concentrations (Goldhaber and Kaplan, 1975; Habicht et al., 2002; Bradley et al., 2015). Both of these variables ultimately contribute to the net reduction rate and carry independent biological thresholds, one of which ultimately becoming rate-limiting (Bradley et al., 2011, 2015). More specifically, variability in these substrates is manifested as changes in the cell-specific rates of MSR in both the laboratory and natural environment (Chambers et al., 1975; Goldhaber and Kaplan, 1975; Leavitt et al., 2013). In laboratory experiments and natural marine and lacustrine systems, volumetric sulfate reduction rates scale primarily as a function of the availability of sulfate relative to common electron donors like organic carbon (Chambers et al., 1975; Goldhaber and Kaplan, 1975; Sim et al., 2011b; Leavitt et al., 2013). Indeed, sulfate can be non-limiting even in environments with as little as μM sulfate (Nakagawa et al., 2012; Gomes and Hurtgen, 2013; Crowe et al., 2014; Bradley et al., 2015), assuming organic matter is more limiting to allow a fractionation to occur (Wing and Halevy, 2014; Bradley et al., 2015). Constrained whole cell (*in vivo*) laboratory experiments demonstrate that when electron donors are limiting, the magnitude of fractionation between sulfate and sulfide ($^{34}\varepsilon$) carries a nonlinear inverse relationship with cell-specific sulfate reduction rates (Harrison and Thode, 1958; Kaplan and Rittenberg, 1964; Chambers et al., 1975; Sim et al., 2011b; Leavitt et al., 2013). Thus, the range of isotopic compositions produced and preserved in natural environments are interpreted as an output of intracellular rates, which scales with enzyme activity associated with microbial sulfate reduction (Goldhaber and Kaplan, 1975; Leavitt et al., 2013).

In addition to following a rate relationship, fractionation in MSR isotope studies often approaches characteristic upper and lower fractionation limits. Recent experimental work at low sulfate reduction rates captures a $^{34}\varepsilon_{MSR}$ (the net isotope effect of microbial sulfate reduction) of nearly 70‰ (Canfield et al., 2010; Sim et al., 2011a). This magnitude of fractionation approaches the theoretical low temperature equilibrium prediction of 71.3 to 67.7‰ between 20° and 30°C (Tudge and Thode, 1950; Farquhar et al., 2003), inspiring research more directly comparing the biologically catalyzed reversibility of MSR enzymes and that of equilibrium (Wing and Halevy, 2014; see also Rees, 1973; Farquhar et al., 2003, 2008; Brunner and Bernasconi, 2005; Johnston et al., 2007; Mangalo et al., 2008; Bradley et al., 2011, 2015; Holler et al., 2011). These studies are fueled by the knowledge that direct (abiotic) equilibration between sulfate and sulfide at Earth surface temperatures is exceedingly slow, with a half-life of exchange estimated at 1.1×10^{10} (at 30°C) to 1.6×10^{12} years (at 20°C; these values are extrapolated from Ames and Willard, 1951). Thus, large fractionations between sulfate and sulfide at Earth surface conditions strongly suggests a role for biology, and likely multiple enzyme catalyzed steps with associated fractionations.

Most experiments with sulfate reducing microorganisms result in isotope fractionations much smaller than would be predicted from abiotic equilibrium estimates. Indeed, more than half a century of research and 648 observations from *in vivo* MSR experiments capture a median isotope fractionation of $^{34}\varepsilon_{MSR} = 16.1‰$ (in both sulfate and sulfite reduction experiments: **Figure 4**). In fact, half of experimental data fall between 10 and 22.5‰. This is consistent with the phenomenology of laboratory experiments being conducted at significantly higher sulfate reduction rates than occur in most natural settings. However, given that all these experiments occurred with the same biochemical network, any enzyme-level explanation for the range of fractionations observed at both high and low sulfate reduction rates must be internally consistent.

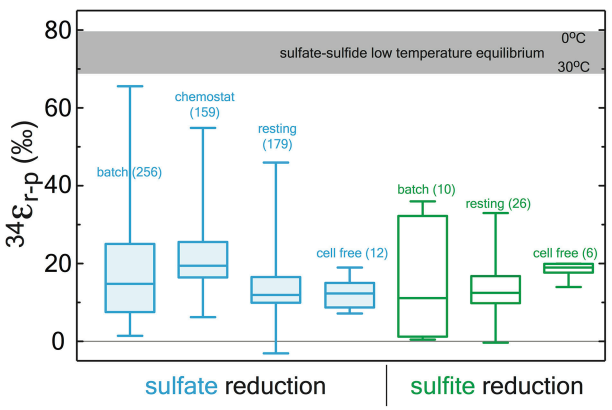

FIGURE 4 | A box and whisker plot of previously published sulfate (blue) and sulfite (green) reduction experiments. All data is binned by experimental approach. The whiskers reflect the entire range of the data, with the boxes reflecting the middle 50% of the data. The median of the data is represented by the bar dividing the box. The bar running across the top is a temperature dependent prediction based on low temperature thermodynamic equilibrium (Farquhar et al., 2003). The statistical method and output are detailed in the Supplementary Material along with the compiled data (http://dx.doi.org/10.6084/m9.figshare.1436115), where all compiled values are from the following sources: (Thode et al., 1951; Ford, 1957; Harrison and Thode, 1957, 1958; Jones and Starkey, 1957; Kaplan and Rittenberg, 1964; Kemp and Thode, 1968; Krouse et al., 1968; Chambers et al., 1975; McCready, 1975; McCready et al., 1975; Smock et al., 1998; Bottcher et al., 1999; Bolliger et al., 2001; Detmers et al., 2001; Farquhar et al., 2003; Kleikemper et al., 2004; Habicht et al., 2005; Johnston, 2005; Canfield, 2006; Hoek et al., 2006; Knöller et al., 2006; Johnston et al., 2007; Mangalo et al., 2007, 2008; Pallud et al., 2007; Davidson et al., 2009; Sim et al., 2011a,b, 2012, 2013; Leavitt et al., 2013, 2014).

Fractionation at the Intracellular Scale

As described above, a suite of enzymes and cofactors drives dissimilatory sulfate reduction. During the reduction of sulfate to sulfide, sulfur isotope effects are likely to result primarily from transformations that involve the making or breaking S related bonds. Initial steps in sulfate reduction, such as transport into the cell and activation via a reaction with ATP to generate APS (**Figure 1**; Fritz, 2002), do not involve the formation of new S linkages, and are not predicted to be associated with primary isotope effects. Influence on the expressed isotopic fractionation due to transport limitation is, however, conceivable. That is, the concentration of sulfate in the cell may influence the expression of downstream isotope effects, altering the net observed $^{34}\varepsilon_{MSR}$. Sulfate transporters may also induce an isotope effect associated with varying membrane fluidity or other strain-specific optima, in response to changing temperature (Kaplan and Rittenberg, 1964; Canfield, 2006), pH (Furusaka, 1961), or as environmental sulfate concentrations become metabolically limiting (Habicht et al., 2005; see discussion in Bradley et al., 2015).

Primary isotope effects are predicted where bonds are made or broken. APS reductase catalyzes a two-electron exchange that breaks a S-O bond during reduction of APS to generate free sulfite. From the crystal structure of ApsR (Fritz, 2002), it is apparent that the enzyme binds with the APS bound sulfur directly on a nitrogen in the FAD (flavin adenine dinucloetide) cofactor. The product sulfite is then available to interact with DsrAB. This heterodimeric enzyme binds sulfite in an active site containing siroheme. The formation of the Fe-S bond between siroheme and sulfite may be the critical reaction controlling isotope fractionation. Following this, sulfite is reduced by the transfer of two electrons to form a S^{2+} intermediate (Santos et al., 2015). Under *in vivo* conditions, the sulfur intermediate was suggested to be withdrawn from the DsrAB complex by the small transfer protein DsrC (Oliveira et al., 2008b; Venceslau et al., 2014), and this has been recently demonstrated (Santos et al., 2015). Under *in vitro* conditions, DsrC is generally absent, and the reduced sulfur in the active site may react with excess sulfite, forming thiosulfate and trithionate (**Figure 1**; Drake and Akagi, 1976). DsrC is independently regulated *in vivo* (Karkhoff-Schweizer et al., 1993), and generates the terminal sulfide from DsrAB bound sulfur derived from sulfite (Venceslau et al., 2014). The relative importance of this protein has only been realized in the last few years (Oliveira et al., 2008b; Venceslau et al., 2014), and has an unconstrained isotope effect.

In general, the magnitude of the thermodynamically predicted sulfur isotope effect scales positively with the number of bonds are made or broken (Tudge and Thode, 1950; Bigeleisen and Wolfsberg, 1958). As described above, sulfite reduction by DsrAB is a central enzyme in MSR, breaking three S-O bonds (Oliveira et al., 2008b; Venceslau et al., 2014), and therefore knowing the fractionation associated with this step is critical to any predictive MSR isotope model (c.f. Rees, 1973; Brunner and Bernasconi, 2005; Farquhar et al., 2007, 2008; Johnston et al., 2007; Bradley et al., 2011, 2015; Wing and Halevy, 2014). Our direct constraint on the fractionation imposed by sulfite reduction indicates that the published assignments of 25‰ (Harrison and Thode, 1958; Rees, 1973) and 53‰ (Brunner and Bernasconi, 2005) for DsrAB are significant over-estimates. It is perhaps not surprising, given that previous appraisals were generated through various indirect approaches (Harrison and Thode, 1958; Rees, 1973; Farquhar et al., 2003; Brunner and Bernasconi, 2005; Johnston et al., 2007). As previously stated (Chambers and Trudinger, 1979), the lack of direct experimental constraints on enzyme-specific fractionation factors leave significant uncertainty in metabolic, geochemical, and geological models that simply assign values to each enzymatic step.

Enzymatic Constrains (This Study)

Our measured $^{34}\varepsilon_{DsrAB}$ value for sulfite reduction (15.3 ± 2.0‰) is large enough to account for a large portion of the fractionations observed in published whole-cell MSR experiments over the last 65 years (median of 16.1‰, n = 648; **Figure 5**). As noted previously, laboratory experiments carry a strong bias toward higher rates of sulfate reduction, and as such, the data compilation should be viewed in this light. As most recently articulated through a series of chemostat experiments (Sim et al., 2011a; Leavitt et al., 2013), the consequence of elevated metabolic rate is a smaller relative $^{34}\varepsilon$. In isotope biogeochemistry, relationships like this often depend on the single slowest overall rate-limiting step within a metabolism (Mariotti et al., 1981; Hayes, 1993). The fractionation limit at high metabolic rates in cultures ($^{34}\varepsilon$ = 17.3 ± 1.3‰), marine sediments ($^{34}\varepsilon$ = 17.3 ± 3.8‰) and DsrAB are statistically indistinguishable (**Figure 5**).

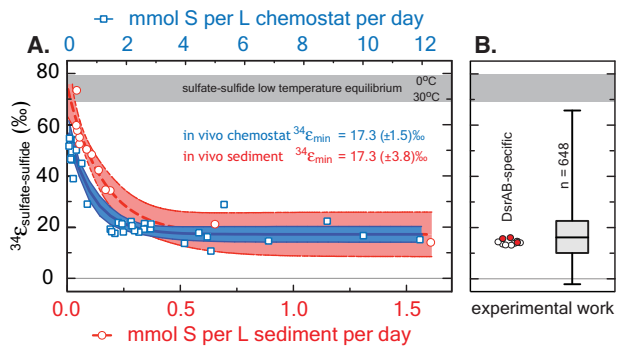

FIGURE 5 | A comparison between modern marine (environmental) and laboratory (experimental) S isotope fractionations, as a function of sulfate reduction rate. These data are further referenced to a statistical distribution of published experimental fractionation data. **(A)** Fractionation as a function of volumetric sulfate reduction rate from axenic continuous culture experiments (blue squares and regression; Leavitt et al., 2013) and modern marine sediments (red circles and regression; Goldhaber and Kaplan, 1975). Solid lines are mean values with shaded regions representing the 95% confidence interval around a non-linear regression. While the upper fractionation limits are offset, perhaps due to differences in biomass per volume of sediment vs. volume of chemostat, the limits approached at high reduction rates are statistically indistinguishable at 17.3‰. **(B)** The fractionation associated with DsrAB experiments, color-coded as in **Figure 3** and on the same isotope scale. Also included is a box-whisker treatment of all measured $^{34}\varepsilon$ (n = 648) sulfate and sulfite reduction experiments compiled in **Figure 4**. Here, the median value is 16.1‰, also statistically indistinguishable from chemostat and modern marine sediments limits at elevated rates of sulfate reduction. Included for reference is the theoretical sulfate-sulfide equilibrium fractionation (gray bar) for 0–30°C (Farquhar et al., 2003).

This similarity is consistent with DsrAB as a rate-limiting step explaining the majority of observed fractionation (**Figure 5**). However, this interpretation omits complexity associated with the metabolic network.

This raises an essential question: how does the DsrAB constraint change our understanding of the possible range of fractionations imposed by MSR? For instance, if we assume that DsrAB is the slowest reaction in MSR, then the metabolic steps preceding sulfite ($SO_4^{2-} \Leftrightarrow$APS $\Leftrightarrow SO_3^{2-}$) will necessarily approach equilibrium (Wing and Halevy, 2014). The thermodynamic predictions would then require an accompanying fractionation approaching 25‰ between sulfate and sulfite at biologically relevant temperatures (the equilibrium fractionation estimate; Farquhar et al., 2003). At its simplest, this effect would be additive with that of DsrAB (25 + 15.3‰, or 40.3‰), which encompasses a majority of experimental MSR isotopic fractionations. However, the lower plateau in fractionation approached at high rates, stemming from the calculations using both modern marine sediment and chemostat data (see the Supplementary Material)—is less than half of this magnitude. That is, the lower plateaus for *in vivo* fractionation at high rates of 17.3‰ allows only a ∼2‰ fractionation partitioned among these upstream steps, if in fact DsrAB is fully expressed. This smaller "upstream" kinetic fractionation is, however, consistent with the few loose estimates from crude cell extracts and resting cell studies (i.e., not purified enzymes), which putatively suggests a $^{34}\varepsilon$ of 4–15‰ for the cumulative activation of sulfate to APS and reduction to sulfite (Ford, 1957; Kemp and Thode, 1968). This may suggest that the sulfate-sulfite conversion (*in vivo* and *in vitro*) reflects a predominately kinetic (rather than equilibrium) control. This requires, however, we loosen the degree to which DsrAB is called upon to fully control the net MSR isotopic fractionation, invoking some delicate balance between upstream reactions and that of DsrAB, but maintaining the model where enzyme kinetics (especially DsrAB) will win out over equilibrium effects as sulfate reduction rates move from low to high.

An alternate explanation is that APS reductase (ApsR) is the rate-limiting step under sulfate replete conditions (Rees, 1973). If this is the case, fractionation imposed by DsrAB is unexpressed, as it is downstream of ApsR (Rees, 1973; Hayes, 2001). If fractionation associated with APS reductase is near 17‰, it could alone account for most of the observed fractionation observed at high sulfate reduction rates. The fractionation imposed by ApsR has not been directly measured, though can be preliminarily estimated from the discussion above. However, evidence against ApsR as the rate-limiting step is shown by studies indicating reversibility of the ApsR (Peck, 1960) and the sulfate reduction pathway (Chambers and Trudinger, 1975; Holler et al., 2011). Recent studies using oxygen isotopes as tracers have demonstrated that some intracellular sulfite is oxidized *in vivo* back to sulfate (Mangalo et al., 2007, 2008; Einsiedl, 2008; Farquhar et al., 2008; Turchyn et al., 2010). These studies demonstrate that sulfite re-oxidation is commonplace in MSR and often quantitatively significant (Antler et al., 2013). This reoxidation is inconsistent with ApsR being rate-limiting under the range conditions tested.

Any explanation for the net MSR isotopic fractionation must also account for the large fractionations observed at low sulfate reduction rates. These large fractionations are common in nature, and require another type of mechanism. These isotopic fractionations approach but do not reach the theoretical equilibrium values for sulfur isotope exchange between sulfate and sulfide (**Figures 4**, **5**; Tudge and Thode, 1950; Farquhar et al., 2003; Johnston et al., 2007). In this context, further analysis to understand intracellular thermodynamics is critical (the redox pairs responsible for various reactions, see Wing and Halevy, 2014), along with measurements of the intrinsic isotope effects of other key enzymes in the metabolic network, including ApsR and DsrC. In that sense, this study represents a key first step.

In parallel to examining the $^{34}\varepsilon$ effects, measuring minor S isotope ($^{33}S/^{32}S$) fractionation provides additional information about the class of reaction mechanism associated with *in vitro* DsrAB activity. In our experiments, the conversion of sulfite to sulfonate carries a $^{33}\lambda$ of from ∼0.496 (±0.012, 2σ), evolving toward 0.510 as the reaction proceeds. Sulfite reduction via DsrAB has an invariant $^{33}\lambda$ of 0.5150 (±0.0012, 2σ). In cases where $^{33}\lambda$ is 0.515, a purely equilibrium fractionation is often inferred but not required, while values less than this require kinetic effects (Young et al., 2002; Farquhar et al., 2003). In this framework, *in vitro* sulfonate formation falls under kinetic control, while formation of reduced S could be interpreted as a kinetic or equilibrium reaction. Thus, specific predictions for the DsrAB enzyme require more detailed modeling of the structure and function of the DsrAB enzymatic active site. This level of analysis—where inroads joining empirical work with theory are constructed—is present in analogous systems (Karsh et al., 2012), but absent within the S cycle. Nonetheless, the work here provides the only triple-isotope constraints on enzyme-specific fractionation factors in both MSR and the global biogeochemical S cycle. Further, this approach may prove useful in other enzymatic systems where elements with ≥3 stable isotopes are involved (e.g., O, Fe, Ca, Mg, Se, Zn, and Mo).

CONCLUSIONS

Direct constraints on enzymatic isotope effects, when placed in context of laboratory and field observations, represent a key step toward improving our understanding of how environmental factors come to control biochemical sulfur isotope fractionations in nature. Experimental results indicate that the kinetic isotope effect generated by dissimilatory sulfite reductase, the enzymatic core of MSR, generates less than a quarter of the maximum fractionation observed in sulfate reduction experiments and modern marine sediments. However, the $^{34}\varepsilon_{DsrAB}$ aligns nicely with the vast majority of experimental data generated over the last 65 years, as well as chemostat and marine sediment studies sampling high rates of sulfate reduction. The consistency between these published fractionations and the DsrAB isotope effect suggests a fundamental role of this enzyme in setting sulfur isotope compositions. This work highlights the need for further consideration of the allied enzymes in MSR and the likelihood of abiological (and/or equilibrium) effects as microbial sulfate reduction rates slow. Though questions remain,

placing quantitative constraints on a core component of sulfate reduction—DsrAB—represent a fundamentally new direction in exploring experimental and environmental sulfur isotope records today and throughout Earth history.

DETAILED METHODS

Operational Definitions of S Moieties

In this study we measured the concentrations of three pools: sulfite, trithionate, and thiosulfate; hydrogen sulfide was not detected. We measured the major and minor sulfur isotopic compositions of three operationally defined pools: "reactant" sulfite (initial and residual), product "sulfonate," and "reduced product" S. What we refer to as the pooled product "sulfonate" sulfurs are known in inorganic chemistry as sulfuryl groups (O_2S-X_2), where one of the X's represents an O^-/OH and the other a S in oxidation state 0 (trithionate) or −1 (thiosulfate), meaning the outer sulfuryl-S's are in approximately oxidation state +5 (thiosulfate) or +4 (trithionate), with initial and residual reactant sulfite sulfur in the standard +4. The sulfonate S differs from sulfite S in that it is bound to either an approximately −1 valent sulfur in thiosulfate (S-$S(O)_{32-}$) (Vairavamurthy et al., 1993) or as two sulfonates each bound to one sulfur of valence approximately 2+, in trithionate ($(O_3S$-S-$SO_3)^{2-}$). In this study we refer to the 0 and −1 oxidation state sulfurs from trithionate and thiosulfate, respectively, as the "reduced product" S pool. They are grouped by our operational extraction (see below). For explicit definitions and nomenclature refer to the "IUPAC Goldbook" (McNaught and Wilkinson, 1997).

Enzyme Purification and *In vitro* Experiments

DsrAB Isolation and Purification

DsrAB was purified from *Desulfovibrio vulgaris* Hildenborough (DSM 644) and *Archaeoglobus fulgidus* cells grown in a 30 or 300 L batch culture in a modified lactate/sulfate medium (Oliveira et al., 2008a) at iBET (Instituto de Biologia Experimental Tecnológica; www.ibet.pt), grown at 37 or 80°C, respectively. The soluble cell fraction was obtained as previously described (Le Gall et al., 1994; Oliveira et al., 2008a). All purification procedures were performed under atmosphere at 4°C using an AKTA FPLC (Amersham Biotech Pharmacia) with two buffers, (A) 20 mM TrisHCl and (B) 50 mM TrisHCl with 1 M of NaCl (both pH 7.6 and containing 10% glycerol). Buffer (A) was used to equilibrate the columns and buffer (B) to generate the ionic strength gradient. The soluble cell fraction was loaded into a Q-Sepharose fast-flow (XK50/30) column, and a stepwise salt gradient applied, with the DsrAB-containing fraction eluting at 300 mM NaCl. The characteristic DsrAB ("desulfoviridin") absorption peak at 630 nm was used to track the protein, as previously described (Wolfe et al., 1994; Marritt and Hagen, 1996). DsrAB-containing fractions were then loaded into a Q-Sepharose fast-flow (26/10) column and eluted in 250 mM NaCl. To verify enzyme purity, the final DsrAB-containing sample was analyzed by 12% SDS-PAGE gel electrophoresis. DsrC is present in the DsrAB preparation from *D. vulgaris*, but remains functionally inactive during *in vitro* assays as previously described (Oliveira et al., 2008b), and also due to the lack of DsrMKJOP (Venceslau et al., 2014). Thus, we refer only to the "DsrAB" fraction in the *D. vulgaris* experiments. In the *A. fulgidus* experiments, DsrAB is free of any DsrC. Protein was quantified by the method of Bradford (Bradford, 1976). The *Desulfovirio gigas* [NiFe] hydrogenase used in all assays was purified as described previously (Romão et al., 1997).

To ensure the activity of purified DsrAB was not strongly influenced by the high initial concentration of sulfite used in the fractionation experiments (10 or 15 mM), we performed small-volume kinetic assays under the same conditions as for isotope measurements. Sulfite alone was measured by HPLC on monobromobimane (MBBr) derivatized samples (Newton et al., 1981). Once the sulfite concentrations for each initial and final (0 and 2 h) time points were sampled, derivatized, measured and calculated, we applied a non-linear regression formulated from the standard Michaelis-Menten equation, solving for the V_{max} and K_m.

D. vulgaris DsrAB *In vitro* Fractionation Experiments in Detail

To determine the DsrAB-specific S isotope fractionation factors we designed and executed a series of batch (closed-system) sulfite reduction experiments. The key considerations in experimental design are: (i) to provide enough sulfite at t_0 to ensure we generate significant enough quantities of all the product pools so we can measure, at high precision and accuracy, and at multiple [time] points on *f*, the multiple S isotopic composition of each pool (i.e., 2 μmols of S per pool per SF_6 measurement on the DI-IRMS, which means 2 μmols per fluorination reaction); (ii) to provide the proper reaction conditions to allow DsrAB optimal activity for goal i (pH = 7.1, T = 20 or 31°C); (iii) to ensure hydrogenase activity is not inhibited by the pH chosen (optimum above pH 7.5, activity significantly depleted below pH 6.5, so we chose pH 7.1, to account for optima of both DsrAB and [NiFe]-Hydrogenase); and finally (*iv*) to ensure the sulfite to hydrogen ratio favors sulfite over reductant capacity (i.e., pH_2 in the headspace relative to $[sulfite]_{t0}$), such that no more than 75% of t_0 sulfite is consumed to all products, and less than 50% to the reduced S (dictated by the amount of H_2 in the headspace. Finally, (v) determining the sampling interval to ensure proper distribution of points along *f*, such that applying a closed system distillation model is possible, and statistically robust. Data plotted in **Figure 3** represents experimental results that met all of these conditions. The full experimental results (33 experiments) are contained as a supplemental file (http://dx.doi.org/10.6084/m9.figshare.1436115).

All experiments were prepared in an anaerobic chamber. *In vitro* reactions were carried out in 100 mL acid-washed, autoclave-sterilized, borosilicate glass bottles sealed with butyl-rubber septa and aluminum crimps. Each bottle contained 50% reaction buffer and 50% gaseous headspace. This was done to sufficient H_2 was present in the headspace to reduce at most 50% of the sulfite, based on an estimate using Henry's law and available solubility constants for H_2 at the given preparation temperatures and headspace pressures. During manipulations in the anaerobic chamber the chamber gas was initially 95:5 N_2:H_2. Upon

removing the reaction mixture-filled bottles from the chamber, these were capped and crimped, and headspace completely exchanged with deoxygenated 100% Ar, then finally exchanged for 100% H_2 to initiate the experiments. Experimental buffer is 50 mM phosphate buffer (KP*i*) prepared at pH 6.9 ± 0.05, with final pH is 7.1 ± 0.05 following the addition of the stock Na_2SO_3 solution (the reaction is therefore initiated at 7.1). All reaction solutions contained the following: 50 mM KP*i* buffer (final pH 7.1 ± 0.05), 10 or 15 mM sodium sulfite, 0.832 mM methyl viologen, 242 nm or 315 nm of *D. vulgaris* DsrAB (calculated to give the same activity depending on the DsrAB aliquot selected), and 8.25 nm [NiFe] hydrogenase (297 U/mg). All experimental mixtures and reagents were prepared in previously boiled 18.2 MΩ water, cooled under O_2-free N_2.

A. fulgidus DsrAB *In vitro* Fractionation Experiments in Detail

To extend our studies to a different taxonomic form of the enzyme, we used DsrAB from the thermophilic archaeon *A. fulgidus*. This enzyme operates at higher temperature and does not have DsrC present in the complex (Schiffer et al., 2008). The results from these experiments are significantly limited compared to those with *D. vulgaris*, due to too few time points to apply the closed-system model (specifically due to significantly low sample sizes of reduced S for isotope measurements, note the effort made to correct the two data points on *A. fulgidus* reduced-S). Nevertheless, the results obtained are comparable, when considering the measured $\delta^{34}S$. The values for these experiments are presented with *D. vulgaris* values in **Figure A2**.

A. fulgidus DsrAB experiments were conducted 15 mM initial sulfite and 65○C, and showed consistent loss of sulfite and accumulation of products between replicates. We selectively precipitated, separated, and directly measured the ^{32}S-^{33}S-^{34}S-^{36}S compositions from the residual reactant ("sulfite S") and the "sulfonate S" ($(SO_3)_x$). Only the $^{34}S/^{32}S$ compositions of the "reduced product S" $[(S)_y]$ reservoirs were measured (again, due to significantly small reduced-S samples recovered). From these experiments we were able to get a complete set of samples (i.e., sulfite, sulfonate, and reduced S) from one time-point and partial sets from another (i.e., sulfite and sulfonate). We are unable to calculate the $^{34}\varepsilon_{DsrAB}$ for *A. fulgidus* directly using our model of sulfite reduction experiments due to the dearth of time points (points on *f*). However, the *A. fulgidus* isotope values agree with those measured sulfite, sulfonate, and reduced S moieties for *D. vulgaris* (**Figure A2**). This general agreement between *D. vulgaris* and *A. fulgidus* DsrAB, independent of temperature or phylogenetic origin is perhaps unsurprising, given that previous theoretical predictions deemphasize the role of temperature in determining the magnitude of *kinetic* isotope effects (Bigeleisen and Wolfsberg, 1958). Furthermore, these enzymes tightly share active site structures (Oliveira et al., 2008b; Parey et al., 2013).

Analytical Methods and Data Handling

Quantification of Dissolved Species

To quantify sulfite and bisulfite concentration in solution we adapted a protocol to quantify SO_2 dissolved in water (Grant, 1947), referred to as the "Fuschin" assay from here foreword. Our protocol is specific to the *in vitro* DsrAB assay conditions. It was determined that matrix matching between samples and standards and the exclusion of oxygen is critical to a successful and reliable assay. Furthermore, we determined trithionate, thiosulfate, sulfate, and zinc sulfide solids do not interact with this color-reagent in the assay. The Fuschin assay is useful over a range of 0–40 nanomoles of sulfite in the final assay volume of 1 mL. Standards of sodium sulfite (Na_2SO_3 anhydrous, analytical grade) were prepared immediately before the assay is performed in deoxygenated water (boiled and degassed with N_2) or KP*i* buffer. The reaction mixture is composed of 0.04% w/v Pararosaniline HCl (analytical grade) in 10% H_2SO_4 (analytical grade) v/v, prepared stored in an aluminum-foil wrapped tube or amber-glass bottle at 4°C; and 3.7% formaldehyde (HCHO) prepared fresh each day by diluting 37% (stock) formaldehyde 1:10 water. The reaction is performed on the bench working under N_2 flow, or in an anaerobic chamber. A detailed step-by-step protocol is available in Leavitt (2014).

Trithonate and thiosulfate were measured by a modified cyanolysis protocol (Sörbo, 1957; Kelly et al., 1969; Kelly and Wood, 1994). We primarily employed the method of Kelly and Wood (1994) modified in the following manner: the reaction volumes were reduced to 10 rather than 25 mL's (still in volumetric flasks) and we used nitric rather than perchloric acid. Nitric acid was used in the original version of this method (Sörbo, 1957), allowing us to avoid the significant hazards of working with significant volumes of perchloric acid. Samples were added to the reaction buffer to fit within the range of ferric thiocyanate standards (prepared from potassium thiocyanate as a simple standard and thiosulfate as a reaction standard) from 5 to 25 μM (final concentration in the 10 mL reaction), as well as "blanks" prepared from the *in vitro* assay reaction buffer (50 mM potassium phosphate buffer at pH 7). This is typically 400 μL of *in vitro* solution added to the 10 mL cyanolysis reaction, in duplicate per method (2X thiosulfate determinations and 2X trithionate determinations). A detailed step-by-step protocol is available in Leavitt (2014).

For sulfide quantifications, we preserved samples in zinc acetate (2% w/v) from each closed system reaction, using a modified Cline method (Cline, 1969). Analytical grade sodium sulfide (>98.9% Na_2S*9H_2O) was used as the standard, and prepared in deoxygenated (boiled and N_2-sparged) *in vitro* reaction buffer, by precipitating the sulfide with excess zinc acetate (anhydrous), mimicking our sampling protocol. A detailed step-by-step protocol is available in Leavitt (2014). In all samples no sulfide was detected above the determined detection limit of 6.25 μM. From the literature reports where membrane fractions were omitted (Drake and Akagi, 1978), signifying a lack of DsrC re-cycling mechanism (Oliveira et al., 2008b; Bradley et al., 2011), we expected little to no sulfide. This is further supported by the closure of S mass balance at each time-point from each experiment, within analytical error (see main text). Blanks were prepared identically to those in the cyanolysis protocol.

Sample Preparation for S Isotope Analysis

All S-bearing samples for S-isotope analyses (ultimately as SF_6 and/or SO_2) were removed from the *in vitro* reaction solution (50 mM potassium phosphate) following a sequential precipitation protocol, inspired by that of Smock et al. (1998). Our protocol reflects our specific experimental setup and the pools we aimed to isolate and purify: sulfite (and any trace sulfate), sulfonate, and reduced product S. Samples of the residual reactant (sulfite) and pooled products (reduced product S and sulfonate S) were removed from the *in vitro* reaction mixture by sequential precipitation and filtration or centrifugation to isolate solid-phases $Ag_2S_{(s)}$ (reduced product), $BaSO_{3(s)}$ (sulfite), $BaSO_{4(s)}$ (sulfonate) by the extraction scheme modified from our recent work (Leavitt et al., 2014) and detailed elsewhere (Leavitt, 2014). Samples were captured as $BaSO_{3(s)}$, $BaSO_{4(s)}$, or $Ag_2S_{(s)}$, respectively. Sub-samples of the reduced product Ag_2S were directly fluorinated (after the below washing steps were carried out to ensure clean Ag_2S), or in the case of the sulfonate S-pool, collected from the AVS residue and converted from $BaSO_4$ to Ag_2S by the method of Thode (Thode et al., 1961), according to the protocol we recently published (Leavitt et al., 2013). Novel to this study: all sulfite samples (reacted as $BaSO_{3(s)}$) were oxidized with peroxide prior to "Thode"-reduction (detailed protocols for these methods are available in Leavitt, 2014). All samples entering the elemental analyzer isotope ratio mass spectrometer (EA-IRMS), and combusted to and analyzed as SO_2, are prepared as dry $BaSO_{3(s)}$, $BaSO_{4(s)}$, or $Ag_2S_{(s)}$. All samples for quadruple S isotope analysis enter the fluorination line as pure dry $Ag_2S_{(s)}$.

Major S-isotope ($^{34}S/^{32}S$) Ratios Measurements

Continuous flow isotope ratio mass spectrometric (CF-IRMS) measurements of the three S-bearing pools of interest, sulfite, sulfonate and reduced product S, were performed as follows: 0.4 mg (±0.05 mg) $BaSO_3$, $BaSO_4$, or Ag_2S were converted to SO_2 by combustion at 1040°C in the presence of excess V_2O_5 (Elemental Analyzer, Costech ECS 4010) and analyzed by continuous flow isotope ratio mass spectrometry ($SD = \pm 0.3‰$; Thermo-Finnegan DELTA V Plus). All samples yielded clean chromatography and most m/z 66 amplitudes (corresponding primarily to the $(^{16}O^{34}S^{16}O)^+$ ionization product) within the range of in-run standards (IAEA: S1, S2, and S3 for Ag_2S or SO5, SO6, and NBS-127 for $BaSO_4$ and $BaSO_3$). Some sulfite precipitates ($BaSO_{3\_sulfite}$), though not any of the sulfate or sulfide precipitates ($BaSO_{4\_sulfonate}$ or $Ag_2S_{\_reduced\ product}$) produced atypical weight to m/z 66 response to what we regularly note with lab standards of $BaSO_3$ or $BaSO_4$ – specifically the signal was less than predicted, likely due to occlusion of phosphates (from the *in vitro* reaction buffer) in the barium sulfite matrix. As a result, we use the m/z 66 to $BaSO_3$ weight ratio (mg of $BaSO_3$ per unit area of the m/z 66 peak) to calculate the desired sample weight to achieve standard signal size, re-weighed and re-combusted/measured the requisite samples, and in all cases achieved m/z 66 peak areas in the range of our IAEA $BaSO_4$ and in-house $BaSO_3$ standards. Each standard is measured at least 4x in-run and each sample 2-3x (when sufficient sample is available). This simplifies the scale-conversion calculation for taking samples referenced in-run to in-house standard tank gas ($HAR1_{SO2}$) and ultimately to the international reference frame (V-CDT).

Multiple S-isotope ($^{33}S/^{32}S$, $^{34}S/^{32}S$, $^{36}S/^{32}S$) Ratio Measurements

Duel-inlet (DI-IRMS) measurements of all four stable S isotopes (^{32}S, ^{33}S, ^{34}S, ^{36}S) from the three S-bearing pools of interest, sulfite, sulfonate and reduced product S, were performed as previously described (Leavitt et al., 2013, 2014). Briefly, all samples for quadruple S-isotope analysis, prepared dry and clean Ag_2S (described above), were fluorinated under 10X excess F_2 to produce SF_6, which is then purified cryogenically (distilled at −107°C) and chromatographically (on a 6′ molecular sieve 5 Å inline with a 6′ HayeSepQ 1/8″-stainless steel column, detected by TCD). Purified SF_6 was measured as SF_5^+ (*m/z* of 127, 128, 129, and 131) on a Thermo-Finnegan Scientific MAT 253 (SD: $\delta^{34}S$ ±0.2, $\Delta^{33}S$ ±0.006‰, $\Delta^{36}S$ ±0.15‰). All isotope ratios are reported in parts per thousand (‰) as experimentally paired sulfates and sulfides measured. Long-term running averages and standard deviations are calculated from measures of IAEA standards: S1, S2, S3 for sulfides or NBS-127, SO5, SO6 for sulfates. Isotope calculations and notation are detailed in the text. Standard deviations for each value is estimated as reported previously (Johnston et al., 2007) with previous inaccuracies in the transcription corrected here.

Scale-Compression Correction Calculations for Small S Samples

Experiments with *A. fulgidus* yielded small amounts of product (0.35 to 0.01 mg), which required additional data handling during isotope analysis. Given the small size of these samples, we ran each sample only once and bracketed the samples (n = 2) with a series of standards: IAEA S1, S2 and S3 (n = 16, 14, and 14, respectively) run over a size series that captured the sample sizes, all by CF-IRMS only. As expected, we observed that the measured isotopic composition of the standards varied non-linearly as a function of signal intensity (monitored as peak integrated areas and peak intensities on m/z 64 and 66 for SO_2^+ and 48 and 50 for SO^+). The size dependence on the isotopic composition (handled as ^{50}R and ^{66}R, which are the 50/48 and 66/64, respectively) scale compression is calculated as a proportional change. For SO (*correction factor* in **Figure A3**) it scales as: $\left|\frac{^{50}R_{predicted} - ^{50}R_{measured}}{^{50}R_{predicted}}\right|$. We focus on SO here as these samples yielded sharper chromatography on slightly different sized signals (due to resistor differences between SO and SO_2 cups $-$ 3×10^{10} Ω and 1×10^{10} Ω respectively). Thus, using the three IAEA standards, we developed a correction whereby we solve (in the standards) for the non-linear features of the data as it relates to signal intensity (here monitored as the peak integrated area on mass 48 $-$ ^{32}SO). This is shown in **Figure A3**. After this correction is applied to $^{50}R_{measured}$, SO data is converted to an SO_2 scale (see **Figure A3**), which is a linear transfer function again derived from IAEA standard data. The final correction places all the data (now on a SO_2 scale against in-house reference SO_2 tank gas) to the V-CDT scale. To review, we perform the following steps (1) correcting the ^{50}R on SO for sample size, (2)

convert ^{50}R to ^{64}R (against tank gas), and finally (3) convert all data to a VCDT scale.

The largest source of error in this treatment is associated with the sample size correction. As such, we propagate the error associated with the fit in **Figure A3** to determine the uncertainty in the final isotope value. As expected, for small samples this error is quite large (**Figure A2**), with the value decreasing in absolute magnitude as signal intensity (peak integrated area) increases. We also compare these error estimates to the calculated shot noise for this measurement (pink line in **Figure A3d**). As is presented below, our regressed error is in excess of the shot noise limit. Similarly, the error on the population of standards that were used in deriving this fit is 1‰ ($n = 44$).

The Closed-System Distillation Model for a More Complex Network

There exists the possible mixing of multiple fractionation factors later in the experiment ($f < 0.85$). The approach outlined in the main text yielded results in which the observed fractionation factor between sulfite and reduced pools appeared to change as a function of *f*, when $f < 0.85$—that is, later in the reaction, when back-reactions are more likely (**Figure A4**). One explanation for this apparent behavior is that the reduced pool is not the product of a single set of reactions but of multiple reactions. The most plausible explanation for this is that some fraction of the reduced pool is derived from the sulfonate pool rather than being derived solely from sulfite, particularly later in the *in vitro* experiment (i.e., at values of $f < 0.85$). Previous work (Drake and Akagi, 1977, 1978; Parey et al., 2010) has demonstrated that DsrAB is capable of reducing trithionate to thiosulfate, and thiosulfate to sulfite and sulfide, which was confirmed with the *D. vulgaris* enzyme.

We can constrain the magnitudes of the fractionation factor related to the conversion of the sulfonate to reduced S through the following steps. First, utilizing the framework given above to solve for α_{red} for the time points where *f* is nearest to 1. As these measurements are obtained at the lowest concentrations of product, we assume that this result gives an estimate for α_{red} that reflects the production of reduced S from sulfite only, with minimal input of reduced S derived from sulfonate. Second, we write an equation for R_{red} as a function of α_{red}, R_{SO3}, and R_{ox}:

$$R_{red} = X_{SO3}\alpha_{red}R_{SO3} + (1 - X_{SO3})\,\alpha_{unk}R_{ox} \tag{7}$$

where X_{SO3} is the fraction of R_{red} generated directly from sulfite and α_{unk} is the unknown fractionation factor between R_{ox} and R_{red}. This equation is then rewritten and solved for α_{unk} as a function of the other parameters over a range of values of X_{SO3} (0.01–0.99). This does not yield a unique solution for the unknown fractionation, but constrains its value given the relative importance of the contribution to the reduced sulfur pool of both sulfonate and sulfite. We assume that the *relative* contribution of the secondary reaction is invariant over the course of the reaction, thereby manifesting as no change in *j*.

Error Propagation Calculation for the Closed System Model Estimates

The error associated with calculations of $^{33}\lambda$ (approximately the slope of a δ^{33}S vs. δ^{34}S line) is highly sensitive to the length of the line (total ^{34}S range, $^{34}\varepsilon$) and modestly related to the residual around a mass-dependent theoretical prediction (the standard deviation on Δ^{33}S is often used here (Farquhar et al., 2003; Johnston et al., 2007). To approximate the standard deviation (σ) associated with our $^{33}\lambda$ calculation, we propagate our measurement errors (δ^{34}S, concentration, etc.). We keep with the presumption that mass-dependence will dictate the δ^{33}S, once the new δ^{34}S is calculated. This stems from the fact that the error in δ^{34}S and δ^{33}S are highly correlated, meaning that the error in Δ^{33}S is significantly smaller (0.008‰) than that for δ^{33}S (0.1‰). As our fractionation factor model is based on a closed-system distillation equation (see above), we perform an error propagation on an equation of the form: $R_f = (R_0)(f^{(\alpha-1)})$, where we are most interested in accounting for the analytical errors on the isotope measurement (σ_R, 0.2‰/1000) and the uncertainty on *f*. The second term is critical here as we are independently determining *f* from concentration measurements in the experiment, with a standard deviation on sulfite concentration measurements of 3%. We use this value moving forward as a metric of σ_f. To simplify the presentation, we let $X = (\alpha - 1)$ and $Z = f$. Following typical error propagation for power law and multiplicative relations (Bevington and Robinson, 2003 p. 43–46), we find:

$$\sigma_Z/Z = \sqrt{\left(X\sigma_f/f\right)^2} \tag{8}$$

which then can substitute into the final form of:

$$\sigma_{R_f}/R_f = \sqrt{\left(\sigma_Z/Z\right)^2 + \left(\sigma_{R_0}/R_0\right)^2} \tag{9}$$

The $\eta\varepsilon\sigma_{Rf}$ is then converted into ‰ units (through multiplying by 1000) so that it can be inserted into the updated (Johnston et al., 2007) error equation for $^{33}\lambda$, presented here:

$$\sigma_\lambda = \sqrt{\sigma^2_{\Delta^{33}S} * \left(\frac{\partial\lambda}{\partial\Delta^{33}S}\right)^2 + \sigma^2_{\delta^{34}S} * \left(\frac{\partial\lambda}{\partial\delta^{34}S}\right)^2}, \tag{10}$$

which can be broken down into:

$$\frac{\partial\lambda}{\partial\Delta^{33}S} = \left\{\frac{1}{\ln\left(\frac{\delta^{34}S}{1000}+1\right)} * \frac{1}{\left(\frac{\Delta^{33}S}{1000} + \left(\frac{\delta^{34}S}{1000}+1\right)^{\lambda_{RFL}}\right)} * \frac{1}{1000}\right\} \tag{11}$$

and

$$\frac{\partial\lambda}{\partial\delta^{34}S} = \left\{\frac{1}{\ln\left(\frac{\delta^{34}S}{1000}+1\right)} * \frac{1}{\left(\frac{\Delta^{33}S}{1000} + \left(\frac{\delta^{34}S}{1000}+1\right)^{\lambda_{RFL}}\right)} * \lambda_{RFL}\left(\frac{\delta^{34}S}{1000}+1\right)^{\lambda_{RFL}-1} * \frac{1}{1000}\right\} +$$

$$\left\{ \ln\left(\frac{\Delta^{33}S}{1000} + \left(\frac{\delta^{34}S}{1000} + 1\right)^{\lambda_{RFL}}\right) * \frac{-1}{\left(\ln\left[\frac{\delta^{34}S}{1000} + 1\right]\right)^2} * \frac{1}{\frac{\delta^{34}S}{1000} + 1} * \frac{1}{1000} \right\}. \quad (12)$$

As noted above, the error on lambda σ_λ is dependent on the δ^{34}S and Δ^{33}S. The subscript *RFL* represents the reference fractionation line, which for $^{33}\lambda$ is 0.515, and for $^{36}\lambda$ is 1.90. Data for δ^{36}S are not discussed in the text, as they yield the same conclusions as δ^{33}S, but are included here in Dataframe S1 (https://github.com/bradleylab/DsrAB_enzyme_models).

In total, this leaves our error estimate a function of the following five variables: $^{34}\varepsilon$, σ_R, f, σ_f, and α. The final error is not an evenly weighted sum of these variables, and in the case presented here, most heavily influenced by the error in concentration data (σ_f). A sensitivity analysis (**Figure A6**) on this exercise demonstrates that the errors in f far outweigh the analytical uncertainty in a measurement of R, and dominate the magnitude of the final σ_{Rf}.

Data Compilations and Statistical Analysis

Compilation and Statistical Analysis of Pure-Culture MSR Fractions

To place our DsrAB enzyme-specific fractionation factor in context with the previous 65 years of pure-culture experimental work, we compile all available observations from studies using axenic cultures of MSR (**Figure 4**), in the following experimental systems: *batch* (closed-system, *in vivo*, whole-cell), *chemostat* (open-system, *in vivo*, whole-cell), *resting* (closed-system, *in vivo*, whole-cell, not growing), *cell-free* (closed-system, *ex vivo* crude cell extracts, not growing). From these four types of experiments we further subdivide experiments into where sulfate was reduced to sulfide or sulfite was reduced to sulfide. We count each experimental determination ($^{34}\varepsilon_{r-p}$) and compile them all in the supplemental data files (http://dx.doi.org/10.6084/m9.figshare.1436115), from experiments where less than 10% of the reactant S-species was consumed. Herein we calculate and present column statistics (box-whisker plots in **Figure 4**) using *Prism5c* (GraphPad, San Diego, CA). The key finding here is that the majority of the means from each set of experiments is significantly less than the previous estimates for the fractionation factor associated with DsrAB (25 to 53‰, Harrison and Thode, 1957; Rees, 1973; Farquhar et al., 2003; Brunner and Bernasconi, 2005; Johnston et al., 2007), and that the mean values from all 650+ experimental determinations, regardless of experiment type or whether it was a sulfate-sulfide or sulfite-sulfide experiments, the grand mean for $^{34}\varepsilon_{r-p}$ falls at 17.9‰ (median at 16.1‰), with the 25th and 75th percentile's falling at 10‰ and 22.5‰, respectively (**Figure 5**)—these are all well within the maximum fractionation accounted for by the sum of our DsrAB value (15.3‰) and our literature derived range for sulfate reduction to sulfite (4 to 15‰), for a total of 19.3 to 30.3‰ (see main text).

Literature Estimates of Fractionation during Sulfate Activation to Sulfite

The upstream kinetic isotope fractionation, the result of enzyme mediated sulfate/sulfite exchange in cell-free extract experiments, is between 4 and 15 ‰ (compilation files: http://dx.doi.org/10.6084/m9.figshare.1436115). The mean of these experiments is $^{34}\varepsilon_{SO4/SO3}$ = 9.5‰, $CI_{95\%}$ = 7.2 to 11.9‰, with and n = 12 (column statistics are also permanently available at: http://dx.doi.org/10.6084/m9.figshare.1436115) (Ford, 1957; Harrison and Thode, 1958; Kaplan and Rittenberg, 1964; Kemp and Thode, 1968). Deconvolving this aggregated fractionation factor ($^{34}\varepsilon_{SO4/SO3}$) *in vitro* is a target for future pure enzyme experiments focusing on the constituent steps (enzyme specific $^{34}\varepsilon$), as well as the minor isotope fractionations associate with each (i.e., $^{33}\lambda$'s).

These values represent the fractionation across the sum of the steps incorporating sulfate activation to APS and its concomitant reduction to sulfite (**Figure 1**). It is important to note that these values were determined using crude-cell extracts, rather than purified enzymes, and not measured over a range of reaction progress (as in **Figure 2**). Further, available data do not allow for the evaluation of mass balance closure, as we have done here for DsrAB. Given our present understanding of the enzymes involved in this process (Bradley et al., 2011; Pereira et al., 2011), sulfate transport into the cytoplasm followed by activation to APS (Sat) are not likely to directly impact S-isotope compositions, whereas the reduction of APS (APSr) most likely does, due to the breaking of a S-O bond. The sum of transport, Sat and APSr fractionations sit immediately upstream of the DsrAB. Both of these constraints ($^{34}\varepsilon_{SO4/SO3}$ and $^{34}\varepsilon_{DsrAB}$) are interpreted in the context of the MSR data compiled from the literature, which includes lab experiments, natural waters and sediments, as discussed in the main text (**Figure 5**).

Statistical Analysis of Laboratory Chemostat and Marine Sediment Fractionations

To apply the compiled sedimentary sulfate reduction rates from Goldhaber and Kaplan (1975), we re-plot their log-scale values to a linear scaling (**Figure 5**) and apply the same non-linear regression one-phase decay model ($Y = (Y_0 - Plateau)\, e^{(-KX)} + Plateau$) from our recent work on fractionation—rate relationships in MSR (Leavitt et al., 2013), minimizing variance to arrive at the following parameters: Y_0 = 73‰, plateau = 17.3‰, and a decay-constant (K) of 6.4 (**Figure 5**). For the chemostat (open-system) MSR data in the study where we derived this regression model (Leavitt et al., 2013), we re-scale the cell-specific MSR rates to basic volumetric fluxes by multiplying out the number of cells at each sampling point, using the chemostat values from our recent study (Leavitt et al., 2013). Applying the same one-phase decay model and minimize variance, we calculate the following parameters: Y_0 = 56.5‰, plateau = 17.3‰, and a decay-constant (K) of 0.054.

All regressions were calculated using *Prism5c* (GraphPad, San Diego, CA).

ACKNOWLEDGMENTS

Thanks to Sofia Venceslau and Fabian Grein for discussions on MSR biochemistry and DsrC cycling; Isabel Pacheco for the purified hydrogenase; to Erin Beirne and Andy Masterson for expert assistance in measurements and separation chemistry. Thanks to Ann Pearson, David Fike and Itay Halevy for comments that greatly improved our interpretations and presentation. We especially thank John Hayes for exceptionally in-depth feedback. This work was funded by an NSF-GRFP (WL), NSF-EAR-1225980 (DJ, IP), the Sloan Foundation (DJ), the Agouron Institute (AB), PTDC/QUI-BIQ/100591/2008 and PTDC/BBB-BQB/0684/2012 (IP), UID/Multi/04551/2013 (to ITQB) funded by Fundacao para a Ciencia e Tecnologia (FCT, Portugal), Washington University in St. Louis (AB) and the Steve Fossett Postdoctoral Fellowship at Washington University in St. Louis (WL).

SUPPLEMENTARY MATERIAL

The Supplementary Material for this article can be found online at: http://journal.frontiersin.org/article/10.3389/fmicb.2015.01392

REFERENCES

Ames, D. P., and Willard, J. E. (1951). The Kinetics of the Exchange of Sulfur between Thiosulfate and Sulfite1. *J. Am. Chem. Soc.* 73, 164–172.

Antler, G., Turchyn, A. V., Rennie, V., Herut, B., and Sivan, O. (2013). Coupled sulfur and oxygen isotope insight into bacterial sulfate reduction in the natural environment. *Geochim. Cosmochim. Acta* 118, 98–117. doi: 10.1016/j.gca.2013.05.005

Bevington, P. R., and Robinson, D. K. (2003). *Data Reduction and Error Analysis*. New York, NY: McGraw–Hill.

Bigeleisen, J., and Wolfsberg, M. (1958). Theoretical and experimental aspects of isotope effects in chemical kinetics. *Adv. Chem. Physics* 1, 15–76.

Bolliger, C., Schroth, M. H., Bernasconi, S. M., Kleikemper, J., and Zeyer, J. (2001). Sulfur isotope fractionation during microbial sulfate reduction by toluene-degrading bacteria. *Geochim. Cosmochim. Acta* 65, 3289–3298. doi: 10.1016/S0016-7037(01)00671-8

Bottcher, M. E., Sievert, S. M., and Kuever, J. (1999). Fractionation of sulfur isotopes during dissimilatory reduction of sulfate by a thermophilic gram-negative bacterium at 60 C. *Arch. Microbiol.* 172, 125–128.

Bradford, M. M. (1976). A rapid and sensitive method for the quantitation of microgram quantities of protein utilizing the principle of protein-dye binding. *Anal. Biochem.* 72, 248–254. doi: 10.1016/0003-2697(76)90527-3

Bradley, A. S., Leavitt, W. D., and Johnston, D. T. (2011). Revisiting the dissimilatory sulfate reduction pathway. *Geobiology* 9, 446–457. doi: 10.1111/j.1472-4669.2011.00292.x

Bradley, A. S., Leavitt, W. D., Schmidt, M., and Knoll, A. H. (2015). Patterns of sulfur isotope fractionation during Microbial Sulfate Reduction. *Geobiology*. doi: 10.1111/gbi.12149. [Epub ahead of print].

Brunner, B., and Bernasconi, S. M. (2005). A revised isotope fractionation model for dissimilatory sulfate reduction in sulfate reducing bacteria. *Geochim. Cosmochim. Acta* 69, 4759–4771. doi: 10.1016/j.gca.2005.04.015

Canfield, D. E. (2001a). Biogeochemistry of sulfur isotopes. *Rev. Mineral. Geochem.* 43, 607–636. doi: 10.2138/gsrmg.43.1.607

Canfield, D. E. (2001b). Isotope fractionation by natural populations of sulfate-reducing bacteria. *Geochim. Cosmochim. Acta* 65, 1117–1124. doi: 10.1016/S0016-7037(00)00584-6

Canfield, D. E. (2006). Models of oxic respiration, denitrification and sulfate reduction in zones of coastal upwelling. *Geochim. Cosmochim. Acta* 70, 5753–5765. doi: 10.1016/j.gca.2006.07.023

Canfield, D. E., and Farquhar, J. (2009). Animal evolution, bioturbation, and the sulfate concentration of the oceans. *Proc. Natl. Acad. Sci. U.S.A.* 106, 8123–8127. doi: 10.1073/pnas.0902037106

Canfield, D. E., Farquhar, J., and Zerkle, A. L. (2010). High isotope fractionations during sulfate reduction in a low-sulfate euxinic ocean analog. *Geology* 38, 415–418. doi: 10.1130/G30723.1

Chambers, L. A., and Trudinger, P. A. (1975). Are thiosulfate and trithionate intermediates in dissimilatory sulfate reduction? *J. Bacteriol.* 123, 36–40.

Chambers, L. A., and Trudinger, P. A. (1979). Microbiological fractionation of stable sulfur isotopes: a review and critique. *Geomicrobiol. J.* 1, 249–293.

Chambers, L. A., Trudinger, P. A., Smith, J. W., and Burns, M. S. (1975). Fractionation of sulfur isotopes by continuous cultures of Desulfovibrio desulfuricans. *Can. J. Microbiol.* 21, 1602–1607.

Cline, J. D. (1969). Spectrophotometric determination of hydrogen sulfide in natural waters. *Limnol. Oceanogr.* 14, 454–458.

Crowe, S., Paris, G., Katsev, S., Jones, C., Kim, S. T., Zerkle, A. L., et al. (2014). Sulfate was a trace constituent of Archean seawater. *Science* 346, 735–739. doi: 10.1126/science.1258966

Cypionka, H. (1994). Sulfate transport. *Methods Enzymol.* 243, 3–14.

Czyzewski, B. K., and Wang, D.-N. (2012). Identification and characterization of a bacterial hydrosulphide ion channel. *Nature* 483, 494–497. doi: 10.1038/nature10881

Davidson, M. M., Bisher, M. E., Pratt, L. M., Fong, J., Southam, G., Pfiffner, S. M., et al. (2009). Sulfur isotope enrichment during maintenance metabolism in the thermophilic sulfate-reducing bacterium desulfotomaculum putei. *Appl. Environ. Microbiol.* 75, 5621–5630. doi: 10.1128/AEM.02948-08

Detmers, J., Brüchert, V., Habicht, K., and Kuever, J. (2001). Diversity of sulfur isotope fractionations by sulfate-reducing prokaryotes. *Appl. Environ. Microbiol.* 67, 888–894. doi: 10.1128/AEM.67.2.888-894.2001

Drake, H. L., and Akagi, J. M. (1976). Product analysis of bisulfite reductase activity isolated from Desulfovibrio vulgaris. *J. Bacteriol.* 126, 733–738.

Drake, H. L., and Akagi, J. M. (1977). Bisulfite reductase of Desulfovibrio vulgaris: explanation for product formation. *J. Bacteriol.* 132, 139–143.

Drake, H. L., and Akagi, J. M. (1978). Dissimilatory reduction of bisulfite by Desulfovibrio vulgaris. *J. Bacteriol.* 136, 916–923.

Einsiedl, F. (2008). Effect of NO2- on stable isotope fractionation during bacterial sulfate reduction. *Environ. Sci. Technol.* 43, 82–87. doi: 10.1021/es801592t

Farquhar, G. D., O'leary, M. H., and Berry, J. A. (1982). On the relationship between carbon isotope discrimination and the intercellular carbon dioxide concentration in leaves. *Funct. Plant Biol.* 9, 121–137.

Farquhar, J., Canfield, D. E., Masterson, A., Bao, H., and Johnston, D. T. (2008). Sulfur and oxygen isotope study of sulfate reduction in experiments with natural populations from Faellestrand, Denmark. *Geochim. Cosmochim. Acta* 72, 2805–2821. doi: 10.1016/j.gca.2008.03.013

Farquhar, J., Johnston, D. T., and Wing, B. A. (2007). Implications of conservation of mass effects on mass-dependent isotope fractionations: influence of network structure on sulfur isotope phase space of dissimilatory sulfate reduction. *Geochim. Cosmochim. Acta* 71, 5862–5875. doi: 10.1016/j.gca.2007.08.028

Farquhar, J., Johnston, D. T., Wing, B. A., Habicht, K. S., Canfield, D. E., Airieau, S., et al. (2003). Multiple sulphur isotopic interpretations of biosynthetic pathways: implications for biological signatures in the sulphur isotope record. *Geobiology* 1, 27–36. doi: 10.1046/j.1472-4669.2003.00007.x

Ford, R. W. (1957). *Sulphur Isotope Effects in Chemical and Biological Processes*. PhD Thesis. McMaster University.

Fritz, G. (2002). Structure of adenylylsulfate reductase from the hyperthermophilic Archaeoglobus fulgidus at 1.6-A resolution. *Proc. Natl. Acad. Sci. U.S.A.* 99, 1836–1841. doi: 10.1073/pnas.042664399

Fritz, P., Basharmal, G. M., Drimmie, R. J., and Ibsen, J. (1989). Oxygen isotope exchange between sulphate and water during bacterial reduction of sulphate. *Chem. Geol.* 79, 99–105.

Furusaka, C. (1961). Sulphate transport and metabolism desulphovibrio desulphuricans. *Nature* 192, 427–429.

Garrels, R. M., and Lerman, A. (1981). Phanerozoic cycles of sedimentary carbon and sulfur. *Proc. Natl. Acad. Sci. U.S.A.* 78, 4652–4656.

Goldhaber, M. B., and Kaplan, I. R. (1975). Controls and consequences of sulfate reduction rates in recent marine sediments. *Soil Sci.* 119, 42–55.

Gomes, M. L., and Hurtgen, M. T. (2013). Sulfur isotope systematics of a euxinic, low-sulfate lake: evaluating the importance of the reservoir effect in modern and ancient oceans. *Geology* 41, 663–666. doi: 10.1130/G34187.1

Grant, W. M. (1947). Colorimetric determination of sulfur dioxide. *Anal. Chem.* 19, 345–346.

Habicht, K., Gade, M., Thamdrup, B., Berg, P., and Canfield, D. E. (2002). Calibration of sulfate levels in the Archean Ocean. *Science* 298, 2372–2374. doi: 10.1126/science.1078265

Habicht, K. S., Salling, L., Thamdrup, B., and Canfield, D. E. (2005). Effect of low sulfate concentrations on lactate oxidation and isotope fractionation during sulfate reduction by archaeoglobus fulgidus strain Z. *Appl. Environ. Microbiol.* 71, 3770–3777. doi: 10.1128/AEM.71.7.3770-3777.2005

Harrison, A. G., and Thode, H. G. (1957). The kinetic isotope effect in the chemical reduction of sulphate. *Transac. Faraday Soc.* 53, 1648–1651.

Harrison, A. G., and Thode, H. G. (1958). Mechanism of the bacterial reduction of sulphate from isotope fractionation studies. *Transac. Faraday Soci.* 54, 84–92.

Hayes, J. M. (1983). "Practices and principles of isotopic measurements in organic geochemistry," in *Organic Geochemistry of Contemporaneous and Ancient Sediments, Great Lakes Section – Society of Economic Paleontologists and Mineralogists*, ed W. G. Meinschein (Bloomington. IN).

Hayes, J. M. (1993). Factors controlling 13 C contents of sedimentary organic compounds: principles and evidence. *Marine Geol.* 113, 111–125.

Hayes, J. M. (2001). Fractionation of carbon and hydrogen isotopes in biosynthetic processes. *Rev. Mineral. Geochem.* 43, 225–277. doi: 10.2138/gsrmg.43.1.225

Hayes, J. M., Strauss, H., and Kaufman, A. J. (1999). The abundance of 13C in marine organic matter and isotopic fractionation in the global biogeochemical cycle of carbon during the past 800 Ma. *Chem. Geol.* 161, 103–125.

Hoek, J., Reysenbach, A.-L., Habicht, K., and Canfield, D. (2006). Effect of hydrogen limitation and temperature on the fractionation of sulfur isotopes by a deep-sea hydrothermal vent sulfate-reducing bacterium. *Geochim. Cosmochim. Acta* 70, 5831–5841. doi: 10.1016/j.gca.2006.07.031

Holland, H. D. (1973). Systematics of the isotopic composition of sulfur in the oceans during the Phanerozoic and its implications for atmospheric oxygen. *Geochim. Cosmochim. Acta* 37, 2605–2616.

Holler, T., Wegener, G., Niemann, H., Deusner, C., Ferdelman, T. G., Boetius, A., et al. (2011). Carbon and sulfur back flux during anaerobic microbial oxidation of methane and coupled sulfate reduction. *Proc. Natl. Acad. Sci. U.S.A.* 108, E1484–E1490. doi: 10.1073/pnas.1106032108

Johnston, D. T. (2005). Multiple sulfur isotope fractionations in biological systems: a case study with sulfate reducers and sulfur disproportionators. *Am. J. Sci.* 305, 645–660. doi: 10.2475/ajs.305.6-8.645

Johnston, D. T., Farquhar, J., and Canfield, D. E. (2007). Sulfur isotope insights into microbial sulfate reduction: when microbes meet models. *Geochim. Cosmochim. Acta* 71, 3929–3947. doi: 10.1016/j.gca.2007.05.008

Jones, G. E., and Starkey, R. L. (1957). Fractionation of stable isotopes of sulfur by microorganisms and their role in deposition of native sulfur. *Appl. Microbiol.* 5, 111.

Kaplan, I. R., and Rittenberg, S. C. (1964). Microbiological fractionation of sulphur isotopes. *J. Gen. Microbiol.* 34, 195–212.

Karkhoff-Schweizer, R. R., Bruschi, M., and Voordouw, G. (1993). Expression of the gamma-subunit gene of desulfoviridin-type dissimilatory sulfite reductase and of the alpha- and beta-subunit genes is not coordinately regulated. *Eur. J. Biochem.* 211, 501–507. doi: 10.1111/j.1432-1033.1993.tb17576.x

Karsh, K. L., Granger, J., Kritee, K., and Sigman, D. M. (2012). Eukaryotic assimilatory nitrate reductase fractionates N and O isotopes with a ratio near unity. *Environ. Sci. Technol.* 46, 5727–5735. doi: 10.1021/es204593q

Kelly, D. P., Chambers, L. A., and Trudinger, P. A. (1969). Cyanolysis and spectrophotometric estimation of trithionate in mixture with thiosulfate and tetrathionate. *Anal. Chem.* 41, 898–901.

Kelly, D. P., and Wood, A. P. (1994). Synthesis and determination of thiosulfate and polythionates. *Methods Enzymol.* 243, 475–501.

Kemp, A., and Thode, H. G. (1968). The mechanism of the bacterial reduction of sulphate and of sulphite from isotope fractionation studies. *Geochim. Cosmochim. Acta* 32, 71–91.

Kim, J. H., and Akagi, J. M. (1985). Characterization of a trithionate reductase system from Desulfovibrio vulgaris. *J. Bacteriol.* 163, 472–475.

Kleikemper, J., Schroth, M., Bernasconi, S. M., Brunner, B., and Zeyer, J. (2004). Sulfur isotope fractionation during growth of sulfate-reducing bacteria on various carbon sources. *Geochim. Cosmochim. Acta* 68, 4891–4904. doi: 10.1016/j.gca.2004.05.034

Knöller, K., Vogt, C., Richnow, H.-H., and Weise, S. M. (2006). Sulfur and oxygen isotope fractionation during benzene, toluene, ethyl benzene, and xylene degradation by sulfate-reducing bacteria. *Environ. Sci. Technol.* 40, 3879–3885. doi: 10.1021/es052325r

Kobayashi, K., Yasuhide, S., and Ishimoto, M. (1974). Biochemical studies on sulfate-reducing Bacteria XIII. Sulfite reductase fromdesulfovibrio vulgaris-mechanism of trithionafe, thiosulfate, and sulfide formation and enzymatic properties. *J. Biochem.* 75, 519–529.

Krouse, H. R., McCready, R. G. L., Husain, S. A., and Campbell, J. N. (1968). Sulfur isotope fractionation and kinetic studies of sulfite reduction in growing cells of salmonella heidelberg. *Biophys. J.* 8, 109–124. doi: 10.1016/S0006-3495(68)86478-1

Laws, E. A., Popp, B. N., Bidigare, R. R., Kennicutt, M. C., and Macko, S. A. (1995). Dependence of phytoplankton carbon isotopic composition on growth rate and [CO 2) aq: theoretical considerations and experimental results. *Geochim. Cosmochim. Acta* 59, 1131–1138.

Leavitt, W. D. (2014). *On the Mechanisms of Sulfur Isotope Fractionation During Microbial Sulfate Reduction*. PhD Thesis. Harvard University.

Leavitt, W. D., Cummins, R., Schmidt, M. L., Sim, M. S., Ono, S., Bradley, A. S., et al. (2014). Multiple sulfur isotope signatures of sulfite and thiosulfate reduction by the model dissimilatory sulfate-reducer, Desulfovibrio alaskensis str. G20. *Front. Microbiol.* 5:591. doi: 10.3389/fmicb.2014.00591

Leavitt, W. D., Halevy, I., Bradley, A. S., and Johnston, D. T. (2013). Influence of sulfate reduction rates on the Phanerozoic sulfur isotope record. *Proc. Natl. Acad. Sci. U.S.A.* 110, 11244–11249. doi: 10.1073/pnas.1218874110

Le Gall, J., Payne, W. J., Chen, L., Liu, M. Y., and Xavier, A. V. (1994). Localization and specificity of cytochromes and other electron transfer proteins from sulfate-reducing bacteria. *Biochimie* 76, 655–665.

Mangalo, M., Einsiedl, F., Meckenstock, R. U., and Stichler, W. (2008). Influence of the enzyme dissimilatory sulfite reductase on stable isotope fractionation during sulfate reduction. *Geochim. Cosmochim. Acta* 72, 1513–1520. doi: 10.1016/j.gca.2008.01.006

Mangalo, M., Meckenstock, R. U., Stichler, W., and Einsiedl, F. (2007). Stable isotope fractionation during bacterial sulfate reduction is controlled by reoxidation of intermediates. *Geochim. Cosmochim. Acta* 71, 4161–4171. doi: 10.1016/j.gca.2007.06.058

Mariotti, A., Germon, J. C., Hubert, P., Kaiser, P., Letolle, R., Tardieux, A., et al. (1981). Experimental determination of nitrogen kinetic isotope fractionation: some principles; illustration for the denitrification and nitrification processes. *Plant Soil* 62, 413–430. doi: 10.1007/BF02374138

Marritt, S. J., and Hagen, W. R. (1996). Dissimilatory sulfite reductase revisited. The desulfoviridin molecule does contain 20 iron ions, extensively demetallated sirohaem, and an S= 9/2 iron-sulfur cluster. *Eur. J. Biochem.* 238, 724–727. doi: 10.1111/j.1432-1033.1996.0724w.x

Mathai, J. C., Missner, A., Kügler, P., Saparov, S. M., Zeidel, M. L., Lee, J. K., et al. (2009). No facilitator required for membrane transport of hydrogen sulfide. *Proc. Natl. Acad. Sci. U.S.A.* 106, 16633–16638. doi: 10.1073/pnas.0902952106

McCready, R. G. L. (1975). Sulfur Isotope Fractionation by Desulfovibrio and Desulfotomaculum species. *Geochim. Cosmochim. Acta* 39, 1395–1401.

McCready, R. G. L., Laishley, E. J., and Krouse, H. R. (1975). Stable isotope fractionation by Clostridium pasteurianum. 1.34 S/32S: inverse isotope effects during SO42-and SO32-reduction. *Can. J. Microbiol.* 21, 235–244.

McNaught, A. D., and Wilkinson, A. (1997). *Compendium of Chemical Terminology, International Union of Pure and Applied Chemistry*. Oxford: Blackwell Science.

Miller, M. F. (2002). Isotopic fractionation and the quantification of 17 O anomalies in the oxygen three-isotope system: an appraisal and geochemical

significance. *Geochim. Cosmochim. Acta* 66, 1881–1889. doi: 10.1016/S0016-7037(02)00832-3

Nakagawa, M., Ueno, Y., Hattori, S., Umemura, M., Yagi, A., Takai, K., et al. (2012). Seasonal change in microbial sulfur cycling in monomictic Lake Fukami-ike, Japan. *Limnol. Oceanogr.* 57, 974–988. doi: 10.4319/lo.2012.57.4.0974

Nakai, N., and Jensen, M. L. (1964). The kinetic isotope effect in the bacterial reduction and oxidation of sulfur. *Geochim. Cosmochim. Acta* 28, 1893–1912. doi: 10.1016/0016-7037(64)90136-X

Newton, G. L., Dorian, R., and Fahey, R. C. (1981). Analysis of biological thiols: derivatization with monobromobimane and separation by reverse-phase high-performance liquid chromatography. *Anal. Biochem.* 114, 383–387.

Oliveira, T. F., Franklin, E., Afonso, J. P., Khan, A. R., Oldham, N. J., Pereira, I. A. C., et al. (2011). Structural insights into dissimilatory sulfite reductases: structure of desulforubidin from desulfomicrobium norvegicum. *Front. Microbiol.* 2:71. doi: 10.3389/fmicb.2011.00071

Oliveira, T. F., Vonrhein, C., Matias, P. M., Venceslau, S. S., Pereira, I. A. C., and Archer, M. (2008a). Purification, crystallization and preliminary crystallographic analysis of a dissimilatory DsrAB sulfite reductase in complex with DsrC. *J. Struct. Biol.* 164, 236–239. doi: 10.1016/j.jsb.2008.07.007

Oliveira, T. F., Vonrhein, C., Matias, P. M., Venceslau, S. S., Pereira, P. M., and Archer, M. (2008b). The crystal structure of Desulfovibrio vulgaris dissimilatory sulfite reductase bound to DsrC provides novel insights into the mechanism of sulfate respiration. *J. Biol. Chem.* 283, 34141–34149. doi: 10.1074/jbc.M805643200

Pagani, M., Liu, Z., LaRiviere, J., and Ravelo, A. C. (2009). High Earth-system climate sensitivity determined from Pliocene carbon dioxide concentrations. *Nat. Geosci.* 3, 27–30. doi: 10.1038/ngeo724

Pallud, C., Meile, C., Laverman, A. M., Abell, J., and Van Cappellen, P. (2007). The use of flow-through sediment reactors in biogeochemical kinetics: methodology and examples of applications. *Marine Chem.* 106, 256–271. doi: 10.1016/j.marchem.2006.12.011

Parey, K., Fritz, G., Ermler, U., and Kroneck, P. M. H. (2013). Conserving energy with sulfate around 100 °C – structure and mechanism of key metal enzymes in hyperthermophilic Archaeoglobus fulgidus. *Metallomics* 5, 302. doi: 10.1039/c2mt20225e

Parey, K., Warkentin, E., Kroneck, P. M., and Ermler, U. (2010). Reaction cycle of the dissimilatory sulfite reductase from Archaeoglobus fulgidus. *Biochemistry* 49, 8912–8921. doi: 10.1021/bi100781f

Park, R., and Epstein, S. (1960). Carbon isotope fractionation during photosynthesis. *Geochim. Cosmochim. Acta* 21, 110–126.

Peck, H. D. Jr. (1959). The ATP-dependent reduction of sulfate with hydrogen in extracts of Desulfovibrio desulfuricans. *Proc. Natl. Acad. Sci. U.S.A.* 45, 701.

Peck, H. D. Jr. (1960). Adenosine 5′-Phosphosulphate as an intermediate in the oxidation of thiosulfate by Thiobacillus thioparus. *Proc. Natl. Acad. Sci. U.S.A.* 46, 1053.

Peck, H. D. (1961). Enzymatic basis for assimilatory and dissimilatory sulfate reduction. *J. Bacteriol.* 82, 933–939.

Peck, H. D. (1962). The role of adenosine-5′-phosphosulfate in the reduction of sulfate to sulfite by Desulfovibrio desulfuricans. *J. Biol. Chem.* 237, 198–203.

Pereira, I. A. C., Ramos, A. R., Grein, F., Marques, M. C., Da Silva, S. M., and Venceslau, S. S. (2011). A comparative genomic analysis of energy metabolism in sulfate reducing bacteria and archaea. *Front. Microbiol* 2:69. doi: 10.3389/fmicb.2011.00069

Piłsyk, S., and Paszewski, A. (2009). Sulfate permeases—phylogenetic diversity of sulfate transport. *Acta Biocim. Pol.* 56, 375–384.

Pires, R. H., Lourenço, A. I., Morais, F., Teixeira, M., Xavier, A. V., Saraiva, L. M., et al. (2003). A novel membrane-bound respiratory complex from Desulfovibrio desulfuricans ATCC 27774. *Biochim. Biophys. Acta* 1605, 67–82. doi: 10.1016/S0005-2728(03)00065-3

Price, M. N., Ray, J., Wetmore, K. M., Kuehl, J. V., Bauer, S., Deutschbauer, A. M., et al. (2014). The genetic basis of energy conservation in the sulfate-reducing bacterium Desulfovibrio alaskensis G20. *Front. Microbiol.* 5:557. doi: 10.3389/fmicb.2014.00577

Rees, C. (1973). A steady-state model for sulphur isotope fractionation in bacterial reduction processes. *Geochim. Cosmochim. Acta* 37, 1141–1162.

Romão, C. V., Pereira, I. A. C., Xavier, A. V., LeGall, J., and Teixeira, M. (1997). Characterization of the [NiFe] Hydrogenase from the Sulfate ReducerDesulfovibrio vulgarisHildenborough. *Biochem. Biophys. Res. Commun.* 240, 75–79. doi: 10.1006/bbrc.1997.7598

Santos, A. A., Venceslau, S. S., Grein, F., Leavitt, W. D., Dahl, C., Johnston, D. T., et al. (2015). A protein trisulfide couples dissimilatory sulfate reduction to energy conservation. *Science* 350, 1541–1545. doi: 10.1126/science.aad3558

Sass, H., Steuber, J., Kroder, M., Kroneck, P., and Cypionka, H. (1992). Formation of thionates by freshwater and marine strains of sulfate-reducing bacteria. *Arch. Microbiol.* 158, 418–421.

Scheller, S., Goenrich, M., Thauer, R. K., and Jaun, B. (2013). Methyl-Coenzyme M reductase from methanogenic archaea: isotope effects on the formation and anaerobic oxidation of methane. *J. Am. Chem. Soc.* 135, 14975–14984. doi: 10.1021/ja406485z

Schiffer, A., Parey, K., Warkentin, E., Diederichs, K., Huber, H., Stetter, K. O., et al. (2008). Structure of the dissimilatory sulfite reductase from the hyperthermophilic archaeon archaeoglobus fulgidus. *J. Mol. Biol.* 379, 1063–1074. doi: 10.1016/j.jmb.2008.04.027

Sim, M. S., Bosak, T., and Ono, S. (2011a). Large sulfur isotope fractionation does not require disproportionation. *Science* 333, 74–77. doi: 10.1126/science.1205103

Sim, M. S., Ono, S., and Bosak, T. (2012). Effects of iron and nitrogen limitation on sulfur isotope fractionation during microbial sulfate reduction. *Appl. Environ. Microbiol.* 78, 8368–8376. doi: 10.1128/AEM.01842-12

Sim, M. S., Ono, S., Donovan, K., Templer, S. P., and Bosak, T. (2011b). Effect of electron donors on the fractionation of sulfur isotopes by a marine Desulfovibrio sp. *Geochim. Cosmochim. Acta*. 75, 4244–4259.

Sim, M. S., Wang, D. T., Zane, G. M., Wall, J. D., Bosak, T., and Ono, S. (2013). Fractionation of sulfur isotopes by Desulfovibrio vulgaris mutants lacking hydrogenases or type I tetraheme cytochrome c3. *Front. Microbiol.* 4:171. doi: 10.3389/fmicb.2013.00171

Smock, A., Bottcher, M., and Cypionka, H. (1998). Fractionation of sulfur isotopes during thiosulfate reduction by Desulfovibrio desulfuricans. *Arch. Microbiol.* 169, 460–463.

Sörbo, B. O. (1957). A colorimetric method for the determination of thiosulfate. *Biochim. Biophys. Acta* 23, 412–416.

Soriano, A., and Cowan, J. A. (1995). Sulfite reductase: active site residues are "noncatalytic." comparison of reaction energetics for enzyme- and siroheme-catalyzed reduction of inorganic substrates. *J. Am. Chem. Soc.* 117, 4724–4725. doi: 10.1021/ja00121a038

Sra, A. K., Hu, Y., Martin, G. E., Snow, D. D., Ribbe, M. W., and Kohen, A. (2004). Competitive 15N kinetic isotope effects of nitrogenase-catalyzed dinitrogen reduction. *J. Am. Chem. Soc.* 126, 12768–12769. doi: 10.1021/ja0458470

Suh, B., and Akagi, J. M. (1969). Formation of thiosulfate from sulfite by desulfovibrio vulgaris. *J. Bacteriol.* 99, 210–215.

Tcherkez, G. G. B., Farquhar, G. D., and Andrews, T. J. (2006). Despite slow catalysis and confused substrate specificity, all ribulose bisphosphate carboxylases may be nearly perfectly optimized. *Proc. Natl. Acad. Sci. U.S.A.* 103, 7246–7251. doi: 10.1073/pnas.0600605103

Thode, H. G., Kleerekoper, H., and McElcheran, D. (1951). Isotope fractionation in the bacteria reduction of sulfate. *Res. (Lond.)* 4, 581–582.

Thode, H. G., Monster, J., and Dunford, H. B. (1961). Sulphur isotope geochemistry. *Geochim. Cosmochim. Acta* 25, 159–174.

Tudge, A. P., and Thode, H. G. (1950). Thermodynamic properties of isotopic compounds of sulphur. *Can. J. Res.* 28, 567–578.

Turchyn, A. V., Brüchert, V., Lyons, T. W., Engel, G. S., Balci, N., Schrag, D. P., et al. (2010). Kinetic oxygen isotope effects during dissimilatory sulfate reduction: a combined theoretical and experimental approach. *Geochim. Cosmochim. Acta* 74, 2011–2024. doi: 10.1016/j.gca.2010.01.004

Vairavamurthy, A., Manowitz, B., Luther Iii, G. W., and Jeon, Y. (1993). Oxidation state of sulfur in thiosulfate and implications for anaerobic energy metabolism. *Geochim. Cosmochim. Acta* 57, 1619–1623.

Venceslau, S. S., Cort, J. R., Baker, E. S., Chu, R. K., Robinson, E. W., Dahl, C., et al. (2013). Redox states of Desulfovibrio vulgaris DsrC, a key protein in dissimilatory sulfite reduction. *Biochem. Biophys. Res. Commun.* 441, 732–736. doi: 10.1016/j.bbrc.2013.10.116

Venceslau, S. S., Stockdreher, Y., Dahl, C., and Pereira, I. A. C. (2014). The "bacterial heterodisulfide" DsrC is a key protein in dissimilatory sulfur metabolism. *Biochim. Biophys. Acta* 1837, 1148–1164. doi: 10.1016/j.bbabio.2014.03.007

Wing, B. A., and Halevy, I. (2014). Intracellular metabolite levels shape sulfur isotope fractionation during microbial sulfate respiration. *Proc. Natl. Acad. Sci. U.S.A.* 115, 18116–18125.

Wolfe, B. M., Lui, S. M., and Cowan, D. (1994). Desulfoviridin, a multimeric-dissimilatory sulfite reductase from Desulfovibrio vulgaris (Hildenborough) Purification, characterization, kinetics and EPR studies. *Eur. J. Biochem.* 223, 79–89. doi: 10.1111/j.1432-1033.1994.tb18968.x

Young, E. D., Galy, A., and Nagahara, H. (2002). Kinetic and equilibrium mass-dependent isotope fractionation laws in nature and their geochemical and cosmochemical significance. *Geochim. Cosmochim. Acta* 66, 1095–1104. doi: 10.1016/S0016-7037(01)00832-8

Conflict of Interest Statement: The authors declare that the research was conducted in the absence of any commercial or financial relationships that could be construed as a potential conflict of interest.

APPENDIX

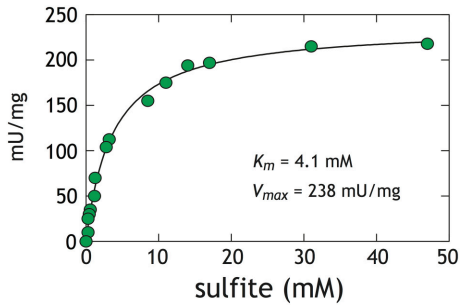

FIGURE A1 | Activity assays with *D. vulgaris* DsrAB. The difference between initial and final concentration of sulfite after 2 h was used to calculate the rate. The Michaelis-Menten equation ($Y = \frac{V_{max} \times X}{K_M + X}$) was solved for experimental K_m and V_{max} under our conditions. The analytical error is less than the size of the symbols ($2\sigma = 1\ \mu$M). One unit (U) is defined as the quantity of enzyme that catalyzes the conversion of one micromol of substrate per minute. At both 10 and 15 mM initial sulfite we are assured to be well above the apparent DsrAB K_m for sulfite. Reaction inhibition was not observed at sulfite concentrations as high as 50 mM (Wolfe et al., 1994; Soriano and Cowan, 1995).

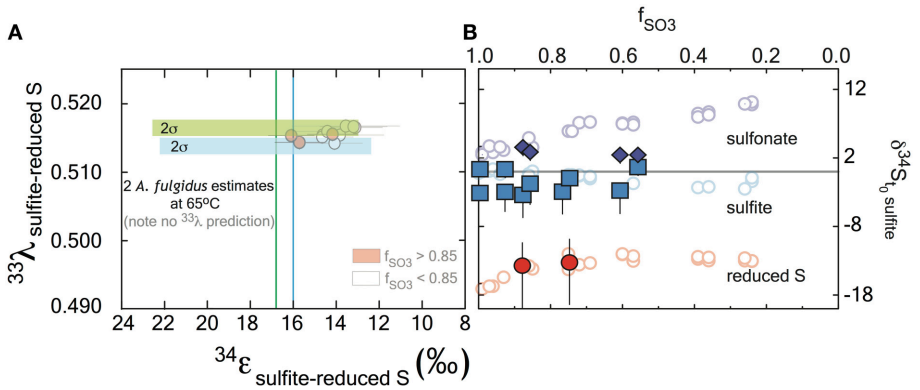

FIGURE A2 | The major isotope ratios ($\delta^{34}S$) reported relative to the composition of sulfite at t_0, for the *A. fulgidus* (closed symbols) and *D. vulgaris* (open symbols) experiments both as a function of reaction progress. The samples sets show a general consistency, particularly at the reduced S sites, despite the significant offet in temperature (20–30°C for *D. vugaris* relative to 65°C for *A. fulgidus*), consistent with kinetic theory (Bigeleisen and Wolfsberg, 1958), where temperature should impart a minimal effect over this range. The asymmetric error bars on reduced S moieties are a function of the non-linear correction for small sample sizes available for isotope.

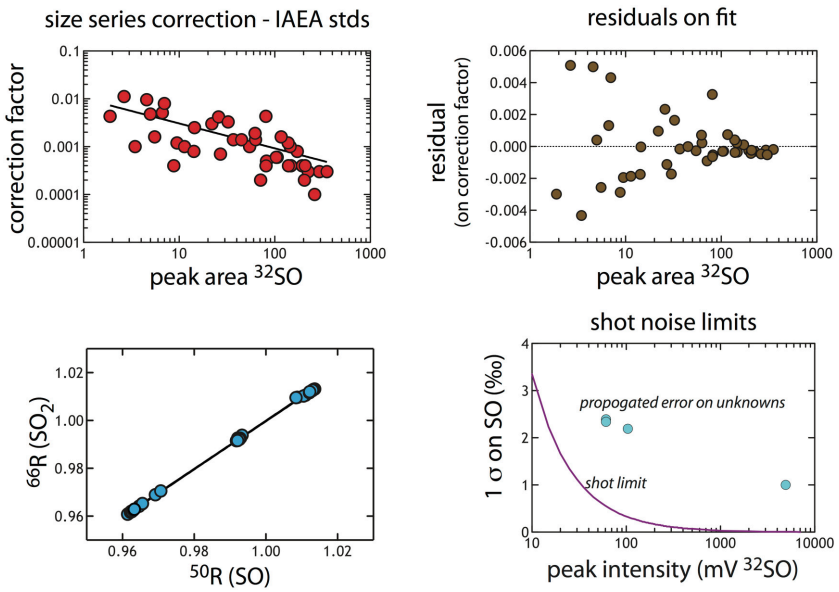

FIGURE A3 | The size series correction calculated from IAEA standards ($n = 44$). (A) Plots the correction (value from $\left|\frac{^{50}R_{predicted} - {}^{50}R_{measured}}{^{50}R_{predicted}}\right|$ against peak-integrated area). **(A)** Shows the calculated residual around that fit, demonstrating a symmetric distribution that scales with peak area. This is an illustration of the goodness of the fit. **(C)** The regression used to convert SO data to an SO_2 scale. **(D)** The calculated shot noise for SO as a function of signal intensity (peak height in mV). This precision limit is below that which we propagate through the correction, and is provided for reference here.

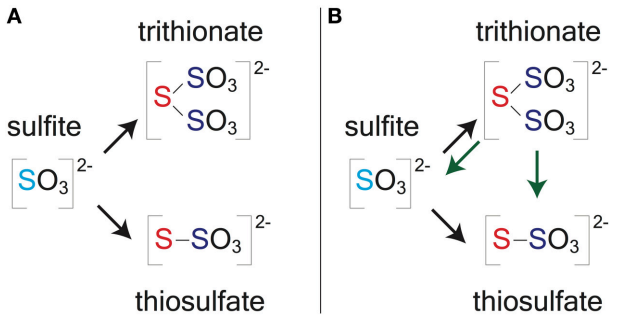

FIGURE A4 | Reaction topology for closed-system models. (A) The simple model for early in the experiments ($f > 0.85$). **(B)** Shows a more complex reaction model that may be applicable later in the closed-system experiments ($f < 0.85$). Sulfite is present in light blue, reduced S is in red and the sulfonate moieties are in purple. Black **(A,B)** arrows represent the simple reduction of sulfite by DsrAB and then formation of thiosulfate and trithionate by combination of that partially reduced S with other sulfite molecules. The green arrows **(B)** represent the more complex scheme in which trithionate is then further reduced, releasing a sulfite and a thiosulfate.

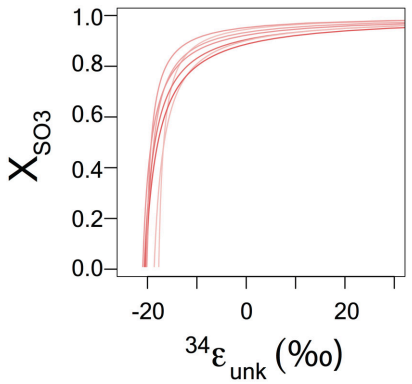

FIGURE A5 | The relationship between the magnitude of a secondary fractionation ($^{34}\alpha_{secondary}$) and the proportion of reduced sulfur deriving directly from sulfite reduction (X_{SO3}). The balance (1- X_{SO3}) is from the parallel reduction of bound sulfonate. Errors estimates are from the propagation calculation, incorporating both isotope and concentration analysis analytical errors (see below).

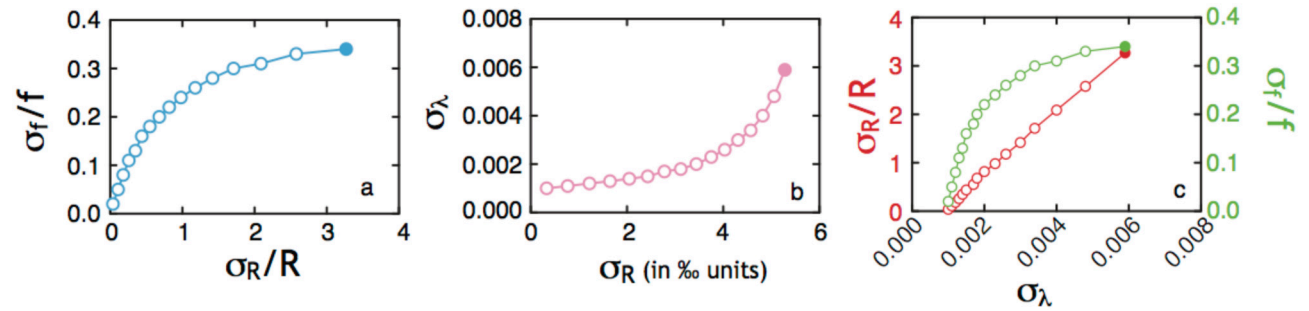

FIGURE A6 | A series of frames (A–C) describing the origin and sensitivity of the controls on the resultant error in δ^{34}S and $^{33}\lambda$ plotted in Figures A2, A3. For this analysis, $^{34}\varepsilon$ is set to 15.3‰ to be consistent with the reductive branch of the DsrAB experiments, the analytical precision of an isotope measurement is 0.2‰ in δ^{34}S and 0.008‰ in Δ^{33}S, and f is allowed to vary from 0.6 to 0.9 in 0.02 increments (noted by circles). This range in f is chosen to reflect the experimental range, and the circle is filled where $f = 0.9$. In **(A)**, the covariance of the relative error in f (σ_f/f) is show to correlate with the error in the relative isotope ratio, σ_R/R. As the calculated error in the R derived from the Rayleigh equation (σ_R) increases, the consequence is an increase in the error in $^{33}\lambda$ **(B)**. Finally, the relationship between the errors in both f and R, as they contribute to the error on $^{33}\lambda$, are presented in frame **C**. Frames **B**,**C** do not approach the origin as a result of f not approaching the limits of 0 and 1, and also due to the multivariate nature of the propagation.

frontiers in Microbiology

ORIGINAL RESEARCH
published: 23 June 2015
doi: 10.3389/fmicb.2015.00596

Microbial- and thiosulfate-mediated dissolution of mercury sulfide minerals and transformation to gaseous mercury

Adiari I. Vázquez-Rodríguez[1], *Colleen M. Hansel*[2]*, *Tong Zhang*[2], *Carl H. Lamborg*[2], *Cara M. Santelli*[3], *Samuel M. Webb*[4] and *Scott C. Brooks*[5]

[1] School of Engineering and Applied Sciences, Harvard University, Cambridge, MA, USA, [2] Department of Marine Chemistry and Geochemistry, Woods Hole Oceanographic Institution, Woods Hole, MA, USA, [3] Department of Mineral Sciences, Smithsonian Institution, National Museum of Natural History, Washington, DC, USA, [4] Stanford Synchrotron Radiation Lightsource, Menlo Park, CA, USA, [5] Environmental Sciences Division, Oak Ridge National Laboratory, Oak Ridge, TN, USA

OPEN ACCESS

Edited by:
Tanja Bosak, Massachusetts Institute of Technology, USA

Reviewed by:
Ulrike Kappler, University of Queensland, Australia
Mustafa Yucel, GEOMAR - Helmholtz Centre for Ocean Research Kiel, Germany

***Correspondence:**
Colleen M. Hansel, Woods Hole Oceanographic Institution, 266 Woods Hole Road, Mailstop 52, Woods Hole, MA 02543, USA
chansel@whoi.edu

Specialty section:
This article was submitted to Microbiological Chemistry and Geomicrobiology, a section of the journal Frontiers in Microbiology

Received: *27 March 2015*
Accepted: *30 May 2015*
Published: *23 June 2015*

Citation:
Vázquez-Rodríguez AI, Hansel CM, Zhang T, Lamborg CH, Santelli CM, Webb SM and Brooks SC (2015) Microbial- and thiosulfate-mediated dissolution of mercury sulfide minerals and transformation to gaseous mercury. Front. Microbiol. 6:596. doi: 10.3389/fmicb.2015.00596

Mercury (Hg) is a toxic heavy metal that poses significant environmental and human health risks. Soils and sediments, where Hg can exist as the Hg sulfide mineral metacinnabar (β-HgS), represent major Hg reservoirs in aquatic environments. Metacinnabar has historically been considered a sink for Hg in all but severely acidic environments, and thus disregarded as a potential source of Hg back to aqueous or gaseous pools. Here, we conducted a combination of field and laboratory incubations to identify the potential for metacinnabar as a source of dissolved Hg within near neutral pH environments and the underpinning (a)biotic mechanisms at play. We show that the abundant and widespread sulfur-oxidizing bacteria of the genus *Thiobacillus* extensively colonized metacinnabar chips incubated within aerobic, near neutral pH creek sediments. Laboratory incubations of axenic *Thiobacillus thioparus* cultures led to the release of metacinnabar-hosted Hg(II) and subsequent volatilization to Hg(0). This dissolution and volatilization was greatly enhanced in the presence of thiosulfate, which served a dual role by enhancing HgS dissolution through Hg complexation and providing an additional metabolic substrate for *Thiobacillus*. These findings reveal a new coupled abiotic-biotic pathway for the transformation of metacinnabar-bound Hg(II) to Hg(0), while expanding the sulfide substrates available for neutrophilic chemosynthetic bacteria to Hg-laden sulfides. They also point to mineral-hosted Hg as an underappreciated source of gaseous elemental Hg to the environment.

Keywords: mercury, metacinnabar, sulfur chemosynthesis, *Thiobacillus*, thiosulfate, mercury sulfide dissolution, sulfur metabolism, sulfur oxidation

Introduction

Mercury (Hg) is a toxic heavy metal that poses significant environmental and human health risks (Wiener et al., 2002; Clarkson and Magos, 2006). Because gaseous elemental Hg travels over hemispheric scales, it is now an internationally recognized priority pollutant in need of global regulation (McNutt, 2013). Mineral associated Hg is the largest Hg reservoir in the environment where it can account for nearly 60% of the total Hg mass inventory (Mason et al., 2012). A large

fraction of this pool is comprised of mercury sulfide minerals (HgS) (Smith-Downey et al., 2010).

The dominant Hg minerals are the two HgS polymorphs cinnabar (α-HgS) and metacinnabar (β-HgS). Metacinnabar is the dominant authigenic phase, where it forms under sulfidic conditions within soils and sediments (Barnett et al., 1997). Under acidic pH conditions (pH∼3), HgS dissolution can be enhanced in the presence of mine tailing-derived microbial cultures (Jew et al., 2014). Under these acidic conditions, bacteria of the genus *Acidithiobacillus* have been implicated in inducing cinnabar dissolution and volatilization of released Hg (Baldi and Olson, 1987). Yet under non-acidic conditions (pH > 4), both HgS phases are considered to be poorly reactive and stable due to their low solubility (e.g., $\log K_{so} \sim -39$) (Dyrssen, 1989) and very slow abiotic dissolution kinetics (Barnett et al., 2001; Holley et al., 2007). There is a growing appreciation, however, for the role of dissolved organic matter in increasing HgS dissolution and inhibiting HgS precipitation and aggregation in the absence and presence of bacterial activity (Ravichandran, 2004; Graham et al., 2012). Nevertheless, HgS minerals are still largely considered as stable Hg phases and microbial-assisted dissolution of HgS at near neutral pH conditions is assumed to be negligible.

Observations of substantial Hg fluxes from unknown sources within terrestrial and marine sulfidic sediments, however, have called into question the validity of this assumption. For instance, HgS minerals have recently been implicated as a source of high dissolved Hg concentrations originating from sulfide-rich deep-sea vent sediments, raising the possibility that chemosynthetic microorganisms mobilize Hg from these low solubility phases (Crespo-Medina et al., 2009). Despite the widespread presence of HgS minerals in both terrestrial and marine sediments, a clear understanding of the extent and mechanisms of HgS dissolution in these systems is lacking. Here we address this knowledge gap by conducting a combination of field and laboratory incubations to identify the potential for metacinnabar as a source of dissolved Hg within near neutral pH environments and the underpinning mechanisms at play.

Materials and Methods

Field Incubations

Metacinnabar and pyrite specimens were obtained from the Harvard Museum of Natural History (HMNH) Mineralogical Collection (specimen #122749). For *in-situ* creek incubations, minerals were cut into sections approximately 2 cm by 2 cm by 1 mm and polished. Mineral sections were mounted on glass slides (2 cm by 2.5 cm), which were then secured into precut holes on a polycarbonate sampler, and covered in mesh to prevent large organisms from interfering with the slabs. This sampler was inserted directly into the East Fork Poplar Creek (EFPC) sediments at a depth of 2.5–5 cm in Oak Ridge, Tennessee, USA at N 36° 00.101', W 084° 15.011', ±18 ft. Minerals were incubated for 6 weeks between September and October 2010 within the aerobic sediments of the EFPC creek channel. The geochemistry of the EFPC porewater near sampler deployment location (EFK 22) has been extensively monitored, and Supplementary Table S1 includes geochemical parameters collected on the day of sampler retrieval.

Once retrieved from the creek, mineral samplers were transported on ice to our laboratory where they were preserved within 24 h. Mineral sections used for DNA extraction and sequencing were stored aseptically at −80°C. Minerals for thin sections were fixed using 4% paraformaldehyde, rinsed twice in PBS solution, and stored at −20°C in a 1:1 (v/v) mixture of PBS and 96% ethanol until further processing.

Molecular Methods

Field-incubated minerals were aseptically crushed and DNA was extracted using the Ultraclean soil DNA kit (Mo Bio Laboratories) using the maximum yield protocol with the following modifications. After minerals were added to the bead solution tubes, tubes were sonicated for 5 min. Following addition of IRS solution, tubes were incubated at 70°C for 10 min, and 200 μg of polyadenylic acid were added (Webster et al., 2003; Santelli et al., 2008), followed by vortexing at maximum speed for 15 min. The 16S rRNA region of environmental DNA was amplified using the 8F and 1492R primer set and conditions used previously (Lane, 1991; Turner et al., 1999; Hansel et al., 2008) in triplicate or quadruplicate to yield sufficient DNA for pyrosequencing. Amplification products were purified using the QIAquick nucleotide removal kit (Qiagen). Bacterial tag-encoded pyrosequencing (bTEFAP) was conducted by the Research and Testing Laboratory, Lubbock, TX using the GS FLX Titanium sequencing platform (Roche Applied Science). Primers 28F (5′GAGTTTGATCNTGGCTCAG) and 519r (5′GTNTTACNGCGGCKGCTG) were used to sequence variable regions V1-V3 of the 16S rRNA gene.

Sequence Processing

Pyrosequencing reads were denoised using AmpliconNoise, and chimeras were removed using Perseus (Quince et al., 2011). Following denoising, the metacinnabar and pyrite sequence library contained 10 846 and 5 177 sequence reads respectively with an average read length of 342 bp. Resulting sample reads were all longer than 150 bp, had a quality score greater than 20, and no ambiguous reads, therefore no further quality filtering was needed. Denoised, single reads were aligned and clustered using the Ribosomal Database Project (RDP) Pyrosequencing Pipeline (Nawrocki et al., 2009) and classified using a naïve Bayesian rRNA classifier, version 2.0, with a bootstrap cutoff of 80% (Wang et al., 2007). Eighty-two percent of denoised metacinnabar reads and 35% denoised pyrite reads were classifiable down to the genus level. Genus level abundances are presented as percent abundance of sequences falling within that genus relative to the total number of sequences classifiable at the genus level.

merA Gene Amplification and Sequencing

Genomic DNA from *T. thioparus* pure cultures was extracted using the Ultraclean soil DNA kit (Mo Bio Laboratories). A 285 bp fragment at the 3′ end of *merA* was amplified using PCR primers A1s-n.F and A5-n.R following previously reported amplification conditions (Chadhain et al., 2006). Gel electrophoresis was used for size separation of the PCR

products, and the expected 285 bp *merA* amplification product was confirmed. The gel purified (QIAquick gel extraction kit, Qiagen) 285 bp amplification product was concentrated (DNA Clean and Concentrator-5, Zymo Research), cloned (StrataClone PCR Cloning Kits, Agilent Technologies) and sequenced. The nucleotide sequence of the *T. thioparus* partial *merA* sequence was analyzed by BLASTN 2.2.31 (Altschul et al., 1997) using the NCBI Genomic Reference Sequences (refseq_genomic) database.

X-ray Absorption Spectroscopy

Fixed field-incubated metacinnabar slabs were air dried and embedded in EpoHeat Epoxy (Buehler). Cross sections (∼500 μm) of the embedded minerals were obtained using a diamond saw, subsequently attached to a high-purity fused quartz slide using Hillquist Thin Section Epoxy A-B (Hillquist), and filed and polished down to 50–100 μm thickness using a microtome and 1000 grit silicon carbide paper (Buehler).

Spatially-resolved (μ-scale) X-ray fluorescence (XRF) and X-ray absorption spectroscopy were conducted at the Stanford Synchrotron Radiation Laboratory (SSRL) by collecting spectra at select points of interest or defining and rastering a defined region. Synchrotron-based μ-XRF on beamline 14-3 at SSRL was used to map the Hg (M-edge) and S (K-edge) spatial distribution within the mineral matrix and oxidation rind. Similarly, beamline 2–3 was used to map the distribution of Fe (K-edge) in relation to Hg. The beam size on the sample at both beamlines was approximately 2 × 2 μm. Total Hg and S distributions were collected at 2495 eV (BL14-3) and 13200 eV (BL2-3). Maps were also collected at several discrete incident energies in continuous raster scanning mode in order to collect the fluorescence at several distinguishing points within the S (2470.7, 2473, 2473.7, 2478.5, 2481.3, and 2483 eV) and Fe absorption edge (7123, 7126, 7128, 7130, 7133 eV) at beamlines 14-3 and 2-3, respectively. X-ray absorption near edge structure (XANES) spectra were collected at spots of interest to confirm the oxidation state at discrete locations and compared to standard spectra. Fluorescence maps and XANES spectra were analyzed using the MicroAnalysis Toolkit (Webb, 2006) and SIXPACK (Webb, 2005), respectively.

For bulk S solid-phase speciation, dried samples were mounted onto S-free Lexan. S XANES spectra were collected within a He-purged sample chamber under a continuous He flow with a Lytle detector at SSRL beamline 4-3. The spectra were calibrated with a thiosulfate standard. Samples were run in a He-purged anaerobic bag surrounding the sample holder chamber within the beamline hutch. XAS scans were averaged, background-subtracted, normalized, and deglitched if necessary using SIXPACK (Webb, 2005). The lineshapes (peak position and peak shape) of the XANES spectra were used to compare the relative proportions of different sulfur species within the sample.

Pure Culture Incubations

Glass serum vials were soaked in 10% Instra-Analyzed HCl (J.T. Baker), and rinsed 4× in nanopure water. Glass vials were not reused following contact with Hg. Vials were loosely capped using similarly acid washed polypropylene caps which allowed air penetration while maintaining a sterile environment. Following contact with Hg caps were cleaned using a previously established protocol (Hammerschmidt et al., 2011). In order to close the system for volatile Hg capture, glass serum vials were capped with rubber stoppers and stainless steel needles were used to direct incoming and outgoing air. All incubation materials were autoclaved prior to use.

Thiobacillus thioparus (ATCC 8158) was incubated aerobically at room temperature in 100 mL glass serum vials in the dark for all experiments in the presence and absence of ground natural metacinnabar. Metacinnabar obtained from the HMNH Mineralogical Collection was sieved (<250 μm) prior to use in incubations, and surface area of processed minerals was determined using the BET Kr adsorption technique (0.1321 ± 0.0007 m^2 g^{-1}).

T. thioparus cultures were pre-grown in a pH 7 buffered basal freshwater medium containing 20 mM $Na_2S_2O_3$, 29 mM KH_2PO_4, 23 mM K_2HPO_4, 3.8 mM Na_2CO_3, 7.5 mM NH_4Cl, 1.0 mM $MgCl_2{\cdot}6H_2O$, 0.3% vitamin solution (Widdel and Bak, 1992), and 0.1% Trace Element Solution (Widdel and Bak, 1992) at 30°C for 5 days. These cells were then centrifuged (5000× g for 10 min at 4°C) and concentrated approximately 30× by re-suspending in spent medium. A 1:100 inoculation of these cells was used for 40 μM, 60 μM, 100 μM and 20 mM initial thiosulfate experiments. For 20 mM initial thiosulfate experiments, a stock solution of sterile Na_2S_2O was prepared and added into incubations. For 40–100 μM initial thiosulfate experiments, no additional thiosulfate was added and the thiosulfate present was carryover from the inoculum, which served as a low level thiosulfate addition in the experiment. For zero thiosulfate experiments, centrifuged cells were re-suspended in thiosulfate-free medium, centrifuged again and then concentrated approximately 30× in the thiosulfate-free medium. A 1:100 or 1:50 inoculation of these cell suspensions was then performed.

Basal freshwater medium containing EDTA was used only for one sample series of aqueous Hg measurements as a function of thiosulfate concentration within incubations containing killed cells and metacinnabar. All other experiments were conducted in the absence of EDTA. Basal freshwater medium containing EDTA was identical to the basal freshwater medium described with the exception that Trace Element Solution was prepared following the T2 Medium for *Thiobacillus* Trace Metals solution (Atlas, 2005) using Na_2MoO_4 instead of $(NH_4)_2MoO_4$. This Trace Element Solution contained 5% w/w EDTA (170 mM) resulting in 0.005% or 170 μM EDTA in the final medium.

Killed controls consisted of autoclaved (121°C, 30 min) concentrated cells or 6-day old pre-grown cultures that were killed with 4% formaldehyde, frozen overnight, thawed, centrifuged down, and re-suspended in thiosulfate-free medium. Similar to the processing for live cells, for killed cell preparations, the washing step was performed once for 40 μM and 20 mM initial thiosulfate experiments, and twice for zero thiosulfate experiments. Experimental inoculum contained elemental sulfur resulting from pre-growth in thiosulfate medium, and was homogenized to minimize differences in this carryover in

the experiments. HgS used in experiments was sterilized by autoclaving under an oxygen-free N_2 atmosphere to prevent mineral oxidation. Mineral loading used in all incubations with metacinnabar was 2 g L^{-1}. Cultures were grown without shaking although vials were swirled prior to aseptically drawing samples for aqueous analyses.

Hg volatilization rates were determined by pumping air into *T. thioparus* incubations at a rate of 1.60 ± 0.2 mL min^{-1}, and then capturing volatile Hg in outflow using gold-coated quartz sand traps. Incoming air was Hg-stripped using an upstream gold-coated sand trap and filtered through a 0.22 μm cellulose filter. Similarly, outflow was filtered upstream of the gold-coated quartz trap. The mass of Hg on traps was subsequently quantified by dual-stage gold amalgamation and the Tekran-2600 cold vapor atomic fluorescence spectrophotometer following previously established modifications (Lamborg et al., 2012). Hg emissions from incubations were sampled in intervals of minutes to hours to collect a Hg mass within the instrument detection range. Total Hg emissions from incubations were then estimated based upon volatilization rates obtained at time intervals throughout the experiment assuming a constant rate of change in volatilization rates. Hg emissions from incubations were sampled more frequently within the first few days of the experiment, with sampling frequency decreasing as the experiment progressed. Hg emissions from incubations started with no exogenous thiosulfate and 40 μM thiosulfate, were sampled daily for 2 and 7 days following inoculation. Sampling frequency was gradually decreased, with weekly sampling by day 19, and every 2 weeks by day 45. Incubations started with 20 mM thiosulfate were sampled daily for 4 and 9 days following inoculations with sampling frequency thereafter reduced to every 10 days.

For comparisons of Hg volatilization rates between natural and synthetic metacinnabar, a commercial synthetic metacinnabar (black HgS, Alfa Aesar) was used. The surface area of this synthetic metacinnabar was 1.2804 ± 0.0045 m^2 g^{-1} as determined by BET Kr adsorption. The same natural metacinnabar used for other incubations was used for comparison. Live cells and incubations were prepared identically to the 40 μM thiosulfate incubations. Killed controls were autoclave killed cells. Incubations were spiked with a 25 mM thiosulfate stock solution every 24 h resulting in a daily 125–132 μM thiosulfate spike, with the range in concentration resulting from the volume change throughout the incubation (this is henceforth referred to as the 100 μM thiosulfate spike). Hg emission rates were quantified 0–16 h following the thiosulfate spike, and are presented as ng Hg per liter of culture volume per day.

Samples to be used for sulfate and thiosulfate quantification were filtered through a 0.22 μm cellulose filter and stored at −20°C until analysis. Sulfate and thiosulfate concentrations were quantified via suppressed anion chromatography with conductivity detection using a Dionex ICS-2000 (AS11 Column) with a KOH eluent generator. An eluent gradient method was employed (flow rate 1.5 mL min^{-1}): beginning for 8 min at 1 mM, followed by a linear ramp to 15 mM over 4 min, another linear ramp to 60 mM over 8 min, followed by a sustained 60 mM for 2 min, and 1 mM for 13 min. A blank was run between all samples and standards to prevent carryover between samples. Samples for total dissolved Hg analysis were oxidized with 1–2% (v/v) bromine monochloride (BrCl) per EPA Method 1631. High thiosulfate samples had greater reducing capacity and were oxidized with either 5 or 10% (v/v) BrCl. Samples for total dissolved Hg analysis were refrigerated between collection and analysis except during the BrCl oxidation step. Calibration of the DMA-80 direct Hg analyzer was performed with a series of dissolved Hg(II) standards and the calibration was regularly verified using reference material from the Quebec National Institute for Public Health (INSPQ) Interlaboratory Comparison Program for Metals in Biological Matrices.

For the determination of total cell abundance, cultures were fixed with a final concentration of 4% formaldehyde and frozen. Prior to enumeration using epifluorescence microscopy, cells were stained using SYBR Green I Nucleic Acid Stain. A 0.1% p-phenylenediamine mounting solution was used to prevent photo bleaching (Noble and Fuhrman, 1998). Cell counts were performed for 20 random fields of view. Viable cell enumeration was conducted by making serial dilutions of the culture in PBS, and then plating onto agar dishes with the same culture medium.

Results and Discussion

Colonization and Oxidation of Metacinnabar in Creek Sediments

We first characterized the microbial colonization and mineralogical transformations of metacinnabar mineral sections that were emplaced below the sediment-water interface (2.5–5 cm) within the aerobic hyporheic zone of a Hg-contaminated creek. Culture-independent analysis of the microbial communities showed that the metacinnabar surfaces were extensively colonized by chemosynthetic bacteria, which accounted for a striking majority (>92%) of the taxonomically classified microbial community (**Figure 1A**, Supplementary Table S2). This chemosynthetic population was composed predominantly of members of the genera *Thiobacillus* (71%), *Sulfuricurvum* (13%), and *Sulfuricella* (8%), genera that have the demonstrated ability to oxidize reduced sulfur compounds. Pyrite surfaces similarly enriched for these organisms, but to a lower relative magnitude (**Figure 1A**). The metacinnabar surface evidently enriched for these sulfur-oxidizing organisms as previous characterization of these creek sediments revealed a microbial community that was phylogenetically diverse and taxonomically distinct from those found on the mineral incubations (Vishnivetskaya et al., 2011). Furthermore, the *Thiobacillus* population on the metacinnabar surface was mainly (>50%) comprised of a single species, *T. thioparus*. *T. thioparus* is a common neutrophilic obligate aerobic sulfur-oxidizing bacterium that couples the oxidation of various sulfur species (e.g., sulfur, thiosulfate, sulfide) to the reduction of oxygen (Kelly and Wood, 2000). This organism (a beta-proteobacterium) is distinct from the iron- and sulfur-oxidizing *Acidithiobacillus* species (gamma-proteobacteria) that have previously demonstrated metacinnabar dissolution at acidic

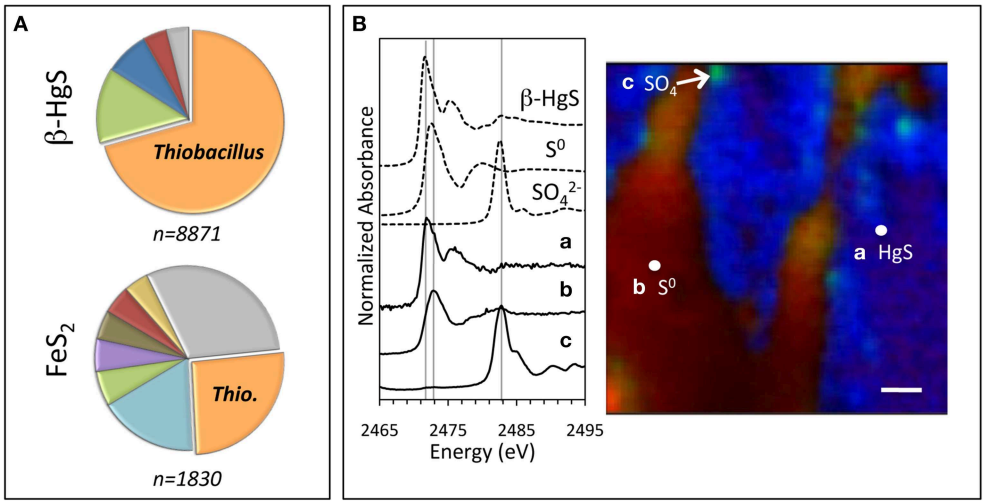

FIGURE 1 | Microbial and mineral composition of incubated mineral sections. Sections were incubated within aerobic hyporheic sediments of the East Fork Poplar Creek for 6 weeks 2.5–5 cm below the sediment-water interface. **(A)** Genus-level classification of 16S rRNA sequences obtained from bacteria colonizing the metacinnabar (top) and pyrite (bottom) mineral sections. Pie chart percentages represent the number of sequences assigned to each genus divided by the total number of classified sequences, which include the known sulfur-oxidizing organisms *Thiobacillus* (orange, β-HgS = 71%, FeS_2 = 26%), *Sulfuricurvum* (green, β-HgS = 13%, FeS_2 = 6%), and *Sulfuricella* (dark blue, β-HgS = 8%), and also the bacterial genera *Methyloversatilis* (red, β-HgS = 4%, FeS_2 = 5%), *Hyphomicrobium* (light blue, FeS_2 = 17%), *Sphingomonas* (purple, FeS_2 = 6%), *Methylotenera* (brown, FeS_2 = 5%), and *Sphingopyxis* (yellow, FeS_2 = 4%). The remainder (gray) represents genera that each comprise less than 4% of the total population. **(B)** Distribution and composition of sulfur (S) in cross sections obtained from the incubated metacinnabar. Left: PCA analysis of the seven energy S K-edge maps indicate that three components account for the S speciation whose XANES spectra match unreacted metacinnabar (*a* = β-HgS), elemental sulfur (*b* = S^0), and sulfate (*c* = SO_4^{2-}). Right: μ-XRF map illustrating the presence of the oxidation product S^0 (red) and isolated spots of sulfate (green) on the HgS surface (blue) (spot size = 5 μm). Scale bar = 60 μm.

pH. Specifically, *T. thioparus* lives solely in circumneutral environments and cannot respire or otherwise oxidize Fe(II). Thus, the proliferation of these organisms on the metacinnabar surface may have ensued due to enhanced access to mineral-hosted sulfur to fuel respiration.

In fact, metacinnabar oxidation is implicated by observations of sulfide oxidation products on the surface of cross sections of the same metacinnabar incubated in the creek sediments (**Figure 1B**). Specifically, principal component analysis (PCA) of X-ray fluorescence maps (XRF) were collected at seven different energies around the sulfur K-edge that are indicative of a full range of organic and inorganic sulfur species. This analysis indicated that three unique components were in the incubated metacinnabar samples. These components were identified as HgS, elemental sulfur (S^0), and sulfate (SO_4) by obtaining spot X-ray absorption near-edge structure (XANES) spectra and comparing them to model compounds (**Figure 1B**). Using unique spectral signatures for these phases, multiple-energy XRF maps for these three spectral components revealed heterogeneous surface rinds on the incubated metacinnabar surface composed primarily of elemental sulfur with isolated sulfate regions (**Figure 1B**). Oxidized sulfur products on the surface of metacinnabar incubated in sterile freshwater were not observed (Supplementary Figure S1).

Further, energy specific XRF maps reveal the presence of oxidized iron, as Fe(III) (hydr)oxides, in isolated regions on the surface of metacinnabar incubated in the creek sediments (**Figure 2**). Iron is present in the metacinnabar primarily as pyritic inclusions (**Figure 2**) and likely also as a trace co-precipitate within the structure. These results indicate that the metacinnabar surface was in fact dissolving leading to the formation of substantial surficial S^0 rinds and Fe (hydr)oxide precipitates. This oxidation may be a direct or indirect consequence of the activity of the chemosynthetic bacterial communities that had extensively colonized the mineral surface. In particular, these elemental sulfur rinds coupled with the extensive colonization of the surface by the obligate sulfur-oxidizer *T. thioparus*, an organism that cannot oxidize Fe(II), point to a role for microbially-mediated sulfur oxidation in the oxidative dissolution of metacinnabar in these incubations.

Metacinnabar Dissolution by *Thiobacillus* Cultures

Incubation of *T. thioparus* axenic cultures with metacinnabar at varying thiosulfate concentrations further points to microbially induced metacinnabar oxidation. In incubations containing an environmentally relevant thiosulfate concentration (initially ~60–100 μM), thiosulfate was consumed by *T. thioparus* within the first 5 days (**Figure 3A**) with the dominant oxidation product being sulfate (**Figure 3B**), formed through a S^0 intermediate (Supplementary Figure S2) as shown previously (Sattley and Madigan, 2006). Following thiosulfate consumption, sulfate concentrations in the presence of metacinnabar continued to increase at a faster rate than in its absence (17 and 10 μM

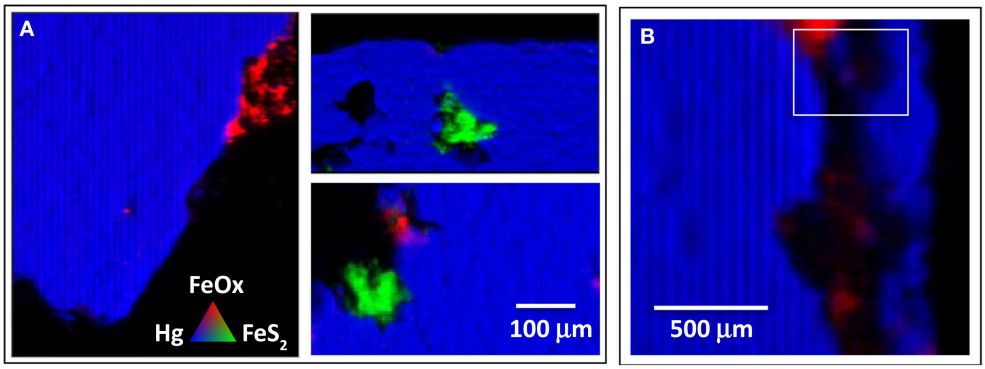

FIGURE 2 | Distribution and composition of Fe and Hg in cross sections obtained from field-incubated metacinnabar. Multiple energy maps were collected on beamline 2-3 at the Stanford Synchrotron Radiation Laboratory (see Methods). PCA analysis of the five energy Fe K-edge maps indicate that only two components account for the Fe speciation. Based on comparison to Fe XANES standard spectra, these components are a ferrihydrite-like Fe (oxy)hydroxide (FeOx) and pyrite (FeS_2). **(A)** These µ-XRF maps illustrate that Fe within the metacinnabar mineral is below detection except for regions containing pyritic inclusions (green). Significant oxidation of regions near the pyritic inclusions is not observed, however iron (oxy)hydroxide precipitates are observed in discrete regions on the metacinnabar surface (as would be expected if small amount of Fe were released from metacinnabar to the aerobic porewater). **(B)** An expanded image of the boxed region shown in **Figure 1**, shows some regions of oxidized iron within the map showing extensive elemental sulfur rinds (**Figure 1**). However, the oxidized iron phases are limited to the upper area of the map (spot size = 5 µm).

day^{-1} sulfate production, respectively, **Figure 3B**). Further, a substantially higher sulfate concentration was observed in the presence of metacinnabar relative to its absence (**Figure 3B**) and was formed in excess of that supported solely by oxidation of added thiosulfate and residual elemental sulfur in the inoculum (see **Table 1**). Together, these results suggest that metacinnabar is in fact fueling sulfur respiration and thereby undergoing microbially mediated oxidative dissolution.

Yet, despite apparent HgS dissolution, negligible levels of aqueous Hg were detected. Dissolved Hg^{2+} was observed in incubations containing killed (formaldehyde-treated or autoclaved) *T. thioparus* cells, with concentrations ranging from 36 nM to more than 500 nM within 10 days (**Figures 3C**, **4**). In contrast, aqueous Hg was below 3 nM in equivalent incubations containing viable cells (**Figures 3C**, **4**) and even after extended periods of time (>11 weeks). The explanation for this is that the aqueous Hg released during metacinnabar dissolution was rapidly volatilized to gaseous Hg^0 in the presence of viable *T. thioparus*. In fact, a substantial amount of gaseous Hg^0 was observed in metacinnabar incubations with viable cells (**Figure 5**). The cumulative gaseous Hg^0 released in the presence of *T. thioparus* varied with reaction time, cell density and initial thiosulfate concentration and ranged from ∼100 to >8000 ng Hg^0 per liter of culture over a 20-day period (**Figures 5A,B**).

Impact of Thiosulfate on Metacinnabar Dissolution

In incubations with initial thiosulfate concentrations of 0 and 60 µM, 48–68% of the excess sulfate production, could be solely attributed to microbial-enhanced HgS dissolution (see **Table 1** and Supplementary Figure S3). Even in the absence of any exogenous thiosulfate, Hg^0 formation was still occurring after 40 days amounting to nearly 400 ng of Hg(0) per liter of culture (**Figure 5C**) and further hinting at sustained microbial respiration and oxidation of metacinnabar-derived sulfur. Meanwhile, minimal volatilization was observed in incubations with killed cells, and with viable cells in the absence of metacinnabar (i.e., background Hg levels in air). The non-metabolic contribution in the killed cell controls is likely due to abiotic Hg(II) reduction by Fe(II) (Wiatrowski et al., 2009; Amirbahman et al., 2013) impurities within the metacinnabar structure (**Figure 2**). Elevated Hg^0 production in the presence of live cells demonstrates that Hg was in fact released from metacinnabar and then volatilized to Hg^0 by *T. thioparus*. Many sulfur-oxidizing organisms possess the enzyme mercuric reductase (Benson et al., 2009), *merA*, which reduces Hg^{2+} to Hg^0 (Barkay et al., 2003). Although *T. thioparus* may also have other strategies or proteins capable of Hg^{2+} reduction, PCR amplification using *mer*-specific primers and sequencing confirmed that *T. thioparus* possesses the *merA* gene. BLAST analysis of the *merA* fragment nucleotide sequence revealed a 98% sequence similarity to *T. thioparus* DSM 505 and 85% similarity to *Thiobacillus denitrificans* ATCC 25259, both containing putative mercuric reductase genes. Supplementary Data S1 includes the 285-bp sequence for the *merA* fragment identified. Hence, the *T. thioparus* strain used in these investigations has the genetic potential to reduce Hg^{2+} as observed in our incubations here.

Addition of higher thiosulfate levels led to enhanced metacinnabar dissolution and volatilization. In the absence of microbial activity (e.g., killed cells), aqueous Hg^{2+} levels increased with increasing initial thiosulfate concentration (**Figure 4**), indicating that thiosulfate stimulated metacinnabar dissolution. Thiosulfate is a strong Hg^{2+} complexing ligand (Crespo-Medina et al., 2009) and MINTEQ modeling indicated that under the experimental conditions tested, nearly all aqueous Hg^{2+} was complexed to thiosulfate, predominantly as $Hg(S_2O_3)_2^{-2}$ (98%) under low (100 µM) thiosulfate conditions

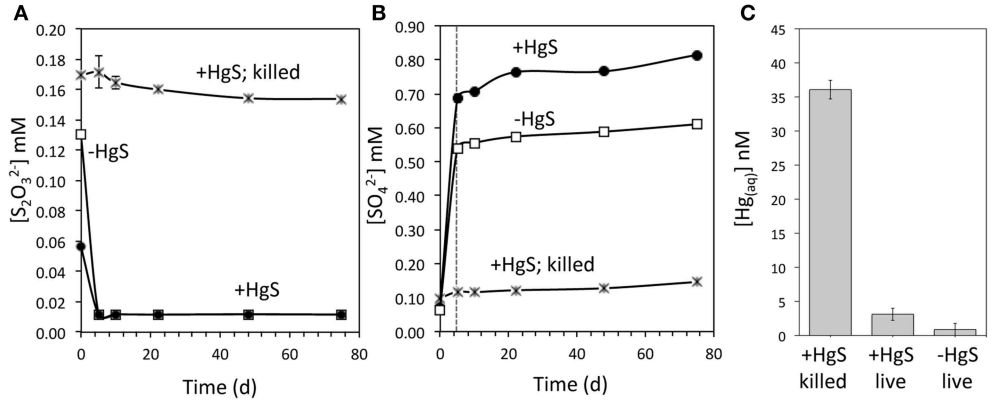

FIGURE 3 | Aqueous sulfur and mercury dynamics in *Thiobacillus* incubations with metacinnabar. Aqueous thiosulfate **(A)**, sulfate **(B)**, and Hg **(C)** concentrations within *Thiobacillus thioparus* incubations initiated with ∼100 μM thiosulfate and metacinnabar. Thiosulfate concentrations are below detection following 5 days of reaction **(A)** corresponding with an increase in the oxidation product sulfate **(B)**. Dashed vertical line in **(B)** indicates time point following which thiosulfate is no longer detected. In the absence of metacinnabar, sulfate production in excess of the stoichiometric amount of sulfate produced from thiosulfate oxidation (2 moles of sulfate produced per mole of thiosulfate), originates from the oxidation of elemental sulfur introduced from the inoculum. Minimal abiotic thiosulfate oxidation and sulfate production are observed in killed controls. A background sulfate level of less than 10 μM is observed accounting for any sulfate carryover from the killed inoculum as well as abiotic oxidative dissolution and release of surface sorbed sulfate (see **Table 1**). In contrast to killed incubations, aqueous Hg concentrations **(C)** in the presence of live *Thiobacillus* cells after 10 days of reaction are significantly lower. Error bars for most time points are smaller than the symbol. Error bars are the standard deviation for method duplicates. In a parallel set of incubations with metacinnabar and the same medium but no cells, aqueous Hg levels are 34 nM after 8 days (similar to 37 nM for killed controls). Further, sulfate production/release in these cell free controls within 10 days is 0.7 μM d^{-1}, again similar to the killed controls (1.7 μM d^{-1}).

TABLE 1 | Microbial contribution to metacinnabar dissolution and microbially mediated dissolution rates.

Initial Thiosulfate Concentration	x days	H_x μM	N_x μM	A_x μM	C_0 μM	M_x μM	Contribution of microbial processes to total HgS dissolution (%)	R μmol (sulfate) m^{-2} d^{-1}
0 μM	11	1024	927	57	7	47	48	16.2
	10	710	560	120	60	90	60	34.1
60 μM	22	760	570	120	60	130	68	22.4
	75	810	610	150	60	110	55	–

The microbial contribution to metacinnabar dissolution observed in our incubations was calculated using sulfate production as a proxy for metacinnabar dissolution as has been reported previously (Barnett et al., 2001; Holley et al., 2007) and calculated using the equation, $M_x = (H_x - N_x) - (A_x - C_0)$, where M_x is the microbial contribution to sulfate production x days after inoculation, H_x is the sulfate produced in live Thiobacillus incubations in the presence of metacinnabar (+HgS), N_x is sulfate produced in live Thiobacillus incubations in the absence of metacinnabar (–HgS), A_x is sulfate produced in killed cell incubations in the presence of metacinnabar (+HgS), and C_0 is the initial sulfate concentration (t = 0) in live Thiobacillus incubations in the absence of metacinnabar (–HgS). The term N_x represents sulfate production attributed to thiosulfate and elemental sulfur oxidation, as well as carryover sulfate from the inoculum, and ($H_x - N_x$) represents sulfate release from metacinnabar from biotic and abiotic processes. The term ($A_x - C_0$) represents abiotic oxidative dissolution and release of any sulfate bound to the metacinnabar surface, with C_0 representing carryover sulfate from the inoculum. M_x, H_x, N_x, A_x, and C_0 are reported in μM. Microbially mediated metacinnabar dissolution rates (R) are calculated by taking into account mineral loading (2 g metacinnabar L^{-1} incubation) and surface area (0.1321 m^2 g^{-1}) and are presented as μmoles (sulfate) m^{-2} d^{-1}.

and $Hg(S_2O_3)_3^{-4}$ (77%) under high (20 mM) thiosulfate concentrations. In the presence of live *T. thioparus*, higher thiosulfate concentrations also led to higher cell densities (Supplementary Figure S4) ultimately resulting in a greater mass of Hg volatilized over a given time period (**Figure 5**). The Hg volatilization rate (∼100–500 ng L^{-1} d^{-1}) after 11–30 days of incubation, when most thiosulfate had been consumed by cells (concentration remaining 0–5 μM), however is similar when normalized to cell abundance (∼50 ag Hg $cell^{-1}$ d^{-1}) for a wide range of initial thiosulfate concentrations (40 μM to 20 mM) (Supplementary Figure S5). Thus, thiosulfate had a dual effect on HgS dissolution, by acting as both a complexing ligand inducing abiotic metacinnabar dissolution before it was consumed through cell respiration and by thereby supporting higher cell densities to stimulate microbially induced dissolution. Our findings demonstrate that at environmentally relevant concentrations, even a small increase in initial thiosulfate abundance (from <4 to 40 μM) resulted in a large enhancement of Hg volatilization (∼35 times, **Figure 5**).

Thiosulfate is a major intermediate sulfur species in environmental systems formed through both oxidative and reductive legs of the sulfur cycle, leading to high thiosulfate fluxes despite variable steady-state concentrations (typically low- to mid-micromolar concentrations, but as high as 3 mM in

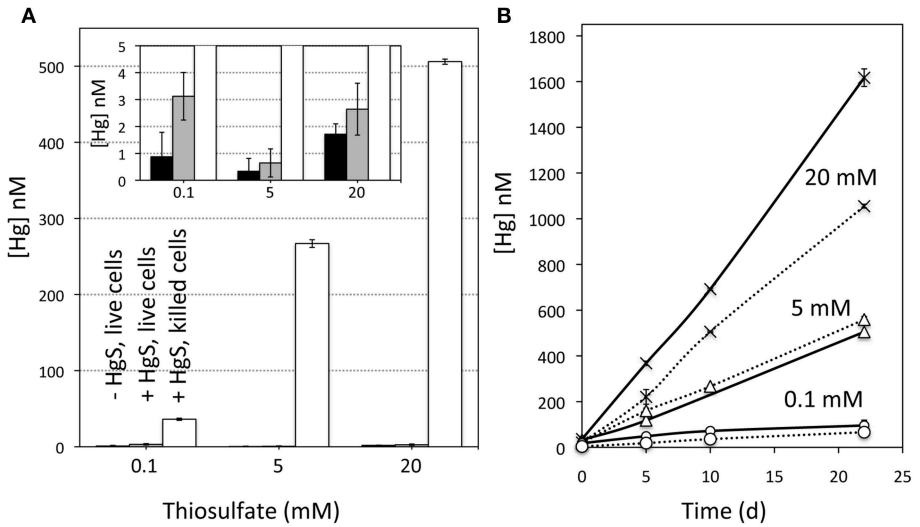

FIGURE 4 | Aqueous Hg concentrations in incubations. (A) Aqueous Hg concentrations (nM) in incubations containing various initial thiosulfate concentrations after 10 days of reaction. The conditions included (black bars) live cells, no metacinnabar; (gray bars) live cells plus metacinnabar, and (white bars) killed cells plus metacinnabar. The inset shows data up to 5 nM Hg to illustrate the differences in the live incubations that are masked in the full range due to the high Hg in killed cell incubations. **(B)** Aqueous Hg concentrations (nM) over time as a function of thiosulfate concentration (0.1, 5, and 20 mM) within incubations containing killed cells and metacinnabar. The solid lines were conducted in a basal freshwater medium containing EDTA, while the dashed lines contained no EDTA. The standard deviation of two method replicates is indicated.

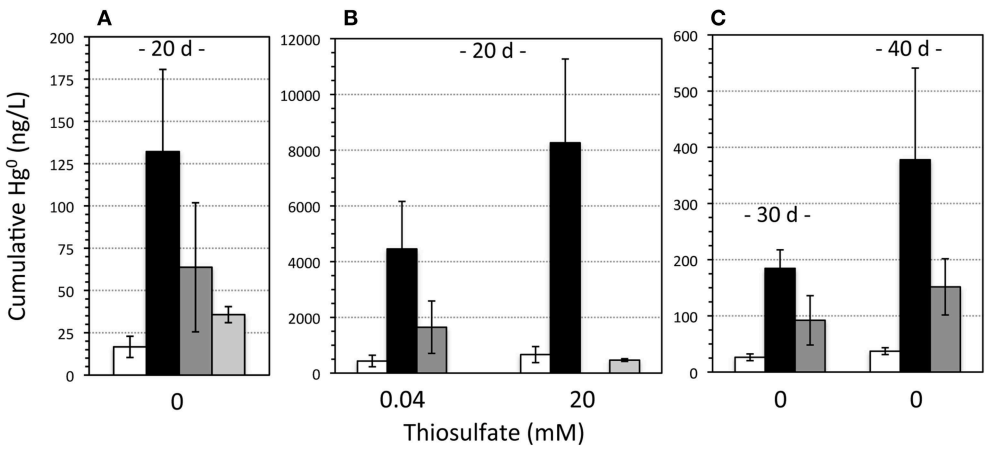

FIGURE 5 | Gaseous mercury (Hg^0) measured in *Thiobacillus* incubations. Concentrations are presented as ng Hg^0 per liter of culture volume. **(A,B)** Gaseous Hg production after 20 days within incubations containing no HgS (white bars), HgS plus live *Thiobacillus* (black bars), HgS plus live *Thiobacillus* at a lower cell density (~10× fewer cells) (dark gray bars), and HgS plus killed *Thiobacillus* cells (light gray bars) and with an initial thiosulfate concentration of **(A)** zero and **(B)** 0.04 or 20 mM thiosulfate. **(C)** Gaseous Hg produced in the zero thiosulfate incubations after 30 and 40 days. Error bars are the standard deviation for two to four biological replicates.

estuarine and marine waters and sediments) (Luther et al., 1986; Jorgensen, 1990a,b; Zopfi et al., 2004; Mullaugh et al., 2008). Accordingly, a subset of experiments was performed to determine the impact of sustained fluxes of thiosulfate on metacinnabar dissolution and Hg volatilization, as well as to compare natural metacinnabar (surface area = 0.1321 ± 0.0007 m^2 g^{-1}) to a synthetic iron-free, finer grained, and higher surface area metacinnabar phase (surface area = 1.2804 ± 0.0045 m^2 g^{-1}). Daily 100 μM thiosulfate spikes were quickly oxidized within hours in the presence of live *T. thioparus* with concomitant sulfate production, while thiosulfate was minimally consumed in killed incubations (**Figure 6**). Dissolved Hg in killed incubations increased over the course of the experiment, due to thiosulfate-induced Hg complexation and dissolution, with a more pronounced increase in natural than in synthetic metacinnabar incubations (**Figure 6**). Dissolved Hg concentrations in natural metacinnabar incubations were ~7× higher than with synthetic metacinnabar, which may be a

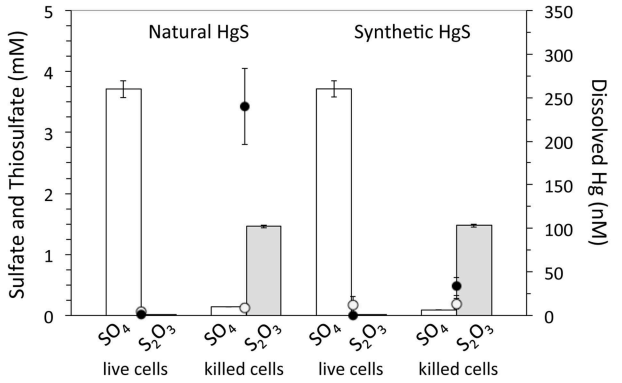

FIGURE 6 | Sulfate, thiosulfate, and dissolved Hg within *T. thioparus* incubations in thiosulfate spike experiments. Sulfate (white bars) and thiosulfate (gray bars) concentrations in live and killed cell incubations 12 days after inoculation and following daily 100 μM additions of thiosulfate. Dissolved Hg measured in incubations 15 h (open circles) and 12 days (solid circles) after inoculation. Error bars indicate the standard deviation of three replicate incubations.

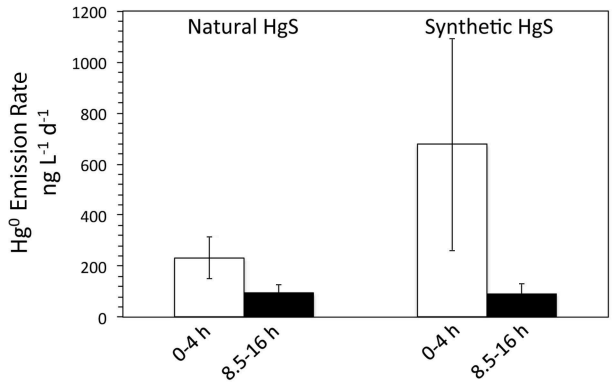

FIGURE 7 | Gaseous Hg emission rates within *T. thioparus* incubations in thiosulfate spike experiments. Average gaseous Hg emission rates within live *T. thioparus* incubations with natural and synthetic metacinnabar and a daily 100 μM thiosulfate spike. Each Hg^0 emission rate displayed represents an average of 5 measurements ($n = 5$) that were taken on 5 different days (days 4–9 during incubation) and grouped for timepoints obtained either 0–4 or 8.5–16 h following the spike. Error bars indicate the standard deviation of measurements taken from three replicate incubations and the five measurements for each time sampling. The high variability in the incubations is due to deviations in the metabolic activity of *Thiobacillus* in the biological replicates and likely also changes in mineral activity/reactivity over the course of the experiment.

consequence of greater Hg adsorption to the higher surface area synthetic phase. Equivalent dissolved Hg levels were obtained for solutions filtered with 0.02 and 0.2 μm filters, indicating that the released Hg from metacinnabar was in fact dissolved Hg and there was no significant nanoparticulate contribution. As expected, gaseous Hg(0) was observed in both the natural and synthetic HgS incubations; albeit with a high degree of variability likely due to an offset in the microbial activity of the biological replicates (**Figure 7**). Overall, a general trend toward decreasing Hg volatilization rates was observed over time following the thiosulfate spike (**Figure 7**).

The timing of thiosulfate additions had a substantial effect on the dynamics of microbially-induced volatilization of mineral-hosted Hg, with release of volatile Hg from natural and synthetic metacinnabar occurring rapidly within the first few hours following the thiosulfate spike, and decreasing volatilization after thiosulfate is consumed by *T. thioparus* (**Figure 7**). Thus, in natural systems where a low continuous flux of thiosulfate is likely present, microbial volatilization of Hg-thiosulfate complexes may lead to substantial metacinnabar dissolution and represent a significant source of gaseous Hg(0). Further, despite synthetic metacinnabar having a higher surface area and thus theoretically higher solubility, enhanced abiotic dissolution of natural metacinnabar here points to more complex controls on metacinnabar dissolution and likely highlights the importance of impurities such as iron.

Conclusion

Here we show that authigenic HgS is not merely a sink for Hg within non-acidic natural environments and instead is a source of gaseous Hg (**Figures 5**, **7**). Volatilization of metacinnabar-hosted Hg is a coupled process involving metacinnabar dissolution (**Figure 4**) and microbial reduction of released Hg (**Figures 5**, **7**). Both microbial activity and thiosulfate enhance Hg release through presumably oxidative and ligand-promoted dissolution processes, respectively. Surprisingly, it appears that metacinnabar could serve as a respiratory source of sulfur in the absence of thiosulfate for *T. thioparus* (**Figure 3**, **Table 1**) and likely other sulfur-oxidizing bacteria (e.g., *Sulfuricurvum* and *Sulfuricella*) explaining their extensive colonization on metacinnabar in sediments (**Figure 1**). Utilizing HgS as a metabolic substrate, however, likely limits the sulfur-oxidizing community to those that can also detoxify the Hg released upon dissolution. Metacinnabar dissolution by thiosulfate (**Figure 4**) or other Hg complexing ligands will also provide sulfide or other S intermediates (e.g., formed via abiotic oxidation of sulfide) further fueling the metabolism of sulfur-oxidizing organisms. Within aerobic systems, as explored here, this volatilized Hg may evade to the atmosphere. Under fluctuating redox conditions, however, methylation may compete for the released Hg from metacinnabar. The ultimate fate of released Hg from metacinnabar will undoubtedly be a function of the system geochemistry and resident microbial community. Regardless of the dissolution mechanisms and fate of Hg, these complex dynamics challenge the notion that metacinnabar serves as a static Hg host within non-acidic sediments.

These findings point to HgS as an underappreciated source of Hg to the environment. Based on these Hg volatilization rates, this process could account for a significant amount of Hg release from sediments and soils into the atmosphere. The microbially enhanced dissolution rates observed here, excluding any abiotic contribution, are 9–1000 times higher than known oxidative dissolution rates (3.15×10^{-2} to 1.90 μmol (sulfate)

m^{-2} d^{-1}) (Barnett et al., 2001; Holley et al., 2007) (see **Table 1**). A reasonable extrapolation for the environmentally relevant Hg volatilization rate from the processes observed in this study is 34 ng Hg m^{-2} h^{-1} (see **Table 1**), which falls within the range of observed emissions from mineral mercury enriched areas (2–440 ng Hg m^{-2} h^{-1}) (Gustin, 2011). Our findings may provide a mechanistic understanding, at least in part, for these field observations. Further, as a first approximation, extrapolating this area normalized rate to an area roughly equivalent to that of all wetlands, redox dynamic systems rich in metal sulfides and thiosulfate, yields a Hg release rate of 1 Mmoles yr^{-1} (see Supplementary Table S3). For scale, total Hg emissions from terrestrial soils are estimated at 15 Mmoles yr^{-1} (Smith-Downey et al., 2010) with the contribution from geologically enriched soils estimated at 2.5–7.5 M yr^{-1} (Gustin, 2011). With that being said, the HgS loadings used in this study were employed to mimic Hg contaminated systems that are common worldwide (Barnett et al., 1997), and thus the application of this process to regional and global scale budgets that take into account also lower HgS environments requires further exploration and validation.

Author Contributions

AV and CH jointly conceived of the study and designed the experiments. AV performed the experiments; AV, TZ, and CH collected the data; CS, SW, and CL assisted in data analysis; SB assisted with fieldwork. AV and CH wrote the manuscript with input from TZ, CL, CS, SW, and SB.

Acknowledgments

This work was supported by the National Science Foundation Graduate Research Fellowship under Grant No. DGE-0644491 awarded to AV. The authors thank R. Perdigão-Henriques and W. D. Leavitt for assistance in processing field samples; C. S. Kim, C. J. Lentini, and J. P. Shine for helpful conversations regarding this study; G. Swarr for assistance with Tekran operation; and N. Lupoli and Z. Dong for assistance with the DMA-80.

Part of this research was conducted at the Stanford Synchrotron Radiation Lightsource. Use of the Stanford Synchrotron Radiation Lightsource, SLAC National Accelerator Laboratory, is supported by the U.S. Department of Energy, Office of Science, Office of Basic Energy Sciences under Contract No. DE-AC02-76SF00515.

Supplementary Material

The Supplementary Material for this article can be found online at: http://journal.frontiersin.org/article/10.3389/fmicb.2015.00596

References

Altschul, S. F., Madden, T. L., Schaffer, A. A., Zhang, J., Zhang, Z., Miller, W., et al. (1997). Gapped BLAST and PSI-BLAST: a new generation of protein database search programs. *Nucleic Acids Res.* 25, 3389–3402. doi: 10.1093/nar/25.17.3389

Amirbahman, A., Kent, D. B., Curtis, G. P., and Marvin-Dipasquale, M. C. (2013). Kinetics of homogeneous and surface-catalyzed mercury(II) reduction by iron(II). *Environ. Sci. Technol.* 47, 7204–7213. doi: 10.1021/es401459p

Atlas, R. M. (2005). *Handbook of Media for Environmental Microbiology*. Boca Raton, FL: CRC Press.

Baldi, F., and Olson, G. J. (1987). Effects of Cinnabar on Pyrite Oxidation by *Thiobacillus ferrooxidans* and Cinnabar Mobilization by a Mercury-Resistant Strain. *Appl. Environ. Microbiol.* 53, 772–776.

Barkay, T., Miller, S. M., and Summers, A. O. (2003). Bacterial mercury resistance from atoms to ecosystems. *FEMS Microbiol. Rev.* 27, 355–384. doi: 10.1016/S0168-6445(03)00046-9

Barnett, M. O., Harris, L. A., Turner, R. R., Stevenson, R. J., Henson, T. J., Melton, R. C., et al. (1997). Formation of mercuric sulfide in soil. *Environ. Sci. Technol.* 31, 3037–3043. doi: 10.1021/es960389j

Barnett, M. O., Turner, R. R., and Singer, P. C. (2001). Oxidative dissolution of metacinnabar (beta-HgS) by dissolved oxygen. *Appl. Geochem.* 16, 1499–1512. doi: 10.1016/S0883-2927(01)00026-9

Benson, D. A., Karsch-Mizrachi, I., Lipman, D. J., Ostell, J., and Sayers, E. W. (2009). GenBank. *Nucleic Acids Res.* 37, D26–D31. doi: 10.1093/nar/gkn723

Chadhain, S. M. N., Schaefer, J. K., Crane, S., Zylstra, G. J., and Barkay, T. (2006). Analysis of mercuric reductase (merA) gene diversity in an anaerobic mercury-contaminated sediment enrichment. *Environ. Microbiol.* 8, 1746–1752. doi: 10.1111/j.1462-2920.2006.01114.x

Clarkson, T. W., and Magos, L. (2006). The toxicology of mercury and its chemical compounds. *Crit. Rev. Toxicol.* 36, 609–662. doi: 10.1080/10408440600845619

Crespo-Medina, M., Chatziefthimiou, A. D., Bloom, N. S., Luther, G. W., Wright, D. D., Reinfelder, J. R., et al. (2009). Adaptation of chemosynthetic microorganisms to elevated mercury concentrations in deep-sea hydrothermal vents. *Limnol. Oceanogr.* 54, 41–49. doi: 10.4319/lo.2009.54.1.0041

Dyrssen, D. (1989). Biogenic sulfur in two different marine environments. *Mar. Chem.* 28, 241–249. doi: 10.1016/0304-4203(89)90198-9

Graham, A. M., Aiken, G. R., and Gilmour, C. C. (2012). Dissolved organic matter enhances microbial mercury methylation under sulfidic conditions. *Environ. Sci. Technol.* 46, 2715–2723. doi: 10.1021/es203658f

Gustin, M. S. (2011). "Exchange of mercury between the atmosphere and terrestrial ecosystems," in *Environmental Chemistry and Toxicology of Mercury*, eds G. Liu, Y. Cai, and N. O'Driscoll (Hoboken, NJ: John Wiley & Sons, Inc.,), 423–451. doi: 10.1002/9781118146644.ch13

Hammerschmidt, C. R., Bowman, K. L., Tabatchnick, M. D., and Lamborg, C. H. (2011). Storage bottle material and cleaning for determination of total mercury in seawater. *Limnol. Oceanogr. Methods* 9, 426–431. doi: 10.4319/lom.2011.9.426

Hansel, C. M., Fendorf, S., Jardine, P. M., and Francis, C. A. (2008). Changes in bacterial and archaeal community structure and functional diversity along a geochemically variable soil profile. *Appl. Environ. Microbiol.* 74, 1620–1633. doi: 10.1128/AEM.01787-07

Holley, E. A., McQuillan, A. J., Craw, D., Kim, J. P., and Sander, S. G. (2007). Mercury mobilization by oxidative dissolution of cinnabar (alpha-HgS) and metacinnabar (beta-HgS). *Chem. Geol.* 240, 313–325. doi: 10.1016/j.chemgeo.2007.03.001

Jew, A. D., Behrens, S. F., Rytuba, J. J., Kappler, A., Spormann, A. M., and Brown, G. E. Jr. (2014). Microbially enhanced dissolution of HgS in an acid mine drainage system in the California Coast Range. *Geobiology* 12, 20–33. doi: 10.1111/gbi.12066

Jorgensen, B. B. (1990a). The Sulfur cycle of freshwater sediments: role of thiosulfate. *Limnol. Oceanogr.* 35, 1329–1342. doi: 10.4319/lo.1990.35.6.1329

Jorgensen, B. B. (1990b). A thiosulfate shunt in the sulfur cycle of marine sediments. *Science* 249, 152–154. doi: 10.1126/science.249.4965.152

Kelly, D. P., and Wood, A. P. (2000). Confirmation of *Thiobacillus denitrificans* as a species of the genus *Thiobacillus*, in the beta-subclass of the Proteobacteria, with strain NCIMB 9548 as the type strain. *Int. J. Syst. Evol. Microbiol.* 50, 547–550. doi: 10.1099/00207713-50-2-547

Lamborg, C. H., Hammerschmidt, C. R., Gill, G. A., Mason, R. P., and Gichuki, S. (2012). An intercomparison of procedures for the determination of total mercury in seawater and recommendations regarding mercury speciation during GEOTRACES cruises. *Limnol. Oceanogr. Methods* 10, 90–100. doi: 10.4319/lom.2012.10.90

Lane, D. J. (1991). "16S/23S rRNA sequencing," in *Nucleic Acid Techniques in Bacterial Systematics,* eds E. Stackbrandt and M. Goodfellow (Chichester: Wiley), 115–175.

Luther, G. W., Church, T. M., Scudlark, J. R., and Cosman, M. (1986). Inorganic and organic sulfur cycling in salt-marsh pore waters. *Science* 232, 746–749. doi: 10.1126/science.232.4751.746

Mason, R. P., Choi, A. L., Fitzgerald, W. F., Hammerschmidt, C. R., Lamborg, C. H., Soerensen, A. L., et al. (2012). Mercury biogeochemical cycling in the ocean and policy implications. *Environ. Res.* 119, 101–117. doi: 10.1016/j.envres.2012.03.013

McNutt, M. (2013). Mercury and Health. *Science* 341, 1430. doi: 10.1126/science.1245924

Mullaugh, K. M., Luther, G. W. III., Ma, S., Moore, T. S., Yucel, M., Becker, E. L., et al. (2008). Voltammetric (micro)electrodes for the *in situ* study of Fe2+ oxidation kinetics in hot springs and S2O32- production at hydrothermal vents. *Electroanalysis* 20, 280–290. doi: 10.1002/elan.200704056

Nawrocki, E. P., Kolbe, D. L., and Eddy, S. R. (2009). Infernal 1.0: inference of RNA alignments. *Bioinformatics* 25, 1335–1337. doi: 10.1093/bioinformatics/btp157

Noble, R. T., and Fuhrman, J. A. (1998). Use of SYBR Green I for rapid epifluorescence counts of marine viruses and bacteria. *Aquat. Microb. Ecol.* 14, 113–118. doi: 10.3354/ame014113

Quince, C., Lanzen, A., Davenport, R. J., and Turnbaugh, P. J. (2011). Removing noise from pyrosequenced amplicons. *BMC Bioinformatics* 12:38. doi: 10.1186/1471-2105-12-38

Ravichandran, M. (2004). Interactions between mercury and dissolved organic matter - a review. *Chemosphere* 55, 319–331. doi: 10.1016/j.chemosphere.2003.11.011

Santelli, C. M., Orcutt, B. N., Banning, E., Bach, W., Moyer, C. L., Sogin, M. L., et al. (2008). Abundance and diversity of microbial life in ocean crust. *Nature* 453, U653–U657. doi: 10.1038/nature06899

Sattley, W. M., and Madigan, M. T. (2006). Isolation, characterization, and ecology of cold-active, chemolithotrophic, sulfur-oxidizing bacteria from perennially ice-covered lake Fryxell, Antarctica. *Appl. Environ. Microbiol.* 72, 5562–5568. doi: 10.1128/AEM.00702-06

Smith-Downey, N. V., Sunderland, E. M., and Jacob, D. J. (2010). Anthropogenic impacts on global storage and emissions of mercury from terrestrial soils: insights from a new global model. *J. Geophys. Res.* 115, G03008. doi: 10.1029/2009JG001124

Turner, S. J., Pryer, K. M., Miao, V. P. M., and Palmer, J. D. (1999). Investigting deep phylogenetic relationships among cyanobacteria and plastids by small subunit rRNA sequence analysis. *J. Eukaryot. Microbiol.* 46, 327–338. doi: 10.1111/j.1550-7408.1999.tb04612.x

Vishnivetskaya, T. A., Mosher, J. J., Palumbo, A. V., Yang, Z. K., Podar, M., Brown, S. D., et al. (2011). Mercury and other heavy metals influence bacterial community structure in contaminated Tennessee Streams. *Appl. Environ. Microbiol.* 77, 302–311. doi: 10.1128/AEM.01715-10

Wang, Q., Garrity, G. M., Tiedje, J. M., and Cole, J. R. (2007). Naive Bayesian classifier for rapid assignment of rRNA sequences into the new bacterial taxonomy. *Appl. Environ. Microbiol.* 73, 5261–5267. doi: 10.1128/AEM.00062-07

Webb, S. M. (2005). SIXPack a graphical user interface for XAS analysis using IFEFFIT. *Phys. Scr.* T115:1011. doi: 10.1238/Physica.Topical.115a01011

Webb, S. M. (2006). *SMAK: Sam's Microprobe Analysis Kit, v.0.25*. Menlo Park, CA: Stanford Synchrotron Radiation Laboratory.

Webster, G., Newberry, C. J., Fry, J. C., and Weightman, A. J. (2003). Assessment of bacterial community structure in the deep sub-seafloor biosphere by 16S rDNA-based techniques: a cautionary tale. *J. Microbiol. Methods* 55, 155–164. doi: 10.1016/S0167-7012(03)00140-4

Wiatrowski, H. A., Das, S., Kukkadapu, R., Ilton, E. S., Barkay, T., and Yee, N. (2009). Reduction of Hg(II) to Hg(0) by Magnetite. *Environ. Sci. Technol.* 43, 5307–5313. doi: 10.1021/es9003608

Widdel, F., and Bak, F. (1992). "Gram-negative mesophilic sulfate-reducing bacteria," in *The Prokaryotes* eds A. Balows, G. Truper, M. Dworkin, W. Harder, and K. H. Schleifer (New York, NY: Springer), 3352–3378.

Wiener, J. G., Krabbenhoft, D. P., Heinz, G. H., and Scheuhammer, A. M. (2002). "Ecotoxicology of mercury," in *Handbook of Ecotoxicology*, *2nd Edn.,* eds D. J. Hoffman, B. A. Rattner, G. A. Burton, Jr., and J. Cairns, Jr. (Boca Raton, FL: CRC Press), 409–464.

Zopfi, J., Ferdelman, T. G., and Fossing, H. (2004). Distribution and fate of sulfur intermediates—sulfite, tetrathionate, thiosulfate, and elemental sulfur—in marine sediments. *Geol. Soc. Am. Spec. Pap.* 379, 97–116. doi: 10.1130/0-8137-2379-5.97

Conflict of Interest Statement: The authors declare that the research was conducted in the absence of any commercial or financial relationships that could be construed as a potential conflict of interest.

Advantages of publishing in Frontiers

OPEN ACCESS
Articles are free to read for greatest visibility and readership

FAST PUBLICATION
Around 90 days from submission to decision

HIGH QUALITY PEER-REVIEW
Rigorous, collaborative, and constructive peer-review

TRANSPARENT PEER-REVIEW
Editors and reviewers acknowledged by name on published articles

Frontiers
Avenue du Tribunal-Fédéral 34
1005 Lausanne | Switzerland

Visit us: www.frontiersin.org
Contact us: info@frontiersin.org | +41 21 510 17 00

REPRODUCIBILITY OF RESEARCH
Support open data and methods to enhance research reproducibility

DIGITAL PUBLISHING
Articles designed for optimal readership across devices

FOLLOW US
@frontiersin

IMPACT METRICS
Advanced article metrics track visibility across digital media

EXTENSIVE PROMOTION
Marketing and promotion of impactful research

LOOP RESEARCH NETWORK
Our network increases your article's readership